

ISSN: 2249-6645

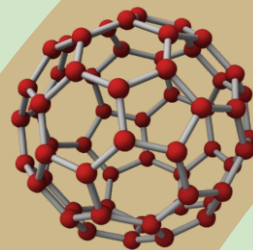


International Journal of Modern Engineering Research (IJMER)

Volume 4

Issue 4

April 2014





International Journal of Modern Engineering Research (IJMER)

Volume : 4 Issue : 4 (Version-1)

ISSN : 2249-6645

April - 2014

Contents :

Study on Bogie and Suspension System of an Electric Locomotive (Wap-4) <i>S. Naveen, C. P. Kiran, M. Prabhu Das, P. Naga Dilip, V. V. Prathibha Bharathi</i>	01-14
Study of Performance of Different Blends of Biodiesel Prepared From Waste Cottonseed Oil <i>Singh Harpreet, Mangla Arunish, Singh Jaspreet</i>	15-20
Securing Data Communication for Node Anonymization Using Location Information <i>Ms. Kanchan P. Kamdi, Mr. G. Rajesh Babu</i>	21-23
Considering User Participation in Light Of level and Stages of Self-Selection in Architectural Design Process (ADP) <i>Mahdi Torabi, Mohammad Pir Mohammadi, Mohsen Roshan, Mahmud Bin Mohd Jusan</i>	24-28
Implementation of FSM Based Automatic Dispense Machine with Expiry Date Feature Using VHDL <i>Mohd. Suhail, Saima Beg</i>	29-33
Palmprint Identification Based on Principle Line Using Machine Learning Techniques <i>Krishnaveni M., Arunpriya C.</i>	34-43
Comparison of Morphological, Averaging & Median Filter <i>Alka Bishnoi</i>	44-45
A Case study for near net Shape – Flashless forging for full yoke (Sleeve Yoke OMNI) <i>Er. O. P. Dwivedi, Er. Dharminder singh</i>	46-64
Some New Operations on Fuzzy Soft Sets <i>Kumud Borgohain, Chittaranjan Gohain</i>	65-68
Measurements Of Dielectric Constant Of Solid Material (Leather Belt) At X-Band And Proposed Wearable Antenna <i>Ambika Singh, Dr. Sudhakar Sahu</i>	69-73

Study on Bogie and Suspension System of an Electric Locomotive (Wap-4)

S. Naveen¹, C. P. Kiran², M. Prabhu Das³, P. Naga Dilip⁴,
V. V. Prathibha Bharathi⁵

^{1,2,3,4} Students of Mechanical Engg, MRCE, Hyderabad

⁵ Associate Prof. of Mechanical Engg, MRCE, Hyderabad

Abstract: This project involves a detailed study on the “**BOGIE AND SUSPENSION SYSTEM OF AN ELECTRIC LOCOMOTIVE (WAP-4)**” in Indian Railways. It involves a list of information on the various parts of a conventional type bogie and also the various advantages of different types of suspension and damping systems installed. Detailed explanation of various electrical and controls of the locomotive were described in the report. Various physical testing methods of springs were focused under suspension chapter. This report isn't just focused on the conventional type loco, but also gives detailed differences observed between the 3-phase bogies from the conventional type loco. In electrified railways, the traction power systems carry power to trains and their reliability is vital to the quality of train services. There are many components in the traction power system, from interface with utility distribution network to contacts with trains, and they are physically located along the rail line. Subject to usage, environment, and ageing conditions of components deteriorate with time. Regular maintenance has to be carried out to restore their conditions and prevent them from failure. However, the decisions on the suitable length of maintenance intervals often lead railway operators to the dilemma of minimizing both risk of failure and operation cost. In the last 20 years, there has been a gigantic acceleration in railway traction development. This has run in parallel with the development of power electronics and microprocessors. What have been the accepted norms for the industry for, sometimes, 80 years, have suddenly been thrown out and replaced by fundamental changes in design, manufacture and operation. Many of these developments are technical and complex. Through this report, we bring to you all the salient features and all important aspects of bogies and suspension system of conventional type Electric Locomotive (WAP-4).

I. Introduction

Indian Railways has a total state monopoly on India's rail transport. It is one of the largest and busiest rail network in the world, transporting 16 million passengers and more than 1 million tones of freight daily. IR is the world's largest commercial or utility employer, with more than 95 lakh employees. The Railways traverse the length and breadth of the country; the routes cover a total length of 63,140 KM (39,233 miles). As of 2002, IR owned a total of 216,717 wagons, 39, 263 coaches and 7,739 locomotives and ran total of 14,444 trains daily, including about 8,702 passenger trains.

1.1 Overview of Electric Locomotive

Due to scarcity of energies like coal, diesel and petrol and also due to increasing environmental pollution, electrification in the railways became a necessity. By electrification the following benefits can be obtained:

1. A pollution free environment
2. Easy and cheap maintenance
3. Saving of essential fuels like coal, diesel etc.
4. Faster, quicker and comfortable transports
5. Smooth starting and stopping

1.2 Trend

The first locomotive was invented by Cornish inventor Richard Trevithick in 1804 & the trend of locomotives started with steam engines, and then developed to diesel engines, which ruled the era for quite a lot of time. The diesel engines were very much flexible and would have a considerable hauling power compared to

the steam ones. But a drastic change influenced the railways with the invention of electrically operated locomotives. These locomotives at the beginning required constraint to be fulfilled, which was to provide electric power always available for the locomotive. This took time and even a huge investment to install electric supply lines all over the areas and also provide adequate and correct amount of power for the loco anywhere it goes. The railway also had to install the sub-stations to boost up the power. Railways signed the contract with state electricity boards, with consent of NTPC which would provide railways a reliable and continual power. After the constraints were fulfilled, the emerging electric locomotives came into applications.

The new invention improved the efficiency of the railway system and moreover reduces the effort of the personal driving the locomotive. Slight modification made the system more and more efficient and flexible, which earned huge profits in the railway sectors. Now, the railways have to surpass the hardship of totally electrifying the network so that the locomotive can run all over.

1.3 Importance of Locomotives

The Locomotive is practically the sole responsible for the smooth running of the whole rail vehicle. It's because of the reason every locomotive is being checked by loco shed department for every 45 days and the maintenance is scheduled for some periods. The initially developed locomotives used power converters, which would convert the received AC power to DC power and feed to DC motors. The new microprocessor controlled locomotives take the AC power and feed the rugged AC induction motors by power conversions criteria these locomotives have surpassed all hardships and also running smoothly as of now. It has been proposed that the new locomotives would replace the old ones with its advantage and comfort for the driver. Making a thorough study of the convention type bogie and suspension of WAP-4 makes the report. The rest of the report portrays the locomotive parts, its working and technical data.

II. Literature Survey

The electric locomotives contain 6 traction motors each driving one shaft. Under each bogie there are three traction motors driving each shaft contain wheels. The conventional DC locos which evolved with the invention of the electric engines use DC series motors. The main transformer fetches AC power from the main power supply. The secondary of the transformer having an auto transformer winding which facilitates the variable voltage supply from the transformer. The secondary stage after the transformer is the reflector block where the sinusoidal supply gets converted to pulsed DC from the power by the bridges from circuited power converters. The power diodes convert the power from AC to DC. After the required Voltage is sent out from the transformer the converter phase is supported by filter network which smoothens the ripples of the DC rectified output. The rectified output is fed to the DC series motors. The DC motor rotates as per the given voltage.

2.1 Description of Locomotive General

1. Locomotives are designed to operate on 25KV AC. Single phase 50 Hz Over Head Lines. Locomotive is of Co-Co type. Consists of single body on two bogies, each having three driving axles.
2. Each bogie is equipped with three axles hung noise supported traction motors to drive the axle through pinion and gear and the body has driving caps at either ends. Inter connections between caps is provided by two corridor on either ends.
3. Current is collected from over head line by pantograph and is fed to an auto transformer through a high voltage circuit breaker is mounted on roof. The transformer steps down the 25KV to 1730V (2 x 865V). It is then converted to DC through two bridged connected Silicon rectifiers and is fed to traction motors.
4. Speed regulation is obtained by varying the voltage at the motor terminals by tap changer. Traction motors are permanently connected in parallel combination.
5. A locomotive is provided with rheostatic braking, besides vacuum and loco air brakes. Rheostatic braking can't be used in case of traction motor isolation and failure of any one of the rectifier.
6. The auxiliary machines are fed from ARNO converters, which convert the incoming AC single phase supply to three-phase at 380V. If one of the rectifier bridges becomes defective, the locomotive will work with other rectifier unit with half power.

2.2 Designation of Locos

Early rudimentary attempts of locomotives were the direct steam engines, direct internal combustion engine system, and the medieval version added to as steam electric system, internal combustion with electric drive, battery electric drive, have all been attempts in enhancing the technology and evolved at the stage of electrification of the track. Locomotives, except for older steam ones have classification codes that identify them. These codes are of the form (gauge, power, load and series). Indian railways engaged only two types of locomotives viz. WAG and WAP locomotives. Locomotives are classified as WAG and WAP depending upon

gear ratios; it means more speed but low hauling capacity for passengers. Locomotives (WAP) and vice versa in case of goods locomotive (WAG), the max.speed of WAP type is about 110 kmph.

1. **WAG** stands for Wide gauge AC Goods.
For example: WAG-1, WAG-2, WAG-4, WAG-5, WAG-7, WAG-9.
2. **WAP**stands for Wide gauge AC Passengers.
For example: WAP-4, WAP-7.

III. Indian Class Wap-4 Electric Locomotive

WAP-4



WAP-4 belonging to Electric Loco Shed, Lallaguda hauling train number 22251

Power type	Electric
Gauge	5 ft 6 in (1,676 mm)
Top speed	Service: 140 km/h (87 mph) Test Runs: 180 km/h (112 mp)
Power output	5,350 hp (3,989 kW)
Tractive effort	32000 kg/force
Career	Indian Railways
Number	Starting from 22069 to 22980

An example of WAP-4:

WAP-4 is a common electric locomotive used in India. It is capable of hauling 26 coaches at a speed of 140 km/h.

The locomotive was developed, after a previous class WAP-1 was found inadequate to haul the longer, heavier express trains(24-26 coaches) that were becoming the mainstay of the Indian Railways network. It was introduced in 1994, with a similar bodyshell to the WAP-1 class, but with Hitachi traction motors developing 5000 hp (5350 hp starting). Electricals are traditional DC loco type tap changers, driving 6 traction motors arranged in Co-Co fashion. This locomotive has proved to be highly successful, with over 800 units in service and more being produced. Newer examples have been fitted with Microprocessor Controlled diagnostics, Static Converter units (instead of arnos) and roof mounted Dynamic (Rheostatic) Brakes. The locomotive can be seen in service across the electrified network of Indian Railways and are homed at 13 sheds (depots).

Design:

The loco has a streamlined twin cab carbody design, with top-mounted headlamps. The first 150 or so units had the headlamp mounted at waist level, with the lights being mounted in a protruding nacelle. Later on the headlamps were placed in a recessed nacelle, and from road # 22579 onward, the headlamps were moved to the top. Newer locos also feature larger windshields, more spacious driver cabin with bucket type seats and ergonomic controls. The control panel also features a mix of digital and analog displays in newer units (all analog display in older versions).

The loco features higher power rated silicon rectifiers and indigenously-designed 5400kVA transformer coupled with Hitachi HS15250 traction motors. Starting power is 5,350 hp (3,990 kW), with 5,000 hp (3,700 kW) being supplied continuously.

Original units were weighed 120 tonnes, which was brought down to 112 tonnes through the usage of lighter material.

WAP-1, WAP-3 and WAP-6 units were rebuilt to WAP-4 specifications after replacing the bogies & electrical.

Performance:

It is used to haul the premier Rajdhani & Shatabdi expresses at 140 km/h. In trials, the locomotive has achieved a top speed of 169 km/h, though Indian Railways limits its top speed to 140 km/hr.

With a 24 coach passenger train, the acceleration time / distances are:

110 km/h - 338 seconds (6.8 km)

120 km/h - 455 seconds (10.5 km)

130 km/h - 741 seconds (20.5 km)

Starting Tractive Effort (Te) - 32000 kg/force

Technical Specifications of WAP-4

Manufacturers	Chittaranjan Locomotive Works
Traction Motors	Hitachi HS15250
Power output	5000hp
Gear Ratio	23:58 (One loco, #22559, is said to have a 23:59 ratio.)
Transformer	5400 KVA, 32 taps
Two silicon rectifiers, (ratings?).	
Axle load	18.8 t
loco weight	113 t
Bogies	Co-Co Flexicoil Mark 1 cast bogies; primary and secondary wheel springs with bolsters
Pantographs	Two high speed Stone India (Calcutta) AM-92 and CCPL IR 03 H.
Current Ratings	1000 A for 10 min, 900 A continuous

VI. Conventional Bogie and Its Components

4.1Bogie:

What is a bogie?

A **bogie** or **truck** is a wheeled wagon or trolley. In mechanics terms, a bogie is a chassis or framework carrying wheels, attached to a vehicle, thus serving as a modular subassembly of wheels and axles.

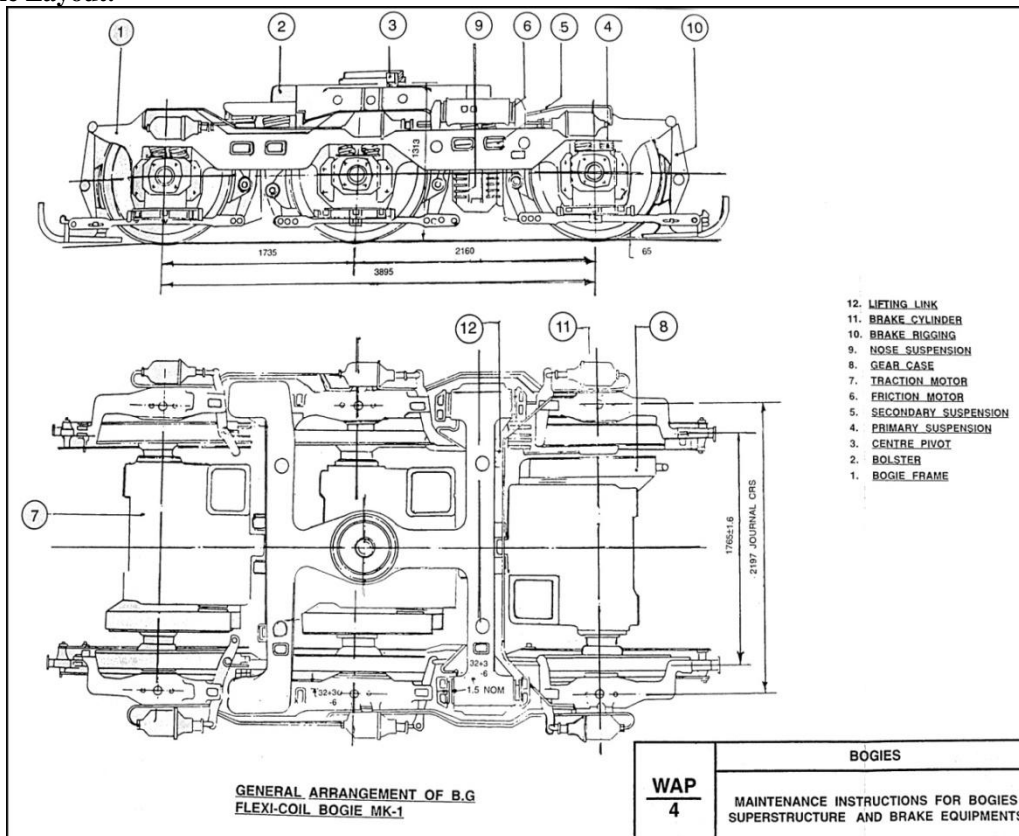


Conventional FLEXICOIL bogie, CO-CO Type of WAP-4 Locomotive.

Table showing types of Locomotive bogies:

S No.	Type of Bogie	Loco Type	Characteristics
1.	B - B	WAG-1 WAG-4	One traction motor in each bogie drives, two wheel sets in each bogie.
2.	BO - BO	WAG-2	Two traction motors in each bogie. Each motor drives individual wheel sets.
3.	CO - CO	WAM-4 WAP-4 WAG-5 WAG-7	3 traction motors drives 3 wheel sets, each motor drives individual wheel sets.
4.	CO - CO Tri mount		3 traction motors drives 3 wheel sets, each motor drives individual wheel sets and loco body rests on CO - CO bogie at 3 places, each displaced triangularly. Centre leading point shares 60% body weight while rest 2 points at High Dynamic Load share 20% body weight each i.e. (20% + 20% = 40% of weight)
5.	CO - CO Flexicoil bogies	WAP-4 WAP-7 WAG-9	Each bogie is having double suspension system namely primary and secondary suspension.

4.2 Bogie Layout:



Components of Bogie

1. Bogie Frame	7. Traction Motor
2. Bolster	8. Gear Case
3. Centre Pivot	9. Nose Suspension
4. Primary Suspension	10. Brake Rigging
5. Secondary Suspension	11. Brake Cylinder
6. Friction Motor	12. Lifting Link

4.3 Design Considerations and description of Bogie:

4.3.1 General Description:

Bogie Frame and Bolster:

The bogie frame and bogie bolster of “FLEXICOIL” bogie Mark-I are of steel casting box type construction manufactures as per the standard laid down by RDSO.

The Locomotive body weight is transferred to the bolster through a centre pivot. The steel – cast “H” type bolster is supported on the steel - cast bogie frame at four corners, by pair of helical springs placed in spring pockets of main longitudinal member of the bogie frame. The bolster is located w.r.t bogie frame by upright pedestals which are integral part of the bogie frame. This arrangement serves to transmit force from bolster to bogie frame and vice-versa. Spring loaded sunbeam piston 2 nos. per bogie made of phenolic material to have high friction between bolster and bogie frame for damping in both vertical and lateral modes of oscillation are also provided in the above pedestal arrangement. Lateral stop are also provided on the bolster as well as on the bogie frame to limit the side movement by flexible action of the spring which is of the order of 32 mm. The bogie frame is in turn supported on the axles by another set of springs resting on the axle boxes .The load of the locomotive superstructure rest on the centre pivot bowl of the bogies. The bowl is fitted with vertical and horizontal liners made of fluon (Vx2) which provides rotational freedom between body and bogie in operation. Two lifting links located diagonally opposite provides the easier accessibility as well as reduce the number of mechanisms to engage or disengage the bogie when installing or removing.



Bogie Frame



Bolster of WAP 4 Locos

4.3.3 Suspension:

This flexicoil bogie Mark-I has two stages of vertical suspension in which helical spring have been used at primary and secondary stages. Primary, between axle box and bogie frame and secondary, between bogie frame and bolster. The transverse flexibility between the body and the bogie has been achieved by the flexicoil action of the helical spring at the secondary stage. The support of the bolster springs have been placed on the wider arm to give better stability in rolling.



A and B are Primary and Secondary suspension systems respectively.

4.3.4 Traction Motor:

The bogies are fitted with HITACHI HS-15250A type Axle-hung, nose-suspended traction motors with the help of suspension tubes with taper roller bearing inside. All the axles are power-driven. The traction motors working on pulsating current are air cooled by external blowers.



4.3.5 Gear Case:

It is a housing which covers the main bull gear and pinion of the traction motor and protects them from foreign material like dust, stones, water etc. It also holds lubricating oil for the relative motion between the bull gear and the pinion.



4.3.6 Nose Suspension Drive:

The nose-suspension drive is the drive mechanism for electric railcars, in which approximately half of the weight of the traction motor is supported by the wheel axle through the suspension limit, and the rest by the bogie frame through the "nose" on the motor frame. The suspension limit does not allow any relative movements between the wheel axle and the motor axle (except for a very limited allowance), which makes it possible to directly connect the two axles by a gearbox.

4.3.7 Brake Rigging:

The means of distributing the braking forces from a brake cylinder to the various wheels on the vehicle. It consists of rods and levers suspended from the underframe and bogies and linked with pins and bushes. Rigging requires careful setting up and regular adjustment to ensure forces are evenly distributed to all wheels. Badly set up rigging will cause wheel flats or inadequate brake force.

4.3.8 Brake Cylinder:

Six (203 dia. x 203 stroke) brake cylinder per bogie are used to operate clasp type brake rigging. Each cylinder piston is connected to the brake lever to actuate the brake on one wheel only. The brake shoe adjustment in service is done by actuating adjusting rod at the bottom. Brake blocks and shoe are of conventional type.



'A' shows brake cylinder.

4.3.9 WheelSet:

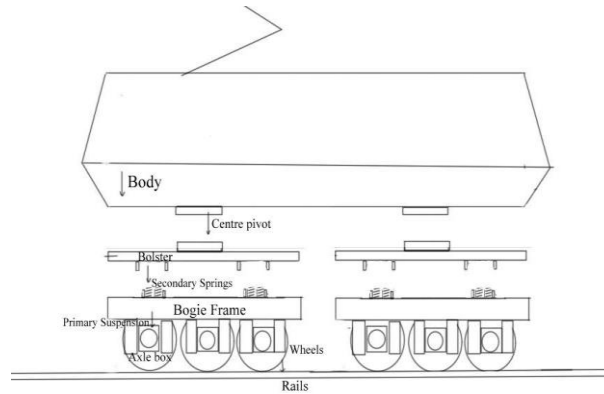
A wheelset is the wheel-axle assembly along with bull gear.



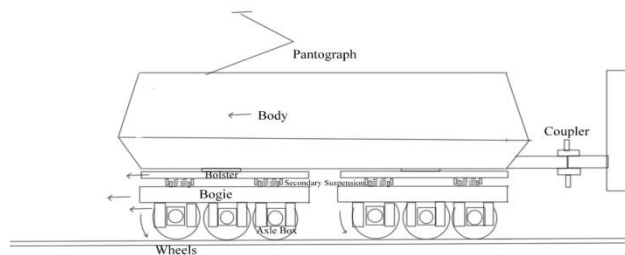
4.4 Weight transfer to wheel axle to provide axle load to improve Adhesion:

WAP-4 Loco:

Locobody rests at centre pivot of bolster; bolster is resting on secondary springs at 4 places. Secondary springs are seated on bogie frame. Bogie frame is resting on primary suspension springs. These primary suspension springs are seated on axle box i.e., axle to wheel weight is transferred to provide axle load to have adhesion.

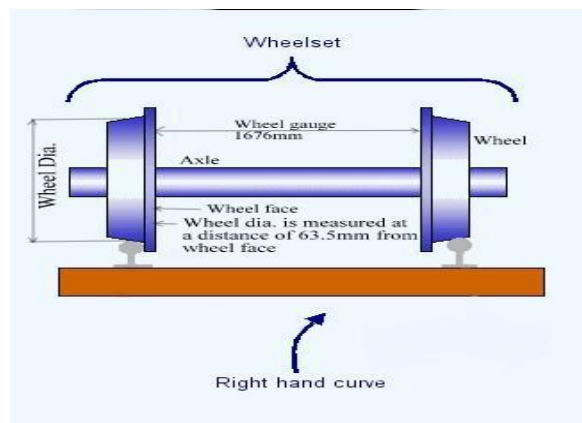


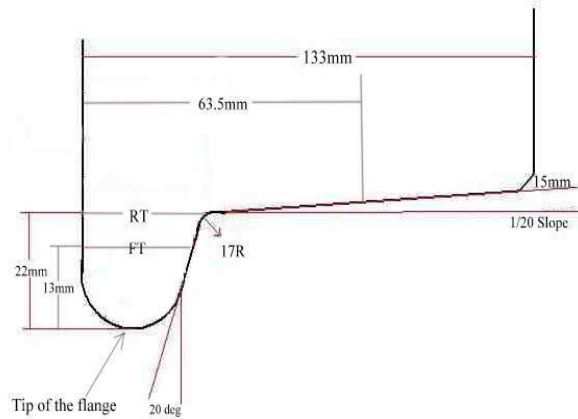
4.5 Mechanical Power Transfer:



1. When traction motor is rotating with input electrical DC power, mechanical power output comes to its pinion.
2. Pinion is engaged with bull gear of axle. When bull gear is rotating, its axle rotates.
3. When axle is rotating wheel rotates, with axle box on the axle. The rotational forces are converted to linear forces due to friction between rail and wheel.
4. These linear forces are shifted to bogie through bogie pedestal at both sides of axle box.
5. From bogie frame to bolster through pedestal at friction damper housing.
6. Now forces are shifted to bolster and from bolster to centre pivot; then centre pivot to loco body.
7. From loco body to centre buffer coupler, haul one train/formation.

4.6 Wheel Profile:





4.6.1 Wheel Profile Table

	New	Condemn	Wear
Root Thickness (RT)	37.5mm	31.5mm	6mm
Flange Thickness (FT)	32mm	29mm	3mm
Tread Wear (TW)	-	6.5mm max.	-
Wheel Dia.	1097mm	1016mm	81mm
Wheel Gauge	1676mm	-	-

NOTE:

1. Root thickness is measured at a height of 22mm from the tip of the flange.
2. Flange thickness is measured at a height of 13mm from the tip of the flange.

V. Suspension System

5.1 Suspension:

Suspension is the term given to the system of springs, shock absorbers and linkages that connects a vehicle to its wheels and allows relative motion between the two. Suspension systems serve a dual purpose — contributing to the vehicle's roadholding/handling and braking for good active safety and driving pleasure, and keeping vehicle occupants comfortable and reasonably well isolated from road noise, bumps, and vibrations, etc.

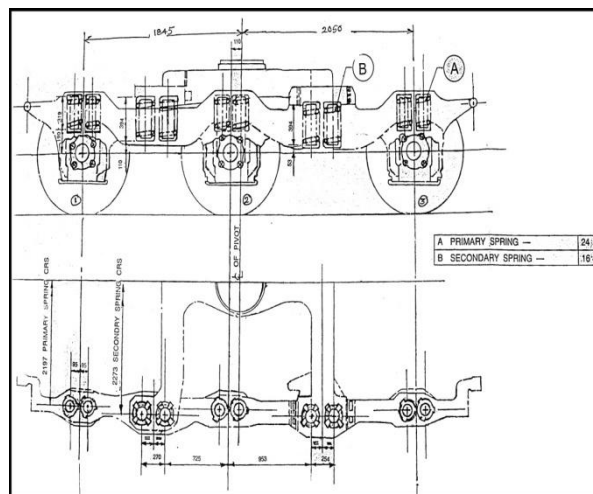
5.2 Suspension in Conventional bogie:

The suspension used in Conventional bogie is **Spring Suspension**.

There are two types of suspension systems used in this conventional type bogie, they are:

1. Primary Suspension
2. Secondary Suspension

The bogie is designed for two stages of suspension to give **flexicoil** action. Various combinations of helical springs are used in **secondary suspension** between bolster and bogie frame and **primary suspension** between axle box and bogie frame.



PRIMARY AND SECONDARY SUSPENSION LAYOUT

5.3 Characteristics of spring suspension:

5.3.1 Principle of a spring:

In distinction to a rigid beam, a spring, regardless of its form or shape, will exert a changing force as it deflects its hornblock. This relationship is linear, with maximum force being applied when the spring is fully compressed (to take the example of a compression spring), and zero force being applied when the spring is in its fully relaxed state – this principle is shown in figure 7. The actual deflection of the spring is directly proportional to a property, the 'springrate' (or 'spring constant') of the particular spring. If a spring relaxes to depress a wheel onto the rail, the reduction in the force applied to the hornblock will be counterbalanced by a distributed increase in the force the loco applies to its other suspension points. Springs absorb and discharge potential energy, and decouple the vertical forces between the wheels and the body.

Thus in a sprung loco traversing uneven track, there is a continuously changing set of forces applying between the wheel tyre and the rail, although the sum of those forces at the railhead is constant. The action of a spring in a prototype loco is related to the weight borne by the particular axle involved, and on the prototype each spring is designed to bear and operate on a specific load. If the spring is too strong, the weight of the loco will not cause it to operate properly over irregularities in the track, while if the spring is too weak the loco is likely to show dynamic instability.

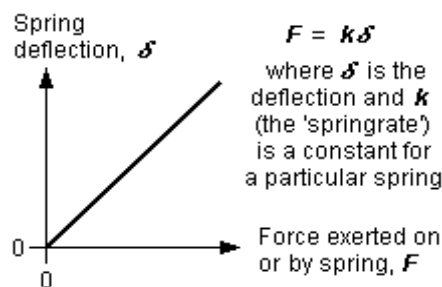


Fig 7 Force v deflection for a spring

5.3.2 Viability of springs in small-scale models:

A prototype loco is suspended, being held up by the strength of the springs. It is generally accepted as being difficult to reproduce the characteristics of prototype springs in small-scale models because:

1. the mass to momentum relationships in the prototype do not scale linearly to models;
2. with the exception of the use of commercial music wire strings as beam springs, it can be difficult to provide the range of model springs appropriate for all the different weights of model locomotives;
3. it can be difficult to adjust the springs so that the loco is both level and at the correct buffer height;
4. it is difficult to assess what the design value of the deflection of a spring should be;
5. Model rail does not deflect under the weight of a model loco like prototype rail does.

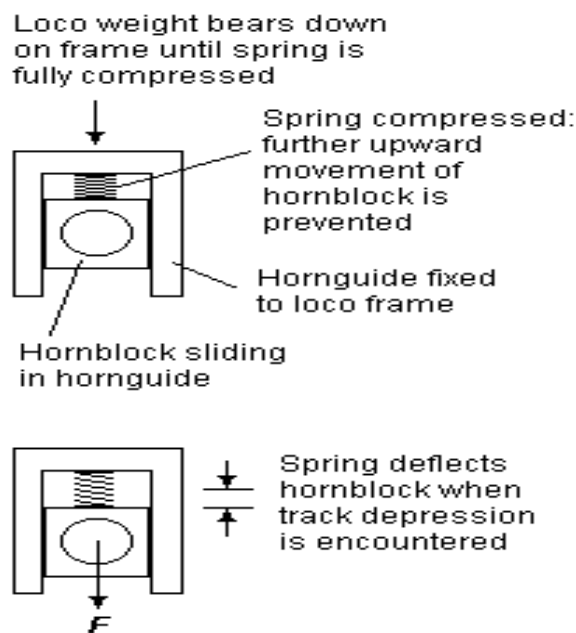


Fig 8 Spring-assisted hornblock (coil)

5.3.3 Spring-assisted hornblocks:

A spring-assisted hornblock is one traditionally containing a coil spring between a hornblock and its hornguide. Under the weight of the loco, the spring compresses either fully (to bind the coils together) or until the hornblock is restrained from further upward movement by some limiter device fitted to the hornguide or the frames of the loco – see **figure 8**. The spring in such a hornblock therefore depresses its axle into depressions of the track, and the deflection is in proportion to the springrate of the particular spring. The downward force of the spring will diminish the greater the depression of the track (see **figure 9**).

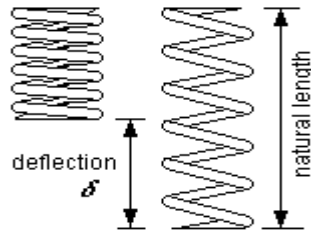


Fig 9 Coil spring deflection

Spring-assisted hornblocks do not provide the equalizing advantages of beams, nor (when in their fully compressed state) the shock-absorbing advantage of properly suspended springs – any upward projection of the track will transmit itself directly and abruptly to a loco chassis fitted with spring-assisted hornblocks. Moreover, if the spring rating is not chosen to match the weight being supported, a loco fitted with spring-assisted hornblocks may show non-optimal haulage, depending on the state of the track.

Note: The above does not imply that all coil spring hornblocks operate in a 'spring-assisted' fashion as described above.

A cantilever leaf spring can also be used to act in a spring-assisted fashion – see **fig 10**.

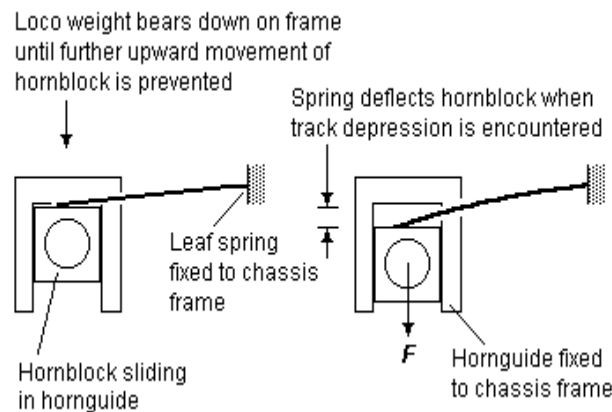
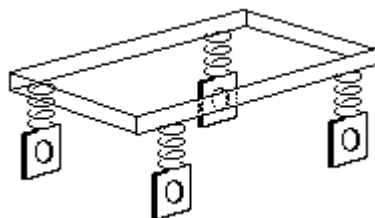
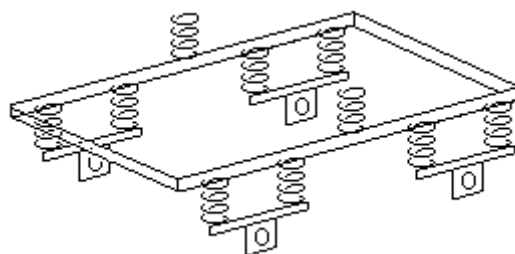


Fig 10 Spring-assisted hornblock (leaf)



(a) Representative suspension points on an 0-4-0



(b) Representative suspension points of a modern prototype bogie

Fig 11 Springing allows multiple suspension points

5.3.4 Suspension points:

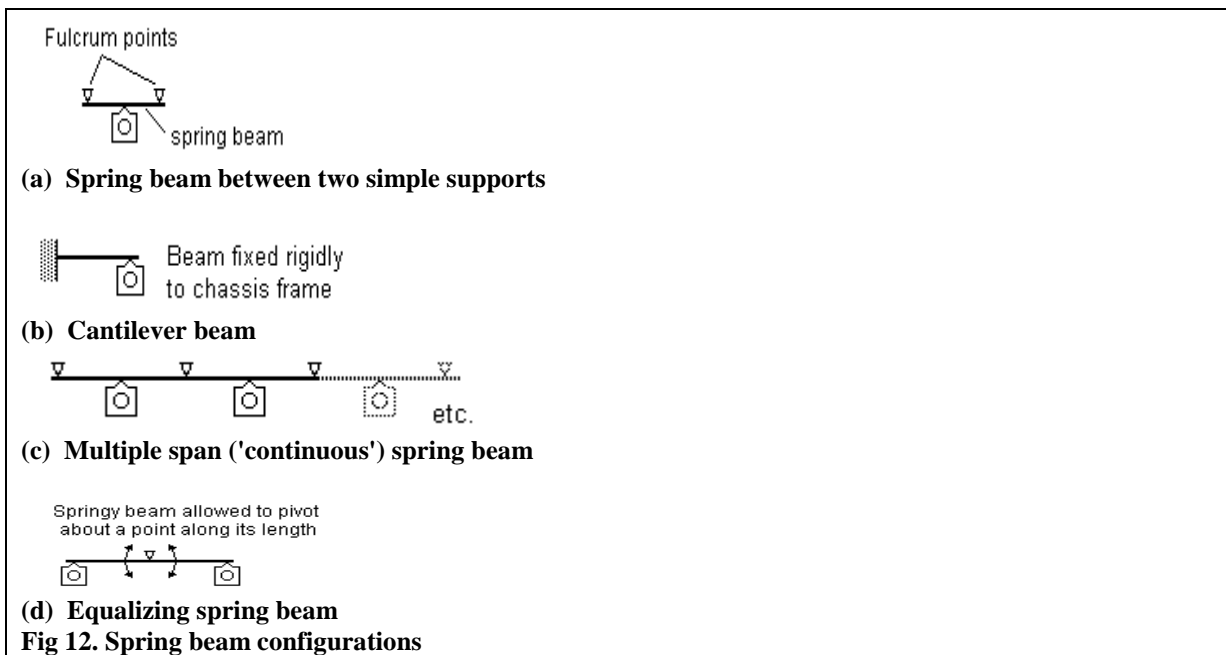
In contrast with rigid beam suspension, there is no limit to the number of primary suspension points allowed for springs. A 0-4-0 has four suspension points (see figure 11(a)), an 0-6-0 or Co bogie has six, an 0-6-2 has eight, and so on. This principle applies to more complicated cases where more than one 'layer' of springing might be involved, and figure 11(b) gives a representation of a prototype example of an EMU/DMU having two main suspension points between each bogie and the body, and two suspension points for each wheel to the bogie frames: in such more complicated cases, the notion of what constitutes the difference between 'primary' and 'secondary' suspension points becomes somewhat academic.

5.3.5 Spring beam configurations:

The deflection of a spring beam varies considerably depending on how it is supported. A common form of support and one that lends itself to being able to control the datum height of the hornblock when under deflection, is where the hornblock spring is restrained loosely against two fulcrum points – see figure 12(a). The beam can slide along and rotate freely around these 'simple' supports, according to the force being applied to the beam. The cantilever spring (see figure 12(b)) is one where the spring is fixed rigidly at one end only. This spring configuration is probably the most difficult to control in terms of being able to set the datum deflection height of the hornblock accurately, but has the virtue of being easily adjustable.

Multiple hornblocks can be supported by using multiple instances of figure 12(a), or by using a continuous single spring beam held against multiple fulcrum points – in figure 12(c) for example, depending on the strength of the spring beam, a significant degree of equalization will be imposed between adjacent hornblocks. Full equalization is given where a single spring beam bearing onto two hornblocks is allowed to pivot about a point (typically the midpoint) along its length. See figure 12(d). The degree of equalization given by the beam will depend on its strength; if it is too weak, it will not act sufficiently to rotate itself about the pivot, and if it is too strong, it will become in effect a rigid beam.

The behavior of all of the above examples of spring configuration will be significantly different from each other, and slight variations in the cross-sectional area of the spring material and distances between fulcrum points will produce very different deflection values.



VI. Conclusion

We have understood the various functions of a bogie of conventional locomotive (WAP-4) and made a detailed study of the suspension system, which involves both primary and secondary suspension systems. We also studied how spring testing is made and segregation of the springs based upon their load bearing capacities (within tolerance limits). Also, we've understood the failures that have been occurring under various circumstances during operation and their solutions have been explained in a detailed manner. We have understood the operating principle of the present day locomotive using traction motors majorly 3-phase induction motors and have drawn a study of bogies and suspension system.

Railway organization is one of the most developed means of transportation in India. It helps the national production, social and industrial development including economics stations of the country. In view of the several advantages over the road transport, the railways got priority of development over highways. Since the introduction of railways in 19th century, India has made considerable progress in developing railway industry as a large scale undertaking. Indian railways are now heading towards modernization of traction, automoval in operations and in tradition of recently introduced technique to meet the requirements of high speed and heavy passengers and goods traffic. Indian Railways is the best system in the world next to USSR.

VII. Bibliography

Maintenance Manual (Volume –II) of Passenger Electric Locomotive [Broad Gauge 5’-6’’ (1676mm)] CO-CO type WAP-4 Class.

REFERNCES

- [1.] http://en.wikipedia.org/wiki/Indian_locomotive_class_WAP-4
- [2.] <http://www.clag.org.uk/41-0rev.html#section8>
- [3.] <http://indiarailinfo.com/faq/post/149>
- [4.] [http://en.wikipedia.org/wiki/Wheelset_\(rail_transport\)](http://en.wikipedia.org/wiki/Wheelset_(rail_transport))

Study of Performance of Different Blends of Biodiesel Prepared From Waste Cottonseed Oil

Singh Harpreet¹, Mangla Arunish², Singh Jaspreet³

^{1,3}Lovely Professional University, Phagwara, Punjab.

²(Lala Lajpat Rai Institute of Engineering and Technology, Moga, Punjab)

Abstract : The use of biodiesel is rapidly expanding around the world, making it imperative to fully understand the impacts of biodiesel on the diesel engine combustion process and pollutant formation. Biodiesel was made by the well-known transesterification process. Waste cottonseed oil was selected for biodiesel production. Three different blends of biodiesel were prepared i.e. B10, B20 and B30. These three blends were fuelled in a compression ignition (C.I.) engine. A maximum of 77% biodiesel was produced with 20% methanol in presence of 0.5% sodium hydroxide. Different parameters for the optimization of biodiesel production were investigated in the first phase of this study, while in the next phase of the study performance test of a diesel engine with neat diesel fuel and biodiesel mixtures are to be carried out. The performance characteristics like brake power (B.P.), brake specific fuel consumption (BSFC) and brake thermal efficiency. This performance was then compared with that of petro diesel.

Keywords: Alternative fuel; Vegetable oil; Biodiesel; Viscosity; Transesterification; Methanol.

I. INTRODUCTION

With self-sufficiency as the most important national energy goal, the options are easily broken down into two fuel types: renewable and non-renewable. Using a combination of the two, that goal is in fact readily achievable. Biodiesel is gaining more and more importance as an attractive fuel due to the depleting fossil fuel resources. Chemically biodiesel is mono-alkyl esters of long chain fatty acids derived from renewable feed stock like vegetable oils and animal fats. It is produced by transesterification in which, oil or fat is reacted with a monohydric alcohol in presence of a catalyst to give the corresponding mono-alkyl esters. The alkali-catalyzed transesterification of vegetable oils proceeds faster than the acid-catalyzed reaction [1]. For an alkali catalyzed transesterification, the triglycerides should have lower free fatty acid (FFA) content, and the alcohol must be anhydrous to render soap formation. Soap formation lowers the yield of esters and renders the separation of esters and glycerol [3, 4, and 5]. Up to about 5% FFA, the reaction can be catalyzed using an alkali catalyst [6]. The extent of transesterification and side reactions depends upon the type of feedstock, catalyst formulation, catalyst concentration, alcohol to-oil ratio, reaction temperature and reaction time [7, 8]. Cottonseed oil was converted into biodiesel by alkali-catalyzed transesterification reaction at different factors. It was found that catalyst concentration 0.75%, temperature 65°C, methanol to oil molar ratio 6:1 and agitation intensity 600 rpm provided optimum condition producing excellent yield (96.9%) of cottonseed methyl ester. [9] The increased viscosity and low volatility of vegetable oils lead to severe engine deposits, injector chocking and piston ring sticking [10]. However, these effects can be reduced or eliminated through transesterification of vegetable oil to form methyl ester [11-14]. Transesterification provides a fuel viscosity that is close to that of No. 2 diesel fuel. Transesterification has shown good potential for reducing engine problems associated with vegetable oils. Transesterification is the process of reaction of a triglyceride with an alcohol in the presence of a catalyst to produce glycerol and fatty acid esters.

The molecular weight of the ester molecule is roughly one-third that of a neat vegetable oil molecule and the ester has a viscosity approximately twice that of diesel fuel [15]. Yamane et al. [20] found that with unwashed biodiesel fuel, the engine is unstable and shows higher exhaust emissions compared with those of washed biodiesel fuel. In the present investigation different parameters for biodiesel production have been investigated and then engine emissions have been studied with neat diesel fuel and the biodiesel mixtures. Here the 100% biodiesel is termed as biodiesel and the different blends of biodiesel with diesel fuel are termed as biodiesel mixtures in the following. The effects of reaction temperature, catalyst percent-ages, alcohol percentages and reaction time for optimum biodiesel production have been studied. The biodiesel from CSO is termed as CSOME. Finally exhaust gas emissions with biodiesel mixtures have been investigated and compared with those of neat diesel fuel.

Nomenclature

B.S.E.C	Brake Specific Energy Consumption	CSOME	Cottonseed Oil Methyl Ester
B.S.F.C	Brake Specific Fuel Consumption	DI	Direct Injection
B.T.D.C	Before Top Dead Center	EL	Engine Load
B.T.E	Brake Thermal Efficiency	FAME	Fatty Acid Methyl Ester
B10	10% Biodiesel + 90% Diesel	FFA	Fat Free Acid
B100	100% Biodiesel	HC	Hydrocarbon
B20	20% Biodiesel + 80% Diesel	IMEP	Indicated Mean Effective Pressure
B30	30% Biodiesel + 70% Diesel	KOH	Potassium Hydroxide
BD	Biodiesel	M	Mass Flow Rate (Kg/S)
BMEP	Brake Means Effective Pressures	NA	Naturally Aspirated
BP	Brake Power	Naoh	Sodium Hydroxide
CA	Crank Angle	NOx	Nitrogen Oxide
CI	Compression Ignition	P	Power (Kw)
CR	Compression Ratio	p	Pressure (Kpa) (Mpa)
CSO	Cotton Seed Oil	Pm	Particulate Matter

II. PURPOSES OF THIS WORK

The purposes of this work were as follows:

1. To produce test quantities of methyl ester (biodiesel) from waste CSO.
2. To determine the fuel properties of the biodiesel fuel.
3. To compare the performances of a diesel engine using neat diesel fuel and biodiesel mixtures separately.

Lots of research works on biodiesel production have been carried out so far, but data on the effect of reaction temperature, effect of catalyst, influence of alcohol on biodiesel production form CSO have not been investigated so far. The authors have an academic interest to investigate different parameters, like reaction temperature, catalyst percentage and alcohol percentage for optimum biodiesel production and the influence of biodiesel on engine Performance.

III. MEASUREMENT OF PROPERTIES OF THE BIODIESEL

Fuel properties of biodiesel such as density, viscosity, flash point and ester etc. of waste cottonseed oil content were determined using the standard test methods. After producing the biodiesel the properties of the biodiesel were determined by using various methods. The following properties were tested:-

Table 0-1 Apparatus used for calculating the properties

Property	Apparatus used
Density	Weighing balance
Kinematic viscosity	Redwood viscometer
Flash point	Flash and fire point apparatus
Fire point	Flash and fire point apparatus
Cloud point	Cloud and pour point apparatus
Pour point	Cloud and pour point apparatus

The observations measured by above methods of bio-diesel B100 fuel properties are compared with the standard petro-diesel fuel properties in the following table.

Table 0-2 Comparative properties of the petro-diesel and biodiesel

Property of oil	ASTM	Diesel Standard	Biodiesel B100 (from Waste CSO)
Density (30 ⁰ C), kg/m ³	-	850	910
Kinematic viscosity, cSt	<5	2.049	3.6
FFA, %	<2.5	-	3.6
Cloud point, ⁰ C	-3 TO 12	<10	-3
Pour Point, ⁰ C	-15 TO 10	-6	-8
Flash point, ⁰ C	>130	78	160
Fire point, ⁰ C	>53	83	165

IV. EXPERIMENTAL SETUP AND PROCEDURE OF EXPERIMENTATION

4.1 Testing of biodiesel in engine

A four stroke, single cylinder variable compression ratio diesel engine is employed for the present study. The detail specification of the engine used is given in table 4.1 below and experimental set up as shown below. The performance tests are carried out on the C.I. engine using various blends of biodiesel and diesel as fuels. The tests are conducted at the constant speed of 1500 rpm at various loads. The experimental data generated are documented and presented here using appropriate graphs. These tests are aimed at optimizing the concentration of ester to be used in the biodiesel-diesel mixture for 1 hr. engine test operation. In each experiment, engine parameters related to thermal performance of engine such as brake power, brake thermal efficiency, break specific fuel consumption.

4.2 Specifications of the engine

The performance characteristics were carried out on variable compression diesel engine. The specifications of the engine are as stated as below.

Table 4-1 Specifications of the engine

Engine	4 stroke, Variable compression diesel engine
No. of cylinders	Single cylinder
Cooling media	Water cooled
Rated capacity	3.5 kW @ 1500 RPM
Cylinder diameter	87.5 mm
Stroke length	110 mm
Connecting rod length	234 mm
Compression ratio	12:1-18:1
Orifice diameter	20 mm
Dynamometer	Eddy current dynamometer
Dynamometer arm length	145 mm

4.3 Experimentation Methodology

First the experimentation is performed with diesel (for getting the base line data of the engine) and then cotton seed oil methyl ester and also its different blends. The performance of the engine is evaluated in terms of brake thermal efficiency, brake specific energy consumption. It also found out economic viability. An eddy current dynamometer, a piezoelectric transducer and digital PT-100 type temperature sensor was calibrated and used in the setup by Apex Innovations. Following parameters were measured from the experimental CI engine setup.

1. Brake power (BP)
2. Brake specific fuel consumption (BSFC)
3. Cooling water temperature (inlet and outlet)
4. brake thermal efficiency
5. Speed of the engine

V. RESULTS AND DISCUSSION

5.1 Performance Parameters

Worldwide, biodiesel is largely produced by methyl transesterification of oils. The recovery of ester as well as its kinematic viscosity is affected by the transesterification process parameters such as catalyst concentration, reaction temperature and reaction time. The above parameters were standardized to obtain methyl ester of waste cotton seed oil with lowest possible kinematic viscosity and highest level of recovery. The engine performance parameters and exhaust gas emission characteristics of B10, B20, B30 and diesel were compared.

5.1.1 Brake Power (BP)

Graph of the brake power (BP) as a function of load obtained during engine operation on different blends of biodiesel i.e. B10, B20 and B30 with diesel (petro diesel) at compression ratio of 18:1 has been shown in Figure 5.1. Brake power of the engine increases with increase in the load on the engine. Brake power is the function of calorific value and the torque applied. Diesel has more calorific value than the biodiesel, so diesel has the highest brake power among the different blends of biodiesel. Due to the more calorific value of B10 blend of biodiesel than B20 and B30, it has the more brake power as shown in figure 5.1.

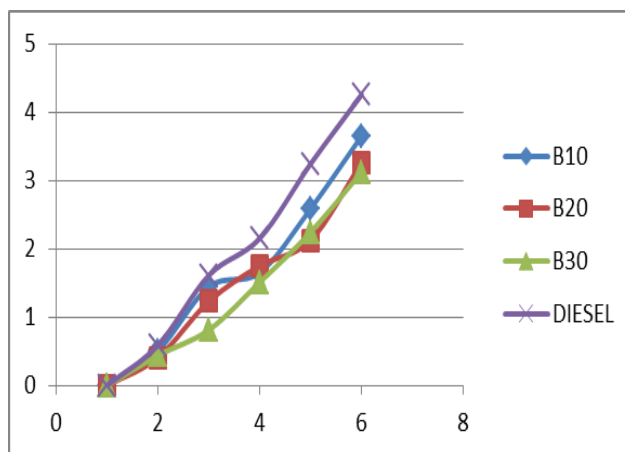


Fig 5-1 Variation in brake power with change in load

It can also be seen that as we increases the load, torque increases and thus there is an increase in brake power with the load.

5.1.2 Brake specific fuel consumption (BSFC)

Graph of the brake specific fuel consumption (BSFC) as a function of load obtained during engine operation on different blends of biodiesel i.e. B10, B20 and B30 with diesel (Petro-diesel) at compression ratio of 18:1 has been shown in Figure 5.2.

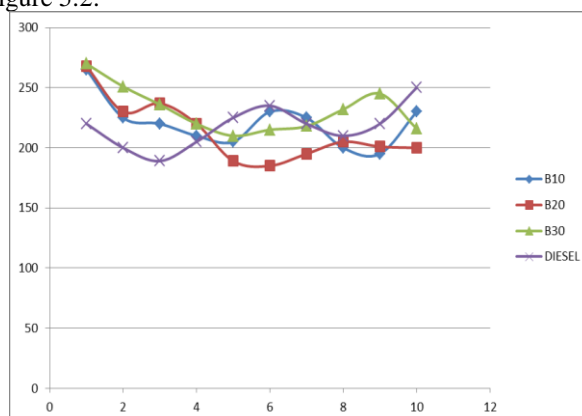


Fig.5-2 Variation in brake specific fuel consumption with change in load

For all blends and petro diesel tested, BSFC decreased with increase in load. One possible explanation for this reduction is the higher percentage of increase in brake power with load as compared to fuel consumption. It can be seen from the figure 5.2 that in case of biodiesel mixtures, the BSFC values were determined to be higher than those of neat diesel fuel. This trend was observed owing to the fact that biodiesel mixtures have a lower heating value than does neat diesel fuel, and thus more biodiesel mixtures was required for the maintenance of a constant power output. It is well known that brake specific fuel consumption is inversely proportional to the brake thermal efficiency. So diesel has the lowest brake specific fuel consumption. Among the three different blends of biodiesel B10 has the lowest value of brake specific fuel consumption.

5.1.3 Brake thermal efficiency (BTE)

Graph of the brake thermal efficiency as a function of load obtained during engine operation on different blends of biodiesel i.e. B10, B20 and B30 with diesel (petro diesel) at compression ratio of 18:1 have been shown in Fig 5.3. In all cases, brake thermal efficiency increases with an increase in load. This can be attributed to reduction in heat loss and increase in power with increase in load. It is also observed that diesel exhibits slightly higher thermal efficiency at most of the loads than CSOME and its blends. The molecules of bio-diesel (i.e. methyl ester of the oil) contain some amount of oxygen, which takes part in the combustion process. Test results indicate that when the mass percent of fuel oxygen exceeds beyond some limit, the oxygen loses its positive influence on the fuel energy conversion efficiency in this particular engine. So the brake

thermal efficiency of diesel is more than that of biodiesel blends. Among the three different blends of biodiesel, B10 has higher brake thermal efficiency than B20 and B30.

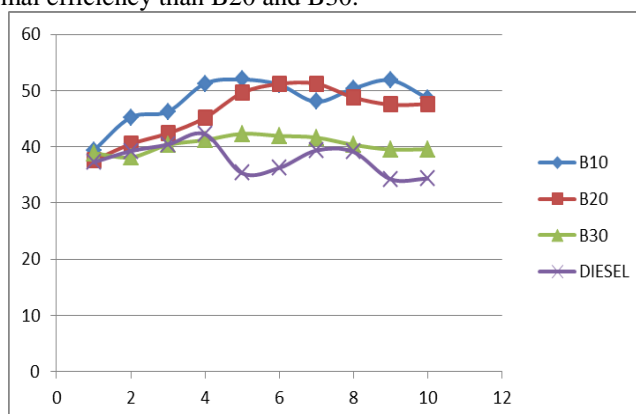


Fig 5-3 Variation in brake thermal efficiency with change in load

VI. CONCLUSION AND FUTURE SCOPE OF WORK

6.1 Conclusions

The overall studies based on the production, fuel characterization, engine performance and exhaust emission of different biodiesel blends of waste cotton seed oil methyl esters were carried out. The following conclusions can be drawn:

1. The recovery of ester by transesterification of waste cotton seed oil with methanol is affected by process parameters such as catalyst concentration and reaction temperature.
2. The graphical results show that diesel has better performance characteristics than biodiesel and biodiesel blends. Among the three different blends of biodiesel, B10 and B20 have the better performance characteristics than B30 blend of biodiesel when fuelled in an internal combustion engine. so we can fuel safely B10 and B20 in internal combustion engine without any modification.
3. The kinematic viscosity of diesel, waste cotton seed oil biodiesel were found as 2.049, 3.6 centistokes respectively at 40°C. The results indicated that the waste cotton seed oil biodiesel had the kinematic viscosity 75.69 percent more than that of diesel.
4. The calorific value of diesel is 42000 KJ/kg and that of waste cotton seed oil is 40000KJ/kg. So the calorific value of waste cotton seed biodiesel is 4.76% less than that of mineral diesel.
5. Waste cotton seed oil biodiesel is non-toxic, biodegradable, environment-friendly, renewable fuels and do not add to global warming.

6.2 Scope of future Work

Biodiesel has distinct advantage as an automotive fuel. Initial cost may be higher but feedstock diversity and multi-feedstock production technologies will play a .2critical role in reductions in production cost and making the fuel economically viable.

The following points may be considered before introducing the fuel in India:

1. Biodiesel may be introduced as a diesel fuel extender or blends (B10, B20 and B30) and not as a sole diesel engine fuel (B100).
2. Government may consider providing support to the activities related to collection of seeds, production of oil from non-edible sources, production of bio-fuels and its utilization for cleaner environment.
3. Legal framework should be there to enforce regulations on bio-fuels.
4. The blends prepared for this project work were utilized within short time span. Thus, long term stability of blends was not studied. So there is scope for study of long term stability of blends.
5. Long-term performance and endurance test evaluate the durability of the engine with prolonged operation on these blends.
6. Energy education on biodiesel program and storing information and database for wider information dissemination among the public at large should be taken up at a larger scale.
7. Further studies can also be carried out on material compatibility, storage and utilization of by-product from biodiesel.

REFERENCES

- [1] Vyas Amish P, Verma Jaswant L, Subrahmanyam N. A review on FAME production processes. *Fuel* 2010;89:1–9.
- [2] Demirbas A. Biodiesel production from vegetable oils via catalytic and non-catalytic supercritical methanol transesterification methods. *Prog Energy Combust Sci* 2005;31:466–87.
- [3] Ma F, Hanna MA. Biodiesel production: a review. *Bioresour Technol* 1999;70:1–15.
- [4] Freedman B, Pryde EH, Mounts TL. Variables affecting the yields of fatty esters from transesterified vegetable oils. *JAOCs* 1984;61:1638–43.
- [5] Muniyappa PR, Brammer SC, Noureddini H. Improved conversion of plant oils and animal fats into biodiesel and co-product. *Bioresour Technol* 1996;56: 19–24.
- [6] Gerpan JV. Biodiesel processing and production. *Fuel Process Technol* 2006;86: 1097–107.
- [7] Anh N, Phan TMP. Biodiesel production from waste cooking oils. *Fuel* 2008;87:3490–6.
- [8] Leung Dennis YC, Xuan Wu, Leung MKH. Review on biodiesel production using catalyzed transesterification. *Appl Energy* 2010;87:1083–95.
- [9] Rashid U, Anwar F, Knothe G. Evaluation of biodiesel obtained from cottonseed oil. *Fuel Process Technol* 2009;90:1157–63.
- [10] G. Velguth, Performance of vegetable oil and their monsters as fuels for diesel engines, SAE Paper 1983: Paper Number 831358.
- [11] S.J. Clark, L. Wagner, M.D. Schrock, P.G. Piennar, Methyl and ethyl soybean esters as renewable fuels for diesel engines, *JAOCs* 61 (10) (1984) 1632–1638.
- [12] M.N. Pestes, J. Stanislaio, Piston ring deposits when using vegetable oil as a fuel, *Journal of Testing and Evaluation* 12 (2) (1984) 61–68.
- [13] L.A. Perkins, C.L. Peterson, Durability testing transesterified winter rape oil (*Brassica napus* L.) as fuel in small bore, multi-cylinder DI diesel engines, SAE Paper, Paper Number 911764, 1991.
- [14] Q.M. Zhang Felderman, C.L. Peterson, Diesel engine durability when fuelled with methyl ester of winter rapeseed oil, ASAE Paper, Paper Number 881562, 1988.
- [15] M. Mittlbach, B. Poktis, A. Silberholz, Production and fuel properties of fatty acid methyl esters from used frying oil, in: *Proceedings of an Alternative Energy Conference*, Nashville, USA, American Society of Agriculture Engineers (ASAE), pp. 74–78, 1992.
- [16] M.J. Nye, P.H. Southwell, Esters from rapeseed oil as diesel fuel, in: *Proceedings from the Vegetable Oil as Diesel Fuel, Seminar III*, Northern Agriculture Energy Center, Peoria, IL, 1983.
- [17] C.L. Peterson, D.L. Reece, B. Hammond, J.C. Thompson, S. Beck, Commercialization of Idaho biodiesel (HySEE) from ethanol and waste vegetable oil, ASAE Paper, Paper Number 6738, 1995.
- [18] J.G. Suryawanshi, Performance and emission characteristics of CI engine fueled by coconut oil methyl ester, SAE Paper, Paper Number 2006-32-0077, 2006.
- [19] F. Karaosmanoglu, K.B. Ciginoglu, M. Tuter, S. Ertekin, Investigation of the refining step of biodiesel production, *Energy and Fuels* 10 (1996) 890–895.
- [20] K. Yamane, T. Kato, H. Okutani, Y. Shimamoto, Effect of refining process in biodiesel fuel production on fuel properties, diesel engine performance and emissions, SAE Paper, Paper Number 2003-01-1930, 2003.
- [21] K. Yamane, A. Ueta, Y. Shimamoto, Influence of physical and chemical properties of biodiesel fuel on injection, combustion and exhaust emission characteristics in a direct injection compression ignition engine, *International Journal of Engine Research* 2 (4) (2001) 249–261.
- [22] S. Suryanarayanan, V.M. Janakiraman, G.L.N. Rao, Comparative study of the performance and emission characteristics of biodiesels from different vegetable oils with diesel, SAE Paper, Paper Number 2008-01-1581, 2008.

Securing Data Communication for Node Anonymization Using Location Information

Ms. Kanchan P. Kamdi¹, Mr. G. Rajesh Babu²

^{1,2}(Assistant Professor & Student, Department of Computer Science & Engineering), Tulsiramji Gaikwad – Patil college of Engineering & technology mohgaon wardha road Nagpur, Maharashtra.

Abstract: MANET is a type of wireless ad-hoc network that usually has a routable networking environment. Mobile Ad Hoc Networks use unidentified routing protocols that hide node identities and routes from outside observers to provide anonymity protection. Our existing anonymous routing protocols depending on either hop-by-hop encryption, redundant traffic either produce high cost or it cannot provide privacy protection to data sources, destinations, and routes. We propose a new location based routing protocol which offers high privacy protection at low cost to sources, destinations, and routes. It also has approaches to effectively counter intersection and timing attacks. The proposed plan ensures the privacy of both route and nodes which we study and simulate the result. This existing protocol achieves better route privacy protection and its lower cost compared to other unidentified routing protocols, and also improving the routing efficiency compared to other geographical routing protocol.

Index Terms: Manets, privacy, routing protocol, geographical routing.

I. Introduction

A "mobile ad hoc network" (MANET) is an autonomous system of mobile routers (an associated hosts) connected by wireless links - the union of which forms an arbitrary graph. Mobile Ad Hoc Networks feature self-organizing and independent infrastructures, which make them an ideal choice for military uses such as communication and information sharing in battlefields. However, the innate on-air nature of MANETs makes them vulnerable to malicious entities that aim to tamper and analyze data and traffic analysis by communication eavesdropping or attacking routing protocols. MANET routing focused on security issues, less attention has been devoted to privacy. Privacy does not mean confidentiality of communication (i.e., data) among MANET nodes.

Anonymous routing protocols are crucial in MANETs to provide secure communications by hiding node identities and preventing traffic analysis attacks from outside observers. Anonymity in MANETs includes identity and location anonymity of data sources (i.e., senders) and destinations (i.e., recipients), as well as route anonymity. Identity and location anonymity of sources and destinations means it is hard if possible for other nodes to obtain the real identities and exact locations of the sources and destinations. For route anonymity, it is important to form an anonymous path between the two endpoints and ensure that nodes en route do not know where the endpoints are, especially in MANETs where location devices may be equipped.

Existing anonymity routing protocols in MANETs can be mainly classified into two categories: hop-by-hop encryption and redundant traffic. Most of the current approaches are limited by focusing on enforcing privacy at a high cost to existing resources because public-key-based encryption and high traffic generate significantly high cost. In addition, many approaches cannot provide all of the aforementioned privacy protections. For example, existing ALARM cannot protect the location privacy of source and destination. SDDR protocol cannot provide route privacy, and ZAP protocol only focuses on destination privacy. Many privacy routing algorithms are based on the geographic routing protocol.

To provide high privacy protection for sources, destination, and route with low cost. We propose an Anonymous Location-based Routing protocol. These routing protocol dynamically partitions a network field into zones and randomly chooses nodes in zones as intermediate relay nodes, which form a non traceable unknown route. Specifically, in each routing step, a data sender partitions the network field in order to separate itself and the destination into two zones. It then randomly chooses a node in the other zone as the next relay node and uses the GPSR [15] algorithm to send the data to the relay node. In the last step, the data is broadcasted to k nodes in the destination zone, providing k-privacy to the destination. It also has a strategy to hide the data sender among a number of senders to strengthen the privacy protection of the source. The proposed routing protocol is also resilient to intersection attacks and timing attacks. We theoretically analyzed proposed system in terms of privacy and efficiency. We also try to do experiments to evaluate the performance of proposed system in comparison with other privacy and geographic routing protocols.

II. RELATED WORK

K.E. Defrawy ,G. Tsudik [2] proposes on privacy aspects of mobility. Unlike most networks, where communication is based on long-term identities (addresses), we argue that the location centric communication paradigm is better-suited for privacy in suspicious MANETs.

Karim El Defrawy and Gene Tsudik [3] proposes the ALARM framework which supports anonymous location-based routing in certain types of suspicious MANETS ALARM relies on group signatures to construct one-time pseudonyms used to identify nodes at certain locations.They show through simulation that node privacy under this framework is preserved even if a portion of the nodes are stationary, or if the speed of movement is not very high.

V. Pathak, D. Yao, and L. Iftode [4] proposes the design of the GSPR secure geographic routing protocol. The overhead of location authentication is investigated under various scenarios through network simulation. Results show that although the presence of malicious nodes increases the routing path length, a data delivery rate of larger than 80% is sustained even if 40% of the nodes are malicious.

Sk.Md.M. Rahman, M. Mambo [5] proposes a new position-based routing protocol which keeps routing nodes anonymous, thereby preventing possible traffic analysis. Time variant Temporary Identifier Temp ID is computed from time and position of a node and used for keeping the node anonymous. Only the position of a destination node is required for the route discovery, and Temp ID is used for establishing the route for sending data: a receiver hand shake scheme is designed for determining the next hop on-demand with use of the Temp ID. hey evaluate the level of anonymity and performance of proposed scheme.Also they clarified the achievement of anonymity and security.

Z. Zhi and Y.K. Choong [6] proposes to preserve location privacy based on the idea of dissociating user's location information with its identity.They also propose an anonymous geographic routing algorithm which includes three components to avoid the explicit exposure of identity and location in communication without compromising the efficiency guaranteed by geographic routing.

III. PROPOSED METHODOLOGY

A. Network Models:

We use two different network models, random way point model and group mobility model. With the random way point model as the default setting, we also compare the performance of anonymous based routing protocol in the group mobility model. In the group mobility model, we set the movement range of each group to 150 m with 10 groups and to 200 m with five groups.

B. Dynamic Pseudonym and Parameter Testing:

The tests were carried out on network simulator using 802.11 as the MAC protocol with a standard wireless transmission range of 250 m and UDP/CBR traffic with a packet size of 512 bytes. The test field in our experiment was set to a1000 m1000 m area with 200 nodes moving at a speed of 2 m/s, unless otherwise specified. The density was set to 50, 100, 150, and 200 nodes per square meters. The duration of each simulation was set to 100 s unless otherwise indicated.

C. Actual Participating Nodes:

The cumulated actual participating nodes in proposed anonymous location based routing protocol, GSPR, ALARM, and AO2P, with 100 and 200 nodes moving at a speed of 2 m/s, respectively. Since ALARM and AO2P are similar to GSPR in the routing scheme and thus have similar number of actual participating nodes, we use GSPR to also represent ALARM and AO2P in discussing the performance difference between them and proposed routing protocol.

D. The Destination Anonymity Protection:

The number of remaining nodes with partitions and a 2 m/s node moving speed when the node density equals 100, 150, and 200, respectively. The figure shows that the number of remaining nodes increases as node density grows while it decreases as time goes on.

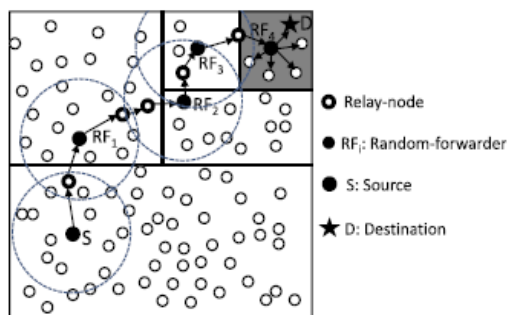


Figure. 1 Routing among the zones.

E. Routing Performance:

The routing performance of Anonymous location based routing protocol compared with GPSR, AO2P, and ALARM in terms of latency, number of hops per packet, and delivery rate. We also conducted tests with and without destination update in location service to show the routing performance of different methods as shown in fig below which shows the actual packet delivery ratio in %. We are trying to improve the packet delivery ratio to 98% to 100%.



Fig. 2 Packet Delivery Ratio

IV. CONCLUSION

Existing anonymous routing protocols, depending on either hop-by-hop encryption or redundant traffic, it produces high cost. And also, some routing protocols are unable to provide complete source, destination, and route privacy protection. Proposed anonymous location based routing protocol is distinguished by its low cost and privacy protection for sources, destinations, and routes. Also we will try to improve the packet loss ratio to 98%.

REFERENCES

- [1] Location-Based Efficient Routing Protocol in MANETs”IEEE Transaction on mobile computing Vol. 12,No.6,June 2013.
- [2] HaiyingShen, Lianyu Zhao, “ALERT: A Anonymous K.E. Defrawy and G. Tsudik, “PRISM: Privacy-Friendly Routing in Suspicious MANETs (and VANETs),” Proc. IEEE Int’l Conf. Network Protocols (ICNP), 2008.
- [3] K.E. Defrawy and G. Tsudik, “ALARM: Anonymous Location- Aided Routing in Suspicious MANETs,” Proc. IEEE Int’l Conf. Network Protocols (ICNP), 2007.
- [4] V. Pathak, D. Yao, and L. Iftode, “Securing Location Aware Services over VANET Using Geographical Secure Path Routing,” Proc. IEEE Int’l Conf. Vehicular Electronics and safety (ICVES), 2008.
- [5] Sk.Md.M. Rahman, M. Mambo, A. Inomata, and E. Okamoto, “An Anonymous On-Demand Position-Based Routing in Mobile Ad Hoc Networks,” Proc. Int’l Symp. Applications on Internet (SAINT), 2006.
- [6] Z. Zhi and Y.K. Choong, “Anonymizing Geographic Ad Hoc Routing for Preserving Location Privacy,” Proc. Third Int’l Workshop Mobile Distributed Computing (ICDCSW), 2005.
- [7] X. Wu, “AO2P: Ad Hoc On-Demand Position-Based Private Routing Protocol,” IEEE Trans. Mobile Computing, vol. 4, no. 4, pp. 335-348, July/Aug. 2005.
- [8] C.-C. Chou, D.S.L. Wei, C.-C. Jay Kuo, and K. Naik, “An Efficient Anonymous Communication Protocol for Peer-to-Peer Applications over Mobile Ad-Hoc Networks,” IEEE J. Selected Areas in Comm., vol. 25, no. 1, pp. 192-203, Jan. 2007.
- [9] L. Zhao and H. Shen, “ALERT: An Anonymous Location-Based Efficient Routing Protocol in MANETs,” Proc. Int’l Conf. Parallel Processing (ICPP), 2011.

Considering User Participation in Light Of level and Stages of Self-Selection in Architectural Design Process (ADP)

Mahdi Torabi¹, Mohammad Pir Mohammadi², Mohsen Roshan³
Mahmud Bin Mohd Jusan⁴

^{1,2,3,4} Department of Architecture, Universiti Teknologi Malaysia, Malaysia

Abstract: Presenting the new definition of self-selection in Architectural Design Process (ADP) needs to clarify the edges of this new concept versus the others, which exist in design area. Referring to conducting content analysis in previous published studies, the general meaning of self-selection is a situation in which user decide to do something for themselves rather than do something that has chosen for them. On the other hand, different users' and designers' vision of self-selection make a connection with End User's Personalization (EUP) and User Centered Design (UCD). Both self-selection and user participation indicate the user decision-making power. Consequently, for earning a high level of user satisfaction, users should allow to contribute partially or totally, in certain decision-making processes, which have normally considered as the typical responsibility of architects. This paper by gathering a close group dissection and using brainstorming method, has attempted to argue the levels and stages of user participation in order to discover and establish the level and stages of self-selection in ADP.

Keywords: Architectural Design Process (ADP), End User's Personalization (EUP), Self-selection, User Centered Design (UCD), User Participation

I. Introduction

Researchers typically try to find a new spot for themselves. All of them know only by studying old concepts and arguing them, the new meaning and definition may come up. After that, the main responsibility of researcher is to clarify similarities and differences of this new concept with the other definitions that already existed. In our case, several design definitions have been taken as the base plate of introducing the entire structure of self-selection in Architectural Design Process (ADP). End users always want to contribute and personalize their own place. Based on this kind of need and desire, End User's Personalization (EUP) is the closest concept of self-selection in ADP [1], [2].

Nevertheless, all design processes have another side too, which wants to control the whole process. Although responsibility of architects should come first in each projects, founded on designer's side, by using the methods of User Centred Design (UCD) as nearest conception of self-selection in ADP, user's values and ideas also can catch [3], [4], and this leads this study to investigate the same pattern of satisfaction in ADP. At last, for explaining the level of contribution of users and the power of architects in ADP, the idea of user participation's stages and levels has been reviewed and argued. Ultimately, in conclusion section, self-selection's stages and level will be presented.

II. Self-Selection

Conferring to primarily studies, the self-selection as self-respect's sub-criteria of human values guide behaviors, meaning that values can guide the people selection or evaluation of behaviors and events [5]. Therefore, normal decision-making is a vital part of what characterizes humans throughout history [6].

Hence, self-selection is selecting of self. It means self-selection is defined as a choice that you make by yourself [7]. Without a doubt, behavioral decisions of people play a fundamental role in better understanding of self-selection. In this area, self-selection is a term used to indicate any situation in which individuals select themselves into a group [8]. Otherwise, self-selection is the best way to describe the decision-making power.

III. User Participation

Participation is a general concept covering different forms [9]. Within the field of design, there is a growing concern with user satisfaction, which benefits from technological innovation in order to identify users' needs and facilitate user participation in the design process [10].

Furthermore, although direct contact between users and designers can be risky if it is not properly structured, user participation is necessary for reaching out diverse ideas for the final decisions that are made during the ADP. However, involving users or stakeholders early and often in the ADP is a key part of delivering

a successful project and so clients need to ensure that this happens [11]. On the other hand, if users take part in the decision-making process of design, they also stand some of the responsibility for the success or the failures. At the end of the day, they cannot turn around and blame the architects for design faults [12]. This participation improves by user needs, values and wants through designer's guidance. In the meantime, designer plays significant part of a controller of what the user thinks. Architect can extend the mental faculties and the imagination of the user by whatever he/she owns of artistic background and experience, which others lack.

3.1 Stages of Participation

Grounded on user participation idea, each ADP has four stages: Planning, Designing, Construction and Evaluation. Although over the recent years these stages have been divided to several parts depending on their time or parts, user participation comes into different levels of them. Description of these stages have mentioned in literature [13], [14], [15], [16] as follows:

3.1.1 Planning

This stage means the stage of policy preparation or the stage of knowing what the user thinks of doing. Therefore, this is the architect's responsibility to know how to allow the user to be participated in the planning process.

3.1.2 Designing

The vital factor in this stage of participation is that the design has to express the user needs and values. Consequently, architect ought to choose and supervise the level of user participation carefully in designing which decisions are the most important ones for ADP to take place in this stage.

3.1.3 Construction

Although numerous users ignore this stage, it is a very important one, as it appears in the self-help project. Regularly, the main purpose is to decrease the cost of the building. Indeed, participation in this stage helps architect manage the budget. Therefore, financial decisions prove that this stage have value position in each projects.

3.1.4 Evaluation

Several researchers do not consider this stage as one of the user participation stages; however, we claim in this paper that Evaluation is one of the significant stages in participation. The aim of this stage is to evaluate the building by User experience (UX) after passing an enough period of living in the building. The architect would ask them the advantages and disadvantages of the building by various questions. The result of this participation would benefit architects to have a better understanding of developing user needs and values in ADP. Ultimately, they will find out how to improve their design in similar future projects.

3.2 Levels of Participation

In any design process, level of participation depends on many factors. According to numerous studies, the most important keys are User, Architect, Project, and Culture of the Community and Democracy in the Community. All of these features make level of participation divides into several portions as to control the architect or the user in ADP. These portions are discussed in [13], [17], [18], which are:

3.2.1 Non-Participating level

The level of participation could be zero. In this level, the architect controls every move in ADP while user participates in none of the four stages. In other words, in this architecture there is no user point, as the diagram below shows.

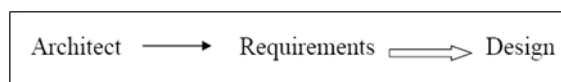


Fig. 1 Non-participating Level

3.2.2 Low Level of Participation

This level means the user participation is small and hence insignificant. The architect takes in his consideration the principle requirements of the project. In this level, architect sets the priorities according to the user ideas and decides which one is helping to improve the ADP.

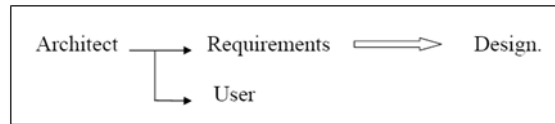


Fig. 2 Low level of Participating

3.2.3 Equally Balanced Level of Participation

In this case, the opinion of the user is equal to the opinion of the architect. The only thing, which they demand is the requirements. Architect and the user cooperate with each other to conduct a project, which expresses the culture of the user and community.

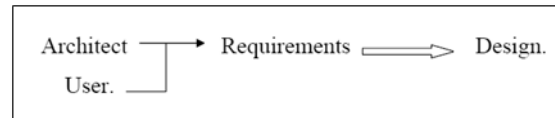


Fig. 3 Equally Balanced Level of Participating

3.2.4 High level of Participation

This level of participation appears when the user has a big power to enables him to administer the stages of the project. It means that user is able to direct the project to the concept of their participation in taking the serious decisions.

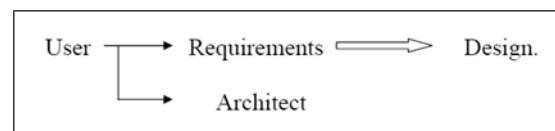


Fig. 4 High Level of Participating

3.2.5 Top level of Participation

In this level, the part of the architect does not exist. The user, who is the chief controller in the project, considers the requirements of ADP. In another manning architecture is without architect.

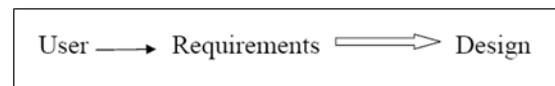


Fig. 5 Top Level of Participating

IV. Discussion

While in concept of participation, user can decide to participate in only one or in all the ADP stages together, there are several doubts in accuracy of self-selection present in these stages. On the other hand, there are five levels of user participation, which can help the architect and user decide the level of contributing in ADP of each unique project. However, by considering whole concept of self-selection from both sides of ADP, which means users' and designers' view, there are a few suspicion to accept these user participation's levels as levels of self-selection in ADP.

4.1 Stages of Self-selection

Recalling the new concept of self-selection in ADP shows that Planning and Designing stages of this process have high potential as the area of User Centered design (UCD). Without any doubt, UCD methods are one of the best ways of user contribution in order to receiving user's values and wants. Nevertheless, from the self-selection point of view, this paper is arguing the possibility of self-selection in Construction stage, which normally has been fixed in the first and second stages of ADP. The only case of an acceptable participation for Construction stage is to admit that these four stages are not dependent on each other.

However, in the last stage of this process, User experience (UX), which is important part of Evaluation stages, helps architects at first, to earn End User's Personalization (EUP) in their own place, and secondly to use this knowledge to the same future ADP with similar users or stakeholders.

4.2 Level of Self-selection

Certainly, it is possible to divide the level of self-selection in different parts such as five levels of user participation, but based on the scientific nature of ADP, without any doubt, architect must take the big role during the design process. This is the merely safe road to earning user's value and needs and using them in ADP.

In the first level of participation, there are no users to choose anything for themselves. Although by absence of user views, most of architects may happily want to follow only their scientific and artistic expression of architecture, for earning best results, user should be encouraged in contributing in, at least, the first stages of participation. Logically, zero participation means no level of self-selection.

In the second level of participation, a bold power of architect exists while contribution of users is weak. In the meantime, responsibility of architect to courage user for expressing their feels and desires is obvious. However, using UCD methods makes this level correct choice for getting high level of satisfaction from both sides in ADP.

In the third level of participation, absence of guidance because of equally balanced level of participation between user and designer leads the project to uncomfortable zone for both sides. It means the only solution is the capability of architects for managing various situations that ought to be considered. Consequently, this level would not right choice as level of self-selection in ADP.

In high levels of participation, user has the power to control every requirements and movements in ADP. It means that user claims that I have enough knowledge to make critical choices in the whole process of design and I do not need to have an architect beside myself. In other words, this level is the same as fifth level of user participation, in which architect does not exist. Subsequently, these last two levels mean Planning, Designing, Construction and Evaluation without any expert.

The only hope of receiving a desired result is that the user must be capable of taking the architect's responsibility. It means user has to be an architect. Finally, this assumption makes these levels as the first level of participation, which does not have an acceptable level of self-selection.

V. Conclusion

In previous studies, the concept of self-selection in ADP that has a strong connection with behavioral decision is guided by people values, needs and desires. Self-selection is a position in which users are allowed to choose and decide something for themselves. In finding of similarities with other existing definitions in design process, grounded on user wills, End User's Personalization (EUP) and based on scientific version of architect's obligations, User Centered Design (UCD) have the best characteristics to explain the unique position of self-selection in ADP.

Both self-selection and user participation are highlighting the user decision-making power and more importantly, the necessity of this contribute in ADP for earning the desirable process and product. Furthermore, several participation studies have emphasized that users have authority to play a part partially or totally in four stages of decisions making process in ADP, which is generally called as common duty of an architect.

Although rereading the main reason of introducing a new concept of self-selection in first place, which wants to highlight the lack of user selection in ADP, has nearest concern to user participation's idea, this paper argues to accept some stages and levels of user contribution in ADP as stages and level of self-selection. Founded on levels of participation some levels let user control all stages of ADP or at least have a significant role or an equal position versus the architect position. Logically, the absence of architect may influence the professional process, as ADP cannot ensure a correct result of user's desires. As result, the only suitable level of self-selection in ADP is the same level as low level of participation.

Besides, in Construction stage of user participation even with mentioning the main purpose of participation, which is to decrease the cost of building, self-selection of user ought to happen in Planning and Designing stages and to be fixed before starting Construction stage. Therefore, this paper discussed that all of the decision-making stages including the financial decisions, which effect the project cost have to takes place during the two early stages of ADP. In other words, no one should allow anyone to change any activities like user self-selection during Construction stage of the project.

Finally, this paper indicates the acceptable stages of ADP for happening self-selection are Planning, Designing and Construction stages. By using User Centered Design (UCD) methods in two early stages and collecting feedback from the end user of building in Evaluation stage by User experience (UX) methods or Usability methods in order to earn End User's Personalization (EUP), architect can use this knowledge in the same future ADP with the same users or stakeholders.

REFERENCES

- [1] Torabi, M., Jusan, M. & Daneshpour. A. (2012). Self-Selection and Personalization in Architectural Design Process (ADP). 6th SEATUC Symposium, King Mongkut's University of Technology Thonburi (KMUTT), Thailand.
- [2] Torabi, M., Jusan, M. & Daneshpour. A. (2012). Effects of Self Selection in Architectural Design Process (ADP); Considering End User's Personalization (EUP). (ICITSBE 2012), Perak, Malaysia
- [3] Torabi, M., Jusan, M. & Daneshpour. A. (2012). The Definition of Self Selection in Architectural Design Process (ADP): Based on User Centered Design (UCD) Method. (ADIC 2012), Malaysia.
- [4] Torabi, M., Jusan, M. & Daneshpour. A. (2012). Effects of Self Selection in Architectural Design Process (ADP); Considering User Centered Design (UCD). (ICITSBE 2012), Perak, Malaysia.
- [5] Schwartz, S. H. & Bilsky, W. (1987). Toward a psychological structure of human values. *Journal of Personality and Social Psychology*, 53, 550-562.
- [6] Lakoff, G. & Johnson, M. (1999). *Philosophy in the flesh: the embodied mind and its challenge to Western thought*. New York, Basic Books.
- [7] Online Dictionary, Available at: <http://www.yourdictionary.com/self-selection>.
- [8] Online Dictionary, Available at: <http://www.wordiq.com/definition/self-selection>.
- [9] Wulz, F. (1990). The concept of participation. *Participatory Design, Theory & Techniques*. By Sanoff, Henry. United States: Bookmasters Inc, pp 39-48.
- [10] Jenkins, P. & Forsyth, L. (2010). *Architecture, Participation and Society*. Routledge Ink, Taylor & Francis Group, London and New York.
- [11] Cabe (2006). Better Public Building. Prime Minister's Award. Available at: www.cabe.org.
- [12] Sanoff, H. (1990). *Participatory Design, Theory & Techniques*. United States, Bookmasters Inc.
- [13] Ahmad Mohammed, A. S. (2006). *Community Participation in Architectural Design, Evaluation of Al-Maageen Housing in Nablus*. Master thesis, An-Najah National University, Nablus, and Palestine.
- [14] Abbott, J. (1996). *Sharing the City, Community Participation in Urban Management*. London: UCL Press.
- [15] Lawrence, R. (1990). Basic principles for public participation in house planning. *Participatory Design, Theory & Techniques*. By Sanoff, Henry. United States: Bookmasters Inc, pp 77-82.
- [16] Lawson, B. (1980). *How Designers Think*. London: The architectural Press Ltd.
- [17] Mikellides, B. (1980). *Architecture for People, explorations in a new humane environment*. Oxford: Aerofilm Ltd.
- [18] Pehnt, W. (1988). *Return of the Sioux. Buildings and Projects*. By Kroll, Lucien. London: Joseph Masterson, pp.7-13.

Implementation of FSM Based Automatic Dispense Machine with Expiry Date Feature Using VHDL

Mohd. Suhail¹, Saima Beg²

^{1,2} (Department of ECE, Integral University, India)

Abstract: In present scenario Automatic Dispense Machine is commonly used in different countries (Like Japan, Germany, U.S. and Singapore e.t.c.) because nowadays everybody wants fast response. In this paper we design and implement Automatic Dispense Machine with expiry date feature. We are using FSM (Finite State Machine) modeling for implement our work. In this paper process of states i.e start, product selection, check expiry date, insert money, dispense product, extra amount returned by machine and feedback are designed by Melay Machine Model. We implement our design for coin as well as currency note. The proposed algorithm is implemented in VHDL. For designing purpose we are using Xilinx ISE 14.2 tool that is also used for synthesis and for verifying results (Simulation) we are using Modelsim 10.2a student addition.

Keywords: VHDL, FSM, Xilinx ISE 14.2, Modelsim 10.2a, Automatic Dispense Machine.

I. INTRODUCTION

Automatic Dispense Machines are used to dispense various products like Cold drink Bottle, Coffee, Chips, and Chocolate etc. when money is inserted into it. Automatic Dispense Machines have been in existence since 1880s. The first commercial coin operated machine was introduced in London and England used for selling post cards. The Automatic Dispense machines are more accessible and practical than the convention purchasing method. Nowadays, these can be found everywhere like at railway stations selling train tickets, in schools and offices Automatic Dispense drinks and snacks, in banks as ATM machine and provides even diamonds and platinum jewellers to customers [4]. This paper proposed approach to design an Automatic Dispense Machine with expiry date features using FSM model by VHDL. The expiry date feature is very useful for user if any product is expire than that product will not dispense and return back the money to the user. We are using FSM (Finite State Machine) modeling to implement our work.

1.1 FSM (FINITE STATE MACHINE)

In a Finite State Machine the circuit's output is defined in a different set of states i.e. each output is a state. A State Register to hold the state of the machine and a next state logic to decode the next state. An output register defines the output of the machine. In FSM based machines the hardware gets reduced as in this the whole algorithm can be explained in one process.

Two types of State machines are:

1. Mealy Machine.
2. Moore Machine.

1.1.1 MEALY MACHINE

In this machine model, the output depends on the present state as well as on the input. The MEALY machine model is shown in fig 1.

In the theory of computation, a Mealy machine is a finite-state machine whose output values are determined both by its current state and the current inputs. A Mealy machine is a deterministic finite state transducer: for each state and input, at most one transition is possible. The Mealy machine is named after George H. Mealy, who presented the concept in a 1955 paper, "A Method for Synthesizing Sequential Circuits".

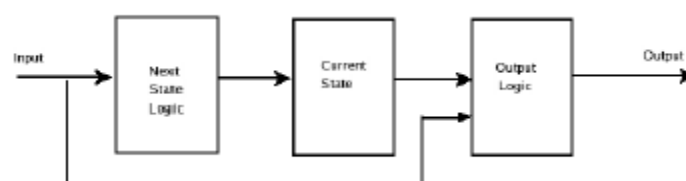


Fig. 1: MEALY Machine Model

1.1.2 MOORE MACHINE

In Moore machine model the output only depends on the present state. The MOORE machine model is shown in fig 2.

In the theory of computation, a Moore machine is a finite-state machine whose output values are determined solely by its current state. This is in contrast to a Mealy machine, whose output values are determined both by its current state and by the values of its inputs. The Moore machine is named after Edward F. Moore, who presented the concept in a 1956 paper, "Gedanken-experiments on Sequential Machines.

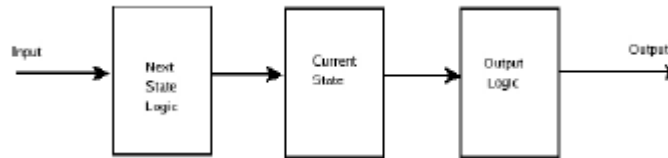


Fig. 2: MOORE Machine Model

II. RELATED WORK

The various researches have been carried out in order to design the Automatic Dispense Machines. A few of them are discussed here as: Fauziah Zainuddin [1] proposes a Automatic Dispense machine for steaming frozen food using conceptual modelling. In which the process of three main states (user selection state, freezer state and steaming state) has been modelled using process approach, which emphasized on the process flow or control logic to construct the model for steamed buns Automatic Dispense machine application. Conceptual modelling is described in [6]. In [7] the concept of automatic mobile payment is discussed. This concept is based on the short message payment with the main control module M68HC11 and GPRS module MC35. These various methods of designing VHDL based machines are discussed in [2], [3] and [8]. Also in [5] the passenger's requirements for ticketing system are given. In [4] a coffee Automatic Dispense machine is designed using single electron encoded logic (SEEL). The designed circuit is tested and its power and switching time is compared with the CMOS technology.

The Cedrone patent (US. Pat. No. 4,776,548) discloses a system for monitoring a vending machine and periodically transmitting information relating to machine conditions, sales and product inventory to a central computer. The Girouard patent (US. Pat. No. 4,982,346) discloses. An automated system for point-of-sale-type advertising and promotional campaigns, having a computer which can display advertisements on a monitor, manage promotional sweepstakes, display product or store locator maps, dispense coupons, accept orders, manage customer surveys, and communicate With a remote host computer.

The Gorog patent (US. Pat. No. 4,947,028) discloses a vending machine that can accept voice commands via a voice recognition system (and communicate with the customer via a voice synthesizer) to accommodate those persons who are unable to perform manual data entry tasks. In addition, the Gorog patent discloses a vending machine that can remotely verify a customer's credit Worthiness prior to permitting a sale on credit to the customer.

III. METHODOLOGY

The In this paper a state diagram is constructed for the proposed Automatic Machine which can vend four products that is cold drink, coffee, chips and chocolate. Four inputs are taken for selection of products. We select the product and input money 8 Rs. for cold drink, 10 Rs for coffee, 20 Rs for chips and 30 Rs for Chocolate. We took 1, 2, 5 as a coin for input as well as 10, 20 as a currency note for respective products. An Expiry date feature is also available in our machine which is used for if any product is out of date then machine will not dispense that product and two output change and ret (Return) are available in our machine for provide the change money to the user and if there is no product available in our machine then return full money. The products with their prices are shown by table 1. There are also two input signal clk and reset. The machine will work on the positive edge of clock and will return to its initial state when reset button is pressed. The proposed vending machine is designed using FSM modeling and is coded in VHDL language.

S. NO.	PRODUCTS	PRICE
1	Cold Drink	8
2	Coffee	10
3	Chips	20
4	Chocolate	30

Table 1: Products with their prices

The state diagram mainly consists of states (Reset, Selection Products, Product available, Expiry date, Insert money, Dispense Product, change and exit). Initially when the reset button is pressed, the machine will be ready for the users to select the product and cold storage has 10 quantities of all products. This state is the initial state of the design. After this the user will select the product to be dispensed. The machine can accept 1, 2, 5 amount of coin and two types of notes i.e. rupees 10/- and 20/-. Let us suppose that the user selects coffee. The machine will firstly check that whether the products are available in the machine or not. After this the control unit will move to check whether product is expire or not, if product is not expiry then insert the sufficient money. Then if rupees 10/- note is inserted then the machine will go to next state and dispense the product. If products are not available in the machine then the control unit will demand for servicing and after service the machine will get reset. This methodology is explained using a flow diagram shown in figure 3.

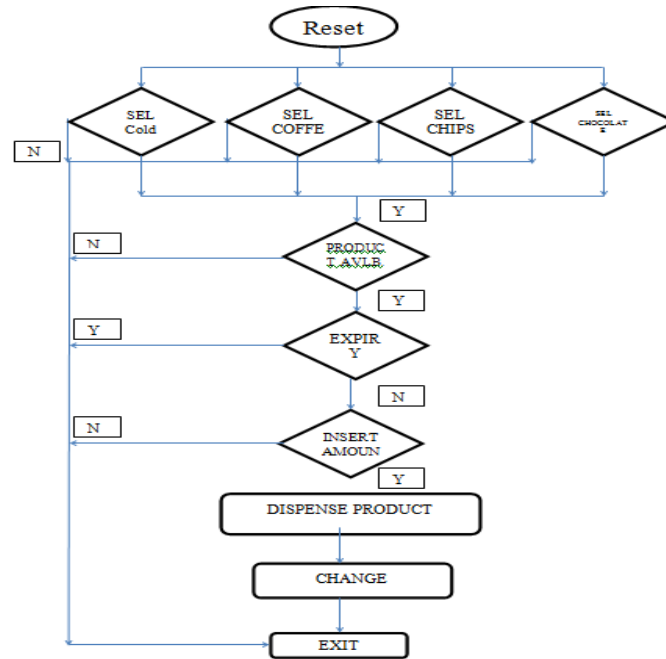


Fig 3: Flow Chart for Automatic Machine

IV. SIMULATION RESULTS

In case of bottle dispense we take reset is '0', input rupees as 8 INR and expiry date (bexpirydate) is '0' then bottle will dispense. We took expiry date as a feedback of product if our product (cold drink bottle) is expire then there is no dispense. If machine has no product then empty signal will be high and return full money. These all operation will perform on positive edge clock. If reset is high then machine will not any do any performance and 10 cold drinks will be stored in cold storage. Fig 4 shows the cold drink dispense.

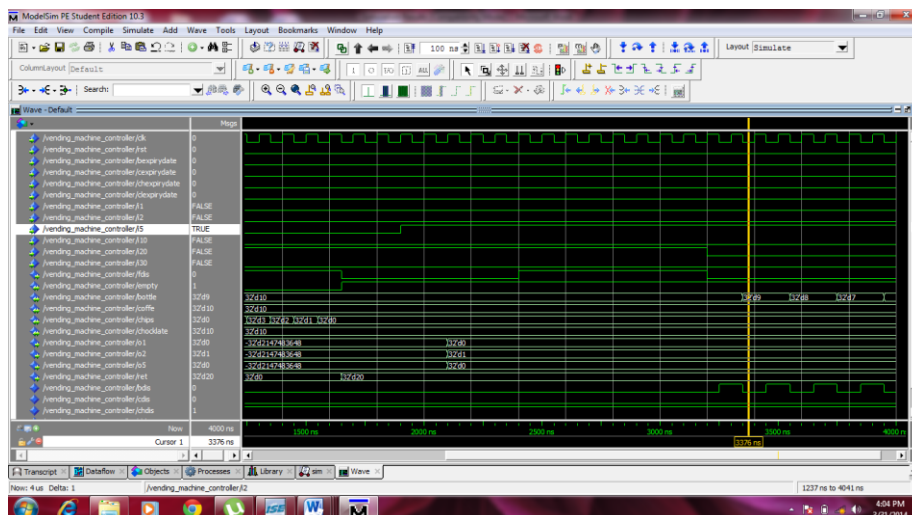


Fig. 4: Simulation result for Cold drink bottle dispance

In case of coffee dispense we take reset is '0', input rupees as 10 INR and expiry date (cexpirydate) is '0' then coffee will dispense. We took expiry date as a feedback of product if our product (coffee) is expire then there is no dispense. If machine has no product then empty signal will be high and return full money. These all operation will perform on positive edge clock. If reset is high then machine will not any do any performance and 10 coffee will be stored in cold storage. Fig 5 shows the coffee dispense.

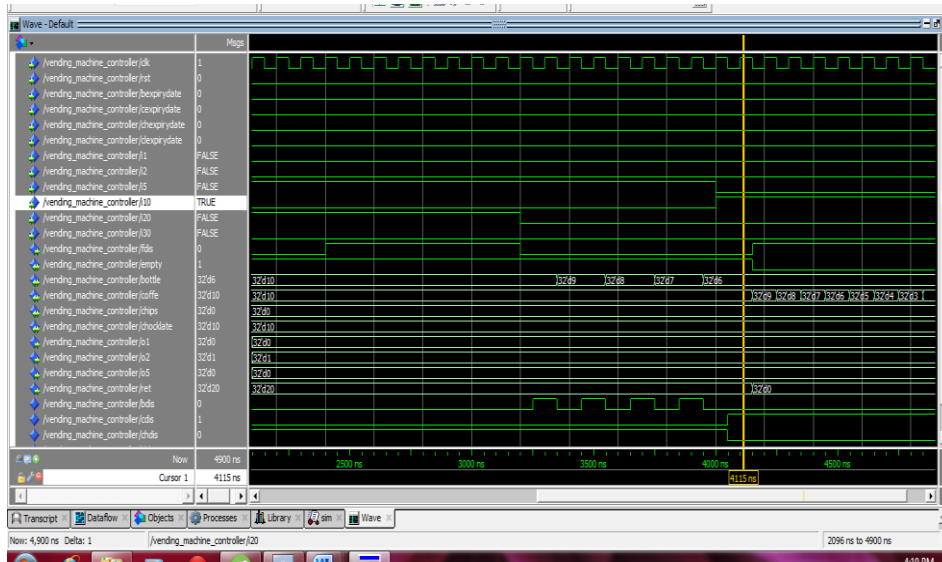


Fig. 5: Simulation result for Coffee dispense

In case of chips dispense we take reset is '0', input rupees as 20 INR and expiry date (chexpirydate) is '0' then chips will dispense. We took expiry date as a feedback of product if our product (chips) is expire then there is no dispense. If machine has no product then empty signal will be high and return full money. These all operation will perform on positive edge clock. If reset is high then machine will not any do any performance and 10 chips will be stored in cold storage. Fig 6 shows the coffee dispense.

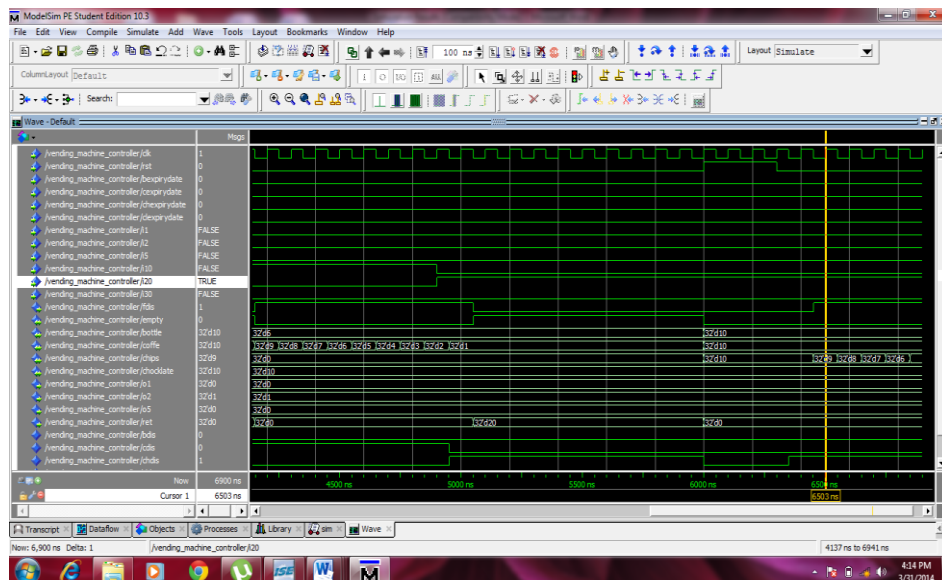


Fig. 6: Simulation result for Chips dispense.

In case of chocolate dispense we take reset is '0', input rupees as 30 INR and expiry date (cexpirydate) is '0' then chocolate will dispense. We took expiry date as a feedback of product if our product (chocolate) is expire then there is no dispense. If machine has no product then empty signal will be high and

return full money. These all operation will perform on positive edge clock. If reset is high then machine will not any do any performance and 10 chocolate will be stored in cold storage. Fig 7 shows the coffee dispense.

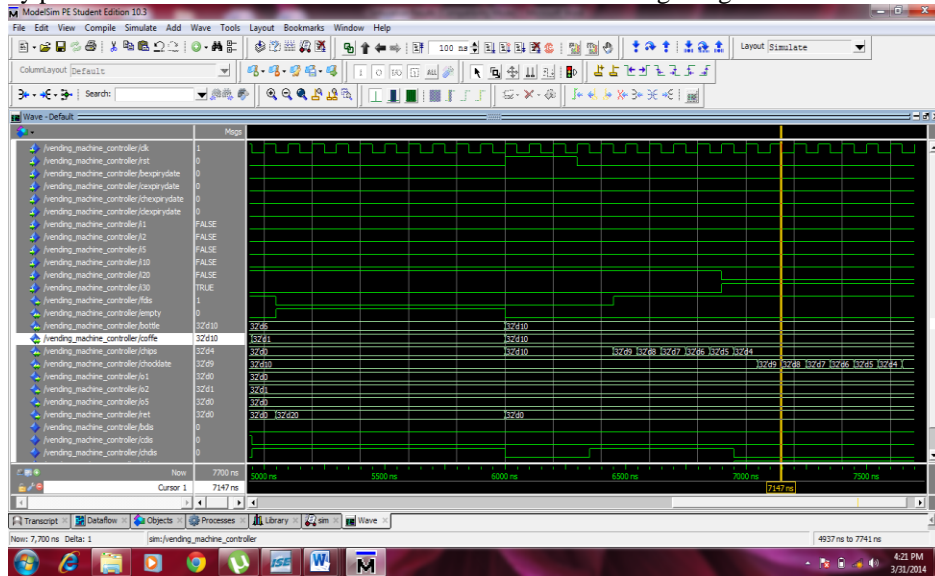


Fig. 7: Simulation result for Chocolate dispense

V. CONCLUSION

We Implement the FSM based automatic dispense machine using Xilinx ISE 14.2. For verification (Simulation) we used Modelsim 10.2a student addition tool from Mentor Graphics Company. We conclude that our design is cost effective and dispense multi products. We also added an expiry date feature that is very useful for common man if any product is out of date or expire machine will not dispense that product and if any person have inserted money for the same product machine will return full amount. At present scenario it is very use full in malls, shopping Complexes, PVRs, railway stations and airports etc.

REFERENCES

- [1] Fauziah Zainuddin, Norlin Mohd Ali, Roslina Mohd Sidek, Awanis Romli, Nooryati Talib & Mohd. Izham Ibrahim (2009) "Conceptual Modeling for Simulation: Steaming frozen Food Processing in Vending Machine" International Conference on Computer Science and Information Technology, University Malaysia Pahang, pp.145-149.
- [2] Xilinx Inc., Spartan 3 Data sheet: <http://www.xilinx.com>.
- [3] Biplab Roy & Biswarup Mukherjee (2010) "Design of Coffee Vending Machine using Single Electron Devices" Proceedings of 2010 International Symposium on Electronic System Design. Pp 38-43.
- [4] M. Zhou, Q. Zhang & Z. Chen (2006), "What Can Be Done to Automate Conceptual Simulation Modelling?" Proceedings of the 2006 Winter Simulation Conference, pp. 809 – 814.
- [5] Zhang Wen & Zhang Xin Long (2010) "Design and Implementation of automatic vending machine Based on the short message payment" International Conference on Information and Communication technology in Electrical Sciences, Neijiang, Sichuan, China.pp.978-981.
- [6] B. Caulfield & M.O Mahony (2005) "Passenger Requirements of a Public Transport Ticketing System" Proceedings of the 8th International IEEE Conference on Intelligent Transportation Systems Vienna, Austria, pp-32-37.
- [7] Peter Minns & Ian Elliott, "FSM-based Digital Design using Verilog HDL", John Wiley & Sons Ltd 2008.
- [8] Bhaskar "VHDL primer" Second Edition.

Palmprint Identification Based on Principle Line Using Machine Learning Techniques

Krishnaveni.M¹, Arunpriya.C²

^{1,2}(Research Scholar, Assistant Professor, Department of Computer Science, PSGR Krishnammal College for Women, India)

Abstract: In this paper, we propose principle line based Palmprint Identification method. In this method to detect principle lines of palm print is with consecutive filtering operations. Smoothing operation is used to remove image noise. Edge detector operation and closing operation are merged to extract the principle lines. Binarization yields the binary principle line. The lines detected with the developed scheme are used to extract textural information using Gray Level Co-occurrence Matrix and Statistical Property Features. Euclidean distance is used for matching to identify the genuine person and the powerful supervised classification techniques namely Support Vector classification Machine and Extreme Learning Machine with kernels like linear, radial basis function is applied to classification. The experimental results on the PolyU palmprint database demonstrate the feasibility and effectiveness of the higher accuracy and reduced execution speed shows that our proposed approach.

Keywords: Biometrics, palmprint extraction, palmprint identification, Principle lines, Machine learning.

I. Introduction

The security of a system has three main components of authentication, authorization, and accountability. Authentication is the most important of these three elements. In the information technology domain, authentication means either the process of verifying the identities of communicating equipment, or verifying the identities of the equipment's users, which are primarily humans. Security plays a very important role in one's life. The accurate identification of the person to access secured application is static challenging due to the limitations imposed by real time applications. Samples of such applications include access to ATM, nuclear facilities, boarding a commercial flight or performing a remote financial transactions etc. The main goal of accurate identification is to prevent the imposter accessing the safe application. There are three methods in which users can be identified such as:

1. Something the user knows—Password, PIN
2. Something the user has—Key, Cards and Tokens
3. Something the user is—Unique Biological properties

Easily lost, stolen, shared or manipulated and there by undermining the intended security. The third way of identifying the person appears to be more secure, so designing a security system based on biological properties cannot be lost, manipulated or stolen. Biometric system can be defined as a pattern recognition scheme, which is capable of finding a Person based on their biological properties. These biological properties can be physical characteristics like face, finger print, hand geometry, palm print, retina, and DNA, ear, iris and hand vein .Behavioral properties like speech, gait and signature.

A biometric is a physical or behavioural feature or attribute that can be measured. It can be used as a means of proving that you are who you claim to be, its means of proving without revealing your identity that you have a definite right.

Apalm print refers to an image acquired of the palm region of the hand. It can be either an online image (i.e. taken by a scanner, or CCD) or offline image where the image is taken with ink and paper. The palm itself consists of principal lines, wrinkles and ridges. It differs to a fingerprint in that it also contains other information such as texture, hollows and marks which can be used when comparing one palm to another.

Palm has unique distinguishing line patterns which can be used to identify people uniquely. It is a physiological biometric. A user is asked to put his/her hand in an surrounded unit having fixed illumination and a platform that restricts hand motion. It may have pegs to further fix the position of the hand. Scanners or cameras can then be used to capture the image. Palm print has high user acceptability with few hygiene based concerns characteristic of all contact based biometric. But there has been a move towards developing contactless recognition systems.

There are two types of palm print recognition research,

1. high resolution
2. low resolution

The high resolution approach employs high resolution images, and is suitable for forensic applications, such as criminal detection. In general, high resolution refers to 400 dpi [1]. In high resolution images, researchers can extract ridges, singular points and minutiae points as features can be detected. The low resolution approach employs low resolution images, and is more suitable for civil and commercial applications such as access control. Palm print images can be acquired with low resolution cameras and scanners and still have enough information to achieve good recognition rates. Low resolution refers to 150 dpi or less. The Low resolution images are generally use principle lines, wrinkles and texture.

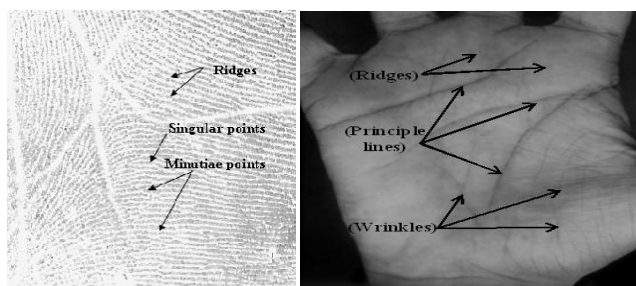


Fig.1 Palm print features in (a) a high resolution image and (b) a low resolution image.

Recognition by iris or retina brings very good results but tolerate very expensive devices of images capture in one hand and on the other hand the possibility of intrusions among the users. Recently, many researchers used verification by face or voice, unfortunately their performance is again far from being satisfactory.

Another technology is based on the geometry of the hand. It uses the geometric information to identify a person, unfortunately these information are very limited with low accurate results. To face the problems encountered in the biometry based on the hand, David Zhang and shuproposed, in 1996, another biometric always based on the hand that is palm prints.

The palmprint, this very large and internal surface of the hand, contains several characteristic features as principle lines, wrinkles, creases and textures. Thanks to this large surface and the abundance of characteristic features, it seems that palm prints are very robust to noise and unique to every individual. Compare to other physical characteristics.

Palmprints identification has several advantages

1. Treatments of low resolution images
2. Few intrusion risks
3. The features of lines are stable
4. High level of acceptance by users.

The Physical characteristics can be fingerprint, palmprint [2,3], face, iris, signature, voice, and gait. Palmprint is an efficient characteristic because of its uniqueness and stableness. In addition, this characteristic gives a lot of biometric information, e.g., principle lines, wrinkles, ridges and datum points which are the unique features of human.

Palmprint-based biometric technology is composed of two steps: feature extraction and recognition. Image features are extracted and collected as input vector while the remaining step is to recognize or classify that vector into the suitable class to identify people.

In recent survey, Sakdanupab et al. [4] have proposed and implemented a palmprint classification method based on principle lines. The phase of principle line extraction is based on profiles of gray values within a window of size 3x3 in four directions (0, 45, 90, and 135 degrees). The principle lines consisting of heart line, head line and life line are extracted and used for recognizing people afterwards. The drawback of this method is that noise is not completely eliminated by the proposed noise reduction process. In addition, their algorithms take too much processing time. The accuracy was achieved 85.49%.

Huang et al. [5] have proposed a palmprint verification approach based on principle lines. In the process of principle line extraction, the lines are extracted by using the modified finite Radon transform. When the transformation is applied, lines in Cartesian coordinate are converted to lines in energy and direction. The energies and directions are used to detect the differences between principle lines and wrinkles. After that, those differences are finally used to verify people. The accuracy was achieved 95%.

Wong et al. [6] have described the palmprint identification based on features from lines in palmprint. In this work, Sobel mask of two sizes (3x3 and 5x5) in four directions together with an appropriate threshold are mainly used to extract feature vectors. Proceedings of the Second International Conference on Knowledge and Smart Technologies 2010 (July, 24-25, 2010)

In 2009, Zhu et al. [7] have applied an approach for major line extraction of palmprint using gradient images in 4 directions which are overlapped, and then merged with canny edge image. To obtain better results, palmprint image will be dilated and blurred with the probable template to get the major lines. The disadvantage of this method is that their algorithm is somewhat complicated to generate the principle palmprints. From our recent survey mentioned, the methods belonging to Huang and Wong are not used the principle lines as main features. The methods attempt to extract features from the whole image instead. The accuracy was achieved 87.04%.

However, the methods from Sakdanupab and Zhu focus on extracting the principle lines directly. This causes the problem because of their complexity and high processing time. In this work, the compact method to detect principle lines of palmprint is proposed with consecutive filtering operations. Smoothing operation is used to remove image noise. Edge detector operation and closing operation are merged to extract the principle lines. Binarization yields the binary principle line. Finally, the postprocessing, removing the connected components with small region, is applied to discard noise.

The Leqing Zhu and RuiXing, proposed a new hierarchical palmprint recognition method [8]. First the gradient images along the four directions are computed. Then these four gradient images are overlapped and de-noised. Edges are detected with canny detector and merged with the de-noised gradient image with and operation. The result is then dilated and blurred with a probable template to get the major line features. The bidirectional method is used for matching.

The Wei Jia, Yi-Hai Zhu, Ling-Feng Liu and De-Shuang Huang, proposed the palmprint retrieval based on principal lines for palmprint recognition [9]. In this principal lines are extracted using modified finite radon transform method. Then key points of principal lines are detected. And direction, position and energy of these are stored in the table. During matching palmprint is retrieved using the table.

The Wei Li, Lei Zhang, David Zhang and Jingqi Yan, proposed the principal line based ICP Alignment for Palmprint Verification [10]. First the modified finite Radon transform (MFRAT) is used to extract principal line. The iterative closest point (ICP) alignment algorithm is used to compute the shifting, rotation and scaling between the ROI images, and then presented an efficient way to combine the alignment result with the competitive code for palmprint recognition.

The Cong Li, Fu Liu and Yongzhongzhang, proposed a method to extract the principal lines based on their cartelistic of roof edges [11]. In this at first gray adjustment and median filtering are used to enhance contrast and weaken noise. Then, palm-lines are detected based on diversity and contrast. And an improved Hilditch algorithm is used to do thinning, an edge tracking approach is applied to get rid of twigs and short lines, and then, the broken lines are connected. Finally, the single pixel principal palm-line image is obtained.

The PatprapaTunkpien, SasipaPanduwareethorn and SuphakanPhimoltares, proposed a simple and fast method to extract the principle lines of palmprint by using consecutive filtering operations related to gradient and morphological operators [12]. A gradient masks and closing operator are used to detect the lines. The results are acceptable with 86.18 % accuracy.

The FengYue, WangmengZuo and David Zhang, proposed the iterative closest point (ICP) algorithm [13] for palmprint alignment before matching. The palm-lines are extracted using steerable filter. However, due to nonlinear deformation and inconsistency of extracted palm line feature, the ICP algorithm using only position information would fail to obtain optimal alignment parameters. To improve its accuracy orientation feature is used, which is more consistent than palm line, to make ICP registration more robust against noise.

II. The Proposed Framework

The proposed method consists of four steps

1. Image Acquisition
2. Image Preprocessing
3. Feature Extraction
4. Matching

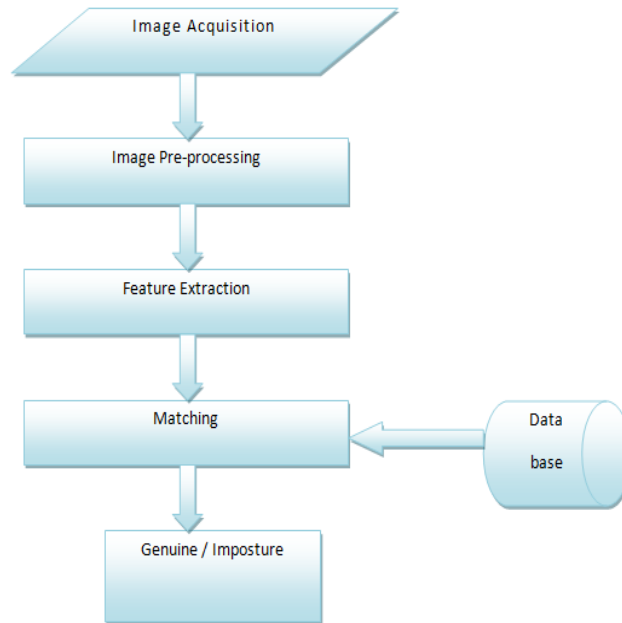


Fig.2 Proposed Architecture

2.1 Image Acquisition

The Poly U Palm print Database [14] is selected for experiment because it is widely used in palm print biometric area. Poly U is the most widely used low-resolution palm print database for algorithmic research considering recognition purposes. It is contained of 7752 images from 386 different persons. Persons provide either the left or the right hand, but then not both. There are 20 samples for each in bitmap file format. Visually, it is possible to identify more variability between images. The ROI of size 150x150 is cropped from each original image to be initially used for extracting the principle lines with filtering procedures based on image processing technique. Those image processing methods filtering algorithms that related to principle lines by employing gradient masks and closing operator to detect the lines and the pre-processing including smoothing, merging with binarization. It will display the principle lines and strong wrinkles.

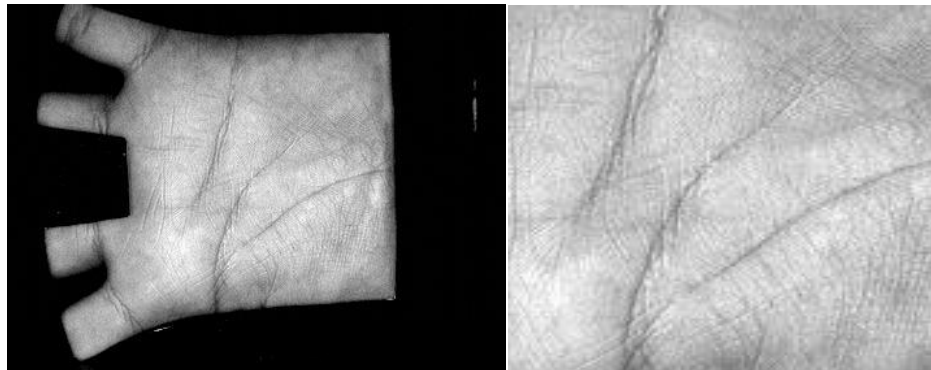


Fig.3 Original image Fig.4 Region of Interest (ROI) of palmprint

2.2 Image Pre-Processing

2.2.1 Smoothing

To blur an image, smoothing filter is applied to eliminate small object in the image for noise reduction purpose. It can also be used to get objects of interest which makes the image easy to detect. The smoothed image can be implemented by applying the mask of standard size, 3x3, with the correlation function as shown in Fig.6

1	1	1
1	1	1
1	1	1

Fig.5 3x3 smoothing filter mask

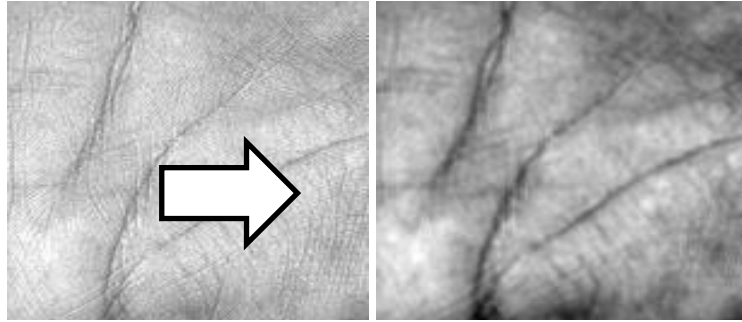


Fig.6 Applying smoothing filter into an ROI

2.2.2 Edge detection

In our research, edge detection is implemented by gradient operator as the second filter in the whole process. Firstly, masks of size 2x2 in two directions (0° and 90°) are used as illustrated in Fig.7. With this small size, edge can be easily detected with simply computation and less processing time. Subsequently, the smoothed image is convolved with the masks in 0° and 90° respectively to enhance the edge in both directions. These results are shown as Fig.7 and Fig.8 Finally, the magnitude of gradient is obtained by taking the root sum square [15] of G_x and G_y :

$$\text{Magnitude of gradient} = \sqrt{G_x^2 + G_y^2}$$

Where G_x and G_y are image gradients in two directions.

$$G_x = \begin{bmatrix} -2 & -2 \\ 2 & 2 \end{bmatrix}$$

$$G_y = \begin{bmatrix} -2 & 2 \\ -2 & 2 \end{bmatrix}$$

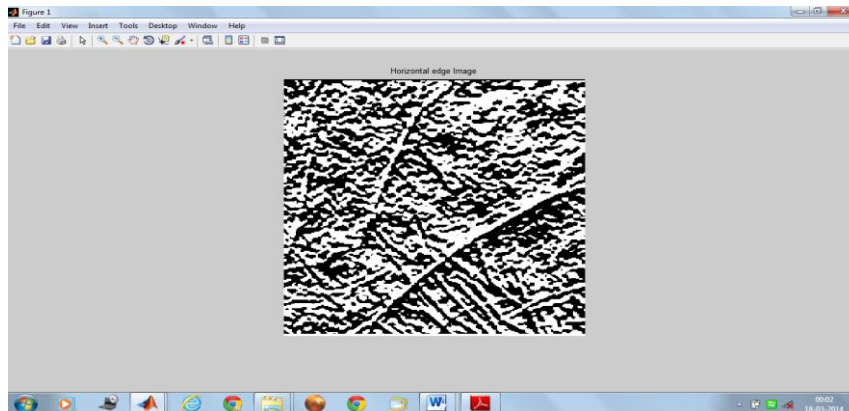


Fig.7 First derivative mask in horizontal directions

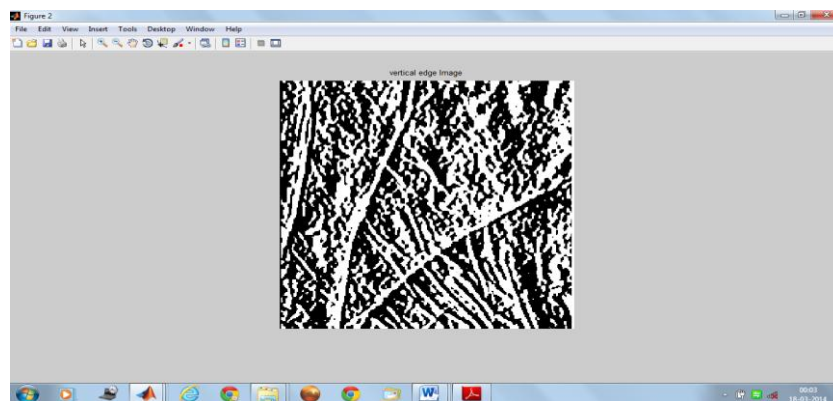


Fig.8 First derivative mask in vertical directions

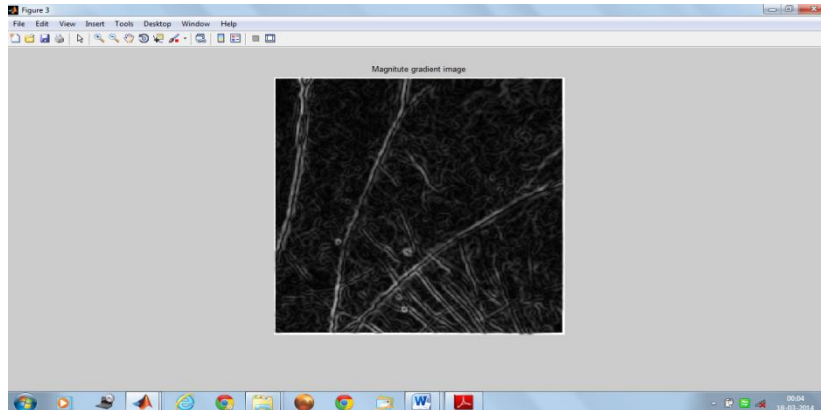


Fig.9 The magnitude gradient obtained from Fig.7 and Fig.8

2.2.3 Closing

Closing [16], the third operator, is the one of morphological operations which uses the basic operations of dilation followed by erosion. The closing of image G by structuring element S is denoted by $G \bullet S$ as follows

$$G \bullet S = (G \oplus S) \ominus S$$

Where \oplus and \ominus are basic mathematical morphology techniques called dilation and erosion. The edge image is performed by closing operator with disk-shape structuring element as demonstrated in Fig.10

Strel =

0	1	0
1	1	1
0	1	0

To smooth contours and fill small holes. After applying closing, the result of image is shown as Fig.11

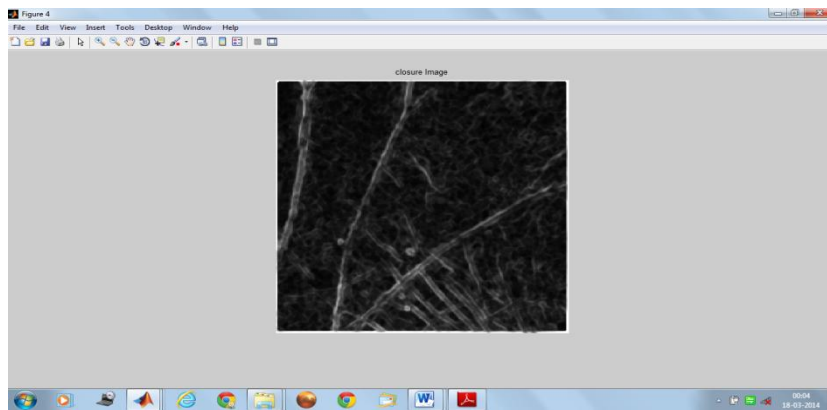


Fig.11 After closing applying result image

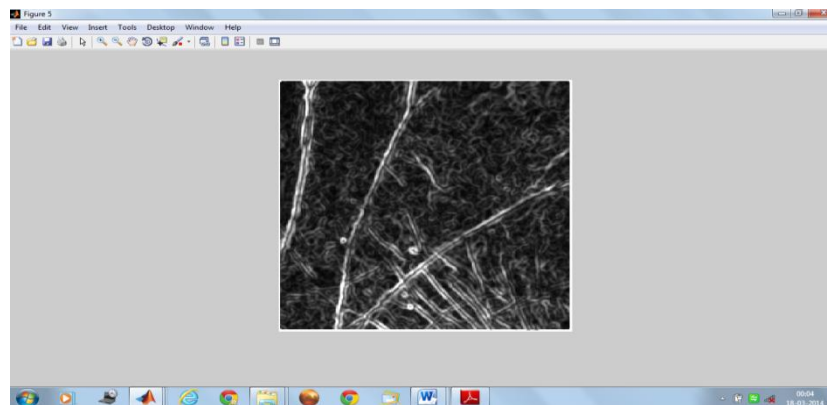


Fig.12 Gradient of an image

3.2.4 Merging

After the image is detected, the principle lines and closing operation is used. Gradient image and closing image are combined by merging with OR [17] operation as shown in Fig.13

This merged image obviously represents the contrast between object and background, so the binarization technique with an automatically pre-defined threshold is employed for enhancing the object from the background.

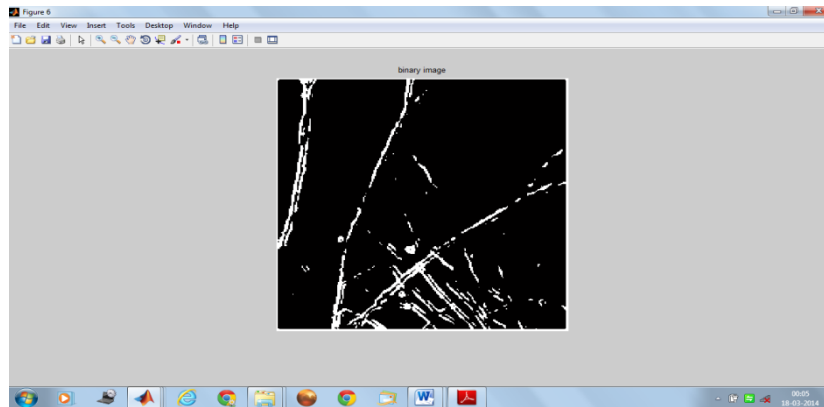


Fig.13 Binarization an image (ie) principle line and strong wrinkles will appear

2.3 Feature Extraction

Features play a significant role in image processing. The transformation of an image into set of features known as Feature Extraction. Features, characteristics of the objects of interest, if selected carefully are representative of the maximum relevant information that the image has to offer for a complete characterization of a region. Feature extraction methodologies analyse objects and images to extract the most prominent features that are representative of the various objects. Features are used as inputs to identify that assign them to the person that they represent. In this work Gray Level Co-Occurrence Matrix (GLCM) features and Statistical Property features are extracted from principal line extracted image.

2.3.1 GLCM (Gray Level Co-Occurrence Matrix) features

The GLCM features extracted in our research work are autocorrelation, contrast, correlation, dissimilarity, homogeneity, entropy, maximum probability, sum of square, sum of variance, sum of entropy, difference of entropy, and difference of variance. These features are developed by Haralick so it is also called Haralick features. Some of the features described above can be calculated using the formula given below.

Energy

Energy returns the sum of squared elements in the Grey Level Co-Occurrence Matrix (GLCM). Energy is also known as uniformity. The range of energy is [0 1]. Energy is 1 for a constant image. The formula for finding energy is given in below equation:

$$E = \sum_{i,j} p(i,j)^2 \quad (1)$$

Contrast

Contrast returns a measure of the intensity contrast between a pixel and its neighbour over the whole image. The range of Contrast is [0 (size (GLCM, 1)-1) ^2]. Contrast is 0 for a constant image. Contrast is calculated by using the equation given below:

$$C = \sum_{i,j} |i - j|^2 p(i,j)^2 \quad (2)$$

Correlation

Correlation returns a measure of how correlated a pixel is to its neighbour over the whole image. The range of correlation is [-1 1]. Correlation is 1 or -1 for a perfectly positively or negatively correlated image. Correlation is NaN (Not a Number) for a constant image. The below equation shows the calculation of Correlation:

$$CORR = \sum_{i,j} \frac{(i-\mu_i)((j-\mu_j)P(i,j)}{\sigma_i \sigma_j} \quad (3)$$

Where $\sigma_i, \sigma_j, \mu_i$ and μ_j are the means and standard deviations of P_i and P_j , the partial probability density functions.

Homogeneity

Homogeneity returns a value that measures the closeness of the distribution of elements in the GLCM to the GLCM diagonal. The range of homogeneity is [0 1]. Homogeneity is 1 for a diagonal GLCM. The homogeneity is evaluated using the equation:

$$H = \sum_{i,j} \frac{P(i,j)}{1+|i-j|} \tag{4}$$

2.3.2 Statistical Properties of a palm image Features

The proposed work discusses about to measure properties of image regions. There are various statistical measurements out of which part of our study and experiment are basic statistical properties of a palm image and are Area, Bounding box and centric.

The description is for the measurement of a set of properties for each connected component (object) in the binary image, BW. The image BW is a logical array; it can have any dimension

Area:

- The Scalar can say an actual number of pixels in the region.

Bounding Box:

- The smallest rectangle containing the region,
- a 1-by-Q *2 vector, where Q is the number of image dimensions: ndims(L), ndims(BW)

Centric:

- It is 1-by-Q vector that specifies the center of mass of the region. Note that the first element of Centric is the horizontal coordinate (or x-coordinate) of the center of mass, and the second element is the vertical coordinate (or y-coordinate). All other elements of Centric are in order of dimension.

These basic statistical properties can be used to measure the statistical property of image region. The calculated values of palm lines extracted image can be useful for palm matching technique. The matching can be done by using basic statistical properties of palm and mostly useful on extracted palm lines image [18].

2.4 MATCHING

2.4.1 Euclidian Distance

One of the most popular similarity distance functions is the Euclidian distance. It is just the sum of the squared distances of two vector values (xi,yi),

$$d_E = \sqrt{\sum_{i=1}^n (x_i - y_i)^2} \tag{5}$$

It is variant to both adding and multiplying all elements of a vector by a constant factor. It is also variant to the dimensionality of the vectors, for example if missing values reduce the dimension of certain vectors produced output will change. Given two data sets of features corresponding to the training and testing samples, a matching algorithm ascertains the degree of similarity between them.

III. Experimental Results

The experiments were implemented in MATLAB 2012 software with Image Processing Toolbox and on a machine with an Intel® Core™ i3-2350M CPU@2.30GHz and 2.00 GB of RAM configured with Microsoft Windows 7. The proposed model of this paper is tested on palmprint database collected by the Poly U from 1000samples for 100 different person left hand palm image (10 images for each person). Among them, eight samples are used for training and remaining two samples are used for testing. For identification, each of the palmprint images was matched with all of the other palmprint images in the database.

The performance of the proposed approach is evaluated using performance metrics i.e. FAR, FRR are shown in Table I and comparative results of Accuracy and execution time using machine learning techniques are shown in Table II.

$$FRR = \frac{\text{Number of rejected verification attempts for a qualified person}}{\text{Number of all verification attempts for a qualified person}} \tag{6}$$

$$FAR = \frac{\text{Number of successful independent fraud attempts against a person}}{\text{Number of all independent fraud attempts against a person}} \tag{7}$$

Table I. Comparative results of the FAR and FRR

P e r s o n	Support vector machine Linear		Support vector machine RBF kernel		Extreme Learning Machine Linear		Extreme Learning Machine RBF kernel	
	FAR	FRR	FAR	FRR	FAR	F R R	FAR	F R R
1	1	1.98	1.5	1.97	0.96	5 2	0.02	9 9
2	0.5	1.9	1	1.98	0.97	5 2	0.05	9 9

Table II. Comparative results of the SVM and ELM classifiers

Classifiers	Kernels	Execution Time (seconds)	Accuracy (%)
SVM	Linear	1.772	88
	Radial basis function(RBF)	1.825	98.1
ELM	Linear	0.0082	99
	Radial basis function(RBF)	0.0103	99

The comparative result shows that the predictive accuracy of Extreme Learning Machine linear is better compared to Support Vector Machine with the kernels like linear and radial basis function. The execution time taken by Extreme Learning Machine Linear is also less than the time taken by the different kernels of Support Vector Machine.

IV. Conclusion

The proposed method to detect principle lines of palm print is with consecutive filtering operations. Smoothing operation is used to remove image noise. Edge detector operation and closing operation are merged to extract the principle lines. Binarization yields the binary principle line. The lines detected with the developed scheme are used to extract textural information using Gray Level Co-occurrence Matrix and Statistical Property Features. Euclidean distance is used for matching to identify the genuine person. The result shows that the accuracy of Extreme Learning Machine linear is better compared to Support Vector Machine with the kernels like linear and radial basis function. The execution time taken by Extreme Learning Machine Linear is also less than the time taken by the different kernels of Support Vector Machine. In future, it will improve the accuracy; reduce the execution time for using other classification techniques.

REFERENCES

- [1] D. Zhang, W.-K. Kong, J. You, and M. Wong, "Online palmprint identification," *IEEE Trans. Pattern Anal. Mach. Intell.*, vol. 25, no. 9, pp. 1041–1050, 2003
- [2] A. Kong, D. Zhang, and M. Kamel, "A survey of palmprint recognition," *Pattern Recognition Letters*, vol. 42, pp. 1408–1418, 2009.
- [3] P.H. Hennings, V. Kumar, and M. Savvides, "Palmprint Classification Using Multiple Advanced Correlation Filters and Palm-Specific Segmentation," *IEEE Proceedings of the Second International Conference on Knowledge and Smart Technologies 2010 (July, 24-25, 2010) Transactions on Information Forensics and Security* vol. 2. no.3. 2007, pp. 613-622.
- [4] M. Sakdanupab and N. Covavisaruch, "An Efficient Approach for Automatic Palmprint Classification," *Proceedings of IEEE International Conference on Signal Image Technology and Internet Based Systems*, 2008, pp. 229-234.
- [5] D. S. Huang, W. Jia, and D. Zhang, "Palmprint verification based on principal lines," *Pattern Recognition*, vol. 4, pp. 1316–1328, 2008.
- [6] K.Y.E. Wong, A. Chekima, J.A. Dargham, and G. Sainarayanan, "Palmprint Identification Using Sobel Operator," *Proceedings of the 10th International Conference on Control, Automation, Robotics and Vision*, Hanoi, Vietnam, 2008, pp. 1338-1341.
- [7] L. Zhu and R. Xing, "Hierarchical Palmprint Recognition Based on Major Line Feature and Dual Tree Complex Wavelet Texture Feature," *Proceedings of the Sixth international Conference on Fuzzy Systems and Knowledge Discovery*, 2009, pp. 15-19.
- [8] Leqing Zhu, S.Z., Rui Xing, Yin Zhang. *Palmprint Recognition Based on PFI and Fuzzy Logic*, in *Fifth International Conference on Fuzzy Systems and Knowledge Discovery*, 2008. FSKD '08. . 2008.
- [9] Wei Jia, Yi-Hai Zhu, Ling-Feng Liu, De-Shuang Huang. *Fast Palmprint Retrieval Using Principal Lines*, *Proceedings of the 2009 IEEE International Conference on Systems, Man, and Cybernetics*, San Antonio, TX,

- USA - October 2009.
- [10] W. Li, L. Zhang, D. Zhang, J.Q. Yan. Principal line based ICP alignment for palmprint verification, in: Proceedings of the International Conference on Image Processing, 2009.
 - [11] Cong Li, Fu Liu and Yongzhongzhang. A Principal Palm-line Extraction Method for Palmprint Images Based on Diversity and Contrast, Third International Congress on Image and Signal Processing (CISP2010),2010.
 - [12] PatprapaTunkpian, SasipaPandu Wadeethorn, SuphakantPhimoltares. Compact Extraction of Principle Lines in Palmprint using Consecutive Filtering Operations, Proceedings of the Second International Conference on Knowledge and Smart Technologies ,July,24-25,2010.
 - [13] FengYue, WangmengZuo, David Zhang. ICP Registration Using Principal line and Orientation features for Palmprint Alignment, Proceedings of 2010 IEEE 17th International Conference on Image Processing September 26-29, 2010, Hong Kong.
 - [14] PolyU Palmprint Database, <http://www.comp.polyu.edu.hk/~biometrics>.
 - [15] A. McAndrew, Introduction to Digital Image Processing with MATLAB, CourseTechnology, Boston, Massachusetts, 2004.
 - [16] R.C. Gonzalez, R.E. Woods and S.L. Eddins. Digital Image Processing using MATLAB, Prentice-Hall, New Jersey, 2002.
 - [17] MATLAB Student Center Tutorial, available at http://www.mathworks.com/academia/student_center/tutorials/intropage.html
 - [18] ShriramD.raut,Dr.vikasT.humbe. Biometric Palmprints features Matching for person Identification ,IJ modern Education and computer science 2012,11,61-69.(<http://www.mecs-press.org/>)

Comparison of Morphological, Averaging & Median Filter

Alka Bishnoi

¹(M.Tech Ece deptt. Suraj Engg. College & Technology Mahendergarh, State-Haryana)

Abstract: Morphological & Averaging filter is proposed in this paper. A comparison between adaptive generalized morphological filter is proposed in this paper. With respect to the interference possibly encountered in image processing power system signal, detailed investigations are carried out through comparison which one is better than other. Morphological filtering are important methods to process and analyze images.

I. Introduction to Morphological Filtering

Morphological filtering theory was created by French mathematicians G.Matheron, J.Sarra and others in the early 80s. As a form of nonlinear filter, morphological filters have been widely applied in the field of digital signal processing. Based on geometric characteristics of signal, filter uses the pre-defined structuring element to match the signal and then achieves the purposes of extracting signal and suppressing noise. There are various forms of morphological filters that have evolved:

II. Morphological open – closing and close -opening filters

In order to suppress the positive and negative impulse noise in images simultaneously, P. Maragos has constructed a morphological open-closing and close-opening filters by using the structuring elements of same size and cascading opening and closing operations in different order [6]. Their definitions are:

Let $f(x)$ denote the input discrete signal and $g(x)$ denote the structuring element. The morphological open-closing (OC) and close-opening (CO) filters are defined respectively as:

$$Oc(f) = (f \circ g \bullet g)(x)$$

$$Co(f) = (f \bullet g \circ g)(x)$$

Morphological open - closing and close – opening filters have all natures of opening and closing operations. Although the morphological open – closing and close – opening filters can filter the positive and negative impulse noise in signal, the output range of open – closing filter will be small for the contractility of opening operation and the output range of close–opening filter will be large for the expansionary of closing operation. The two basic filters all have statistical bias phenomenon.

2.1 Generalized open - closing and close – opening filters

At present, the morphological filters adopted are mainly the morphological opening and closing operations and the cascade forms of them. Although these filters can suppress the positive and negative impulse noise synchronously, the statistical bias phenomenon will exist during the signal filtering process for the anti-expansion of morphological opening and the expansion of morphological closing. The bias phenomenon will go against the suppression of impulse noise and the filters cannot suppress the white noise effectively.

In order to overcome this drawback, literature [12] has constructed a sort of generalized open-closing and close-opening filters by using the structuring elements of different size and cascading opening and closing operations. Their definitions are:

Let $f(x)$ denote the input discrete signal and g_1, g_2 denote the structuring elements. It is further assumed that $g_1 \subseteq g_2$; The generalized open-closing and close-opening filters are defined respectively as:

$$GOC(f) = (f \circ g_1 \bullet g_2)(x)$$

$$GCO(f) = (f \bullet g_1 \circ g_2)(x)$$

2.2 Spatial Domain Filtering

Filtering operation that is performed directly on the pixels of the image is called spatial domain filtering. The process consists of simply moving the filter mask from point to point in an image. At each point (x,y) the response of the filter at that point is calculated using a predefined relationship.

In smoothing linear filters the output of a smoothing linear spatial filter is simply the average of the pixels contained in the neighborhood of the filter mask. These filters are sometimes called the **averaging filters** and also the low pass filters. Spatial averaging filter in which all the coefficients are equal are sometimes called a **box filter**.

Weighted average, in which pixels are multiplied by different coefficients, thus giving more importance to some pixels at the expense of others.

Order statistics filters are the nonlinear spatial filters whose response is based on the ordering the pixels contained in the image area encompassed by the filter and then replacing the value of the center pixel by the value determined by ranking result e.g. median filter.

Median filter replaces the value of pixel by the median of the gray levels in the neighborhood of that pixel. Median filters are quite popular for their effectiveness in case of impulse noise (salt or pepper noise) because of its appearance as black and white dots superimposed on an image.

Gaussian noise:-

Gaussian noise is statistical noise that has a probability density function (abbreviated pdf) of the normal distribution (also known as Gaussian distribution). In other words, the values that the noise can take on are Gaussian-distributed. It is most commonly used as additive white noise to yield additive white Gaussian noise (AWGN). White means its power spectral density is independent of the operating frequency. White is used in the sense that white light contain all the frequency components.

$BW=(0.75*BW3oc)+(0.3*BW3co);$

III. Comparison of morphological, median and averaging filter

For an image containing noise i.e. 'gaussian', the results are obtained by using morphological, median and Averaging filters. These have different quality and also, their mean errors are different. This comparison is shown in Figure 4.10.

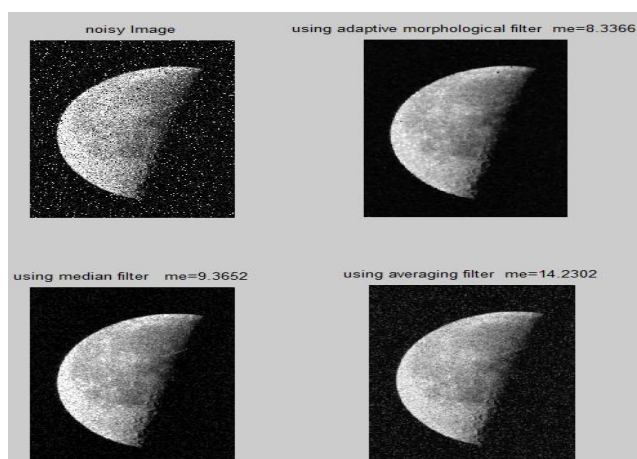


Fig 4.10 Comparison of results of morphological, median and averaging filters

IV. Conclusion

We have proposed filtering using mathematical morphology to improve the performance of detection of various noises in highly corrupted images. The proposed method is based on mathematical morphology. The morphological residue detector powerfully determinates the noises with a low percentage error. The simulation results indicate that the proposed filter performances better than median and averaging filtering techniques.

References

- [1.] 1.Rafael C. Gonzalez and Richard E. Woods "Digital Image Processing", Third Edition
- [2.] 2.WANG Jing, LIU Pan, LIU Di-chen "The design and analysis of improved adaptive generalized morphological filter(2008),(School of Electrical Engineering of Wuhan University, Wuhan 430072, China)
- [3.] 3.Rafael C. Gonzalez and Richard E. Woods "Digital Image Processing using Matlab", Third Edition
- [4.] 4.MATLAB 7.0.4 (help)
- [5.] 5.John C.Russ "The image Processing Handbook" Fifth edition
- [6.] 6.Image Processing Toolbox For Use with MATLAB User's Guide ,Version 2 ,The mathswok.inc
- [7.] 7.<http://www.mathworks.com/access/helpdesk/help/toolbox/images/index.html>.

A Case study for near net Shape – Flashless forging for full yoke (Sleeve Yoke OMNI)

Er. O. P. Dwivedi¹, Er. Dharminder singh²

¹(GM (mfg) GNA UDYOG Ltd, Bundala, M. tech (P/T) RIET/PTU, Phagwara/jalandhar ,Punjab,India)

²(Lecturer in Ramgharia polytechnic Phagwara, M. tech (P/T) PTU, jalandhar)

Abstract: Forging is a metal forming process commonly used in industry. Forging process is strongly affected by the process parameters. In a progressive press forging process, an initial block of metal (billet) is compressed between two dies halves in each stage to produce a complex part. The shape of the initial billet is crucial in achieving the desired characteristics in the final forged part. The metallurgical property as well as the geometry of the final product are strongly dependent on the shape of initial work piece as well as on the perform shapes at each of the subsequent forming stages. The major issue, which restricts imparting large deformation to the billet are the tensile stress, which later results in cracking. Bulge is also undesirable from near net shape manufacturing point of view, as it will require secondary processing like trimming. Traditionally, an experienced designer uses his or her expertise and design data handbooks for optimizing the initial billet shape. Design of the optimum preform for near net shape forging is a crucial step in the design of many forging products. In this study, the same is arrived at using profile map, which is generated using the results of FE simulations of varying geometrical and processing parameters. It is shown that preform map offers a powerful tool for near net shape forging

Keyword: finite element ,preform, press forging; profile map; near net shape

I. Introduction

1.1 In metal forming process, Net shape forging can be defined as the process of forging components to final dimensions with no post forging machining necessary. Near-net shape forged components, on the other hand, are forged as close as possible to the final dimensions of the desired part, with little machining or only grinding [1] after forging and heat treatment. Automotive industry is the main customer of near net shape forging components. Today's market is characterized by requirements for short delivery times, low costs and high quality. The supplier is confronted with smaller production and delivery batch sizes and an increasing type variation of part types. Automobile producers are more and more interested in parts which need minimal machining or are ready to assemble. Near Net shape forging parts can fulfill these requirements. The preform design used in near net shape forging processes is an important aspect for improving product quality and decreasing production cost. In the past, preform design was accomplished by empirical design, approximate analysis and trial-and-error. This task is now supported by the finite-element method and the backward tracing scheme [2]. Preform is material part that has undergone preliminary shaping but is not yet in its final form. In preform all process parameter and part geometry is defined in advance by which near net shape is easily found. through the use of simulation technique. This computer- aided simulation will reduce number of expensive die tryouts[3]

1.2 **Background:** This product is the main part in propeller shaft's universal joint as shown in PHOTO 1 . In PHOTO 1(a) the final product full yoke is presented. The product is forged in 4 multistage [4] operation steps. Each operation consists of a stroke between a male and female die. The 4 multi stage-operation method is based on the flashless die technology, developed in the press forge [4]. Flashless forging technology means that the external material during production is as less as possible. Earlier the part is manufactured by drop forging process in three stages (fullering, blocker and finisher) as shown in Fig 2 . Design is provided with minimum of 15% flash margin and 1.5mm minimum machining allowances per side which can be controlled to 3% flash and 0.5mm machining margins per side by flashless/near net shape forging concept .Fig. 2a and Fig. 2b shows the old hammer dies and produced forging part.



Photo 1 1, Photo 1 2
Fig 1a Prop. Shaft Omni
Photo (1) Prop. Shaft Omni



Photo (1a) Final forged part

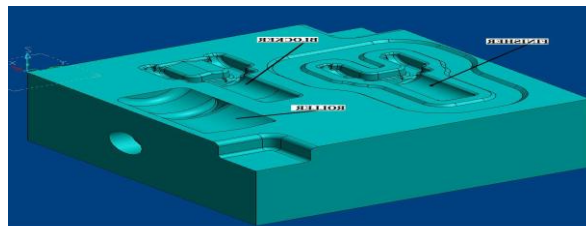


Fig (2a) Old Drop forging die design



Fig (2b) Drop forged part

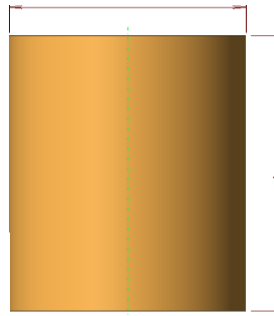


Fig (3a) STAGE -1 (Blank)

Figures showing the Drop forging process stages

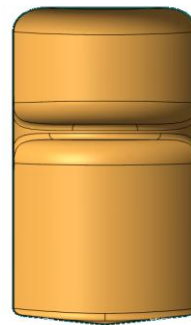
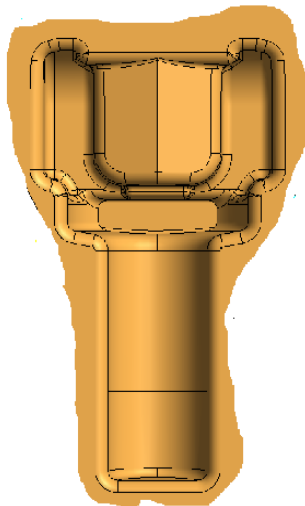


Fig (3b) STAGE -2 (Fullering)

Fig. (3c) STAGE -3 (Blocker)



Fig. (3d) STAGE -4 (Finished)

Comparison Table 1

Parameters	Drop Hammer	FE Model
Material	C-45	C-45
Blank weight (kg)	1.450	0.993
Blank size (mm)	Φ50 X 84	Φ 48X70
Temperatu(°c)	1250	950
Max Load (N)	2000	340
Allowances	15%	3%

1.3 Design Research

1.3.1 Design Research – 1

To achieve near net shape / flash less forging, the design was changed to vertical forging where the contact area between the top punch, bottom die and the work piece was minimized so that minimum flash could be achieved [5]. To achieve this Preform Design it was conceptualized that the stem portion will be in one cavity only and there would be no contact of the other half of the die. The other half which would be in contact and where there will be flash formation will only be in the yoke portion. So the conceptualized photo is as shown in the Fig.(4a) & (4b)

1.3.1.1 Operation 1

Gathering or upsetting is done in the top head keeping the stem diameter same which is as per the volume required for making yokes with 3% (Burning and Flash) allowance as shown in Fig (4a)



Fig (4a) STAGE -1

1.3.1.2 Operation 2

Turning the vertical piece at right angle and slight upset so that the sufficient material is achieved for yoke filling up.



Fig (4b) STAGE -2)

1.3.1.3 Operation 3

Again turning the piece to right angle and forging it to final shape.

Result: - The yoke found unfilled and huge flash formed unevenly as shown in the Fig (4c)

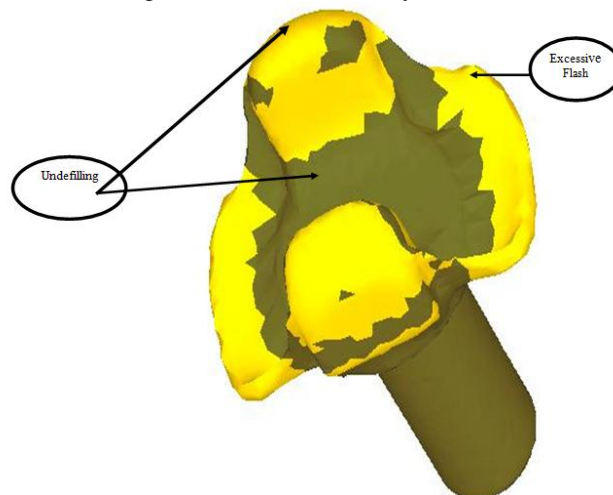


Fig. (4c) STAGE -3

1.3.2 Design Research – 2

To overcome the problem of underfilling and excess flash in design research 1, design research 2 was conceptualised as shown below from Fig (5a) to (5e)

1.3.2.1 Design and development approach



Fig (5a) Stage -0 (billet)

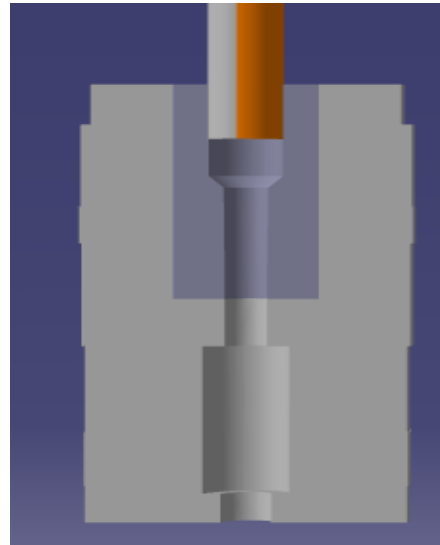


Fig (5b) Stage -1 (forward extrusion- FE model)

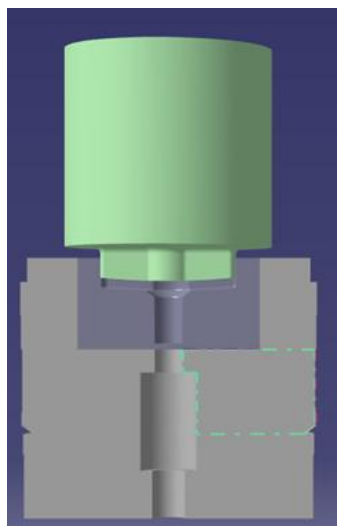


Fig (5c) stage2 T- formation (FE model)



Fig(5c) T – formed

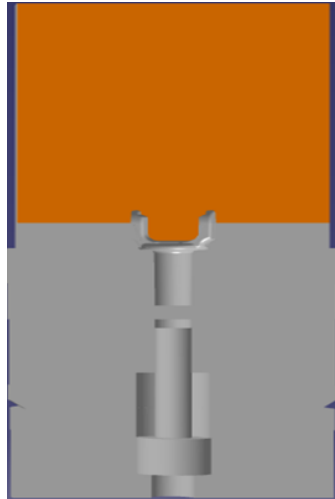


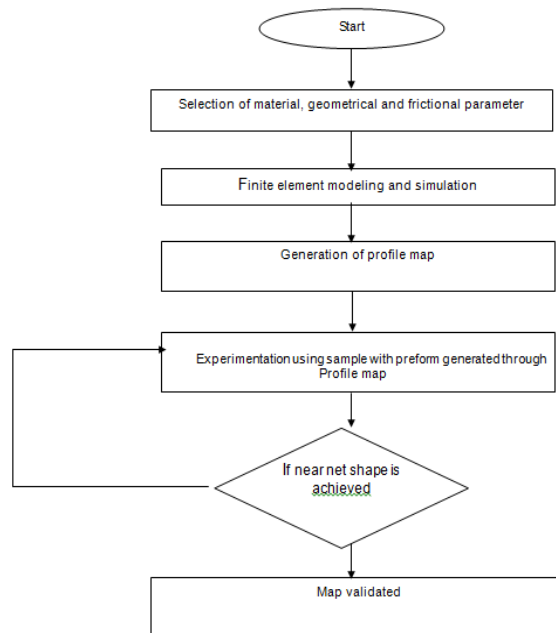
Fig (5d) Stage -3 Bending of T (FE model)



Fig (5e) Stage -4 (Finished yoke)

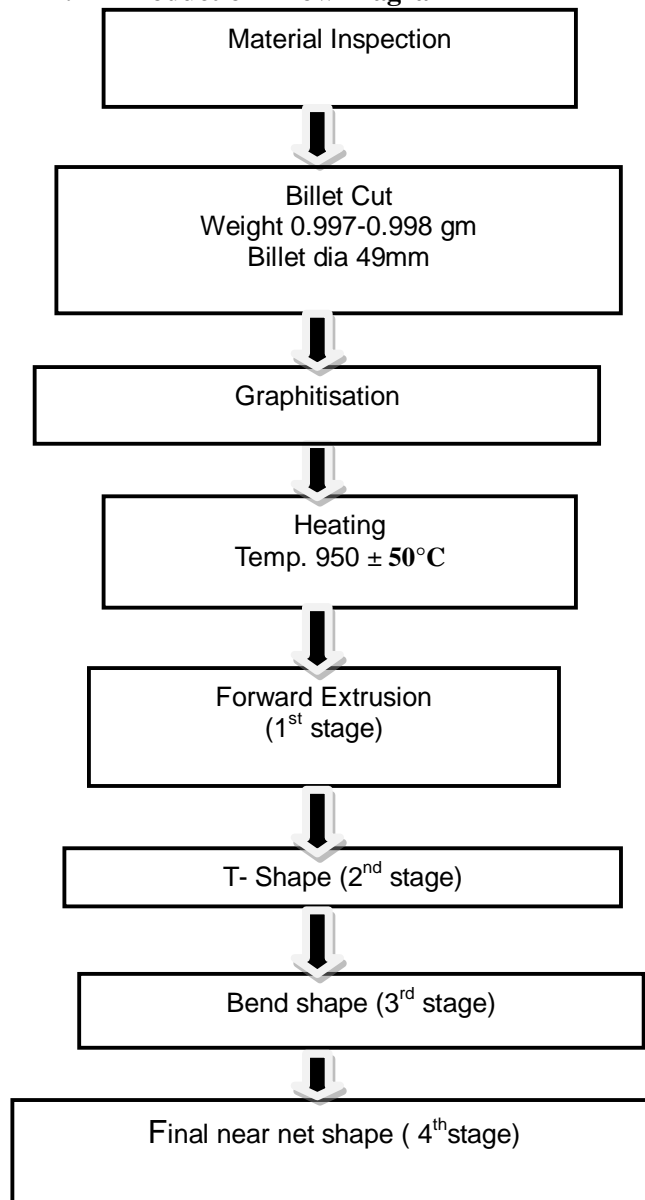
II. Methodology

Methodology followed during the tenure of this study is given in the form of flowchart as followed-



Flow chart 1

III. Production Flow Diagram



Flow Chart 2



Fig. 6 a (Near net shape Forged Part)



Fig. 6 b (FE Model)

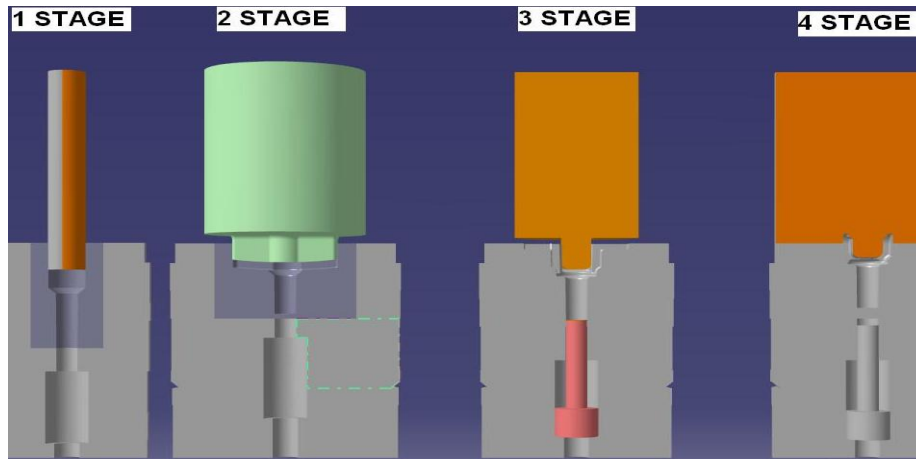


Fig 7a (Four stages die design)

IV. Deform Simulation / FE Models

The FE model for all four stages consist of three parts i.e. top, bottom and part geometry . Part geometry [6] used in each operation is the output of previous operation. The top and bottom dies are selected as rigid bodies while the part is in plastic form. Because the die blocks have to retain their shape.

In Table 2 the friction parameters [7] in all stages are presented:

Stage 1		
Contact	Friction Coefficient	Heat Transfer Coefficient
Lower die	0.3	11(N/sec/mm/C)
Upper die	0.3	11(N/sec/mm/C)
Piece	0.3	11(N/sec/mm/C)

Stage 2		
Contact	Friction Coefficient	Heat Transfer Coefficient
Lower die	0.3	11(N/sec/mm/C)
Upper die	0.3	11(N/sec/mm/C)
Piece	0.3	11(N/sec/mm/C)

Stage 3		
Contact	Friction Coefficient	Heat Transfer Coefficient
Lower die	0.3	11(N/sec/mm/C)
Upper die	0.3	11(N/sec/mm/C)
Piece	0.3	11(N/sec/mm/C)

Stage 4		
Contact	Friction Coefficient	Heat Transfer Coefficient
Lower die	0.3	11(N/sec/mm/C)
Upper die	0.3	11(N/sec/mm/C)
Piece	0.3	11(N/sec/mm/C)

Table 2

V. Production explanation

In this chapter, the complete production of product (full yoke) will be explained. All the possible problems that appear in the production will be described. Each operation is defined clearly so a good idea about the main problem of this subject can be made

5.1 Preparation: The starting product consist of a steel alloy cylinder with a diameter of 48 [mm] and a height of 70 [mm]. The cylinder will be called in the future piece. The piece is preheated in an induction furnace till it has the temperature of 950°C. This means also that the volume of the epiece changes because of the big temperature difference. With the formula the new volume can be calculated. (1) With expansion coefficient $\alpha = 0.000012 [1/K]$ and $\Delta T = 950 [K]$, the diameter increases to 48.633 [mm] and the height increases to 70.924 [mm]. So these lengths have to be used in the FE model well as in first operation die, After heating the cylinder cools for 18 seconds, because in that time the cylinder is transported from the induction heater to the first operation place, After that the piece has to be placed in the center of the die of the first operation, this is very important for the good centering of the product. This takes atleast 1.5 secs. The 19.5 secs of transportation and cooling has to be simulated as well in the numerical simulation

5.2 operation1: After positioning of the piece, the first stroke takes place. This operation is the forward extrusion operation [8] and has a couple of aims. First of all it removes the scale and redistribute the material to the shape of the end product. Next to that, it also rejects the piece if the weight tolerance is exceeded. Because if the weight tolerance is exceeded, the piece will not fit in the die of the second operation. Further it ensures the exact positioning in the die of the second operation

The final distance between the upper and lower die is 24.435 [mm]. In figure7(a), the upper and lower dies of operation 1 are presented. The parameters, which can be changed for the research, are given in Fig(7a) ,Only the height can be changed, because by changing the height, also the angle shall change. This will ensure to keep the same volume between the two dies

In Fig (8a) the filling of the original geometry after operation 1 is presented. After the stroke, the upper die will go up and the piece will be transported to the lower die of operation 2. This takes 1.5 seconds and in this time, the piece will cool again.

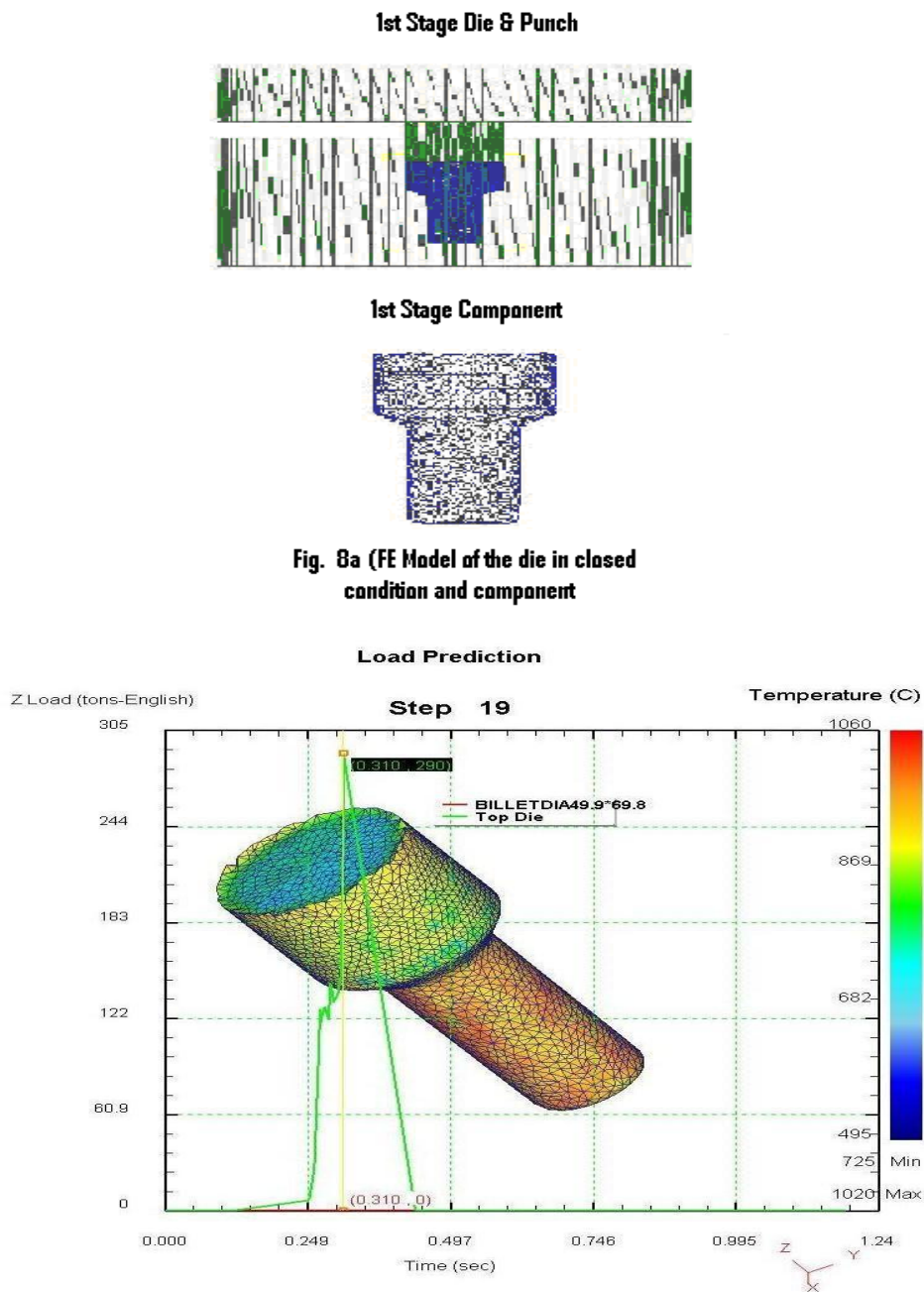


Table 3 State variable parameters for Stage 1

Stage1			
Sr. No	contents	minimum value	maximum value
1	Effective Strain (mm/mm)	0.01120	3.20000
2	Effective Stress (Mpa)	39.5	440.0
3	Effective Strain rate (mm/mm/sec)	0.06490	769.00000
4	Temperature (°C)	725	1016
5	Volume (mm ³)	135773.43	
6	Displacement (mm)	48.95130	98.30460
7	Velocity (mm/sec)	18.66	2492.72

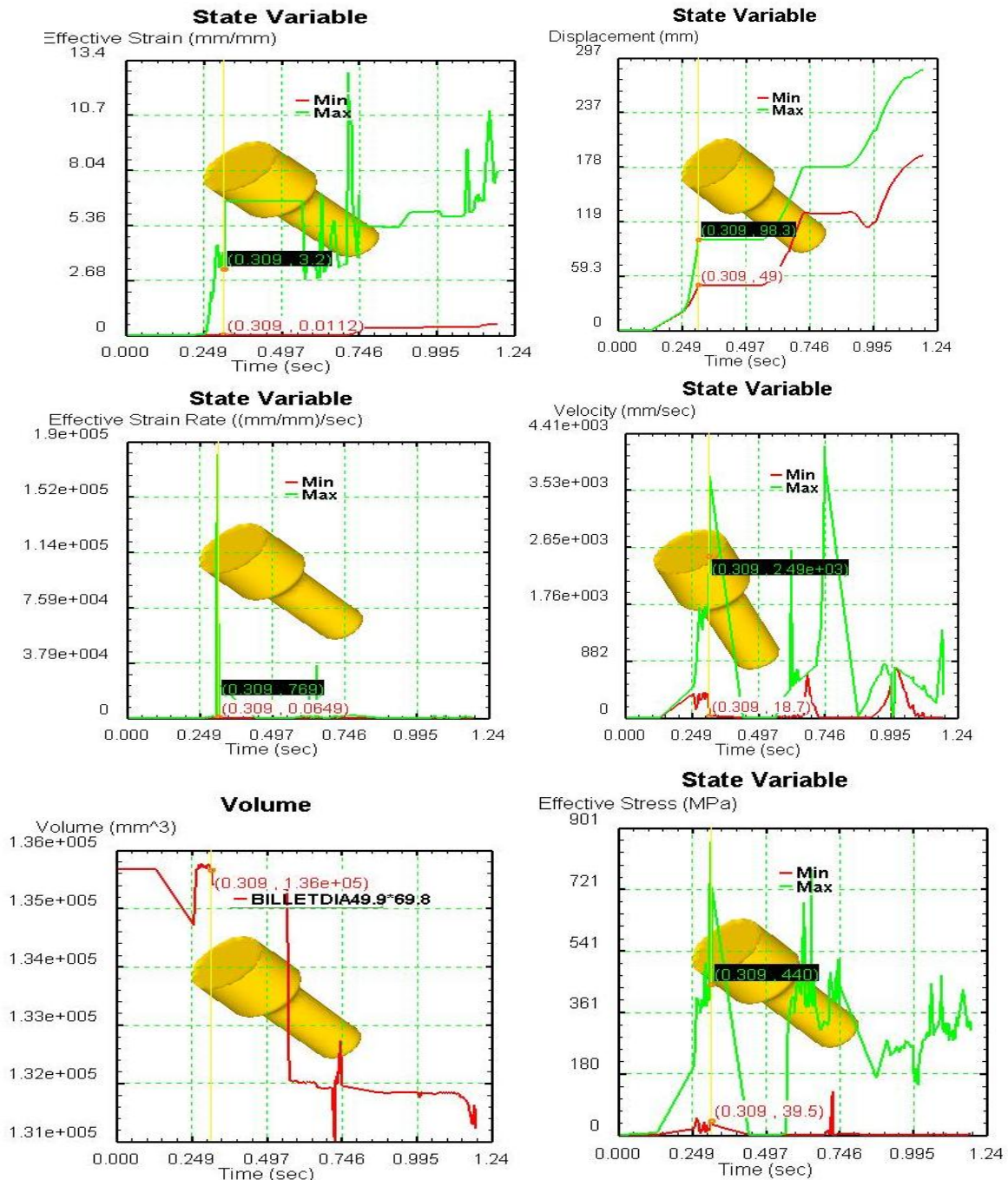


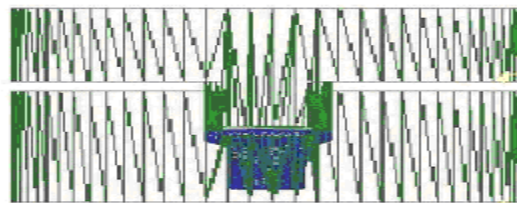
Fig. 8b State variable & graph for operation 1

5.3 operation 2: After the transportation of the operation1 , the piece will be placed in the lower die of operation 2, which also takes 1.5 seconds. The second operation is the preforming operation in T shape and has also a couple of aims. First of all it creates arms equal to calculated length of forks the side walls of the die would restrict the flow of material and control the width of forks without any flash. Thickness of forks can be adjusted by adjusting the stroke length

In Fig(9a), the upper and lower dies of operation 2 are presented. In this operation a lot of parameters can be changed. This is also the reason that the solution first has to be found in the second operation.

Now the second stroke takes place. The final distance between the upper and lower die depends on the filling of the point where the upper and lower die comes together. See the arrow at Fig (9a) The filling of the corner has to be approximately the same as the filling in Fig(5c). A shape in the corner like that, gives a good filling in the top of the die and also a good flashless filling at the end of operation 4.

2- STAGE DIE & PUNCH



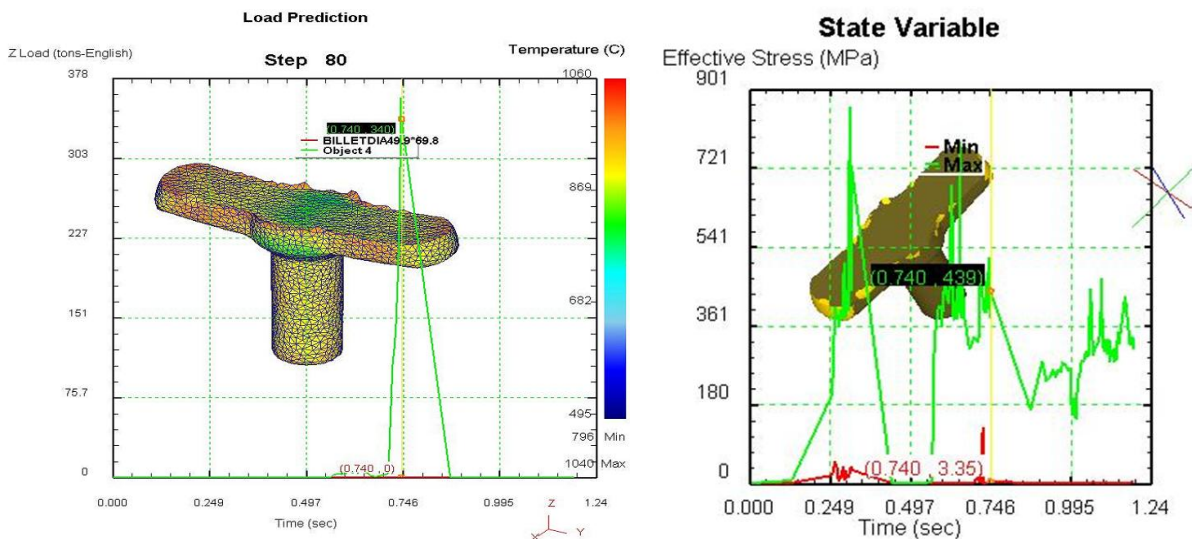
2- STAGE COMPONENT



Fig. 9a FE Model of the die in closed condition and preform in T Shape

Table 4 State Variable parameters for Stage 2

SR.NO	CONTENTS	MINIMUM VALUE	MAXIMUM VALUE
1	Effective strain(mm/mm)	0.35200	5.33000
2	Effective stress(mpa)	3.34	439.0
3	Effectivestarin rate(mm/mm/sec)	0.01570	2356.0000
4	Teperature(°c)	796.38	1042.58
5	Volume (mm³)	131827.26	
6	Displacment(mm)	127.2800	177.48000
7	Velocity(mm/sec)	0.0463	3950.0



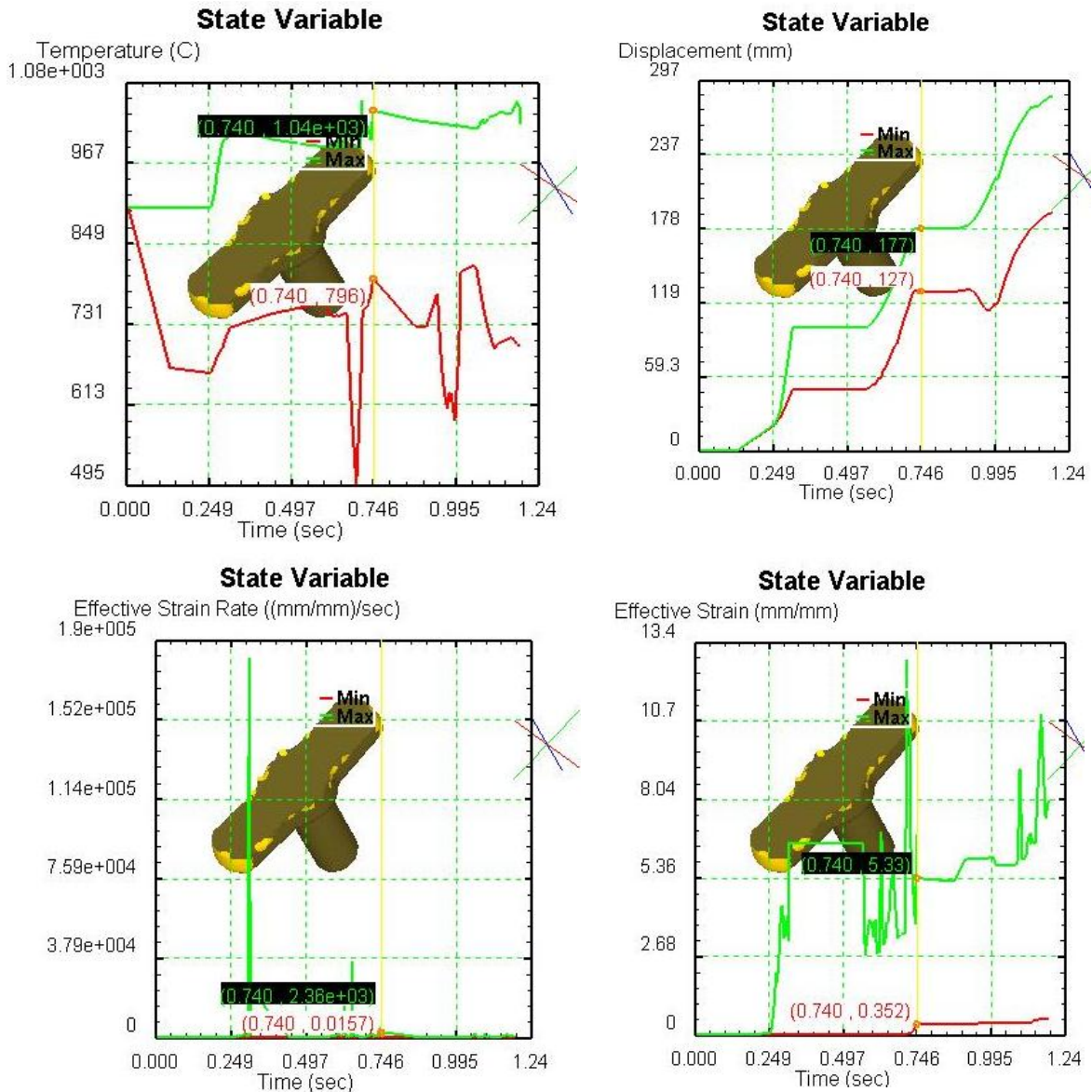


Fig. (9b) State variable graph for operation 2

5.4 Operation 3

After the operation 2, the piece will be transported in the lower die of operation 3, which also takes 1.5 seconds. In Fig (10a), the upper and lower dies of operation 3 are presented. In this operation only one parameter can be changed. This because of the fact that the shape of the end product is prescribed. Now the third stroke takes place. The final distance between the upper and lower die depends upon the proper bending of piece in the die. If the whole die is filled, it isn't necessary to press further. In DEFORM [9] this is easily seen with the graphical function of the normal pressure.

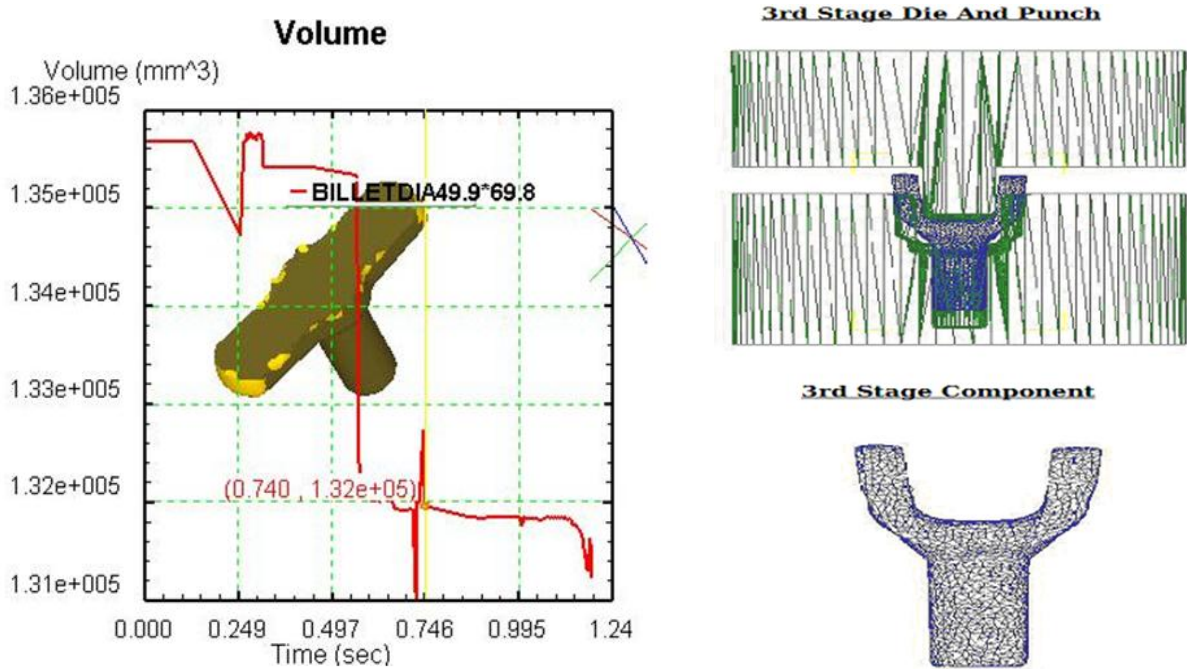
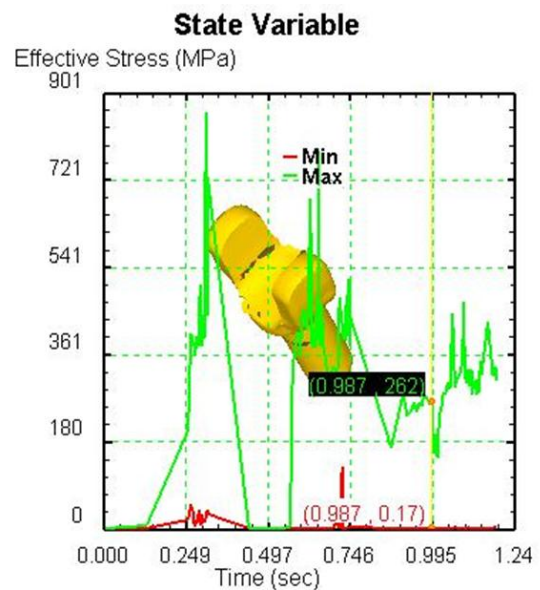
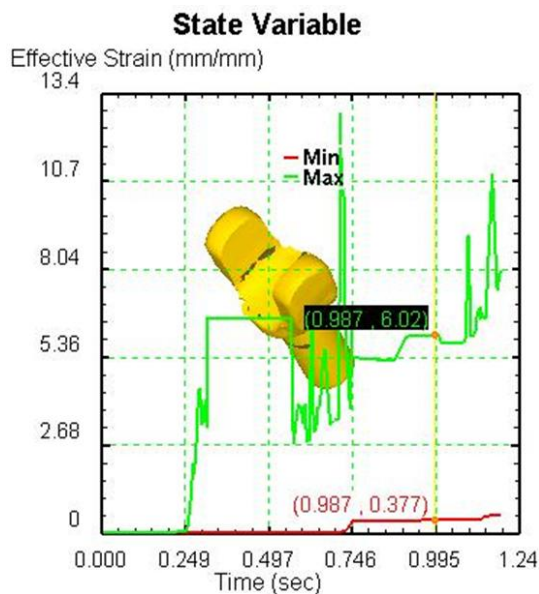


Fig 10a FE Model of die in closed condition and perform after bending of T

STAGE 3

SR.NO	CONTENTS	MINIMUM VALUE	MAXIMUM VALUE
1	Effective strain(mm/mm)	0.37700	6.0200
2	Effective stress(mpa)	0.17	282.0
3	Effectivestarin rate(mm/mm/sec)	1.87000	62.27000
4	Temeperature(°c)	589.00	1020.00
5	Volume (mm³)	131704.50	
6	Displacment(mm)	117.35000	217.58000.
7	Velocity(mm/sec)	490.1200	680.43

Table 5 : Stage Variable Parameters for Stage 3



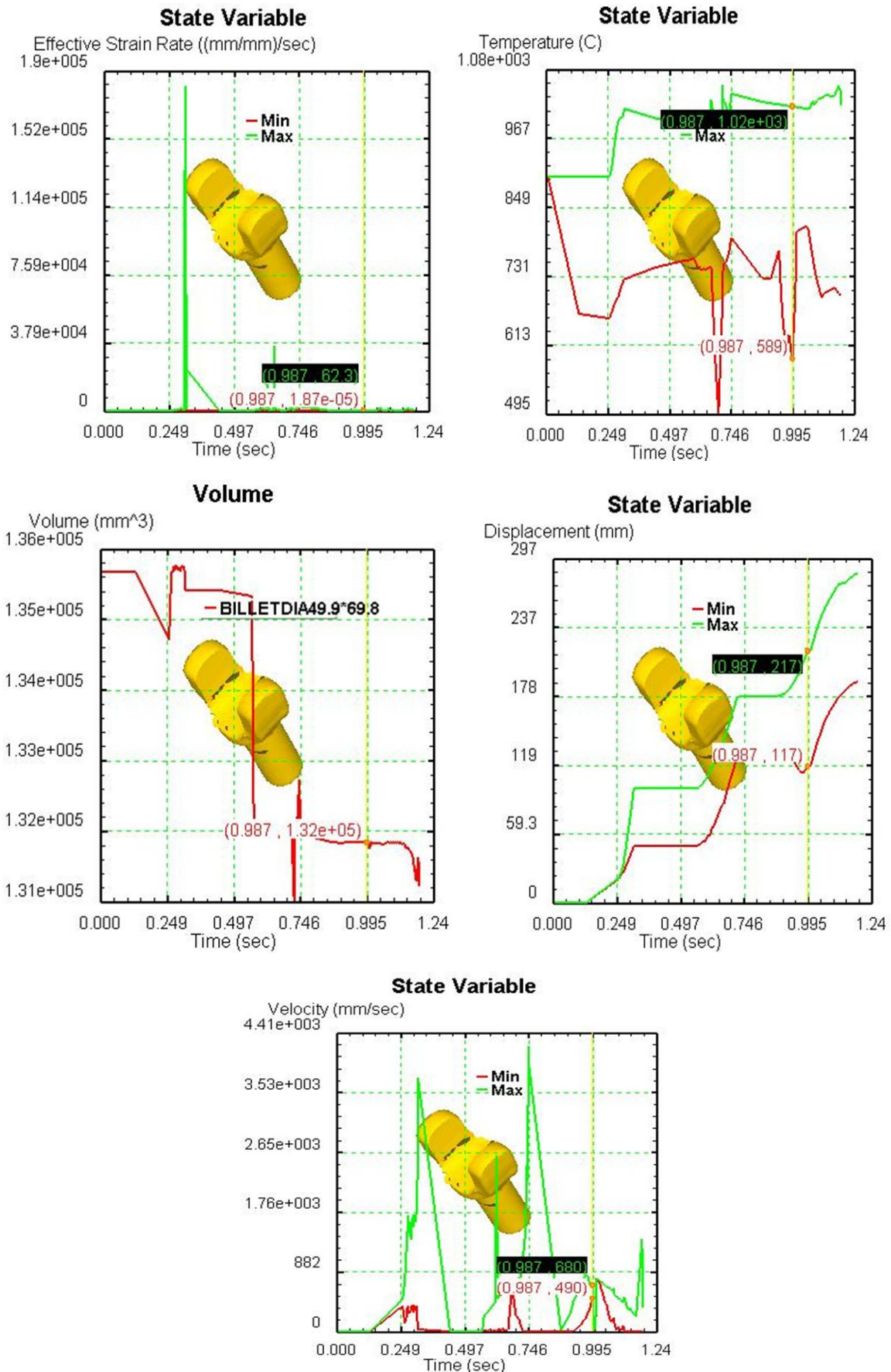


Fig. 10b State variable graph for operation 3

5.4 operations 4 After the Operation 3, the piece will be transported in the lower die of operation 4, which also takes 1.5 seconds. In figure 7, the upper and lower dies of operation 4 are presented. In this operation only one parameter can be changed. This because of the fact that the shape of the end product is prescribed.

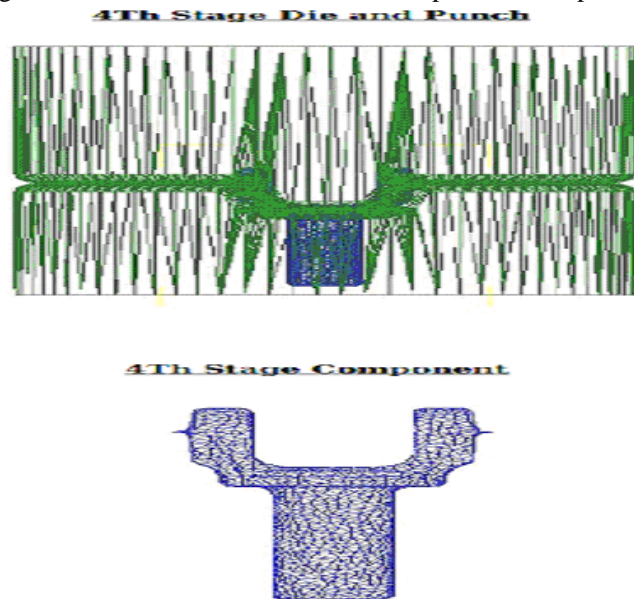


Fig. 11a FE Model of the die in closed condition and final near net shape Full Yoke

Now the fourth stroke takes place. The final distance between the upper and lower die **depends on the filling of the top of the die**. If the whole die is filled, and the total length is achieved it isn't necessary to press further. In DEFORM 3D this is easily to see with the graphical function of the normal pressure.

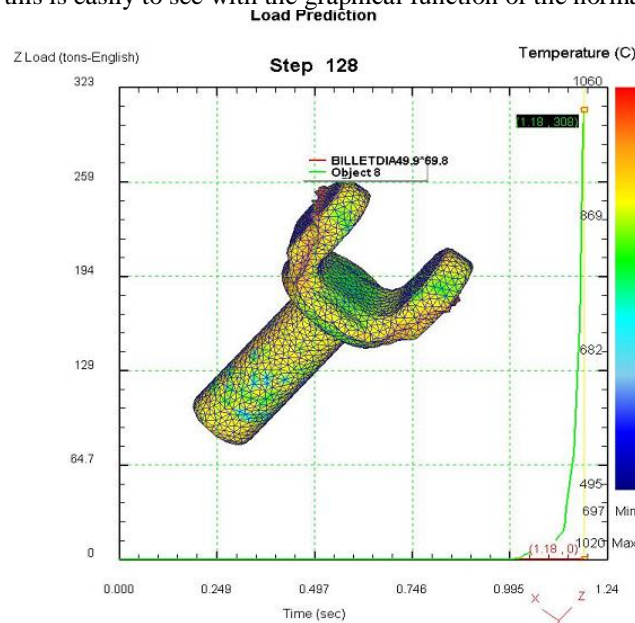
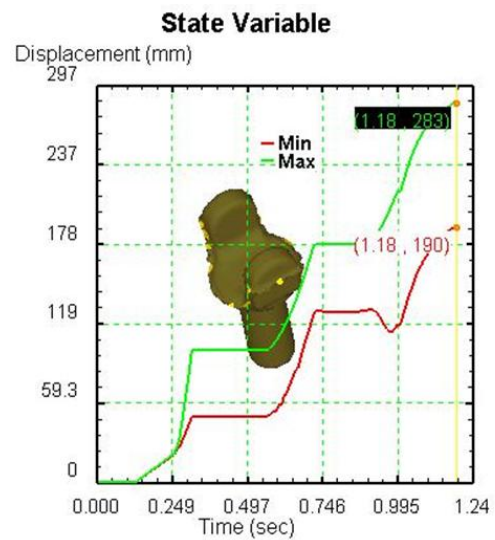
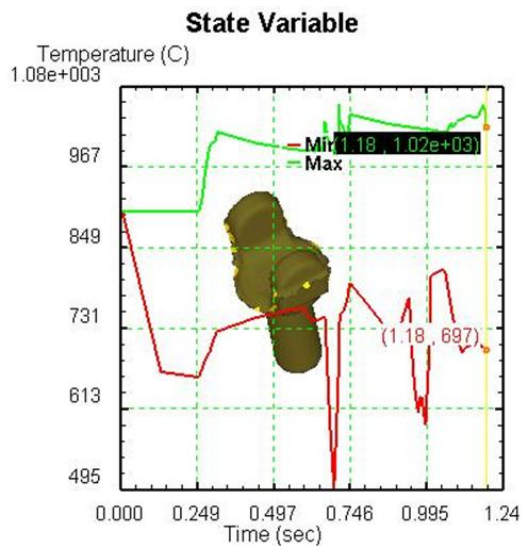
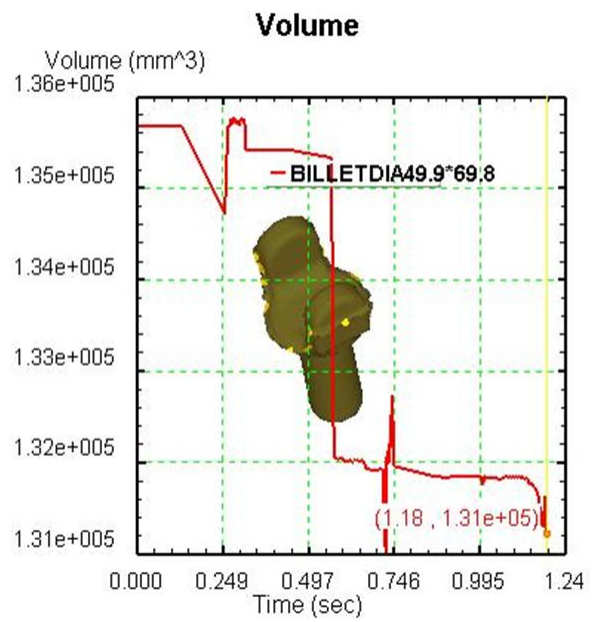
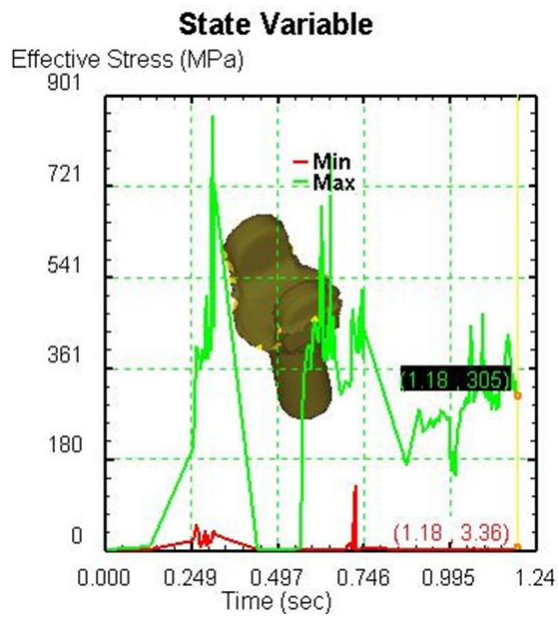
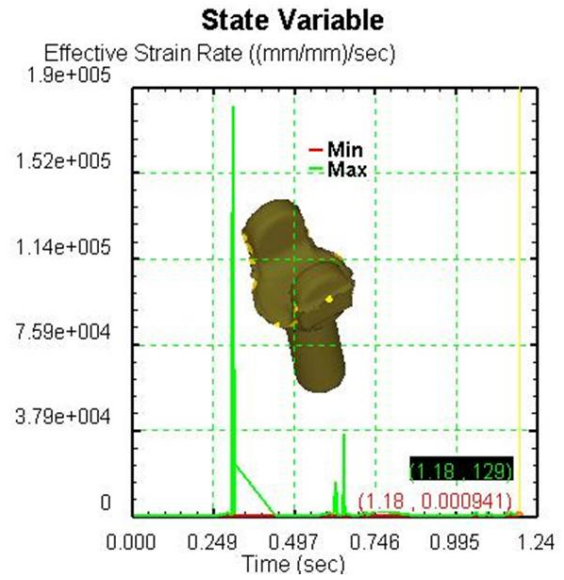
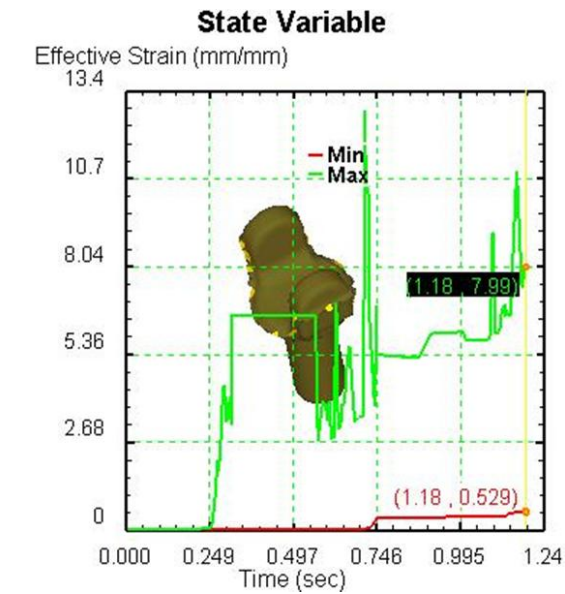


Table 6 State variable parameters for stage 4

SR.NO	CONTENTS	MINIMUM VALUE	MAXIMUM VALUE
1	Effective strain(mm/mm)	0.52800	7.99400
2	Effective stress(mpa)	3.3638	305.1160
3	Effectivestarin rate(mm/mm/sec)	0.00094	62.27000
4	Temperature(°c)	589.00	12874.00000
5	Volume (mm³)	131035.59	
6	Displacment(mm)	190.01100	282.54000.
7	Velocity(mm/sec)	0.0100	348.26



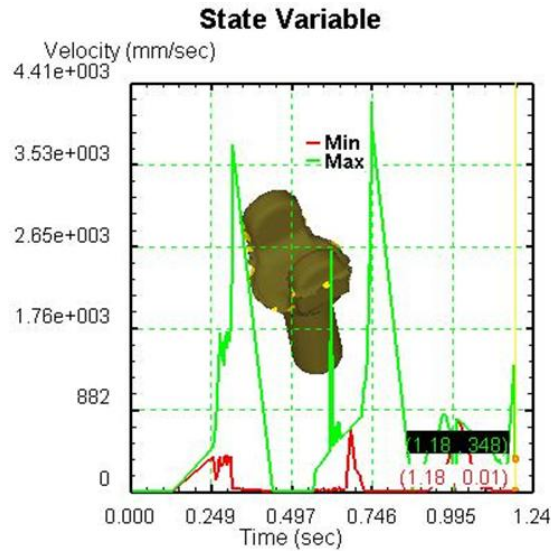
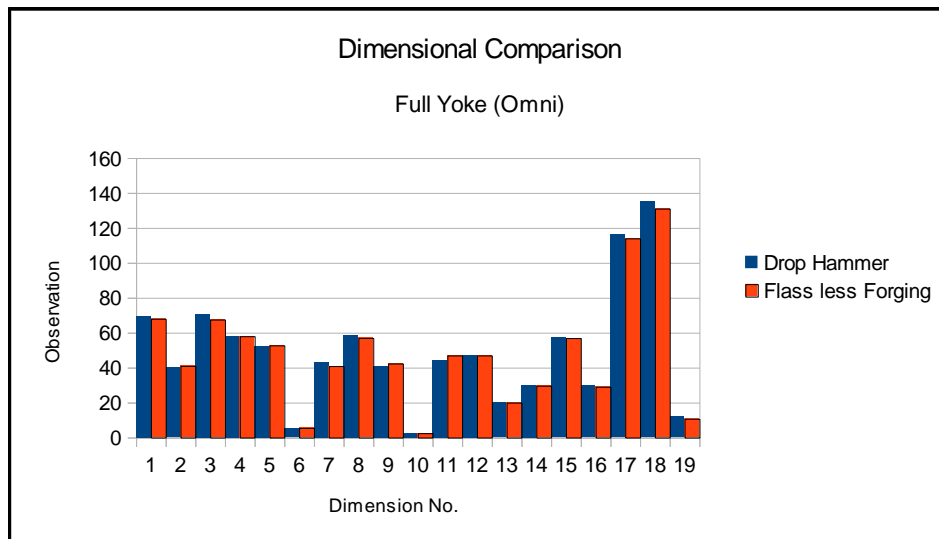


Fig. (11 b) State variable Graph for operation 4

VI. Result & Comparison

Sr No	Dimensions Obtained Through(hammer forging route) (mm)	Dimensions Obtained Throughflashless forging route (Press forging)(mm)
1	69.5	67.91
2	40.00	41.00
3	70.50	67.60
4	58.00	58.00
5	52.20	52.75
6	5.00	5.50
7	43.00	40.90
8	58.40	57.00
9	40.73	42.36
10	2.30	2.50
11	44.2	46.98
12	47.00	47.00
13	19.80	19.96
14	29.80	29.64
15	57.00	56.90
16	29.50	29.00
17	116.00	114.00
18	135.00	131.00
19	11.80	10.70

Table 7



Graph 1

6.1 Metallurgical Test Reports and Comparison

DATE	METALLURGICAL PROPERTIES	HAMMER	PRESS (1500 TON)
17/9/2012	HARDNESS	197 BHN	229 BHN
	TENSILE (DATA AS PER HARDNESS VALUE)	68 kgf/mm ²	79 kgf/mm ²
	IMPACT	22 Joule	44 Joule
	GRAIN SIZE	6-8 ASTM	5-8 ASTM
	GRAIN FLOW	OK	OK

Table 8

SLEEVE YOKE-CARRY-FORGING (HOT)

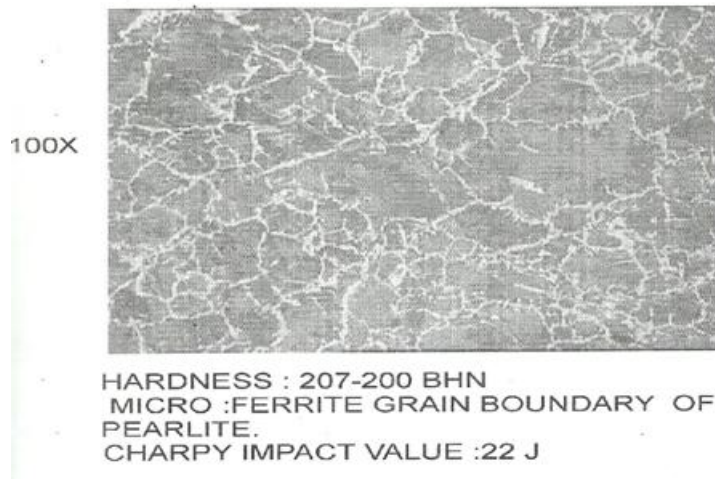


Photo 2 (Micro Structure of Hot Forging on Hammer)

SLEEVE YOKE -WORM FORGE

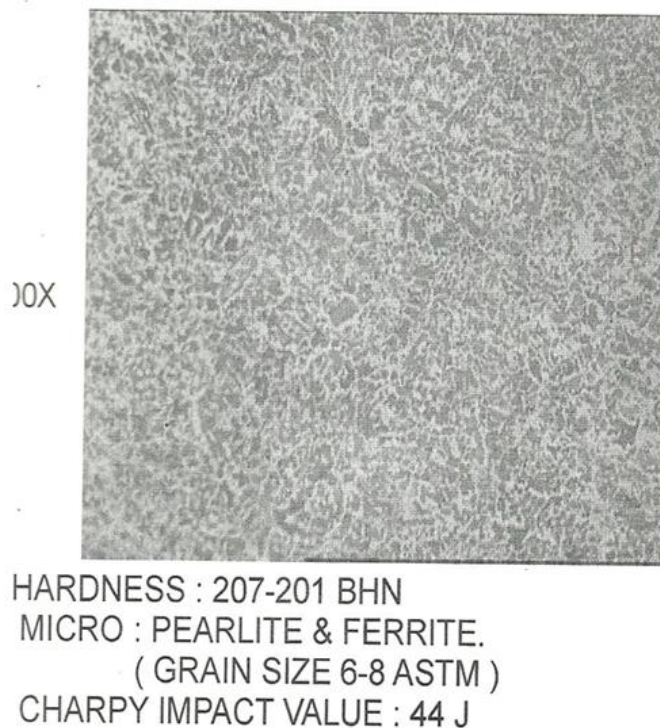


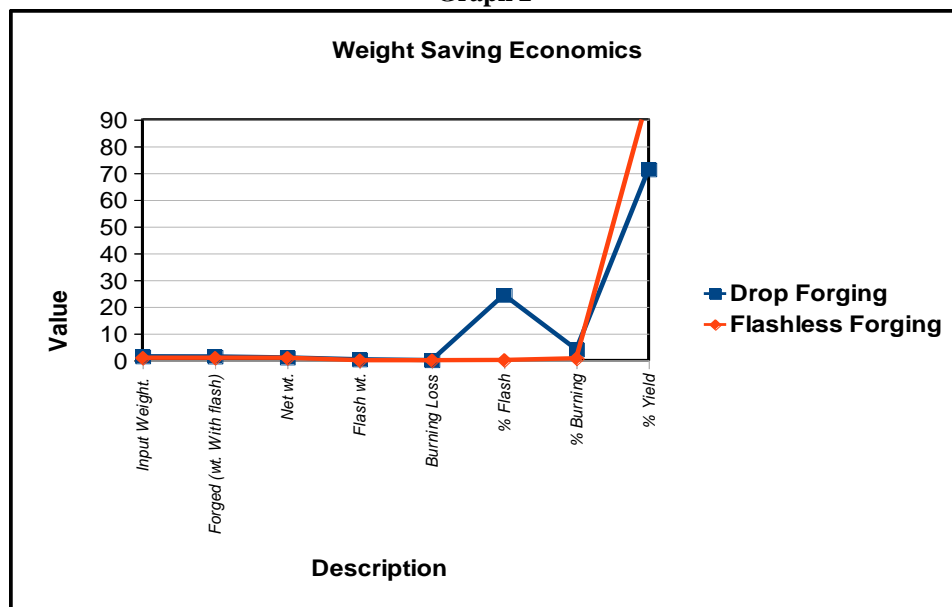
Photo 3 (Micro Structure of Near Net Shape forging on 1500MT Multi Station Press)

6.2 Weight saving Economics Reports and comparison

WEIGHT SAVING ECONOMICS					
SR.NO	Description	Drop Forging (kg)	Flashless Forging (kg)	Wt. Saving	% Saving
1	Input Weight.	1.47	0.945	0.525	35.71
2	Forged (wt. With flash)	1.41	0.938	0.472	
3	Net wt.	1.05	0.937	0.113	7.69
4	Flash wt.	0.36	0.001	0.359	
5	Buming Loss	0.06	0.007	0.053	
6	% Flash	24.49	0.11		24.38
7	% Buming	4.08	0.74		3.34
8	% Yield	71.4	99.2		27.7

Table 9

Graph 2



VII. Conclusion

The aim of this project is reached at GNA Udyog Ltd.. It will be used as a prototype for all other Yoke flashless or Near Net shape forging. In this case a study has been carried out for near net shape – flashless forging for full yoke omni, a child part to be fixed in propeller shaft of omni vehicle (a LCV) made by Maruti Suzuki Ltd (India). In this study the preform die design changes required for flashless forging of sleeve yoke through warm forging route is carried out. It has been concluded that preform design plays a very important role to achieve near net shape – flashless forging, the yield improved from 71.4 % (closed die hot forging through hammer route) to 99.2% flashless/near net shape warm forging through press forging route. Finite element analysis is carried out for different stages of preform & finisher forging for the elements – effective strain rate, effective stress, temperature, volume displacement & velocity. Such application of preforms & simulation techniques will help achieve optimum utilisation of material resulting in economical utilisation of components.

References

- [1] ohio.edu [on line], 2005, available at <http://www.ent.ohio.edu/~raub/Manufacturing/forging.htm>
- [2] Guoqun Zhao, Zhenduo Zhao, Tonghai Wang, Ramana V. Grandhi, *Journal of Materials Processing Technology*, 84, 193–201, (1998).
- [3] Altan taylan, *Metal Forming Fundamental and Application*, ASM International, 180- 181 (1983).
- [4] Bramley A.N., Mnaors D., *Materials and Design*, 21, 279-286, (2000)
- [5] Chitkara Naunit R, Young J. Kim, *International Journal of Machine Tools & Manufacture*, 41, 225-246, (2001).
- [6] Ou H, Lan J., Armstrong C.G Price M.A *Journal of Materials Processing Technology*, 151, 208-216, (2004)
- [7] Lu B., Ou H., Armstrong C.G, Rennie. A, *Materials and Design*, 30, 2490–2500, (2009).
- [8] Kondo, K “some reminiscences of the development of precision technology process “, *Advanced Technology of Plasticity*, vol 1, Proceedings of the 7th ICTP, oct 28=31, 2002 Yokhame japan
- [9] User’s manual, Deform 3D software, Version 6.1

Some New Operations on Fuzzy Soft Sets

Kumud Borgohain¹, Chittaranjan Gohain²

¹Deptt. of Mathematics, Dhemaji College, Assam, India

² Deptt. of Mathematics, Duliajan College, Assam, India

Abstract: Fuzzy soft set is one of the recent topics developed for dealing with the uncertainties present in most of our real life situations. The parameterization tool of soft set theory enhances the flexibility of its application. In this paper, we have studied membership grade, power set, α -cut set, strong fuzzy α -cut set, some standard operation fuzzy soft set, degree of subset hood and proposed some results with examples.

Keywords: Fuzzy set, Soft sets, fuzzy soft class, standard union fuzzy soft set, standard intersection fuzzy soft set

I. Introduction

In many complicated problems arising in the fields of engineering, social science, economics, environment, medical science etc. have various uncertainties. Fuzzy soft sets are very useful structures arising in many areas of mathematics and computer science. The theory soft sets was initiated by Molodtsov[4] in 1999 for modeling uncertainty present in real life. Roughly speaking a soft set is a parameterized classification of the objects of the universe. He has shown several applications of soft sets in different areas like integration, decision making etc. In 2003, Maji, Biswas and Ray [5] studied the theory of soft sets initiated by Molodtsov. They defined equality of two soft sets, subset and super set of a set, complement of a soft set, null soft set and absolute soft set with examples. Soft binary operations like AND, OR and also the operations of union, intersection were also defined. In 2005, Pie and Miao [10] and Chen et al [2] improved the work of Maji et al [5]. In 2012, Borah, Neog and Sut [9] studied the theory of soft sets initiated by Molodtsov [4] and put forwarded some more propositions regarding fuzzy soft set. In this paper, an analysis has been made to discuss about some properties related to fuzzy soft sets along with examples and proofs of certain results.

II. Preliminaries

Definition 2.1[1]

Let U be an initial universal set and E be a set of parameters. Let $P(U)$ denote the power set of U . A pair (F, A) is called a soft set over U if F is a mapping given by $F: A \rightarrow \mathcal{P}(U)$, Where $A \subseteq E$

Definition 2.2[6]

Let U be a universe and E a set of attributes. Then the pair (U, E) denotes the collection of all fuzzy soft sets on U with attributes from E and is called a fuzzy soft class.

Definition 2.3[6]

For two fuzzy soft sets (F, A) and (G, B) over a common universe U , we say that (F, A) is a fuzzy soft subset of (G, B) if

- i) $A \subseteq B$
- ii) For all $\epsilon \in A$, $F(\epsilon)$ is a sub set $G(\epsilon)$ and is written as $(F, A) \subseteq (G, B)$

Definition 2.4[6]

For two fuzzy soft sets (F, A) and (G, B) over a common universe U are said to be soft set equal if (F, A) is a soft subset of (G, B) and (G, B) is a soft subset of (F, A)

Definition 2.6[6]

Intersection of two fuzzy soft sets (F, A) and (G, B) over a common universe U is a fuzzy soft set (H, C) , Where $C = A \cap B$ and $\epsilon \in C$, $H(\epsilon) = F(\epsilon) \cap G(\epsilon)$ and is written as $(F, A) \cap (G, B) = (H, C)$

III. Main Result

Definition 3.1

let $X = \{x\}$ be a collection of objects denoted by x than a fuzzy soft set \check{A} in X is a set of ordered pairs $\check{A} = \{x, \mu_{\check{A}}(x): x \in X\}$, where $\mu_{\check{A}}(x)$ is called the membership grade of x in \check{A} .

Example 3.1

Let $X = \{p, q, r, s\}$ and $A: X \rightarrow I$ defined $A(p)=0.1, A(q)=0.2, A(r)=0.3, A(s)=0.4$. Then fuzzy soft set A can be written as $A = \{(p, 0.1), (q, 0.2), (r, 0.3), (s, 0.4)\}$

Definition 3.2

Let X be a domain. Then set of all fuzzy soft subsets of X is called the fuzzy soft power set.

Example 3.2 Let $X = \{a, b\}$ be a fuzzy soft set Then fuzzy soft power set is $\{\emptyset, [a], [b], [a, b]\}$

Definition 3.3

A fuzzy soft set a is defined on X . The α -cut set ${}^\alpha A$ is made up of members X . Whose members grade is not less than α , therefore ${}^\alpha A = \{x \in X, A(x) \geq \alpha\}$ Where $\alpha \in [0, 1]$

Example 3.3 Let $x = \{p, q, r, s\}$ and fuzzy soft set $A = \frac{0.9}{p} + \frac{1.0}{q} + \frac{0.2}{r} + \frac{0.1}{s}$ and α -cut set for

$\alpha = 0.1, 0.2, 0.9, 1.0$ then ${}^{1.0}A = \{q\}, {}^{0.9}A = [p, q], {}^{0.2}A = \{p, q, r\}, {}^{0.1}A = \{p, q, r, s\} = X$

Definition 3.4

Let A be a fuzzy soft set on X . Then strong fuzzy soft α -cut set ${}^{\alpha+}A$ is made up of member of X . whose membership grade is greater than α i. e ${}^{\alpha+}A = \{x \in X, A(x) > \alpha\}$ where $\alpha \in [0, 1]$

Example 3.4 In Example 3.3 the strong α -cut set is ${}^{1.0+}A = \{q\}, {}^{0.9+}A = \{q\}, {}^{0.2+}A = [p, q], {}^{0.1+}A = \{p, q, r\}$

Definition 3.5

The set of all levels $\alpha \in [0, 1]$ that represents distinct α -cut set of a given fuzzy soft set A is called a fuzzy soft level set of A then $\Lambda(A) = \{\alpha : A(x) = \alpha \text{ for all } x \in X\}$

Example 3.5 Let $X = \{a, b, c, d\}$ and fuzzy soft set $A = \frac{0.1}{a} + \frac{0.4}{b} + \frac{0.3}{c} + \frac{0.5}{d} + \frac{0.3}{e}$ then fuzzy soft level set of $A = \{0.1, 0.3, 0.4, 0.5\}$

Definition 3.6

The support of a fuzzy soft set A over the universal set X is the crisp set that contains all the elements that have non-zero membership grades in A and is denoted by $\text{Supp}(A)$ i.e. $\text{Supp}(A) = \{x \in X, A(x) > 0\}$

Definition 3.7

Let A be a fuzzy soft set over universal set X . then the set of all those elements of X whose membership grade is 1 called core of fuzzy soft set A and is denoted by $\text{core}(A)$ i. e $\text{core}(A) = \{x \in X, A(x) = 1\}$

Definition 3.8

Let A be a fuzzy soft set over a universal set X . Then the height of A is the largest membership grade obtained by any element in that set and is denoted by $h(A)$ i.e $h(A) = \sup_{x \in X} A(x)$

Example 3.6 If $A = \{0, 0.2, 0.8\}$ then $h(A) = 0.8$

Definition 3.9

A fuzzy soft set A of a classical set X is called fuzzy soft normal if there exists an $x \in X$ such that $A(x) = 1$

Example 3.7 If $a = \{0, 0.1, 0.2, 1.0\}$ then $A(x) = 1$

IV. Standard Operation Of Fuzzy Soft Set

Definition 4.1

Let A be a fuzzy soft subset of a nonempty set X . Then the complement of A is denoted by \bar{A} and is denoted by $\bar{A} = 1 - A(x) \forall x \in X$

Definition 4.2

Let A and B are two fuzzy soft subset over nonempty set X . Then the standard union of A and B are denoted by $(A \tilde{\cup} B)(x) = \max[A(x), B(x)] \forall x \in X$

Definition 4.3

Let A and B are two fuzzy soft subset over nonempty set X . Then the standard intersection of A and B are denoted by $(A \tilde{\cap} B)(x) = \min[A(x), B(x)] \forall x \in X$

Proposition 4.1 Let A, B be fuzzy soft sets over a universal set X then $|A| + |B| = |A \tilde{\cup} B| + |A \tilde{\cap} B|$

$$\begin{aligned}
 \text{Proof : } |A \cup B| &= \sum_{x \in X} \max[A(x), B(x)] \\
 |A \cap B| &= \sum_{x \in X} \min[A(x), B(x)] \\
 |A \cup B| + |A \cap B| &= \sum_{x \in X} \max[A(x), B(x)] + \sum_{x \in X} \min[A(x), B(x)] \\
 &= \sum_{x \in X} [A(x) + B(x)] \text{ or } \sum_{x \in X} [B(x) + A(x)] \\
 &= \sum_{x \in X} A(x) + \sum_{x \in X} B(x) \\
 &= |A| + |B|
 \end{aligned}$$

Definition4.4

Let A be a fuzzy soft subset over a finite set X then scalar cardinality is denoted by $|A| = \sum_{x \in X} A(x)$

Example4.4 If A= {0.1, 0.2, 0.3} be a fuzzy soft set then $|A| = 0.1+0.2+0.3+0.6$

Definition4.5

Let A be a fuzzy soft set over a finite set X is obtained by computing the magnitude of fuzzy soft set A with the universal set X and is denoted by $\|A\| = \frac{|A|}{|X|}$

Example4.4 If A= {0.1, 0.2, 0.8, 0.3} be a fuzzy soft set then $|A| = 0.1+0.2+0.8+0.3=1.4$

$$|x| = 4, \text{ therefore } \|A\| = \frac{|A|}{|X|} = \frac{1.4}{4} = .35$$

V. Degree Of Subset Hood

Definition5.1

The support of a fuzzy soft set A over a finite universal set X is the crisp set that contains all elements of X that have non zero membership grades in A i.e. $\text{supp}(A) = \{x \in X, A(x) > 0\}$

Definition5.2

The height of a fuzzy soft set A is the largest membership grades obtained by any element in that set and is denoted by $h(A) = \text{sup}(A)$

Definition5.3

Let A and B are two fuzzy soft sets of universal set X. Then degree of subset hood denoted by S(A,B) is defined as $S(A, B) = \frac{1}{|A|} [|A| - \sum_{x \in X} \max[0, A(x) - B(x)]]$

Proposition 5.13 Let A and B are two fuzzy soft sets of universal set X . Then degree of subset hood denoted by S(A,B) is defined as $S(A, B) = \frac{1}{|A|} [|A| - \sum_{x \in X} \max[0, A(x) - B(x)]]$ or $S(A, B) = \frac{|A \cap B|}{|A|}$

Proof: $S(A, B) = \frac{1}{|A|} [|A| - \sum_{x \in X} \max[0, A(x) - B(x)]] \dots\dots\dots(1)$

$$\begin{aligned}
 \text{We have } & [|A| - \sum_{x \in X} \max[0, A(x) - B(x)]] \\
 &= [\sum_{x \in X} A(x) - \sum_{x \in X} \max[0, A(x) - B(x)]] \\
 &= \sum_{x \in X} [A(x) - \max[0, A(x) - B(x)]] \\
 &= \sum_{x \in X} \min[A(x) - 0, A(x) - \{A(x) - B(x)\}]
 \end{aligned}$$

$$= \sum_{x \in X} \min[A(x), B(x)]$$

$$= |A \cap B| \dots \dots \dots (2)$$

From (1) and (2), we get $S(A, B) = \frac{|A \cap B|}{|A|}$

VI. Conclusion

In this paper, we have given definitions of power soft set, core of fuzzy soft set, strong fuzzy α -cut set, standard operations of fuzzy soft set and illustrate with some examples. We have introduced the concept fuzzy soft set, degree of subset hood. It is hoped that our findings will help enhancing this study on fuzzy soft sets for the researchers.

REFERENCES

- [1] Borah M.J, Neog. T.J, Sut. D.K. ‘Fuzzy Soft Matrix Theory and its Decision Making’ International Journal of Modern Engineering Research. Vol.-2 Issue.2 March-April, pp121-127,2012
- [2] Chen,D. Tsang,E.C.C, Yeung.D.S, Wang.X “The parameterization reduction of soft sets and its Applications”Vol.49, No.-5-6,pp757-763,2005
- [3] Chetia.B, Das.P.K “On Fuzzy Soft Matrix Theory” JAAM, Vol.2 pp 71-83,July-2010
- [4] Molodstov. D.A soft set theory ‘First Result’ Computers and Mathematics with Applications Vol.37, pp 19-31, 1999
- [5] Maji. P.K, Biswas.R, and Roy A.R, ‘Soft set Theory’ Computers and Mathematics with Applications. Vol.45 pp-555-562, 2003
- [6] M.I.Ali,Feng.F, LiU.X.Y,Min.W.K, Shabir.M “ On Some New operations in soft set theory” Computers and Mathematics with Applications,57,pp1547-1553,2009
- [7] Majumdar P ‘Soft Multisets’ Journal of Mathematics and Computer ScienceVol.2 pp1700-1711,2012
- [8] Majumder P. & Samanta, ‘Generalized Fuzzy soft Set’ Comput. Math. With Application Vol.59, pp 1425-1432,2010
- [9] Neoga T.J and Sut. D.K ‘ A new Approach to the theory of soft sets’ International Journal of computer Applications. Vol-32, pp1-6, 2011
- [10] Pie .P and Miao. D, “From Soft Sets to International Systems” In proceeding of the IEEE, International Conference on Granular Computing. Vol.2 pp 617-621, 2005
- [11] Ray. S.R , Saradha. M. ‘Properties of Fuzzy Soft Set’ International Journal for Basic Science and Social Science.pp112-118,2013.

Measurements Of Dielectric Constant Of Solid Material (Leather Belt) At X-Band And Proposed Wearable Antenna

Ambika Singh¹, Dr. Sudhakar Sahu²

¹ambikasingh1991@gmail.com, ²ssahufet.kiit.ac.in

(¹M.Tech, ²Associate Professor, School of Electronics Engineering, KIIT University, Bhubaneswar, India)

Abstract: This article discusses the experimental measurement technique for dielectric constant (i.e. permittivity) of leather belt at X-band. This measurement play selection of dielectric constant for antenna substrate. This leather can be used as flexible substrate of wearable microstrip antenna. This measurement system consist of solid state klystron power supply, isolator, VSWR meter, frequency meter, solid dielectric cell (XC-501). This data may be interested in flexibility wearable microstrip antenna studies and design.

Keywords: Solis dielectric cell; leather belt; Ansoft HFSS

I. INTRODUCTION

Recently, as the number of system using high frequency electromagnetic wave has increased, serious electromagnetic compatibility (EMC) problem have become apparent. This has lead to search for electromagnetic wave absorbing material useful in microwave frequencies.

The permeability and permittivity of a Leather belt plays an important role to determine reflection properties. It is very essential to determine accurately the dielectric constant of Leather material. Such type of absorbing materials have varied application such as construction of wearable microstrip antenna, improvement of antenna pattern and improvement in wearable antenna performance[13].

In this paper we determine dielectric constant of Leather and used as wearable antenna substrate. Emerging trends in monitoring people (patients, soldiers, athletes, etc.) have led to numerous recent advances in body area communication networks (BAN). Wireless sensor communication opens up tremendous potential for wireless patient monitoring. Body centric wireless networks use RF sensor nodes in close proximity to the human body. Body networks include on body, body to body and off body communication. Antenna design and analysis plays an important part in the development of sensors for BAN. Antennas for on-body communication include the inverted F antenna, wearable (fabric) antennas [9]-[12]. In this paper we discuss a low cost, nearly circularly polarized truncated patch antenna design on Zelt [8] fabric and Felt substrate for performing off body communication centered at 0.8344 GHz for Leather and 0.9029 GHz for Felt for monitoring patients after operation. This low cost antenna provides good return loss comparable to the fabric antennas.

II. MEASUREMENT USING RECTANGULAR WAVEGUIDES X- BAND

A representative study was carried on leather belt. In this work the thickness of dielectric sample of leather 2.2 cm. [1]. The accuracy of sample largely depends upon smoothness of the sample in waveguide and care which has been taken to ensure that its surface are properly squared with respect to each other.[2]. The machine sample has taken very carefully for smoothness, the size and squared surfaces.

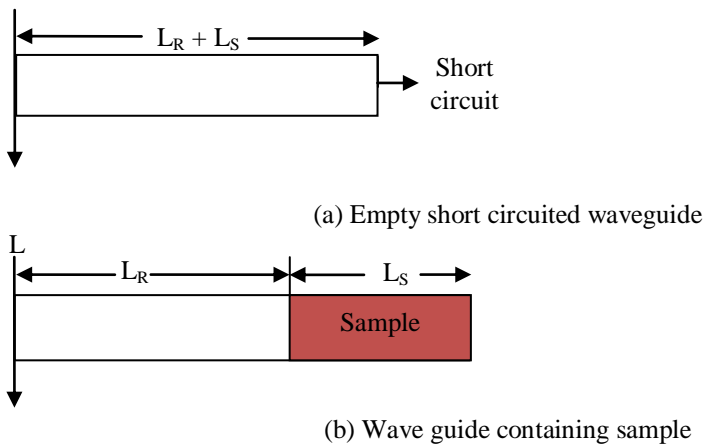
The figure 1(a) shows an empty short circuited waveguide with probe located at voltage minimum L_R Figure 1(b) the sample waveguide containing sample of length L_S with a probe located at new voltage minimum L [13].

Factor affecting Dielectric Constant of Leather

Electromagnetically a leather is, in general a three component dielectric mixture consisting of air, rawhide, bound water. Due to forces acting upon it the bound water molecule interacts with an incident electromagnetic wave in a manner dissimilar to that free water molecule, thereby exhibiting a dielectric dispersion spectrum, very different from that of free water molecule. Therefore, the dielectric constant of leather mixture is greatly influenced by a number of factors such as total water content due to humidity of environment, frequency, temperature etc.[6].

Many of the studies on dielectric properties of leather have been carried out in laboratory conditions. In general, it has been observed that dielectric constant of leather primarily related to leather moisture content [7]. Dielectric constant of water is 80, hence variation in leather moisture content makes significant in dielectric properties of leather[13].

PROCEDURE



Where

- L_R = empty cavity length
- L_S = sample (i.e. dielectric material) length

Fig1. Figure shows waveguide with dielectric and without dielectric sample

The basic arrangement of equipment were connected as shown in Fig. 2.

1. Connect the equipment as shown in Fig. 2
2. With no sample dielectric in the short circuited line, measure L_R position of the minimum in the slotted line with respect to arbitrary chosen reference plane ($L = 0$), was find out.
3. The guide wavelength (λ_g) was obtained by measuring distance between alternate in the slotted line.
4. The dielectric , i.e. the leather sample in this case was inserted in the short circuit in such a manner that it touches the end of the sample.
5. Measure D , the position of minima in the slotted with respect to the reference plane.

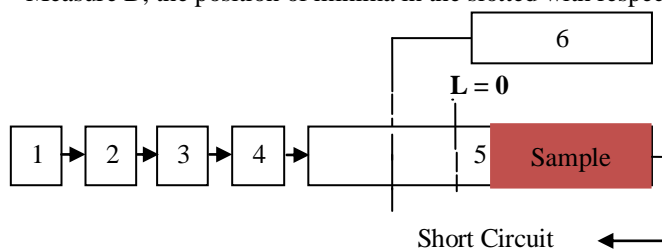


Fig. 2 Experimental Set Up for Dielectric Constant measurement

1. Microwave Source (Klystron power supply)
2. Isolator
3. Frequency meter
4. Variable attenuator
5. Wave containing sample
6. Detector

III. Waveguide inside a Dielectric

The wavelength in a dielectric medium is always smaller than free space wavelength. The wavelength in any unbounded dielectric medium λ_d is

$$\lambda_d = \frac{\lambda_0}{\sqrt{k'\mu'}}$$

Where

- k' = dielectric constant of the medium (i.e. leather belt)
- μ' = permeability of the medium
- λ_c = cut-off wavelength of the waveguide
- λ_0 = wavelength in vacuum

For most of the dielectric materials $\mu' = 1$ and therefore

$$\lambda_d = \frac{\lambda_0}{\sqrt{k'}}$$

The wavelength λ_g in the air field rectangular waveguide is given by

$$\lambda_g = \frac{\lambda_0}{\sqrt{\left[1 - \left(\frac{\lambda_0}{\lambda'_c}\right)^2\right]}}$$

Where

λ_c = cut-off wavelength of the waveguide.

If the waveguide is filled with a medium of dielectric constant k' the new wavelength λ'_g in the waveguide is given by

$$\lambda'_g = \frac{\lambda_0}{\sqrt{\left[k' - \left(\frac{\lambda_0}{\lambda'_c}\right)^2\right]}}$$

Where,

$$\lambda'_g = \frac{\lambda_g}{\sqrt{k'}}$$

$$\lambda'_c = \sqrt{k'}\lambda_c$$

after solving these equation we obtain dielectric constant of leather belt (i.e. k') of leather sample is 1.6587[13].

IV. Antenna Design and Geometry

Fig. 3 illustrates the geometry of the proposed printed antenna with rectangular radiator and a finite - size system ground plane. One of the main criteria for choosing material for fabric antenna design is the ease with which it can be incorporated. the second criteria is that the fabric material for antenna and the ground plane must have good conductivity. The third criteria is that the fabric material substrate must have constant thickness and stable permittivity. Based on the basic properties required for textile antenna, Felt and Leather were chosen for the antenna substrate, where as Zelt is used as antenna material. The material properties of the fabrics and Leather are given in Table 1.

Table 1: Properties of Zelt , Felt and Leather materials

Properties	Leather	Zelt [8]	Felt
Conductivity (S/m)		1×10^6	
Resistivity (ohm/sq)		0.01	
Loss Tangent			0.023
Permittivity	1.6587		1.38
Substrate Thickness (mm)	2.2		2.2

This is based on a simple microstrip patch design (Zelt is also used as a ground plane) and backing behind the blue Felt in Figure 3. The corners were truncated to provide circular polarization. Commercially available electromagnetic solver Ansoft HFSS was used during design . As the design criterion, we look at return loss characteristics. Truncation and feed optimization were performed for obtaining a well matched, left hand circular polarization (LHCP) truncated patch design.

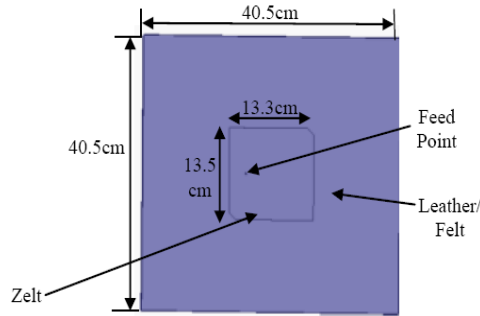


Fig3: Truncated patch antenna using Zelt fabricoc for antenna a Felt and leather substrate.

V. Simulation Result

In this section we compare simulated antenna characteristics for two different dielectric materials Felt ($h = 2.2$ mm and $\epsilon_r = 1.38$) and Leather ($h = 2.2$ mm and $\epsilon_r = 1.6587$) which is used as antenna substrate. The Simulated return loss (S_{11}) is compared in figure 4 and shows excellent agreement. The simulated antenna has return loss of about -32.7696 dB at 0.8244GHz for Leather and -38.9001dB at 0.9029 GHz for Felt substrate. The simulated antenna has a 10 dB-bandwidth of 0.0353GHz for Leather substrate and 0.0413 GHz for Felt substrate.

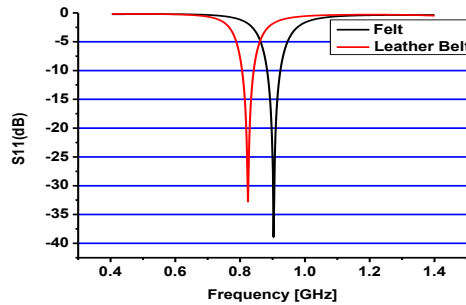
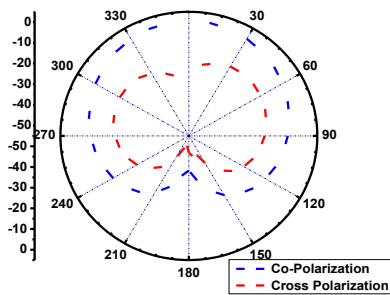


Fig 4: Simulated return loss (S_{11}) dB comparison between two material

The measured normalized co-polarized and cross polarized E-plane and H-plane radiations of the patch antenna at 0.8244GHz are shown in Fig. 5

1. For Leather Belt Gain Theta and Phi at $\Phi = 0^\circ$



2. For Leather Belt Gain Theta and Phi at $\Phi = 90^\circ$

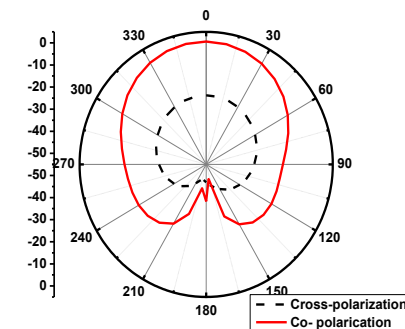


Fig. 5 Simulated E-plane (Co-pol(solid line)) and Cross pol(dotted line)) radiation pattern is at 0.8244 GHz for Leather.

IV. Conclusion

In this paper measurement of dielectric constant of leather belt determined. From the computed result it is conclude that dielectric constant depends on thickness of the sample and at lower frequency dielectric constant are high. This paper also simulates an inexpensive fabric antenna for performing communications from sensors on the human body to a near by receiver. The antenna well matched at 0.8244 GHz for leather and at 0.9029GHz for Felt substrate. It is nearly LHCP in the frequency band of nearest. The effect of antenna flexing as well as the presence of human body along with designs with improved antenna efficiency.

V. Acknowledgement

Author is thankful to Associate Prof (Dr) K.K Verma, Associate Prof (HOD) R.K Tiwari, Department of Physics & Electronics, Dr. Ram Manohar Lohia Avadh University, Faizabad, India, for his valuable support. The authors also would like to thanks Laxman Mekala, Indian Institute of Technology, Bombay ; Rajesh Pedamallu , IIT Delhi for the constructive suggestions.

REFERENCES

- [1] R. M. Redheffer "The Measurements of dielectric constants " in technique of microwave measurements, C. G. Montgomery, Ed., vol. 2. New York: Dover. 1966. pp. 591-659.
- [2] P. K. Kadaba. "Simultaneous measurement of complex permittivity and permeability in the millimeter region by a frequency domain technique " IEEE Trans. Instrum. Means., vol. IM-33, pp. 336-340,1984.
- [3] A. R Von Hippel. Dielectric Materials and its Applications. New York: Wiley, 1954, pp. 134-135, 310-332.
- [4] T. L. Blakney, "Automatic measurement of complex dielectric constant and permeability at microwave frequency " proceeding of the IEEE. No. 1, January 1974.
- [5] M. Young, The Technical Writer's Handbook. Mill Valley, CA: University Science, 1989.
- [6] M.F.T. Hallikainen, M.C. Ulb'ey, M. Dobson, Rayes EI and L.K Wu. (1985). Microwave Dielectric Behaviour of Wet soil Part-I: Empirical Model and Experimental Observations. IEEE trans. Remote Sensing, 23: 25-35.
- [7] G.C. Topp, J.L. Davis and A.P. Annan (1980). Electromagnetic determination of soil water content: measurement of coaxial transmission lines, Water resource. Res., 16: 574-585.
- [8] Zhu S., Langely R., "Dual band antenna for EBG substrates", Electronic Letters, Vol.43, No.3, Feb 2007
- [9] I Khan, P.S. Hall, A.A Serra, A.R. Guraliuc, P. Nepa, "Diversity Performance analysis for On-body Communication Channels at 2.45 GHz", IEEE Transactions on Antennas and Propagation, Vol. 57, No. 4, April 2009
- [10] Carla Hertleer, Hendrik Rogier, Luigi Vallizzi and Lieva Van Langenhove. "A Textile Antenna for Off-Body Communication Integrated Into Protective Clothing for Firefighters." IEEE Transactions and Antennas and Propagation, Vol. 57, NO. 4, April 2009: 919-925.
- [11] Amir Galehdar and David V. Thiel. "Flexible, Light-Weight Antenna at 2.4 GHz for Athlete Clothing." IEEE Antenna and Propagations, 2007: 4160-4163
- [12] Jaime G Santas, Akram Alomainy and Yang Hao. "Textile Antennas for On-Body Communications: Techniques and Properties." IEEE Antenna and Propagation, 2007: 1-4
- [13] Ambika Singh, Shashanka Sekhar Behera, Anand Maheshwari, Sudhakar Sahu, Pravanjana Behera, Dinbandhu Mandal " Characterization of dielectric constant of solid materials (Leather belt) at X- Band", American Journal of Engineering Research, e-ISSN : 2320-0847 p-ISSN : 2320-0936 , Volume-03, Issue-02, pp-84-89.



Ambika Singh received his B.Sc (Mathematics and Physics) from DAVPG College, Gorakhpur, Uttar Pradesh, India, M.Sc (Electronics) in Department of Physics and Electronics, Dr.Ram Monahar Lohia Avadh University, Faizabad, Uttar Pradesh and M.Tech Electronics (Communication Engineering) student in School of Electronics Engineering of Bhubaneswar, Kalinga Institute of Technology University, Bhubaneswar, India. His area of interest lies in the field of Wearable Microstrip Technology, Electromagnetics, RF and Microwave, Computational Electromagnetic.



International Journal of Modern Engineering Research (IJMER)

Volume : 4 Issue : 4 (Version-2)

ISSN : 2249-6645

April - 2014

Contents :

Performance Analysis of Single Phase Inverter <i>Anas Mansoor, Pratibha Tiwari</i>	01-07
Design of HDLC Controller with CRC Generation Using VHDL <i>Mahfooz Ahmad, Saifur Rahman</i>	08-12
An Enhanced Security System for Web Authentication <i>Rajnish Kumar, Akash Rana, Aditya Mukundwar</i>	13-20
Design of Coaxial Rotor Micro Air Vehicle <i>Manoj J. Watane, Dushyant B. Pawar</i>	21-25
Minimization Of Inter Symbol Interference Based Error in OFDM System Using Adaptive Decision Mechanism by SNR Estimation <i>Swati Sengar, Anil Sharma</i>	26-31
Theoretical Analysis for Energy Consumption of a Circulation-Type Superheated Steam Degreasing System Applied to Oily Metal Waste Recycling <i>Naoki Maruyama, Youhei Watanabe, Hiroaki Ito, Masafumi Hirota</i>	32-39
Material Optimization of Leaf Spring of Tractor Trolley by FEA <i>Narendra Yadav, Mr. Praveen Tandon, Mr. S.A.K. Jilani</i>	40-44
A CONTROL APPROACH FOR GRID INTERFACING INVERTER IN 3 PHASE 4 WIRE DISTRIBUTION SYSTEM WITH POWER-QUALITY IMPROVEMENT FEATURES <i>Remya A. V., Rinku Scaria</i>	45-54
MK-Prototypes: A Novel Algorithm for Clustering Mixed Type Data <i>N. Aparna, M. Kalaiarasu</i>	55-62
Two Stage Reversible Data Hiding Based On Image Interpolation and Histogram Modification <i>Nice Mathew, Dr. A. Grace Selvarani</i>	63-68

Performance Analysis of Single Phase Inverter

Anas Mansoor¹, Pratibha Tiwari²

^{1,2}(Department of Electrical & Electronics Engineering, Shepherd School of Engineering & Technology,
Sam Higginbottom Institute Of Agriculture Technology & Sciences Allahabad, India)

Abstract: In this paper performance of Single Phase Inverter is discussed. In this case IGBT & GTO switches are used with Sinusoidal Pulse Width Modulation technique. First of all two models are developed using SIMULINK toolbox of MATLAB software and SIMULATE both models. After the simulation performance of both Inverter is compared. Finally it indicates that IGBT based Inverter is more suitable.

Keywords: DC Source. GTO. IGBT. PWM. RLC Load. SIMULINK. SIMULATION.

I. Introduction

The process of conversion of a DC power into AC power at a desired output voltage and frequency is called inversion. This can be done by a fully controlled converter (using thyristors) connected to ac mains. When a thyristor based inverter supplies an ac power to an isolated load forced commutation techniques are required. This makes the inverter bulkier and costlier. Therefore thyristor based inverter are used only in high power applications. For low and medium power inverter gate controlled turn OFF device such as Power BJT, Power MOSFET, IGBT, GTO and SIT etc. are used. In addition to being fully controlled these have high switching frequencies. Therefore these devices may be very efficiently employed in inverters. Where the output voltage is to be controlled using the pulse width modulation (PWM) technique. Inverter can be broadly classified into two types based on their operation.

1. Voltage Source Inverter (VSI)
2. Current Source Inverter (CSI)

1. Voltage Source Inverter (VSI)

Type of inverter is fed by a dc source of small internal impedance. Looking from the ac side terminal voltage remains almost constant irrespective of the load current drawn. Depending on the circuit configurations VSI may be classified as half bridge and full bridge inverters. VSI may further be classified as square wave inverter and pulse width modulation inverter.

2. Insulated Gate Bipolar Transistor (IGBT)

It is used for medium power application. It is developed to remove drawbacks of power BJT and power MOSFET. It is a minority carrier device its switching speed is slightly inferior to that of a power MOSFET. It has many appealing features of both power BJT and MOSFET e.g. low conduction voltage drop ease of drive wide SOA, peak current capability, no turn off saturation time, no second breakdown and ruggedness. It has a high impedance gate (like a MOSFET), low on state voltage drop (like a BJT), and bipolar voltage blocking capability (like a thyristor/SCR).

3. Gate Turn OFF Thyristor (GTO)

It is also used for medium power application. It is a member of thyristor family. It can be turned ON by a positive gate pulse (like a SCR) and turned OFF by a high power negative gate pulse. Since no separate forced commutation circuit is required (as in case of SCR), cost size and weight of controllers reduce where as the efficiency improves. It has high efficiency and high power handling capability. But requires a large gate power source (negative) to turn it OFF $I_G = I_A/3$.

4. Pulse Width Modulation (PWM)

To achieve voltage control with in inverter and to reduce the harmonic contents in the output voltage pulse width modulation techniques are used. In PWM technique width of output pulses are modulated to achieve the voltage control. Among the large number of modulated technique simple modulation techniques are-

- a. Single Pulse Width Modulation
- b. Multiple or Uniform Pulse Width Modulation
- c. Sinusoidal Pulse Width modulation

5. Sinusoidal Pulse Width Modulation

Sinusoidal PWM pulse can be achieved by comparison of high frequency triangular signal with required frequency sinusoidal signal. In this modulation technique width of pulses varies in proportion to the magnitude of a sine wave.

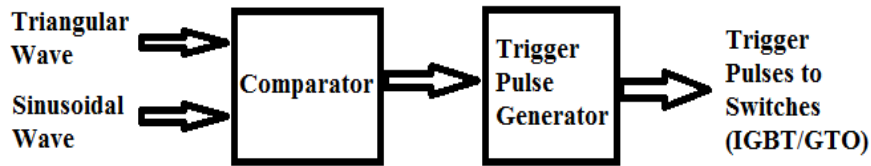


Fig. 1

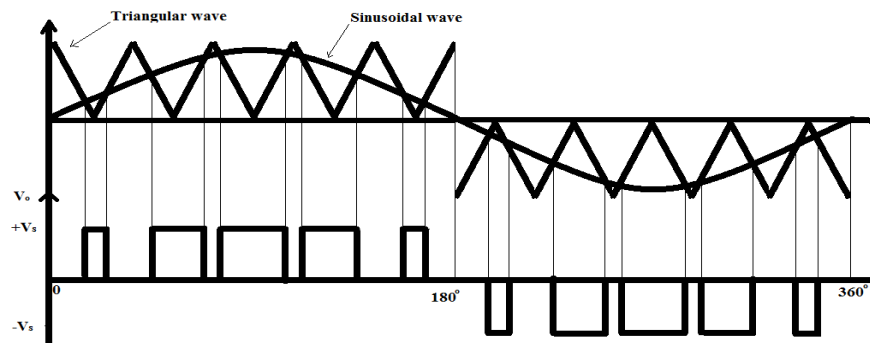


Fig. 2

6. Total Harmonic Distortion (THD)

A total harmonic distortion is a measure of closeness in a shape between the output voltage waveform and its fundamental component.

II. Simulation

In this section basic SIMULINK blocks which are used to make Inverter models are shown. And both IGBT and GTO based SIMULINK models are also shown. Load voltage and load current waveform which are obtained after SIMULATION are also given.

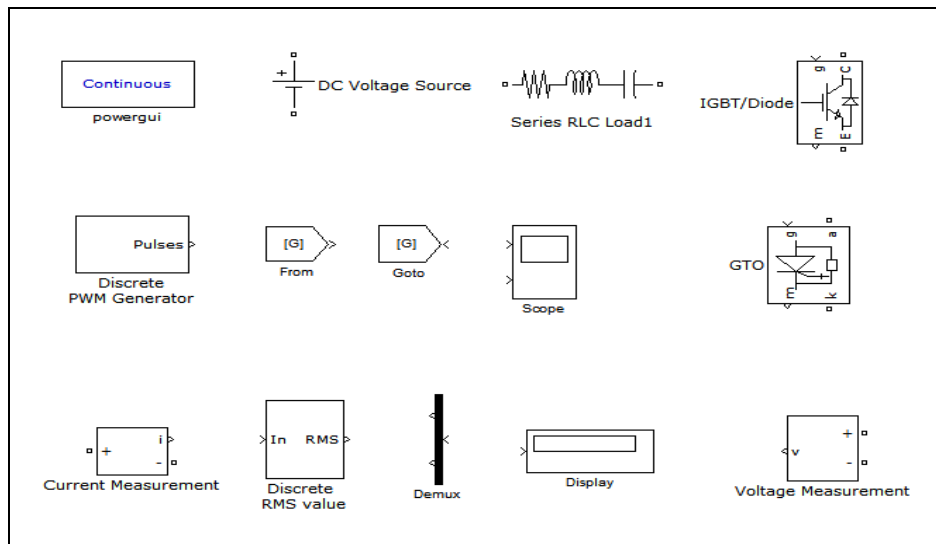


Fig. 3 Simulink Blocks

Block Name	Details
D C Voltage Source	400 Volt
Series RLC Load	Nominal Voltage V_n (Vrms) 230V, Nominal frequency f_n 50Hz, Active power (P) 1000W, Inductive Reactive Power (Q_L) 750Var, Capacitive Reactive power (Q_c) 150Var, Capacitor Initial Voltage 0V, Inductor Initial Current 0 A.
IGBT	Internal Resistance (R_{on}) 0.009 ohms, Snubber Resistance (R_s) 9000ohms, Snubber Capacitance (C_s) 10micro F
GTO	Resistance (R_{on}) 0.001ohms, Inductance (L_{on}) 0H, Forward Voltage (V_f) 1V, Current 10% fall time(T_f) 10 micro Sec., Current tail time (T_t) 20micro sec., Snubber Resistance (R_s) 120ohms, Snubber Capacitance (C_s) 10micro F, Initial Current (I_c) 0A.
Discrete PWM Generator	Carrier Frequency 1080Hz, Frequency of Output voltage 50Hz, Sample time 5 micro sec., Modulation index 0.4 to 1, Phase of output voltage(degrees) 0

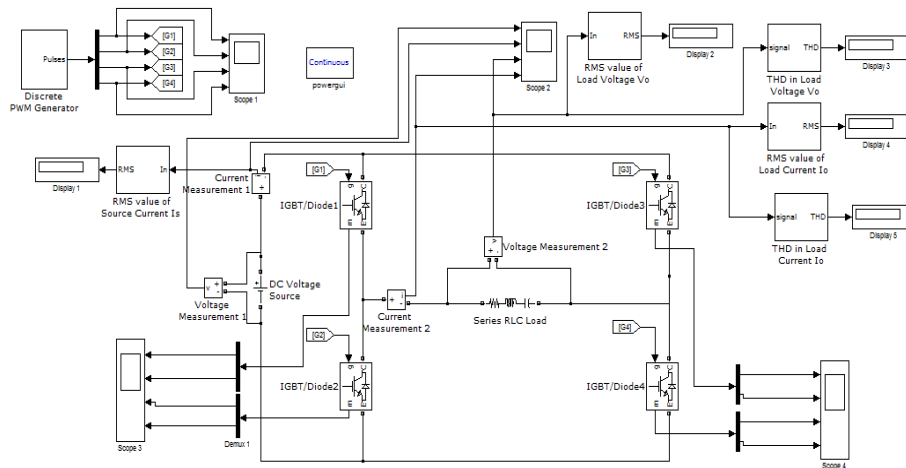


Fig. 4(A) Simulation model for IGBT based Inverter

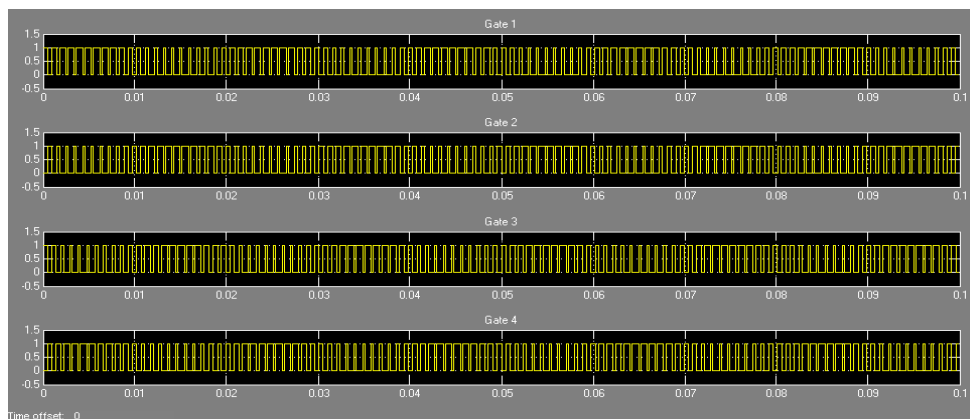


Fig. 4(B) Waveform of PWM Pulses

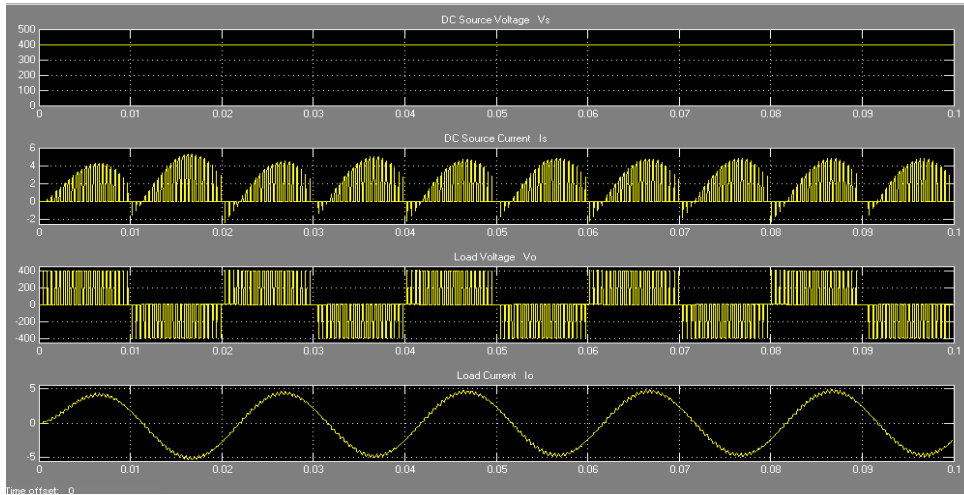


Fig. 4(C) Waveform of Source & Load

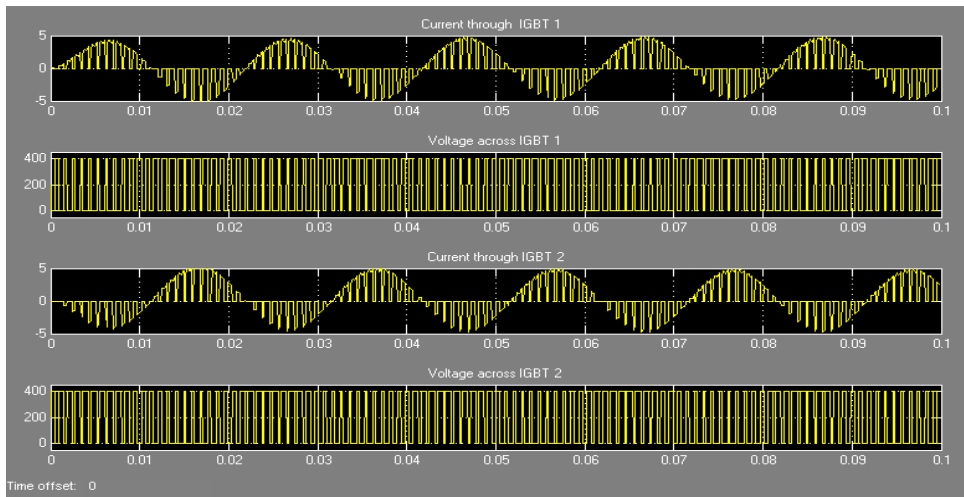


Fig. 4(D) Waveform of IGBT1 & IGBT2

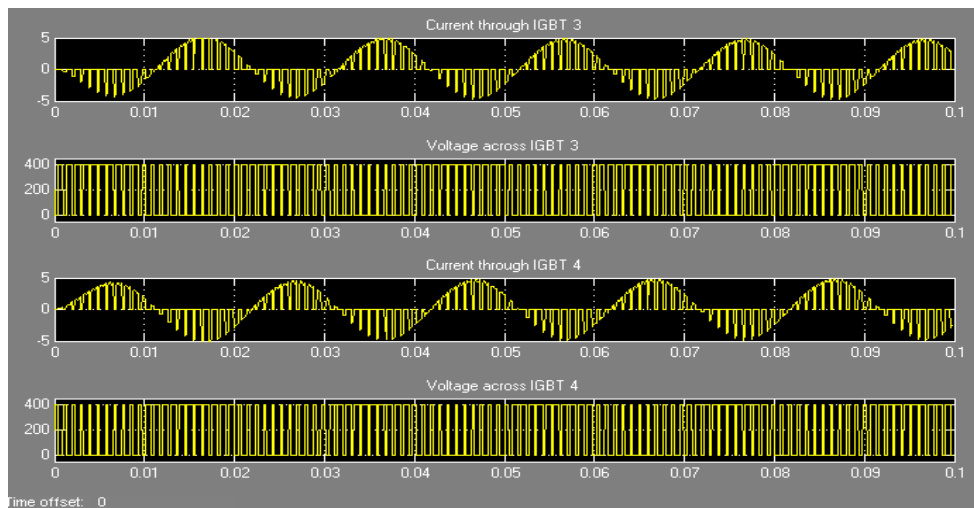


Fig. 4(E) Waveform of IGBT 3 & IGBT 4

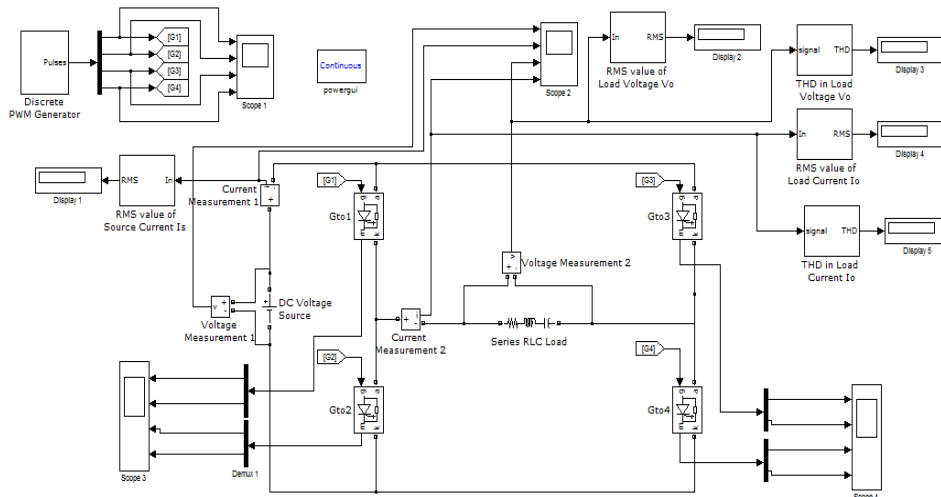


Fig. 5(A) Simulation model for GTO based Inverter

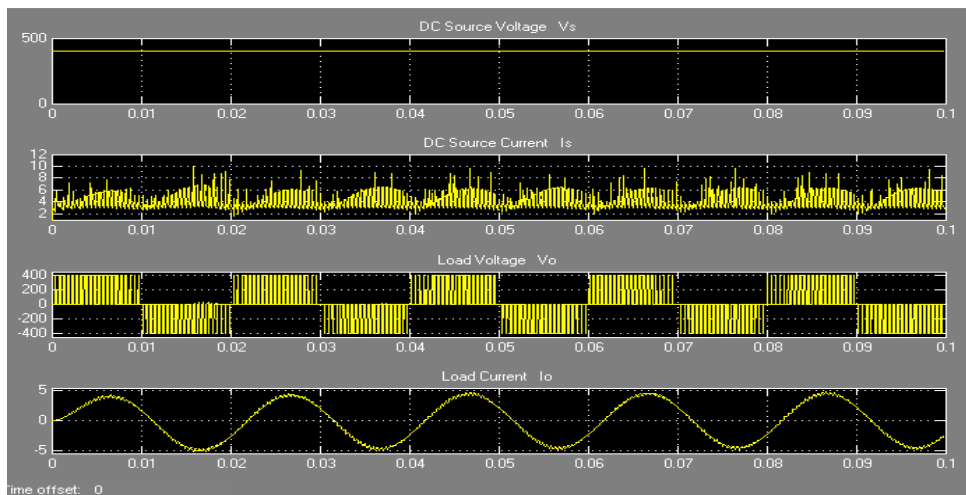


Fig. 5(B) Waveform of Source & Load

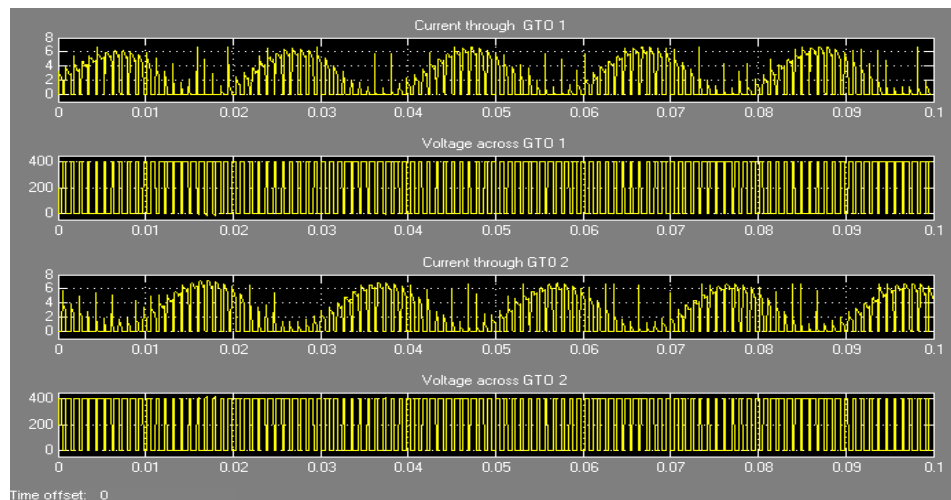


Fig. 5(C) Waveform of GTO 1 & GTO 2

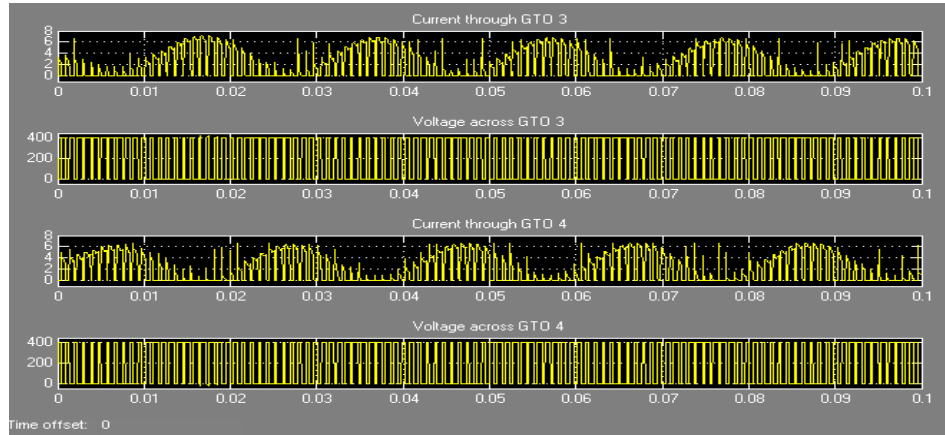


Fig. 5(D) Waveform of GTO 3 & GTO 4

III. Tables

By increasing modulation index (0.4 to 1) we find various value of load voltage and load current with the help of simulation. Here power factor in all these case becomes 0.8.

DC Source Voltage Vs Volt	Modulation Index m	Load Voltage Vo Volt	THD Vo %	Load Current Io Amp	THD Io %	Power Factor
400	0.4	203	147	2.494	4.347	0.8
	0.5	228	122.4	3.117	3.793	
	0.523	229.8	121.3	3.26	3.67	
	0.55	234.9	115.3	3.428	3.53	
	0.6	244.9	105.8	3.74	3.279	
	0.7	266.8	89.57	4.363	2.774	
	0.8	283.5	76.03	4.985	2.28	
	0.9	299.9	63.96	5.607	1.848	
1	315.5	50.15	6.235	1.511		

Table 1. for IGBT

DC Source Voltage Vs Volt	Modulation Index m	Load Voltage Vo Volt	THD Vo %	Load Current Io Amp	THD Io %	Power Factor
400	0.4	202	147	2.483	4.345	0.8
	0.5	226.9	122.3	3.102	3.792	
	0.523	228.6	121.3	3.245	3.67	
	0.55	233.8	115.4	3.41	3.533	
	0.6	243.7	106.9	3.7	3.337	
	0.7	265.8	94.2	4.244	3.136	
	0.8	282.9	83.57	4.797	2.936	
	0.9	299.8	72.58	5.386	2.783	
1	315.9	58.73	6.021	2.84		

Table 2. for GTO

IV. Conclusion

From the tables we see that value of Load voltage and Load current in case of IGBT based inverter is more as comparison to GTO based inverter and also value of Total Harmonic Distortion (both Load voltage and current) in case of IGBT based inverter is less as comparison to GTO based inverter. After these comparison we can say that IGBT is more suitable for inverter as compared to GTO. This paper will help to select proper switch for designing inverter. In future many other switch's performance may be discussed.

REFERENCES

Journal Papers:-

- [1] M.Murugesan, R.Sakthivel, E. Muthukumar and R.Sivakumar, "Sinusoidal PWM Based Modified Cascaded Multilevel Inverter" International Journal Of Computational Engineering Research (IJCER) Vol. 2 | Issue No.2 |529-539 Mar-Apr 2012
- [2] Omokere, E. S and Nwokoye, A. O. C, "Evaluating the Performance of a Single Phase PWM Inverter Using 3525A PWM IC" International Journal of Engineering Research & Technology (IJERT) Vol. 1 Issue 4, June – 2012
- [3] Pankaj H Zope, Pravin G.Bhangale, Prashant Sonare,S. R.Suralkar "Design and Implementation of carrier based Sinusoidal PWM Inverter" International Journal of Advanced Research in Electrical, Electronics and Instrumentation Engineering (IJAREEIE) Vol. 1, Issue 4, October 2012.
- [4] A. Hemant Mehar, "MATLAB Simulation Techniques in Power Electronics" IEEE Technology and Engineering Education (ITEE),VOL.7,NO.4 December, 2012
- [5] C.S.Sharma, Tali Nagwani, "Simulation and Analysis of PWM Inverter Fed Induction Motor Drive" International Journal of Science Engineering and Technology Research (IJSETR) Volume 2, Issue 2, February 2013.
- [6] Sunil Kumar Mahapatro, "MPPT Based Solar PV System for 3 Phase Grid connected IGBT Inverter System using POWER-GUI Environment" International Journal of Engineering Research & Technology (IJERT) Vol. 2 Issue 4. April-2013.
- [7] G. Pandian, S. Rama Reddy, "Simulation and Implementation of PWM Inverter Fed Induction Motor Drive" International Journal of Innovative Research in Science Engineering and Technology Vol.2,Issue 11, November 2013.

Books:

- [8] M.S.Jamil Asghar, Power Electronics (Ashoke K. Ghosh:Prentice-Hall of India Private Limited, 2006).

Websites :-

- [9] Prof. Sabyasachi Sengupta and et.all, "NPTEL Power Electronics Notes" [Online]. Available: nptel.iitm.ac.in
- [10] P.J. van Duijsen; P.Bauer; B. Davat; "Simulation and Animation of Power Electronics and Drives, Requirements for Education" [Online]. Available: www.simulation-research.com



Anas Mansoor is a research scholar pursuing M.Tech in Power Electronics from Sam Higginbottom Institute Of Agriculture Technology & Sciences Allahabad, (U.P) India. He secured degree of B.Tech. in Electrical Engineering from Aligarh Muslim University, Aligarh (U.P), India in 2010.



Pratibha Tiwari presently working as Assistant Professor in Electrical & Electronics Engineering at Sam Higginbottom Institute of Agriculture Technology & Sciences, Allahabad, (U.P) India. The degree of B.Tech secured in Electrical & Electronics Engineering from United College of Engineering and Research, Allahabad in 2002 and M.Tech. in Control and Instrumentation from Moti Lal Nehru National Institute of Technology, Allahabad in 2006. Research interest includes Control and Instrumentation and Power Electronics.

Design of HDLC Controller with CRC Generation Using VHDL

Mahfooz Ahmad¹, Saifur Rahman²

^{1,2}(Department of ECE, Integral University, Lucknow, India)

Abstract: In this paper we design the High-level Data Link Control to permit synchronous, code transparent data transmission. The control information is always in the same position and specific bit patterns which used for control differ dramatically from those representing data that reduces the errors chances. The transmission rate and data stream are controlled by the network node. This eliminates additional synchronization and buffering of the data at the network interface. Some common applications include terminal-to-terminal, terminal to CPU, satellite communication, packet switching and other high-speed data links. In system, which require expensive cabling, and interconnection hardware. So this core can be used to simplify interfacing by going serially, thereby reducing interconnects hardware cost. The HDLC Controller MEGACELL is a high performance module for the bit oriented, switched, non-switched packet transmission module. It supports half duplex and full duplex communication lines, point-to-point and multipoint channels.

Keywords: HDLC Controller, VHDL, CRC, OSI Model and Bit stuffing.

I. INTRODUCTION

HDLC [High-level Data Link Control] is a group of protocols for transmitting [synchronous] data [Packets] between [Point-to-Point] nodes. In HDLC, data is organized into a frame. HDLC protocol resides with Layer 2 of the OSI model, the data link layer. It is an efficient layer2 protocol standardized by ISO for point-to-point and multipoint data links. HDLC provides minimal overhead to ensure flow control, error control, detection and recovery for serial transmission.

The HDLC frame is synchronous and therefore relies on the physical layer to provide method of clocking and synchronizing the transmission and reception of frames. The frames are separated by HDLC flag sequences that are transmitted between each frame and whenever there is no data to be transmitted. To inform the receiving station that a new packet is arriving and synchronizes the receive clock with the transmitted clock a specific bit pattern is added at the front and the back of the packet. The header of the packet contains an HDLC address and an HDLC control field. The specific bit pattern is used to affix with the packet in the case of HDLC Controller is 01111110. The length of the address field is normally 0, 8 or 16 bits in length. In many cases the address field is typically just a single byte, but an Extended Address [EA] bit may be used allowing for multi-byte addresses. A one residing in the LSB bit indicates [the end of the field] that the length of the address field will be 8 bits long. A zero in this bit location [now the first byte of a multi-byte field] indicates the continuation of the field [adding 8 additional bits].

The Control field is 8 or 16 bits and defines the frame type; Control or Data To guarantee that a flag does not appear inadvertently anywhere else in the frame, HDLC uses a process called bit stuffing. Every time the user wants to send a bit sequence having more than 5 consecutive 1s, it inserts (stuffs) one redundant 0 after the fifth 1. The trailer is found at the end of the frame, and contains a Cyclic Redundancy Check (CRC), which detects any errors that may occur during transmission. A CRC value is generated by a calculation that is performed at the source device. The destination device compares this value to its own calculation to determine whether errors occurred during transmission. First, the source device performs a predetermined set of calculations over the contents of the packet to be sent. Then, the source places the calculated value in the packet and sends the packet to the destination. The destination performs the same predetermined set of Calculations over the contents of the packet and then compares its computed value with that contained in the packet. If the values are equal, the packet is considered valid. If the values are unequal, the packet contains errors and is discarded. The receiver can be configured into transparent mode, effectively disabling the HDLC protocol functions [2]. In normal HDLC protocol made, all received frames are presented to the host on the output register. A status register is provided which can be used to monitor the status of the receiver channel, and indicates if the packet currently being received includes any errors.

II. RELATED WORK

The layered concept of networking was developed to accommodate changes in technology. Each layer of a specific network model may be responsible for a different function of the network. Each layer will pass information up and down to the next subsequent layer as data is processed. [1]

2.1 OSI 7 LAYERS REFERENCE MODEL FOR NETWORK COMMUNICATION

Open Systems Interconnection (OSI) model is a reference model developed by ISO (International Organization for Standardization) in 1984, as a conceptual framework of standards for communication in the network across different equipment and applications by different vendors. It is now considered the primary architectural model for inter-computing and internetworking communications. Most of the network communication protocols used today have a structure based on the OSI model. The OSI model defines the communications process into 7 layers, which divides the tasks involved with moving information between networked computers into seven smaller, more manageable task groups. A task or group of tasks is then assigned to each of the seven OSI layers. Each layer is reasonably self-contained so that the tasks assigned to each layer can be implemented independently. This enables the solutions offered by one layer to be updated without adversely affecting the other layers. [1]

The following list details the seven layers of the Open System Interconnection (OSI) reference model:

1. Layer 7—Application
2. Layer 6—Presentation
3. Layer 5—Session
4. Layer 4—Transport
5. Layer 3—Network
6. Layer 2—Data link
7. Layer 1—Physical

2.2 NETWORK PROTOCOL AND STANDARD

A protocol in the context of networking is essentially a system of rules which define how data is transferred from a source to a destination, at different levels of abstraction from the physical level of electrical pulses carried via cables or wireless, or fiber-optical signals, to the more abstract level of messages sent by an application such as email. In order for computers with different hardware and operating systems to be able to communicate effectively over a network or an internet, it is clearly important for there to be a uniform set of protocols and standards which the communicating systems and applications will conform to. This in turn suggests a need for organizations with commonly recognized authority that will develop, define and publish standards in different domains [3].

2.3 DATA LINK LAYER SPECIFICATIONS

The physical layer takes care of getting data on the wire and off of it again. At the data link layer, we must take this incoming stream of data from higher or lower layers and create frames from it. Handling the data requires a solid protocol that can perform better error checking and more efficient throughputs. The first to really address these needs was the Synchronous Data Link Control (SDLC) protocol from IBM. Developed for their Systems Network Architecture (SNA) systems, IBM created what is known as a bit-oriented protocol. This meant that specific bits themselves had meaning. Information wasn't formed just on the byte level. [4]

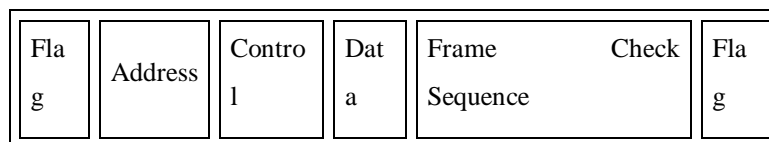


Fig. 2: SDLC Data Frame

2.4 ETHERNET SYSTEM

Ethernet was originally conceived of in the early 70s by Xerox designers. Its successful use in the Xerox Alto PC led two a consortium of three companies who wanted to be able to interlink various minicomputers. The companies were Digital Equipment Company (DEC), Intel Corporation and Xerox Corporation. Intel took on the task of providing the chips for NICs. Xerox wrote the software to operate it and DEC stepped in to make use of the technology for its minicomputers. The result was a high-speed connection that provided an alternative to IBM's networking architectures. In 1980 these companies released a

specification for Ethernet Version 1. This version was followed by a second version in 1982. These early versions comprise the standard we should refer to as "Ethernet" today. [5]

2.5 STANDARD ORGANIZATION

A wide variety of organizations contribute to internetworking standards by providing forums for discussion, turning informal discussion into formal specifications, and proliferating specifications after they are standardized. Most standards organizations create formal standards by using specific processes: organizing ideas, discussing the approach, developing draft standards, voting on all or certain aspects of the standards, and then formally releasing the completed standard to the public.

Some of the best-known standards organizations that contribute to internetworking standards include these [1]:

1. International Organization for Standardization (ISO)—ISO is an international standards organization responsible for a wide range of standards, including many that are relevant to networking. Its best-known contribution is the development of the OSI reference model and the OSI protocol suite.
2. American National Standards Institute (ANSI)—ANSI, which is also a member of
3. the ISO, is the coordinating body for voluntary standards groups within the United States. ANSI developed the Fiber Distributed Data Interface (FDDI) and other communications standards.
4. Electronic Industries Association (EIA)—EIA specifies electrical transmission standards, including those used in networking. The EIA developed the widely used EIA/TIA-232 standard (formerly known as RS-232).
5. Institute of Electrical and Electronic Engineers (IEEE)—IEEE is a professional organization that defines networking and other standards. The IEEE developed the widely used LAN standards IEEE 802.3 and IEEE 802.5.
6. International Telecommunication Union Telecommunication Standardization Sector (ITU-T)—formerly called the Committee for International Telegraph and Telephone (CCITT), ITU-T is now an international organization that develops communication standards. The ITU-T developed X.25 and other communications standards.
7. Internet Activities Board (IAB)—IAB is a group of internetwork researchers who discuss issues pertinent to the Internet and set Internet policies through decisions and task forces. The IAB designates some Request For Comments (RFC) documents as Internet standards, including Transmission Control Protocol/Internet Protocol (TCP/IP) and the Simple Network Management Protocol (SNMP).

III. METHODOLOGY

The whole design is organized as a collection of 2 sections that work together to efficiently perform the operation as shown in fig. 3. These units are:

1. Transmitter section

The Transmit Data Interface provides a byte wide interface between the transmission host and the HDLC Protocol core. Transmit data is loaded into the core on the rising edge of clk when the write strobe input asserted. The start and end bytes of a transmitted HDLC frame are indicated by asserting the appropriate signals with the same timing as the data bytes. The HDLC core will, on receipt of the first byte of a new packet, issue the appropriate flag sequence and transmit the frame data calculating the FCS. When the last byte of the frame is seen, the FCS is transmitted along the closing flag. Extra zeroes are inserted into the Bit stream to avoid transmission of the control flag sequence within the frame data. The transmit data is available on the TxD pin with appropriate setup to be sampled by clk. If TxEN is reasserted, the transmit pipeline is stalled, and the TxD pin is tristated. A transmit control register is provided which can enable or disable the channel, select transparent mode where the HDLC protocol is disabled, and specify the HDLC core action on transmit FIFO under runs. In addition, it is possible to force the transmission of the HDLC Abort sequence. This will cause the currently transmitted frame to be discarded. The transmit core can be configured to automatically restart after an abort, with the next frame, or to remain stalled until the host microprocessor cleared the abort or transmit FIFO under run condition.

2. Receiver section

Receiver accepts a bit stream on port RxD. The data is latched on the rising edge of clk under the control of the enable input RxEN. The flag detection block stream for the flag sequence in order to determine the frame boundaries. Any stuffed zeroes are detected and removed and the FCS is calculated and checked. Frame data is placed on the receiver data interface and made available to the host. In addition, flag information

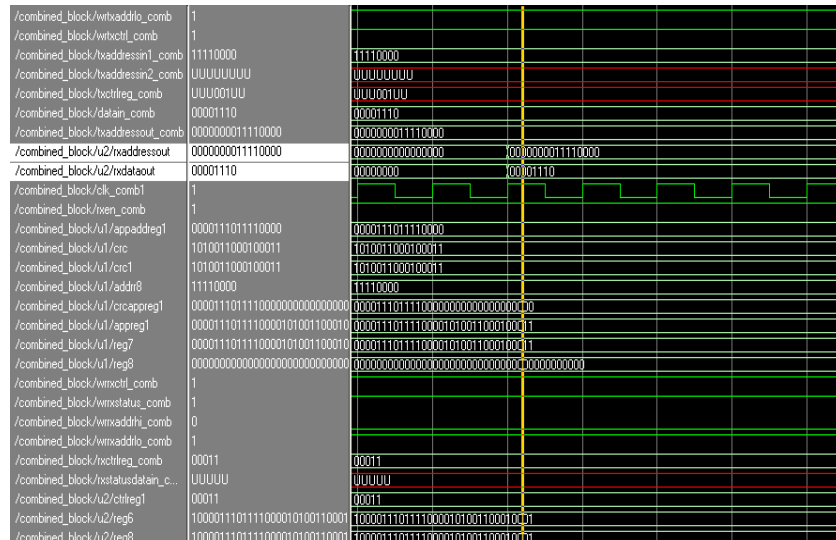


Fig. 5: Simulation result for O/P at the receiver for 16 bit address and 8 bit data

VI. CONCLUSION

Finally we conclude that HDLC Controller has been developed has the capability to operate in full duplex and half duplex mode. Controller can automatically check frame sequence generation using cyclic redundancy check i.e. CRC-16 and CRC-32 to ensure error free transmission. It is compatible with all the protocols present at the physical layer i.e.X.25 protocol and network layer i.e. Internet protocol (IP protocol). It has the capability to work in normal mode and asynchronous response mode. HDLC uses a process called bit stuffing where it stuffs a zero whenever it finds 5 consecutive 1's. VHDL model for the HDLC Controller has also been developed.

REFERENCES

- [1] Guozheng Li Nanlin Tan State Key Lab. of Rail Traffic Control & Safety, Beijing Jiaotong Univ., Beijing, China "Design and Implementation of HDLC Protocol and Manchester Encoding Based on FPGA in Train Communication Network", Information and Computing (ICIC), 2010 Third International Conference.
- [2] Arshak, K. Jafer, E. McDonagh, D. Ibalá, C.S. Univ. of Limerick, Limerick, "Modelling and simulation of wireless sensor system for health monitoring using HDL and Simulink mixed environment" Computers & Digital Techniques, IET Sept. 2007
- [3] Gheorghiu, V., S. Kameda, T. Takagi, K. Tsubouchi and F. Adachi, 2008. "Implementation of frequency domain equalizer for single carrier transmission," In Proceedings of the 4th International Conference on Wireless Communications, Networking and Mobile Computing, WiCOM '08.
- [4] Jun Wang; Wenhao Zhang; Yuxi Zhang; Wei Wu; Weiguang Chang; Sch. of Electron. & Inf. Eng., Beihang Univ. (BUAA), Beijing, China "Design and implementation of HDLC procedures based on FPGA", Anti- counterfeiting, Security, and Identification in Communication, 2009. ASID 2009. 3rd International Conference, 20-22 Aug. 2009
- [5] Meng, X. and V. Chaudary, 2009. "Boosting data throughput for sequence database similarity searches on FPGAs using an adaptive buffering scheme," Parallel Computing, 35(1): 1-11.

An Enhanced Security System for Web Authentication

Rajnish Kumar¹, Akash Rana², Aditya Mukundwar³

^{1,2,3}(Department of Computer Engineering, Sir Visvesvaraya Institute of Technology, Nashik, India)

Abstract: Web authentication has low security in these days. Today, for authentication purpose, textual passwords are commonly used; however, users do not follow their requirements. Users tend to choose meaningful words from dictionaries, which make textual passwords easy to break and vulnerable to dictionary or brute force attacks. Also, textual passwords can be identified by 3rd party software's. Many available graphical passwords have a password space that is less than or equal to the textual password space. Smart cards or tokens can be stolen. There are so many biometric authentications have been proposed; however, users tend to resist using biometrics because of their intrusiveness and the effect on their privacy. Moreover, biometrics cannot be evoked. In this paper, we present and evaluate our contribution, i.e., the OTP and 3-D password. A one-time password (OTP) is a password that is valid for only one login session or transaction. OTPs avoid a number of shortcomings that are associated with traditional (static) passwords. The most important shortcoming that is addressed by OTPs is that, in contrast to static passwords, they are not vulnerable to replay attacks. It means that a potential intruder who manages to record an OTP that was already used to log into a service or to conduct a transaction will not be able to abuse it, since it will be no longer valid. The 3-D password is a multifactor authentication scheme. To be authenticated, we present a 3-D virtual environment where the user navigates and interacts with various objects. The sequence of actions and interactions toward the objects inside the 3-D environment constructs the user's 3-D password.

Keywords: OTP, FTP, AES, 3D Virtual Environment.

I. INTRODUCTION

Due to fast technology and evaluation in internet, all type of organization such as business, educational, medical and engineering and even all are having a website. User registers on that website and create an account. They use textual passwords to login but this textual passwords can be easily hacked by many ways such as using 3rd party software's, by guessing so for authentication purpose, An OTP password should be required for only one session and this OTP password should come on User's registered Mobile Number or Email Id. This type of security system can enhance the Web Authentication.

In this paper, we present and evaluate our contribution, i.e., the OTPS and 3-D password. A proposed system combines the 3 different password authentication systems. First is Normal and old textual password system, after successfully login to textual password system, server will send Password in decrypted form through SMS to valid User. Once the user enter correct password which he had received from server user will successfully pass through OTPS (i.e. One Time Password System) phase, and user will enter to 3D authentication phase.

One-time password systems provide a mechanism for logging on to a network or service using a unique password which can only be used once, as the name suggests this prevents some forms of identity theft by making sure that a captured username/password pair cannot be used a second time. Typically the user's login name stays the same, and the one-time password changes with each login. One-time passwords are a form of so-called strong authentication, providing much better protection to on-line bank accounts, corporate networks and other systems containing sensitive data. The 3-D password is a multifactor authentication scheme. To be authenticated, we present a 3-D virtual environment where the user navigates and interacts with various objects. The sequence of actions and interactions toward the objects inside the 3-D environment constructs the user's 3-D password. The design of the 3-D virtual environment and the type of objects selected determine the 3-D password key space. The proposed system is multilevel authentication system for Web which is a combination of three authentication systems and in turn provides more powerful authentication than existing authentication system.

II. LITERATURE SURVEY

For any project, Literature Survey is considered as the backbone. Hence it is needed to be well aware of the current technology and systems in market which is similar with the system to be developed. The dramatic increase of computer usage has given rise to many security concerns. One major security concern is authentication, which is the process of validating who you are to whom you claimed to be. In general, human

authentication techniques can be classified as knowledge based (what you know), token based (what you have), and biometrics (what you are). Knowledge-based authentication can be further divided into two categories as follows: 1) recall based and 2) recognition based. Recall-based techniques require the user to repeat or reproduce a secret that the user created before. Recognition based techniques require the user to identify and recognize the secret, or part of it, that the user selected before.

Existing System

These are the following Existing System:

- 1. Textual Password System**
- 2. Token Based System**
- 3. Graphical Based Password System**
- 4. Biometric System**

1. Textual Password System

Textual passwords are commonly used. One major drawback of the textual password is its two conflicting requirements: the selection of passwords that are easy to remember and, at the same time, are hard to guess. Even though the full textual password space for eight-character passwords consisting of letters and numbers is almost $2 * 10^{14}$ possible passwords; it is easy to crack 25 percent of the passwords by using only a small subset of the full password space. Many authentication systems, particularly in banking, require not only what the user knows but also what the user possesses (token-based systems). However, many reports have shown that tokens are vulnerable to fraud, loss, or theft by using simple techniques.

2. Token Based System

A token is a physical device that an authorized user of computer services is given to ease authentication. The term may also refer to software tokens. Security tokens are used to prove one's identity electronically (as in the case of a customer trying to access their bank account). The token is used in addition to or in place of a password to prove that the customer is who they claim to be. The token acts like an electronic key to access something.

3. Graphical Based Password System

Graphical passwords can be divided into two categories as follows:

- Recognition based
- Recall based.

Various graphical password schemes have been proposed. Graphical passwords are based on the idea that users can recall and recognize pictures better than words. However, some of the graphical password schemes require a long time to be performed. Moreover, most of the graphical passwords can be easily observed or recorded while the legitimate user is performing the graphical password; thus, it is vulnerable to shoulder surfing attacks. Currently, most graphical passwords are still in their research phase and require more enhancements and usability studies to deploy them in the market.

4. Biometric System

Many biometric schemes have been proposed; fingerprints, palm prints, hand geometry, face recognition, voice recognition, iris recognition, and retina recognition are all different biometric schemes. Each biometric recognition scheme has its advantages and disadvantages based on several factors such as consistency, uniqueness, and acceptability. One of the main drawbacks of applying biometrics is its intrusiveness upon a user's personal characteristic. Moreover, retina biometric recognition schemes require the user to willingly subject their eyes to a low-intensity infrared light. In addition, most biometric systems require a special scanning device to authenticate users, which is not applicable for remote and Internet users.

Proposed System

A proposed system is a multilevel authentication system in which we combine the 3 different password authentication systems that are textual, OTPS and 3D password authentication system. Following are the proposed system:

- 1. OTPS (One Time Password System)**
- 2. 3D Password System**

1. OTPS (One Time Password System)

One-time password systems provide a mechanism for logging on to a network or service using a unique password which can only be used once, as the name suggests. There are two entities in the operation of the OTP one-time password system. The generator must produce the appropriate one-time password from the user's secret pass-phrase and from information provided in the challenge from the server. The server must send a challenge that includes the appropriate generation parameters to the generator, must verify the one-time password received, must store the last valid one-time password it received, and must store the corresponding one-time password sequence number. The server must also facilitate the changing of the user's secret pass-phrase in a secure manner.

The OTP system generator passes the user's secret pass-phrase, along with a seed received from the server as part of the challenge, through multiple iterations of a secure hash function to produce a one-time password. After each successful authentication, the number of secure hash function iterations is reduced by one. Thus, a unique sequence of passwords is generated. The server verifies the one-time password received from the generator by computing the secure hash function once and comparing the result with the previously accepted one-time password. This technique was first suggested by Leslie Lamport.

2.3D Password System

It is the user's choice to select which type of authentication techniques will be part of their 3D password. This is achieved through interacting only with the objects that acquire information that the user is comfortable in providing and ignoring the objects that request information that the user prefers not to provide. For example, if an item requests an iris scan and the user is not comfortable in providing such information, the user simply avoids interacting with that item. Moreover, giving the user the freedom of choice as to what type of authentication schemes will be part of their 3-D password and given the large number of objects and items in the environment, the number of possible 3-D passwords will increase. Thus, it becomes much more difficult for the attacker to guess the user's 3-D password.

It is easier to answer multiple-choice questions than essay questions because the correct answer may be recognized. To be authenticated in 3D password authentication stage, we present a 3-D virtual environment where the user navigates and interacts with various objects. The sequence of actions and interactions toward the objects inside the 3-D environment constructs the user's 3-D password. The design of the 3-D virtual environment and the type of objects selected determine the 3-D password key space.

III. SYSTEM ARCHITECTURE

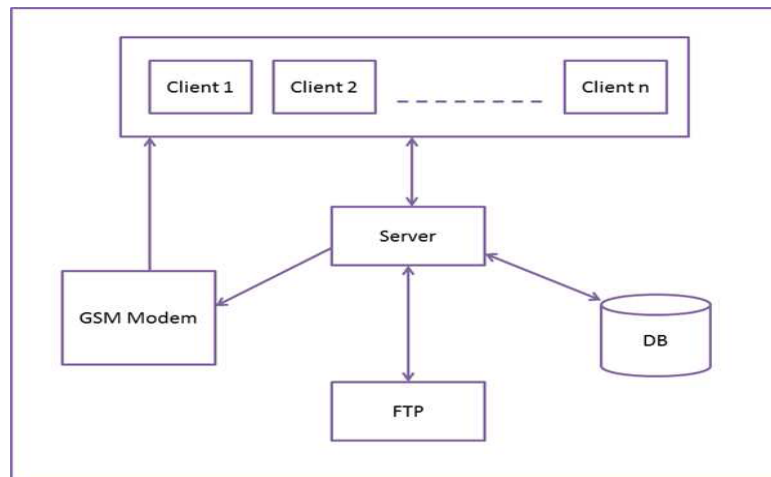


Figure 3.1: System Architecture

There are two modules in the System Architecture:

1. Client Module

When user wants to interact with system or user wants to use the services of the system first time, he has to register himself. During registration phase, user needs to provide his or her basic information including personal mobile number and at the time of login user needs to provide his valid username which is string of alphanumeric characters and special symbols in order to get access to the resources.

During login phase user needs to pass successfully through Textual, OTP and 3D password phases. On which user can receive OTP passwords on his/her mobile. Also he has to select one unique username. And at the same time user has to create 3D password, which user will use at the time of login.

2. Server Module

At the time of login when user login successfully to the textual password phase, user will enter into second stage i.e. OTP. In this phase server will generate OTP password which will be stored in encrypted form in database using AES algorithm and at the same time it will be displayed on user's mobile in decrypted form. And at the time of verification password entered by user will be encrypted first and then will be matched with the password stored in database, if it matches then server will remove the OTP password from database as it is valid only for one session. Now the last stage is 3D password. In this phase at the time of registration 3D chess board virtual environment will be provided to user from which user will select his 3D password which will be stored in encrypted form in database and at the time of login user needs to recall his previously recorded password which is encrypted and matched with the stored encrypted password and if it matches with the stored password then the user will get access to the system. And after that user can perform transaction and can use the services which particular bank will provide.

IV. MODULES & ALGORITHM

Modules

Proposed system contains different modules such as:

1. Registration module
2. Textual Login module
3. OTP Login module
4. 3D Login module
5. FTP Access module
6. Setting modules
7. Service module

1. Registration Module:

When user wants to access the system first time, then registration module is used for registering himself. And it also stores the details of user like name, address, mobile no., email id etc. in database.

2. Textual Login Module:

This module is used for accepting the username from end user and sends it to server module for validating purpose.

3. OTP Login Module:

This module is used for accepting the OTP password which he/she had received on his/her mobile from the system after providing valid username to textual login module. And that password is sent to server side for matching with password stored in the database.

4. 3D Login Module:

After providing valid information in textual as well as OTP login module, in 3D login module the 3D chessboard environment will be provided to the end user. In this, user will perform different actions and interactions towards 3D objects which will create user's 3D password that will be stored in database in encrypted form.

5. FTP Access Module:

This module will be available to the user if and only if user successfully passes through login phases. In this module FTP services will be provided to the end user where user can upload or download to or from server.

6. Setting Module:

Setting module allows user to update contact details, reset 3D password as well as notification settings according to end user's choice.

7. Service Module:

This module is implemented at server side which is used for providing the services to user. And also maintains the log of requested users. This module will listen the request from the client side and will provide response accordingly.

Algorithms

1. Proposed System Algorithm

This System contains the combination of textual, OTP and 3D Password Authentication Techniques. User can use this system if and only if he has registered himself. If not then user has to register himself before using system first time.

Steps:

1. Registration Process:

In this step, user needs to provide following four types of information.

(a) Users Personal Information:

In this, user will provide his/her personal info like Full Name, Address, State, and City.

(b) Users Contact Details:

In this, user will provide his/her contact no., mobile no. and emailid.

(c) Credential Details:

At this section, user will provide his/her username and also create 3D password from the 3D virtual environment which is provided in the GUI.

(d) Notification Details:

In this final section, user will select notification options such as login notification, update notification, and reset notification according to user's choice.

2. Login Process:

When user is already registered then for login into system he/she has to pass successfully from several stages.

(a) Textual Login:

In this, user will provide his/her valid username, after that server system will verify that username. And if it is valid then system will allow user to enter into next stage.

(b) OTP Login:

After successfully passed through textual login stage user will get OTP password on his/her mobile and if user enter valid OTP password then he/she will enter into last stage.

(c) 3D Password Login:

Here user has to interact with the 3D chessboard environment and needs to repeat same movements which he/she had done at the time of registration. After doing valid movements user will login successfully.

3. FTP Services:

User login successfully into the system then he/she can access the FTP services where user can upload or download files.

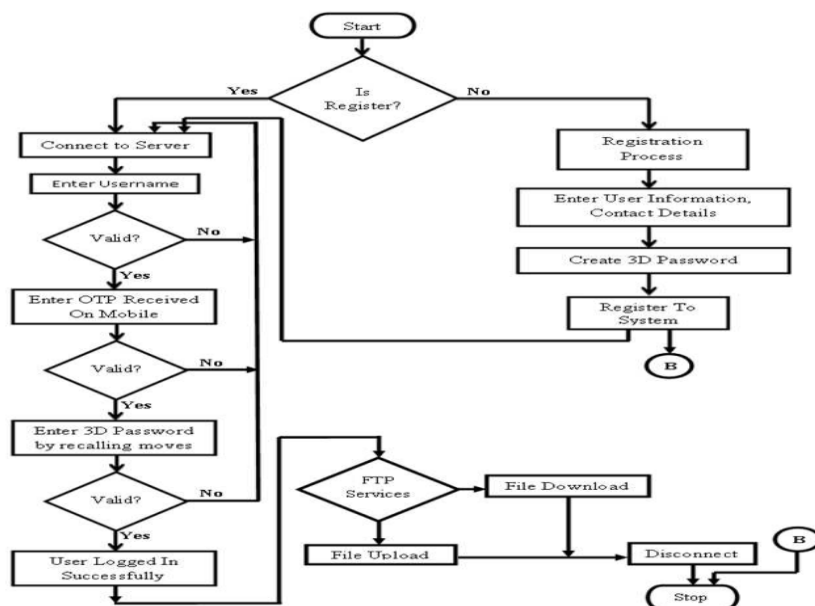


Figure 4.1: System Flow

4. AES Algorithm

In cryptography, the Advanced Encryption Standard (AES) is an encryption standard adopted by the U.S. government. The standard comprises three block ciphers, AES-128, AES-192 and AES-256, adopted from a larger collection originally published as Rijndael. The Rijndael cipher was developed by two Belgian cryptographers, Joan Daemen and Vincent Rijmen, and submitted by them to the AES selection process. Each AES cipher has a 128-bit block size, with key sizes of 128, 192 and 256 bits, respectively. The AES ciphers have been analysed extensively and are now used worldwide, as was the case with its predecessor, the Data Encryption Standard (DES).

Steps of AES Algorithm:

1. Key Expansion:

Round keys are derived from the cipher key using Rijndael’s key schedule(to expand a short key into a number of separate round keys).

2. Initial Round - AddRoundKey:

Each byte of the state is combined with the round key using bitwiseXOR.

3. Rounds

(a) SubBytes:

SubBytes is used at the encryption site. To substitute a byte, weinterpret the byte as two hexadecimal digits.The SubBytes operationinvolves 16 independent byte-to-byte transformations using lookup table.

(b) ShiftRows:

The ShiftRows step operates on the rows of the state; it cyclicallyshifts the bytes in each row by a certain offset. For AES, the first rowis left unchanged. Each byte of the second row is shifted one to theleft. Similarly, the third and fourth rows are shifted by offsets of twoand three respectively. For blocks of sizes 128 bits and 192 bits, theshifting pattern is the same. Row n is shifted left circular by n-1 bytes.

(c) MixColumns:

In the MixColumns step, the four bytes of each column of the stateare combined using an invertible linear transformation. TheMixColumnsfunction takes four bytes as input and outputs four bytes, where eachinput byte affects all four output bytes. Together with ShiftRows, Mix-Columns provides diffusion in the cipher.

(d) AddRoundKey:

In the AddRoundKey step, the subkey is combined with the state.For each round, a subkey is derived from the main key using Rijndael’skey schedule. The subkey is added by combining each byte of the statewith the corresponding byte of the subkey using bitwise XOR.

4. Final Round (no MixColumns):

(a) SubBytes

(b) ShiftRows

(c) AddRoundKey

V. SCREEN SHOTS

5.1 Server Side Home page

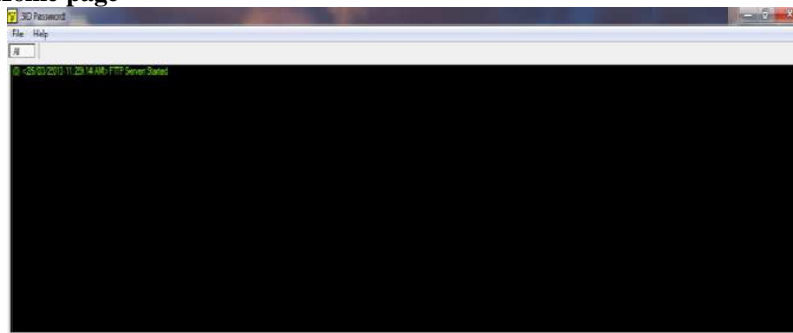


Figure 5.1: Server Side Home Page

5.2 Client Side Main Form



Figure 5.2: Client Side Main Form

5.3 Textual Login Window



Figure 5.3: Textual Login Window

5.4 OTP Login Form



Figure 5.4: OTP Login Form

5.5 3D Login Form



Figure 5.5: 3D Login Form

VI. TECHNICAL SPECIFICATION

Hardware Requirement

1. Processor: Intel Dual Core.
2. Hard Disk: 40 GB. (Client System), 60 GB. (Server System).
3. RAM: 512 MB. (Client System), 2 GB. (Server System).

Software Requirement

1. Database: Oracle 10g
2. Coding language: Java

Advantages

1. Not easy to write down on paper
2. Difficult to crack and Avoid Attacks
3. Large password space

Disadvantages

1. Not feasible for blind people
2. Shoulder surfing attack is possible

Applications

1. Critical server
2. Nuclear and military facilities
3. Air-planes and jetfighters
4. E-Banking& ATMs

VII. CONCLUSION

In Market, there are so many authentication schemes available. Some techniques are based on user's physical characteristics as well as behavioral properties, and some other techniques are based on user's knowledge such as textual and graphical passwords. However, as mentioned before, both authentication schemes are vulnerable to certain attacks. This system is multilevel authentication system for Web because it combines three different authentication system i.e. textual password, one time password and 3D password. So it is difficult to break the system and also provides large password space over alphanumeric password. The proposed system avoids different types of attacks like brute force attack, dictionary attack and well-studied attack. One-time password systems provide a mechanism for logging on to a network or service using a unique password which can only be used once, as the name suggests.

VIII. FUTURE SCOPE

These are the possible future scopes:

1. Enhancing and Improving the User Experience for the 3-D Password
2. Gathering Attackers from different backgrounds to break the system

REFERENCES

- [1] Prof. Sonkar S. K., Dr. Ghungrad S. B., "Minimum Space and Huge Security in 3D Password Scheme", International Journal of Computer Applications (0975-8887), vol. 29-No. 4, Sept. 2011.
- [2] Young Sil Lee, "A study on efficient OTP generation using stream cipher with random digit", Advanced Communication Technology (ICACT), 2010 The 12th International Conference, vol. 2, pp 1670-1675. Feb. 2010.
- [3] Renaud, K. (2009). "On user involvement in production of images used in visual authentication". J. Vis. Lang. Comput. 20(1):1-15.
- [4] Haichang, G. L. Xiyang, et al. (2009). "Design And Analysis of Graphical Password scheme", Innovative Computing, Information and Control (ICICIC), 2009 fourth, International Conference On Graphical Password.
- [5] Fawaz A. Alsulaiman and Abdulmotaleb El Saddik, "Three-Dimensional Password for More Secure Authentication," IEEE, <http://ieeexplore.ieee.org>, Last Updated 6 Feb 2008.
- [6] Soon Dong Park, JoongChae Na, Young-Hwan Kim, dong Kyue Kim, "Efficient OTP (One Time Password) Generation using AES based MAC," Journal of Korea Multimedia Society, vol. 11, No. 6, pp. 845-851, June. 2008.
- [7] S. Wiedenbeck, J. Waters, J.-C. Birget, A. Brodskiy, and N. Memon, "Pass Points: Design and longitudinal evaluation of a graphical password system," Int. J. Human-Comput. Stud. (Special Issue on HCI Research in Privacy and Security), vol. 63, no. 1/2, pp. 102127, Jul. 2005.
- [8] S. Wiedenbeck, J. Waters, J.-C. Birget, A. Brodskiy, and N. Memon, "Authentication using graphical passwords: Basic results," in Proc. Human-Comput. Interaction Int. Las Vegas, NV, Jul. 2527, 2005.

Design of Coaxial Rotor Micro Air Vehicle

Manoj J. Watane¹, Dushyant B. Pawar²

^{1,2}(Mechanical Engineering Department, Dr. Sau Kamaltai Gawai Institute of Engineering & Technology Darapur, Dist. Amravati State: Maharashtra, India)

Abstract: The main objective of this paper is the systematic description of the current research and development of small or miniature unmanned aerial vehicles and micro aerial vehicles, with a focus on rotary wing vehicles. In recent times, unmanned/Micro aerial vehicles have been operated across the world; they have also been the subject of considerable research. In particular, UAVs/MAVs with rotary wings have been expected to perform various tasks such as monitoring at fixed points and surveillance from the sky since they can perform not only perform static flights by hovering but also achieve vertical takeoffs and landing. Helicopters have been used for personnel transport, carrying goods, spreading information, and performing monitoring duties for long periods. A manned helicopter has to be used for all these duties. On the other hand, unmanned helicopters that can be operated by radio control have been developed as a hobby. Since unmanned helicopters are often superior to manned helicopters in terms of cost and safety, in recent years, accomplishing tasks using unmanned helicopters has become popular. Considerable expertise is required to operate unmanned helicopters by radio control, and hence, vast labor resources are employed to train operators. Moreover, it is impossible to operate unmanned helicopters outside visual areas because of lack of radio control, and the working area is hence limited remarkably. For solving the above problems, it is necessary to realize autonomous control of unmanned helicopters. However, no general method for designing the small unmanned helicopters has been developed yet – today, various design techniques by different study groups using different helicopters exist. In this paper the conceptual design process is explained.

Keywords: Micro air vehicle, coaxial rotor, vertical takeoff & landing (VTOL)

I. INTRODUCTION

Autonomous unmanned aircraft equipped with autonomous control devices called unmanned aerial vehicles & micro aerial vehicles. This is generally called as autonomous flying robots. Micro- and nano air vehicles are defined as “extremely small and ultra-lightweight air vehicle systems” with a maximum wingspan length of 15 cm and a weight less than 20 grams. In 1997, DARPA started a program called “MAV-project” where they presented some minimal requirements. In particular, they set the maximum dimension to be around 15 cm long, and the weight, including payload, to be less than 100 g. Furthermore, flight duration should be 20 to 60 minutes.

Many research institutions are actively studying and developing new air vehicles, reducing size and weight while improving performance, and adding more functionality.

Examples here are Harvard Micro-robotics Laboratory in the USA, Department of Aeromechanics and Flying Engineering from Moscow Institute of Physics and Technology in Russia, Aircraft Aerodynamics and Design Group at Stanford University (USA), the Autonomous Systems Laboratory at ETH Zurich (Switzerland), and Department of Precision Instrument and Mechanology at Tsinghua University in China. Several companies and agencies also play an important role in the manufacturing and development of AVS. Examples here are DARPA from USA, Prox Dynamics from Norway, and Syma from USA. AVS applications span a wide range, and the majority of them are military. AVS are capable to perform both indoor missions and outdoor missions in very challenging environments. The main applications are intelligence, surveillance, and reconnaissance (ISR) missions.

These systems can provide a rapid overview in the area around the personnel, without exposing them to danger. Infrared (IR) cameras can give detailed images even in the darkness. Furthermore, NAVs, thanks to their reduced dimensions, are perfect for reconnaissance inside buildings, providing a very useful tactical advantage. As reported in, such small vehicles are currently the only way to remotely “look” inside buildings in the battlefield.

II. History of Unmanned Aerial Vehicles

The first UAV was manufactured by the Americans Lawrence and Sperry in 1916. It is shown in Fig.1. They developed a gyroscope to stabilize the body, in order to manufacture an auto pilot. This is known as the beginning of “attitude control,” which came to be used for the automatic steering of an aircraft. They called their device the “aviation torpedo” and Lawrence and Sperry actually flew it a distance that exceeded 30 miles. However, because of their practical technical immaturity, it seems that UAVs were not used in World War I or World War II. The development of UAVs began in earnest at the end of the 1950s, taking advantage of the Vietnam War or the cold war, with full-scale research and development continuing into the 1970s. Figure 2 shows a UAV called Fire bee. After the Vietnam War, the U.S. and Israel began to develop smaller and cheaper UAVs. These were small aircraft that adopted small engines such as those used in motorcycles or snow mobiles. They carried video cameras and transmitted images to the operator’s location. It seems that the prototype of the present UAV can be found in this period.

The U.S. put UAVs into practical use in the Gulf War in 1991, and UAVs for military applications developed quickly after this. The most famous UAV for military use is the Predator, which is shown in Fig.3. On the other hand, NASA was at the center of the research for civil use during this period. The most typical example from this time was the ERAST (Environmental Research Aircraft and Sensor Technology) project. It started in the 1990s, and was a synthetic research endeavor for a UAV that included the development of the technology needed to fly at high altitudes of up to 30,000 m, along with a prolonged flight technology, engine, sensor, etc. The aircraft that were developed in this project included Helios, Proteus, Altus, Pathfinder, etc., which are shown in Figs. 4–6. These were designed to carry out environmental measurements. To take-off and land, or catapult launching.

Table1: Types of Unmanned Aerial Vehicles

Sr No.	Figure	Name	Sr No.	Figure	Name
1		First UAV in the world, 1916	4		Civil use UAV by NASA (Helios)
2		UAVs in the 1960s and 1970s (Fire bee)	5		Civil use UAV by NASA (Helios)
3		Predator in military use	6		Civil use UAV by NASA (Altus)

III. Configurations of UAV

Fixed-wing UAVs, as shown in fig (7) which refer to unmanned airplanes (with wings) that require a runway. Rotary-wing UAVs, as shown in fig (8) also called rotorcraft UAVs or vertical take-off and landing (VTOL) UAVs, which have the advantages of hovering capability and high maneuverability. These capabilities are useful for many robotic missions, especially in civilian applications. A rotorcraft UAV may have different

configurations, with main and tail rotors (conventional helicopter), coaxial rotors, tandem rotors; multi-rotors, etc.

Micro aerial vehicles (MAV): In the last few years, micro aerial vehicles, with dimensions smaller than 15 cm, have gained a lot of attention. These include the Black Widow manufactured by AeroVironment, the Micro Star from BAE, and many new designs and concepts presented by several universities, such as the Entomopter (Georgia Institute of Technology), Micro Bat (California Institute of Technology), and MFI (Berkeley University), along with other designs from European research centers fig 10.

Fig 7. Some configurations of fixed-wing UAVs



Fig 8. Examples of rotary-wing UAVs



Fig 10 Unmanned aerial vehicles, from big platforms to micro flying robots.



IV. Design Procedure for Micro Air Vehicle

The designer must go through a preliminary design procedure where the overall size and shape of the vehicle will be determined. This conceptual process is the focus of this paper and it is outlined Figure 11.

4.1. Components and Take-Off Weight

One advantage of MAV design over conventional full-scale aircraft design is that the calculation of take-off weight can be performed with relatively little use of empirical data. This is due to the fact that most of the components to be carried, as well as their size and weight, are known. Consider here take of weight as 40 gram. (W_o)

4.2. Estimation of Cruise Velocity

With the take-off mass defined, the next step in the design procedure is to determine the Cruise speed of the MAV. This step is particularly difficult because, there will be no experimental data of the thrust of the engine selected versus airspeed.

Relation for calculating Cruise velocity is taken as

$$V_c^{\text{Coaxial UAV}} = 99.5 \cdot W_o^{0.268} \quad \text{where } V_c \text{ is cruise velocity \& } W_o \text{ is the gross weight}$$

$$V_c^{\text{Coaxial UAV}} = 99.5 \cdot (0.04)^{0.268} = 0.699 \text{ m/sec}$$

4.3. Required Lift Coefficient

With the take-off weight and estimated airspeed known, it is possible to calculate the lift coefficient required to sustain level flight. That is,

$$C_{L,req} = W_0 / 0.5\rho V^2 S$$

$$C_{L,req} = 40 / 0.5 \times 1.29 \times (0.699)^2 \times 3.14 \times (0.125)^2$$

$$= 2.58$$

Where W is the weight of the aircraft, V is the estimated cruise speed, and S is the wing area.

4.4. Selection of Wing Plan form Shape:

In order to determine which wing shape is best suited for a micro aerial vehicle, wind tunnel experimental data is to be used to develop an empirically-based design and analysis procedure.

The results obtained from the University of Notre Dame’s MAV entry to the 2000 Micro Aerial Vehicle Student Competition was used as the best wing plan form shape for a MAV. These results were summarized in a report written by Gabriel Torres and Thomas J. Mueller, entitled, “Micro Aerial Vehicle development: Design, Components, Fabrication, and Flight-testing”. Torres and Mueller used wind tunnel experiments, which were used to develop an empirically-based design and analysis procedure, to determine the optimal wing shape for a MAV. In these experiments four different wing shapes were tested, shown in Fig. 11. All had zero camber, a thickness-to-chord ratio of 1.96% and aspect ratios of 1 and 2 (Mueller 2000). [4]

4.5. Selection of Aspect Ratio and Wing Area:

Having determined the optimum shape the next task will be to size it: that is, to select the aspect ratio and wing area. As is discussed earlier, this step is difficult to do accurately due to the uncertainty of the estimated airspeed, the assumptions used in the generation of the interpolation model, and the fact that a thin wing with zero camber will have different lift and drag characteristics than a ready-to-fly MAV with a fuselage and wings with camber and thickness.

Relation to calculate aspect ratio
$$AR = \frac{b^2}{S}$$

As can be seen from Eq. 5 using a small aspect ratio, the MAV can maximize its wing area (Francis and McMichael 1997). It was found that a wing with AR=1.5 was close to the most efficient use of maximum dimension for a wing platform, similar in shape to the inverse Zimmerman wing

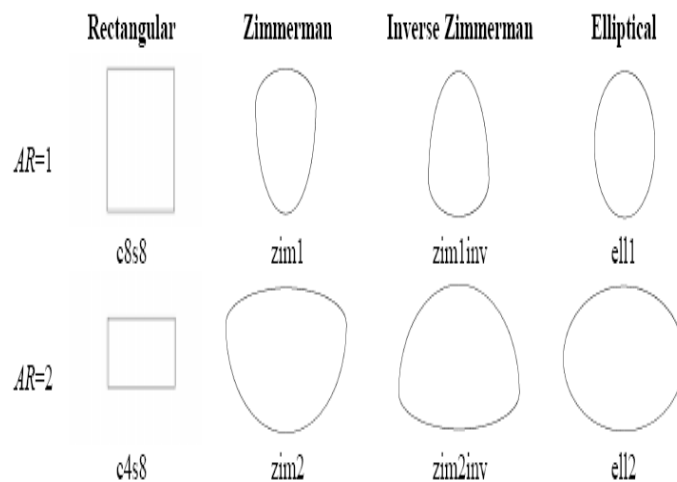
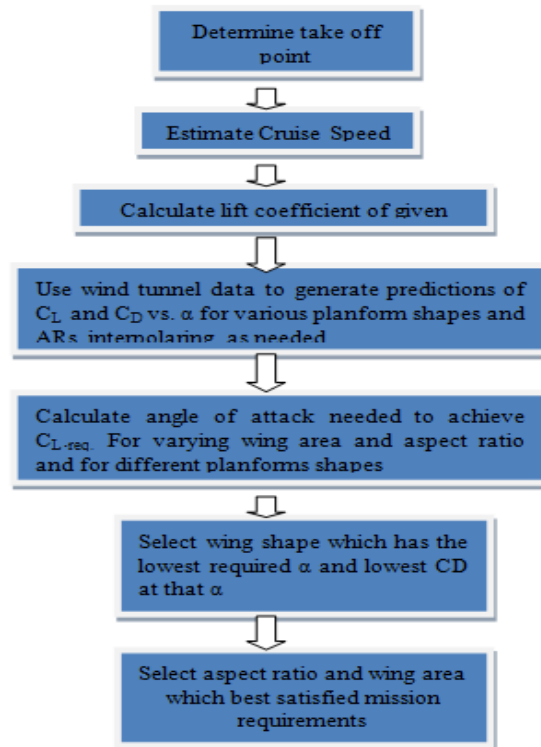


Figure 10. Shapes of the wings which were tested in the wind tunnel tests.

Figure 11: Design Procedure for Micro Aerial Vehicle



V. Applications

Potential civil applications of UAVs are

1. Inspection of terrain, pipelines, utilities, buildings, etc.
2. Surveillance of coastal borders, road traffic, etc.
3. Disaster and crisis management search and rescue.
4. Environmental monitoring.
5. Agriculture and forestry.
6. Fire fighting.
7. Communications relay and remote sensing.
8. Aerial mapping and meteorology research by university laboratories

VI. Conclusion

From above design method it is concluded that we can design a micro air vehicle ranging from 20 gram to 100 gram. Selecting density of air & gross weight of vehicle to be lift coefficient of lift will be obtained, force required to lift a vehicle i.e equal to gross weight of vehicle will be calculated.

REFERENCES

Books:

- [1] Autonomous Flying Robots (Unmanned Aerial Vehicles and Micro Aerial Vehicles) by Kenzo Nonami Farid Kendoul • Satoshi Suzuki Wei Wang • Daisuke Nakazawa.

Journal Papers:

- [2] Micro- and Nano-Air Vehicles: State of the Art Luca Petricca , and Christopher Grinde.
- [3] Micro aerial vehicle development: design, Components, fabrication, and flight-testing by Gabriel Torres and Thomas J. Mueller.

Journal Papers:

- [4] Samantha Hearne 'Minimum Structural Weight of a Micro Aerial Vehicle' University of New South Wales at the Australian Defence Force Academy, October 2008.

Minimization Of Inter Symbol Interference Based Error in OFDM System Using Adaptive Decision Mechanism by SNR Estimation

Swati Sengar¹, Anil Sharma²

^{1,2}(Department of Electronics and Communication Engineering, Mangalayatan University Aligarh, India)

Abstract: In the wireless multimedia applications OFDM modulation is a promising approach for establishing a high bit rates. Modern OFDM systems uses channel estimation and tracking, instead of differential phase-shift keying (DPSK) it provides a 3-dB SNR loss compared with normal coherent phase-shift keying (PSK). In this article we have improved the performance of OFDM systems in coherent PSK modulation schemes; we implemented a channel estimation technique for OFDM communication. We designed an algorithm based on mean-square-error (MSE) channel estimator by use of calculations based on the time and frequency-domain received signals of the frequency response obtained after passing through time-varying dispersive Rayleigh fading channels distorted with AWGN. We have considered the uncertainty of channel statistics that results in mismatch of the estimator-to-channel statistics and proposed a robust channel estimator that is independent to uncertainty of channel performance statistics. The robust channel estimator response are further used to run a modulation decision scheme logic that can significantly improve the performance of OFDM systems in noisy Rayleigh fading channel by minimizing BER and inter symbol interference.

Keywords: Adaptive Decision, OFDM, Fading Channel, SNR estimation, PSK/QAM.

I. Introduction

Orthogonal frequency division multiplexing (OFDM) [1]–[3] in recent years has collected high popularity due to its performance features like its robustness to multipath delay spread and AWGN noise, it has quality of high data transmission rate with improved bandwidth efficiency, and its application of adaptive equalization and power allocation in between the subcarriers in accordance of the channel conditions. OFDM is used in wire line applications like Asymmetric Digital Subscriber Line [4], broadcasting services Digital Audio Broadcasting [5], Terrestrial Digital Video Broadcasting [6] and (Terrestrial Integrated Services Digital Broadcasting) [7], high rate wireless LAN standards (ETSI Hiper LAN 2 and IEEE 802.11) and multimedia wireless services like Multimedia Mobile Access Communications [8], [9].

In the non-coherent OFDM system the system complexity is reduced at the cost of 3–4 dB performance loss [10] but in coherent OFDM system channel estimation is a major requirement along with the pilot symbols incorporation in channel estimation. Pilot preambles are pre inserted in all subcarriers forming an OFDM training symbol, these training symbols are transmitted at an appropriate data rate with respect to the time varying response of the wireless channel.

Channel estimation is a very important part in wireless communications systems. Pilot-signal-based channel estimation as discussed above is enormously used in packet-data base communications. In single-carrier systems, optimal periodic or a periodic sequences based channel estimation analyzed in [10]-[11] references. An optimal training sequences for pilot symbols for orthogonal frequency division multiplexing (OFDM) channel estimation were proposed in [12][13]. The Optimal placement location and training symbols energy allocation for single-carrier and OFDM systems are described in [14] for frequency-selective Rayleigh block-fading channel. The training signal placement location is such that it maximizes a lower bound on the capacity training-based signal with the assumption that all pilot symbols have the same energy. It has been found that in OFDM systems, in the frequency domain the optimally best placement location of pilot tones is equal spaced positioning scheme. Optimal design and placement of pilot symbols for frequency-selective block-fading channel estimation are addressed in [15] by considering SISO as well as MIMO single-carrier systems by minimizing the Cramer-Rao bound. The same challenge is also addressed in [16] by maximizing a lower bound on the average capacity.

We have implemented an adaptive decision feedback decision logic scheme for in OFDM using the channel estimates obtained from periodic block-type pilots. We have investigated the performances of seven

different modulation scheme by measuring bit error rate for QAM and MPSK variants in the presence of multi-path Rayleigh fading and AWGN noise channels combination as channel models.

In this paper, we have shown the performance of schemes by applying 16QAM (16 Quadrature Amplitude Modulation), QPSK (Quadrature Phase Shift Keying and BPSK (Binary Phase Shift Keying) etc. as modulation schemes with Rayleigh fading. We have designed the MATLAB/Simulink model of the OFDM system using method of pilot channel estimation. In Section III, the estimation of the channel based on block-type pilot arrangement is discussed. In this model the estimation of the channel at pilot frequencies is calculated in the simulation environment and results are analyzed for determining the thresh level of SNR estimate at which a modulation scheme starts to give minimum BER.

II. OFDMA System Design And BER Minimization

2.1. OFDM Transceiver without Channel Estimation

In an OFDM transceiver communication design without any channel estimation there is no insertion of pilot symbols. Hence, 200 out of 256 carriers are allocated for data, in which number of used sub-channels (FFT size) is 256. The main parameters for this design can be shown in Table 1.

Simulation parameters	parameter value
Bandwidth (MHz)	10
Fs (MHz)	11.2
FFT	Size 256
Left Guard Interval	28
Right Guard Interval	27
DC Carrier Index	Central
Used Carriers	201 (Including a DC carrier)
Data Carriers	200
Cyclic Prefix	1/8

In our basic OFDM simulink model, extra functional blocks are also added to form mobile system module as shown in Fig 1. This blocks model is implemented according to IEEE 802.16-2005. To study the effect of Doppler shift and multipath fading, a multipath channel is be added to the system shown in figure 2.

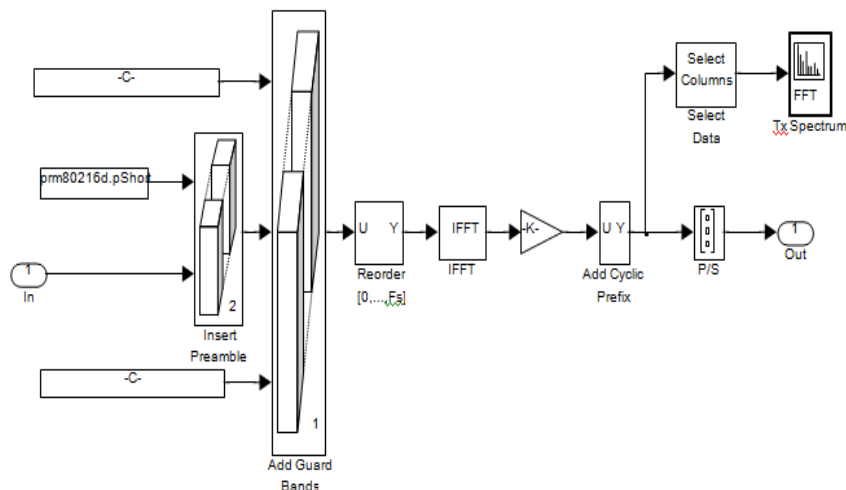


Fig 1: Simulink Model of designed OFDM system

We have used MATLAB/Simulink contains Rayleigh and AWGN Channel model. We have thus tested the data distortion effects by multipath propagation in Non line of sight transmission, environment. In Fig 3 the OFDMA system with modulation mapping scheme is shown with adding multipath Rayleigh and AWGN channel in which ITU- channel models are used. The parameters of Multipath Rayleigh fading channel in our model are :

Maximum Doppler shift (Hz): A positive scalar that indicates the maximum Doppler shift.

Sample time: The period of each element of the input signal. It is set to 1/1152.

Delay vector (s): A vector that specifies the propagation delay for each path.

Gain vector (dB): A vector that specifies the gain for each path. Normalize gain vector to 0 dB overall gain: Checking this box causes the block to scale the Gain vector parameter so that the channel's effective gain (considering all paths) is 0 decibels.

Initial seed: The scalar seed for the Gaussian noise generator.

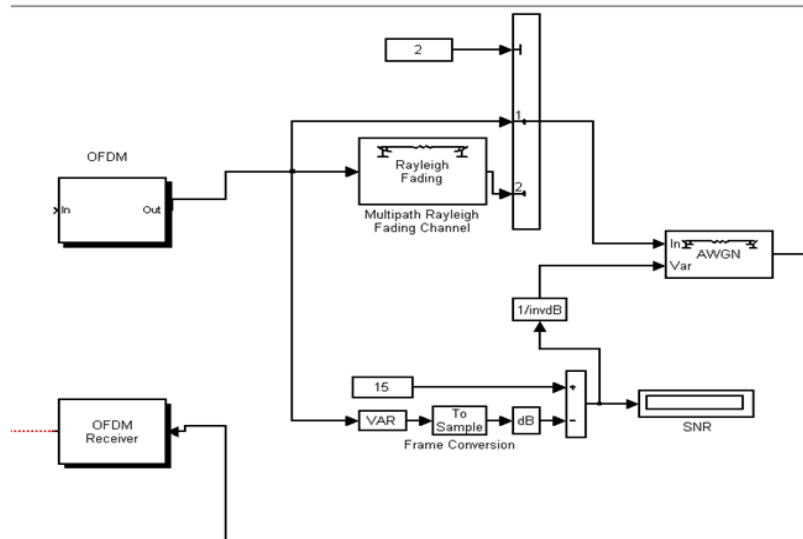


Fig 2: Channel Model consist of Rayleigh fading prior to AWGN channel.

Thus, the modified OFDMA transceiver system as shown in Figure 3 has pilot symbols (on pilot subcarriers) embedded in between the data symbols (on data subcarriers), which provides the channel information at the receiver. However, at the receiver, the values of channel estimation are interpolated over the data subcarriers whereas data symbols are decoded. In both time and frequency domain, the interpolation depends much on subcarrier spacing, symbol time and pilot location. The interpolation will not be accurate if the channel characteristics are changed significantly between pilot subcarriers. The model simulation is carried out at fixed step discrete configuration with the SIMULINK environment using communication blocksets. The system in the simulation is subjected to AWGN channel and Rayleigh fading with AWGN at different SNR.

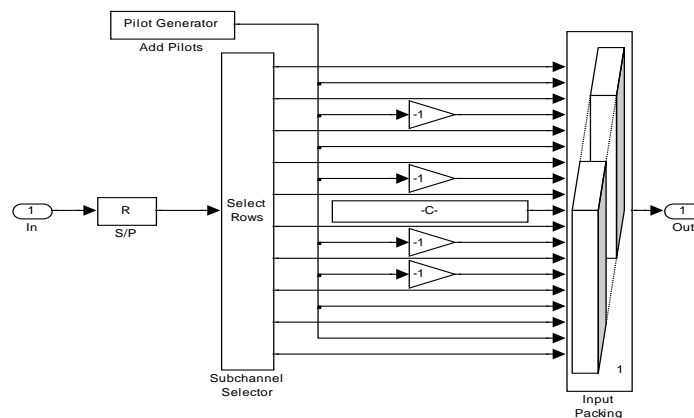


Fig 3: Pilot insertion to the modulated data block prior to OFDM.

III. Results And Discussion

We have developed our simulation model for investigating physical layer performance of IEEE 802.16e (WiMax communication model) using simulink tool of MATLAB 2010. We have improved the performance of OFDM technique by using channel SNR and response estimation. We have considered 3 cases. In 1st case, we have considered 7 different modulation scheme related to PSK I/O Mapping in presence of AWGN only and AWGN with multipath Rayleigh fading. In 2nd case, we have applied OFDM methodology on all 7 cases to check the benefit of OFDM based multi carrier system in reducing inter symbol interference to improve multipath propagation in mobile wireless communication system. In 3rd case we have develop a model that can evaluate a model that can evaluate channel SNR and it attenuation factor along with phase delay for every frame using the error in preamble symbol insert prior to OFDM application. This case include an adoptive decision mechanism control block that can switch over in between different PSK modulation scheme in order to get a final modulation scheme. For developing adoptive decision mechanism, we investigated the result of case1 case 2 for selecting the value of SNR at which each of 7 modulation scheme starts to show minimum bit

rate(BR). We have take different modulation scheme named as BPSK ,QPSK ½,QPSK¾,16QAM1/3,16 QAM ¾,64QAM2/3,64QAM¾ and our result consist of scatter plots, BER values at different SNR for energy modulation scheme.

This fig 4 shows that our input data is random data source generated using Bernoulli generator block having sample time 8.3333e-008 and sample per frame 864.The Bernoulli generator block pass to the modulation bank. It consist of 3 main operations coding interleaving and modulation using PSK or QAM mapping. Data generated from Bernoulli generator is padding by zero's to construct the frame 64 prior to encoding.

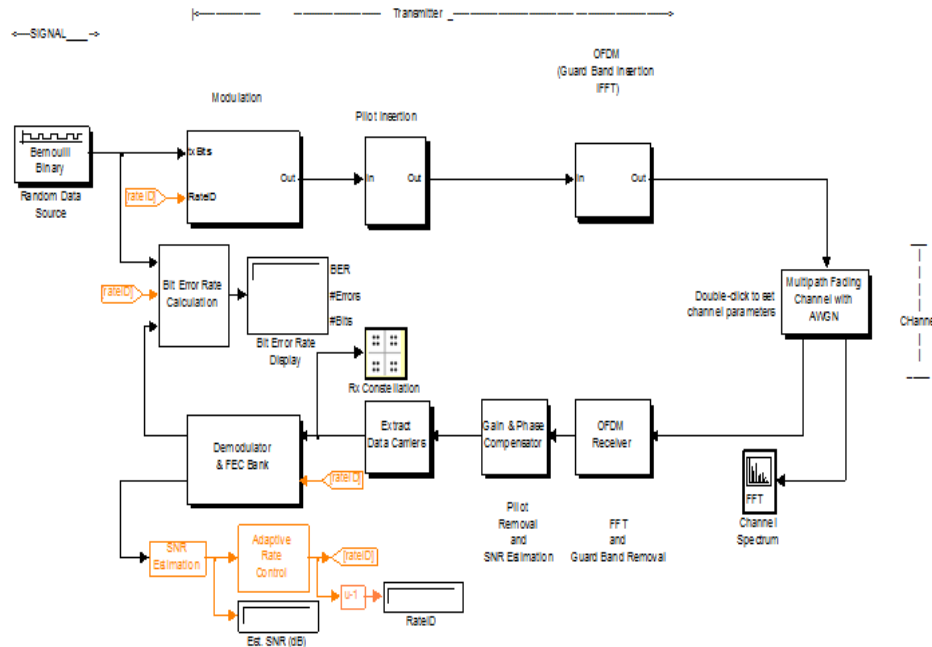


Fig. 4 Complete OFDM simulink model for SNR channel estimation and adaptive decision mechanism

The encoder consist of the poly2trellis structure having specification (7, [171 133]).It represent that, this encoder will generate to 2 encoded schemes as per the octal number representation of 177,133 XOR gate connection. In this way after encoding, we get the packet of bits 1048 that is double of size of packet bits or interleaving ,the number of subchannel are taken as 16 with Ncbps=192 and Ncpc=1.These interleaving signals are pass through the BPSK modulation having the output packet size. For different modulation scheme the polytrellis structure is same ,but the parameter of interleaver is changed allow with the padding data showing in following table 1.

Modulation Scheme and rate id	No. of subchannels	No. of coded bits per subchannel (Ncbps)	No. of coded bit per subcarrier(Ncpc)
BPSK (0)	16	192	1
QPSK ½(1)	16	384	2
QPSK ¾(2)	16	384	2
16 QAM1/2(3)	16	768	4
16 QAM3/4(4)	16	768	4
64 QAM 2/3(5)	16	1152	6
64 QAM ¾(6)	16	1152	6

Table 1: Configuration for different modulation scheme

We have shown our results in tabular form for all three cases. Table1 shows the obtained in our model when no channel estimation and OFDM is applied.

We have changed the SNR of AWGN channel in presence of noise and also in noise along with fading. Both results for all the seven modulation schemes are shown in this table.

Case 1:

S N R	AWGN(BER) WITHOUT FADDING							AWGN (BER)WITH FADDING							
	BP SK	QPS K 1/2	QPSK ¾	16Q AM 1/2	16Q AM ¾	64Q AM 2/3	64Q AM ¾	BPS K	QPSK 1/2	QPS K ¾	16Q AM ½	16Q AM ¾	64Q AM 2/3	64 QA M ¾	
5	0	0.025 26	0.2669	0.487	0.495 9	0.499 8	0.49 39	0.49 6	0.498 7	0.49 81	0.498 6	0.499 7	0.499 8	0.4 997	
10	0	0	0.0002 778	0.123 1	0.467 6	0.488 6	0.49 37	0.50 1	0.498 5	0.49 77	0.498 6	0.499 6	0.499 6	0.4 997	
15	0	0	0	0	0.312 2	0.305 6	0.41 36	0.49 5	0.498 5	0.49 76	0.498 7	0.499 6	0.499 6	0.4 998	
20	0	0	0	0	0	0	0.01 69	0.49 5	0.498 8	0.49 8	0.498 7	0.499 8	0.499 7	0.4 997	
25	0	0	0	0	0	0	0	0.49 7	0.498 4	0.49 78	0.499 7	0.499 7	0.499 7	0.4 996	
30	0	0	0	0	0	0	0	0.49 9	0.497 9	0.49 88	0.498 8	0.499 8	0.499 7	0.4 996	

Table 1: Communication Model Performance without applying OFDM

Case 2:

S N R	AWGN(BER WITH OFDM) WITHOUT FADDING							AWGN (BER WITH OFDM)WITH FADDING							
	BP SK	QPS K 1/2	QPS K ¾	16Q AM 1/2	16Q AM ¾	64Q AM 2/3	64QA M ¾	BP SK	QP SK 1/2	QP SK ¾	16Q AM ½	16Q AM ¾	64Q AM 2/3	64 QA M ¾	
5	0	0.08 437	0.34 61	0.49 27	0.49 5	0.49 77	0.501 2	0.3 033	0.4 927	0.4 979	0.49 88	0.50 27	0.49 98	0.4 99 8	
10	0	0	0.00 066	0.21 74	0.43 22	0.49 21	0.499 8	0.4 371	0.5 062	0.4 977	0.50 04	0.49 62	0.50 05	0.4 98 4	
15	0	0	0	0.09 633	0.01 348	0.37 54	0.449 2	0.5 163	0.4 987	0.5 005	0.49 69	0.50 19	0.49 93	0.5 01 4	
20	0	0	0	0	0	0.00 150	0.042 65	0.5 428	0.5 003	0.4 977	0.49 76	0.49 92	0.49 98	0.5 03 3	
25	0	0	0	0	0	0	0	0.5 519	0.3 485	0.3 913	0.50 5	0.50 22	0.49 98	0.5 01 8	
30	0	0	0	0	0	0	0	0.3 788	0.4 938	0.4 284	0.49 93	0.50 31	0.50 08	0.5 00 2	

Table 2: Communication Model Performance with applying OFDM but without gain and phase compensation

Case 3:

SNR	AWGN WITH Adaptive decision scheme			
	Without fading		With fading	
	BER	RATid	BER	RATid
5	0.001249	0	0.1173	0
10	0	1	0.02536	0
15	0	3	0.03427	1

20	0	3	0.0117	1
25	0	5	0.01081	3
30	0	6	0.01227	2

Table 3: Communication Model Performance with applying OFDM with gain and phase compensation and adaptive modulation decision.

We can see that in table 2 we have applied OFDM using IFFT-FFT in the pilot inserted symbol. But since we have not utilized the information obtained by channel estimation that is why there is no improvement in system performance. On applying gain and phase compensation along with adaptive decision mechanism we can see that the modulation rate id is changing and increases as we increase the SNR in order to maintain a modulation scheme at which we get minimum BER.

IV. Conclusion

In this paper, a design analysis for the pilot based channel estimation is performed for OFDM communication system. Our model uses the channel estimation based SNR prediction from the pilot arrangement preamble with or without adaptive modulation scheme decision mechanism. Channel estimation based on pilot arrangement is applied by giving the channel estimation methods at the pilot frequencies and the investigation of the Rayleigh channel with AWGN channel at data frequencies response is performed. The simulation results are obtained for three different cases using MATLAB/SIMULINK environment. The performance of our model gives a minimum BER of the range of 0.01 at different SNR. This was expected because the pilot arrangement helps in the tracking of fast fading channel and adaptive decision scheme utilizes the mean-square error between the interpolated points and their actual values to choose a modulation id that provides minimized BER.

REFERENCES

- [1] R. W. Chang, "Synthesis of band-limited orthogonal signals for multichannel data transmission," Bell Syst. Tech. Journal, vol. 45, Dec. 1966.
- [2] L. J. Cimini, Jr., "Analysis and simulation of a digital mobile channel using orthogonal frequency-division multiplexing," IEEE Trans. Commun., vol. 33, no. 7, pp. 665–675, July 1985.
- [3] J. A. C. Bingham, "Multicarrier modulation for data transmission: An idea whose time has come," IEEE Commun. Mag., vol. 28, no. 5, pp. 5–14, May 1990.
- [4] Asymmetric digital subscriber line (ADSL) metallic interface, American National Standards Institute (ANSI), Dec. 1995.
- [5] P. Shelswell, "The COFDM modulation system: The heart of digital audio broadcasting," Elec. Commun. Eng. Journal, pp. 127–136, June 1995.
- [6] U. Reimers, "Digital video broadcasting," IEEE Communications Magazine, vol. 36, no. 6, pp. 104–110, June 1998.
- [7] M. Uehara, M. Takada, and T. Kuroda, "Transmission scheme for the terrestrial ISDB system," IEEE Trans. on Consumer Electronics, vol. 45, no. 1, pp. 101–106, Feb. 1999.
- [8] R. van Nee and G. Awater, "New high-rate wireless LAN standards," IEEE Communications Magazine, pp. 82–88, Dec. 1999.
- [9] N. Morinaga and A. Hashimoto, "Technical trend of multimedia mobile and broadband wireless access systems," IEICE Trans. Commun., vol. E82-B, no. 12, pp. 1897–1905, Dec. 1999.
- [10] Y. Li, N. Seshadri, and S. Ariyavisitakul, "Channel estimation for OFDM systems with transmitter diversity in mobile wireless channels," IEEE Journal on Select. Areas in Comms., vol. 17, no. 3, pp. 461–470, Mar. 1999.
- [11] A. Milewski, "Periodic sequences with optimal properties for channel estimation and fast start-up equalization," IBM Journal of Research and Development, Vol. 27, No. 5, Sept. 1983, pp. 426-431.
- [12] J.C.L. Ng, K.B. Letaief, and R.D. Murch, "Complex Optimal Sequences with Constant Magnitude for Fast Channel Estimation Initialization," IEEE Trans. Commun., Vol. 46, No. 3, Mar. 1998, pp. 305-308.
- [13] R. Negi and J. Cioffi, "Pilot tone selection for channel estimation in a mobile OFDM system," IEEE Trans. Consumer Electronics, Vol. 44, No. 3, pp. 1122-1128, Aug., 1998.
- [14] J.H. Manton, "Optimal training sequences and pilot tones for OFDM systems," IEEE Commun. Let., Vol. 5, No. 4, Apr. 2001, pp. 151-153.
- [15] S. Adireddy, L. Tong, and H. Viswanathan, "Optimal Placement of Training for Frequency-Selective Block-Fading Channels," IEEE Trans. Info. Theory, Vol. 48, No. 8, Aug. 2002, pp. 2338-2353.
- [16] M. Dong and L. Tong, "Optimal design and placement of pilot symbols for channel estimation," IEEE Trans. Signal Processing, Vol. 50, No. 12, Dec. 2002, pp. 3055-3069.

Theoretical Analysis for Energy Consumption of a Circulation-Type Superheated Steam Degreasing System Applied to Oily Metal Waste Recycling

Naoki Maruyama¹, Youhei Watanabe², Hiroaki Ito³, Masafumi Hirota⁴
^{1, 2, 3, 4}(Division of Mechanical Engineering, Graduate School of Engineering, Mie University, Japan
1577 Kurimamachiya-cho, Tsu, 514-8507, Mie, Japan)

Abstract: Recycled waste material has recently become of interest because of the huge amount of natural resource consumption worldwide. It is necessary to introduce a material recycle system in municipal and industrial waste management. Quality improvement of oily metal waste disposed from metalworking factories as recycling materials is one of the issues. Here, the degreasing system plays an important role. In this paper, energy consumption of a circulation-type superheated steam degreasing system was applied to oily metal waste disposed from a metalworking factory. This system was compared to a once-through type superheated steam degreasing system. Flow rates of materials applicable to the degreasing system were estimated based on preliminary experiments, and heat and energy balances from the system were theoretically evaluated and compared between once-through and circulation type systems. As a result, a circulation-type superheated steam waste degreasing system that can process oily metal waste provides a promising energy-saving waste metal recycle system.

Keywords: Circulation, Degreasing, Energy balance, Material recycle, Once-through, Superheated steam

I. INTRODUCTION

An increase in the world's population and an improvement in quality of human life cause natural resource depletion. Fossil fuel depletion has been of particular interest globally. However, material resource depletion has also become a serious issue. Generally, oily metal waste disposed from metalworking factories is melted directly by an electric steelmaking furnace or blast furnace, and recycled as low grade material, which includes impurities. Some removable methods, such as centrifugal separation or chemical dissolution, are introduced to remove oil from metal waste. A centrifugal separation method can not remove oil well enough from metal because metal waste has a complex shape. Oil gathering in a recess remains on a metal waste. On the other hand, if oil is removed with chemicals, the oil dissolves into a chemical substance and becomes difficult to separate from the chemical agent. In addition, it is also difficult to dispose of liquid waste that includes a chemical substance into the surroundings from an environmentally-conscious standpoint.

Superheated steam has been a very popular heat source for industrial and municipal applications, such as air conditioning and boilers. In particular, most of the electric power supply is generated by using superheated steam turbine systems in a power plant. Superheated steam is a gas generated by heating saturated steam until it exceeds the boiling point [1, 2]. For industrial application, the superheated steam is applied to drying several kinds of materials, like wood, coffee beans, vegetables, and waste materials, based on special characteristics such as inactive gas and condensation heat transfer [3-5]. A drying system using superheated steam plays an important role in high-moisture material drying procedures due to the steam's high thermal efficiency. This kind of steam creates several advantages, such as inactive gas and high specific enthalpy, for material processing systems. Accordingly, the system using superheated steam has been very useful in waste processing [6-8]. The superheated steam was introduced to improve the quality of metal waste disposed from metalworking factories as recycling materials [9-11]. The superheated steam evaporates waste oil and removes it from the metal. Nonetheless, in order to obtain a superheated steam, a large amount of latent heat for water evaporation is required. Generally, superheated steam is condensed after it passes through a processing section where the latent heat is exhausted into the surroundings, resulting in low thermal efficiency. In this paper, a practical circulation-type superheated steam degreasing system is proposed for oily metal waste recycling disposed from metalworking factories, and the system's energy consumptions are theoretically evaluated and compared to the results from a once-through type system.

II. CHARACTERISTICS OF SUPERHEATED STEAM FOR AN INDUSTRIAL APPLICATION

Superheated steam is an atmospheric vapor heated until it reaches 100 °C or higher. Generally, superheated steam is available in a higher efficiency at around 170 °C or more for an industrial application compared to the efficiency of hot air at the same temperature. This temperature is called the inversion temperature [12, 13]. The superheated steam can heat the materials by convection, radiation and condensation heat transfers, as shown in Fig. 1. The condensation heat transfer is a special feature of superheated steam heat transfer, especially for moisture materials, in which hot air heat transfer cannot be encouraged. When the material's surface temperature, which will be processed, is lower than 100 °C, superheated steam can push large amounts of condensation heat into the material and the steam contains several prominent advantages, especially for waste processing, since the gas is an inactive gas. When the processing chamber is filled with the superheated steam, a chemical reaction, such as ignition, can be prevented since the steam does not contain O₂. Hence, fires or explosions cannot take place in the processing apparatus, and safety in the waste processing is finally ensured. Similarly, this gas also presents useful features for waste disposal, including sterilization, degreasing and deodorization.

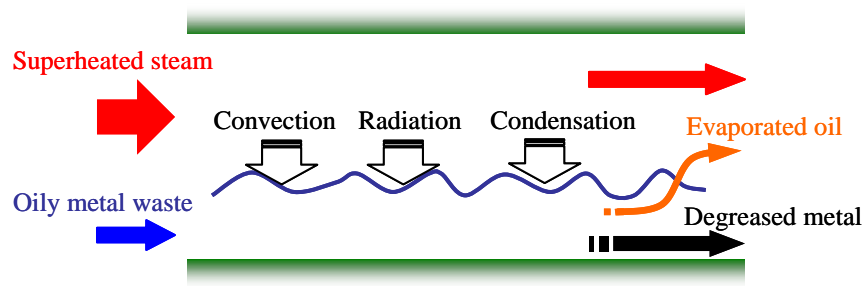


Fig. 1 Superheated steam and material flow in an open-type processing section applied to an oily metal degreasing system

III. THEORETICAL ANALYSIS FOR HEAT AND ENERGY BALANCE

3.1. System Configuration of Superheated Steam Degreasing System

Figure 2 shows an oily metal waste degreasing system using superheated steam. Once-through type and circulation-type degreasing systems are assumed, and their heat and energy consumptions are compared. First, air in the processing chamber is displaced by superheated steam, which comes from the superheated steam generator. Next, oily metal waste is transferred into a chamber, and is processed. At the low oxygen concentration field, even in the high temperature field, the oily metal does not ignite. While the superheated steam passes through the processing chamber, the oily metal is stirred with superheated steam by use of the rotary kiln. Here, the induction heating is applied to heat superheated steam and waste materials. Oil is evaporated and mixed with steam, and the gas flows out from the chamber. On the other hand, degreased metal is discharged from the chamber. After that, superheated steam with evaporated oil passes through a cyclone for dust extraction, and flows into an oil-steam separator. If the system is a once-through type, evaporated oil and steam are simultaneously condensed by a cooling unit at the oil-steam separator, and these substances are collected in a liquid state, as shown in Fig. 2(a). A blower is introduced in order to promote the system's gas flow.

In contrast, only the evaporated oil is condensed at an oil-steam separator, and steam passes through the separator at the superheated steam state in a circulation type system, as shown in Fig. 2(b). The steam is pressurized by a blower and heated by a super heater again. After that, the heated steam flows into the processing chamber, while the steam that comes from the generator is closed in a steady state condition. Finally, the superheated steam is circulated in the degreasing system.

Figure 3 shows a demonstration of the superheated steam degreasing system and an example of waste material. The theoretical estimation in this paper was applied to this system. The system is composed of the equipment shown in Fig. 2. The system configuration can be changed for a once-through or a circulation-type system only by operation valves. The ducts and equipment were coated with a thick layer of heat-insulation material. Typical temperatures in the system were measured by K-type thermocouples and recorded by a multi-channel data logger.

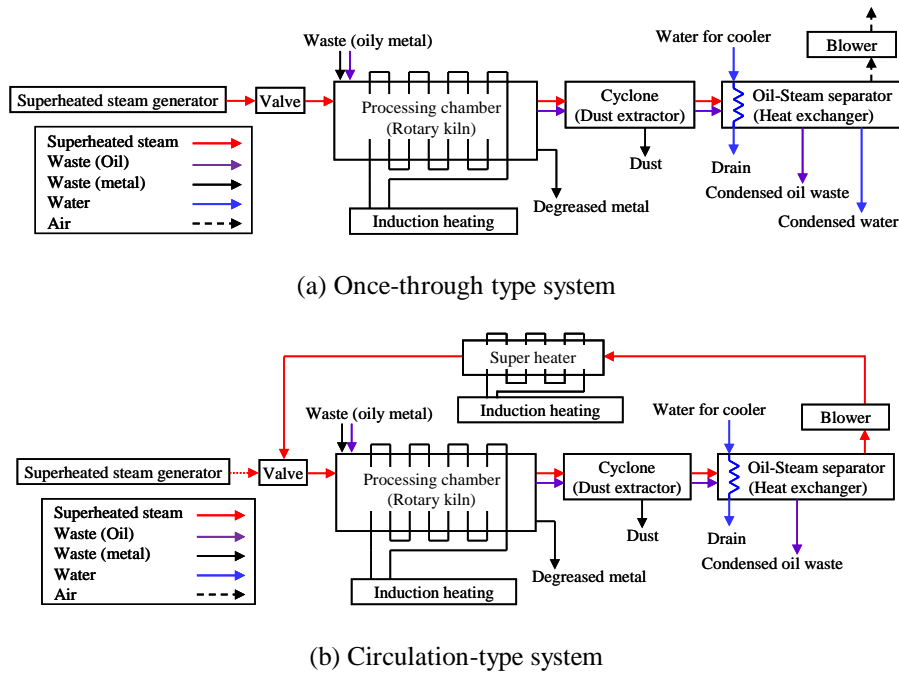


Fig. 2 System configuration of degreasing system using superheated steam

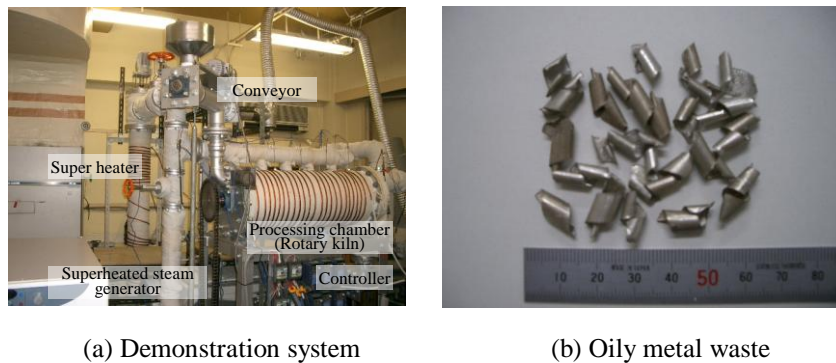


Fig. 3 Superheated steam degreasing demonstration system and example of waste material

3.2. Material Flow of Degreasing System

Material flow of this degreasing system was estimated based on the system shown in Fig. 2. Oily metal waste flowed into the processing chamber. The volume flow rate was assumed by defining 1/5 of the processing chamber capacity as filled by waste material, and the length of time for waste to pass through the processing chamber was assumed to be 10 minutes. The adhesion rate of oil was assumed to be 2.5 wt% of the metal waste. These assumptions were observed by a preliminary experiment. Oily metal waste was heated by the high temperature superheated steam and induction heating in the processing chamber. After processing, the degreased metal is discharged from the processing chamber, and superheated steam with evaporated oil flows out from the chamber. The volume flow rate of metal is $\dot{Q}_{v,m}$; thus, the mass flow rate becomes $\dot{m}_m = \rho_m \dot{Q}_{v,m}$. The mass flow rate of oil is assumed to be $\dot{m}_o = 0.025\dot{m}_m$ in this estimation.

3.3. Energy Balance of Degreasing System

The heat balance and energy consumption of the once-through type and the circulation-type systems are estimated based on Fig. 4. Electricity was supplied to each type of equipment in order to operate the system. However, the electric consumption of the main apparatus was taken into account in this estimation.

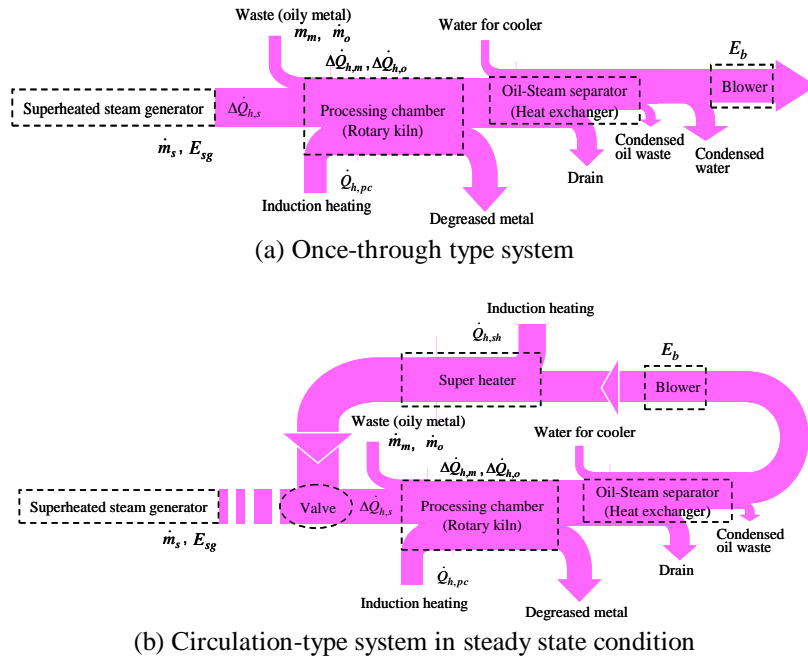


Fig. 4 Heat and energy balance of degreasing system using superheated steam

3.3.1. Once-through type system

The schematic heat and energy balance diagram of the once-through type system is presented in Fig. 4(a). Superheated steam enters the processing chamber in order to evaporate oil. Metal waste and oil temperatures at the processing chamber inlet and exit are $T_{m,1}$, $T_{o,1}$ and $T_{m,2}$, $T_{o,2}$, and the superheated steam temperature at the processing chamber inlet and exit are defined as $T_{s,1}$ and $T_{s,2}$, respectively. Oily metal waste must be heated to $T_{s,2}$ when it passes through a processing chamber. Therefore, heat added to the oily metal can be expressed as:

$$\Delta\dot{Q}_{h,m} = \dot{m}_m c_m (T_{m,2} - T_{m,1}) \quad (\text{for metal}) \quad (1)$$

$$\Delta\dot{Q}_{h,o} = \dot{m}_o \{c_o (T_{o,2} - T_{o,1}) + L_o\} \quad (\text{for oil}) \quad (2)$$

where, $T_{m,1} = T_{o,1}$ and $T_{m,2} = T_{o,2} = T_{s,2}$.

On the other hand, heat supplied by the superheated steam generator is consumed to increase the temperature of the oily metal waste as follows:

$$\Delta\dot{Q}_{h,s} = \dot{m}_s (h_{s,2} - h_{s,1}) \quad (3)$$

If $(\Delta\dot{Q}_{h,m} + \Delta\dot{Q}_{h,o}) < \Delta\dot{Q}_{h,s}$, oil is evaporated and separates from the metal waste. However, additional heat $\dot{Q}_{h,pc}$ needs to be supplied by induction heating in the processing chamber if $(\Delta\dot{Q}_{h,m} + \Delta\dot{Q}_{h,o}) > \Delta\dot{Q}_{h,s}$. Steam with evaporated oil will be cooled by additional water at a temperature below evaporation and condensed to a liquid state in the oil-steam separator. Condensed steam and oil are separated by using the specific gravity separation method. Generally, heat loss from the equipment must not be neglected in this system. The additional heat will be supplied by the heater to the equipment and ducts.

3.3.2. Circulation-type system

The schematic heat and energy balance of the circulation-type system is shown in Fig. 4(b). For the circulation-type system, energy flow after the processing chamber is different from the once-through type

system. After the waste materials pass through the processing chamber, the gas is cooled in the oil-steam separator. Only evaporated oil is condensed and steam remains in a superheated steam condition in the oil-steam separator. Following this, steam is pressurized by a blower and reheated by the super heater. The additional heat from the super heater is estimated as:

$$\dot{Q}_{h,sh} = \dot{m}_s (h_{s,4} - h_{s,3}) \quad (4)$$

If the steam temperature is increased by the super heater upon the inlet temperature $T_{s,1}$, high enthalpy steam can perform the oily metal waste processing. The steam flow rate is kept constant by using a high pressure blower, and the steam circulates without a superheated steam generator in a steady state condition, as shown in Fig. 4(b).

IV. APPLICATION FOR DEMONSTRATION SYSTEM

The heat and energy flow described in Fig. 4 will be applied to the demonstration system to establish an energy balance. The theoretical conditions of the energy balance analysis are shown in Table 1. The size of the processing chamber in this system was 0.30 dia. \times 1.0 m in length. Hence, the optimum volume and mass flow rates of metal are estimated as $\dot{Q}_{v,m} = 2.4 \times 10^{-5} \text{ m}^3/\text{s}$ and $\dot{m}_m = 7.0 \times 10^{-3} \text{ kg/s}$, respectively. Here, the density of a waste metal is measured as $\rho_m = 2.9 \times 10^2 \text{ kg/m}^3$ by a preliminary experiment. In this case, the mass flow rate of oil is $\dot{m}_o = 1.7 \times 10^{-4} \text{ kg/s}$, which corresponds to 2.5 wt% of the metal flow rate.

Table 1 Theoretical conditions of energy balance analysis based on preliminary experimental results

Temperature		
Metal and oil at the processing chamber inlet	$T_{m,1}, T_{o,1}$	15 °C
Superheated steam at the processing chamber inlet	$T_{s,1}$	400 °C
Metal, oil and superheated steam at the processing chamber exit	$T_{m,2}, T_{o,2}, T_{s,2}$	250 °C
Superheated steam at the super heater inlet	$T_{s,3}$	150 °C
Superheated steam at the super heater exit	$T_{s,4}$	400 °C
Enthalpy of superheated steam		
at the processing chamber inlet at 0.1 MPa, $T_{s,1}$	$h_{s,1}$	3.28 MJ/kg
at the processing chamber exit at 0.1 MPa, $T_{s,2}$	$h_{s,2}$	2.97 MJ/kg
at the super heater inlet at 0.1 MPa, $T_{s,3}$	$h_{s,3}$	2.78 MJ/kg
at the super heater exit at 0.1 MPa, $T_{s,4}$	$h_{s,4}$	3.28 MJ/kg
Mass flow rate		
Superheated steam	\dot{m}_s	$1.25 \times 10^{-3} \text{ kg/s}$
Metal	\dot{m}_m	$7.0 \times 10^{-3} \text{ kg/s}$
Oil	\dot{m}_o	$1.7 \times 10^{-4} \text{ kg/s}$
Specific heat		
Metal (Aluminum)	c_m	0.9 kJ/(kg·K)
Oil (cutting oil)	c_o	2.1 kJ/(kg·K)
Evaporative latent heat of oil	L_o	320 kJ/(kg·K)

For the once-through type system, the energy balance is estimated based on Fig. 4(a). The evaporation temperature of the cutting oil has an observation range between 150 - 250 °C. The exit temperature of material from the processing chamber is assumed to be $T_{m,2} = T_{o,2} = 250 \text{ °C}$. The initial temperature of the material and the evaporation temperature of oil are assumed to be 15 °C and less than 250 °C, respectively. The heat required to heat waste material is estimated as:

For metal:

$$\begin{aligned} \Delta \dot{Q}_{h,m} &= \dot{m}_m c_m (T_{m,2} - T_{m,1}) \\ &= 7.0 \times 10^{-3} \times 0.90 \times 10^3 \times (250 - 15) = 1,480 \text{ W} \end{aligned} \quad (5)$$

For oil:

$$\Delta \dot{Q}_{h,o} = \dot{m}_o \{c_o (T_{o,2} - T_{o,1}) + L_o\}$$

$$= 1.7 \times 10^{-4} \times \{2.1 \times 10^3 \times (250-15) + 320 \times 10^3\} = 140 \text{ W} \quad (6)$$

Therefore, it is estimated for the waste material as:

$$\Delta \dot{Q}_{h,w} = 1,480 + 140 = 1,620 \text{ W} \quad (7)$$

The superheated steam generator employed in this demonstration system can produce 4.5 kg/h of steam at 450 °C, 0.3 MPa, and its electric consumption is $E_{sg} = 5.0$ kW. Heat required to heat the waste material is supplied by the superheated steam generated by the superheated steam generator, $\Delta \dot{Q}_{h,s}$, and the induction heating through the processing chamber, $\dot{Q}_{h,pc}$. Heat supplied by superheated steam is estimated as:

$$\begin{aligned} \Delta \dot{Q}_{h,s} &= -\dot{m}_s (h_{s,2} - h_{s,1}) \\ &= -1.25 \times 10^{-3} \times \{2.97 \times 10^6 - 3.28 \times 10^6\} = 390 \text{ W} \end{aligned} \quad (8)$$

It was found that only 390 W is available to heat waste material, even if the superheated steam generator consumes 5.0 kW. Residual energy, 4.6 kW, is exhausted and the superheated steam generator is inflected to replace air with steam inside a processing system. Therefore,

$$\begin{aligned} \dot{Q}_{h,pc} &= \Delta \dot{Q}_{h,w} - \Delta \dot{Q}_{h,s} \\ &= 1,620 - 390 = 1,230 \text{ W} \end{aligned} \quad (9)$$

has to be supplied by induction heating through the processing chamber. The inverter and conversion efficiency of induction heating are assumed to be 0.95 and 0.60 respectively. Electric consumption of the induction heating is estimated as:

$$E_{pc} = \frac{\dot{Q}_{h,pc}}{\eta_i \eta_c} = 2,160 \text{ W} \quad (10)$$

In addition, a blower is employed for the system. The electric consumption of the blower is measured by a preliminary experiment. The demonstration system employs a 750 W high pressure blower. The measured electric consumption of the blower is:

$$E_b = 600 \text{ W} \quad (11)$$

Consequently, the total energy consumption of the once-through type, E_{ot} , is estimated as:

$$\begin{aligned} E_{ot} &= E_{sg} + E_{pc} + E_b \\ &= 5.0 + 2.2 + 0.6 = 7.8 \text{ kW} \end{aligned} \quad (12)$$

$$e_{ot} = \frac{E_{ot}}{\dot{m}_m + \dot{m}_o} = 1.1 \text{ MJ/kg} \quad (13)$$

For the circulation-type degreasing system at a steady state condition, only energy consumed in a circulation area is estimated in Fig. 4(b). The required heat to increase the temperature of waste material was determined earlier using Eq. (7). The circulation-type system also supplies heat to the processing chamber by induction heating. Here, the steam mass flow rate is assumed to be the same as that of the once-through type system. The discharged steam with evaporated oil from the processing chamber is cooled in the oil-steam separator. Gas is cooled at a temperature between that of water evaporation and under that of oil condensation. The condensing temperature of oil is assumed to be 150 °C in this estimation. Steam remains as superheated steam at 150 °C. Therefore, the discharged steam from the oil-steam separator is superheated by the super heater. The required heat and electric consumption are estimated as:

$$\begin{aligned}\dot{Q}_{h,sh} &= \dot{m}_s(h_{s,4} - h_{s,3}) \\ &= 1.25 \times 10^{-3} \times (3.28 \times 10^6 - 2.78 \times 10^6) = 625 \text{ W}\end{aligned}\quad (14)$$

$$E_{sh} = \frac{\dot{Q}_{h,sh}}{\eta_i \eta_c} = 1.1 \text{ kW}\quad (15)$$

As a result, the total energy consumption of the circulation type, E_{ci} , is estimated as:

$$\begin{aligned}E_{ci} &= E_{pc} + E_{sh} + E_b \\ &= 2.2 + 1.1 + 0.6 = 3.9 \text{ kW}\end{aligned}\quad (16)$$

$$e_{ci} = \frac{E_{ci}}{\dot{m}_m + \dot{m}_o} = 0.54 \text{ MJ/kg}\quad (17)$$

The energy consumption estimated from the circulation-type superheated steam degreasing system is smaller than the amount of the once-through type system.

It was also found that heat loss from the circulation-type system increases compares to the once-through type system because the path length of steam becomes longer. These results were obtained based on the main equipment of these systems. Therefore, additional energy, such as a duct heater or rotary kiln operation, should be added for each of the estimations. However, these results show the advantages of introducing a circulation-type decreasing system.

V. CONCLUSION

Energy consumption of the circulation-type superheated steam degreasing system is compared with the results of the once-through type system. Both system configurations are assumed and the heat and energy balance are estimated. The prototype processing system was constructed and the energy consumption with a heat balance was estimated. For the superheated steam processing system, the once-through type system consumes a sufficient amount of energy compared to the circulation-type system because the latent heat of water is higher than the electric consumption of additional equipment for the circulation-type system. As a result, the circulation-type superheated steam oily metal waste degreasing system serves as an adequate system for industrial application.

Acknowledgements

This work was supported in part by JSPS KAKENHI Grant Number 23560228.

NOMENCLATURE

c :	Specific heat at a constant pressure [J/(kg · K)]
E :	Electric consumption [W]
e :	Specific electric consumption [J/kg]
h :	Specific enthalpy [J/kg]
L :	Latent heat [J/kg]
\dot{m} :	Mass flow rate [kg/s]
\dot{Q}_h :	Heat [W]
\dot{Q}_v :	Volume flow rate [m ³ /s]
T :	Temperature [°C]
η :	Efficiency [-]
ρ :	Density [kg/m ³]

Subscripts

- 1: processing chamber inlet
- 2: processing chamber exit
- 3: super heater inlet

4: super heater exit
b: blower
c: work coil
ci: circulation type
i: inverter
m: waste metal
o: waste oil
ot: once-through type
pc: processing chamber
s: steam
sg: superheated steam generator
sh: super heater
w: waste material

REFERENCES

- [1] A. M. Lane and S. Stern, Application of Superheated-Vapor Atmospheres to Drying, *Mechanical Engineering*, 78, 1956, 423-426.
- [2] Y. Tatemoto, Y. Bando, K. Oyama, K. Yasuda, M. Nakamura, Y. Sugimura and M. Shibata, Effects of Operational Conditions on Drying Characteristics in Closed Superheated Steam Drying, *Drying Technology*, 19(7), 2001, 1287-1303.
- [3] A. S. Mujumdar, Superheated Steam Drying, in A. S. Mujumdar (Ed.), *Handbook of Industrial Drying*, (2nd Ed.), 35 (New York: Marcel Dekker, 1995) 1071-1086.
- [4] H. Shibata, and A. S. Mujumdar, Steam Drying Technologies: Japanese R & D, *Drying Technology*, 12(6), 1994, 1485-1524.
- [5] T. Kudra and A. S. Mujumdar, Special Drying Techniques and Novel Dryers, *Handbook of Industrial Drying*, (2nd Ed.), 36 (New York: Marcel Dekker, 1995) 1087-1149.
- [6] N. Maruyama, Y. Ichihashi and D. Tanaka, Material Resource Recycle System from High Water Content Waste to Solid Fuel using Superheated Vapor, Proc. of 5th International Energy Conversion Engineering Conference (IECEC2007), Paper No. AIAA 2007-4785, CD-ROM, 2007, 1-8.
- [7] N. Maruyama, D. Tanaka, N. Kanamori and T. Shimizu, Environmental Assessment of Re-fuel System to Process High Water Content Waste to Solid Fuel using Superheated Steam, Proc. of 6th International Energy Conversion Engineering Conference (IECEC2008), Paper No. AIAA-2008-5677, CD-ROM, 2008, 1-11.
- [8] N. Maruyama, D. Tanaka, M. Tamada, T. Shimizu, and M. Hirota, Waste Recycle using Superheated Steam and Its Environmental Evaluation, Proc. of 7th International Energy Conversion Engineering Conference (IECEC2009), Paper No. AIAA-2009-4638, CD-ROM, 2009, 1-11.
- [9] N. Maruyama, Y. Watanabe, H. Ito, Y. Achawangkul and M. Hirota, Theoretical Analysis for Energy Balance of Material Recycle using Circulation Type Superheated Steam Evaporation System, Proc. of the Fifth International Conference on Science, Technology and Innovation for Sustainable Well-Being (STISWB V), Paper No. MME23, CD-ROM, 2013, 1-6.
- [10] N. Maruyama, Y. Watanabe, H. Ito, Y. Achawangkul and M. Hirota, Theoretical Analysis for Energy Balance of Circulation-type Superheated Steam Degreasing System, Proc. of International Symposium on EcoTopia Science (ISETS'13), Paper No. P-5-20, CD-ROM, 2013, 1.
- [11] N. Maruyama, Y. Watanabe, H. Ito, Y. Achawangkul and M. Hirota, Oily Waste Metal Recycle using Circulation-type Superheated Steam Degreasing System, International Conference and Utility Exhibition on Green Energy for Sustainable Development (ICUE 2014), CD-ROM, 2014, 1-7.
- [12] T. Yoshida and T. Hyodo, Evaporation of Water in Air, Humid Air, and Superheated Steam, *Industrial & Engineering Chemistry Process Design and Development*, 9(2), 1970, 207-214.
- [13] M. Haji and L. C. Chow, Experimental Measurement of Water Evaporation Rates into Air and Superheated Steam, *Transactions of the American Society of Mechanical Engineers, Journal of Heat Transfer*, 110, 1988, 237-242.

Material Optimization of Leaf Spring of Tractor Trolley by FEA

Narendra Yadav¹, Mr. Praveen Tandon² Mr. S.A.K. Jilani³

^{1, 2, 3}(M E Scholar, Associate Professor, Associate Professor, Department of Mechanical Engineering, RCET, Bhilai-India)

Abstract: Leaf Spring (LS) is an indispensable machine element of the automobile sector. In this particular work we are analyzed a LS with the help of Finite Element Method when subjected to static loads and appropriate boundary conditions. The LS taken into consideration is that of a Tractor Trolley having a Gross Vehicle Weight of 20 ton. According to the existing dimension of simple leaf spring it has modeled in solid works 2013. after that cad model has used to discretized in to small no of element and nodes to perform the required finite element analysis. Initially analysis has done for three different materials and taken the most economic and suitable material for leaf spring in the optimization stages. Comparison of material was perform on the basis of result obtained from the analysis of leaf spring like von mises stress, strain and deflection.

Keywords: leaf spring (LS), Finite Element Analysis (FEA), Camber, Leaf Span, Static loading, Computer Aided Engineering (CAE)

I. Introduction

Leaf springs are crucial suspension elements used on light passenger vehicle, mini loader and truck necessary to minimize the vertical vibrations impacts and bumps due to road irregularities and to create a comfortable ride. Leaf springs are widely used for automobile and rail road suspensions. The leaf spring should absorb the vertical vibrations and impacts due to road irregularities by means of variations in the spring deflection so that the potential energy is stored in spring as strain energy and then released slowly so increasing the energy storage capabilities of a leaf spring and ensures a more compliant suspension system. Three dimensional finite element analysis of the leaf spring consists of a computer model or design that is stressed and analyzed for specific results.

The leaf spring is analyzed for static strength and deflection using 3D finite element analysis. The general purpose finite element analysis software ANSYS is used for present study. The variation of bending stress and displacement values are predicted. With the Indian market becoming global and advent of multinationals in the market, a cut throat competition has a rise between the Indian companies and the Multinational company .thus to remain in the contest it has become necessary for the Indian industries to improve and innovate their product.

II. Material

The existing material of tractor trolley leaf spring is 50Cr1V23 and we had applied three different materials for analysis of leaf spring like 55Si2Mn90, 38Si6 and 50Cr1. The material used for the experimental work is 55Si2Mn90.

Tab.1 Parameters of the steel leaf spring

Material options	Material	Input Properties	
	Spring Steel	Tensile Yield Strength (MPa)	Ultimate Tensile Strength (M6Pa)
Existing	50Cr1V23	1800	2050
Option 1	50Cr1	1650	1950
Option 2	38Si6	1050	1300
Option 3	55Si2Mn90	1800	1950

III. Three Dimensional Solid Model

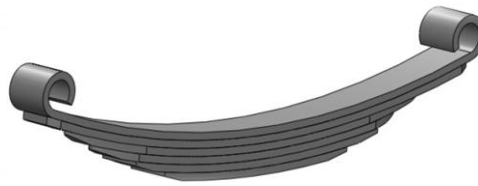


Fig. 1: Three Dimensional CAD Model

IV. Finite Element Analysis

Analysis of leaf spring is done by Finite Element Method in software ANSYS Workbench. Finite element method (FEM) is a numerical method for solving a differential or integral equation. It has been applied to a number of physical problems, where the governing differential equations are available. The method essentially consists of assuming the piecewise continuous function for the solution and obtaining the parameters of the functions in a manner that reduces the error in the solution. In this article, a brief introduction to finite element method is provided. The method is illustrated with the help of the plane stress and plane strain formulation

The first phase for applying the method of Finite Elements is Meshing or Discretization. Meshing is basically the process of breaking the CAD model into very small elements. It is also known as piecewise approximation. Meshing are of different types, it may be comprising of 1D, 2D or 3D elements. In present case selected is shown in Table-2

Mesh			Element type	
S.N.	Entity	Size	Connectivity	Statistics
1	Nodes	9201	Connectivity	Statistics
2	Elements	4185	TE10	4185 (100%)

V. Results from FEA

The following result we obtained by applying FEA on the leaf spring assembly.

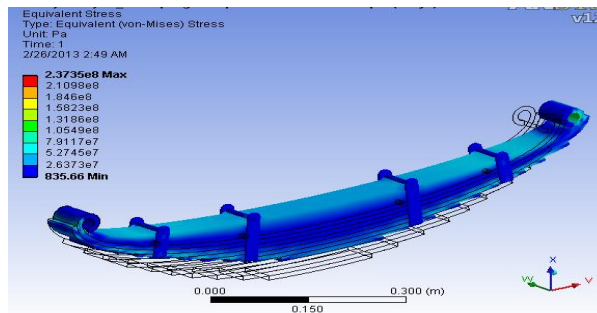


Fig. 2 Stress Analysis (Material-50Cr1V23)

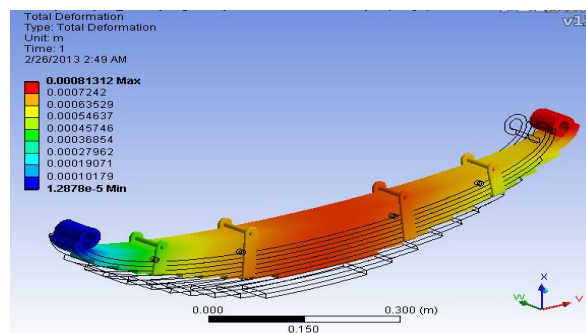


Fig 3 Deflection Analysis (Material-50Cr1V23)

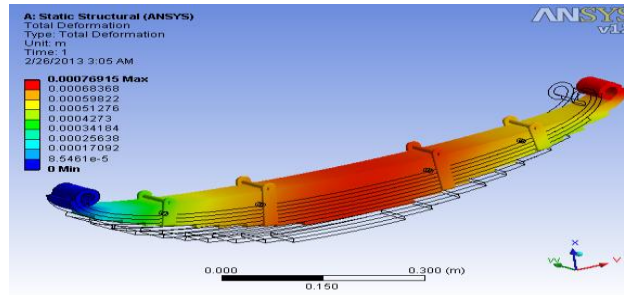


Fig 4 Deflection Analysis (Material-38Si6)

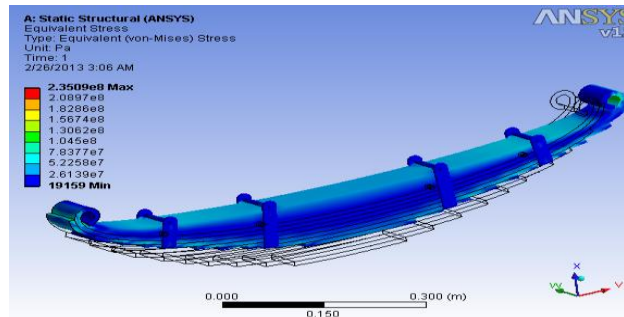


Fig 5 Stress Analysis (Material-38Si6)

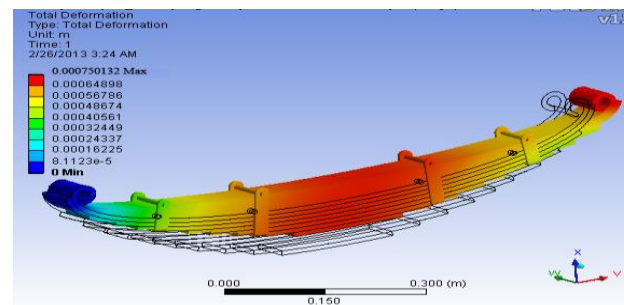


Fig 6 Deflection Analysis (Material-50Cr1)

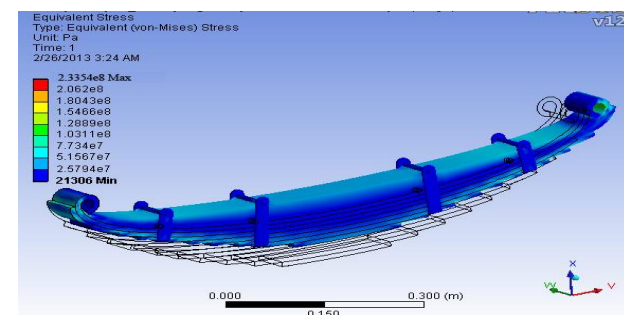


Fig 7 Stress Analysis (Material-50Cr1)

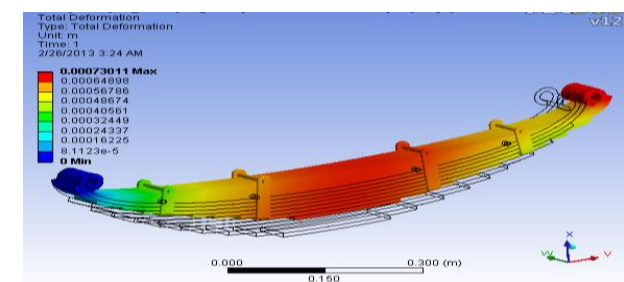


Fig 8 Deflection Analysis (Material-55Si2Mn90)

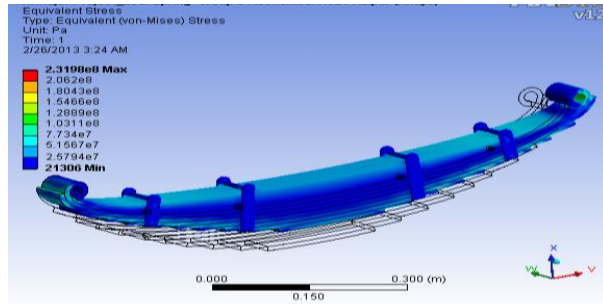


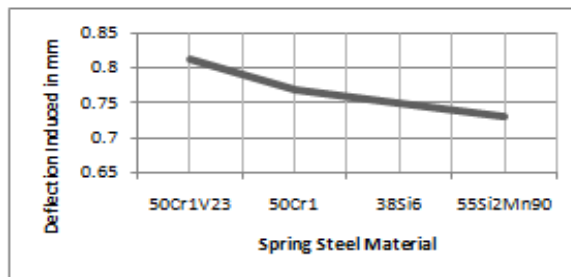
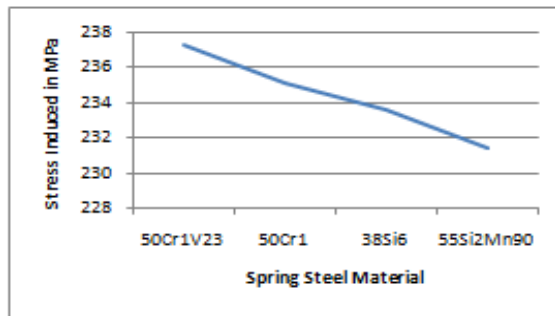
Fig 9 Stress Analysis (Material-55Si2Mn90)

After the analysis of leaf spring gives the above result for different materials.

Material options	Material	Input Properties		Analysis Result	
	Spring Steel	TYS (MPa)	UTS (MPa)	Stress (MPa)	Deflection mm
Existing	50Cr1V23	1800	2050	237.30	0.81312
option 1	50Cr1	1650	1950	235.09	0.76915
option 2	38Si6	1050	1300	233.54	0.75010
option 3	55Si2Mn90	1800	1950	231.38	0.73011

VI. Conclusion

As per the result obtained from Finite Element Analysis in ANSYS we found that leaf spring provides good performance when it is made up of Spring Steel 55Si2Mn90 the results are-



In this work the main focus was to create a method wherein the load carrying capacity of leaf spring can be computed, and in this context FEA turned out to be very effective. The work elucidated is completely devoted to the conglomeration of Mechanical Engineering Design & Computer Aided Engineering.

REFERENCES

- [1] Dewangan Ritesh, Patnaik Manas and Yadav Narendra.” Minimization of Stress of a Parabolic Leaf Spring by Simulated Annealing Algorithm”, International Journal of Engineering Research and Applications (IJERA), Vol. 2, Issue 4, July-August 2012, pp.457-460.
- [2] Patnaik Manas Dewangan Ritesh and Yadav Narendra.”, “Estimation of Maximum Load Carrying Capacity of a Parabolic Leaf Spring by Design of Experiments” International Journal of Engineering Research and Applications (IJERA), Vol. 2, Issue 4, July-August 2012
- [3] Gulur Siddaramanna Shiva Shankar, Sambagam Vijayarangan, “Mono Composite Leaf Spring for Light Weight Vehicle Design, End Joint Analysis and Testing”, J. of Materials Science, Vol. 12, pp. 220-225, Issue 3, 2006.
- [4] Patnaik Manas, Yadav Narendra, Dewangan Ritesh,” Study of a Parabolic Leaf Spring by Finite Element Method & Design of Experiments”, International Journal of Modern Engineering Research (IJMER), Vol.2, Issue 4, July-Aug 2012 pp-1920-1922.
- [5] G. Wagle Sachin, Satish S. Oesai, Wadkar S. B., “Optimized Design & Analysis of Parabolic Leaf Spring Considering Braking, Cornering & Bump loads”, National Conference of computational methods in Mechanical Engineering, pp. 47-52 , September 2005.
- [6] Kanbolat Ahmet , Murathan Soner, Mustafa Karaagaç, Tolga Erdogus, “Parabolic Leaf Spring Optimization and Fatigue Strength Evaluation on The Base of Road Load Data, Endurance Rig Tests and Non Linear Finite Element Analysis”, SAE International, 2011
- [7] Kumar Krishan and Aggarwal M.L. “A Finite Element Approach for Analysis of a Multi Leaf Spring using CAE Tools”, Research Journal of Recent Sciences, Vol. 1, pp. 92-96, December 2012.
- [8] Yadav Narendra, Dewangan Ritesh, Patnaik Manas,” Minimization Of Stress In A Parabolic Leaf Spring By Local Algorithm For Constant & Priorities, International Journal of Engineering Research and Applications (IJERA), Vol. 2, Issue4, July-August 2012, pp.1897-1899.
- [9] Dhoshi N.P., Ingole N.K., Gulhane U.D., “Analysis and Modification of Leaf Spring of Tractor Trailer Using Analytical and Finite Element Method”, International Journal of Modern Engineering Research, Vol. 1, pp. 719-722, Issue 2, December 2012.
- [10] Kothari Dakshraj, Sahu Rajendra and Satankar Rajesh, “Comparison of Performance of Two Leaf Spring Steels Used For Light Passenger Vehicle”, International Journal of Mechanical, Automobile & Production Engineering, Vol. 2, pp. 9-16, Issue 1, 2012.
- [11] Kumar Krishan, Aggarwal M.L, “Computer Aided FEA Comparison of Mono Steel And Mono GRP Leaf Spring”, International Journal of Advanced Engineering Research and Studies, Vol. 1, pp. 155-158, Issue 2, January-March, 2012.
- [12] Clarke C.K. and Borowski G.E., “Evaluation of a Leaf Spring Failure”, Journal of Failure Analysis and Prevention, Vol. 5, pp. 54-63, Issue 6, December 2005.
- [13] Jadhav K.K. and Dalu R.S., “Experimental Investigation & Numerical Analysis of Composite Leaf Spring”, International Journal of Engineering Science and Technology, Vol. 3, pp. 4759-4764, Issue 6, June 2012.
- [14] Arora Vinkel, Bhushan Gian and Aggarwal M.L., “Eye Design Analysis of Single Leaf Spring In Automotive Vehicles Using CAE Tools”, International Journal of Applied Engineering and Technology, Vol. 1, pp. 88-97, Issue 1, October-December, 2011.
- [15] Douglas C. Montgomery, Design & Analysis of Experiments, JOHN WILEY & SONS INC, 5th Edition, 2001, pp 8-19.
- [16] Jiju Antony, Design of Experiments for Scientists & Engineers, Elsevier Science & Technology Books, 1st Edition, 2003, pp 6-24.
- [17] G.R. Liu & S.S. Quek, The Finite Element Method, Butterworth-Heinemann (Imprint of Elsevier Science), 1st Edition, 2003, pp 3-65.
- [18] Klaus-Jurgen Bathe, Finite Element Procedures, Prentice Hall, 1st Edition, 1996, pp 78-96.

A CONTROL APPROACH FOR GRID INTERFACING INVERTER IN 3 PHASE 4 WIRE DISTRIBUTION SYSTEM WITH POWER-QUALITY IMPROVEMENT FEATURES

Remya.A.V¹, Rinku Scaria²

^{1,2}(M.Tech Student, Assistant professor ,Department of Electrical and Electronics Engineering, Federal Institute of Science and Technology (FISAT), MG University, Kerala, India)

Abstract: With the increase in load demand, the Renewable Energy Sources (RES) are increasingly connected in the distribution systems which utilizes power electronic Converters/Inverters. Nowadays, 3-phase 4-wire distribution power system has been widely used in residential and office buildings, manufacturing facilities, schools etc This paper presents a novel control strategy for achieving maximum benefits from the grid-interfacing inverters when installed in 3-phase 4-wire distribution systems. The inverter can thus be utilized as: 1) power converter to inject power to the grid, and 2) shunt APF to compensate current unbalance, load current harmonics and load neutral current. All of these functions may be accomplished either individually or simultaneously. This new control concept is demonstrated with extensive MATLAB/Simulink simulation studies

Keywords: Active power filter (APF), distributed generation (DG), grid interconnection, power quality(PQ),renewable energy

I. INTRODUCTION

Due to increasing air pollution, global warming concerns, diminishing fossil fuels and their increasing cost have made it necessary to look towards Renewable Energy Sources (RES) as a future energy solution. Since the past decade, there has been an enormous interest in many countries on renewable energy for power generation since the past decade, there has been an enormous interest in many countries on renewable energy for power generation. However, the extensive use of power electronics based equipment and non-linear loads at PCC generate harmonic currents, which may deteriorate the quality of power. The widespread increase of non-linear loads nowadays, significant amounts of harmonic currents are being injected in to power systems.

The utility is concerned due to the high penetration level of intermittent RES in distribution systems as it may pose a threat to network in terms of stability, voltage regulation and power-quality (PQ) issues. Therefore, the DG systems are required to comply with strict technical and regulatory frameworks to ensure safe, reliable and efficient operation of overall network. In [8] Power quality problems associated with distributed power (DP) inverters, implemented in large numbers onto the same distribution network, are investigated. The general objective is to investigate the power quality problems and the interaction of the inverters with the distribution network. However, the extensive use of power electronics based equipment and non-linear loads at PCC generate harmonic currents, which may deteriorate the quality of power

Generally, current controlled voltage source inverters are used to interface the intermittent RES in distributed system. Recently, a few control strategies for grid connected inverters incorporating PQ solution have been proposed. In [11], a control method is presented which enables equal sharing of linear and nonlinear loads in three-phase power converters connected in parallel, without communication between the converters. But the exact calculation of network inductance in real-time is difficult and may deteriorate the control performance

The loads based on power electronic devices generally pollute the nearby network by drawing non sinusoidal currents from the source. The rapid switching of electronic devices creates additional problems. This makes voltages and currents at point of common coupling (PCC) highly distorted. One of the best solutions to compensate both current and voltage related problems, simultaneously, is the use of Unified Power Quality Conditioner (UPQC). Reference [6] is based on a unified approach for load and source compensation using Unified Power Quality Conditioner (UPQC).Performance of this UPQC has been evaluated with a typical industrial load with realistic parameters supplied by a polluted distribution network.

Usually, the fuel cell and photovoltaic energy sources generate power at variable low dc voltage, while the variable speed wind turbines generate power at variable ac voltage. Thus, the power generated from these renewable sources needs power conditioning (i.e., dc/dc or ac/dc) before connecting on dc-link [3]–[5]. In [3] an overview of the structures for the DPGS based on fuel cell, photovoltaic, and wind turbines are presented. In addition, control structures of the grid-side converter are presented, and the possibility of compensation for low-order harmonics is also discussed. In [5], the behavior of grid-coupled DG units during voltage dips in low voltage distribution grids will be investigated. The impact of DG units on the retained grid voltage (the lowest rms voltage during the event) is strongly dependent on the voltage level, and thus the grid impedance, of the concerned grid. This will focus on small-scaled DG units connected to the low voltage distribution grid.

In [4] new trends in power-electronic technology for the integration of renewable energy sources and energy-storage systems are presented. This describes the current technology and future trends in variable-speed wind turbines and also present power-conditioning systems used in grid-connected photovoltaic (PV) generation plants. The continuously decreasing prices for the PV modules lead to the increasing importance of cost reduction of the specific PV converters. Energy storage in an electricity generation and supply system enables the decoupling of electricity generation from demand

In this paper, a approach in which a shunt active filter acts as active conductance to damp out the harmonics in distribution network is performed. It is shown that the grid-interfacing inverter can effectively be utilized to perform following important functions: 1) transfer of active power harvested from the renewable resources 2) current harmonics compensation at PCC; and 3) current unbalance and neutral current compensation in case of 3-phase 4-wire system. The PQ constraints at the PCC can therefore be strictly maintained within the utility standards without additional hardware cost.

II. SYSTEM MODELING

The proposed system consists of RES connected to the dc-link of a grid-interfacing inverter as shown in Fig. 1. This topology has proved better controllability than the classical three-leg four-wire. The RES may be a DC source or an AC source with rectifier coupled to dc-link. The dc-link capacitor decouples the dc source from grid and also allows independent control of converters on either side of dc-link. The voltage source inverter is a key element of a DG system as it interfaces the source to the grid and delivers the generated power.

Active power filters are power electronic devices that cancel out unwanted harmonic currents by injecting a compensation current which cancels harmonics from the nonlinear harmonics is achieved with the voltage source inverter in the current controlled mode and an interfacing filter. Shunt active power filters compensate load current harmonics by injecting equal-but opposite harmonic compensating current. Generally, four-wire APFs have been conceived using four leg converters loads. The current wave form for canceling the PQ constraints at the PCC can be strictly maintained within the utility standards without additional hardware cost. The desired current waveform is obtained by accurately controlling the switching of the insulated gate bipolar transistors (IGBT's) in the inverter. The driving voltage across the interfacing inductance determines the maximum di/dt that can be achieved by the filter .A large inductor is better for isolation from the power system and protection from transient disturbances. However, the larger inductor limits the ability of the active filter to cancel higher order harmonics.

2.1 DC Link Capacitor

The dc-capacitor decouples the source from grid and also allows independent control of converters on either side of dc-link. Here the DC link is connected between a constant DC source and three phase 4 leg grid interfacing inverter. The switching network on the output side generates very large transients at the switching frequency. The Ripple effects the life and reduces the energy in the DC source (Battery, Fuel Cell).The capacitor provides a low impedance path for harmonics/transients (ripple).The DC link capacitor helps to keep these transients from radiating back to the input.

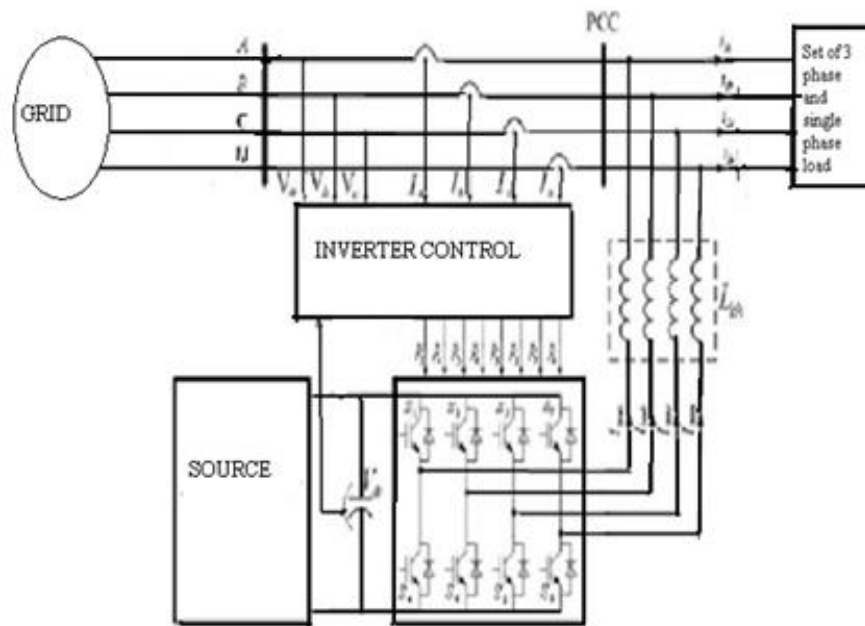


Fig.1. Schematic of renewable based distributed generation system.

2.2 Voltage Source Converter (VSC)

The voltage source inverter is a key element of a DG system as it interfaces the source to the grid and delivers the generated power. In this a 3 three phase 4 leg voltage source converter is used. The fourth leg of inverter is used to compensate the neutral current of load. If the output voltage of the VSC is greater than AC bus terminal voltages, is said to be in capacitive mode. So, it will compensate the reactive power through AC system. The type of power switch used is an IGBT in anti-parallel with a diode. The three phase four leg VSI is modeled in Simulink by using IGBT.

2.3 L filter

The output filter reduces the harmonics in generated current caused by semiconductor switching. The L-filter is the first order filter with attenuation 20 dB/decade over the whole frequency range. Therefore the application of this filter type is suitable for converters with high switching frequency, where the attenuation is sufficient. On the other side inductance greatly decreases dynamics of the whole system converter.

2.4 Grid

Grid energy storage refers to the methods used to store electricity on a large scale within an electrical power system. Electrical energy is stored during times when production (from power plants) exceeds consumption and the stores are used at times when consumption exceeds production. In this way, electricity production need not be drastically scaled up and down to meet momentary consumption – instead, production is maintained at a more constant level.

2.5 Non linear load

Applies to those ac loads where the current is not proportional to the voltage. The nature of non-linear loads is to generate harmonics in the current waveform. This distortion of the current waveform leads to distortion of the voltage waveform. Under these conditions, the voltage waveform is no longer proportional to the current

III. PROPOSED CONTROL OF GRID INTERFACING INVERTER

The control diagram of grid- interfacing inverter for a 3-phase 4-wire system is shown in Fig. 2. The fourth leg of inverter is used to compensate the neutral current of load. While performing the power management operation, the inverter is actively controlled in such a way that it always draws/ supplies fundamental active power from/ to the grid. If the load connected to the PCC is non-linear or unbalanced or the combination of both, the given control approach also compensates the harmonics, unbalance, and neutral current.

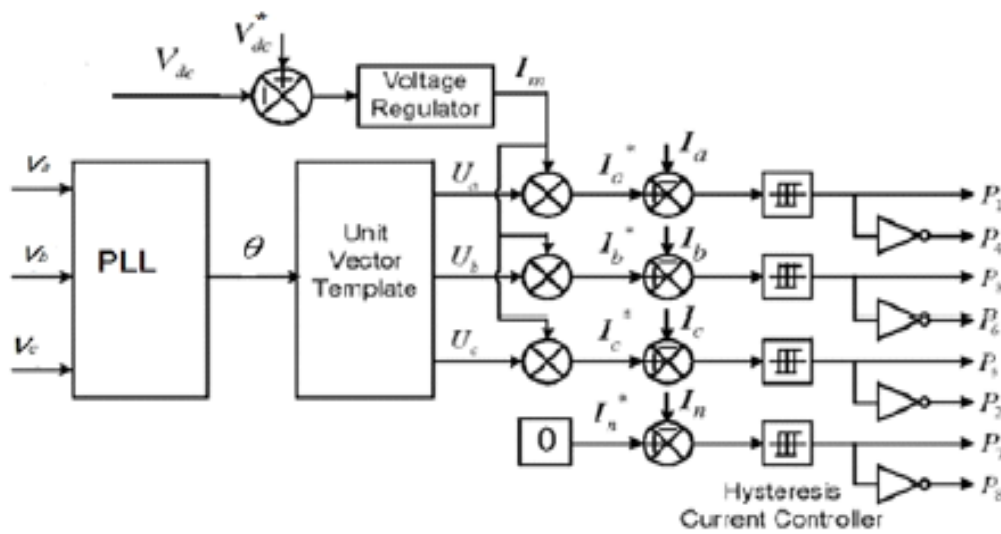


Fig. 2. Block diagram representation of grid-interfacing inverter control

3.1 Phase-Locked Loop

A phase-locked loop or phase lock loop (PLL) is a control system that generates an output signal whose phase is related to the phase of an input signal. While there are several differing types, it is easy to initially visualize as an electronic circuit consisting of a variable frequency oscillator and a phase detector. The oscillator generates a periodic signal. The phase detector compares the phase of that signal with the phase of the input periodic signal and adjusts the oscillator to keep the phases matched.

The grid synchronizing angle (θ) obtained from phase locked loop (PLL) is used to generate unity vector template as

$$U_a = \sin(\theta) \quad (1)$$

$$U_b = \sin(\theta - 2\pi/3) \quad (2)$$

$$U_c = \sin(\theta + 2\pi/3) \quad (3)$$

3.2 PI Controller

PI controller will eliminate forced oscillations and steady state error resulting in operation of on-off controller and P controller respectively. The difference of the filtered dc-link voltage and reference dc-link voltage V_{dc}^* is given to a discrete-PI regulator to maintain a constant dc-link voltage under varying generation and load conditions. The output of the PI controller is denoted as I_m . The dc-link voltage error $V_{dcerr}(n)$ at n^{th} sampling instant is given as:

$$V_{dcerr}(n) = V_{dc}^* - V_{dc}(n) \quad (4)$$

The output of discrete-PI regulator at n^{th} sampling instant is expressed as

$$I_{m(n)} = I_{m(n-1)} + K_{PV_{dc}} (V_{dcerr}(n) - V_{dcerr}(n-1)) + K_{IV_{dc}} V_{dcerr}(n) \quad (5)$$

where $K_{PV_{dc}} = 10$ and $K_{IV_{dc}} = .05$ are proportional and integral gains of dc-voltage regulator.

The reference current templates (I_a^* , I_b^* , and I_c^*) are obtained by multiplying the peak value (I_m) by the three-unit sine vectors (U_a , U_b and U_c) in phase with the three source voltages. These unit sine vectors are obtained from the three sensed line to neutral voltages. The reference grid neutral current (I_n^*) is set to zero, being the instantaneous sum of balanced grid currents. Multiplication of magnitude I_m with phases (U_a , U_b , and U_c) results in the three phase reference supply currents (I_a^* , I_b^* , and I_c^*).

The instantaneous values of reference three phase grid currents are compute as

$$I_a^* = I_m \cdot U_a \quad (6)$$

$$I_b^* = I_m \cdot U_b \quad (7)$$

$$I_c^* = I_m \cdot U_c \quad (8)$$

The neutral current, present if any, due to the loads connected to the neutral conductor should be compensated by forth leg of grid-interfacing inverter and thus should not be drawn from the grid. In other words, the reference current for the grid neutral current is considered as zero and can be expressed as

$$I_n^* = 0 \tag{9}$$

The reference grid currents (I_a^*, I_b^*, I_c^* and I_n^*) are compared with actual grid currents (I_a, I_b, I_c and I_n) to compute the current errors as

$$I_{aerr} = I_a^* - I_a \tag{10}$$

$$I_{berr} = I_b^* - I_b \tag{11}$$

$$I_{cerr} = I_c^* - I_c \tag{12}$$

$$I_{nerr} = I_n^* - I_n \tag{13}$$

These error signals are given to hysteresis current controller then generates the switching pulses for six IGBTs of the grid interfacing inverter.

3.3 Hysteresis current control

The hysteresis current control (HCC) is the simplest control method available so forth to implement the shunt APF with three phase current controlled VSI and is connected to the AC mains for compensating the current harmonics and the VSI gate control signals are brought out from hysteresis band current controller where a hysteresis current controller is implemented with the closed loop control system and waveforms which are shown in figure 3.

Here a error signal is used to control the switches in a voltage source inverter and the error is the only difference between the desired current and the current being injected by the inverter and when the error exceeds the upper limit of the hysteresis band the upper switch of the inverter arm is turned off and the lower switch is turned on as a result of which the current starts decaying. When the error crosses its defined lower limit of the hysteresis band then the lower switch of the inverter arm is turned off and the upper switch is turned on as a result of which the current gets back into the hysteresis band and the minimum and maximum values of the error signal are e_{min} and e_{max} respectively and the range of the error signal $e_{max} - e_{min}$ directly controls the amount of ripple in the output current from the VSI.

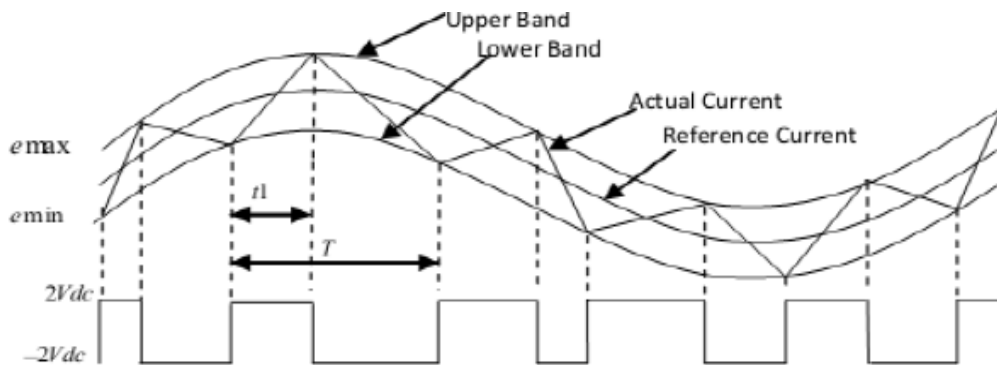


Figure 3 Waveform of Hysteresis current controller

IV. SIMULATION RESULTS

In order to verify the proposed control approach to achieve multi-objectives for grid interfaced DG systems connected to a 3-phase 4-wire network, an extensive simulation study is carried out using MATLAB/Simulink. A 4-leg current controlled voltage source inverter is actively controlled to achieve balanced sinusoidal grid currents at unity power factor (UPF) despite of highly unbalanced nonlinear load at PCC. Here 3 cases are simulated

- Case 1: When Balanced load directly connected to grid without RES
- Case 2: When Unbalanced load directly connected to grid without RES
- Case 3: When Unbalanced load connected to grid with grid interfacing inverter control

4.1 System Parameters

- Grid (3 phase supply) in r.m.s $V_g = 170V(\text{r.m.s}), 50\text{Hz}$
- 3 phase load $R = 26.66\Omega$
- 1-Phase Non linear Load (A-N) $R = 36.66\Omega, L = 10\text{mH}$
- 1-Phase Non linear Load (C-N) $R = 26.66\Omega, L = 10\text{mH}$
- Dc link voltage $V_{dc} = 300V$
- Coupling inductance $L_{sh} = 5\text{mH}$
- DC link capacitance $C_{dc} = 3000\mu F$

4.2 Balanced load directly connected to grid without RES

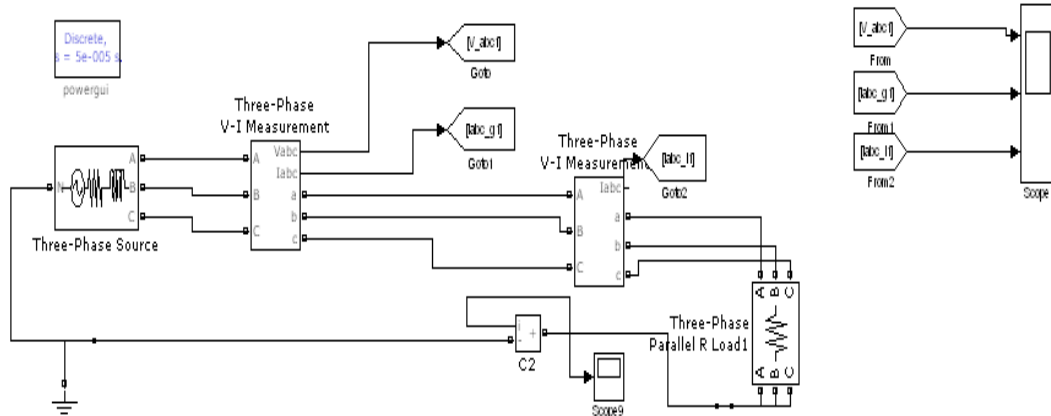


Figure 4. Simulink model when balanced load directly connected to grid without RES

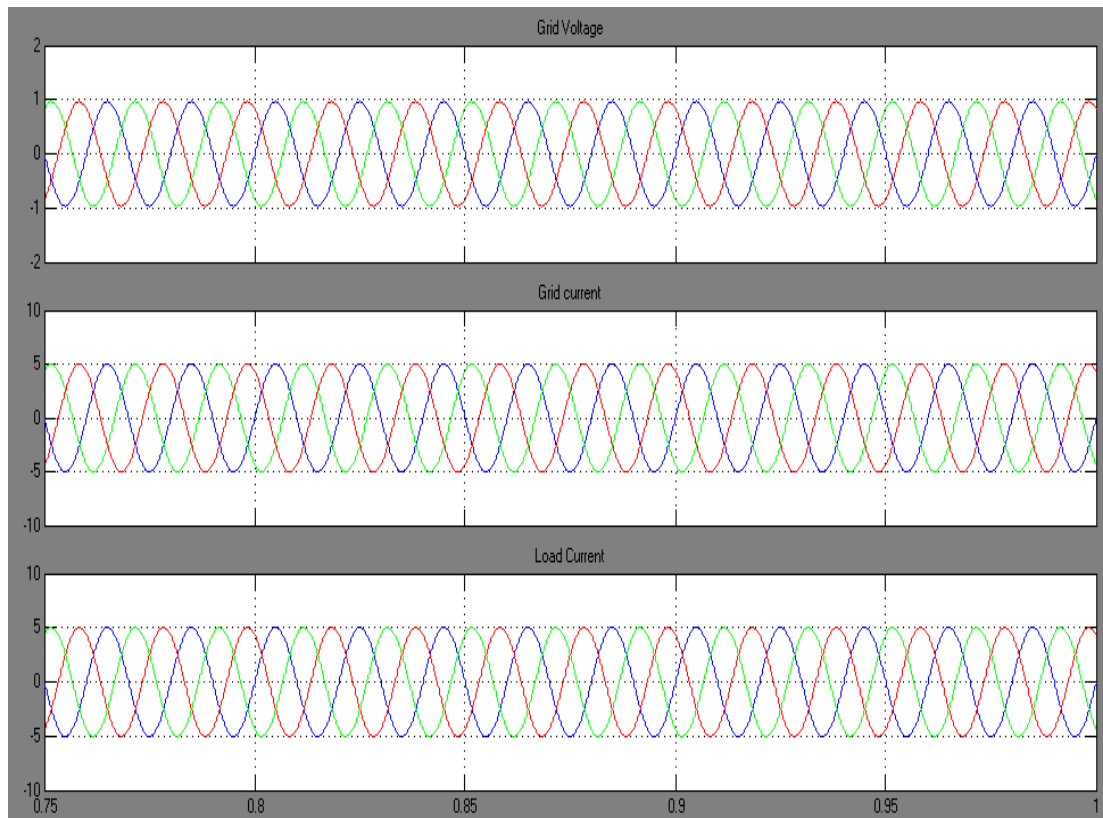


Figure 5. Simulation results: (a) Grid voltages, (b) Grid Currents (c) load currents when balanced load directly connected to grid without RES

The waveforms of grid voltage, grid currents and load current are shown in figure 5. It shows that the grid voltage grid currents and load currents are balanced when balanced nonlinear load connected directly to the grid.

4.3 Unbalanced load directly connected to grid without RES

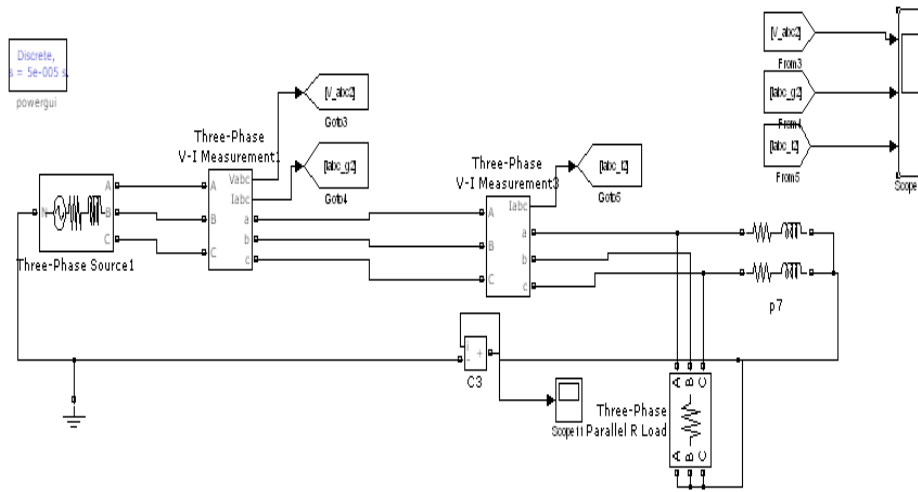


Figure 6. simulink model when unbalanced load directly connected to grid without RES

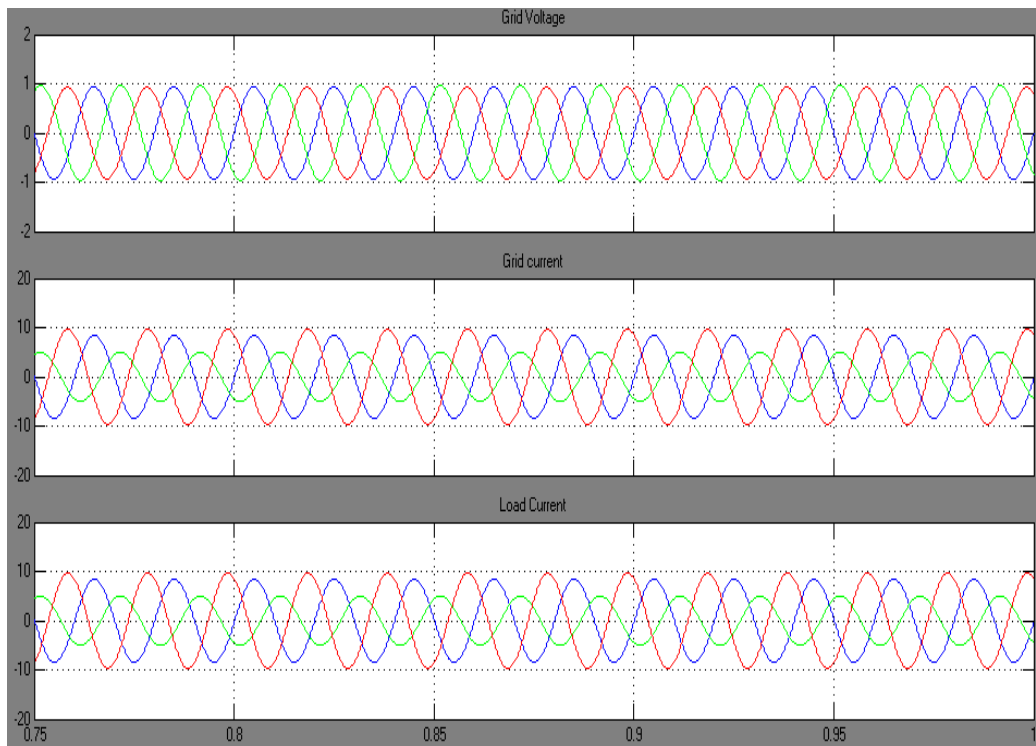


Figure 7. Simulation results: (a) Grid voltages, (b) Grid Currents (c) load currents when unbalanced load directly connected to grid without RES

The waveforms of grid voltage, grid currents and load current when unbalanced load directly connected to grid without inverter are shown in figure 7. It shows that the grid currents and load currents become unbalanced when a set of 3 phase balanced linear and 1 phase unbalanced nonlinear loads are connected directly to the grid.

4.4 Unbalanced load connected to grid with grid interfacing inverter control

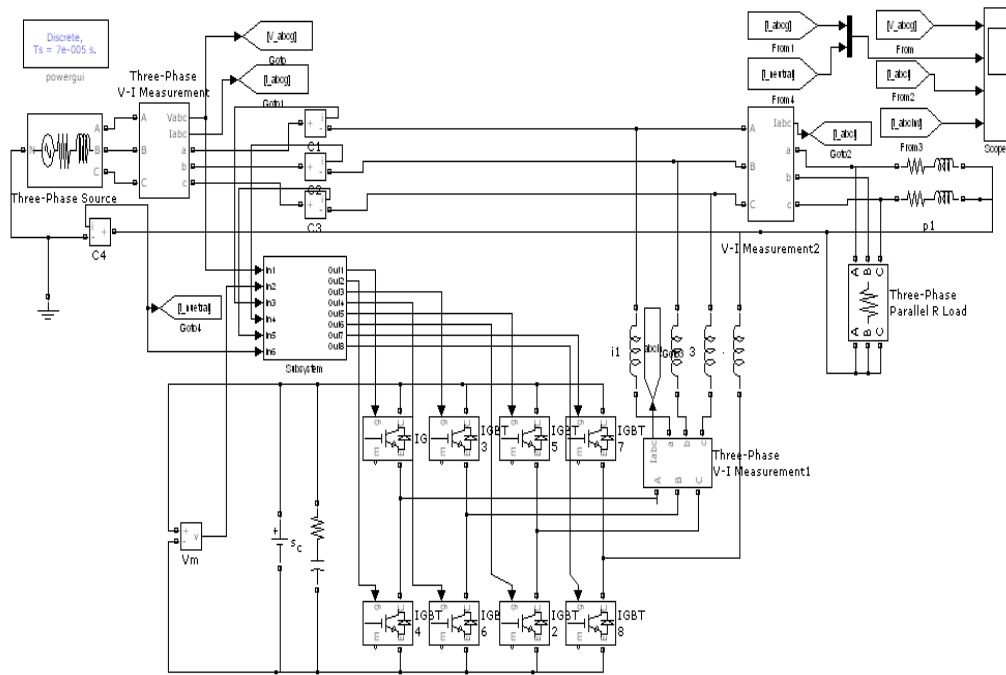


Figure 8. simulink model when unbalanced load connected to grid with grid interfacing inverter control

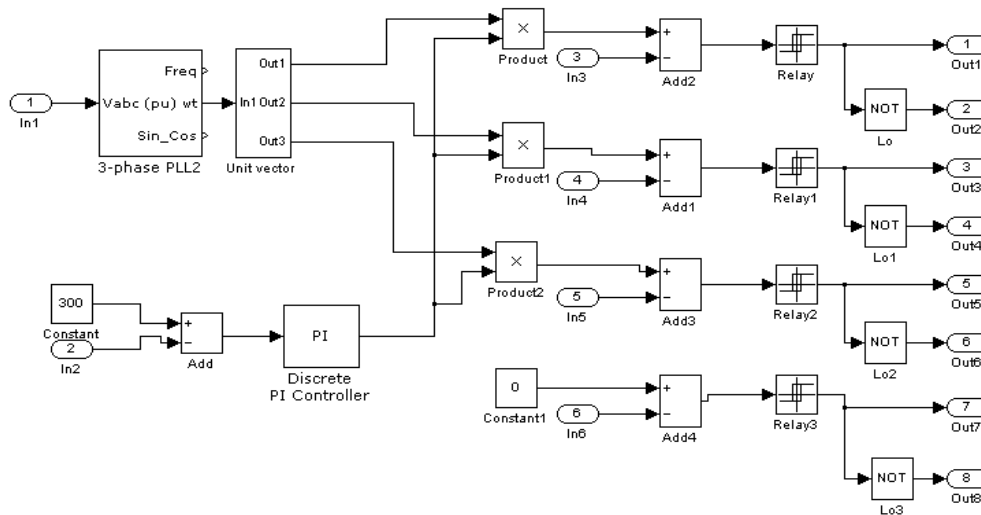


Figure.9 simulink control model when unbalanced load connected to grid with grid interfacing inverter control

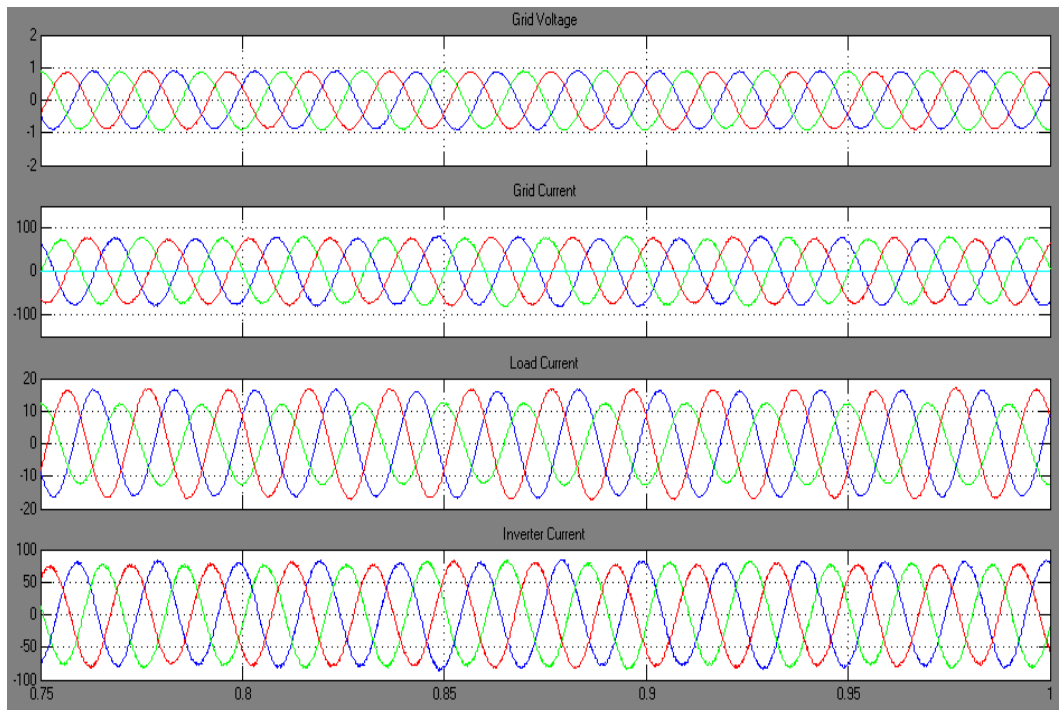


Figure.10 Simulation results: (a) Grid voltages, (b) Grid Currents (c) load currents and d) Inverter current when unbalanced load directly connected to grid with inverter control

The waveforms of grid voltage, grid currents and load current when Unbalanced load directly connected to grid with inverter control are shown in figure 10. It shows that the Grid voltage and grid currents are get balanced when a set of 3phase balanced linear and 1 phase unbalanced nonlinear loads are connected to the grid with grid interfacing inverter control method.. The dc-link voltage across the grid- interfacing inverter during different operating condition is maintained at constant level. Thus from the simulation results, it is evident that the grid-interfacing inverter can be effectively used to compensate the current unbalance and current harmonics.

V. CONCLUSION

This thesis has presented a novel control of an existing grid interfacing inverter to improve the quality of power at PCC for a 3-phase 4-wire DG system. It has been shown that the grid-interfacing inverter can be effectively utilized for power conditioning without affecting its normal operation of real power transfer. The grid-interfacing inverter with this approach can be utilized to: 1) inject real power to the grid, and/or, 2) Operate as a shunt Active Power Filter (APF). This approach thus eliminates the need for additional power conditioning equipment to improve the quality of power at PCC. Extensive MATLAB/Simulink simulation results have validated this approach and have shown that the grid-interfacing inverter can be utilized as a multi-function device.

REFERENCES

- [1] Mukhtiar Singh, Vinod Khadkikar, Ambrish Chandra and Rajiv K. Varma "Grid Interconnection of Renewable Energy Sources at the Distribution Level With Power-Quality Improvement Features" IEEE Transactions on Power Delivery, vol. 26, no. 1, January 2011
- [2] M. Singh and A. Chandra, "Power maximization and voltage sag/swell ride through capability of PMSG based variable speed wind energy conversion system," in Proc. IEEE 34th Annu. Conf. Indus. Electron. Soc., 2008, pp. 2206–2211.
- [3] F. Blaabjerg, R. Teodorescu, M. Liserre, and A. V. Timbus, "Overview of control and grid synchronization for distributed power generation systems," IEEE Trans. Ind. Electron., vol. 53, no. 5, pp. 1398–1409, Oct. 2006.
- [4] J. M. Carrasco, L. G. Franquelo, J. T. Bialasiewicz, E. Galván, R. C. P. Guisado, M. Á. M. Prats, J. I. León, and N. M. Alfonso, "Power-electronic systems for the grid integration of renewable energy sources: A survey," IEEE Trans. Ind. Electron., vol. 53, no. 4, pp. 1002–1016, Aug. 2006.

- [5] B. Renders, K. De Gusseme, W. R. Ryckaert, K. Stockman, L. Van-develde, and M. H. J. Bollen, "Distributed generation for mitigating voltage dips in low-voltage distribution grids," *IEEE Trans. Power Del.*, vol. 23, no. 3, pp. 1581–1588, Jul. 2008.
- [6] V. Khadkikar, A. Chandra, A. O. Barry, and T. D. Nguyen, "Application of UPQC to protect a sensitive load on a polluted distribution network," in *Proc. Annu. Conf. IEEE Power Eng. Soc. Gen. Meeting*, 2006, pp. 867–872.
- [7] J. M. Guerrero, L. G. de Vicuna, J. Matas, M. Castilla, and J. Miret, "A wireless controller to enhance dynamic performance of parallel inverters in distributed generation systems," *IEEE Trans. Power Electron.*, vol. 19, no. 5, pp. 1205–1213, Sep. 2004.
- [8] J. H. R. Enslin and P. J. M. Heskes, "Harmonic interaction between a large number of distributed power inverters and the distribution network," *IEEE Trans. Power Electron.*, vol. 19, no. 6, pp. 1586–1593, Nov. 2004.
- [9] P. Jintakosonwitt, H. Fujita, H. Akagi, and S. Ogasawara, "Implementation and performance of cooperative control of shunt active filters for harmonic damping throughout a power distribution system," *IEEE Trans. Ind. Appl.*, vol. 39, no. 2, pp. 556–564, Mar./Apr. 2003.
- [10] K. J. P. Macken, M. H. J. Bollen, and R. J. M. Belmans, "Mitigation of voltage dips through distributed generation systems," *IEEE Trans. Ind. Appl.*, vol. 40, no. 6, pp. 1686–1693, Nov./Dec. 2004.
- [11] U. Borup, F. Blaabjerg, and P. N. Enjeti, "Sharing of nonlinear load in parallel-connected three-phase converters," *IEEE Trans. Ind. Appl.*, vol. 37, no. 6, pp. 1817–1823, Nov./Dec. 2001.
- [12] J. P. Pinto, R. Pregitzer, L. F. C. Monteiro, and J. L. Afonso, "3-phase 4-wire shunt active power filter with renewable energy interface," presented at the *Conf. IEEE Renewable Energy & Power Quality*, Seville, Spain, 2007.
- [13] P. Rodríguez, J. Pou, J. Bergas, J. I. Candela, R. P. Burgos, and D. Boroyevich, "Decoupled double synchronous reference frame PLL for power converters control," *IEEE Trans. Power Electron.*, vol. 22, no. 2, pp. 584–592, Mar. 2007.
- [14] H. Zhu, B. Arnet, L. Haines, E. Shaffer, and J.-S. Lai, "Grid synchronization control without ac voltage sensors," in *Proc. IEEE APEC*, 2003, vol. 1, pp. 172–178.
- [15] J. Svensson, "Synchronisation methods for grid-connected voltage source converters," *Proc. Inst. Electr. Eng.—Gener. Transm. Distrib.*, vol. 148, no. 3, pp. 229–235, May 2001.

MK-Prototypes: A Novel Algorithm for Clustering Mixed Type Data

N. Aparna¹, M. Kalaiarasu²

^{1,2}(Department of Computer Science, Department of Information Technology, Sri Ramakrishna Engineering College, Coimbatore)

Abstract: Clustering mixed type data is one of the major research topics in the area of data mining. In this paper, a new algorithm for clustering mixed type data is proposed where the concept of distribution centroid is used to represent the prototype of categorical variables in a cluster which is then combined with the mean to represent the prototype of clusters with mixed type variables. In the method, data is observed from different views and the variables are grouped into different views. Those instances that can be viewed differently from different viewpoints can be defined as multiview data. During clustering process the differences among views are ignored in usual cases. Here, both views and variables weights are computed simultaneously. The view weight is used to determine the closeness or density of view and variable weight is used to identify the significance of each variable. With the intention of determining the cluster of objects both these weights are used in the distance function. In the proposed method, enhancement to the k-prototypes is done so that it automatically computes both view and variable weights. The proposed algorithm MK-Prototypes algorithm is compared with two other clustering algorithms.

Keywords: clustering. mixed data. multiview. variable weighting. view weighting. k-prototypes.

I. Introduction

Clustering is a fundamental technique of unsupervised learning in machine learning and statistics. It is generally used to find groups of similar items in a set of unlabeled data. The aim of clustering is to divide a set of data objects into clusters so that those data objects that belongs to the same cluster are more similar to each other than those in other clusters [1-4]. In real world, datasets usually contain both numeric and categorical variables [5,6]. However, most existing clustering algorithms assume all variables are either numeric or categorical, examples of which include the k-means [7], k-modes [8], fuzzy k-modes [9] algorithms. Here, the data is observed from multiple outlooks and in multiple types of dimensions. For example, in a student data set, variables can be divided into personal information view showing the information about the student's personal information, the academic view describing the student's academic performance and the extra-curricular view which gives the extra-curricular activities and achievements made by the student.

Traditional methods take multiple views as a set of flat variables and do not take into account the differences among various views [10], [11], [12]. In the case of multiview clustering, it takes the information from multiple views and also considers the variations among different views which produces a more precise and efficient partitioning of data.

In this paper, a new algorithm Multi-viewpoint K-prototypes (MK-Prototypes) for clustering mixed type data is proposed. It is an enhancement to the usual k-prototypes algorithm. In order to differentiate the effects of different views and different variables in clustering, the view weights and individual variables are applied to the distance function. Here while computing the view weights, the complete set of variables are considered and while calculating the weights of variables in a view, only a part of the data that includes the variables in the view is considered. Thus, the view weights show the significance of views in the complete data and the variables weights in a view shows the significance of variables in a view alone.

II. Related Works

Till date, there exist a number of algorithms and methods to directly deal with mixed type data. In [13], Cen Li and Gautam Biswas proposed an algorithm, Similarity-based agglomerative clustering (SBAC) that works well for data with mixed attributes. It adopts a similarity measure proposed by Goodall [14] for biological taxonomy. In this method, while computing the similarity, higher weight is assigned to infrequent attribute value matches. It does not make any suppositions on the underlying features of the attribute values. An agglomerative algorithm is used to generate a dendrogram and a simple distinctness heuristic is used to extract a partition of the data. Hsu and Chen proposed CAVE [15], a clustering algorithm based on the Variance and Entropy for

clustering mixed data. It builds a distance hierarchy for every categorical attributes which needs domain expertise. Hsu et al. [16] proposed an extension to the self-organizing map to analyze mixed data where the distance hierarchy is automatically constructed by using the values of class attributes.

In [17] Chatziz proposed KL-FCM-GM algorithm in which data derived from the clusters are in the Gaussian form and is designed for the Gauss-Multinomial distributed data.

Huang presented a k-prototypes algorithm [18] where k-means is integrated with k-modes to partition mixed data. Bezdek et al. considered the fuzzy nature of the objects in his work the fuzzy k-prototypes [19] and Zheng et al. proposed [20] an evolutionary type k-prototypes algorithm by introducing an evolutionary algorithm framework.

III. Proposed System

The motivation for the proposed system is on one hand to provide a better representation for the categorical variable part in a mixed data since the numerical variables can be well represented using the mean concept itself. On the other hand it considers the importance of view and variables weights in the process of clustering. The concept of distribution centroid represents the cluster centroid for the categorical variable part. Huang's strategy of evaluation is used for the computation of both view weights and variable weights.

A. The distribution centroid

The idea of distribution centroid for a better representation of categorical variables is stimulated from fuzzy centroid proposed by Kim et al. [21]. It makes use of a fuzzy scenario to represent the cluster centers for the categorical variable part.

For $\text{Dom}(V_j) = \{v_i^1, v_i^2, v_i^3, \dots, v_i^t\}$, the distribution centroid of a cluster o , denoted as C'_o , is represented as follows

$$C'_o = \{c'_{o1}, c'_{o2}, \dots, c'_{oj}, \dots, c'_{om}\} \quad (1)$$

where

$$c'_{oj} = \{\{b_j^1, w_{oj}^1\}, \{b_j^2, w_{oj}^2\}, \dots, \{b_j^k, w_{oj}^k\}, \dots, \{b_j^t, w_{oj}^t\}\} \quad (2)$$

In the above equation

$$w_{oj}^k = \sum_{i=1}^n \mu(x_{ij}) \quad (3)$$

where

$$\mu(x_{ij}) = \begin{cases} \frac{u_{io}}{\sum_{i=1}^n u_{io}} & \text{if } x_{ij} = b_j^k \\ 0 & \text{if } x_{ij} \neq b_j^k \end{cases} \quad (4)$$

Here, u_{io} is assigned the value 1, if the data object x_i belongs to cluster o and as 0, if the data object x_i do not belong to cluster o

From the above mentioned equations it is clear that the computation of distribution centroid considers the number of times each categorical value repeat in a cluster. Thus to denote the center of a cluster it takes into account the distribution features of categorical variables

B. Weight calculation using Huang's approach

Weight of a variable identifies the effect of that variable in clustering process. In 2005, Huang et al. proposed an approach to calculate the weight of variable [22]. According to their method, the weight is computed by minimizing the value of objective function.

The standard for assigning weight of variable is to allocate a larger value to a variable that has a smaller sum of the within cluster distances (WCD), and vice versa. This principle is given by

$$w_j \propto \frac{1}{D_j} \quad (5)$$

where w_j is the significance of the variable j , \propto is the mathematical symbol denoting direct proportionality, and D_j is the sum of the within cluster distances for this variable.

C. Multiview concept

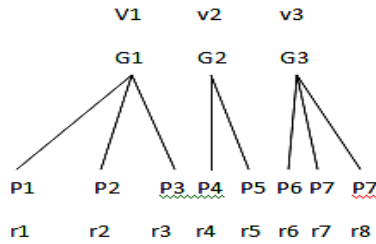


FIGURE 1 : Multiview concept

In 2013, Chen Et Al [23] proposed Tw-K-Means where the concept of multiview data was introduced. The above figure illustrates the multiview concept. During the process of clustering, the differences among different views are not considered. In the process of multiview clustering, in addition to variable weights, the variables are grouped according to their characteristic properties. Each group is termed as a view and a weight is assigned to each view. The view weight is assigned according to Huang’s approach.

D. The proposed algorithm

The proposed algorithm, MK-prototypes put together the concepts in section 3.1, section 3.2, section 3.3. The figure 2 describes the steps involved in the algorithm:
Steps in the proposed algorithm:

1. Compute the distribution centroid to represent the categorical variable centroid
2. Compute the mean for the numerical variables
3. Integrate the distribution centroid and mean to represent the prototype for the mixed data
4. Compute the view weights and variable weights.
5. Measure the similarity between the data objects and the prototypes
6. Assign the data object to that prototype to which the considered data object is the closest
7. Repeat steps 1-6 until an effective clustering result is obtained.

E. The optimization model

The clustering process to partition the dataset X into k clusters that considers both view weights and variable weights is represented according to the framework of [23] as a minimization of the following objective function.

$$P(U, Z, R, V) = \sum_{o=1}^k \sum_{i=1}^n \sum_{t=1}^Q \sum_{s \in G_t} u_{i,o} v_t r_s d(x_{i,s}, z_{o,s}) \tag{6}$$

subject to $\sum_{o=1}^k u_{i,o} = 1, u_{i,l} \in \{0,1\}, 1 \leq i \leq n$

$$\sum_{i=1}^Q v_t = 1, \quad 0 \leq v_t \leq 1, \quad 0 \leq r_j \leq 1, \quad 1 \leq t \leq Q, \quad \sum_{j \in G_t} r_j = 1$$

where U is an n x k partition matrix whose elements $u_{i,o}$ are binary where $u_{i,o} = 1$ indicates that object i is allocated to cluster o. $Z = \{Z_1, Z_2, \dots, Z_k\}$ is a set of k vectors on behalf of the centers of the k clusters. $V = \{V_1, V_2, \dots, V_Q\}$ are Q weights for Q views. $R = \{r_1, r_2, \dots, r_s\}$ are s weights for s variables. $d(x_{i,s}, z_{o,s})$ is a distance or dissimilarity measure on the s^{th} variable between the i^{th} object and the center of the o^{th} cluster.

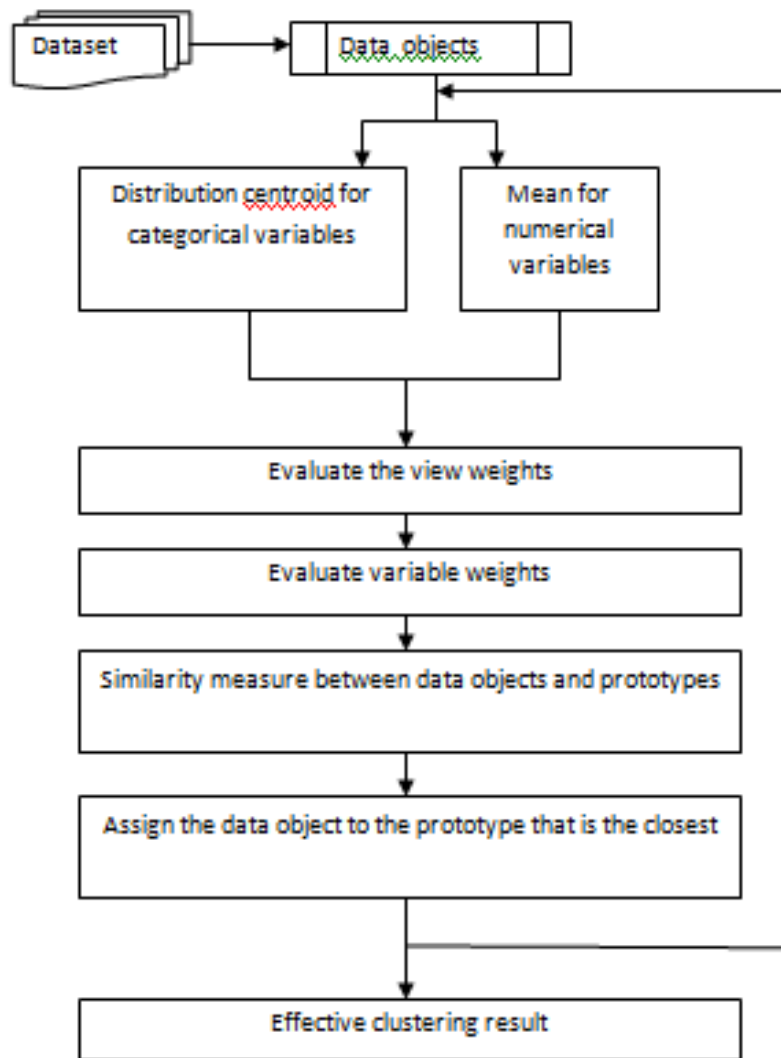


FIGURE 2. Flowchart for the proposed algorithm

In order to minimize the equation, the problem is divided into four sub-problems:

1. Sub-problem 1: Fix $Z=Z^{\wedge}, R=R^{\wedge}$ and $V=V^{\wedge}$ and solve the reduced problem $P(U, Z^{\wedge}, R^{\wedge}, V^{\wedge})$.
2. Sub-problem 2: Fix $U=U^{\wedge}, R=R^{\wedge}$ and $V=V^{\wedge}$ and solve the reduced problem $P(U^{\wedge}, Z, R^{\wedge}, V^{\wedge})$.
3. Sub-problem 3: Fix $Z=Z^{\wedge}, U=U^{\wedge}$ and $V=V^{\wedge}$ and solve the reduced problem $P(U^{\wedge}, Z^{\wedge}, R, V^{\wedge})$.
4. Sub-problem 4: Fix $Z=Z^{\wedge}, R=R^{\wedge}$ and $U=U^{\wedge}$ and solve the reduced problem $P(U^{\wedge}, Z^{\wedge}, R^{\wedge}, V)$.

The sub-problem 1 is solved by:

$$u_{i,o} = 1 \tag{7}$$

if

$$\sum_{s=1}^m v_t r_s d(x_{i,o}, z_{i,0}) \leq \sum_{s=1}^m v_t r_s d(x_{i,o}, z_{e,0}) \tag{8}$$

where $1 \leq e \leq k$

$$u_{i,o} = 0 \text{ where } e \neq o$$

The sub-problem 2 is solved for the numeric variable by

$$z_{o,s} = \frac{\sum_{i=1}^n u_{i,o} x_{i,s}}{\sum_{i=1}^n u_{i,o}} \quad (9)$$

and for the categorical variables by $z_{o,s} = c'_{i,s}$ which is already defined.

$d(x_{i,s}, z_{o,s}) = |x_{i,s} - z_{o,s}|$ if the sth variable is a numeric variable .

$d(x_{i,s}, z_{o,s}) = \varphi(x_{i,s}, z_{o,s})$ if the sth variable is a categorical variable .

where $\varphi(x_{i,s}, z_{o,s}) = \sum_{k=1}^t \delta(x_{i,s}, b_j^k)$ and $\delta(x_{i,s}, b_j^k)$ is 0 if $x_{i,s} \neq b_j^k$ and $w_{o,j}^k$ if $x_{i,s} = b_j^k$.

The solution to the sub-problem 3 is as followed:

Let $Z=Z^\wedge$, $U=U^\wedge$ and $V=V^\wedge$ be fixed . Then the reduced problem $P(U^\wedge, Z^\wedge, R, V^\wedge)$ is minimized if

$$r_s = \frac{1}{\sum_{h \in G_t} \left[\frac{D_s}{D_h} \right]^\gamma} \quad (10)$$

where

$$D_s = \sum_{o=1}^k \sum_{i=1}^n u'_{i,o} w'_t d(x_{i,s}, z'_{o,s}) \quad (11)$$

Sub-problem 4 is solved as follows

$$w_t = \frac{1}{\sum_{t=1}^h \left[\frac{F_s}{F_t} \right]^\mu} \quad (12)$$

where

$$F_s = \sum_{o=1}^k \sum_{i=1}^n \sum_{s \in G_t} u'_{i,o} r'_s d(x_{i,s}, z'_{o,s}) \quad (13)$$

Having presented the detailed computations required for calculating the important variables, the proposed algorithm

MK-Prototypes can be described as given below:

1. Choose the number of iterations, number of clusters k, value of μ and γ , randomly choose k distinct data objects and convert them into initial prototypes and initialize the view weights and variable weights.
2. Fix Z', R', V' as Z^t, R^t, V^t respectively and minimize the problem $P(U, Z', R', V')$ to obtain U^{t+1} .
3. Fix U', R', V' as U^t, R^t, V^t respectively and minimize the problem $P(U', Z, R', V')$ to obtain Z^{t+1} .
4. Fix U', Z', V' as U^t, Z^t, V^t respectively and minimize the problem $P(U', Z', R, V')$ to obtain R^{t+1} .
5. Fix U', Z', R', V as U^t, Z^t, R^t respectively and minimize the problem $P(U', Z', R', V)$ to obtain V^{t+1} .
6. If there is no improvement in P or if the maximum iterations is reached, then stop. Else increment t by 1 , decrement number of iterations by 1 and go to Step 2.

IV. Experiments on Performance Of Mk-Prototypes Algorithm

In order to measure the performance level of the proposed algorithm, it is used to cluster a real-world dataset Heart (disease). The dataset is taken from UCI Machine Learning Repository.

The proposed algorithm is compared with k-prototypes and SBAC algorithm. They are well known for clustering mixed type data. In this paper, the clustering accuracy is measured using one of the most commonly used criteria. The clustering accuracy r is given by

$$r = \frac{\sum_{i=1}^k a_i}{n} \quad (14)$$

where a_i is the number of data objects that occur in both the i th cluster and its corresponding true class and n is the number of data objects in a data set.

Higher the value of r , the higher the clustering accuracy. A perfect clustering gives a value of $r=1.0$.

A. Dataset description

The Heart disease data set is a mixed dataset. It contains 303 patient instances. The actual data set contains 76 variables out of which 14 are considered usually. In the proposed algorithm, in order to define three views 19 out of 76 variables are considered here. It consists of seven numeric variables and twelve categorical variables.

These 19 variables can be naturally divided into 3 views.

1. Personal data view: It includes those variables which describes a patient’s personal data.
2. Historical data view: It includes those variables which describes a patient’s historical data like the habits.
3. Test output view: It includes all those variables which describes the results of various tests conducted for the patient.

Here, G_1, G_2, G_3 represents the three views personal, historical, test output respectively.

B. Results and analysis

Below are the graphical representations of the clustering results. Fig 3 shows the variation in variable weights for varying μ values and fixed γ values. Fig 4 shows the variation in view weights for varying μ values and fixed γ values.

From Table 1, it is observed that as μ increased, the variance of V decreased rapidly. This result can be explained from equation (10) as μ increases, V becomes flatter. The graphical representation of the Table 1 has been shown below.

Table 1: Variable weights vs γ value For fixed μ value

$\mu \backslash \gamma$	1	4	12
10	0.01	0	0
15	0	0.01	0
20	0.7	0	0.05
25	0.03	0.4	0.1
30	0	0.1	0.02
35	0.02	0	0

Table 2 shows that as γ increased, the variance of view weights decreased rapidly. This result can be explained from equation (11) as γ increases, W becomes flatter. The graphical representation has been shown below.

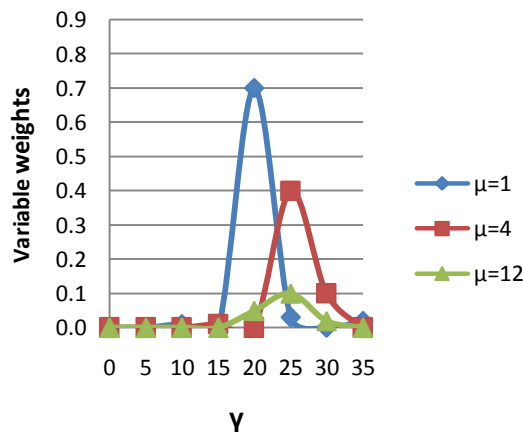


Fig 3: Variable weights vs γ value for fixed μ value

Table 2: View weights vs μ value for fixed γ value

$\mu \backslash \gamma$	1	4	12
10	0.05	0.075	0.01
20	0.075	0.14	0.015
30	0.095	0.05	0.04
40	0.16	0.06	0.01
50	0.04	0.07	0.005
60	0.05	0.04	0.02
70	0.07	0.035	0.01

From above analysis, it can be summarized that the following method can be used to control two types of weight distributions in MK-Prototypes algorithm by setting different values of γ and μ .

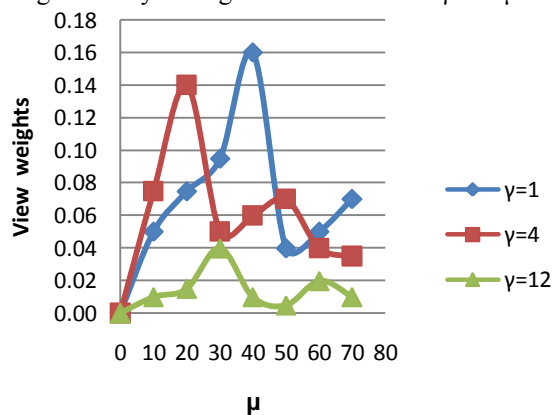


Figure 4: View weights vs μ value for fixed γ value

The experiments have been conducted for three different values of μ and γ for varying values of γ and μ respectively.

1. Large μ makes more variables contribute to the clustering while small μ makes only important variables contribute to the clustering.
2. Large γ makes more views contribute to the clustering while small γ makes only important views contribute to the clustering.

Table 3: Comparison of accuracy rates of dataset considering all views

Algorithms	Clustering accuracy %
k-prototypes	0.521
SBAC	0.747
MK-Prototypes	0.846

From the above table, it is clear that the proposed algorithm has a better clustering accuracy than the existing k-prototypes and SBAC.

V. Conclusion

Mixed type data are encountered everywhere in the real world. In this paper, a new algorithm, Multiview point based clustering algorithm for mixed type data has been proposed. When compared with the existing algorithms the proposed algorithm has many significant contributions. The proposed algorithm encapsulates the characteristics of clusters with mixed type variables more efficiently since it includes the distribution information of both numeric and categorical variables.

It also takes into account the importance of various variables and views during the process of clustering by using Huang’s approach and a new dissimilarity measure.

It can compute weights for views and individual variables simultaneously in the clustering process. With the two types of weights, dense views and significant variables can be identified and effect of low-quality views and noise variables can be reduced.

Because of these contributions the proposed algorithm obtains higher clustering accuracy, which has been validated by experimental results.

REFERENCES

- [1] Z.X. Huang, Extensions to the k means algorithm for clustering large datasets with categorical values, *Data Min. Knowl. Discovery* 2 (3) (1998) 283–304.
- [2] A.K.Jain, R.C.Dubes, *Algorithms for Clustering Data*, Prentice-Hall, New Jersey, 1988.
- [3] A.K.Jain, M.N.Murty, P.J.Flynn, Data clustering: a survey, *ACM Comput. Surv.* 31 (3) (1999) 264–323.
- [4] J.W.Han, M.Kamber, *Data Mining Concepts and Techniques*, Morgan Kaufmann, San Francisco, 2001.
- [5] C.Hsu, Y.P.Huang, Incremental clustering of mixed data based on distance hierarchy, *Expert Syst. Appl.* 35 (3) (2008) 1177–1185. [6] C.Hsu, S.Lin, W.Tai, Apply extended self-organizing map to cluster and classify mixed-type data, *Neurocomputing* 74 (18) (2011) 3832–3842.
- [7] S.Lloyd, Least squares quantization in PCM, *IEEE Trans. Inf. Theory* 28 (2) (1982) 129–137.
- [8] Z.X.Huang, Extensions to the k-means algorithm for clustering large datasets with categorical values, *Data Min. Knowl. Discovery* 2 (3) (1998) 283–304. [9] Z.X.Huang, M.K.Ng, A fuzzy k-modes algorithm for clustering categorical data, *IEEE Trans. Fuzzy Syst.* 7 (4) (1999) 446–452.
- [10] J. Mui and K. Fu, “Automated Classification Of Nucleated Blood Cells Using A Binary Tree Classifier,” *IEEE Trans. Pattern Analysis And Machine Intelligence*, Vol. 2, No. 5, Pp. 429-443, May 1980.
- [11] J. Wang, H. Zeng, Z. Chen, H. Lu, L. Tao, And W. Ma, “Recom: Reinforcement Clustering Of Multitype Interrelated Data Objects,” *Proc. 26th Ann. Int’l ACM SIGIR Conf. Research And Development In Informaion Retrieval*, Pp. 274-281, 2003.
- [12] S. Bickel And T. Scheffer, “Multi-View Clustering,” *Proc. IEEE Fourth Int’l Conf. Data Mining*, Pp. 19-26, 2004.
- [13] C.Li, G.Biswas, Unsupervised Learning with Mixed Numeric And Nominal Data, *IEEE Trans. Knowl. Data Eng.* 14 (4) (2002) 673–690.
- [14] D.W.Goodall, A New Similarity Index Based On Probability, *Biometrics* 22 (4) (1966) 882–907.
- [15] C.C.Hsu, Y.C.Chen, Mining Of Mixed Data With Application To Catalog Marketing, *Expert Syst. Appl.* 32 (1) (2007) 12–27.
- [16] C. Hsu, S.Lin, W.Tai, Apply Extended Self-Organizing Map To Cluster And Classify Mixed-Type Data, *Neurocomputing* 74 (18) (2011) 3832–3842.
- [17] S.P.Chatzis, A Fuzzy C-Means-Type Algorithm For Clustering Of Data With Mixed Numeric And Categorical Attributes Employing A Probabilistic Dissimilarity Functional, *Expert Syst. Appl.* 38 (7) (2011) 8684–8689.
- [18] Z.X.Huang, Clustering Large Datasets with Mixed Numeric and Categorical Values, In: *Proceedings Of The First Pacific-Asia Knowledge Discovery And Data Mining Conference*, 1997, Pp.21–34.
- [19] J.C.Bezdek, J.Keller, R.Krisnapuram, *Fuzzy Models And Algorithms For Pattern Recognition And Image Processing*, Kluwer Academy Publishers, Boston, 1999. [25].
- [20] Z.Zheng, M.G.Gong, J.J.Ma, L.C.Jiao, Unsupervised Evolutionary Clustering Algorithm For Mixed Type Data, In : *Proceedings Of The IEEE Congresson Evolutionary Computation (CEC)*, 2010, Pp.1–8.
- [21] W.Kim, K.H.Lee, D.Lee, Fuzzy Clustering Of Categorical Data Using Fuzzy Centroid, *Pattern Recognition Lett.* 25 (11) (2004) 1263–1271.
- [22] Z.X.Huang, M.K.Ng, H.Q.Rong, Z.C.Li, Automated Variable Weighting In K-Means Type Clustering, *IEEE Trans. Pattern Anal. Mach. Intell.* 27 (5) (2005) 657–668.
- [23] Xiaojun Chen, Xiaofei Xu, Joshua Zhexue Huang, And Yunming Ye, Tw-K-Means: Automated Two-Level Variable Weighting Clustering Algorithm For Multiview Data, *IEEE Transactions On Knowledge And Data Engineering*, Vol. 25, No. 4, April 2013, pp 932-945

Two Stage Reversible Data Hiding Based On Image Interpolation and Histogram Modification

Nice Mathew¹, Dr. A. Grace Selvarani M. E²

^{1,2}(PG Scholar, Professor & HOD, Department of CSE (PG), Sri Ramakrishna Engineering College, Coimbatore)

Abstract: In this paper a two stage reversible data hiding technique is proposed. At the first stage, an interpolation technique is used to generate a cover image from the input image. The difference values from input image and cover image is used as the carrier to embed data. At the second stage, a histogram modification is applied on a difference image to embed data. The extraction process also works in two stages. The proposed algorithm is expected to increase the embedding capacity as two techniques are combined. The interpolation technique helps to keep the distortion low. Experimental results show that the new method has higher embedding capacity than other existing methods.

Keywords: Reversible data hiding, two stage embedding, image interpolation, histogram modification.

I. Introduction

Digital steganography and watermarking are the two kinds of data hiding technology to provide secure communication and authentication. Steganography means hiding a secret message in such a way that an outsider cannot detect the presence of the hidden message. Today the growth in the IT field, especially in computer networks, has opened new opportunities in scientific and commercial applications. But this progress has also led to many serious problems such as duplications, hacking and malevolent usage of digital information [1]. Steganography is sometimes confused with cryptography, but there are some notable and distinctive differences between the two concepts. In some situations steganography is often preferred to cryptography. This is because in cryptography the cipher text is a scrambled output of the plaintext and the attacker can guess the presence of encryption has been performed and hence can employ decryption techniques to acquire the hidden data. Also, cryptographic techniques often require high computing power to perform encryption which may affect devices that lack enough computing resources to implement encryption. On the other hand, steganography is the process of masking the sensitive data in any cover media like still images, audio or video. This way the attacker does not feel the presence of the data being transmitted since it is hidden to the naked eye and impossible to distinguish from the original media.

Steganography involves 4 steps:

- a. Selection of the cover media used for data hiding.
- b. The secret message or information that is needed to be embedded in the cover image.
- c. A function that will be used to hide the data value in the cover media and its inverse function to retrieve the hidden data.
- d. An optional key or the password to authenticate or to embed and extract the data.

To avoid the interception of sensitive information by a malicious user during transmission, data hiding has attracted significantly much attention in recent years [2,3,4]. The philosophy of data hiding is to embed the secret data into a cover image and to generate quality stego-image with PSNR higher than 30dB. Since the stego-image with PSNR higher than 30dB is imperceptible to human's recognition, the malicious user will not be able to recognize whether the secret data is embedded in stego-image or not. Only the authorized user can extract the secret data from the stego-image.

Many RDH methods have been proposed in recent years, e.g., the methods based on lossless compression [5,6], difference expansion technique (DE) [7,8,9], histogram shifting (HS) method [14,15,16], and integer transform [18,19], etc. All these methods aim at increasing the embedding capacity (EC) as high as possible while keeping the carrier distortion low. Tian's DE algorithm [7] is an important work in the field of RDH. In DE algorithm, the host image is divided into pixel pairs, and the difference value of two pixels in each pair is expanded to carry one data bit. This method can provide an embedding rate (ER) up to 0.5 bits per pixel (BPP) and outperforms previous compression-based works. In particular, Tian used a location map to record all expandable locations, and afterwards, the technique of location map is widely used by most RDH algorithms. Later on, Tian's method has been improved in many aspects. Alattar [10] generalized DE to a triple or a quad of pixels which can raise the maximum ER from 0.5 BPP to 0.75 BPP. Kamstra and Heijmans [8] utilized low-pass image to predict expandable locations so that the location map can be compressed remarkably. Thodi and

Rodriguez [9] achieved a major improvement by incorporating DE with HS. In addition, instead of the difference value, Thodi and Rodriguez suggested the use of the prediction-error for expansion embedding since this can better exploit local correlations within neighboring pixels. In [11], as an extension of Thodi and Rodriguez's work, Hu et al. proposed a method by constructing a location map dependent on payload. Recently, Hu et al.'s method is further investigated by Li et al. [12] by considering adaptive embedding in which smooth pixels are embedded with more data bits than other pixels. Another improvement of Hu et al.'s method is the work of Zhou and Au [13] by introducing a different capacity parameters determination strategy.

Ni et al.'s HS-based algorithm [14] is another important work of RDH, in which the peak value of image histogram is utilized to embed data. In this method, each pixel value is modified at most by 1, and thus it keeps the visual quality of marked image. In [15], Lee et al.'s proposed a method by utilizing the histogram of difference image. This method performs better than Ni et al.'s by improving both EC and visual quality. The spatial correlation of natural images is exploited in Lee et al.'s method and thus a more correct histogram is obtained. In [16], Hong et al. proposed a new HS-based method by modifying the histogram of prediction-error. This method can well exploit the image redundancy and can thus achieve a much better performance compared with the previously introduced DE-based methods. Recently, Wu and Huang [17] proposed a novel HS-based method where the histogram bins used for expansion embedding are specifically selected to make the embedding distortion minimum as possible. In general, HS-based RDH is implemented by modifying host image's histogram.

Image interpolation [20,21] is usually used to generate a high-resolution image from its low-resolution one, that is, it scales up an image. The original image and interpolated pixels result to some difference values and data hiding can be applied by taking this as an advantage. There are a number of simple interpolation methods, such as nearest neighbor, bilinear, nearest neighbor mean interpolation etc.

II. Related Works

2.1. Neighbor mean interpolation

In 2009, Jung and Yoo [22] proposed a new interpolation technique called "Neighbor mean interpolation (NMI for short)". It is having a low-time complexity and high-calculation speed. The data hiding scheme by Jung and Yoo scales down the input image into 1/4 of its actual size, which then becomes the original image. The scheme then uses NMI to enlarge this original image into a cover image, which has the same size as the original input image. Secret data are embedded into the scaling-up cover image. The authorized receiver can extract embedded secret message from the stego-image and restore the original image from the cover image.

2.2. Ni et al's method

In 2006, Ni [14] proposed a novel reversible data hiding algorithm, which can recover the original image without any distortion from the marked image after the hidden data have been extracted, is presented by Ni et al. This algorithm utilizes the zero or the minimum point of the histogram of an image and slightly modifies the pixel grayscale values to embed data bit into the image. It can embed more data than many of the reversible data hiding algorithms existing at that time.

For a grayscale cover image C with size of $M \times N$, let a grayscale value with the maximum number of pixels in C as the maximum point denoted as P ; let a grayscale value with no pixels or the minimum number of pixels in C as the zero point denoted as Z . Assume $P < Z$, histogram modification method shifts the values within the range $[P + 1, Z - 1]$ of the histogram to the right-hand side by one unit. It leaves the grayscale value $(P + 1)$ empty. A bit b which is extracted from the secret data will be embedded in the selected pixels, and the output stego-image, S is obtained.

2.3. Yongjian Hu's method

In this paper, [23] they investigated the problem of the overflow location map, which is an important issue in DE-based RDH. In order to increase embedding capacity, the compressibility of the overflow location map is improved by designing a new embedding scheme. The overflow location map depends on the payload. Unlike other (overflow) location maps, it contains two types of overflow locations: one from data embedding and the other from pixel shifting. Since the constraint on shifting is looser, it results in fewer overflow locations than that on embedding. Therefore, our overflow location map matrix is often sparser than others.

This feature makes the overflow location map to have higher compressibility. Interleaving histogram shifting scheme also enhances capacity control capability and it benefits image quality. The proposed algorithm often has better resilience to different images and larger embedding capacity.

III. Proposed System

A two-stage reversible data hiding method with high capacity and good visual quality based on image interpolation and histogram modification techniques is proposed. At the first stage, a high-quality cover image using the developed enhanced neighbour mean interpolation is generated. Then take the difference values from input and cover pixels as a carrier to embed secret data. At the second stage, a histogram modification technique is applied on the difference image to further increase the embedding capacity and preserve the image quality without distortion. The extraction is also two staged. After extracting the whole hidden data the cover image is restored. The architecture can be shown as in fig (1).

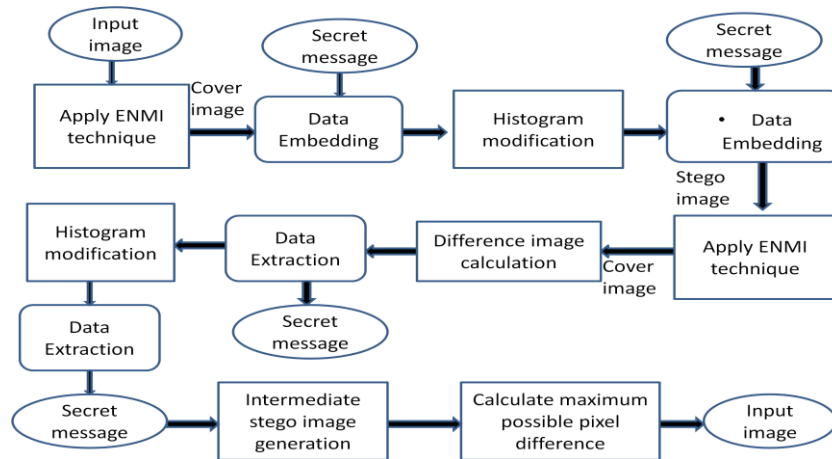


Figure 1: System architecture

3.1. Data embedding

The proposed data hiding algorithm, including two stages with interpolation based data hiding and histogram modification, are shown next in details. The first embedding groups a number of bits and embed its decimal equivalent into pixels. Second embedding is a bit-wise embedding based on histogram modification.

Step 1. For an input image $I(N \times N)$, the ENMI algorithm is applied to generate the corresponding cover image C as given in Eq (1).

for $i = 0$ to $N-1$ do
 for $j = 0$ to $N-1$ do

$$C(i, j) = \begin{cases} I(i, j), & \text{if } i \bmod 2 = 0 \text{ and } j \bmod 2 = 0 \\ I(i, j - 1), & \text{if } j = N - 1 \\ I(i - 1, j), & \text{if } i = N - 1 \\ \frac{I(i, j-1) + I(i, j+1)}{2} & \text{if } i \bmod 2 = 0 \text{ and } j \bmod 2 = 1 \\ \frac{I(i-1, j) + I(i+1, j)}{2} & \text{if } i \bmod 2 = 1 \text{ and } j \bmod 2 = 0 \\ \frac{I(i-1, j-1) + I(i-1, j+1) + I(i+1, j-1) + I(i+1, j+1)}{4}, & \text{otherwise} \end{cases} \quad (1)$$

End for

End for

Step 2. Afterward, a difference image $D0$ can be computed from input image and cover image as shown in Eq (2).

$$D0(i, j) = C(i, j) - I(i, j) \quad (2)$$

Step 3. The number of bits that can be embedded in a pixel, says n is calculated by using Eq (3).

$$n = \lfloor \log_2 |D0(i, j)| \rfloor - 1 \quad (3)$$

Step 4. The first segment of binary secret data $W1$ needs to be partitioned into sub-streams, say w , with n bits before they are hidden. Each sub-stream is extracted out from secret segment $W1$. A single bit "1" called the leading bit is padded to the left-hand side of sub-stream w . An integer value d is calculated from the sub-stream w and its leading bit.

Step 5. Now the integer value d can be embedded into the cover pixel $C(i, j)$. A stego-image $S1$ is generated by adding or subtracting d to or from the cover pixel $C(i, j)$. This helps to make the stego-pixel value closer to the input pixel $I(i, j)$. The embedding rule is shown in Eq (4).

$$S1(i, j) = \begin{cases} C(i, j), & \text{if } i \bmod 2 = 0 \text{ and } j \bmod 2 = 0 \\ C(i, j) + d, & \text{if } I(i, j) \geq C(i, j) \\ C(i, j) - d, & \text{if } I(i, j) < C(i, j) \end{cases} \quad (4)$$

Step 6. The second stage of embedding procedure produces another difference image D1 for increasing the embedding capacity as referred in Eq (5).

$$D1(i, j) = S1(i, j) - C(i, j). \quad (5)$$

Step 7. Then a histogram is constructed based on the difference values D1. Two peak points are chosen where $P2 < 0 < P1$. It is worth mentioning that 0 is not choosing as a peak value as it is necessary to represent the changes of reference pixels when the pixel-shifting in the histogram modification of D1 are carried out. The statute for shifting values in the histogram of D1 is shown in Eq (6).

$$D'1(i, j) = \begin{cases} D1(i, j) + 1, & \text{if } D1(i, j) > P1 \\ D1(i, j) - 1, & \text{if } D1(i, j) < P2 \\ D1(i, j), & \text{otherwise} \end{cases} \quad (6)$$

Step 8. Sequentially scan the difference image D'1 from left-to-right. If the value D'1(i, j) equals to one of the peak values, then one bit w' from the second segment of binary secret data W2 can be embedded in D'1(i, j). The second stage of embedding statute is listed in Eq (7).

$$D''1(i, j) = \begin{cases} D1(i, j) + w', & \text{if } D1(i, j) = P1 \\ D1(i, j) - w', & \text{if } D1(i, j) = P2 \\ D1(i, j), & \text{otherwise} \end{cases} \quad (7)$$

Step 9. The difference value D''1(i, j) can be added to the cover pixel C(i, j) to generate the stego-pixel S(i, j). This is shown in Eq (8).

$$S(i, j) = C(i, j) + D''1(i, j). \quad (8)$$

3.2. Data extraction

Data extraction is the process of separating the secret message from the stego image. There are two stages needed to be performed for extracting the whole hidden data and restoring cover pixels.

Step 1. The procedure first scans the stego-image S and introduces the ENMI algorithm to obtain C by the Eq (9).

$$C(i, j) = \begin{cases} S(i, j) & \text{if } i \bmod 2 = 0 \text{ and } j \bmod 2 = 0 \\ \frac{S(i, j-1) + S(i, j+1)}{2}, & \text{if } i \bmod 2 = 0 \text{ and } j \bmod 2 = 1 \\ \frac{S(i-1, j) + S(i+1, j)}{2}, & \text{if } i \bmod 2 = 1 \text{ and } j \bmod 2 = 0 \\ \frac{S(i-1, j-1) + S(i-1, j+1) + S(i+1, j-1) + S(i+1, j+1)}{4}, & \text{otherwise} \end{cases} \quad (9)$$

Step 2. Now construct a difference image by subtracting C from S by applying Eq (10).

$$D''1(i, j) = S(i, j) - C(i, j). \quad (10)$$

After that, the extraction procedure sequentially scans the difference image D''1 from left-to-right for extracting a segment of secret message by referencing to the values around the peak points.

Step 3. The first stage of extraction initializes W2 as an empty set in advance. A secret bit has been embedded in D''1(i, j) if its value equals to P1, P1 + 1, P2, or P2 - 1. Now the secret data bit w' can be extracted from difference image as in Eq (11).

$$w' = \begin{cases} 0, & \text{if } D''1(i, j) = P1 \text{ or } D''1(i, j) = P2 \\ 1, & \text{if } D''1(i, j) = P1 + 1 \text{ or } D''1(i, j) = P2 - 1 \end{cases} \quad (11)$$

Append the secret bits to W2 in the way that $W2 = W2 || w'$. After that, the histogram modification method is applied on the difference image D''1 as given in Eq (12).

$$D1(i, j) = \begin{cases} D''1(i, j) - 1, & \text{if } D''1(i, j) > P1 \\ D''1(i, j) + 1, & \text{if } D''1(i, j) < P2 \\ D''1(i, j), & \text{otherwise} \end{cases} \quad (12)$$

Step 4. The next is to convert the integer D1(i, j) to its binary format, say b. The first bit which must have been the leading bit "1" of the string b. The secret sub-stream is obtained by discarding the leading bit and takes the rest of the string b. However, when D1(i, j) = 1 is encountered, it means the absence of secret data.

Step 5. Finally, all the secret sub-streams are appended to obtain the secret segment W1. The whole secret message W is obtained by appending W2 to W1. ie, $W = W1 || W2$.

Step 6. The input image can be obtained by applying the ENMI technique on cover image.

IV. Experimental Results

Peak signal-to-noise ratio, often abbreviated PSNR, is an expression for the ratio between original image and noise. It is most commonly used to measure the quality of reconstruction. PSNR measurement is most easily defined via the mean squared error (MSE) value. The mean squared error (MSE) for practical purposes allows comparing the “true” pixel values of our original image to our degraded marked image. The MSE represents the average of the squares of the "errors" between original image and noisy image. The error is the amount by which the values of the original image differ from the noisy image. Given a noise-free $m \times n$ image I and its noisy approximation K, MSE is defined as in Eq. (13) [24].

$$MSE = \frac{1}{mn} \sum_{i=0}^{m-1} \sum_{j=0}^{n-1} [I(i, j) - K(i, j)]^2 \tag{13}$$

The PSNR can be defined as given in Eq. (14):

$$PSNR = 20 \log_{10} \left(\frac{MAX_f}{\sqrt{MSE}} \right) \tag{14}$$

where MAX_f is the maximum possible pixel value of the image. When the pixels are represented using 8 bits per pixel, this is 255. In the absence of noise, the two images I and K are identical, and thus the MSE becomes zero. In this case the PSNR is undefined.

The test images selected for evaluation are shown in Fig:1

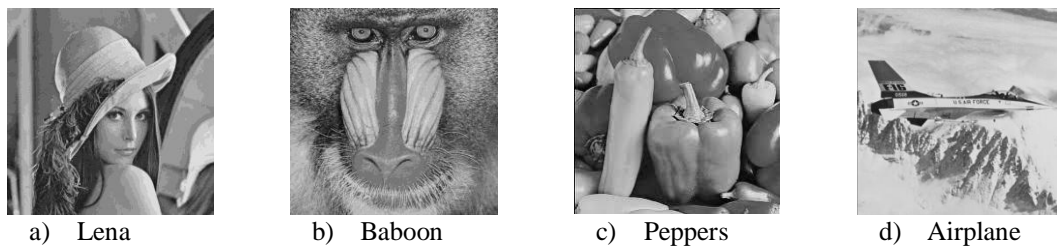


Figure 2: Test images

The algorithm is evaluated by comparing it with some already existing works. Four test images are taken for comparing the algorithms. The PSNR value obtained for different algorithms for each test image can be shown in table I.

Table I. Comparison of PSNR(in dB) for the proposed method with some existing methods for a payload of 20000 bits.

Test image (512x512)	Ni et al's method	Jung and Yoo	Proposed system
Lena	43.21	32.94	44.72
Baboon	41.19	35.71	43.86
Air plane	39.93	33.85	42.04
Peppers	43.92	32.77	44.38

V. Conclusion

The proposed method is a two stage reversible data hiding. It combines the image interpolation technique and histogram shifting. The payload embedding capacity can be increased considerably by the proposed work. The secret message can be completely extracted out at the receiver. The scheme ensures that the distortion due to embedding is kept to be low. In future, more advanced histogram shifting techniques can be combined with interpolation of image to achieve high embedding capacity and low distortion. The technique can be also applied to image after partition it into blocks. This can also increase the efficiency of data hiding.

REFERENCES

[1] C. K. Chan, L. M. Cheng Hiding data in images by simple LSB substitution. Pattern Recognit 37(3), 2004, 469–474
 [2] C. C. Lin, W. L. Tai, and C. C. Chang, Multilevel Reversible Data Hiding based on Histogram Modification of Difference Images, Pattern Recognition, Vol. 41, pp., 2008, 3582-3591.
 [3] H. W. Tseng, Y. M. Tsai, Reversible Data Hiding Scheme Based on Hierarchy Prediction, International Journal of Advanced Information Technologies, Vol.5, 2011, pp.73-90.

- [4] C. C. Chang, W. C. Wu, and Y. C. Hu, Lossless Recovery of a VQ Index Table with Embedded Secret Data, *Journal of Visual Communication and Image Representation*, Vol. 18, 2007, pp 207-216.
- [5] T. Kalker and F. M. J. Willems, Capacity bounds and constructions for reversible data hiding, *Security Watermarking Multimedia Contents V*, vol. 5020, 2003, pp 604-611.
- [6] M. U. Celik, G. Sharma, A. M. Tekalp, and E. Saber, Lossless generalized-LSB data embedding, *IEEE Trans. Image Process.*, vol. 14, no. 2, 2005, pp 253-266.
- [7] J. Tian, Reversible data embedding using a difference expansion, *IEEE Trans. Circuits Syst. Video Technol.*, vol. 13, no. 8, 2003, pp 890-896.
- [8] L. Kamstra and H. J. A. M. Heijmans, Reversible data embedding into images using wavelet techniques and sorting, *IEEE Trans. Image Process.*, vol. 14, no. 12, 2005, pp 2082-2090
- [9] D. M. Thodi and J. J. Rodriguez, Expansion embedding techniques for reversible watermarking, *IEEE Trans. Image Process.*, vol. 16, no. 3, 2007, pp. 721-730.
- [10] A. M. Alattar, Reversible watermark using the difference expansion of a generalized integer transform, *IEEE Trans. Image Process.*, vol. 13, no. 8, 2004, pp. 1147-1156.
- [11] Y. Hu, H. K. Lee, and J. Li, DE-based reversible data hiding with improved overflow location map, *IEEE Trans. Circuits Syst. Video Technol.*, vol. 19, no. 2, 2009, pp. 250-260.
- [12] X. Li, B. Yang, and T. Zeng, Efficient reversible watermarking based on adaptive prediction-error expansion and pixel selection, *IEEE Trans. Image Process.*, vol. 20, no. 12, 2011, pp. 3524-3533.
- [13] J. Zhou and O. C. Au, Determining the capacity parameters in PEE based reversible image watermarking, *IEEE Signal Process. Lett.*, vol. 19, no. 5, 2012, pp. 287-290.
- [14] Z. Ni, Y. Q. Shi, N. Ansari, and W. Su, Reversible data hiding, *IEEE Trans. Circuits Syst. Video Technol.*, vol. 16, no. 3, 2006, pp. 354-362.
- [15] S. K. Lee, Y. H. Suh, and Y. S. Ho, Reversible image authentication based on watermarking, in *Proc. IEEE Int. Conf. Multimedia Expo*, Jul. 2006, pp. 1321-1324.
- [16] W. Hong, T. S. Chen, and C. W. Shiu, Reversible data hiding for high quality images using modification of prediction errors, *J. Syst. Softw.*, vol. 82, no. 11, 2009, pp. 1833-1842.
- [17] H.-T. Wu and J. Huang, Reversible image watermarking on prediction errors by efficient histogram modification, *Signal Process.*, vol. 92, no. 12, Dec. 2012, pp. 3000-3009,.
- [18] D. Coltuc and J. M. Chassery, Very fast watermarking by reversible contrast mapping, *IEEE Signal Process. Lett.*, vol. 14, no. 4, Apr. 2007, pp. 255-258,.
- [19] X. Wang, X. Li, B. Yang, and Z. Guo, Efficient generalized integer transform for reversible watermarking, *IEEE Signal Process. Lett.*, vol. 17, no. 6, Jun. 2010, pp. 567-570,.
- [20] Jan SR, Hsu SJ, Chiu CF, Chang SL, An improved data hiding method using image interpolation, seventh international conference on intelligent information hiding and multimedia signal processing, 2011, pp 185-188.
- [21] Yalman Y, Akar F, Erturk I, An image interpolation based reversible data hiding method using R-weighted coding, 13th IEEE international conference on computational science and engineering, 2010, pp 346-350
- [22] Jung KH, Yoo KY Data hiding method using image interpolation. *Comput Stand Interfaces* 31(2), 2009, pp 465-470.
- [23] Y. Hu, H. K. Lee, and J. Li, DE-based reversible data hiding with improved overflow location map, *IEEE Trans. Circuits Syst. Video Technol.*, vol. 19, no. 2, Feb. 2009, pp. 250-260.
- [24] Salomon, David, *Data Compression: The Complete Reference* (4 ed.). Springer. p. 281. ISBN 978-1846286025, 2007.



International Journal of Modern Engineering Research (IJMER)

Volume : 4 Issue : 4 (Version-3)

ISSN : 2249-6645

April - 2014

Contents :

Comparative Study of ECONOMISER Using the CFD Analysis <i>K. Sainath, Mohd Salahuddin, Mohammed Shafi, Dr. T.K.K Reddy</i>	01-06
On πGr-Separation Axioms <i>C. Janaki, V. Jeyanthi</i>	07-13
Design of Image Projection Using Combined Approach for Tracking <i>Ms. Pooja Pandey, Ms. V. N. Katkar</i>	14-17
Assessing Water Demand And Supply For Srinagar City (J&K) India, Under Changing Climatic Scenarios Using Water Evaluation And Planning Model (WEAP) <i>Muzaffar A. Malla, Umar Firdous Ahmad, Manzoor A. Rather, Muzafar N. Teli, Nisar A. Kuchhay</i>	18-26
Low Power Design of Standard Digital Gate Design Using Novel Sleep Transistor Technique <i>Kusum Tomar, A.S.M. Tripathi</i>	27-33
Disrepair of Earth Moving Equipment: Causes and Remedies <i>David O. Obada, Emmanuel B. Lucas, Bernard A. Otegbayo, Tosin I. Orogun, Ibraheem A. Samotu, Chike V. Chira</i>	34-39
Office Security System <i>Bhagare Pradeep M., Prof. Mrs. Laturkar A. P.</i>	40-45
Effect of Hardness and Wear Resistance on En 353 Steel by Heat Treatment <i>Navin A. Astunkar, A. S. Bonde</i>	46-49
Accelerating Real Time Applications on Heterogeneous Platforms <i>Vivek Vanpariya, Prof. S. Ramani</i>	50-55
Strengthening Of PCC Beams by Using Different Types of Wire Mesh Jacketing <i>Er. Arote P. S., Er. Dhindale G. B., Er. Malunjkar J. A., Er. Umbare A. S.</i>	56-58

Comparative Study of ECONOMISER Using the CFD Analysis

K. Sainath¹, Mohd Salahuddin², Mohammed Shafi³, Dr. T.K.K Reddy⁴

^{1,2,3}Mechanical Engineering Department Sreyas Institute of Engineering & Technology, Nagole,
Hyderabad-500 085, INDIA

⁴Mechanical Engineering Department Jawaharlal Nehru Tech. University Hyderabad, Kukatpally,
Hyderabad -500 085, INDIA

Abstract: This paper presents a simulation of the economizer zone, which allows studying the flow patterns developed in the fluid, while it flows along the length of the economizer. The past failure details reveal that erosion is more in U-bend areas of Economizer Unit because of increase in flue gas velocity near these bends. But it is observed that the velocity of flue gases surprisingly increases near the lower bends as compared to upper ones. The model is solved using conventional CFD techniques by FLUENT software. In which the individual tubes are treated as sub-grid features. A geometrical model is used to describe the multiplicity of heat-exchanging structures and the interconnections among them. The Computational Fluid Dynamics (CFD) approach is utilised for the creation of a three-dimensional model of the economizer coil of single column tube. With equilibrium assumption applied for description of the system chemistry. The flue gas temperature, pressure and velocity field of fluid flow within an economizer tube using the actual boundary conditions have been analysed using CFD tool. This study is a classic example of numerical investigation into the problem of turbulent flows in U-bends for the pressure drop and velocity variation in the flow so that it helps in design the economizer with low pressure losses for the thermal power plants.

Keywords: Economizer, flow efficiencies, CFD, pressure drops, FLUENT, fluid dynamics.

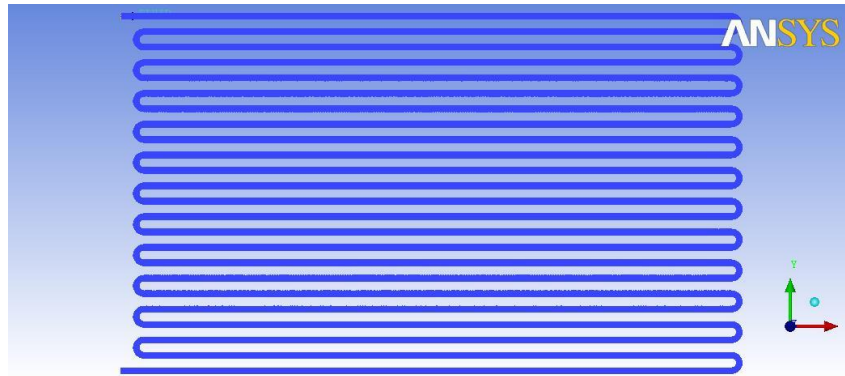
I. Introduction

In boilers, economizers are heat exchange devices that heat fluids, usually water, up to but not normally beyond the boiling point of that fluid. Economizers are so named because they can make use of the enthalpy in fluid streams that are hot, but not hot enough to be used in a boiler, thereby recovering more useful enthalpy and improving the boiler's efficiency. Using an economizer can increase feed water temperature and reduce the amount of heat required in a boiler. The amount of heat that can be transferred and the upper limit of feed water temperature depend primarily on boiler (steam) pressure and temperature of flue gases discharged from the boiler. Transferring heat from the flue gases to the feed water will lower flue gas temperature. Economizer reduces operating costs or economies on fuel by recovering extra energy from the flue gas. The ultimate goal of economizer design is to achieve necessary heat transfer at minimum cost. A key design criterion for economizer is maximum allowable flue gas velocity. Higher velocity provides better heat transfer and reduces capital cost. The control over the fluid flow is absolute to increase the efficiency of the economizer. And CFD modelling is a good tool to study the fluid flow, to improve the efficiency of economizer by reducing the number of tubes of existing model. The strategy of how to recover this heat depends in part on the temperature of the waste heat gases and the economics involved. Large quantity of hot flue gases is generated from Boilers, Kilns, Ovens and Furnaces. If some of this waste heat could be recovered, a considerable amount of primary fuel could be saved. CFD has evolved as important tool for modelling of coal fired boiler and it can be useful to quantify the fluid flow field and pressure distribution with the boiler economizer. Hence FLUENT software was used to study the velocity and pressure distribution of the working fluid inside the economizer.

II. Describing the Model and Simulations

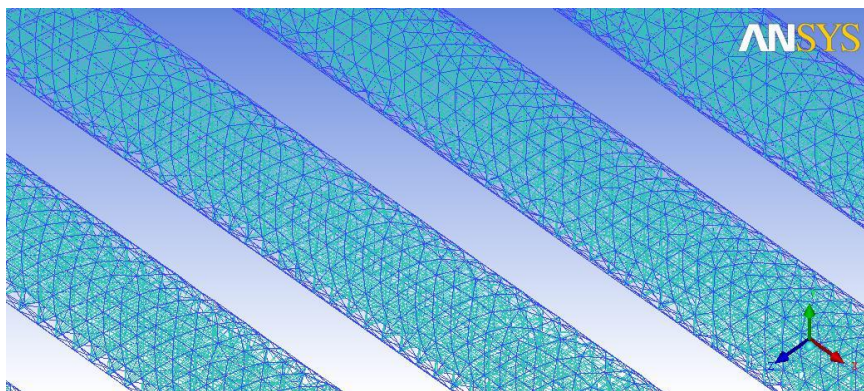
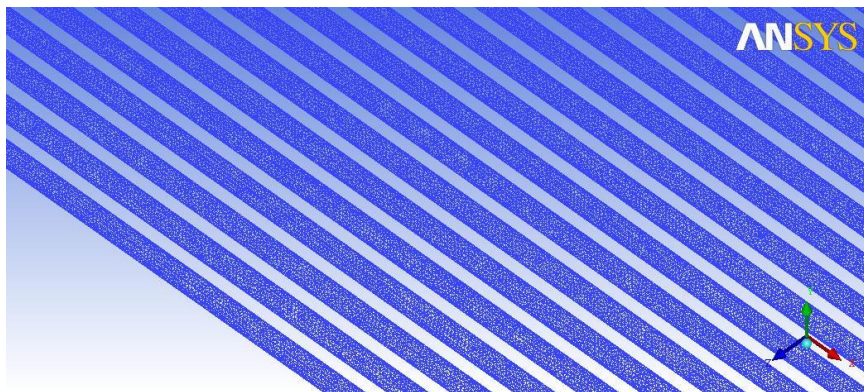
A three dimensional model of an economizer is model with the standard specifications and dimensions from an industry, by using the software tool ICEM CFD. In the ICEM CFD, the economizer was modelled and meshed with the tetrahedral scheme. For this analysis, single unit of economizer is considered and modelled to observe the flow phenomenon and pressure drop in each step tube and the overall pressure drop of the economizer unit.

It consists of 12 parallel pipes of 30 meters long and 23 C-shaped connecting tubes on either side of the parallel tube as shown in figure 1.



III. Meshing & Solving

The modelled geometry was under gone discretization process, with the help of Mesh tool available in the ICEM CFD tool. On meshing the geometry in the ICEM CFD tool, it was observed to had quality of 0.72 in the relevance standards of the ICEM CFD tool. With the satisfactory mesh quality, it is found that it has:



IV. Boundary Conditions

On discretising the geometry, the specific boundary conditions should be assigned to the surface of the elements, which decides the behaviour of the element to the solver. The following working and boundary conditions are to evaluate the performance between the right angled and circular tube pipes. In the fluent solver, the following boundary and solver conditions are used:

Model:

Solve under energy equation with viscosity k-epsilon equation with standard wall function, with the possibility of viscous heating.

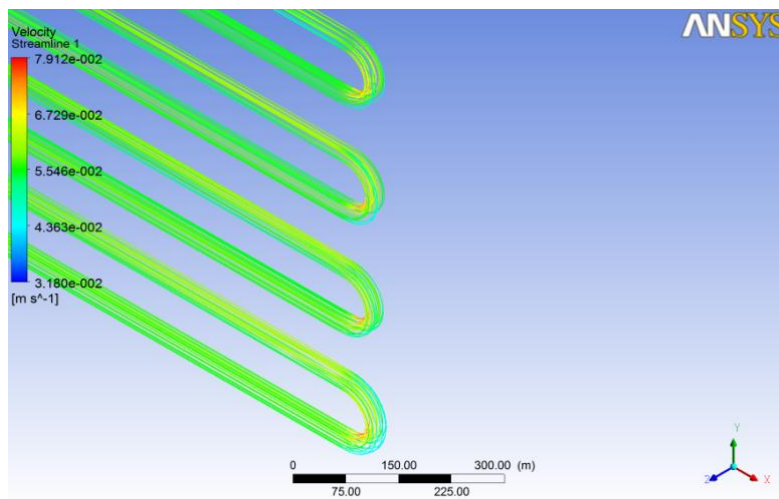
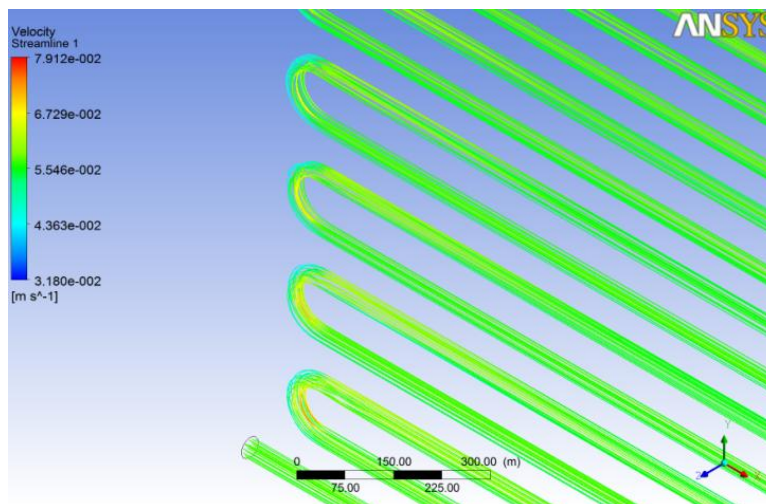
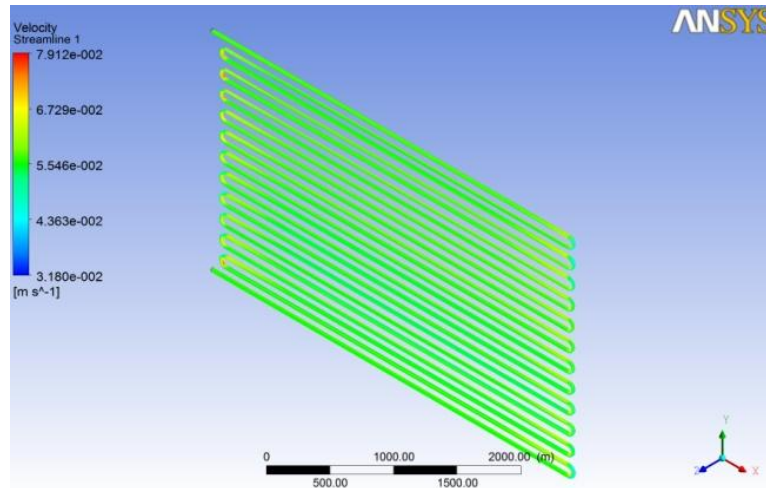
Material:

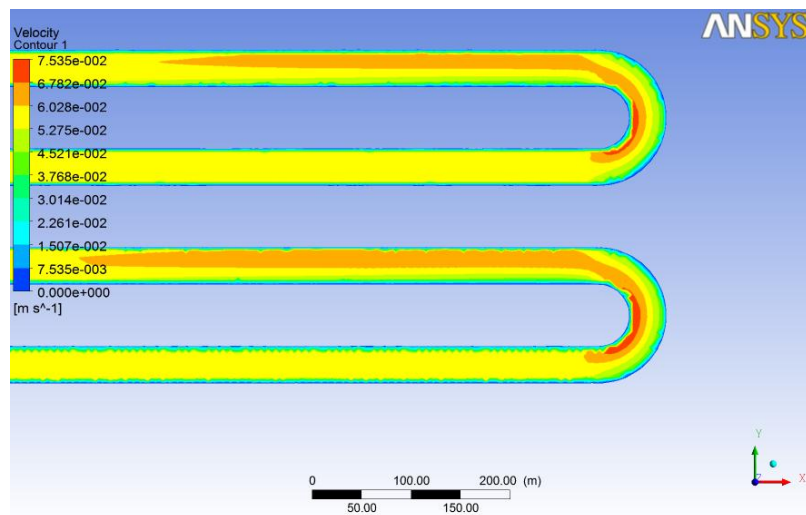
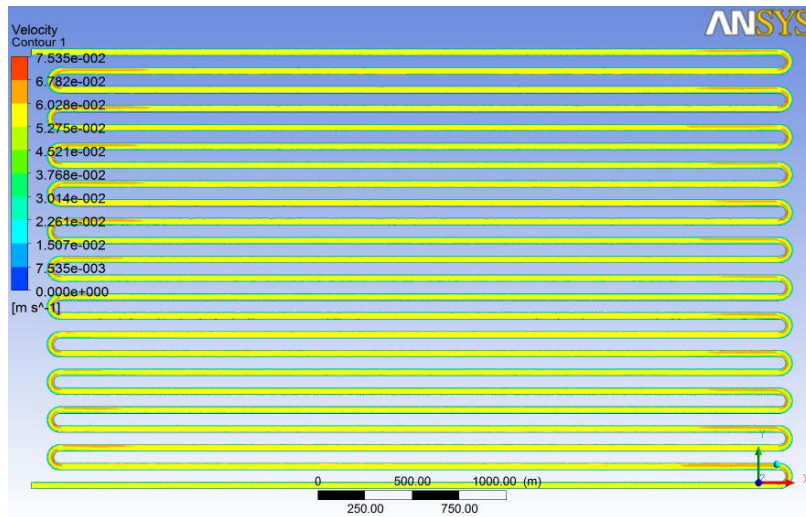
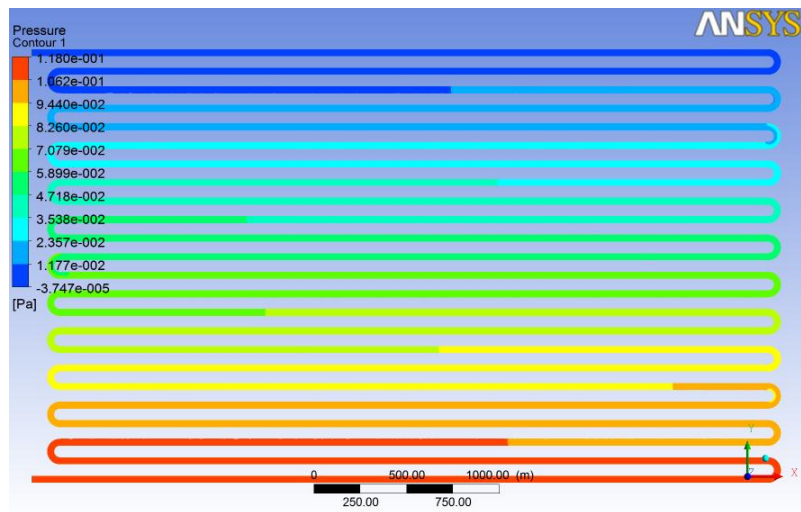
Steel for the pipe wall and water vapour for the volumetric domain (fluid).

Boundary conditions:

Inlet as mass flow rate as 71.5572 kg/s; with inlet pressure as 450000; with temperature 531 K; and with turbulent kinetic energy 1 m²/s²; turbulent dissipation rate 1 m²/s³; outlet as default outflow conditions and the wall temperature as 300 K.

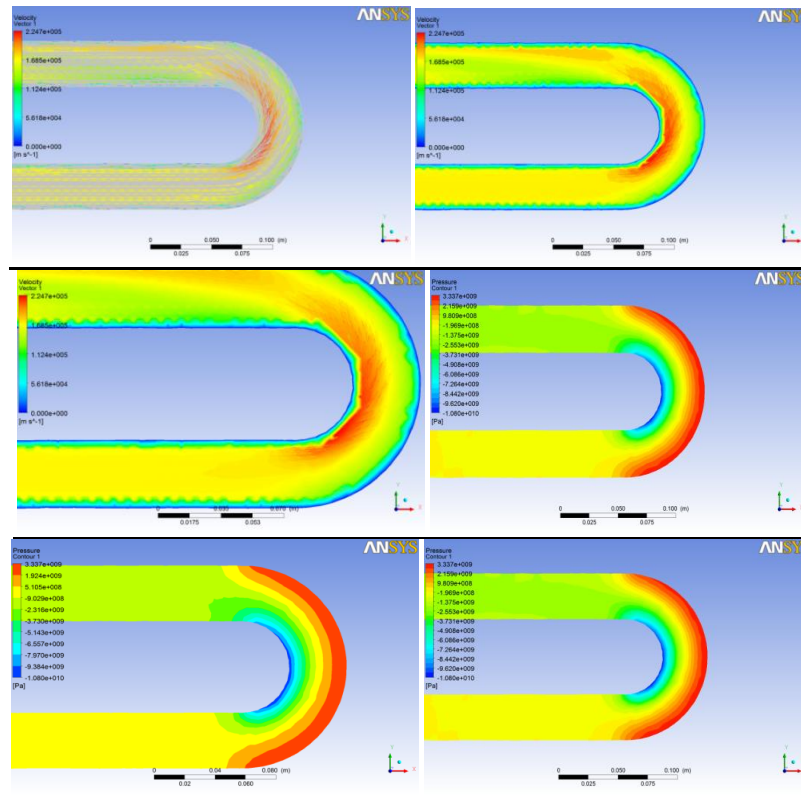
V. Results



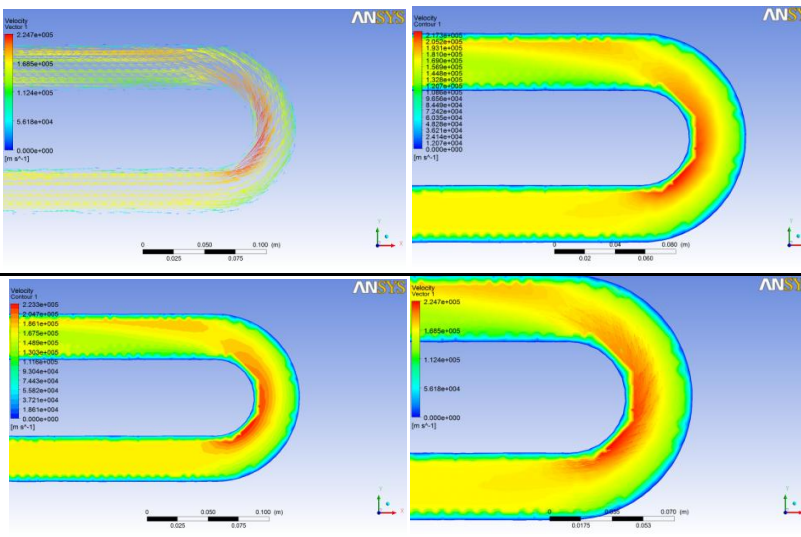


VI. Thermal Analysis

The velocities and pressure profiles:



Temperature profiles:



VII. Summary

From the obtained results, it is observed that the working fluid is accelerated at the C sections of the economizer tube. It was also observed from the obtained contour plots, the stream tube of the flow decreases in the C-section pipe, and resulting in the increase in velocity, which evident to the conservation of continuity equation. It has the maximum and minimum velocity magnitude as $7.535e-2$ and $7.23e-3$ respectively. Due to inertia of the fluid, to change its direction, the stream tube cross sectional area modifies to change its direction. Since considering working fluid as incompressible fluid, to compensate the change in cross sectional area, the fluid gets accelerate inside the stream tube, in the physic principle of mass conservation, which in other words, its satisfied the continuity equation. The pressure drop simulated in the economizer is that, it has the drop of 2.3 a, with reference pressure of 476000 Pa for every pipe. The overall pressure drop is measured 23 Pa across inlet and outlet.

REFERENCES

- [1.] Recovery boilers, American Forest & Paper Association, Tappi Press, Atlanta, 1997, ISBN 0-9625985-3.
- [2.] Adams T.N., and Frederick W.J., Kraft recovery boiler physical and chemical processes.
- [3.] American Paper Institute, New York, NY, 1988.
- [4.] Backman R., Hupa M., and Hyöty P., Tappi J., 67 (12): 60-64, 1984.
- [5.] Björklund H., Warnquist B., Pettersson B., Inside a Kraft recovery boiler – combustion of (high sulfidity) black liquor at high solids content, Tappi/CPPA 1989 International Chemical Recovery Conference Proceedings, Tappi Press, Atlanta, pp. 177-182, 1989.
- [6.] Blasiak W., Vaclavinek J., and Collin, R., Investigation of the flow conditions in a recovery boiler with respect to gases, droplets and dust, Project number: 1192, Department of Heat and Furnace Technology, Royal Institute of Technology, 1992.
- [7.] Coulson J.M., and Richardson J.F., Chemical engineering, Volume 1; Fluid flow, heat transfer and mass transfer, 6th edition, The Bath Press, Bath, Great Britain, 2000.
- [8.] FLUENT user guide, Fluent inc., 2001.
- [9.] Grace T.M., Lien S., Schmidl W., Tse D., Abdullah Z., and Salcudean M., Validation of CFD-based recovery furnace models, International Chemical Recovery Conference, 1998.
- [10.] Grimison E.D., Correlation and utilization of new data on flow resistance and heat transfer for cross flow of gases over tube banks, Trans. ASME, 59: 583-594, 1937.
- [11.] Hupa M., Backman R., Skrifvars B.-J., Tappi J., 73(6): 185-189, 1990.
- [12.] Idelchik I.E., Handbook of hydraulic resistance, 3rd ed., Begell House, 1996, ISBN 1-56700-074-6.
- [13.] Jacoby J., AF-Process AB, personal communication, 2005.
- [14.] Jakob M., Heat transfer and flow resistance in cross flow of gases over tube banks, Trans ASME, 60: 384, 1938.
- [15.] Kawaji M., Shen X.H., Tran H.N., Esaki S., and Dees C., Prediction of heat transfer in the Kraft recovery boiler superheater region, Tappi J., 78(10): 214-221, 1995.
- [16.] Lundborg S., AF-Process AB, personal communication, 2005.
- [17.] Patankar S.V., and Spalding, Heat exchangers: design and theory sourcebook, Scripta Book Co., Washington, D.C., pp.155-176, 1974.70
- [18.] Salcudean M., Modelling of industrial processes using computational fluid dynamics, Canadian Metallurgical Quarterly, 37(3-4): 251-263, 1998.
- [19.] Saviharju K., Pakarinen L., Wag K., and Välipakka I., Numerical modelling feedback in recovery boilers, International Chemical Recovery Conference, 2004.
- [20.] Shen X.H., Kuhn D.C.S., Tran H.N., Mostaghimi, J., and Dees C., Simulation of flue gas flow in the upper furnace of a recovery boiler, Pulp & Paper Canada, 96(5): T171-T175, 1995.
- [21.] Smook G.A., Handbook for pulp & paper technologists, 2nd edition, Angus Wilde Publications, 1992.
- [22.] Tao L., and Blasiak W., Numerical simulation of a Kraft recovery boiler using rotation firing method, Modelling of Kraft recovery boilers - collection of publications (1), Division of Heat and Furnace Technology, Royal Institute of Technology, 1996.
- [23.] Tran H.N., Tappi J., 69 (11): 102, 1986.
- [24.] Tse D., Matys P., Nowak P., Abdullah Z., Salcudean M., and Gartshore I., Flow and heat transfer modelling in the upper furnace of a Kraft recovery furnace, Department of Mechanical Engineering, University of British Columbia, Vancouver, B.C., Canada, 1996, in the 1998 final year report of Black liquor combustion validated recovery boiler modeling.
- [25.] The Institute of Paper Science and Technology, Oregon State University, the University of British Columbia and Babcock & Wilcox Company.
- [26.] Vakkilainen E.K., Adams T.N., and Horton R.R., The effect of recovery furnace bullnose designs on upper furnace flow and temperature profiles, Proc. of 1992 International Chemical Recovery Conference, J101-J112, Seattle, USA, 1992.
- [27.] Vakkilainen E.K., Nikkanen S., Hautamaa J., and Anttonen T., Flows in the upper region of recovery boilers, AIChE Forest Products Symposium, 1991, pp. 125-134.
- [28.] Versteeg H.K. & Malalasekera W., An introduction to computational fluid dynamics – the finite volume method, Addison Wesley Longman Limited, 1995, ISBN 0-582-21884-5.

On π Gr-Separation Axioms

C.Janaki¹, V.Jeyanthi²

¹Asst.Professor, Department of Mathematics, L.R.G. Govt. Arts College for Women, Tirupur-4

²Asst.Professor, Department of Mathematics, Sree Narayana Guru College, Coimbatore- 105

Abstract: In the present paper, we introduce and study the concept of π gr- T_i - space (for $i = 0, 1, 2$) and obtain the characterization of π gr-regular space, π gr- normal space by using the notion of π gr-open sets. Further, some of their properties and results are discussed.

Key Words: π gr- T_0 -space, π gr- T_1 - space, π gr- T_2 -space, π gr- Normal, π gr- Regular.

AMS Subject Classification: 54A05, 54D10, 54D15.

I. Introduction

In 1970, Levine[8] introduced the concept of generalized closed set and discussed the properties of closed and open maps, compactness, normal and separation axioms. Later in 1996 Andrijivic [1] gave a new type of generalized closed set in topological space called b closed sets. The concept of regular continuous functions was introduced by Arya.S.P and Gupta.R [3]. Later Palaniappan.N and Rao. K.C[12] studied the concept of regular generalized continuous functions. Also, the concept of generalized regular closed sets in topological space was introduced by Bhattacharya.S[4,5].Zaitsev [14] defined the concept of π -closed sets and a class of topological spaces called quasi- normal spaces. Dontchev and Noiri [6] defined the notion of π g-closed sets and used this notion to obtain a characterization, preservation theorem for quasi- normal spaces. Maheswari and Prasad[10,11] first defined the notion of S-normal spaces by replacing open sets in the definition of normal spaces by semi-open sets due to Levine[9]. In 1973, Singal and Singal [13] introduced a weak form of normal spaces called mildly normal spaces. In 1990, Arya and Nour[2] studied the characterizations of s-normal spaces. In 2012, Jeyanthi.V and Janaki.C[7] introduced π gr-closed sets in topological spaces.

The purpose of this paper is to introduce and study π gr-separation axioms in topological spaces. Further we introduced the concepts of π gr-regular space, π gr-Normal Space and study their behaviour.

II. Preliminaries

Throughout this paper (X, τ) , (Y, σ) (or simply X , Y) always mean topological spaces on which no separation axioms are assumed unless explicitly stated.

For a subset A of a topological space X , the closure and interior of A with respect to τ are denoted by $Cl(A)$ and $Int(A)$ respectively.

Definition: 2.1

A subset A of X is said to be regular open [12] if $A = \text{int}(cl(A))$ and its complement is regular closed.

The finite union of regular open set is π -open set[6,14] and its complement is π -closed set. The union of all regular open sets contained in A is called $\text{rint}(A)$ [regular interior of A] and the intersection of regular closed sets containing A is called $\text{rcl}(A)$ [regular closure of A]

Definition: 2.2

A subset A of X is called π gr-closed[7] if $\text{rcl}(A) \subset U$ whenever $A \subset U$ and U is π -open. The complement of π gr-closed set is π gr-open set. The family of all π gr-closed subsets of X is denoted by $\pi\text{GRC}(X)$ and π gr-open subsets of X is denoted by $\pi\text{GRO}(X)$

Definition: 2.3

The intersection of all π gr-closed containing a set A is called π gr-closure of A and is denoted by $\pi\text{gr-Cl}(A)$. The union of π gr-open sets contained in A is called π gr-interior of A and is denoted by $\pi\text{gr-int}(A)$.

Definition: 2.4

A function $f: (X, \tau) \rightarrow (Y, \sigma)$ is called

1. Continuous [9] if $f^{-1}(V)$ is closed in X for every closed set V in Y .
2. Regular continuous (r -continuous) [3] if $f^{-1}(V)$ is regular-closed in X for every closed set V in Y .
3. An R -map[6] if $f^{-1}(V)$ is regular closed in X for every regular closed set V of Y .
4. π gr-continuous[7] if $f^{-1}(V)$ is π gr-closed in X for every closed set V in Y .
5. π gr-irresolute[7] if $f^{-1}(V)$ is π gr-closed in X for every π gr-closed set V in Y .

Definition: 2.5

A space X is called a π gr- $T_{1/2}$ space [7] if every π gr-closed set is regular closed.

Definition: 2.6

A map $f: X \rightarrow Y$ is called

1. Closed [9] if $f(U)$ is closed in Y for every closed set U of X .
2. R-closed (i.e., regular closed) [12] if $f(U)$ is regular closed in Y for every closed set U of X .
3. rc-preserving [6] if $f(U)$ is regular closed in Y for every regular closed set U of X .

Definition: 2.7

A map $f: X \rightarrow Y$ is called

1. π gr-open map if $f(V)$ is π gr-open in Y for every open set V in X .
2. strongly π gr-open map (M - π gr-open) if $f(V)$ is π gr-open in Y for every π gr-open set V in X .
3. Quasi π gr-open if $f(V)$ is open in Y for every π gr-open set V in X .
4. Almost π gr-open map if $f(V)$ is π gr-open in Y for every regular open set V in X .

Definition: 2.8

A space X is said to be R-regular [10] if for each closed set F and each point $x \notin F$, there exists disjoint regular open sets U and V such that $x \in U$ and $F \subset V$.

Definition: 2.9

A space X is said to be R-Normal [11,13] (Mildly Normal) if for every pair of disjoint regular closed sets E and F of X , there exists disjoint open sets U and V such that $E \subset U$ and $F \subset V$.

III. π Gr Separation Axioms

In this section, we introduce and study π gr-separation axioms and obtain some of its properties.

Definition: 3.1

A space X is said to be π gr- T_0 -space if for each pair of distinct points x and y of X , there exists a π gr-open set containing one point but not the other.

Theorem: 3.2

A space X is π gr- T_0 -space iff π gr-closures of a distinct points are distinct.

Proof: Let x and y be distinct points of X . Since X is a π gr- T_0 -space, there exists a π gr-open set G such that $x \in G$ and $y \notin G$.

Consequently, $X - G$ is a π gr-closed set containing y but not x . But π gr-cl(y) is the intersection of all π gr-closed sets containing y . Hence $y \in \pi$ gr-cl(y), but $x \notin \pi$ gr-cl(y) as $x \notin X - G$. Therefore, π gr-cl(x) \neq π gr-cl(y).

Conversely, let π gr-cl(x) \neq π gr-cl(y) for $x \neq y$.

Then there exists at least one point $z \in X$ such that $z \notin \pi$ gr-cl(y).

We have to prove $x \notin \pi$ gr-cl(y), because if $x \in \pi$ gr-cl(y), then $\{x\} \subset \pi$ gr-cl(y)

$\Rightarrow \pi$ gr-cl(x) $\subset \pi$ gr-cl(y). So, $z \in \pi$ gr-cl(y), which is a contradiction. Hence $x \notin \pi$ gr-cl(y). $\Rightarrow x \in X - \pi$ gr-cl(y), which is a π gr-open set containing x but not y . Hence X is a π gr- T_0 -space.

Theorem: 3.3

If $f: X \rightarrow Y$ is a bijection, strongly- π gr-open and X is a π gr- T_0 -space, then Y is also π gr- T_0 -space.

Proof: Let y_1 and y_2 be two distinct points of Y . Since f is bijective, there exists points x_1 and x_2 of X such that $f(x_1) = y_1$ and $f(x_2) = y_2$. Since X is a π gr- T_0 -space, there exists a π gr-open set G such that $x_1 \in G$ and $x_2 \notin G$. Therefore, $y_1 = f(x_1) \in f(G)$, $y_2 = f(x_2) \notin f(G)$. Since f is strongly π gr-open function, $f(G)$ is π gr-open in Y . Thus, there exists a π gr-open set $f(G)$ in Y such that $y_1 \in f(G)$ and $y_2 \notin \pi$ gr- T_0 -space.

Definition: 3.4

A space X is said to be π gr- T_1 -space if for any pair of distinct points x and y , there exists π gr-open sets G and H such that $x \in G, y \notin G$ and $x \notin H, y \in H$.

Theorem: 3.5

A space X is π gr- T_1 -space iff singletons are π gr-closed sets.

Proof: Let X be a π gr- T_1 -space and $x \in X$. Let $y \in X - \{x\}$. Then for $x \neq y$, there exists π gr-open set U_y such that $y \in U_y$ and $x \notin U_y$.

Conversely, $y \in U_y \subset X - \{x\}$.

That is $X - \{x\} = \bigcup \{U_y : y \in X - \{x\}\}$, which is π gr-open set.

Hence $\{x\}$ is π gr-closed set.

Conversely, suppose $\{x\}$ is π gr-closed set for every $x \in X$. Let $x, y \in X$ with $x \neq y$. Now, $x \neq y \Rightarrow y \in X - \{x\}$. Hence $X - \{x\}$ is π gr-open set containing y but not x . Similarly, $X - \{y\}$ is π gr-open set containing x but not y . Therefore, X is a π gr- T_1 -space.

Theorem: 3.6

If $f : X \rightarrow Y$ is strongly π gr -open bijective map and X is π gr - T_1 -space, then Y is π gr- T_1 - space.

Proof: Let $f : X \rightarrow Y$ be bijective and strongly- π gr-open function. Let X be a π gr- T_1 -space and y_1, y_2 be any two distinct points of Y .

Since f is bijective, there exists distinct points x_1, x_2 of X such that $y_1 = f(x_1)$ and $y_2 = f(x_2)$. Now, X being a π gr- T_1 -space, there exists π gr-open sets G and H such that $x_1 \in G, x_2 \notin G$ and $x_1 \notin H, x_2 \in H$. Since $y_1 = f(x_1) \in f(G)$ but $y_2 = f(x_2) \notin f(G)$ and $y_2 = f(x_2) \in f(H)$ and $y_1 = f(x_1) \notin f(H)$.

Now, f being strongly- π gr-open, $f(G)$ and $f(H)$ are π gr-open subsets of Y such that $y_1 \in f(G)$ but $y_2 \notin f(G)$ and $y_2 \in f(H)$ and $y_1 \notin f(H)$. Hence Y is π gr- T_1 -space.

Theorem: 3.7

If $f : X \rightarrow Y$ is π gr -continuous injection and Y is T_1 , then X is π gr- T_1 - space.

Proof: Let $f : X \rightarrow Y$ be π gr- continuous injection and Y be T_1 . For any two distinct point x_1, x_2 of X , there exists distinct points y_1, y_2 of Y such that $y_1 = f(x_1)$ and $y_2 = f(x_2)$.

Since Y is T_1 - space, there exists open sets U and V in Y such that $y_1 \in U$ and $y_2 \notin U$ and

$$y_1 \notin V, y_2 \in V.$$

i.e. $x_1 \in f^{-1}(U), x_1 \notin f^{-1}(V)$ and $x_2 \in f^{-1}(V), x_2 \notin f^{-1}(U)$

Since f is π gr - continuous, $f^{-1}(U), f^{-1}(V)$ are π gr -open sets in X .

Thus for two distinct points x_1, x_2 of X , there exists π gr - open sets $f^{-1}(U)$ and $f^{-1}(V)$ such that $x_1 \in f^{-1}(U), x_2 \notin f^{-1}(V)$ and $x_2 \in f^{-1}(V), x_2 \notin f^{-1}(U)$.

Therefore, X is π gr - T_1 - space.

Theorem : 3.8

If $f : X \rightarrow Y$ be π gr -irresolute function, and Y is π gr - T_1 - space, there X is π gr - T_1 -space.

Proof: Let x_1, x_2 be distinct points in X . Since f in injective, there exists distinct points y_1, y_2 of Y such that $y_1 = f(x_1)$ and $y_2 = f(x_2)$.

Since Y is π gr - T_1 -space, there exists π gr- open sets U and V in Y such that $y_1 \in U$ and $y_2 \notin U$ and $y_1 \notin V, y_2 \in V$.

i.e. $x_1 \in f^{-1}(U), x_1 \notin f^{-1}(V)$ and $x_2 \in f^{-1}(V), x_2 \notin f^{-1}(U)$.

Since f is π gr- irresolute, $f^{-1}(U), f^{-1}(V)$ are π gr - open sets in X .

Thus, for two distinct points x_1, x_2 of X , there exists π gr- open sets $f^{-1}(U)$ and $f^{-1}(V)$ such that $x_1 \in f^{-1}(U), x_1 \notin f^{-1}(V)$ and $x_2 \in f^{-1}(V), x_2 \notin f^{-1}(U)$.

Hence X is π gr - T_1 - space.

Definition: 3.9

A space X is said to be π gr- T_2 -space, if for any pair of distinct points x and y , there exists disjoint π gr-open sets G and H such that $x \in G$ and $y \in H$.

Theorem: 3.10

If $f : X \rightarrow Y$ be π gr -continuous injection, and Y is T_2 -space, then X is π gr - T_2 -space.

Proof: Let $f : X \rightarrow Y$ be the π gr continuous injection and Y be T_2 . For any two distinct points x_1 and x_2 of X , there exists distinct points y_1, y_2 of Y such that $y_1 = f(x_1), y_2 = f(x_2)$. Since Y is T_2 -space, there exists disjoint open sets U and V in Y such that $y_1 \in U$ and $y_2 \in V$.

i.e. $x_1 \in f^{-1}(U), x_2 \in f^{-1}(V)$.

Since f is π gr - continuous, $f^{-1}(U) \& f^{-1}(V)$ are π gr - open sets in X .

Further f is injective, $f^{-1}(U) \cap f^{-1}(V) = f^{-1}(U \cap V) = f^{-1}(\phi) = \phi$.

Thus, for two disjoint points x_1, x_2 of X , there exists disjoint π gr-open sets $f^{-1}(U) \& f^{-1}(V)$ such that $x_1 \in f^{-1}(U)$ and $x_2 \in f^{-1}(V)$. Hence X is π gr- T_2 -space.

Theorem: 3.11

If $f : X \rightarrow Y$ be the π gr irresolute injective function and Y is π gr- T_2 -space, then X is π gr- T_2 -space.

Proof : Let x_1, x_2 be any two distinct points in X . Since f in injective, there exists distinct points y_1, y_2 of Y such that $y_1 = f(x_1)$ and $y_2 = f(x_2)$.

Since Y is π gr- T_2 , there exist disjoint π gr-open sets U and V in Y such that $y_1 \in U$ and $y_2 \in V$.

i.e, $x_1 \in f^{-1}(U), x_2 \in f^{-1}(V)$.

Since f is π gr-irresolute injective, $f^{-1}(U), f^{-1}(V)$ are disjoint π gr-open sets in X .

Thus, for two distinct points x_1, x_2 of X , there exists disjoint π gr-open sets $f^{-1}(U)$ and $f^{-1}(V)$ such that $x_1 \in f^{-1}(U)$ and $x_2 \in f^{-1}(V)$.

Hence X is π gr- T_2 -space.

Theorem: 3.12

In any topological space, the following are equivalent.

1. X is π gr- T_2 -space.
2. For each $x \neq y$, there exists a π gr-open set U such that $x \in U$ & $y \notin \pi$ gr-cl(U)
3. For each $x \in X$, $\{x\} = \bigcap \{\pi$ gr-cl(U): U is a π gr-open set in X and $x \in U\}$.

Proof: (1) \Rightarrow (2): Assume (1) holds.

Let $x \in X$ and $x \neq y$, then there exists disjoint π gr-open sets U and V such that $x \in U$ and $y \in V$. Clearly, $X-V$ is π gr-closed set. Since $U \cap V = \emptyset$, $U \subset X-V$.

Therefore, π gr-cl(U) \subset π gr-cl($X-V$)

$Y \notin X-V \Rightarrow y \notin \pi$ gr-cl($X-V$) and hence $y \notin \pi$ gr-cl(U), by the above argument.

(2) \Rightarrow (3): For each $x \neq y$; there exists a π gr-open set U such that $x \in U$ and $y \notin \pi$ gr-cl(U)

So, $y \notin \bigcap \{\pi$ gr-cl(U): U is a π gr-open set in X and $x \in U\} = \{x\}$.

(3) \Rightarrow (1): Let $x, y \in X$ and $x \neq y$.

By hypothesis, there exists a π gr-open set U such that $x \in U$ and $y \notin \pi$ gr-cl(U).

\Rightarrow There exists a π gr-closed set V set $y \in V$. Therefore, $y \in X-V$ and $X-V$ is a π gr-open set.

Thus, there exists two disjoint π gr-open sets U and $X-V$ such that $x \in U$ and $y \in X-V$.

Therefore, X is π gr- T_2 -space.

IV. π Gr- Regular Space

Definition: 4.1

A space X is said to be π gr-regular if for each closed set F and each point $x \notin F$, there exists disjoint π gr-open sets U and V such that $x \in U$ and $F \subset V$.

Theorem: 4.2

Every π gr-regular T_0 -space is π gr- T_2 .

Proof : Let $x, y \in X$ such that $x \neq y$.

Let X be a T_0 -space and V be an open set which contains x but not y .

Then $X-V$ is a closed set containing y but not x . Now, by π gr-regularity of X , there exists disjoint π gr-open sets U and W such that $x \in U$ and $X-V \subset W$.

Since $y \in X-V$, $y \in W$.

Thus, for $x, y \in X$ with $x \neq y$ there exists disjoint open sets U and W such that $x \in U$ and $y \in W$.

Hence X is π gr- T_2 -space.

Theorem: 4.3

If $f: X \rightarrow Y$ is continuous bijective, π gr-open function and X is a regular space, then Y is π gr-regular.

Proof: Let F be a closed set in Y and $y \notin F$. Take $y=f(x)$ for some $x \in X$.

Since f is continuous, $f^{-1}(F)$ is closed set in X such that $x \notin f^{-1}(F)$. (since $f(x) \notin F$)

Now, X is regular, there exists disjoint open sets U and V such that $x \in U$ and $f^{-1}(F) \subset V$.

i.e. $y=f(x) \in f(U)$ and $F \subset f(V)$.

Since f is π gr-open function, $f(U)$ and $f(V)$ are π gr-open sets in Y .

Since f is bijective, $f(U) \cap f(V) = f(U \cap V) = f(\emptyset) = \emptyset$.

$\Rightarrow Y$ is π gr-regular.

Theorem: 4.4

If $f: X \rightarrow Y$ is regular continuous bijective, almost π gr-open function and X is R -regular space, then Y is π gr-regular.

Proof:

Let F be a closed set in Y and $y \notin F$.

Take $y=f(x)$ for some $x \in X$.

Since f is regular continuous function, $f^{-1}(F)$ is regular closed in X and hence closed in X .

$\Rightarrow x = f^{-1}(y) \notin f^{-1}(F)$.

Now, X is R -regular, there exists disjoint regular open sets U and V such that $x \in U$ and $f^{-1}(F) \subset V$.

i.e. $y=f(x) \in f(U)$ and $F \subset f(V)$.

Since f is almost π gr-open function $f(U)$ and $f(V)$ are π gr-open sets in Y and also f is bijective, $f(U) \cap f(V) = f(U \cap V)$

$=f(\emptyset) = \emptyset$.

$\Rightarrow Y$ is π gr-regular.

Theorem: 4.5

If $f: X \rightarrow Y$ is continuous, bijective, strongly π gr-open function (quasi π gr-open) and X is π gr-regular space, then Y is π gr-regular (regular).

Proof: Let F be a closed set in Y and $y \in F$.

Take $y = f(x)$ for some $x \in X$.

Since f is continuous bijective, $f^{-1}(F)$ is closed in X and $x \notin f^{-1}(F)$.

Now, since X is π gr-regular, there exists disjoint π gr-open sets U and V such that $x \in U$ and $f^{-1}(F) \subset V$.

i.e. $y = f(x) \in f(U)$ and $F \subset f(V)$.

Since f is strongly π gr-open (quasi π gr-open) and bijective, $f(U)$ and $f(V)$ are disjoint π gr-open (Open) sets in Y .

$\therefore Y$ is π gr-regular (regular).

Theorem: 4.6

If $f: X \rightarrow Y$ is π gr-continuous, closed, injection and Y is regular, then X is π gr-regular.

Proof: Let F be a closed in X and $x \notin F$.

Since f is closed injection, $f(F)$ is closed set in Y such that $f(x) \notin f(F)$.

Now, Y is regular, there exists disjoint open sets G and H such that $f(x) \in G$ and $f(F) \subset H$.

This implies $x \in f^{-1}(G)$ and $F \subset f^{-1}(H)$.

Since f is π gr-continuous, $f^{-1}(G)$ and $f^{-1}(H)$ are π gr-open sets in X .

Further, $f^{-1}(G) \cap f^{-1}(H) = \emptyset$.

Hence X is π gr-regular.

Theorem : 4.7

If $f: X \rightarrow Y$ is almost π gr-continuous, closed injection and Y is R -regular, then X is π gr-regular.

Proof: Let F be a closed set in X and $x \notin F$. Since f is closed injection. $f(F)$ is closed set in Y such that $f(x) \notin f(F)$. Now, Y is R -regular, there exists disjoint regular open sets G and H such that $f(x) \in G$ and $f(F) \subset H$.

$\Rightarrow x \in f^{-1}(G) \text{ \& } F \subset f^{-1}(H)$

Since f is almost π gr-continuous, $f^{-1}(G)$ & $f^{-1}(H)$ are π gr-open sets in X .

Further, $f^{-1}(G) \cap f^{-1}(H) = \emptyset$.

Hence X is π gr-regular.

Theorem: 4.8

If $f: X \rightarrow Y$ is π gr-irresolute, closed, injection and Y is π gr-regular, then X is π gr-regular.

Proof: Let F be a closed set in X and $x \notin F$. Since f is closed injection, $f(F)$ is closed set in Y such that $f(x) \notin f(F)$.

Now, Y is π gr-regular, there exists disjoint π gr-open sets G and H such that $f(x) \in G$ and $f(F) \subset H$.

$\Rightarrow x \in f^{-1}(G) \text{ \& } F \subset f^{-1}(H)$.

Since X is π gr-irresolute, $f^{-1}(G)$ and $f^{-1}(H)$ are π gr-open sets in X .

Further, $f^{-1}(G) \cap f^{-1}(H) = \emptyset$ and hence X is π gr-regular.

V. π Gr-Normal Spaces

Definition: 5.1

A space X is said to be π gr-Normal if for every pair of disjoint closed sets E & F of X , there exists disjoint π gr-open sets U & V such that $E \subset U$ and $F \subset V$.

Theorem: 5.2

The following statements are equivalent for a Topological space X :

1. X is π gr-normal.
2. For each closed set A and for each open set U containing A , there exists a π gr-open set V containing A such that π gr-cl(V) $\subset U$
3. For each pair of disjoint closed sets A and B , there exists π gr-open set U containing A such that π gr-cl(U) $\cap B = \emptyset$.

Proof: (1) \Rightarrow (2): Let A be closed set and U be an open set containing A .

Then $A \cap (X - U) = \emptyset$ and therefore they are disjoint closed sets in X .

Since X is π gr-normal, there exists disjoint π gr-open sets V and W such that $A \subset V$, $X - U \subset W$. i.e. $X - W \subset U$.

Now, $V \cap W = \emptyset$, implies $V \subset X - W$

Therefore, π gr-cl(V) $\subset \pi$ gr-cl($X - W$) = $X - W$, Because $X - W$ is π gr-closed set.

Thus, $A \subset V \subset \pi$ gr-cl(V) $\subset X - W \subset U$.

i.e. $A \subset V \subset \pi$ gr-cl(V) $\subset U$.

(2) \Rightarrow (3): Let A and B be disjoint closed sets in X , then $A \subset X - B$ and $X - B$ is an open set containing A . By hypothesis, there exists a π gr-open set U such that $A \subset U$ and π gr-cl(U) $\subset X - B$, which implies π gr-cl(U) $\cap B = \emptyset$

(3) \Rightarrow (1): Let A and B be disjoint closed sets in X. By hypothesis (3), there exists a π gr-open set U such that $A \subset U$ and $\pi\text{gr-cl}(U) \cap B = \emptyset$ (or) $B \subset X - \pi\text{gr-cl}(U)$.

Now, U and $X - \pi\text{gr-cl}(U)$ are disjoint π gr-open sets such that $A \subset U$ and $B \subset X - \pi\text{gr-cl}(U)$.

Hence X is π gr-normal.

Definition: 5.3

A space X is said to be mildly π gr-Normal if for every pair of disjoint regular closed sets E & F of X, there exists disjoint π gr-open sets U & V such that $E \subset U$ and $F \subset V$.

Theorem: 5.4

If $f: X \rightarrow Y$ is continuous bijective, π gr-open function from a normal spaces X onto a space Y, then Y is π gr-normal.

Proof: Let E and F be disjoint closed sets in Y,

Since f is continuous bijective $f^{-1}(E)$ and $f^{-1}(F)$ are disjoint closed sets in X.

Now, X is normal, there exists disjoint open sets U and V such that $f^{-1}(E) \subset U, f^{-1}(F) \subset V$.

i.e. $E \subset f(U), f \subset f(V)$.

Since f is π gr-open function, $f(U)$ and $f(V)$ are π gr-open sets in Y and f is injective, $f(U) \cap f(V) = f(U \cap V) = f(\emptyset) = \emptyset$. Hence Y is π gr-Normal.

Theorem: 5.5

If $f: X \rightarrow Y$ is regular continuous bijective, almost π gr-open function from a mildly normal space X onto a space Y, then Y is π gr-normal.

Proof: Let E and F be disjoint closed sets in Y, Since f is regular continuous bijective $f^{-1}(E)$ and $f^{-1}(F)$ are disjoint regular closed sets in X.

Now, X is mildly normal, there exists disjoint regular open sets U and V, such that $f^{-1}(E) \subset U, f^{-1}(F) \subset V$.

i.e. $E \subset f(U), F \subset f(V)$. Since f is almost π gr-open function, $f(U)$ & $f(V)$ are π gr-open sets in Y and f is injective, $f(U) \cap f(V) = f(U \cap V) = f(\emptyset) = \emptyset$.

Thus, Y is π gr-Normal.

Theorem: 5.6

If $f: X \rightarrow Y$ is π gr-continuous, closed, bijective, and Y is normal, then X is π gr-normal.

Proof: Let E and F be disjoint closed sets in Y, since f is closed injection, $f(E)$ and $f(F)$ are disjoint closed sets in Y.

Now Y is normal, there exists disjoint open sets G and H such that $f(E) \subset G, f(F) \subset H$.

$\Rightarrow E \subset f^{-1}(G) \text{ \& } F \subset f^{-1}(H)$.

Since f is π gr-continuous, $f^{-1}(G)$ and $f^{-1}(H)$ are π gr-open sets in X.

Further, $f^{-1}(G) \cap f^{-1}(H) = \emptyset$. Hence X is π gr-Normal.

Theorem: 5.7

If $f: X \rightarrow Y$ is almost π gr-continuous, R-closed injective, and Y is R-normal, then X is π gr-normal.

Proof: Let E and F be disjoint closed sets in Y. Since f is R-closed injection, $f(E)$ and $f(F)$ are disjoint regular closed sets in Y.

Now Y is Mildly Normal, (i.e, R-normal), there exists disjoint regular open sets G and H such that $f(E) \subset G, f(F) \subset H$.

$\Rightarrow E \subset f^{-1}(G) \text{ \& } F \subset f^{-1}(H)$.

Since f is almost π gr-continuous, $f^{-1}(G)$ and $f^{-1}(H)$ are π gr-open sets in X.

Further, $f^{-1}(G) \cap f^{-1}(H) = \emptyset$.

Hence X is π gr-Normal.

Theorem: 5.8

If $f: X \rightarrow Y$ is almost π gr-irresolute, R-closed injection, and Y is π gr-normal, then X is π gr-normal.

Proof: Let E and F be disjoint closed sets in Y. Since f is R-closed injection, $f(E)$ and $f(F)$ are disjoint regular closed sets in Y.

Now Y is π gr-Normal, there exists disjoint π gr-open sets G and H such that $f(E) \subset G, f(F) \subset H$.

This implies $E \subset f^{-1}(G)$ and $F \subset f^{-1}(H)$.

Since f is π gr-irresolute, $f^{-1}(G)$ and $f^{-1}(H)$ are π gr-open sets in X.

Further, $f^{-1}(G) \cap f^{-1}(H) = \emptyset$.

\Rightarrow X is π gr-Normal.

Theorem: 5.9

If $f: X \rightarrow Y$ is continuous, bijective, M - π gr-open (quasi π gr-open) function from a π gr-normal space X onto a space Y , then Y is π gr-normal (normal).

Proof: Let E and H be disjoint closed sets in Y . Since f is continuous bijective, $f^{-1}(E)$ and $f^{-1}(H)$ are disjoint closed sets in X . Now, X is π gr-normal, there exists π gr-open sets U and V such that $f^{-1}(E) \subset U$ and $f^{-1}(H) \subset V$. That is $E \subset f(U)$ and $H \subset f(V)$. Since f is M - π gr-open (quasi π gr-open) function, $f(U)$ and $f(V)$ are π gr-open sets (open sets) in Y and f is bijective,

$$f(U) \cap f(V) = f(U \cap V) = f(\emptyset) = \emptyset.$$

Hence Y is π gr-normal (normal).

BIBLIOGRAPHY

- [1] D.Andrijevic, Semi-pre open sets mat.Vesnik 38 (1) 1986, 24-32.
- [2] S.P.Arya and T.Nour, Characterizations of s -normal spaces, Indian J.Pure and Applied Maths 21 (8) (1990) 717-719.
- [3] Arya. S.P and Gupta.R (1974), On Strongly Continuous function. Kyungpook Math . J., 14:131-143.
- [4] Bhattacharya.S (2011), On Generalized Regular Closed sets, Int. J. Contemp. Math .sciences, 6: (3) 145-152.
- [5] P.Bhattacharya and B.K.Lahiri, Semi-generalized closed sets on topology, Indian J.Maths 29 (3) (1987) 375-382.
- [6] J.Dontchev and T.Noiri, Quasi π -normal and π g-closed sets, Acta Math . Hungar, 89(3)(2000), 211-219.
- [7] Jeyanthi.V and Janaki.C, “ π gr-closed sets in topological spaces”, Asian Journal of Current Engg. And Maths, 1:5 Sep 2012, 241-246.
- [8] N.Levine, Generalized closed sets in topology, Tend Circ., Mat. Palermo (2) 19 (1970), 89-96.
- [9] N.Levine, Semi-open sets and semi-continuity in topological spaces, Amer.Math. Monthly 70 (1963), 36-41
- [10] S.N. Maheswari and R.Prasad, On S -regular spaces, Glasnik Math., 10(30): 347:350, 1975.
- [11] S.N. Maheswari and R.Prasad, On S -normal spaces, Bull. Math. Soc. Sci. R.S. Roumanie, 22(70); 27:29, 1978.
- [12] Palaniappan .N and Rao.K.C (1993), Regular Generalized Closed Sets, Kyungpook Math, J. ,33: (2) 211-219.
- [13] Singal M.K, Singal A.R, Mildly Normal spaces, Kyungpook Math J 1973: 13:27-31.
- [14] V. Zaitsav, On Certain classes of topological spaces and their bicompaifications, Dokl Akad Nauk SSSR(178), 778-779.

Design of Image Projection Using Combined Approach for Tracking

Ms. Pooja Pandey¹, Ms. V. N. Katkar²

^{1,2}(Department of computer science and engineering, G. H. Raisoni Institute of engineering and technology for Women's, Nagpur)

Abstract: Over the years the techniques and methods that have been used to interact with the computers have evolved significantly. From the primitive use of punch cards to the latest touch screen panels we can see the vast improvement in interaction with the system. There are many new ways of projection and interaction technologies that can reshape our perception and interaction methodologies. Also projection technology is very useful for creating various geometric displays. In earlier generations, the projector technology was used for projecting images and videos on single screen, using large and bulky setup. To overcome the earlier limitations we are designing "Wireless Image Projection Tracking", which is a system that uses IR (Infrared) technology to track the body in the IR range and uses their movements for image orientation and manipulations like zoom, tilt/rotate, and scale. We are presenting a method of mapping IR light source position and orientation to an image. By using this system we can also track single and multiple IR light source positions and also it can be used effectively to see the image projection in 3D view. Extension in this technology can further be useful for future tracking capabilities to implement the touch screen feature for commercial applications.

Index Terms: image projection, object's location detection, detection of x, y and z-axis values.

I. INTRODUCTION

Today, computers and computer-generated images are occupied and used in many aspects of our daily life. Computer imagery especially is found in many media and activities such as presentation materials, newspapers, weather reports, and surgical procedures. The image visualization technology significantly improves the quality and intuitiveness of output information, but input part still depends on some traditional ways such as keyboard typing, mouse pointing and remote controlling. Recently, advancements in input technology in game and mobile fields provide the potential power for inventing more intuitive, natural and easier-to-use human-computer interaction (HCI) methods.

The proposed system allows users to track their finger movements in 3D space by using the Wiimote's built-in infrared camera with an LED array and reflectors. Head tracking is based on a simple concept that there is a base position in which your head is at the center in front of the screen and at a certain distance (predefined) from the screen. Moving left, right, up, down, towards or away from the camera results in the detection of other coordinates (this can be seen as an offset from the center). The values are calculated in coordinates and then its location is calculated by the localization scheme. Also this design will ensure that we can see the 3D image from the 2D input image.

Wiimote is a smart device used for developing a unified human computer interface. It is a handheld device resembling a television remote, but in addition to buttons, it contains a 3-axis accelerometer, a high-resolution high speed IR camera, motion sensor and wireless Bluetooth connectivity. This technology makes the Wii remote one of the most sophisticated PC compatible input devices available today.

The aim of this research is to improve the projector technology in a way that it can be easily applicable at places where more number of projectors are used and the image can be minimized, maximized, tilted, rotated and its 3D view can be viewed. In this research we are proposing a scheme to implement (Infrared) IR light source tracking system which can be used for tracking single and multiple IR light source positions and can be used effectively in optical tracking problems such as tracking head position which is a basic requirement in a Virtual Reality System. We are designing a system that uses IR (Infrared) technology to track the body in the IR range and uses their movements for image manipulations like zoom, tilt/rotate, and scale.

We are presenting a method of mapping IR light source position and orientation to an image. By using this system we can also track single and multiple IR light source positions and also it can be used to see the image projection in 3D view.

II. Literature Survey

Since the introduction of the “Wiimote” work has been done in the area of wireless communication by Johnny Chung Lee, the further researches improved the use of Wiimote. Wiimote is a multipurpose device as it contains multiple devices included with it like IR camera tracker, accelerometer, LEDs, speaker, vibration motor, Bluetooth connectivity, internal flash memory, batteries, expansion port and buttons. The wireless remote also nicknamed as “Wiimote” is a smart device which has multiple features [1].

For converting the Wiimote readouts to the position and orientation of the corresponding mobile unit based on major axes identification, coordinate transformation, and position updating. The scheme and the algorithm are validated by tracking the Wiimote location on a two-axis linear servomotor. The 2D IR source location sensing was designed by D. Gu, Y.-T. Fu, K.-S. Ou and K.-S. Chen [2].

The head location tracking is used with Wiimote to track the head behind a computer screen. Also the tracking method was used in Windows with the use of Windows based OpenGL and made it as a library which can be used in any OpenGL application. The application is created with the use of Direct X and the Microsoft Windows operating system was presented by Bharat L, Shashank S, Nageli V S, Sangeeta Shrivastava and S Rakshit [3].

The two handed surface-less interaction for presentation based on infrared based point tracking was then developed. It contributed a robust method for pairing and pinching that allowed to detect hands and their actions. It was useful to work with slide decks, images and videos. Luc Vlaming, Jasper Smit, and Tobias Isenberg presented this interaction with hands which showed rotation and scaling using hand gestures and movements of fingers and handle the images videos and slide presentations. It also presented geometric transformation methods for rotation of objects and also for translation and scaling [4].

Hector Vragas, Enrique Preza, and Ramiro Velazquez proposed a method to detect the working area of the Wiimote and also useful for tracking positioning and tracking of the small aerial vehicles. It also showed a method of 3D tracking using the Wiimote [5].

Thus by surveying the previous work done we are proposing a design for wireless image projection tracking.

III. Research Methodology

Infrared communication has high directionality and can identify the person with whom you are communicating. Compared with the wireless communication with a maximum speed of about 100 Mbps, the infrared communication has a potential of 1 Gbps. The IR LEDs are used as IR sources and as IR sensor we used Wii Remote. IR is used to provide a range for the system such that it can be used inside that particular range only. Using the Wii Remote’s built-in camera, the position and orientation of the Wii Remote in 3D space can be calculated by tracking four known infrared (IR) LEDs (LED - Light Emitting Diode) positions and then relating these values to the reported position retrieved from the camera. It can be utilized as a tracking device. We can set up expressions that linearly transform IR LEDs from a known position in the global coordinate space into the camera’s coordinate space.

Bluetooth is a wireless technology standard for exchanging data over short distances. Bluetooth operates in the range of 2400–2483.5 MHz. This is in the globally Industrial, Scientific and Medical (ISM) 2.4 GHz short-range radio frequency band. Bluetooth is used to establish the communication between the IR transmitter, smart device and the computer. Communication is established using the Bluetooth protocol. The software aspect of this communication is handled by the Bluetooth Stack which should be installed in the system.

Object positioning is used to track the position of the objects in the form of IR reflectors. Smart device is proposed to act as finger and gesture tracking sensor to manipulate the image operations like scaling, rotating and zooming. The position and orientation of the corresponding object is based on major axes identification, coordinate transformation, and position updating. These values are used to locate the object and image processing will be used for image manipulations.

For head tracking the camera detects two IR points which are placed on the two sides of the goggle and translates these to two coordinates onto the plane. The camera takes in the coordinates of the IR sources and translates this into an absolute movement with respect to the default position of the head.

The present module is the communication between the computer and the wiimote. It consists of the interfacing program. The interface here is Bluetooth technology. With the help of the Bluetooth technology it becomes easier to both track and transfer the information. The next module is the event activation which is the activation of the buttons in the wiimote. The future module is the finger tracking and its related events activation. It will be an approach for wireless mouse. The final module will be the 3D view generation. It consists of the generation of the Z-axis of the 2D plane.

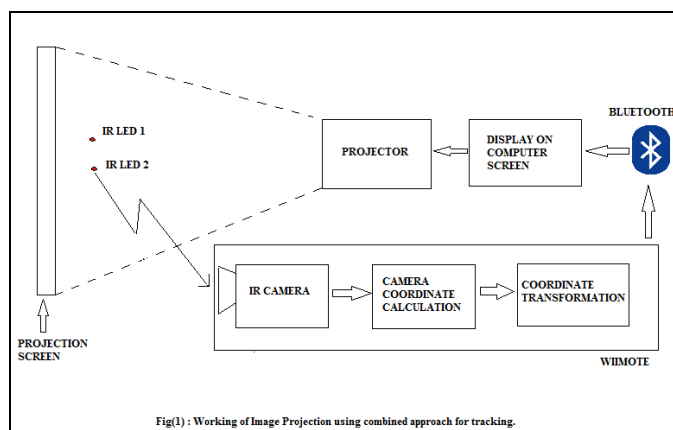
The modules work in combination to form the Projection of wireless image using tracking. Hence every parameter to be measured and calculated is to be accurate for the proper functioning of the whole system.

In order to operate the system, the WiiMote must be connected to the operating laptop. The WiiMote communicates with the laptop via Bluetooth, therefore the laptop must have accessibility to Bluetooth devices, in case the laptop doesn't have that ability, it is necessary to connect a Bluetooth USB dongle that will enable the Bluetooth connections. Generally the Bluetooth accessibility is inbuilt in the today's laptops still for accurate working of the setup we use Bluetooth dongle.

The idea is that the detected distance between the object vs. the distance of the center of the other object from the IR camera is being mapped. Then a curve fitting is being used to find a good approximation formula that will represent the distance from the screen by detecting the distance between the two objects.

IV. Working Diagram

The working diagram shows the generalized working of the image projection of image using combined approach for tracking.



The fig.(1) has a wiimote which consist inbuilt camera and the camera coordinates are calculated by the wiimote. The calculated values are sent to the computer using Bluetooth. These calculated values are given to the computer or laptop for viewing. This laptop or computer is connected to a projector which projects this tracked values and operates according to the tracked operation.

V. Algorithm

The algorithm for this system is as follows:

1. Detect the object in the range of the camera. Check whether the object is detected by the camera by seeing the help of a dot point in the detection screen.
2. If object is detected then keep the wiimote stationary and record the coordinate values in a table.
3. Now change the location of the object and then repeat the step 2.
4. Keep changing the wiimote location and record the x, y and z coordinate values.
5. Check the events of the wiimote by pressing each of the buttons and also check whether the appropriate box gets clicked or not.
6. If the events are properly working then we will use this device to operate as wireless mouse and run paint application by using its events buttons.

This algorithm is the modification of the base paper's algorithm [1]. The existing algorithm was only using this for head tracking but its modified version is used for the projection and tracking in our experiment.

VI. Expected Outcome

The result of this research will be that we can have an easy and efficient interaction between human and computer also it will reduce the bulky setup and improve the projector technology. Manipulation of the image and 3D view will be projected on the screen.

VII. Future Scope

In future this research will be helpful in the following ways:

1. Image can be stored in the viewer's screen.
2. Image can be transmitted to other communication systems.
3. Can be copied on the projector itself.
4. Outputs to multiple screens.

REFERENCES

- [1] Johnny Chung Lee, "Hacking the Nintendo Wii remote", *Pervasive Computing*, (3):39-45, IEEE 2009.
- [2] D. Gu, K.-S. Ou, Y.-T. Fu, K.-S. Chen "Design of Wiimote Indoor Localization Technology for Omni-directional Vehicle Trajectory Control" IEEE 2012.
- [3] Bharat L, Shashank S, Nageli V S, Sangeeta Shrivastava, S Rakshit, "Tracking Method for Human Computer Interaction using Wii Remote", IEEE 2010.
- [4] Luc Vlaming, Jasper Smit and Tobias Isenberg, "Presenting using Two-Handed Interaction in Open Space" IEEE International Workshop on Horizontal Interactive Human Computer System (TABLETOP) 2008.
- [5] Hector Vragas, Enrique Preza, and Ramiro Velazquez, "A Combined Wiimote-Camera Tracking System for Small Aerial Vehicles", *Electronics, Robotics and Automotive Mechanics Conference*, IEEE Computer Society 2009.
- [6] Po-Wei Chen, Kuang-Shun Ou "IR Indoor Localization and Wireless Transmission for Motion Control in Smart Building Applications based on Wiimote Technology" SICE Annual Conference August, 2010.
- [7] David Bradshaw and Kia Ng, "Tracking Conductors Hand Movements Using Multiple Wiimotes", *International Conference on Automated solutions for Cross Media Content and Multi-channel Distribution by ICS 2008*.
- [8] D Balakrishna, PV Sailaja, RVV Prasad Rao, Bipin Indurkha, "A Novel Human Robot Interaction using the Wiimote", *Proceedings of the 2010 IEEE International Conference on Robotics and Biomimetics*, Tianjin, China, December, 14-18, 2010.

Assessing Water Demand And Supply For Srinagar City (J&K) India, Under Changing Climatic Scenarios Using Water Evaluation And Planning Model (WEAP)

Muzaffar A. Malla¹, Umar Firdous Ahmad², Manzoor A. Rather³,
Muzafar N. Teli⁴, Nisar A. Kuchhay⁵
^{1, 2, 3, 4, 5}(State Remote Sensing Centre J&K Government)

Abstract: The study holds significance keeping in view the global climatic concerns, which began to cast their shadows on the climate of Jammu and Kashmir as well. In order to accomplish the present study, WEAP (water evaluation and planning model) of Stockholm Environment Institute was used. This model is a tool for integrated water resource management and planning like, forecasting water demand, supply, inflows, outflows, water use, reuse, water quality, priority areas and Hydropower generation, etc.. During the present study discharge data from 1979-2010 (past thirty years) of our study rivers i.e., Dachigam Stream and Sindh Stream was used as supply to our demand sites and also to find the impacts of changing climatic conditions over them. Due to availability of data upto year 2010 only therefore the scenarios were generated from year 2011 onwards. The water demands for Srinagar i.e., irrigation demands for agriculture and water supply demands for our domestic needs was analyzed, industrial demands were not analyzed as we have negligible demands in this sector. The water supplied to our demand sites was mostly contributed by our study rivers and a little demand was met by ground water. Data was collected from various agencies like PHE Srinagar, Census data of 2011, Meteorology department etc. This collected and generated data was given as input to the WEAP model. The model generated the trends for discharge of our study rivers for next 15 years and at the same time also generated scenarios calculating our demands and supplies for the future. The model results reveal that there will be shortages in the requirements met in the urban water needs for some years like 2016, 2017, 2018 and 2020. The results generated from the model outputs will help us in predicting whether our water resources are going to suffice our growing water needs or not in future. The results will help in drafting policies for future regarding water supplies and demands under changing climatic scenarios.

Keywords: Climate change scenarios, Demand sites, Discharge data, Global Climate Change, WEAP

I. INTRODUCTION

The recent scientific assessment by the Intergovernmental Panel on Climate Change (IPCC) concludes that, since the late 19th century, anthropogenically induced emissions of gases such as carbon dioxide (CO₂) that trap heat in the atmosphere in the manner of a greenhouse have contributed to an increase in global mean surface air temperatures of about 0.3 to 0.6⁰ C. Moreover, based on the IPCC's mid-range scenario of future greenhouse gas emissions and aerosols and their best estimate of climate sensitivity, a further increase of 2⁰ C is expected by the year 2100 [1]. The purpose of this paper is to examine the likely impacts of a Climate change on the supply and demand for water and the resulting socioeconomic implications.. The consequences of these global climatic changes are already being witnessed in several Himalayan areas where glaciers and glacial lakes are changing at alarming rates. Climate change is affecting the temperatures, amount of snow and ice in the Himalayan region as well as rainfall patterns [2]. Due to global warming, the Indo-Gangetic basin of the Indian subcontinent, where water supply is dominated by melting snow and glacier ice, will be faced with severe environmental problems. Negative impacts, including seasonal shifts in water supply, flood risks and increased precipitation variability, will eventually offset benefits incurred by short term increases in runoff from glacier melt [3]. According to Dr Shakeel Ramshoo, convener of the Climate Change Research working group of

Kashmir University, the Kolahai glacier has been melting at the rate of about 80 sq m per year over the last three decades since 1976 and has shrunk from 13.87 sq km to 11.24 sq km. Situated at an altitude of 3600 m, the Kolahai is the source of water for Lidder and Sindh, two major fresh water streams in the Jhelum basin. Dr Ramshoo says that the melting is due to the climate change, "The increase in the Kashmir temperature has been 1°C, which is much more than the 0.72°C rise in global temperature over the past century. The result is less snowfall and less formation of glaciers." [4] Keeping in view the decreasing water supplies and increasing demands in Kashmir valley in general and Srinagar district in particular the current study holds great significance as our domestic water demands are increasing with the increase in the population and standard of living of the people with each passing day.

In order to prepare for future in advance, an attempt was made to calculate our water demands and the supply which we have at present, the trends and climatic scenarios of water demands and supply were drawn from WEAP Model, of Stockholm Environment Institute. WEAP Model is a microcomputer tool for integrated water resources management and planning. It provides a comprehensive, flexible and user-friendly framework for policy analysis [5]. Operating on the basic principle of water balance accounting, WEAP is applicable to municipal and agricultural systems, single sub-basins or complex river systems [6]. In the present study following objectives were accomplished analyzing the trends in the discharge data of our study rivers, evaluation of water resources available to Srinagar city, evaluating all water demands and supplies, and to manage the water resources in accordance to changing climate scenarios.

II. STUDY AREA

Srinagar lies between the coordinates 34° 01' N to 34° 27' N latitude and 74° 36' E to 75° 30' E, it is around 77 km long and 40 km wide, the average elevation of the valley is 1600 m above sea level spread over an area of 1862 sq km located approximately 1730 m above the sea level. Srinagar is surrounded by Budgam district in the west, Pulwama in South and Ganderbal in north. The valley of Jammu & Kashmir as a whole is an asymmetrical fertile basin, stretching from south-east to north-westerly direction. Its diagonal length (from SE to SW corner) is 187 km, while the breadth varies considerably, being 115.6 km along the latitude of Srinagar, the altitude of the floor of valley at Srinagar is 1600 m and the highest peak among its surrounding mountains is that of the Kolahoi or Kwashiorkor (Alt.5420m).

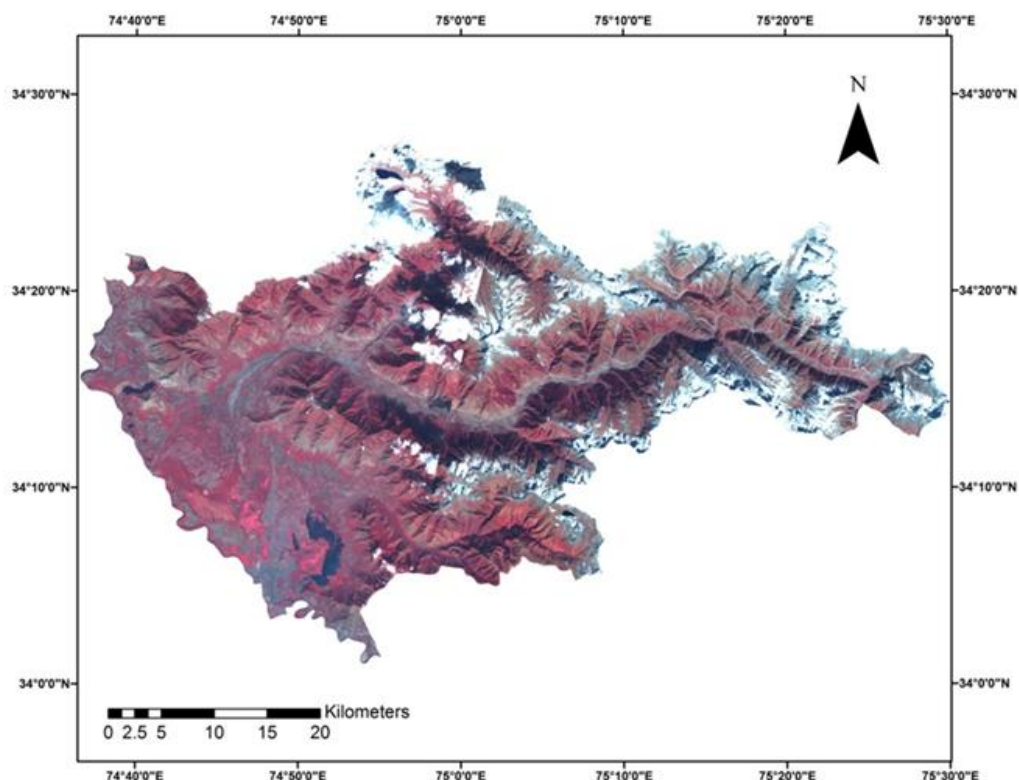


Figure 1: Location of Study Area.

III. METHODOLOGY

The methodology that was employed for current research involved use of satellite/remote sensing data in a GIS environment combined with field investigation, hydrological data, digital elevation data, secondary/ancillary data, and simulation modeling. The study relied on two fold methodologies wherein firstly the necessary datasets required to simulate future climatic scenarios were generated and later these generated datasets were given as input to WEAP Model. Detailed methodology consisting of schematic flow chart of the methods used to address the research objectives is shown in Fig.2 below:

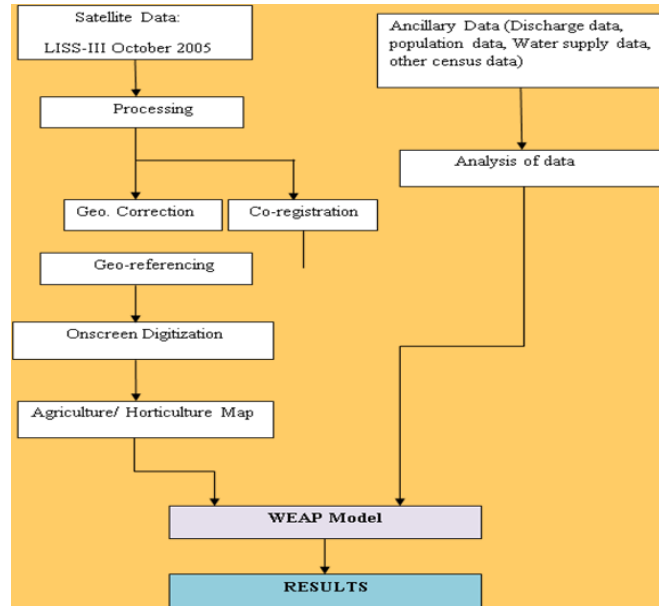


Figure 2: Methodology Flowchart

LISS III image of October 2005 was geometrically corrected and registered using ERDAS IMAGINE 8.4 software. Arc view 3.2 software was used for on-screen digitization. At the same time other data related to the study area viz: ancillary data like census data of 2011, Ground water potential and its usage, PHE water supply data and discharge data of study rivers was preprocessed and analysed and then put as input to WEAP Model to generate the final results.

IV. RESULTS & DISCUSSIONS

The basic datasets to generate the model results were generated firstly by analyzing the discharge data of our three demand sites viz: Dachigam Stream, Sindh Stream and Srinagar city from (1979- 2010). From the analysis of discharge data of each demand site individually it was found that mean yearly discharge and monthly data of Dachigam Stream from 1979- 2010 showed an overall decreasing discharge trend or negative trend, depicting that the discharge in the river is decreasing. Maximum discharge was observed for year 1981 and for year 1999 lowest discharge was observed.

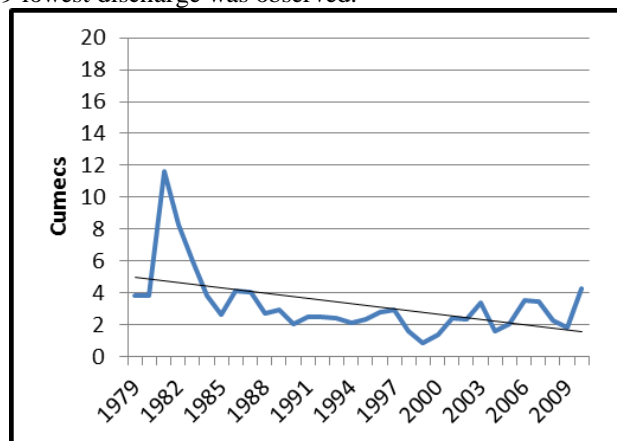


Figure 3: Mean Yearly Discharge Data of Dachigam Stream

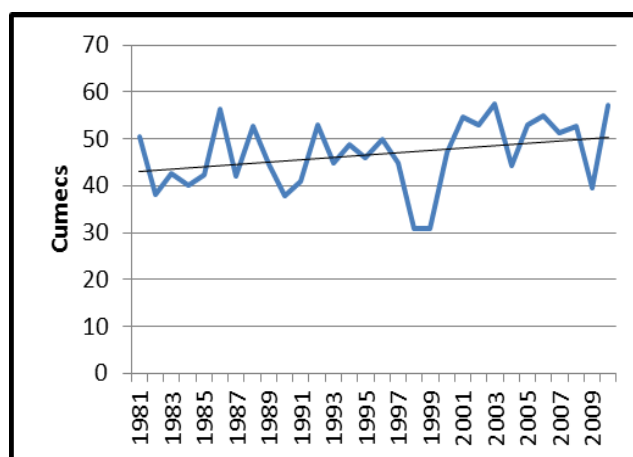


Figure 4: Mean Yearly Discharge Data of Sindh Stream

The results of analysis for Dachigam Stream showing average mean yearly discharge is shown in the Fig. 3. The months June, July, August are of much significance as the demand is increased due to irrigation needs for rice cultivation. The discharge trends for these months are decreasing in the same manner as the yearly discharge trends show decreasing trends. In case of Sindh Stream it was found that overall discharge over the past years is increasing, the reason may be attributed to fast melting of glaciers [3].

1. Domestic Water demands: It was found that Srinagar City has a population of 1269751 (2011 census). 98% of the population uses Tap water (2011 census). Water usage per person is about 111 m³/yr or 304 L/day (100 m³ from tap water and 11 m³ from ground water - PHE Srinagar). 79 MGD of water are supplied to 1.27 million people in the city from PHE supply and 1.58 MGD is harnessed from ground water. This accounts for 299 L/day/person of the water supplied from PHE supply and 5.9 L/day/person for the supply from the ground water and other sources. Water consumption per capita is much higher in Srinagar than the overall average in India, as J&K state is rich in water resources and tap water supply is available 24x7.
2. Irrigation Water Demands: Total area irrigated by Dachigam stream was found to be about 2300 hectares and the abundant crop was paddy, Minimum Water demand per hectare = 3,000 m³ (SKUAST). Rate of change of agriculture to horticulture/urban was found to be 18% per decade from the analysis of past satellite data. Present water demand for agriculture is found to be 12 Million Cubic Meters. Present agriculture is 1205 hectares and accordingly it will be left to 917 ha in 2026. In case of overflowing the paddy fields demand per hectare is 10,000 m³. About 45% of water is consumed in the first month for sowing and transplanting i.e., 1st stage of paddy growth [7].
3. Water Demand and Supply Analysis for Agriculture Sindh: Total area under paddy cultivation = 10000 hectares. Water demand for Sindh agriculture was found to be 101.7 Million Cubic Meters. Sindh has large discharges rates and the volume that is available is able to satisfy the demand fully for agriculture.

4.1 Model Results

The various parameters which were fed to WEAP model in order to generate various simulations were, census data (2011) PHE (Public Health Engineering data to see overall water supply to Srinagar, discharge data of past 30 years (1979-2010), total agricultural land to see agricultural demands, water requirements per hectare in our demand sites was found from Sher-I-Kashmir University of Agricultural Technology (SKUAST). All the data was compiled and brought in the format acceptable to model and the model simulations were run for 16 years. Fig below shows the overall results generated by the model in the form of overall inflows, outflows from the rivers, supply requirements and the un-met demands for the three demand sites for the city of Srinagar. It includes four water nodes for inflows i.e., Dachigam Stream, Jhelum River, Sindh Stream and the ground water. From these nodes water is supplied to demand sites. The Outflows from Areas includes the water that comes out of the demand sites when their needs are fulfilled. The Supply requirements are generated for three demand sites that include Domestic water demands for Srinagar City, Irrigation water demands for Dachigam agriculture and Sindh agriculture. The next scenario generated was for Unmet water demands in thousand meter cube for three demand sites.

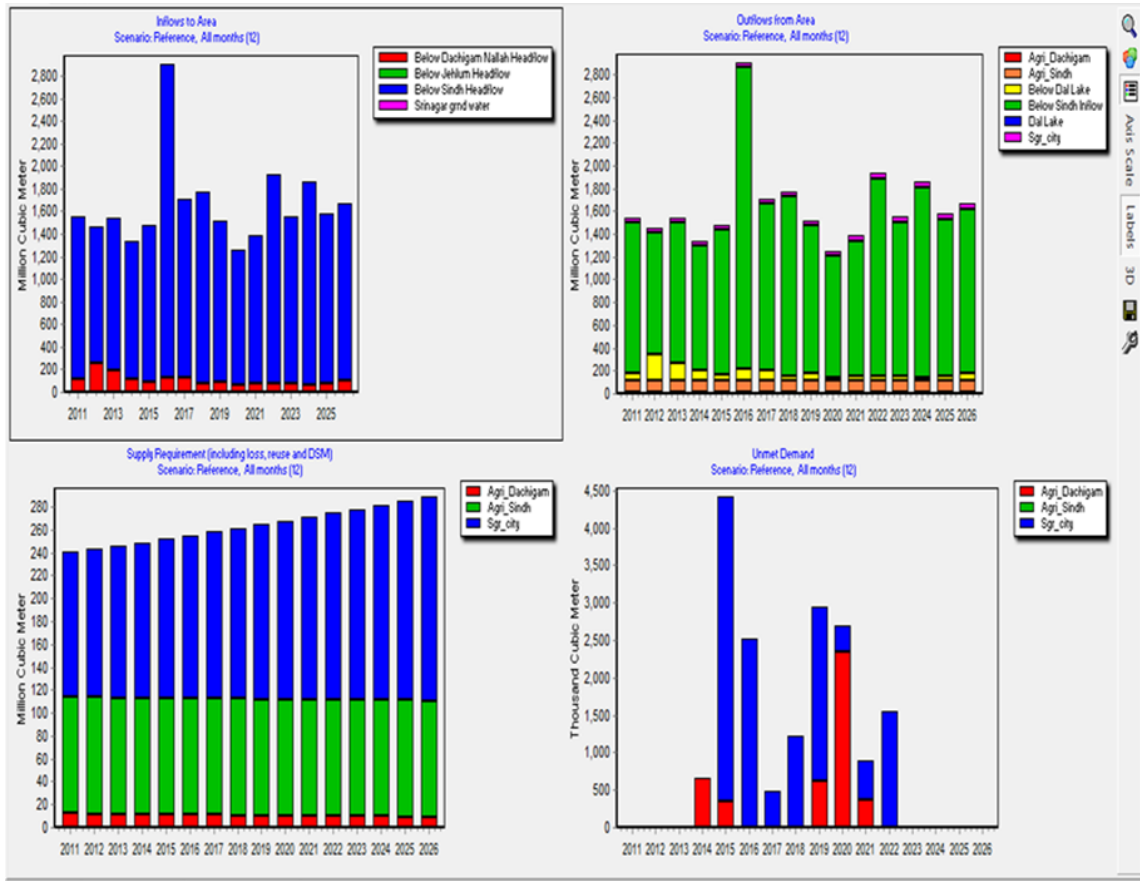


Figure 5: The Overall Results Generated by The Model Up to Year 2026

4.1.1 Discharge Trend

The Discharge trend that was generated by WEAP model is based on the previous discharge trend, of thirty years that was given as input to the model. High discharge years as simulated by model are 2016 for river Sindh and 2012 for Dachigam Stream, probably due to fast melting of glaciers due to global warming, whereas low discharge years as simulated by the model were 2026 for River Sindh and 2015, 2016, 2018, 2020, probably because of shrinkage of glacier areas.

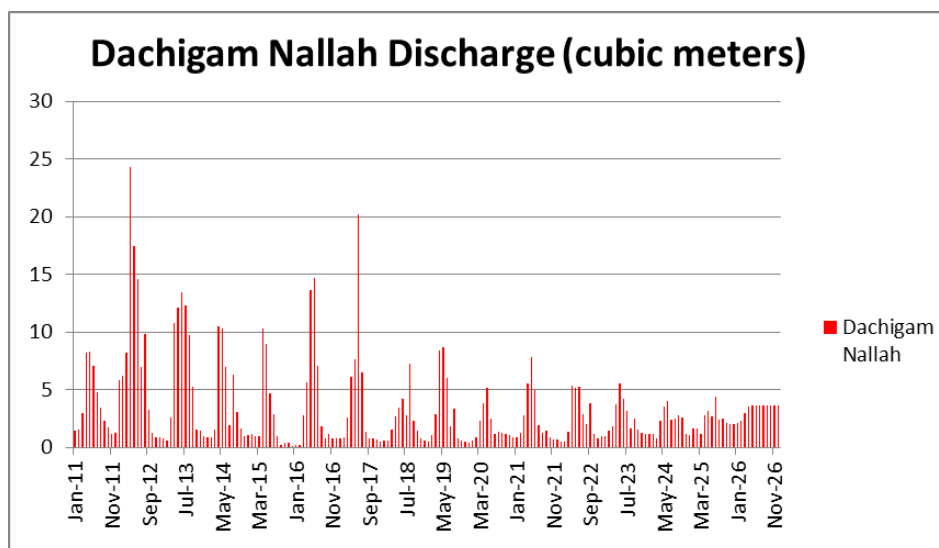


Figure 6: Discharge Data for Dachigam Stream 2011-2026 as generated by Model.

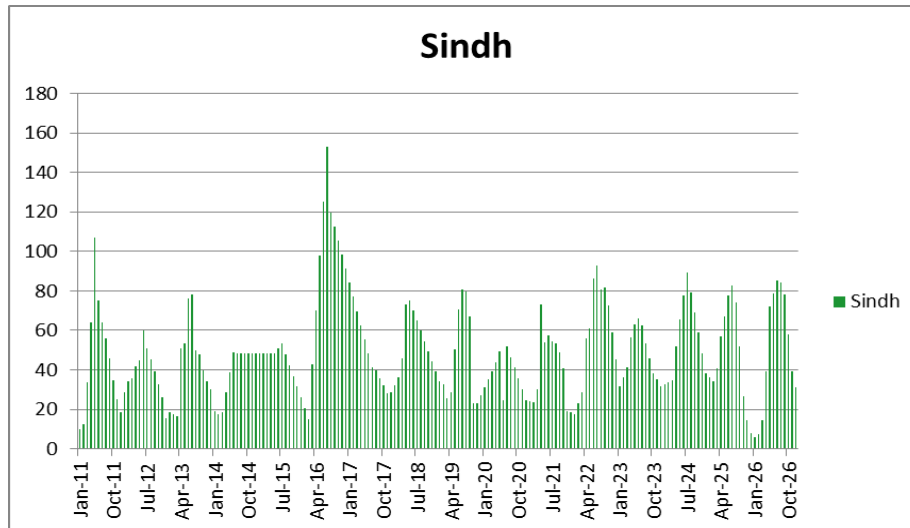


Figure 7: Discharge Data for Sindh Stream 2011-2026 as generated by Model

4.1.2 Supply Requirement

WEAP Model has generated the water requirement for three demand sites for next 15 years. It is evident from the table that water requirements for Srinagar city increase from (127-176) Million cubic meters from 2011 to 2026. The demand for Srinagar city is increasing due to increasing population and urbanization, whereas the demand for Agriculture Dachigam is decreasing (12-9.1) Million cubic meters, due to conversion of agriculture land to horticulture and urbanization. The demand for Sindh agriculture is constant due to no changes in the area of agriculture land.

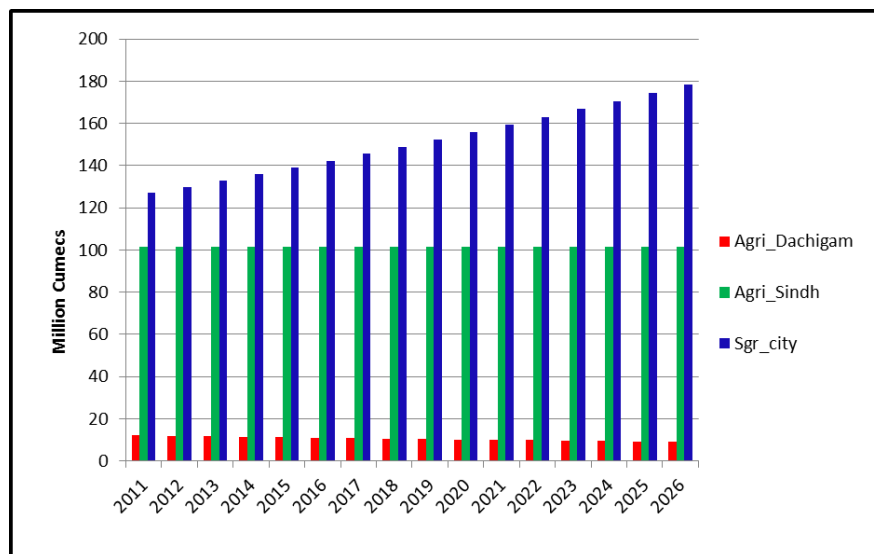


Figure 8: Water Supply Requirements for Srinagar City in Million Cubic Meters (Model Results)

4.1.3 Supply delivered

Supply delivered to the demand sites is shown below in the table. Supply delivered to the demand sites is varying as is prevalent from the model results above, it is delivered 100% in some years while as in some years there is shortage of the supply. In some years there is reduced discharge in the study rivers as analyzed by the study, which affects the supply.

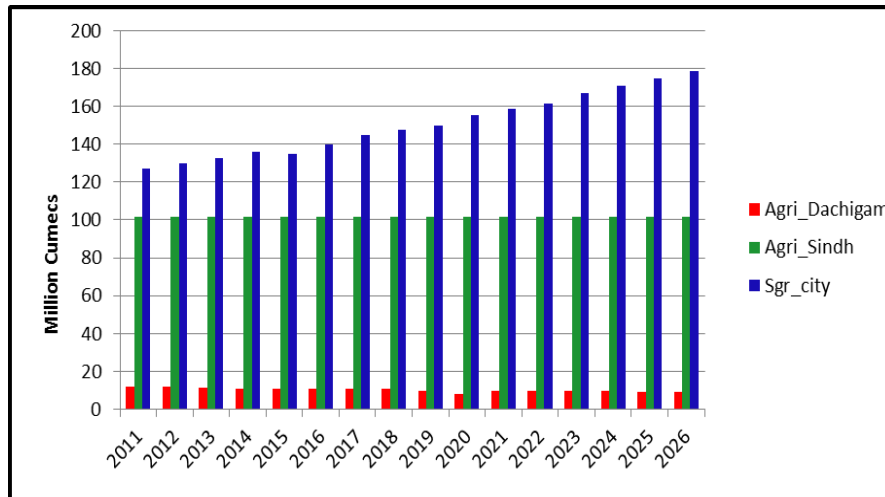


Figure 9: Water Supply delivered to the demand sites (Million cubic meters).

4.1.4 Un-Met water Demands

The figure below shows the results of unmet demands for three demand sites from 2012-2026, generated from WEAP model. On the basis of results generated it was found out that Srinagar city has an un-met demand of almost 4 Million meter cube for the year of 2015 while as Agriculture Dachigam has a shortage of almost 3 Million meter cube. The un-met water demands are shown in Figure 10.

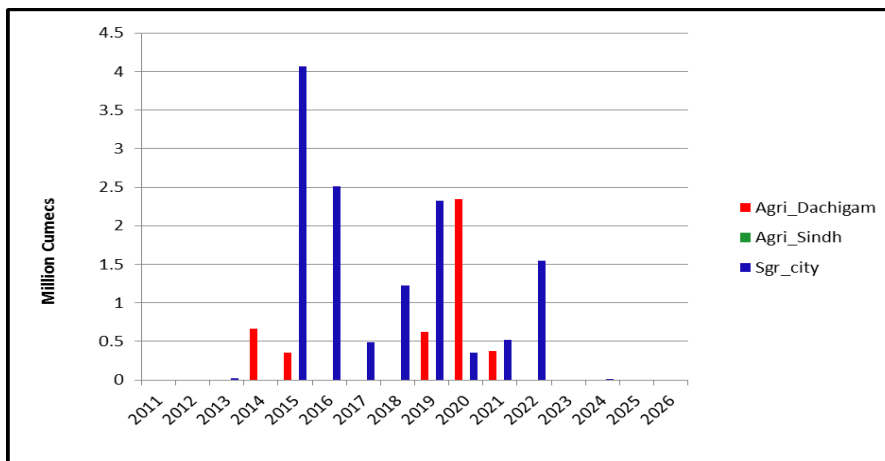


Figure 10: Un-met Water Demands (Thousand Cubic Meters)

Site Reliability:

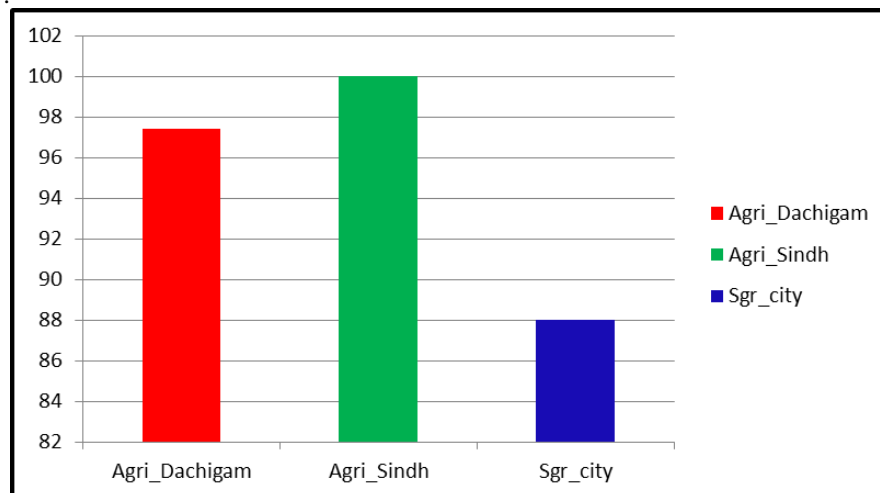


Figure 11: Site Reliability for The Demand Sites

It shows that Agriculture Sindh has 100% reliable site i.e., its demands are fully fulfilled. While as the water sources that fulfill the demands of the Srinagar city are only 88% reliable. 12% of the demands are not fulfilled.

V. CONCLUSION

On the basis of the results formulated from the current study, following main conclusions can be drawn:

1. Discharge data analysis for the Dachigam stream revealed that the flow has decreased from 1979-2010.
2. Agriculture demands for Dachigam area are facing shortage even in minimum requirement scenario because of reduction of almost 10 times discharge from the year of 1979-2010 in the Dachigam stream. Agriculture Dachigam faces shortage mostly in the month of July. In order to meet the domestic water needs, the Dachigam Stream fed agriculture must be irrigated efficiently.
3. Dachigam fails to provide even 15% of the water supplied to Srinagar City. On the contrary discharge data analysis for the Sindh stream revealed that the flow has increased from 1979-2010. Therefore Sindh Stream has the potential to meet the growing water demands of Srinagar city.
4. From the WEAP model predictions, it is assumed that urban water supply met to city will be only 85% in 2016 and 90-95% in 2017-2019 and 2022.
5. It is also predicted that the urban water supply met to city will likely to face shortage in winter months.

VI. RECOMMENDATIONS

From the analysis of the results, it is found that Sindh stream has the potential of meeting the growing demands of water supply to Srinagar city in future, therefore judicious use of water from Sindh stream and restoration of this water stream by checking the illegal encroachments along its course is necessary. It is also recommended to make water storage reservoirs at various places along this stream, so as to store the water for meeting the demands of water during the winter months to the Srinagar city.

REFERENCES

Journal Papers:

- [1] Intergovernmental Panel on Climate Change. 1996. Climate Change 1995: The Science of Climate Change: Contribution of Working Group I to the Second Assessment Report of the Intergovernmental Panel on Climate Change, Cambridge University Press.
- [2] UNEP. Recent Trends in Melting Glaciers, Tropospheric Temperatures over the Himalayas and Summer Monsoon Rainfall over India, UNEP 12/2009.
- [3] S.I. Hussain, Impact of melting glaciers in the Himalaya. The International Journal for Rural Development: Rural 21, 04/2009.
- [4] Himanshu Thakkur, Water Sector Options for India in a Changing Climate. South Asia Network on Dams, Rivers & People, March 2012.
- [5] Stockholm Environment Institute, SEI. WEAP: Water evaluation and planning system –user guide. Boston, USA. 2001.
- [6] Yates, D., J. Sieber, D. Purkey, and A. Huber-Lee, WEAP21—A demand priority and preference driven water planning model. Part 1, Water Int (2005b).
- [7] FAO, Corporate Documentary Repository. Irrigation Water Management: Irrigation scheduling...
- [8] A.K. Chapagain and A.Y. Hoekstra, The green, blue and grey water footprint of rice from both a production and consumption perspective, ELSEVIER March 2010
- [9] A.K. Chapagain and A.Y. Hoekstra, Water footprints of nations, Volume 1: UNESCO-IHE Main Report, Volume 2: Appendices November 2004.
- [10] Bryson Bates, Zbigniew W. Kundzewicz, Jean Palutikof, IPCC Technical Paper VI Climate change and water, 2008.
- [11] Duguay, C.R. and Co-authors, Ice-cover variability on shallow lakes at high latitudes: model simulations and observations. Hydrol. Process 2003.
Lillesand, T.M., R.W. Kiefer, and J.W. Chipman. Remote Sensing and Image Interpretation. New York: John Wiley & Sons (2004).
- [12] M.L. Parry, O.F. Canziani, J.P. Palutikof, P.J. van der Linden and C.E. Hanson, Climate Change Impacts, Adaptation and Vulnerability. Contribution of Working Group II to the Fourth Assessment Report of the Intergovernmental Panel on Climate Change, 2007.
- [13] Sieber, J., Huber-Lee, A., & Raskin, P. WEAP:Water Evaluation And Planning System User Guide for WEAP 21, Stockholm Environmental Institute—Boston, Boston, USA. (2002).
- [14] Singh and Kumar, Run off discharge trends, J. Hydrol., 1997.

- [15] R. K. Mall, Akhilesh Gupta, Water resources and climate change: An Indian perspective, CURRENT SCIENCE, VOL. 90, NO. 12, 25, June 2006.
- [16] Pant, G. B. and Rupakumar, K., Climates of South Asia, John Wiley, UK, 1997.
- [17] Stern, N., The Economics of Climate Change: The Stern Review. Cambridge University Press, Cambridge, 2007.
- [18] Yates, D., D. Purkey, J. Sieber, A. Huber-Lee, H. Galbraith, J. West, and S. Herrod-Julius, A physically-based, water resource planning model of the Sacramento Basin, California USA, J. Water Resource Planning Manage, 2008.
- [19] Woodworth, P.L. and D.L. Blackman, Evidence for systematic changes in extreme high waters since the mid-1970s. J. Climate, 2004.

Low Power Design of Standard Digital Gate Design Using Novel Sleep Transistor Technique

Kusum Tomar¹, A.S.M.Tripathi²

^{1,2}(Department of Electronics and Communication Engineering, Mangalayatan University Aligarh, India)

Abstract: In the nanometer range design technologies static power consumption is very important issue in present peripheral devices. In the CMOS based VLSI circuits technology is scaling towards down in respect of size and achieving higher operating speeds. We have also considered these parameters such that we can control the leakage power. As process model design are getting smaller the density of device increases and threshold voltage as well as oxide thickness decrease to maintain the device performance. In this article two novel circuit techniques for reduction leakage current in NAND and NOR inverters using novel sleepy and sleepy property are investigated. We have proposed a design model that has significant reduction in power dissipation during inactive (standby) mode of operation compared to classical power gating methods for these circuit techniques. The proposed circuit techniques are applied to NAND and NOR inverters and the results are compared with earlier inverter leakage minimization techniques. All low leakage models of inverters are designed and simulated in Tanner Tool environment using 65 nm CMOS Technology (1volt) technologies. Average power, Leakage power, sleep transistor

Keywords: Adaptive Decision, OFDM, Fading Channel, SNR estimation, PSK/QAM.

I. Introduction

In modern electronics the peripheral circuits based on SRAM like input drivers, word line drivers, and output drivers etc. occupy major portion of on chip caches in processors. Due to this tremendous attention is given towards savings of leakage power in peripheral circuits for improving the device performance. The on chip memory utilization involves long inactive states during cache misses. Thus a large time is spent in sleep modes in various functions. It indicates that static power reduction is getting an important issue of concern for memory utilization based peripheral device.

For a CMOS circuit the power dissipation occurs during the active mode of operation due to dynamic and static components but in the standby mode, the power dissipation is due to the standby leakage current [2] [3]. In the hand held devices based on nanometer technologies static power consumption is a prime concern. Due to down scaling in the size down along with the improvement in operating speeds of CMOS VLSI circuits; the leakage power is increased with the growth of technology. We have found in various literatures that as the geometries are getting smaller threshold voltage as well as oxide thickness decrease to maintain the device performance.

Hence with the successive growth of technology reduction in channel length has decreased the requirement of levels of threshold voltage and gate oxide thickness. Due to reduction in threshold voltage the consequences are observed in the form of exponential increase in leakage current. For fulfilling the purpose of successive down scaling of transistors leakage current is going to be a limiting factor [1]. In nanometer range based technology feature sizes are very small due to this smaller length of channels causes increase in sub threshold current because the transistors are not kept completely switched off.

In the growing technology the number of transistors is rising, transistors leakage occurs even they are not activated this causes significant dissipation of power during the inactive state of circuits for a given area. Hence with the successive growth of the technology leakage power in an integrated circuit is also increasing.

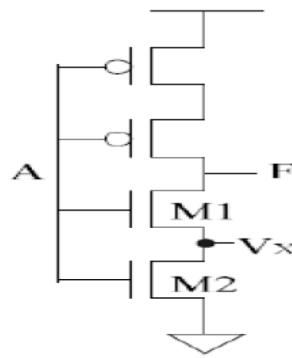


Fig 1: Transistor stack Connection for Forced Inverter

II. Related Work

From above discussion it can be observed that it is very necessary to reduce the idle mode operation static power in the peripheral circuits that utilizes SRAM for cache memory based functions. In all the processors SRAMS are integral and very important components. In addition to this in Embedded Systems SRAMS occupies a larger area on chips. So it is required to apply various leakage power reduction methods to SRAMS to increase valuable battery usage time in hand held mobile devices. We have analyzed many VLSI techniques that can help for leakage power reduction. Some of the techniques are such that they can provide a very perfect approach to reduce leakage power; but every technique has some disadvantages that implements limitations in the application of each technique. We have sorted out two new approaches that can be proposed to apply to reduce total power consumption, thus this can help in getting a new choice for low-leakage power VLSI design techniques. We have also studied previous techniques and compared with the two new methods presented in this report.

The method that has already proved its advantages in reducing leakage power in inverters is the making use of transistor stacking [4]. With more than one transistor in the stack is kept in turned off state it has been found that sub threshold leakage current flow reduces in a stack of series connected transistors as shown in figure 1. This phenomenon is called as stacking effect. In the article [5] it has been proposed that the use of sleep transistors helps in leakage reduction, it is also known as gated-VDD and gated-GND techniques. This technique is used to cut off pull-up or pull-down or both networks from supply voltage or ground using sleep transistors. In this technique either i) an additional NMOS sleep transistor is used between pull-down network and ground or/and an additional PMOS sleep transistor is used between pull-up network and VDD.

2.1. Proposed Method

The sleep transistor is turned on during active mode of operation and turned off during idle or standby mode of operation. When the sleep transistor is off the virtual ground terminal VG will be at a nonzero potential. The gate to source voltage of off transistor M2 becomes negative and its threshold voltage increases. This has an effect of reducing sub threshold current flowing between drain and source of the transistor. The substrate to source voltage and drain to source voltage also reduce and give rise to higher threshold voltage. All these effects cumulatively add up to lowered sub threshold current that flows in the off transistors.

In this work we have proposed two novel techniques for reduction of leakage current in inverters with and without application of state retention property. We have used these techniques for the reduction of power dissipation during inactive (standby) mode of operation. The reduced power is compared to traditional power gating methods for circuit techniques.

As we have discussed before that in CMOS circuit power dissipation occurs due to dynamic and static components during the active mode of operation and standby condition the power dissipation is by the standby leakage current.

The dynamic switching power (PD) and leakage power (PLEAK) can be evaluated by following equations:

$$P_D = \alpha f c V_{DD}^2 \dots\dots\dots (1)$$

$$P_{LEAK} = I_{LEAK} V_{DD} \dots\dots\dots (2)$$

In the above equations the various terms are described below:

α : switching activity

f : operation frequency

C : the load capacitance

VDD : supply voltage and

I_{LEAK} : the cumulative leakage current due to all the components of the leakage current.

For CMOS Inverters current flows from Source to Drain in ideal conditions when $V_{GS} > V_T$. But in the case of real transistors current instead of cut-off abruptly below a given threshold it drops exponentially. This type of exponential drop off conduction is called as leakage conduction and it causes an undesired conduction in a state when transistor is considered as nominally off. This leakage current is also taken as sub threshold or weak inversion current that flows from drain to source when the transistor is off during the state when gate voltage is kept below the threshold voltage. The leakage current depends on various process parameters in the MOSFETs, like the transistor size, the quiescent state of the circuit [3] etc.

In this work we have considered various methods to reduce the sub threshold leakage current by increasing threshold voltage V_{TO} , increasing V_{SB} and reduction of V_{GS} , V_{DS} and lowering the temperature.

We have observe that the reduction in leakage current can be achieved using both process- and circuit-level techniques. In the process level the reduction in leakage current can be obtained by governing the dimensions like length, oxide thickness, junction depth and doping profile of the CMOS transistors and in the circuit level, threshold voltage and leakage current of transistors can be effectively controlled by controlling the voltages of different device terminals named as drain, source, gate and substrate body.

In this paper we have applied novel static power reduction method in inverters and SRAM memory peripheral circuits. This proposed method has tremendous scope in extending it for. Application related to peripheral devices like write data drivers, decoders etc.

The proposed design of novel low leak inverter uses new power gating technique in which PMOS transistor is used in the pull down path and NMOS transistor in the pull up path as sleep transistors. Both the sleep transistors are kept on during the active mode of operation. The PMOS pull down transistor holds the virtual ground (VG) node at a higher potential than ground and the NMOS pull-up transistor maintains the virtual power (VP) node at a lower potential.

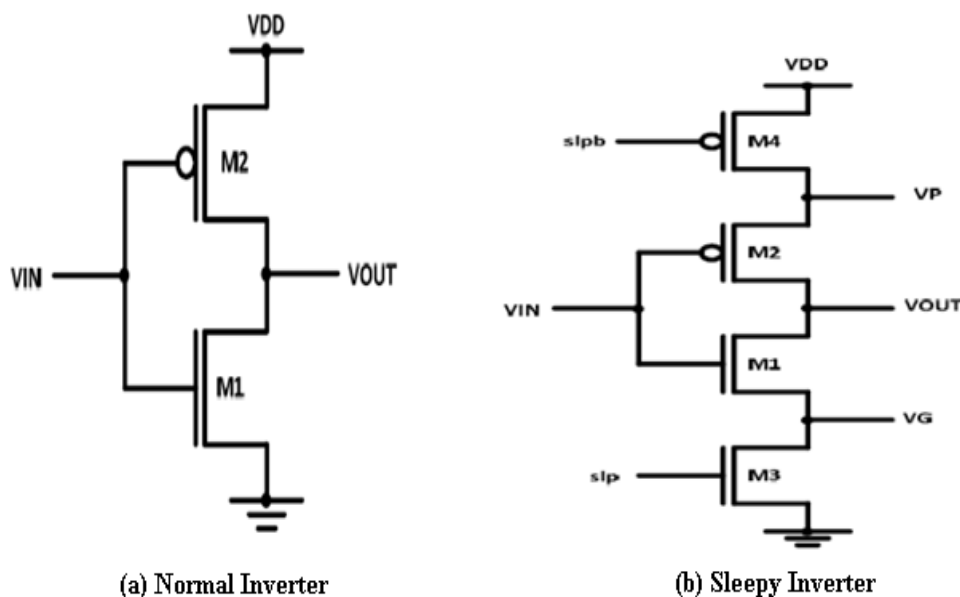


Fig 2: Connection Diagram for a normal inverter and sleep inverter using transistor stack connection.

This helps the current flowing in the circuit to reduce and causes lower power dissipation during active mode. During the idle mode the sleep transistors are off. This provides a very large impedance path establishment across the nodes VP and VG in comparison to the traditional power gating method.

This method provides maximum reduction in static power during periods of inactivity or sleep state. However the output states during active mode of operation will not be at good logic1 and logic 0 values. To obtain good logic output levels during active mode of operation and to achieve the retention of previous output state, state retention transistors are introduced across the sleep control transistors. This state retention technique has resulted in state retention at lower total power dissipation as compared to previous best known techniques. This work also addresses leakage power reduction in buffer chains. Word line drivers have been designed with novel low leak inverters.

2.1.1. Low leakage Novel sleepy NAND, NOR inverter modeling

The novel technique based sleepy inverter for low leakage applications is shown in figure 2b. This novel sleepy inverter gives very good reduction in leakage power but if we consider the output voltage levels they are not at good logic1 and logic 0 values. The large amount of reduction in leakage power has uses in inverter chains provided in the peripheral circuits of SRAM related memory devices and systems like data/ address I/O driver, row pre decoder, word line driver, etc. if reduced voltage level is not as a constrain for limiting factor.

The novel sleepy inverter consist of PMOS transistor for giving pull down sleep transistor actions and NMOS transistor for pull up operations of sleep transistor. During active mode the sleep signal slp is logic 0 and sleep bar signal slpb is logic 1. In the active period duration the sleep transistors M3 and M4 are on. The node VG at higher potential with respect to ground and VP is at a lower potential with respect to VDD. In this manner the inverter circuit has lower potential difference for node VP and VG. In this way current though the circuit is reduced and power dissipation also get reduced. During operations in standby mode the slp signal is at logic 1 and signal slpb is logic 0. In this case M3 and M4 transistor are off and gives very high impedance between the path of VDD and ground and in this way leakage current is lowered consequently. It has been found that the power dissipation in standby mode duration operation is lowest. In this article we have described a design based on novel sleepy transistor based NAND and NOR inverter. The SLEEPY NAND GATE technique for low leakage operation of an inverter is shown in below figure 3. This inverter provides significantly leakage power reduction as compared to design of the conventional NAND using CMOS for leakage power reduction using 65nm technology with power supply V_{dd} (Vpwr) 1v and also considering the speed of the devices.

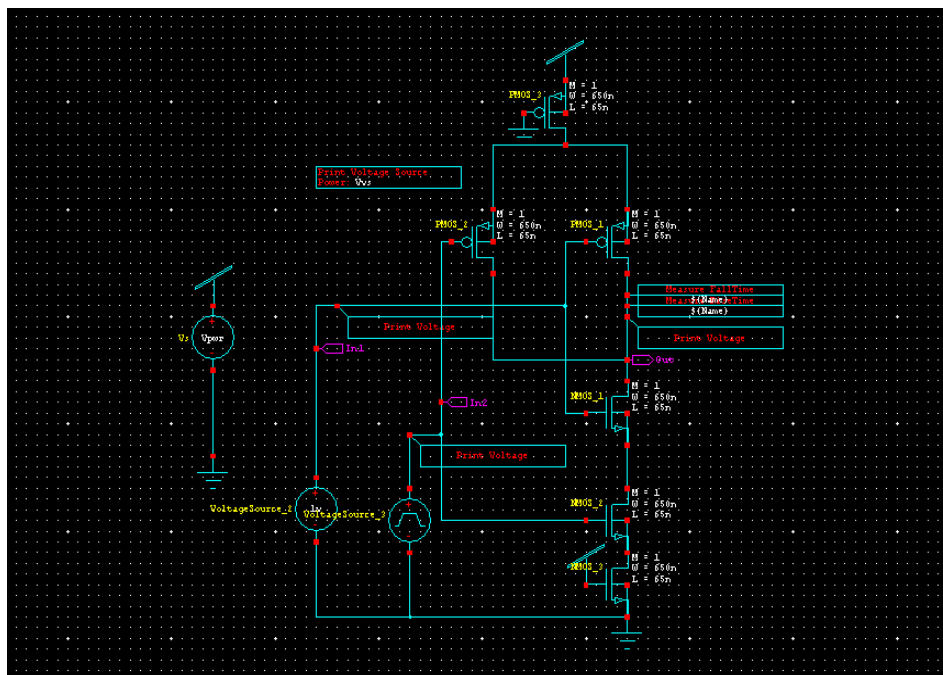


Figure 3: Sleepy NAND inverter for active MODE (slp=1, slpb=0).

The SLEEPY NOR gate for low leakage operation of an inverter is shown in below figure 4.

Figure 4 shows Sleepy NOR for active mode. During normal operation the sleep signal slp is held at logic 1 voltage level and complementary sleep signal slpb is held at logic 0 voltage levels. When inverter has to function in stand-by or sleep mode the signal slp is held at logic 0 and signal slpb is held at logic 1.

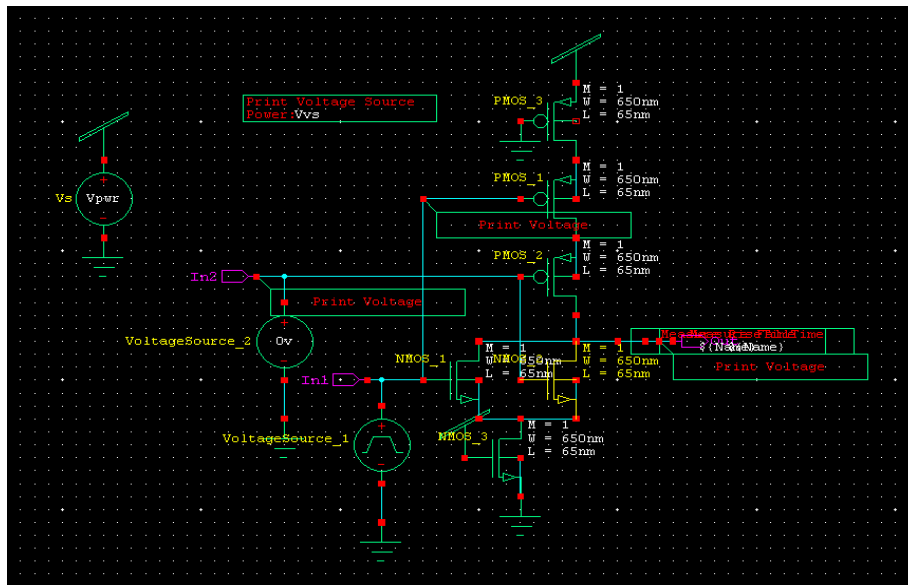


Fig 4: Sleepy NOR For Normal mode (slp=1, slpb=0)

The Novel SLEEPY NAND Inverter technique for low leakage operation of an inverter is depicted in below figure. This inverter though provides significantly leakage power reduction.

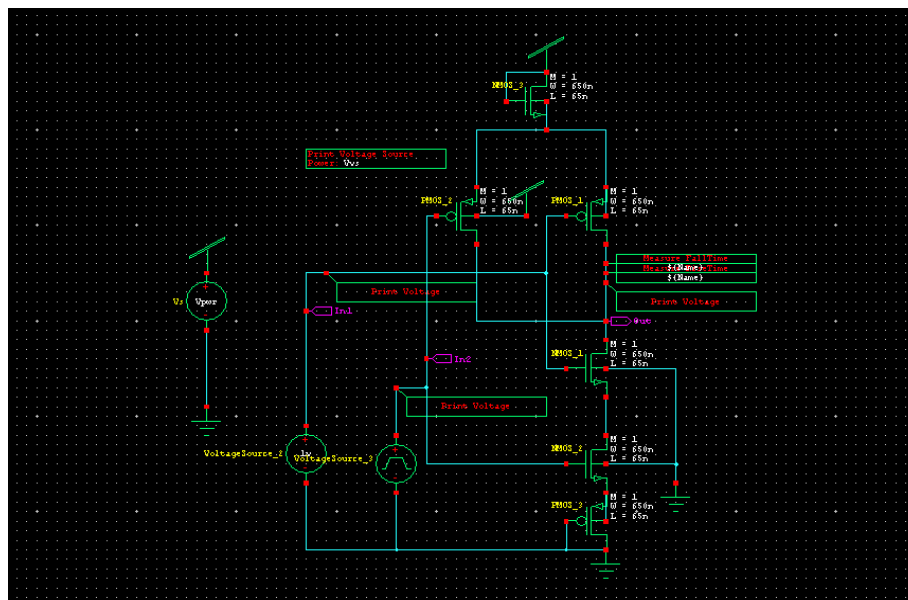


Fig 5: Novel Sleepy NAND Inverter for Normal Mode (slp=0, slpb=1)

Above figure 5 shows Novel Sleepy NAND gate for active mode. During normal operation the sleep signal slp is held at logic 0 voltage levels and complementary sleep signal slpb is held at logic 1 voltage level. When inverter has to function in stand-by or sleep mode the signal slp is held at logic 1 and signal slpb is held at logic 0. Similarly NOVEL SLEEPY NOR gate for low leakage operation of an inverter is shown in below figure 6. This inverter also provides significant leakage power reduction.

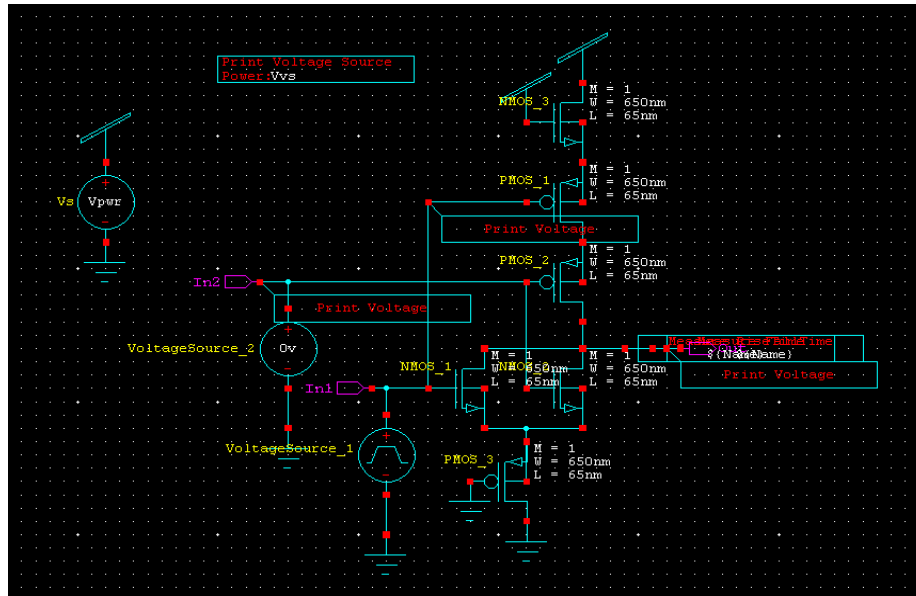


Fig 6: Novel Sleepy NOR Inverter for normal mode(Slp=0,slpb=1)

III. Results And Discussion

The circuit design is carried out using 65 nm CMOS NAND and NOR Gate technology files. All the designs are done and simulation is performed in Tanner design environment. The total (average) power dissipation is measured using Tanner tools. The power dissipation is measured both during active mode and standby mode of operations, for all the GATE and drivers and also considers the speed of all Gates in terms of rise time and fall time.

The simulation of Gate and driver circuits is performed by applying slp and slpb signals with 12nanosecond period and variable pulse widths. Active mode operation is observed by keeping these signals in the logic states. Long sleep (standby) period is also introduced to observe the performance during inactive period. The CMOS NAND and NOR Gate using sleepy, novel technique has exhibited lower leakage current and lower power. However during active mode lower output voltage is observed at correct functionality.

The average power dissipation during all operating modes is measured by using Tanner result browser and calculator. Table 1 and 2 compares the total power dissipation of all the NAND and NOR Gate during active mode i.e. when sleep control signals slp and slpb hold the respective sleep transistors in the on state and the logic inverter behaves as a normal NAND and NOR Gate.

TABLE 1. CMOS NAND Gate Total (Average) Power Dissipation (ACTIVE MODE):

S.No.	Inverter	Power (Watt.) O/P=0V(in:0,1)	Rise Time(s)	Fall Time(s)
1.	NAND Gate	3.214 E-6	1.859 E-10	1.584 E-10
2.	Sleepy NAND Gate (slp=1,slpb=0)	2.44 E-6	1.95 E-10	1.74 E-10
3.	Novel Sleepy NAND Gate (slp=0,slpb=1)	8.58 E-7	6.58 E-9	4.29 E-9

TABLE 2. CMOS NOR Gate Total (Average) Power Dissipation (Active Region):

S.No.	Inverter	Power (Watt.) O/P=0V(in:0,1)	Rise Time(s)	Fall Time(s)
1.	NOR Gate	3.15 E-6	1.92 E-10	1.92 E-10
2.	Sleepy NOR Gate (slp=1,slpb=0)	2.59 E-6	2.32 E-10	2.05 E-10
3.	Novel Sleepy NOR Gate (slp=0,slpb=1)	9.21 E-7	6.47 E-9	4.75 E-9

TABLE 3. CMOS NAND Gate Total (Average) Power Dissipation (SLEEP MODE):

S.No	GATE	Power (Watt.) O/P		Rise Time(s)	Fall Time(s)
		0V(in:1,1)	1V(in:1,0)		
1.	NAND Gate	4.78 E-8	3.60 E-8	N.A	N.A
2.	Sleepy NAND Gate (slp=0,slpb=1)	4.21 E-9	2.50 E-8	N.A	N.A
3.	Novel Sleepy NAND Gate (slp=1,slpb=0)	1.83 E-8	1.84 E-8	N.A	N.A

TABLE 4. CMOS NOR Gate Total (Average) Power Dissipation (SLEEP MODE):

S.No.	GATE	Power (Watt.) O/P		Rise Time(s)	Fall Time(s)
		0V(in:0,1)	1V(in:0,0)		
1.	NAND Gate	2.184 E-8	1.66 E-7	N.A	N.A
2.	Sleepy NAND Gate (slp=0,slpb=1)	4.00 E-9	1.546 E-8	N.A	N.A
3.	Novel Sleepy NAND Gate (slp=1,slpb=0)	1.844 E-8	1.88 E-8	N.A	N.A

Table 3 and 4 provides the total power dissipation during sleep mode of operation for all the NAND and NOR Gate.

The sleep signal slp is in the pull down path and sleep signal slpb is used in the pull up path. Depending upon whether PMOS or NMOS sleep transistor is driven, slp and slpb assume logic states to make them on or off. The logic values of these sleep signals for different modes of operation in case of different inverters are provided in the tables of observation.

IV. Conclusion

In this article we have simulated the circuit design using 65 nm CMOS NAND and NOR Gate technology files. All the designs are developed in Tanner design environment with the total (average) power dissipation measurement. The novel sleepy transistor based design provides very good reduction of leakage power but it shows low levels of output. This proposed method can be utilized in situations which do not have requirements of good voltage levels and the circuit remains standby (inactive) mode for most of its operation time. The leakage power during active and standby mode is found to be better for novel method compared to sleepy and sleepy inverts using NAND and NOR.

REFERENCES

- [1] International Technology Roadmap for Semiconductors, <http://public.itrs.net>.
- [2] Kaushik Roy, Saibal Mukhopadhyay, Hamid Mahmoodi-Meimand "Leakage Current Mechanisms and Leakage Reduction Techniques in Deep Submicrometer CMOS Circuits", Proceedings of the IEEE, vol. 91, No. 2, February 2003.
- [3] Neil Weste, David Harris, Ayan Banerjee "CMOS VLSI Design: A Circuits And Systems Perspective" Text. III Edition, Pearson Education.
- [4] Chen, M. Johnson, L. Wei and K. Roy, "Estimation of Standby Leakage Power in CMOS Circuits Considering Accurate Modelling of Transistor Stacks," International Symposium on Low Power Electronics and Design, pp. 239-244, August 1998.
- [5] M.D. Powell, S.H. Yang, B. Falsafi, K. Roy and T.N. Vijaykumar, "Gated -VDD: A Circuit Technique to reduce Leakage in cache memories", Proceedings of the 2000 International Symposium on Low Power Electronics and Design, July 2000.
- [6] J.C. Park, V. J. Mooney III and P. Pfeiffenberger, "Sleepy Stack Reduction of Leakage Power," Proceeding of the International Workshop on Power and Timing Modelling, Optimization and Simulation, pp. 148-158, September 2004.

Disrepair of Earth Moving Equipment: Causes and Remedies

David O. Obada¹, Emmanuel B. Lucas², Bernard A. Otegbayo³, Tosin I. Orogun⁴, Ibraheem A. Samotu⁵, Chike V. Chira⁶

^{1, 5, 6} Department of Mechanical Engineering, Ahmadu Bello University, Zaria, Nigeria.

² Department of Mechanical Engineering, LAUTECH, Ogbomoso, Nigeria.

³ Department of Mechanical Engineering, University of Greenwich at Medway, United Kingdom.

⁴ National Veterinary Research Institute, Vom, Jos, Nigeria.

Abstract: This study examines the causes of earth-moving equipment breakdown in construction sites in Nigeria using Kwara State, Ilorin as a case study. Efforts were put in place to survey the reasons why many earth moving equipment were abandoned in a state of disrepair on sites using questionnaire, interview and physical observation. Five different types of earth movers were studied and relevant data were collected and analyzed. The results of data obtained identified some subsystems of the equipment which are prone to failure leading to quick breakdown of the entire equipment. Among the subsystems, hydraulic and fuel system contributed significantly to incessant breakdown of the equipment examined, while traction, electrical and cooling system showed the least tendency to breakdown. Possible reasons for abandoning the equipment in their states of disrepair include scarcity of faulty part, expensive maintenance cost, lack of proper training of operator, nonchalant attitude among workers and improper handling of the repair processes, while the reasons for equipment malfunctioning include use of wrong tools by technicians, illiteracy amongst operators and technicians and impatience of operators as identified by the research.

Keywords: earth-moving equipment, maintenance, repair, sub-systems, operators, technicians.

I. Introduction

Earth-moving equipment are large engineering vehicles consisting of articulated parts atop an undercarriage with tracks or wheels. They are used in heavy construction, especially civil engineering projects, which often require the moving of millions of cubic meters of earth. Earth-moving equipment comes with different attachments which serve as the major distinguishing factor to the uses to which they can be put to. Some types of earth-moving equipment are Bulldozer, Pay-loader, Motor-grader, Excavator, Paver-Machine, Tractor and Dump truck. In order to ensure the best performance and profitable utilization of the earthmoving equipment, it is essential that adequate maintenance of the equipment be observed.

The biggest distinction from a cost standpoint is classification of repair as major or a minor repair. A major repair can alter the depreciation of equipment value due to an extension in service life while a minor repair is normal maintenance. Many construction and civil engineering companies had experienced problems and invariably folded up due to incessant scarcity of earthmoving equipment spare parts during servicing.



Fig1: Motor Grader in its State of Disrepair (Source: Construction Site, Ilorin)



Fig 2: Backhoe Loader in its State of Disrepair (Source: Construction Site, Ilorin)

According to Beppler and Hummedia (1983), the accumulated repair cost in the United States is as high as 1.6 times of the purchase price with inability of the local equipment assembly plants to produce spare parts. These equipment are not produced in the country (Nigeria), so huge capital investment is needed to purchase them. [1,2]. When considered individually, the various components of earth-moving machines such as links, pins, bushings, sprockets, rollers, idlers, shoes and frames seem relatively simple parts, but when these components are assembled into a system that supports and propels a track-type machine, the equipment becomes a complex mechanism which might account for half (or more) of the equipment's lifetime repair bill. Gene (1983) and Adigun (1987) classified the component systems of earthmoving equipment into 8 sub-systems viz, engine, transmission, hydraulic, cooling, electrical, lubrication, fuel and traction sub-systems. [3]

1.1 Ergonomics

Operator conveniences can have a large impact on the efficiency of a project because, the more comfortable and efficient the operator is, the quicker and better the project will go. Some common ergonomic considerations include air suspension seats, windshield wipers, beverage holders, storage trays, rearview mirrors and other detail. [4]

1.2 Serviceability

Earth moving equipment manufacturers continually strive to make their products easier to service. Some conveniences include such things like air filters on the same side of the engine, rear-tilting engine hoods, and so on. [4]

1.3 Auxiliary systems

Current auxiliary systems on an earth-moving machine such as an air conditioner, cooling fans, or pilot pumps, are powered by the engine of the earth moving machine. The auxiliary systems are belt or gear driven systems which are connected to the engine.

The auxiliary systems are driven at a speed dictated by the speed of the engine. For example, the speed of the engine can vary between low idle, i.e. 700rpm, and high idle, i.e. 2400rpm. The variance in the engine speed is dependent on the particular work function the machine is performing, as well as the load that the engine is carrying. [4]. The major aim of this work is to survey some heavy-duty automobiles in their states of disrepair in Kwara State for their serviceability situation and make recommendations on how to obtain the best use and maintenance of these machines at the cheapest cost obtainable.

Therefore, the specific objectives include:

1. To identify the nature of premature disrepair and their causes in the selected equipment as to make recommendations that would contribute to the improvement and performance of the equipment.
2. To recommend the best maintenance practices to ensure prolonged useful life of the earth-moving equipment.

II. Methodology

The methodology employed in this work was basically the use of questionnaire and analysis of detailed information obtained on various types of earthmoving equipment. Their usage and maintenance procedures were collected from respondents, also personal observations were made. A survey was carried out on three types of earthmoving equipment in Ilorin, Kwara State, Nigeria. These equipment are:

1. Backhoe Loader
2. Motor Grader
3. Bulldozer

Details of the methodology adopted are highlighted under the following sub-headings.

1. Questionnaire formation
2. Physical observation
3. Photographic presentation

2.1 Questionnaire

To identify the nature and state of disrepair and causes, a questionnaire was prepared (see appendix) which was administered to the following group of people:

1. Owners of the equipment.
2. Technicians engaged in repair of equipment.
3. Operators of the equipment.

2.2 Physical Observation

Information was also gathered from visual observation of the use of these equipments on site during visits to some construction companies in Ilorin. Inspection and observations were made to consolidate questionnaire information. Interviews were also conducted at sites. Besides the physical observation of the earthmoving machine, photographs of some of the equipment, parts and worksites were taken (see Figures 1 and 2) to properly document the findings.

III. Results and Discussion

It was found out from the questionnaire administered to the owners that all the earth-moving equipment were purchased as fairly used. Most of the equipment (about 70 %) had a few issues at the point of purchase. This complains ranged from bad tackle system to faulty transmission system. They were however purchased by the owners with the intention of putting them in order by buying missing parts and replacing bad ones.

Findings also indicated that some parts are more prone to damage in these equipment thereby causing untimely breakdown of the equipment, the parts include:

1. Transmission pump, hydraulic pump, primer pump
2. Gear
3. Nozzle
4. Nose
5. Radiator
6. Fuel Filter, Oil Filter, Magnetic Strainer
7. Air Cleaner.

The relevance of these parts to the smooth operation of the equipment is discussed below.

Pumps

The transmission, hydraulic and primer pumps are important as they help in coordinating the motions of other parts and sometimes the machine as a whole. Leakages in pumps result in breakdown of the equipments. These leakages result from bad or rusted hose clips or poor clipping of hoses to pipes. This can be corrected by checking hose clips during weekly maintenance and replacing them if they are bad or likely to go bad soon. Leakages can also be caused by high oil level, excessive foaming of lubricant and loose drain plug.

Gear system

The gear system needs maintenance other than periodic oil changes. However, when repair is carried out on a gear system, it is important to examine the whole gear train to locate worn or faulty parts and repair or replace them at that time. This will prevent a breakdown and the need to disassemble the transmission once again.

Therefore, some flaws to look for during maintenance are:

1. Excessive gear tooth wear or broken teeth.
2. Worn-out bearings.
3. Damaged or plugged transmission oil lines or passage in shafts.

Trouble-shooting the gear system

This trouble shooting chart is given as a general guide to common gear system or transmission system failures. They list what the causes might be, and the remedies.

Table 1: Transmission noisy in neutral

S/n	Possible Cause	Remedy
1.	Transmission not aligned with engine	Align
2	Dry, badly worm or broken bearings	Lubricate or replace

Table 2: Transmission noisy while in gear

S/n	Possible Cause	Remedy
1.	Low transmission oil level	Refill
2.	Worn gear-tooth	Replace gear
3.	Defective engine vibration damper	Replace or adjust

Table 3: Transmission slips out of gear

S/n	Possible Cause	Remedy
1	gear loose on shaft	Replace shaft or gear
2.	gear teeth worn	Replace gear

Nozzle

Nozzle heat-up and expand when the engine is running. They expand to cause leakages when they have been in use for a long time. Regular replacement of hoses during maintenance will help prevent breakdown.

Filters and cleaners

Filters and cleaners cannot be prevented from damage but must be replaced at regular intervals.

3.1 Analysis

According to the questionnaire and interviews, equipment owners prefer a cost effective approach in solving problems encountered on the equipment. The issue of buying fairly used parts as against new ones is a common practice. It was also found out from observation of work site areas that some of the equipment were used for jobs way beyond their capacity, and thus resulting in damage of different parts of the machines.

3.2 Reason for Equipment Disrepair

The parts mentioned, are often abandoned when they go bad bringing about equipment being abandoned whenever a fault develops. This is mostly due to scarcity of faulty parts, expensive maintenance cost, inadequate training of operators, nonchalant attitude amongst workers, and improper handling of the repair processes.

3.3 Factors that Led to Equipment Malfunctioning

Some factors were identified as causes of equipment malfunctioning during the cause of the research, they include:

Technicians

Most of the technicians usually make use of wrong tools when repairing or working on faulty equipment. For example, tools like hammer and screwdrivers are used on bolts and nuts as against the

conventional spanner designed for the purpose. More so, their workshops are not arranged to allow systematic, convenient and correct handling of tools, servicing and repair of equipment. Due to the fact that replaceable scraps are not guaranteed in the warehouse, practice of cannibalization has become very necessary.

Illiteracy

It was also observed that one of the reasons for most equipment going into disrepair is as a result of little or no educational background of the operators and technicians. Necessary periodic maintenance in order to prevent the likelihood of equipment not meeting the optimum working condition is not considered important among the operators. At times, wrong practice of cannibalization or economization on equipment repairs result to malfunctioning of equipment.

Impatience

This was inferred from the information collected. Some technicians/operators, in order to hasten their work do not bother to follow manufacturers' specification and correct order to routing maintenance and repairs.

Overuse and wrong use of equipment

Overuse of equipment and nonchalant attitude towards the equipment capacity and flywheel power results to untimely breakdown of equipment. Wrong use of equipment for a particular job can also result in its malfunctioning. For instance, the use of a pay-loader to dig instead of an excavator will bring about its untimely breakdown.

3.4 Precautions to Reduce Disrepair and Scrap Items

1. During servicing and repairs, it is very important that the established equipment guidelines for part replacement or repair are followed. Operators and technicians should be made to undergo proper training. This will reduce nonchalant attitude towards their work
2. Proper inventory must be done, since its shortage results to wrong practice or cannibalization, which may not be economical.
3. Routine maintenance and repair policy should be implemented to suit manufacturers' specification

IV. Conclusions and Recommendations

4.1 Conclusions

The present study examined the causes of earth-moving equipment breakdown in Kwara state. Five (5) different types of earth movers were observed and relevant data were collected. The result of data obtained on the vehicles indicated that hydraulic and fuel system contributed significantly to incessant breakdown of the equipment examined. The results also indicated that traction, electrical and cooling system showed the least tendency to breakdown.

Possible reasons for abandoning the equipments in their states of disrepair include scarcity of faulty part, expensive maintenance cost, lack of proper training of operator, nonchalant attitude among workers and improper handling of the repair processes while the reasons for equipment malfunctioning include use of wrong tools by technicians, illiteracy among operator and technician and impatience of operators during operations as identified by the research.

4.2 Recommendations

The following recommendations can be made:

- a) **Maintenance:** In order to prolong the life span of the machine, it is necessary that some preventive and corrective maintenance procedures are adhered to. These include daily checking of the machine's engine oil, transmission oil, hydraulic oil as well as water in the radiator before starting and operating the machine. Apart from regular check, maintenance such as servicing, lubrication and repairs should also be performed.
- b) **Servicing:** These involve changing of filters and draining of oil from either engine, transmission or hydraulic depending on the period the machine had worked. It should be divided into:
 1. 250 hrs service: involves changing engine oil and filters.
 2. 500 hrs service: involves changing engine oil and filters.
 3. 750 hrs service: involves changing engine oil and filter.
 4. 1000 hrs service: involves changing engine, transmission and hydraulic oil and filters.

A proper inventory of spare parts must be maintained for effective maintenance. Service and operators manuals should be constantly used by operators and maintenance personnel. This is in agreement with conclusion in an earlier research reported [5].

- c) **Lubrication:** Proper and regular lubrication must be ensured. This must entail the changing of oil and greasing of movable parts of the machine with correct amount of oil. Also, the use of correct type of oil for the engine, transmission and greasing of movable part to prevent rubbing of metals in order to ensure proper meshing of the gears and to reduce heat and friction.
- d) **Repair:** regular check up should be done on the equipment to notice any damage or imperfection in the machines .Examples include leakage of hydraulic boost while machine is at work and not noticed in time, this may lead to total damage of the pump.

REFERENCES

- [1] Beppler and Hummedie (1983), eight years of cost monitoring. Paper no 74- 1544. ASAE.
- [2] Peterson Anderson Incorporate (2007). Tractor maintenance cost (Trinidad) vol. 1 page 67
- [3] Gene (1983) and Adigun (1987). Maintenance culture: The Nigeria Situation. The Nigeria Journal of Engineering Management 1 (4):38 - 43.
- [4] Earth Moving Equipment Guide (2008)
- [5] Trewite Philip (1999). Towards Building Better Engineering Services Design.

APPENDIX I Questionnaire

Department of Mechanical Engineering, Ladoke Akintola University of Technology, Ogbomoso, Oyo State, Nigeria. Sample of a Filled Questionnaire on State Of Disrepair of Earth Moving Equipment In Ilorin, Kwara State.

SECTION A

NAME OF COMPANY	Bulletin Construction Company Ilorin
DATE OF VISIT	13 th August 2008
NAME OF EQUIPMENT	Loader/ Backhoe
DATE OF PURCHASE	2007
DATE OF MANUFACTURE	2004
NAME OF MANUFACTURER	ALLMAND
MODEL NAME	2004 ALLMAND 235
CAPACITY	1.3 TON (Mini- Loader)
NATURE OF WORK DONE BY EQUIPMENT	Digging holes, landscaping, breaking asphalt, paving roads, small demolition amongst others.
NATURE OF LOCATION OF WORK	Dry land
LEVEL OF EXPERIENCE OF OPERATOR	2-3 years
AVERAGE NUMBER OF HOURS OF USE PER WEEK	36 hours
AVERAGE NUMBER OF HOURS OF USE BEFORE SERVICING	250 hours
MAINTENANCE CARRIED OUT ON MACHINE	Deferred Maintenance
MOST FREQUENT REASON FOR BREAKDOWN	Hydraulic problems

SECTION B

NAMES OF PARTS AND PROBLEMS OF MAINTENANCE

NAME OF PART	FUNCTION	AVERAGE NUMBER OF HOURS OF USAGE BEFORE CHANGE	MOST FREQUENT REASON FOR CHANGE
Back hoe	It is used to dig up hard compact material usually earth	2,200 hours	Hydraulic problems
Bucket	It operates from the rear. It is used to pick up large amount of waste material.	1,400 hours	Wear of Bucket blade
Loader	It is used to pick up large amount of waste material. e.g sand.	-	-

Office Security System

Bhagare Pradeep M¹, Prof. Mrs. Laturkar A. P.²
^{1,2} (Department of E&TC, PES Modern College of Engineering, Pune)

Abstract: In this Office Security System project, image is captured by web camera, detected image is compared with original data base for face recognition. If recognized image is known face then open the door, otherwise sent the unknown image through LAN for displaying a new visitor, to all over the network in various Departments. If the new visitor is to any one of the related person of staff member then he will give the instruction to open door for the same visitor.

The Cortex M-3 system can measure all kind of electrical and thermal parameters RTD and so on. The measured data can be displayed on the LCD/TFT of the system and at the same time can be transmitted through RS – 485, or Ethernet N/W to remote DAS or DCS monitoring system by using mod bus / RTU or mod bus / TCP control, The system has N/W with long distance communication function which can ensure the disturbance rejection capabilities and reliability of the communication network. Hardware platform use 32 bit embedded arm microprocessor and software platform use the microcontroller and real time multitasking operating system which is open source. By using all these different port's functioning parameters of the Cortex M-3, Office Security System is developed.

Keywords: Discrete Cosine Transform, Face detection, Face Recognition, Discrete Cosine Transform coefficients, Threshold, Principle Components Analysis, Eigen faces.

I. INTRODUCTION

Now a day's security matter is very important. Also day by day its getting critical. Security is different for different locations and situations with time. By considering all insecurity parameters in society, also by considering advanced updated technology Office Security System is one of the solution for this problem. In Office Security System by considering general parameters of the unknown/visitor, staff, persons face recognition is done. For real time application and low cost high speed purpose cortex controller is used. Since it gives a very large scope for future expansion, development.

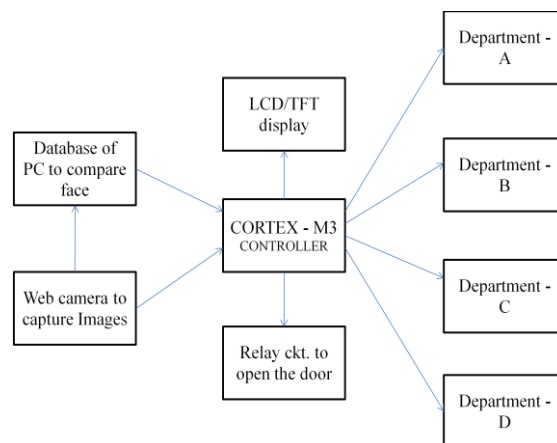


Fig 1: Main Block Schematic

II. Working

PART: 1 (To open door for known person)

This project is basically for security purpose. In this, initially the known staff/employees' images are stored as data base in PC . When a person enters via main gate the image will be captured by web camera. The captured image will be sent for detection of image through serial port. If this image is recognized or the image is matching with our original data base then and then only PC will sent signal to activate the controller so that it

will switch ON the relay of Motor. This will open the door. Thus the door will open for known staff/ persons only.

Flow chart (Complete Project)

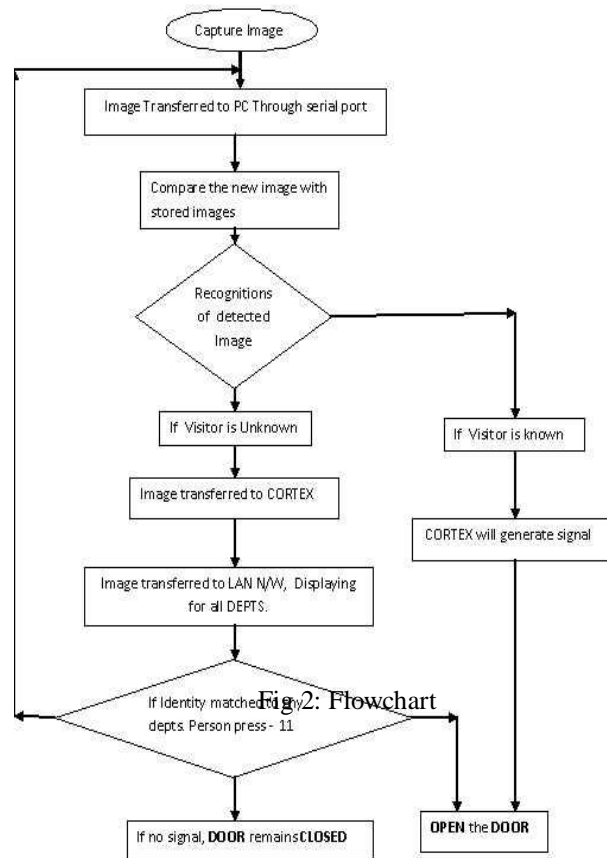


Fig.2: Flowchart

PART: 2 (Face Detection & Recognition part)[1, 2, 3]
Block Diagram with Explanation

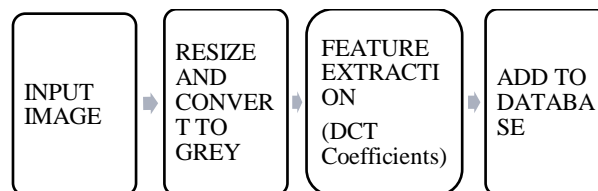


Fig.3 : Block Diagram of Face detection

The captured image by web camera is compared with the original data base which is already stored in PC. Now the process of face recognition is done. The captured image is resized in (200*180) predefined format. The RGB image is converted in to gray image. Apply the discrete cosine transform on this gray scale image. We do not required all the frequency components of complete face but only the high frequencies are required. After applying DCT only high frequency components get separate out i.e. only the face borders. Out of these frequency components only few which are required for Euclidian distance are picked up for comparison with original data base. If this Euclidian distance is less than threshold then the face is identified or it indicates that is face of known person i.e. face matching.

Give the instruction for controller to open the door. Thus due to the real time application and to reduce processing time of processor. Only required Frequency components are taken for consideration of Euclidian distance calculations.

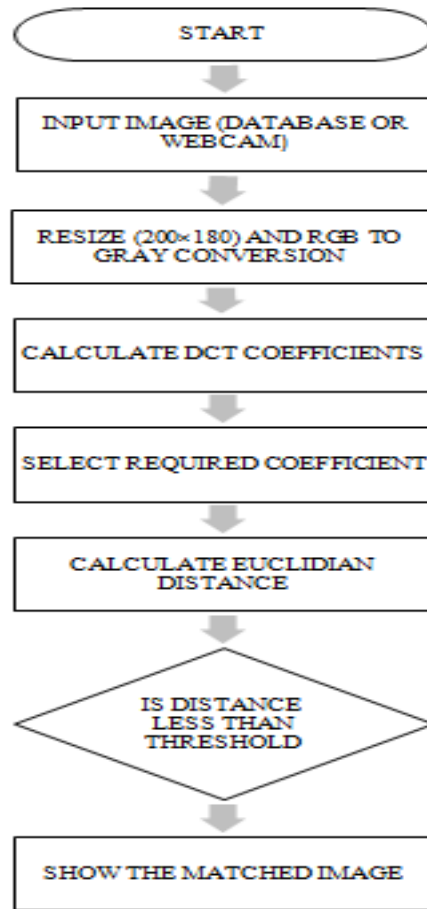


Fig.4: Flow chart for face recognition



Fig. 5: Block diagram to Calculate Euclidian Distance

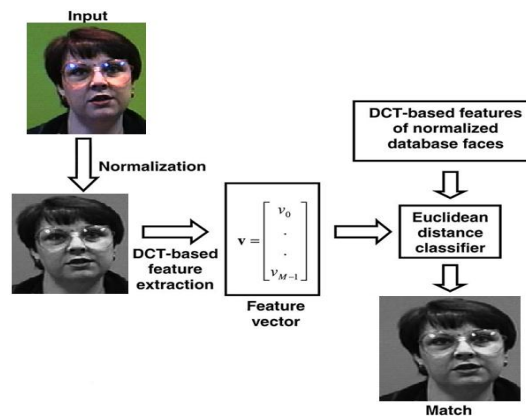


Fig. 6: Block diagram to Calculate DCT coefficients [Courtesy: IEEE images]

III. Calculation

Calculation of Euclidian Distance:[2, 4]

$$D = \sqrt{[(f_0 - v_0)^2 + (f_1 - v_1)^2 + \dots + (f_m^{-1} - v_m^{-1})^2]}$$

where

$$v = [v_0, v_1, v_2, \dots, v_m^{-1}]$$

T = Input image DCT coefficient vector

$$f = [f_0, f_1, f_2, f_3, \dots, f_m^{-1}]$$

T = DCT coefficients vector of image to be compared.

After calculating the Euclidian distance the match is found on the basis of the shortest Euclidian distance in data base.

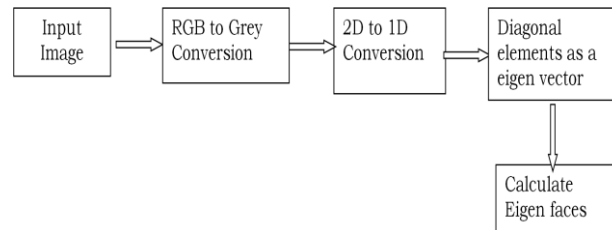


Fig.7: Block diagram to Calculate Eigen faces

PART: 3 Controller (LPC 1768) & LAN [5]

If the visitor/unknown persons want to enter through Main-gate. The image will be captured by web camera. The image sent to the data base for comparison of face, and reply of the controller will be not matching of face. In such case, the image will be transferred to departmental LAN which is connected to cortex controller. Thus unknown person will see on the screen of departmental PC. Thus you can see the face of the unknown visitor who is stood in front of the security gate which is far away from the different departments. Thus we can capture, stored the unknown visitors image for our information.

If identity or introduction of image or photo copy of this unknown person is matched to any of the dept's / staff member then that person will convey to security dept. to open the door / main gate. Thus door will not open for unknown person and unknown person will not be allowed to enter without identity is the major part of controller.

Technical Features of LPC 1768

1. ARM Cortex-M3 processor, running at frequencies of up to 100 MHz A Memory Protection Unit (MPU) supporting eight regions is included. And available as 100-pin LQFP package.
2. ARM Cortex-M3 built-in Nested Vectored Interrupt Controller (NVIC).
3. Up to 512 kB on-chip flash programming memory. Enhanced flash memory accelerator
4. Enables high-speed 100 MHz operation with zero wait states.
5. In-System Programming (ISP) and In-Application Programming (IAP) via on-chip Boot loader software.
6. On-chip SRAM includes:
7. 32/16 kB of SRAM on the CPU with local code/data bus for high-performance CPU access.
8. Two/one 16 kB SRAM blocks with separate access paths for higher throughput. These SRAM blocks may be used for Ethernet (LPC1768/66/64 only), USB, and DMA memory, as well as for general purpose CPU instruction and data storage.
9. Eight channel General Purpose DMA controller (GPDMA) on the AHB multilayer matrix that can be used with the SSP, I2S-bus, UART, the Analog-to-Digital and Digital-to-Analog converter peripherals, timer match signals, and for memory-to-memory transfers.
10. Multilayer AHB matrixes interconnect provides a separate bus for each AHB master. AHB masters include the CPU, General Purpose DMA controller, Ethernet MAC (LPC1768/66/64 only), and the USB interface. This interconnect provides communication with no arbitration delays.
11. Split APB bus allows high throughput with few stalls between the CPU and DMA.
12. Serial interfaces:
13. Ethernet MAC with RMI interface and dedicated DMA controller (LPC1768/66/64 only).
14. USB 2.0 full-speed device/Host/OTG controller with dedicated DMA controller and on-chip PHY for device, Host, and OTG functions. The LPC1764 includes a device controller only.
15. Four UARTs with fractional baud rate generation, internal FIFO, DMA support, and RS-485 support. One UART has modem control I/O, and one UART has IrDA support.

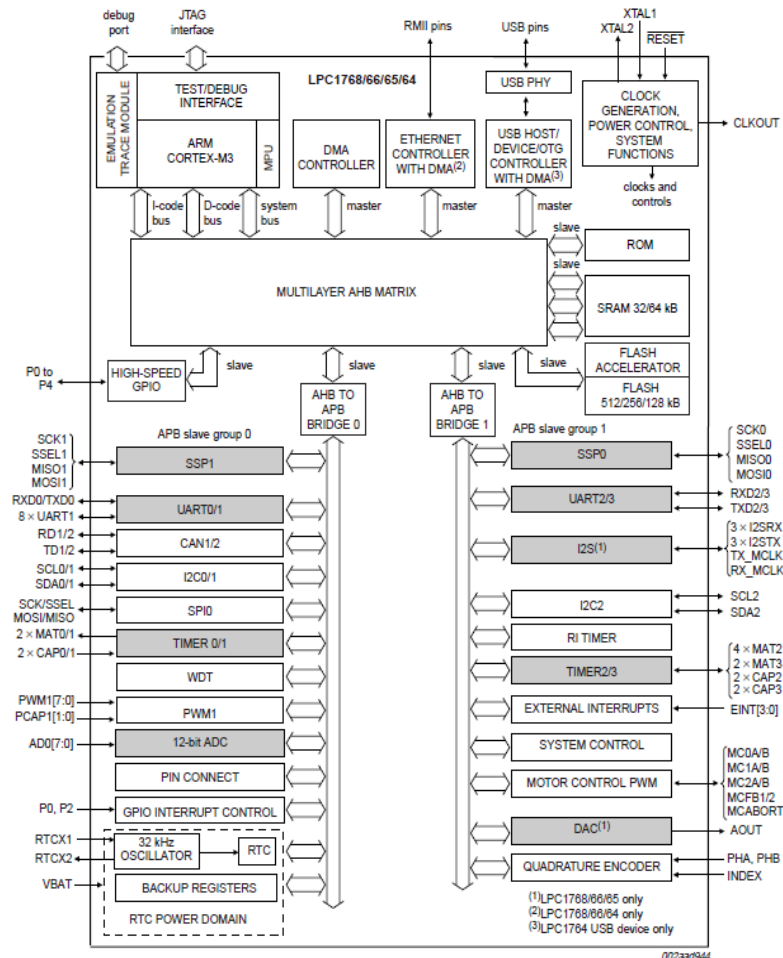


Fig. 8: Block schematic of LPC 1768

16. CAN 2.0B controller with two channels.
17. SPI controller with synchronous, serial, full duplex communication and programmable data length.
18. Two SSP controllers with FIFO and multi-protocol capabilities. The SSP interfaces can be used with the GPDMA controller.
19. Two I2C-bus interfaces supporting fast mode with a data rate of 400 Kbits/s with multiple address recognition and monitor mode.
20. One I2C-bus interface supporting full I2C-bus specification and fast mode plus with a data rate of 1 Mbit/s with multiple address recognition and monitor mode.
21. On the LPC1768/66/65 only, I2S (Inter-IC Sound) interface for digital audio input or output, with fractional rate control. The I2S-bus interface can be used with the GPDMA. The I2S-bus interface supports 3-wire and 4-wire data transmit and receive as well as master clock input/output.
22. Other peripherals:
23. 70 General Purpose I/O (GPIO) pins with configurable pull-up/down resistors and a new, configurable open-drain operating mode.
24. 12-bit Analog-to-Digital Converter (ADC) with input multiplexing among eight pins, conversion rates up to 1 MHz, and multiple result registers. The 12-bit ADC can be used with the GPDMA controller.
25. 10-bit Digital-to-Analog Converter(DAC) with dedicated conversion timer and DMA support (LPC1768/66/65 only).
26. Four general purpose timers/counters, with a total of eight capture inputs and ten compare outputs. Each timer block has an external count input and DMA support.
27. One motor control PWM with support for three-phase motor control.
28. Quadrature encoder interface that can monitor one external quadrature encoder.
29. One standard PWM/timer block with external count input.
30. RTC with a separate power domain and dedicated RTC oscillator. The RTC block includes 64 bytes of battery-powered backup registers.

31. Watchdog Timer (WDT) resets the microcontroller within a reasonable amount of time if it enters an erroneous state. System tick timer, including an external clock input option.
32. Repetitive interrupt timer provides programmable and repeating timed interrupts.
33. Each peripheral has its own clock divider for further power savings.
34. Standard JTAG test/debug interface for compatibility with existing tools. Serial Wire Debug and Serial Wire Trace Port options.
35. Emulation trace module enables non-intrusive, high-speed real-time tracing of instruction execution.
36. Integrated PMU (Power Management Unit) automatically adjusts internal regulators to minimize power consumption during Sleep, Deep sleep, Power-down, and Deep Power-down modes.
37. Four reduced power modes: Sleep, Deep-sleep, Power-down, and Deep power-down.
38. Single 3.3 V power supply (2.4 V to 3.6 V).
39. Four external interrupt inputs configurable as edge/level sensitive. All pins on PORT0 and PORT2 can be used as edge sensitive interrupt sources.
40. Non-maskable Interrupt (NMI) input.

IV. Conclusions

Cortex M-3 (LPC 1768) is a universal controller with the help of this we can perform or interface all kinds of modern devices and perform different applications as per requirements. In Office Security System, using different communication ports, images are transferred for face recognition. The unknown image is transferred for identification for all departments through LAN port. The decision of opening a door is completely controlled by Cortex M-3 controller with the help of predefined programmed criteria. Thus an intelligent Office Security System will be achieved with the help of Cortex M-3 controller.

V. Future Work

- 1) We can modify this for Iris detection.
- 2) We can modify this for Metal detection.
- 3) We can modify this for Finger print detection.
- 4) If our controller is connected to Police Stations then unknown images will be compared with WANTED person's images and the system will give information of WANTED persons to police stations automatically. Thus the system will help for the security of society.

REFERENCES

- [1] DerzuOmaia, JanKees v. d. Poel, Leonardo V. Batista "Low – Memory Requirement and Efficient Face Recognition System Based on DCT Pyramid", IEEE Transactions on Consumer Electronics, Vol. 56. 3, August 2010.
- [2] DerzuOmaia, JanKees v. d. Poel, Leonardo V. Batista, "2D- DCT Distance Based Face Recognition Using Reduced Number of Coefficients", October 11-October 15 2009 IEEE International Conference on DCT Page(s) 1-8. Rio de Janeiro, Brazil.
- [3] Shah Ronak, Venkat Reddy, Rahul kumar Mishra, Tamakuwala Jimmy B. "Fingerprint Recognition using Discrete Cosine Transform", November 2009
- [4] Swarup Ku. Dandpat, Sukadev Meher, "New Technique for DCT-PCA Based Face Recognition", IEEE International Conference On DCT – PCA, 2009.
- [5] S.R. Shridhara, Di Renzo, S. Lingum, S. J. Lee, R. Blazquize, J. Maxey, S. Ghanem, Y. H. Lee, R. Abdalla, P. Singh and M. Goel, "Microwatt Embedded Processor platform for medical System on chip applications," IEEE Symp. VLSI Circuits Dig. Paper 15-16, 2010

Effect of Hardness and Wear Resistance on En 353 Steel by Heat Treatment

Navin A. Astunkar¹, A. S. Bonde²

^{1,2}(M.Tech 2ndyr. (Prod.Engg), Department of Mechanical engineering, Yeshwantrao Chavan College of Engineering, Nagpur, India)

Abstract: En 353 steel is an easily available and cheap material that is acceptable for heavy duty applications. Heat treatment on En 353 steel is improved the ductility, toughness, strength, hardness and relive internal stress in the material. Spectrographic method is used to analyze the composition of the alloy material. The experimental results of hardness and dry wear testing on pin-on-disc are done to get idea about heat treated En 353 steel. It is found that the hardness and wear resistance of the En 353 steel is improved after the heat treatment and the microstructure is changed from ferrite to martensite.

Keywords: En 353 steel. Heat treatment. Hardness. Wear resistance. Pin-on-disc.

I. INTRODUCTION

En 353 steel has carbon content of 0.17% and the most common form of steel as it provides material properties that are acceptable for many automobile applications such as heavy duty gear, shaft, pinion, cam shafts, gudgeon pins. It is neither externally brittle nor ductile due to its lower carbon content and lower hardness. As the carbon content increases, the metal becomes harder and stronger. The process of heat treatment is carried out first by heating the metal and then cooling it in water or oil or air. The purpose of heat treatment is, to enhances the transformation of austenite to martensite i.e. (soft material to hard material), to change the grain size, to modify the structure of the material and relive the stress set up in the material. It is a one-time permanent treatment process and it is change the entire cross section of the material. The martensitic phase transformation is usually used to increase the hardness of the steels. The various heat treatment processes are annealing, normalizing, hardening, quenching and tempering.

According to this work basically focus on carburizing; it is a process of improving carbon on case. These are done by exposing the part to carbon rich atmosphere at the high temperature (close to melting point) and allow diffusion to transfer the carbon atoms into the steel. So, these work concentrations go through gas carburizing which is widely used in mass production. The carburizing process does not harden the steel it only increases the carbon content. In heat treatments, both chemical composition and microstructure properties of a case can be changed.

The aim of this paper is to examine the hardness, wear resistance and effect of microstructure of before and after heat treatment on En 353 steel. In heat treatment, the machined specimens are loaded in the gas carburizing chamber. Carburizing takes places at 920°C for 120 minutes then it is cooled by air and relaxing time is 75 minutes. The purpose of the relaxing time is to arrest the in and out of the carbon and it is followed by oil quenching at 820°C for 30 minutes, oil temperature is below 80°C then by tempering at 250°C for 90 minutes. In general, the untempered material structure has the high hardness and also more brittle. Hence the tempering process should be done to reduce the brittleness, to relieve the internal stress and to increase the toughness and ductility of the material.

Nomenclature:

- AHT - After Heat Treatment
- BHT - Before Heat Treatment
- CHT - Conventional Heat Treatment
- HV - Vickers Hardness test

II. Methodology

After heat treatment, the specimens for structure investigations are conventionally prepared and etched using nital. The specimen with a diameter of 10 mm and a length of 50 mm are subjected to the Hardness test using the MH6 machine. The specimen with same size are subjected to wear testing using Pin-on-disc apparatus. The Leica DM 2500 M microscope is used to the observations of obtained structures before and after the heat treatment.

III. Results And Discussion

3.1 Chemical Analysis

In order to ensure the material of the specimen is done with help of the optical emission spectroscope (OES). The result is obtain from the chemical analysis, carbon - 0.169 %, silicon - 0.234 %, manganese - 0.712 %, phosphorus - 0.015 %, sulphur - 0.030 %, Chromium – 1.617 %, Nickel - 1.574 %, molybdenum - 0.265 %, copper - 0.243%, Aluminum -0.034% and remaining percentage is iron respectively. A sample of $\phi 20 \times 10$ mm is polished using 60 grit papers and two sparks is introduced on the surface to find the chemical composition of the material. After ensuring the chemical composition, the raw material is machined according to the dimension for various tests.

3.2 Hardness

Vickers hardness measurement is done on the specimen as per the IS 1501-2008 procedures by using Vickers hardness tester (MH6). Hardness measurement is made with 100 g loads, dwell time of 10 seconds and diamond indenter is used for test. The impression is done on the circular faces at the centre of the specimen. The hardness values are taken corresponding to the diagonal length of the indentation. Two samples (i.e. BHT and AHT) and four readings are taken from the each sample from case to core. The average value is calculated from four readings. The hardness values of BHT (case and core) samples are, 244.25 and 244.77 HV respectively. The hardness values of AHT (case and core) samples are 671 and 417.2 HV respectively. It is clearly noticed that the base material (BHT) has the low hardness. The AHT specimen has high hardness when compared to the BHT sample as shown in Fig. 1.

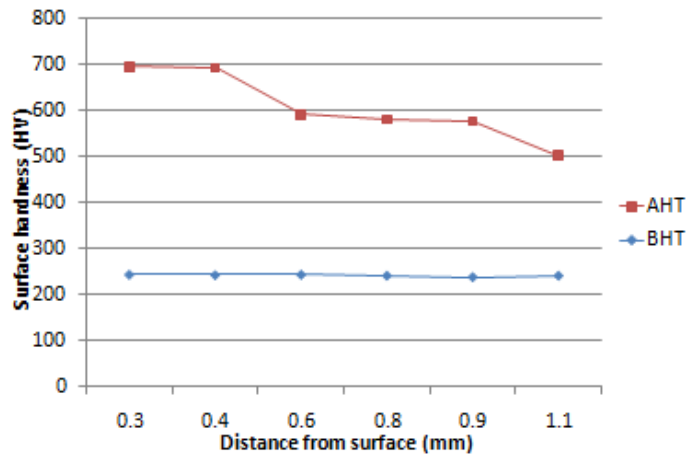


Fig.1: Hardness Profile of En353 steel BHT and AHT

3.3 Wear Resistance

wear resistance measurement is done on specimen by using dry wear on pin-on-disc testing in accordance with the ASIM G99-95standrds.the experimental results of wear carried out in laboratory gives values of initial and final weight, before and after wear of specimen. wear test carried out with the 40N load, 400rpm velocity, 40mm track radius, 1000m sliding distance for 10 minutes. the experimental result of wear test are analyzed by the Archad's (Hutchings,1995)or Rabinowicz's equation (rabinowicz,1965) that assess the wear rate and wear coefficient, relating the cumulative lost volume per sliding distance with the wear resistance through the linear equation as follows.

$$Q\left(\frac{\text{mm}^3}{\text{m}}\right) = \frac{V}{S} = K \frac{F_N}{H} \dots\dots\dots(\text{equation 1})$$

where,

- Q - wear rate
- V - cumulative lost volume
- S - sliding distance
- F_N - normal load
- H - hardness (HRC)

from Eq.(1), wear coefficient is given by,

$$K = \frac{QH}{F_N} \dots\dots\dots(\text{equation2})$$

and in general wear coefficient is defined as 1/K.

Readings are taken from two samples average value calculated from readings. results obtain are shown in following tables.

Sr. no.	Specimen	wear rate $Q=V/S(\text{mm}^3/\text{m})$ (*10 ⁻³)	mean value Q	wear coefficient(K) (*10 ⁻³)	mean value(K)	wear resistance(1/K)	mean value(1/K)
1	BHT	8.81	8.81*10 ⁻³	5.1	5.1*10 ⁻³	196.1	196.1
2		8.81		5.1		196.1	
1	AHT	1.23	1.23*10 ⁻³	9.04	9.04*10 ⁻⁴	1106.2	1106.2
2		1.23		9.04		1106.2	

Table 1: results of wear resistance BHT and AHT

3.4 Microstructure

The change of microstructure in the material due to conventional heat treatment (CHT) is the main reason for the improved mechanical properties. Hence the microstructure examination is carried out to find the structure of BHT and AHT. The samples are polished using SiC emery paper of grit 280 and velvet cloth using white kerosene as coolant. These samples are etched with nital and dried in air. Finally, microstructure examination is carried out using optical microscope.

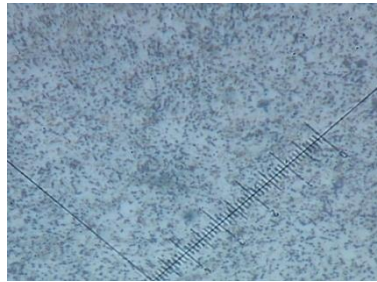


Fig. 2: spheroidized annealed structure at Mag. 1000X BHT

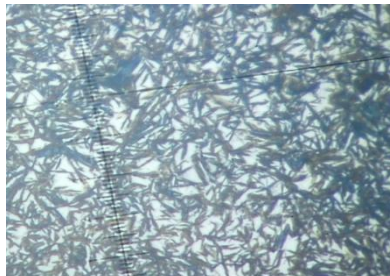


Fig. 3: about 45% retained austenite in the matrix of martensite at Mag. 1000X AHT

Fig. 2 show the microstructure of BHT is ferrite and spheroidized annealed structure with at the grain boundaries distributed throughout the structure and Fig. 3 show the microstructure of AHT is fine martensite, with retained austenite and traces of ferrite distributed throughout the structure.

IV. Conclusion

Before and after the heat treatment process the mechanical properties of the En 353 steel are examined. The results obtain under the experimental conditions of this work the following conclusion are drawn.

1. High hardness is obtained in carburizing 120 minutes at 920°C for En 353 steel.
2. Micro hardness values of AHT are found to be higher than BHT.
3. Wear resistance values AHT are found to be higher than BHT.
4. The specimen is having greater hardness on case sample than the core sample.
5. Pictorial view of case/core microstructure indicates that the heat treated specimen is martensite.
6. Thus life of material can be enhanced by the conventional heat treatment process.

REFERENCES

- [1] B. Selcuk, R. Ipek, M.B. Karamis, A study on friction and wear behaviour of carburized, carbonitrided and borided AISI 1020 and 5115 steels, *Journal of Materials Processing Technology* 141 (2003) 189–196
- [2] R. Ipek, B. Selcuk, The dry wear profile of cam shaft, *Journal of Materials Processing Technology* 168 (2005) 373–376
- [3] M. Preciado, P.M. Bravo, J.M. Alegre, Effect of low temperature tempering prior cryogenic treatment on carburized steels, *Journal of Materials Processing Technology* 176 (2006) 41–44
- [4] B. Selcuk, R. Ipek, M.B. Karamis, V. Kuzucu, An investigation on surface properties of treated low carbon and alloyed steels (boriding and carburizing) *Journal of Materials Processing Technology* 103 (2000) 310-317
- [5] Boyel, D.O. Northwood, R.bowers, X. Sun, P.bauerle, The effects of initial microstructure and heat treatment on the core mechanical properties of carburized automotive steel, *material forum volume 32-2008*
- [6] Sandor, L. T.; Politori, I.; Gonçalves, C.S.; Uehara, A.Y.; Leal, C.V.; Sato, M.; Ferreira, Fatigue Crack Propagation in Nine Steels, Type SAE 43XX, from 0.20 to 1.00 % C, for the Simulation of the Fatigue Behavior in a Carburized Layer of the SAE 4320, *Procedia Engineering* 2 (2010) 735–742
- [7] S.Ilayaveial, A. Venkatesan, The wear behavior of manganese phosphate coating applied to AISI D2 steel subjected to different heat treatment processes *Procedia Engineering* 38 (2012) 1916-1924.
- [8] J.D. Bressan, D.P. Daros, A.Sokolowski, R.A. Mesquita, C.A. Barbosa., Influence of hardness on wear resistance of 17-4 PH stainless steel evaluated by the pin-disc testing, *journal of material processing technology* 205 (2008) 353-359 .
- [9] Michael A. Klecka, Ghatu Subhash, Nagaraj K. Arakere, Determination of sub surface hardness gradient in plastically graded materials via surface indentation, *Journal of Tribology* 133 (2011) 1-5.
- [10] Manoj V, K Gopinath and G Muthuveerappan Rolling contact fatigue studies on case carburized and cryogenic treated en 353 gear material, *International Symposium of Research Students on Material Science and Engineering* 22 (2004) 1-8.
- [11] Jason J. Spice and David K. Matlock Greg Fett, Optimized Carburized Steel Fatigue Performance as Assessed with Gear and Modified Brugger Fatigue Tests, *Society of Automotive Engineers*, 1003 (2002) 1-9.

Accelerating Real Time Applications on Heterogeneous Platforms

Vivek Vanpariya¹, Prof. S. Ramani²
^{1,2} (SCSE, VIT University, Vellore, India)

Abstract: In this paper we describe about the novel implementations of depth estimation from a stereo images using feature extraction algorithms that run on the graphics processing unit (GPU) which is suitable for real time applications like analyzing video in real-time vision systems. Modern graphics cards contain large number of parallel processors and high-bandwidth memory for accelerating the processing of data computation operations. In this paper we give general idea of how to accelerate the real time application using heterogeneous platforms. We have proposed to use some added resources to grasp more computationally involved optimization methods. This proposed approach will indirectly accelerate a database by producing better plan quality.

Index Terms: Graphics processing unit (GPU), depth estimation, and video analysis.

I. INTRODUCTION

General purpose CPU performance scaling has opened up a new direction for computer scientist and architect. Scaling performance of new generation GP-CPU has not as predicted by Gordon moor. After observing it closely the throughput for sequential code in GP-CPU is getting fluctuated between subsequent processor generations. This problem has motivated the scientist to innovate the high performance and cost effective hardware. As a solution computer scientist comes up with a low level GP-GPU core which has features like out of order execution and lack branch prediction to optimize the sequential code [1]. Khronos has a framework and standard set for heterogeneous parallel computing on cross-vendor and cross-platform hardware [7]. It provides an abstraction layer via which code can scale from simple embedded microcontrollers to GP-CPU's from Intel and AMD, up to massively-parallel GP-GPU hardware pipelines, all without modifying code [8]. Most important task of graphical processing unit (GPU) is to accelerate the graphical applications. It contains large amount of streaming processors for commutations when compared to Central Processing Unit (CPU). Also GPU have high-bandwidth for data transfer. Graphics processing unit's hasty increase in both programmability and capability has spawned a researcher's community that has effectively mapped a broad range of computationally demanding, complex problems to the GPU. In other words GPU computing is using it as to boost up central processing units for general-purpose scientific and engineering computations. It can be achieved by offloading some of the intensive and overwhelming portions of the code and the remaining part of the code will remain in the CPU. From user's view point, the application run more rapidly because of the extremely parallel processing power of the general purpose unit to boost performance which is well-known as "heterogeneous" or "hybrid" computing. Some critical factors like power, cost, bandwidth on which we have to focus when we working on GPU.

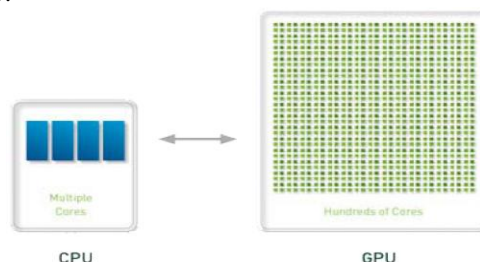


Figure 1: CPU vs. GPU

II. GPU ARCHITECTURE

Graphics processing units will be able to process independent fragments and vertices, but also can process many of them in parallel. This comes handy when the programmer needs to process many vertices or fragments in the same way. In this logic, GPUs are stream processors also called as stream at once. Stream can be said as collection of records that requires similar kind of computation.

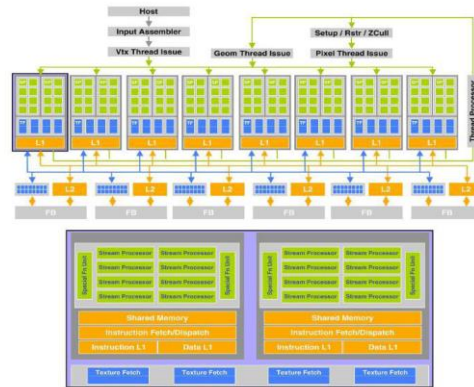


Figure 2: GPU Architecture

The 8800 is composed of 128 stream processors each rotating at the rate of 1350 Mhz. Each processor is capable to do calculation like MAD and MUL per clock cycle. Each processor need 4 cycles for executing specials instructions like EXP, LOG, RCP, RSQ, SIN, COS which is managed by an additional unit.

III. OPEN COMPUTING LANGUAGE

Open CL is popularly known as one of the free of royalty standard for general purpose parallel programming across CPUs, GPUs and other processors, giving software developer’s transportable and capable access to the power of these assorted processing platforms. OpenCL consists of an application programming interface for coordinating parallel computation across heterogeneous processors and a cross-platform programming language with a well précised computation background.

Standards of Open CL:

- It supports data-based and task-based parallel programming models.
- It utilizes a rift of ISO C99 with extensions for parallelism.
- It defines steady numerical supplies based on IEEE 754.
- It defines a configuration report for handheld and embedded devices.
- It efficiently interoperates with OpenGL, OpenGL ES and other graphics APIs.

OPENCL memory model

Open CL framework provides the distributed memory. As shown in figure 3, each processor has its own private memory and each core has its own local memory.

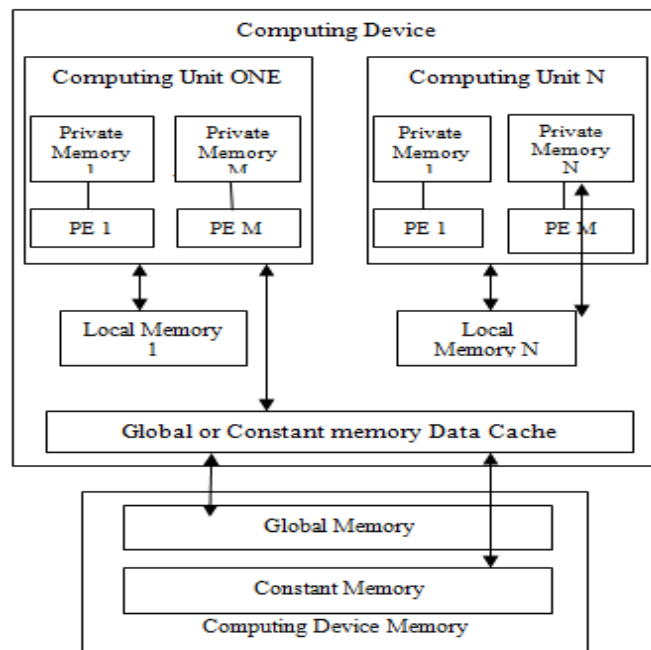


Figure 3: Architecture of Conceptual Open CL device having processing elements (PE), computing units and devices.

IV. TEST CASE FOR SERIAL VS PARALLEL CODE

In this section we give the basic comparison of serial and parallel code performance. If we take simple example of matrix multiplication in which each element is computed sequentially from the row of the first matrix and column of the second matrix. Same matrix multiplication can be done on parallel environment because there will be no previous data dependency. The below discussion give knowledge how to write parallel code using Open CL.

Parallel code of matrix multiplication is ported on Storm which is a tool of STMicroelectronics, which provide the parallel environment with 64 parallel processing units.

No. of Data Elements per matrix	No. of Cycles required for sequential code to run	No. of Cycles required for parallel code to run	Speed Up
16x16	1654850	32230	51
32x32	13185830	212402	62
48x48	44479008	701355	63
64x64	105413896	1653468	63
128x128	843161792	13180778	64
256x256	6744844288	105394568	64
512x512	53957111808	843086272	64

Table 2: Comparison table of Serial vs Parallel code of Matrix multiplication.

Tools have got 4 clusters and each cluster contains 16 processing elements (cores). Above table give comparison chart of matrix multiplication using Storm. If we take the advantage of local memory and memory bandwidth for accessing the data from host part to device part then we can get better speedup i.e., speed of data transfer from global memory to compute device is slower than the speed of data transfer from local memory to compute device. Because local memory is more near to clusters and it is local to each clusters. Memory coalscaling is another feature of parallel processing. Suppose my bit transfer capacity from host to device is 32 bit's then why should I transfer 8 bit at a time. Fetch 32 bit's at a time and store it on device local memory until four bytes process.

No. of Data Elements per matrix	No. of Cycles using Global Memory	No. of Cycles using Local Memory	Speed Up
16x16	32230	20477	1.57
32x32	212402	114949	1.85
48x48	701355	368612	1.90
64x64	1653468	860118	1.92

Table 3: Comparison table of global vs serial memory for Matrix multiplication.

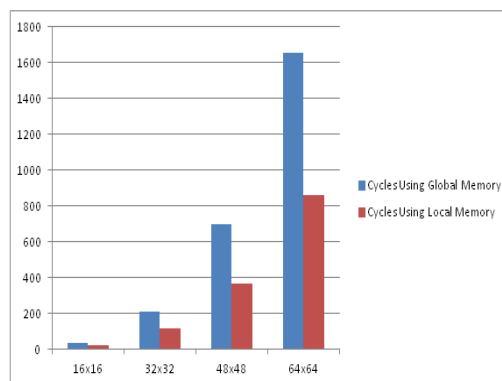


Figure 4: Cycles Needs for Global Vs. Local Memory for Matrix Multiplication

V. REAL TIME APPLICATION

Real time applications like depth estimation for stereo images, video analytics for surveillance and etc. are the good applications on image processing technology where repetitive work on pixels is needed. For this we are concentrating on throughput rather than the latency. Filtering and/or convolution for images are one of the important modules for depth estimation or in video analytics. In below discussion we briefly discuss convolution and result analysis after porting it on NVIDIA's Quadro FX 4600 and Storm tool of STMicroelectronics.

Convolution

Kernel: It is a collection of numbers in the matrix form which is used in convolution of images. They are available in different size having different number patterns producing different results. The dimension of each kernel is subjective but most often 3x3 is preferred.

A convolution is usually performed by doing the multiplication of a pixel and its adjacent pixels color value by a matrix.

Convolve is likely used to Enhance, Sharpen or smoothing the image.

We have the formulae for doing convolution of image $f(x, y)$ and kernel $k(x, y)$ represented as

$$f(x,y) * k(x,y) = \int_{-\infty}^{\infty} \int_{-\infty}^{\infty} f(u,v) k(x-u,y-v) du dv \dots(1)$$

In discrete form,

$$f(x,y)*k(x,y) = \sum_{i=0}^{w-1} \sum_{j=0}^{H-1} f(i,j) k(x-i, y-j) \dots(2)$$

W, H is the width and height of image respectively.

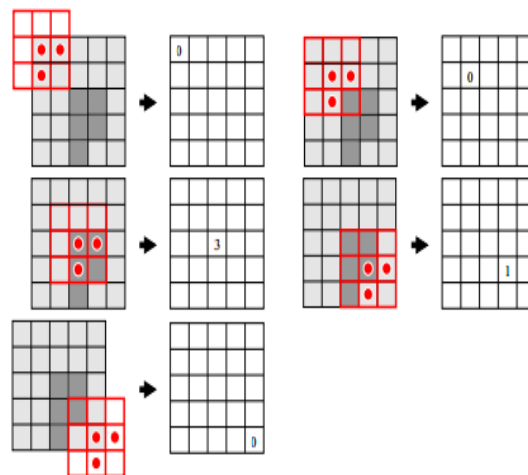


Figure 5: Masking on image.

VI. RESULT ANALYSIS

Function Name	Time require for assembly code (ms)	Time require for C/C++ code (ms)	Time require for Parallel code (ms)
convolve_cols_3x3	50	360	136
convolve_121_row_3x3_16bit	10	50	30
convolve_101_row_3x3_16bit	20	60	23

Table 4: Time analysis for assembly, serial and parallel code (using NVIDIA device).

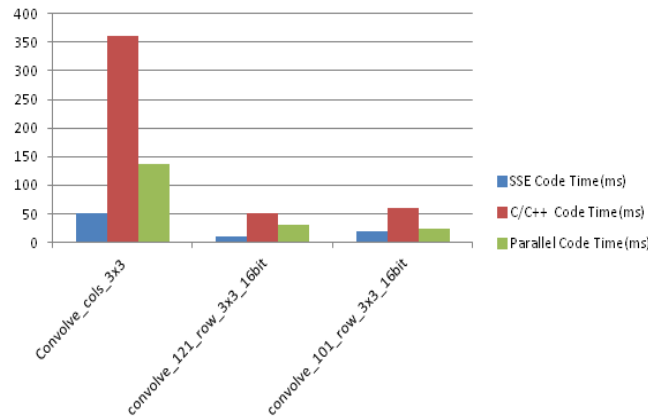


Figure 6: Comparison graph for table 4

Function Name	Time require for Assembly Code (ms)	Time require for C/C++ Code (ms)	Time require for Parallel Code on xp70(ms)
convolve_cols_3x3	50	360	128
convolve_121_row_3x3_16bit	10	50	28
convolve_101_row_3x3_16bit	20	60	20

Table 6: Time analysis for assembly, serial and parallel code (using Sthorm device).

VII. CONCLUSION AND FUTURE WORK

In this paper we have discussed the behavior of serial and parallel code with respect to different heterogeneous platforms. OpenCL has lot of task like getting a platform, kernel setting, memory/buffer initialization, filling the read buffer with input data, taking the device information, setting the work group and work items etc.. Due to this, performance results are not expected for small size data. By analyzing the comparison tables, we can accelerate the sequential code with the help of parallel computing elements on heterogeneous platforms.

In future related work, one can apply the optimization technique like memory co-aliasing, vector data types and pipeline futures on complex real time applications.

REFERENCES

- [1] I. Blthoff, H. Blthoff, and P. Sinha. "Topdown influences on stereoscopic depth-perception". *Nature Neuroscience*, 1:254.257.
- [2] S. Das and N. Ahuja. "Performance analysis of stereo, vergence, and focus as depth cues for active vision". *IEEE Trans PAMI*, 17:1213.1219.
- [3] A. Smolic and P. Kauff, "Interactive 3-D video representation and coding technologies," *Proc. IEEE, Special Issue on Advances in Video Coding and Delivery*, vol. 93, no. 1, pp. 98–110, Jan. 2005.
- [4] K. Mueller, P.Merkle, H. Schwarz, T. Hinz, A. Smolic, T. Oelbaum, and T. Wiegand, "Multi-view video coding based on H.264.MPEG4-AVC using hierarchical B pictures," in *Proc. PCS' 2006*, Apr. 2006, paper SS3–3. [Online.] <http://www.engineeringvillage2.org>.
- [5] Niem W, Buschmann R, "Automatic Modelling of 3D Natural Objects from Multiple Views", *European Workshop on Combined real and synthetic image processing for broadcast and video productions*, 23–24. 11. 1994, Hamburg, Germany.
- [6] L. Falkenhagen, A. Kopernik, M. Strintzis, "Disparity Estimation based on 3D Arbitrarily Shaped Regions", *RACE Project Deliverable*, R2045/UH/DS/P/023/b1.
- [7] Y. Yakimovski, R. Cunningham, "A System for Extracting 3D Measurements from a Stereo Pair of TV Cameras", *CGVIP*, Vol. 7, 1978, pp. 195 – 210.
- [8] Koch, R., "3-D Scene Modelling from Stereoscopic Image Sequences", *European Workshop on Combined real and synthetic image processing for broadcast and video productions*, 23–24. 11. 1994, Hamburg, Germany.



Vivek Vanpariya received his B.E degree from A.D Patel institute of Technology affiliated to Sardar Patel University, Gujrat, India. He did his M. Tech in Computer Science and Engineering from VIT University Vellore, India. His area of interests includes Computer Network, Algorithms and Operating Systems.



Ramani S received his M.Tech degree from Bharathidasan Institute of Technology affiliated to Bharathidasan University, TamilNadu, India. He is pursuing his Ph. D from VIT University Vellore, India. His area of interests includes Database, Web Technologies and Data Mining.

“Strengthening Of PCC Beams by Using Different Types of Wire Mesh Jacketing”

Er. Arote P.S.¹, Er. Dhindale G.B.², Er. Malunekar J.A.³, Er. Umbare A.S.⁴
^{1, 2, 3, 4}(Department of Civil Engineering, Amrutvahini College of Engineering, Sangamner,
Maharashtra, India. 422608.)

Abstract: This paper presents the effect of the use of different types of wire mesh jacketing to the PCC beams. The experimental work is mainly concerned with the study of flexural strength of concrete by different types of wire mesh jacketing. This study brings out the importance of use of strengthening of existing structure technology by using locally available wire mesh. In this paper, the beams of plain cement concrete are bonded with locally available wire mesh to strengthen of structural member for increase its strength. The method mention in this paper is most suited for strengthening and retrofitting due to their easy availability, economy and their property of being cast to any shape without needing significant formwork.

Keywords: Flexural strength. Wire mesh jacketing. Strengthening. Retrofitting.

I. Introduction

It is well-known that reinforced concrete beams which have been subjected to a fire will lose a major part of their strength and stiffness parameter. These two factors (strength and stiffness) are a major concern relating to the safety of concrete structures after fire. Generally, post-heated concrete structures are capable of being repaired economically rather than completely demolished and re-built. The most common technique for repairing fire damaged reinforced concrete beams is using a wire mesh jacket.

In recent years the easy handling and speedy repairing technique, with numerous advantages, are making the wrapping system of locally available wire mesh jackets the preferred technique for the repair and strengthening of a large number of projects. It has been found previously that wire mesh jacket can provide an effective confinement of reinforced concrete beams and therefore, it has a great potential to be used as a strengthening material.

A wire mesh jacket consists of a thin wire, wrapped around various beam shapes, in which finely divided wire meshes are distributed spatially. The distribution of such small diameter wires closely and uniformly spaced improves the overall properties of the beam member, such as impact resistance, fatigue resistance, tensile strength, toughness, flexural strength. Although labourintensive, the workmanship required for the fabrication of wire mesh is fairly low level and its constituents are typically locally available.

II. Objectives

The objectives of the project are in the form of the following things:

1. Technical aspects related to results:

- To increase the flexural strength of concrete beam by using wire mesh.
- Comparison of beams containing different types of wire mesh and different types of its orientations with PPC M30.

III. Experimental Investigation

3.1 Test materials and mix proportions

Portland pozzolan cement with ISI mark was used for tests on fresh and hardened concrete. The compressive strength was 28.04 MPa and 46.35MPa at 7 and 28 days respectively. Local river sand and coarse aggregate with fineness modulus of 3.61 and 4.58 respectively were used. The coarse aggregates with basaltic origin, maximum size 20 mm were from local stone crusher. Potable water, with pH of 7.1, was used. The designed mix M30 with proportion 1:1.48:2.69 (Cement: Fine aggregate: Coarse aggregate) for concrete. The mix design was done as per IS 10262:2009. Water cement ratio of 0.45 kept constant for both the types of concrete and for all specimens. Rectangular opening and hexagonal opening wire meshes are used for this research. The diameter of wire is 0.9mm for hexagonal mesh with 43.7 mm² opening area and diameter of wire is 0.6mm for rectangular mesh with 24 mm² opening area. The both types of wire mesh are with thin wires and woventype. Wire mesh adhered with concrete surface by using Epoxy.

3.2 Specimen Details

There were two series. PCC beams with one side wire mesh other is three side wire mesh PCC beams. For each series six beams (150mm x 150mm x 700mm) in that three are of hexagonal openings and other is rectangular openings, were cast as control specimens. Specimens were cured for 28 days. Two types of wire mesh as denoted by 1RWMC, 3RWMC, 1HWMC, 3WHMC. 1- denotes one side wire mesh similarly, 3- denotes three side wire mesh, R-denotes rectangular openings, H- denotes hexagonal mesh openings, W- denotes wire, M- denotes mesh, C- denotes concrete.

3.3 Testing

Testing was carried out on 6 beams of both series for flexure. For flexural strength beams were simply supported on constant effective span of 900 mm under two point concentrated symmetrical loads for both series. All the beams were having constant overall span and width of 1000 mm and 150 mm respectively.

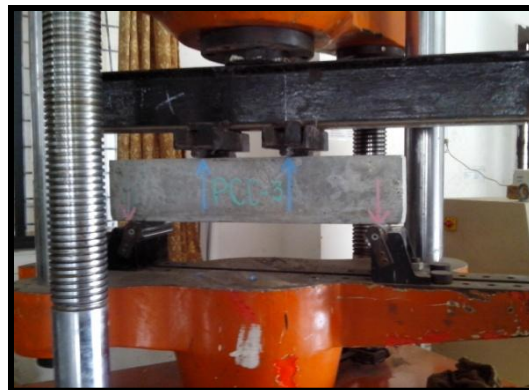


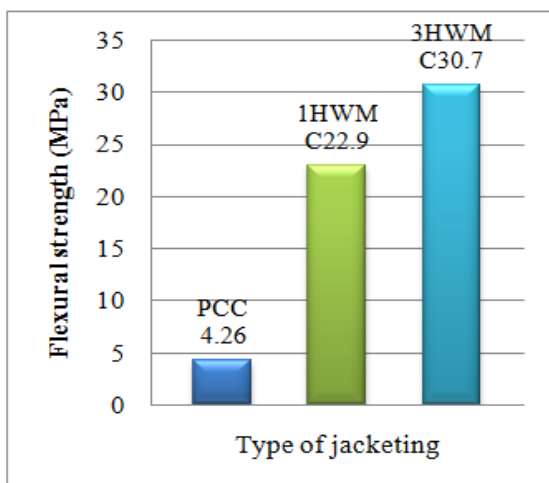
Figure 1: Flexural test setup

The beams were kept on universal testing machine. The beams were tested under gradually applied two points loading on Universal Testing machine (UTM) as shown in Fig. 1 for flexural strength. Ultimate load and modes of failure of beam were noted.

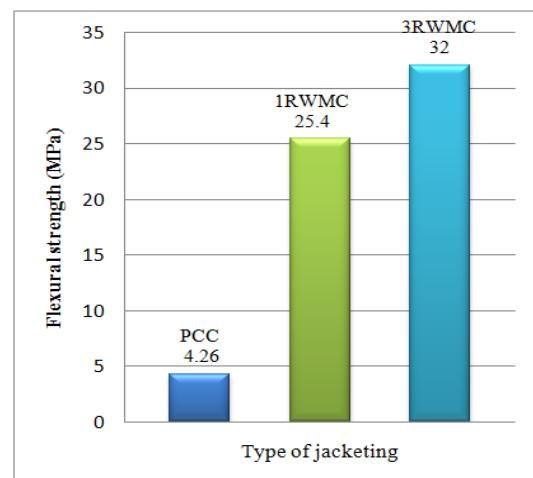
IV. Discussion and result

4.1 Flexural Strength

It is observed that all the beams are failed in flexure and the flexural strength of concrete increases by jacketing with locally available wire mesh. Plain cement concrete has very low tensile strength whereas locally available wire mesh has a good tensile strength as compared to concrete. After adhering locally available wire mesh to a concrete surface, makes the concrete able to transmit bending stresses from concrete to wire mesh which further increase a flexural strength and improve overall behavior of concrete.



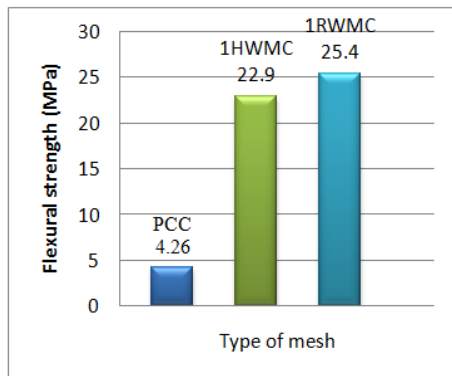
Graph no.1: Flexural strength of hexagonal wire mesh jacketing



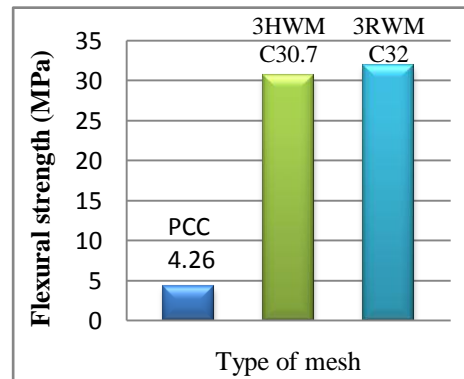
Graph no.2: Flexural strength of rectangular wire mesh jacketing

We have used the different types of wire mesh to check performances of concrete under the flexural strength. It is observed that wire mesh jacketing to three sides of concrete surface gives more flexural strength compared to single side (bottom side) jacketing. Because, the test results and the crack patterns of tested specimens show that all three sides jacketing techniques are effective to overcome the bending stresses problem of one side jacketing. Among all jacketing techniques considered in this study 3RWM type jacketing shows the best performance in carrying concentric loading than the 3HWM.

There is no bond failure at the end of the grid systems was observed in these beams up to the ultimate load, debonding area is more in hexagonal opening wire mesh as compared to rectangular opening wire mesh.



Graph no.3: Flexural strength of one side wire mesh jacketing



Graph no.4: Flexural strength of three side wire mesh jacketing

V. Conclusions

1. This method has been utilized as an alternative repair/ strengthening technique for increasing flexural strength of plain cement concrete.
2. All the jacketed beams are failed in ductile manner, as the bending stresses transmit from concrete to wire mesh which further increase a flexural strength and improve overall behavior of concrete.
3. A test result shows that, Flexural strength of 1HWM beam and 1RWM beam is increased by 4.37 times and 4.96 times than that of Plain cement concrete respectively.
4. A test result shows that, Flexural strength of 3HWM beam and 3RWM beam is increased by 7.2 times and 7.5 times than that of Plain cement concrete respectively.
5. A test result shows that, Flexural strength of 1RWM beams is increased by 10.92% than that of 1HWM beams and flexural strength of 3RWM beams is increased by 4.23% than that of 3HWM beams.
6. A test result shows that, Flexural strength of 1HWM beams is increased by 34.06% than that of 3HWM beams and flexural strength of 1RWM beams is increased by 25.98% than that of 3RWM beams.

REFERENCES

- [1.] GopalCharanBehera, RaoT.D.Gunneswar and Rao C.B.K, "Torsional strength of ferrocement "U" wrapped normal strength beams with only Transverse Reinforcement". The 2nd International Conference on Rehabilitation and Maintenance in Civil Engineering, published by Proceedia Engineering vol. 54 (2013), pp 752 – 763.
- [2.] YasmeenTalebObaidat, Susanne Heyden, Ola Dahlblom, Ghazi Abu-Farsakh, Yahia Abdel-Jawad, "Retrofitting of reinforced concrete beams using composite laminates". Construction and Building Materials Published by science direct vol. 25 (2011), pp 591–597.
- [3.] Hani H. Nassif, HusamNajm, "Experimental and analytical investigation of ferrocement–concrete composite beams". Cement & Concrete Composites, Published by science direct vol. 26 (2004), pp 787–796.
- [4.] ShrutiRatnaparkhe, AshishNim and SonamChandore, "A study on ferrocement-concrete composites".Published by VSRD International Journal of Civil Engineering, Vol. 3 No. 2 February 2013.
- [5.] Ghojarah, H. AbouElfath, "Rehabilitation of a reinforced concrete frame using eccentric steel Bracing". Published byEngineering Structures science direct vol. 23 (2001), pp 745–755.
- [6.] 6.Ibrahim Erdema, UgurhanAkyuzb, UgurErsoyb, GuneyOzcebe, "An experimental study on two different strengthening techniques for RC frames". Published by Engineering Structures science direct vol.28 (2006), pp 1843–1851.
- [7.] M.R. Islam, M.A. Mansur, M. Maalej, "Shear strengthening of RC deep beams using externally bonded FRP systems". Cement &Concrete Composites Published byscience direct vol. 27 (2005), pp 413–420.



International Journal of Modern Engineering Research (IJMER)

Volume : 4 Issue : 4 (Version-4)

ISSN : 2249-6645

April - 2014

Contents :

Performance Evaluation of Friction Belt Apparatus Using Indigenous Materials <i>Durowoju M. O., Sangotayo E. O., Orowole I. A.</i>	01-09
Short Term Load Forecasting Using Multi Layer Perceptron <i>S. Hema Chandra, B. Tejaswini, B. Suneetha, N. Chandi Priya, P. Prathima</i>	10-14
Calculating Voltage Instability Using Index Analysis in Radial Distribution System <i>J. K. Garg, Pallavi Swami</i>	15-26
Modified Procedure for Construction and Selection of Sampling Plans for Variable Inspection Scheme <i>V. Satish Kumar, M. V. Ramanaiah, Sk. Khadar Babu</i>	27-31
Speech Compression Using Wavelets <i>P. Srinivasa rao, G. Krishnaveni, G. Prasanna kumar, G. Satyanandam, CH. Parimala, K. Ramteja</i>	32-39
Accelerometer based Robot control using Renesas Microcontroller <i>S. Hemachandra, T.K.S Ravi Kiran, B. Gowri Prasad, S. M. Mazhar</i>	40-48
A New Technique of Extraction of Edge Detection Using Digital Image Processing <i>Balaji S.C.K.</i>	49-54
An Analytical Study of International Standards on Minority Rights <i>Vikrant Sopan Yadav</i>	55-62
Image Denoising Based On Wavelet for Satellite Imagery: A Review <i>Bhosale Narayan P., Ramesh R. Manza, K. V. Kale</i>	63-68
Pose and Illumination in Face Recognition Using Enhanced Gabor LBP & PCA <i>Manit Kapoor, Sumit Kapoor</i>	69-74

Performance Evaluation of Friction Belt Apparatus Using Indigenous Materials

Durowoju M.O¹, Sangotayo E. O², Orowole I. A³

^{1, 2, 3} (Department of Mechanical Engineering, LAUTECH, Ogbomoso-Nigeria)

Abstract: This project presents performance evaluation of a designed and constructed friction belt apparatus, using locally available materials. The aim is to explore the possibility of producing cheaper alternative testing apparatus for quality control laboratories and institutions in Nigeria. The locally produced friction belt apparatus has the main body frame ; pulley ; bearing ; stud ; hangers ; masses; Tommy bar ; and belts as components. The apparatus was tested with V-belt and flat belt with constant load as T_1 (kg) and varying load masses as T_2 (kg) at different angles of wrap and thereafter compared with results using similar procedures on fabricated apparatus and standard imported friction belt apparatus. The comparisons were done, using graphical presentation to study the trend and t-Test was used to investigate the significant difference in the results. t-Test shows that, for flat belt experiment, t-Stat value (1.378189195303) is lesser than the critical value (2.17898812792408) and also for V-belt experiment, t-Stat value (1.06852895427649) is lesser than the critical value (2.17881279240828), for two tail analysis. These confirmed that there is no significant difference between the two results. (t-stat value < critical value). It was established that the result of the friction belt apparatus obtained for all the experiments carried out using standard imported apparatus and locally produced apparatus have no significant difference at 95% confidence limit. The production cost of the locally produced apparatus is ₦33,520.00k, as against the sum of \$960.00 for the purchase of standard imported apparatus.

Keywords: Friction, belt, performance evaluation, Analysis of variance and t-test.

I. Introduction and Concept

Man's quest for a better life has led him to various technological breakthroughs. Some of these breakthroughs are recorded in machine design, particularly in the area of power transmission in engines. Power transmission is a function of belt tension. Fatigue, more so than abrasion, is the culprit for most belt problems, due to stress from rolling around the pulleys. High belt tension, excessive slippage, adverse environmental conditions and belt overloads caused by shock, Vibration or belt slapping, all contribute to belt fatigue. (Attaway et al 1999). In some cases in machine design, in the past, belt tension with respect to the pulley diameter and surface on which the belt moves were not taken into cognizance therefore slip occurred and therefore maximum power transmission could not be achieved. Belt tension should be adjusted to belt type, size, and speed and pulley diameter. The equation that describes the relationship between tension ratio and angle of wrap is given as:

$$\mu = \frac{\ln(T_1/T_2)}{\theta}$$

Where μ describes the coefficient of friction, T_1 is the initial tension, while T_2 is that required to overcome friction, θ is the angle of wrap and μ is the coefficient of friction. It has been reported that for technological development in Nigeria to succeed, development and manufacture of most of the needed equipment and machines must be based on indigenous designs. (Charles – Owaba, 2009; Ismaila, 2008 and Akintayo, 2009). These will ensure conservation of foreign exchange earnings, maintainability and affordability to average Nigerians. In view of importance of the control of the friction between belts and pulley at various angles of wrap, to optimum power transmission of machine in Nigeria, it is therefore pertinent to explain the possibility of constructing an equipment to measure the tension require to overcome the coefficient of friction of different angles of wrap, using different types of belt such as Flat belt and V-belt. With the availability of this apparatus in the laboratories on large scales, Engineer will be equipped with the right information before lurching to go into the field of construction as properties of different belt at different angles of wrap with respect to apply tension would be known. This project present the performance evaluation of locally produced friction belt apparatus for the purpose of laboratory teaching aids and industrial application using indigenous materials in the Department of Mechanical Engineering, Ladoke Akintola university of technology, Ogbomoso. The apparatus was tested using two different belts viz: flat belt and V-belt.

Belt Theory

A change in belt tension due to friction forces will cause the belt to elongate or contract and move relative to the surface of the pulley. This motion is caused by elastic creep and is associated with static friction as opposed to static friction. The action at the driving pulley, through that portion of the angle of contact that is actually transmitting power is just that the belt moves slowly than the surface speed of the pulley because of the elastic creep Firbank et al (2001).

Belt Tension

In practice a spring loaded wheel pushing against the belt is used to tension the belt. The tension will be the same along its whole length and equal to F . When transmitting power, the driven wheel will be reluctant to turn and the driving wheel has to pull it and exert a torque on it. Consequently, the tension in the side pulling will increase to T_1 but the tension in the other side will decrease to T_2 . The increase in tension on the tight side of the belt is equal to decrease on the slack side so the sum of the tensions remains the same (<http://www.freestudy.co.uk>).

Maximum Power Transmitted in Pulleys

The (tension) in a pulley belt increases with torque and power. The maximum power that a pulley system can transmit is ultimately limited by the strength of the belt material. If this is a problem then more than one belt should be used to share the load. If the belt does not break then the possibility of the belt slipping exists and this depends upon the angle of lap and the coefficients of friction is the same on both wheels, then slippage will occur first on the smaller wheel. The power at which the belt slips is not the absolute maximum power that can be transmitted as more power can be transmitted with slippage occurring by using higher wheel speed.

The friction between the belt and the wheel is further affected by centrifugal force which tends to lift the belt off the wheel. This increases the likelihood of slippage. The friction between the belt and the wheel may be increased by the shape of the belt. A V-section or round section belt in a V-groove will grip better than a flat belt and is less likely to slip.

II. Materials and Methods

2.1 Material Selection

The materials used for the fabrication of the apparatus for measuring the friction belt apparatus were sourced locally. This is aimed at producing the machine at affordable and economic price, to make it readily available to Nigerians for quality control. The materials were selected based on the following factors: strength, availability, cost and comfort. The frame work of the apparatus is as shown in Figures 1.0.

2.2 Pulley

The construction of the pulley of the friction belt apparatus, mild steel was used which is readily available, even at cheaper cost. It has two machined grooves to suit a flat or V-belt and a rope. The pulley was made of diameter 150mm from mild-steel of a cylindrical pipe which also has thickness of 5mm. It has grooves for Flat belt and V-belt cut on it. At the centre was also cut a slot of 15mm inside which the bearing was tightly fitted.

2.3 Bearing

They are manufactured to take pure radial loads, pure thrust loads, or a combination of two kinds of loads. A ball bearing is a type of rolling element bearing that uses balls to maintain the separation between the moving parts of the bearing. The purpose of ball bearing is to reduce friction and support radial and axial loads. It achieves this by using at least two races to contain the balls and transmit the loads through the balls. McGraw-Hill (2002),

2.4 Belt

This is a band of flexible material used in machinery to transmit motion or power. Flat belt and V-belt were used.

2.5 Hanger

The hanger which is made of mild-steel was fabricated using a cylindrical rod and sheet metal. This cylindrical rod was cut size to size and bents into shape of hanger to the top.

2.6 Beam

The beam of the apparatus was fabricated by welding cut-to-size sheet of the mild-steel. The length is 227mm, breadth 226mm and the width 60mm. The base is rectangular in shape, with specification of 227 x 226 x 60mm. A slot of 7mm was cut at the centre to accommodate the shaft force fitted into the pulley bearing.

2.7 Frame

This was made of wood where the apparatus was mounted. The apparatus was bolted to the top of the frame to carry the apparatus to be tested. The masses which are the weight to be placed on the beam were purchased and was used in its original form and not fabricated.

2.8 Experimental Methods

The apparatus was subjected to various testing condition in the laboratory using different belts such as Flat belt and V-belt separately. A constant load T_1 was loaded on the side of the apparatus and varying mass T_2 was loaded on the hanger on the other side of the apparatus gradually until the exact mass that will overcome friction posed by constant mass 15 kg hanging on the belt against the pulley. The procedure was repeated five times for each angle of wrap such as 30° , 60° , 90° , 120° , 150° , 180° , and 210° respectively.

All the procedures adopted for the fabricated apparatus were repeated for the standard apparatus. The results of standard apparatus and fabricated apparatus were compared using t-Test to indicate if there is significant difference between the results. This apparatus consists of a wall mounted fixed pulley with a loaded belt. The equipment is part of a range design to both demonstrate and experimentally confirm basic engineering principles. It is used to carry out experiments which help to investigate: the ratio of belt tension when a rope passes over pulleys of different V-angles, to determine the coefficient of friction between the pulley and cotton rope, and to assess the variation of belt tension ratio with lap angle.

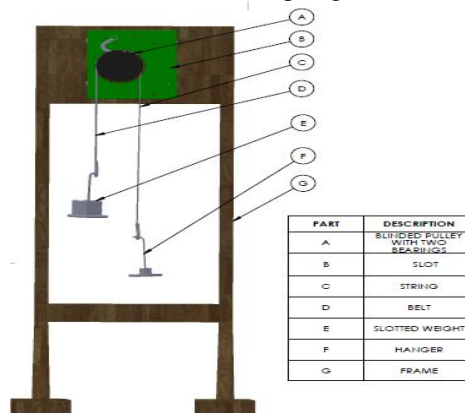


Figure 1.0 Experimental set-up of friction belt apparatus

III. Result And Discussion

Five consecutive experiments were done for each angles of wrap using 15kg as constant mass T_1 and values for T_2 were obtained for Flat belt as indicated in Figure 2.0 for the standard apparatus and Figure 3.0 for the fabricated apparatus. Figure 2.0 and 3.0 show that effect of angle of wrap, θ on the overcoming tension T_2 of a flat belt, it shows that increase in the angle of wrap from 30° to 210° reduces the overcoming tension in both apparatus.

The results obtained on the two apparatus using V-belt are shown in characteristics profile in Figure 4.0 for the standard apparatus and Figure 5.0 for the fabricated apparatus. It is evident that overcoming tension T_2 is inversely proportional to the angle of wrap, θ that is increase in angle of wrap yields decrease in overcoming tension in the pulley for V-belt.

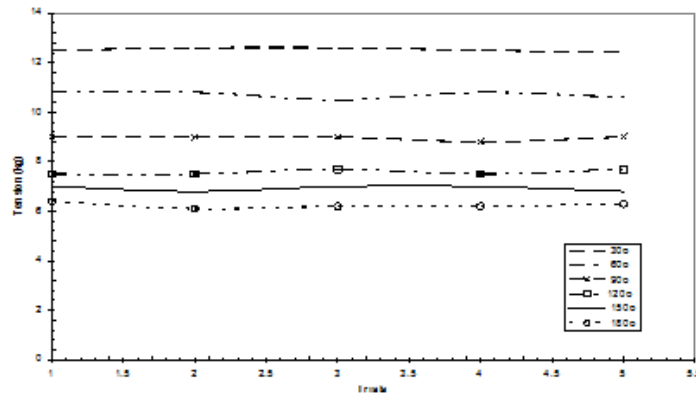


Figure 2.0 Plot of varying angles of rap and tension in flat belt of the standard apparatus

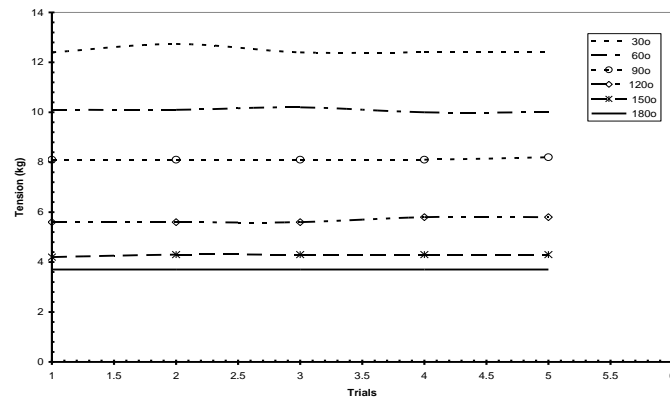


Figure 3.0 Plot of varying angles of rap and tension in flat belt of the fabricated apparatus

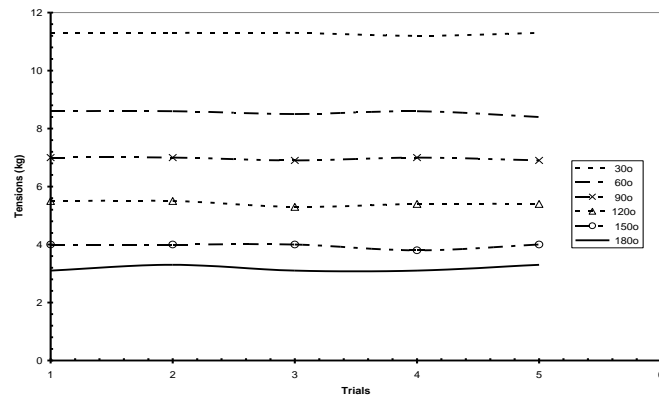


Figure 4.0 Plot of varying angles of rap and tension in V - belt of the standard apparatus

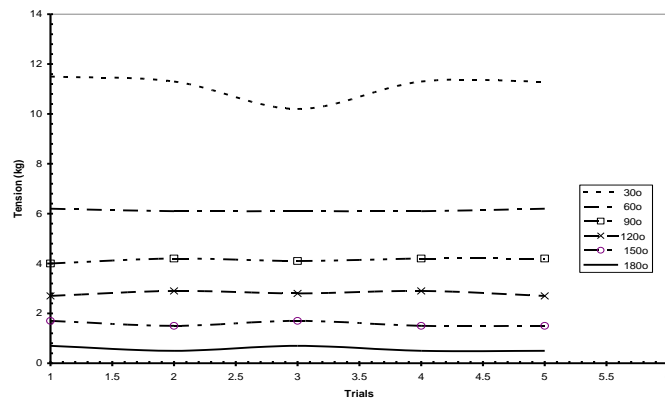


Figure 5.0 Plot of varying angles of rap and tension in V - belt of the fabricated apparatus

The natural logarithms for the tension ratio for each angle of wrap were obtained on the apparatus (imported and locally fabricated) using flat and V -belt. The results are presented in Figure 6.0 and Figure 7.0. Figure 6.0 shows graphical comparison of $\ln(T_1/T_2)$ for standard apparatus and fabricated apparatus results using flat belt. Figure 7.0 shows graphical comparison of $\ln(T_1/T_2)$ for standard apparatus and fabricated apparatus results using V belt. The two figures show characteristics performance profile for both imported apparatus and locally fabricated apparatus using flat belt and V belt has the same trend pattern. The results were further subjected to statistical test to affirm if there is any significant difference in the results obtained in locally fabricated and imported apparatus as shown in Table 1.0 and Table 2.0.

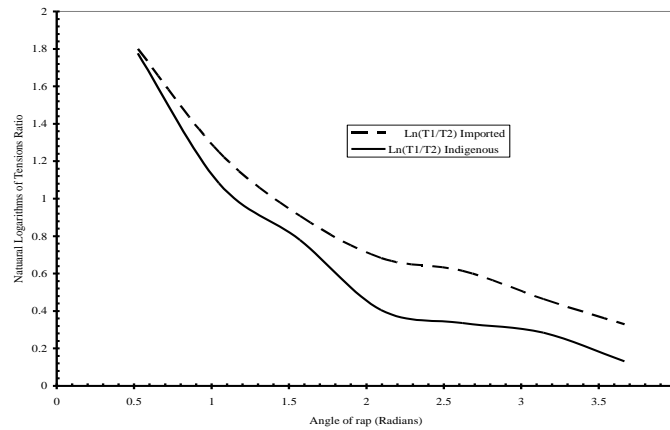


Figure 6.0 Plot of natural logarithms of the tension ratio against angle of wrap using flat belt

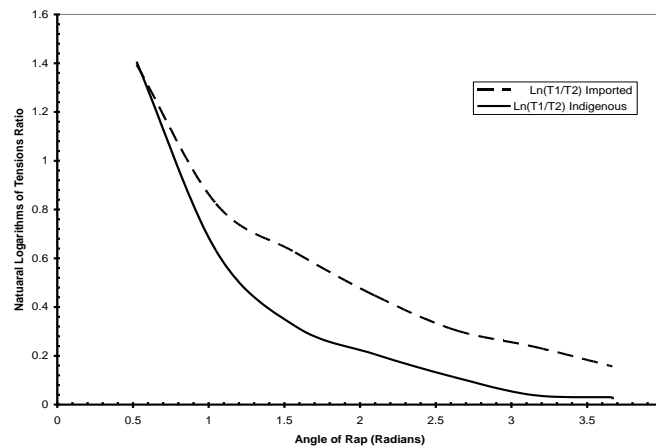


Figure 7.0 Plot of natural logarithms of the tension ratio against angle of wrap using V belt

Table 1.0 shows t-test result analysis for comparing of $\ln(T_1/T_2)$ obtained on the two apparatus using flat belt at 95% confidence limit and Table 2.0 shows t-test result analysis for comparing $\ln(T_1/T_2)$ obtained on the two apparatus using V belt at 95% confidence limit

Table 1.0: t – Test Analysis Results Obtained for Flat Belt Experiment

	<i>Imported</i>	<i>Indigenous</i>
Mean	0.864142857	0.685
Variance	0.26133581	0.337671
Observations	7	7
Hypothesized Mean Difference	0	

Df	12
t Stat	0.612396411
P(T<=t) one-tail	0.275851878
t Critical one-tail	1.782287548
P(T<=t) two-tail	0.551703756
t Critical two-tail	2.178812827

Table 1.0 shows that the values of t-Stat Calculated, 1.378189195303 is less than the critical values 1.782286744856 and 2.17898812792408 for both one tail and two tails respectively. This implies that there is no significant difference in the results of natural logarithms of the tension ratio for varying angle of wrap on the two apparatuses (imported and locally fabricated) using flat belt.

Table 2.0: t-Test Analysis Results Obtained for V-Belt Experiment

	<i>Imported</i>	<i>Indigeous</i>
Mean	0.518625	0.346375
Variance	0.180101125	0.225523125
Observations	8	8
Hypothesized Mean Difference	0	
Df	14	
t Stat	0.764966239	
P(T<=t) one-tail	0.228496832	
t Critical one-tail	1.761310115	
P(T<=t) two-tail	0.456993663	
t Critical two-tail	2.144786681	

Table 2.0 shows that the values of t-Stat calculated 1.06852895427649 is less than the critical values 1.78228674485581 and 2.17881279240828 for one tail and two tails respectively. This implies that there is no significant difference in the results of natural logarithms of the tension ratio for varying angle of wrap on the two apparatuses (imported and locally fabricated) using flat belt at 5% significant level.

The coefficients of friction for varying angle of wrap were determined on the two apparatuses (imported and locally fabricated) using flat and V -belt. The results are presented in Figure 8.0 and Figure 9.0. Figure 8.0 shows graphical comparison of coefficients of friction for varying angle of wrap on standard apparatus and fabricated apparatus results using flat belt. Figure 9.0 shows graphical comparison of coefficients of friction for varying angle of wrap on standard apparatus and fabricated apparatus results using V belt. The two figures show characteristics performance profile for both imported apparatus and locally fabricated apparatus using flat belt and V belt has the same trend pattern. The results were further subjected to statistical test to affirm if there is any significant difference in the results obtained in locally fabricated and imported apparatus as shown in Table 3.0 and Table 4.0.

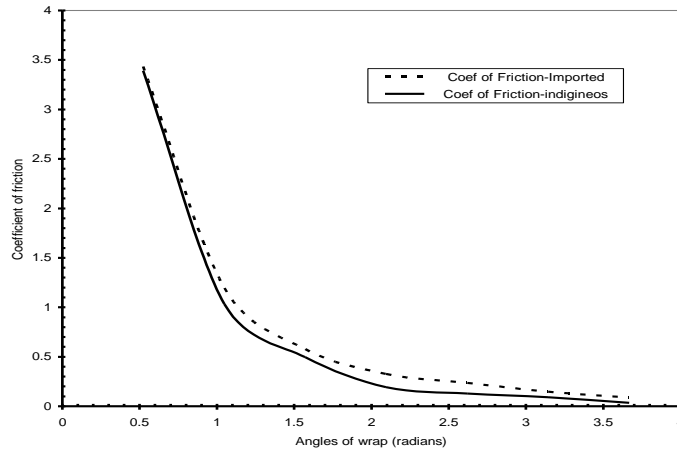


Figure 8.0 Plot of Coefficient of friction versus varying angles of wrap for flat belt

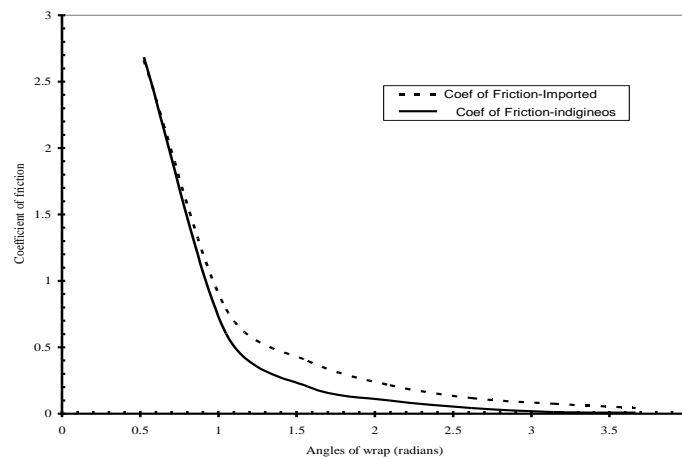


Figure 9.0 Plot of coefficient of friction versus varying angles of wrap using V belt

Table 3.0 shows t-test result analysis for comparing of coefficient of friction obtained on the two apparatus using flat belt at 95% confidence limit and Table 2.0 shows t-test result analysis for comparing coefficient of friction obtained on the two apparatus using V belt at 95% confidence limit

Table 3.0: t – Test Analysis of coefficient of friction Results Obtained for Flat Belt Experiment

	<i>Imported</i>	<i>Indigenous</i>
Mean	0.857717707	0.766791288
Variance	1.433038168	1.45995789
Observations	7	7
Hypothesized Mean Difference	0	
Df	12	
t Stat	0.1414377	
P(T<=t) one-tail	0.444935432	
t Critical one-tail	1.782287548	
P(T<=t) two-tail	0.889870865	
t Critical two-tail	2.178812827	

Table 3.0 shows that the values of t-Stat Calculated, 0.1414377 is less than the critical values 1.782287548 and 2.178812827 for both one tail and two tails respectively. This implies that there is no significant difference in the coefficient of friction for varying angle of wrap on the two apparatuses (imported and locally fabricated) using flat belt.

Table 4.0: t – Test Analysis of coefficient of friction Results Obtained for V Belt Experiment

	<i>Imported</i>	<i>Indigenous</i>
Mean	0.542022416	0.457470814
Variance	0.795965552	0.848989142
Observations	8	8
Hypothesized Mean Difference	0	
Df	14	
t Stat	0.186461796	
P(T<=t) one-tail	0.427378777	
t Critical one-tail	1.761310115	
P(T<=t) two-tail	0.854757554	
t Critical two-tail	2.144786681	

Table 2.0 shows that the values of t-Stat calculated 0.186461796 is less than the critical values 1.761310115 and 2.144786681 for one tail and two tails respectively. This implies that there is no significant difference in the coefficient of friction for varying angle of wrap on the two apparatuses (imported and locally fabricated) using V belt at 5% significant level.

Table: 5.0 Bill of Engineering Measurement and Evaluation for the Apparatus as at 04 05 2012

S/N	Description	Quantity	Unit Cost (₦)	Cost (₦)
1	Pulley	1	7000	7000
2	Bearing	1	500	500
3	Shaft	1	200	200
4	Plate	2	1,250	2,500
5	Frame	1	2,000	2,000
6	Painting			500
7	Belt			1,800
	Contingency			1,450
	Overhauling			1,550
	Workmanship			2,000
	Total Cost			₦19, 500.00k

IV. Conclusions

It has been established that the results of friction of belt obtained when using standard imported apparatus and locally fabricated apparatus with indigenous materials have the same characteristic performance profile trend pattern and there is no significant difference in the results from the two apparatuses at 95% confidence limit, for all experiments carried out. Hence the locally fabricated apparatus is reliable.

The economic feasibility of fabricated apparatus with indigenous available materials is better compared to the exorbitant cost of standard foreign apparatus which many Nigerians cannot afford. The fabricated apparatus with indigenous material is affordable to an average Nigeria at the production cost of ₦19,500.00k compared to the cost of standard apparatus which sells for \$ 960, approximately ₦144,000. It does not include the cost of importation.

REFERENCES

- [1.] Akintayo, J.A. (2009): Workshop on Professional Membership and Registration; Paper on Engineer in Society, Nigerian Society of Engineers, Ibadan Branch, Ibadan.
- [2.] Arthur, P., Richard, J., (2001): Engineering Mechanics, USA, Brooks/Cole.
- [3.] Attaway, S., Stephen W., (1999): The Mechanics of Friction in Rope, Tudor Times Ayer Publishing, dorth dakota.
- [4.] Charles-Owaba, E. O. (2009): Industrial Capacity Building: Role of Engineers; A lecture Presented at the Induction Ceremony of Graduate Engineers, LAUTECH, Ogbomoso, Faculty of Engineering and Technology.
- [5.] Ferdinand, B., (2008): Vector Mechanics for Engineers, McGraw-Hill Publishing Company, limited New Delhi, sTata.
- [6.] Graw, M., (2002): Mechanical Engineering Design, McGraw-Hill Publishing company limited New Delhi, Tata.
- [7.] Ismaila, S.O. (2008): Guidelines to Registration as an Engineer, Kay Concept Printing Press, Ibadan, ISBN: 978-169-
- [8.] Kakani, S.L., Hemrajani, C., Shubhra, K., (2006) : Mechanics, Kundili New Delhi,.
- [9.] Mann Herman (2005): Belt Friction, Ruhur Universitate. <http://www.esr.ruhur.nibochum.de/rt1/currentcourse/node57.html>.
- [10.] Onawumi, A.S., Olafimihan, E.O., Asafa, T.B., Sangotayo E.O., (2007): Fundamentals of Engineering Mechanics, Wole Alabi Press Ogbomoso.
- [11.] Belt available on URL <http://www.free.study.uk.co.uk/> 2006/01/07.
- [12.] Belt Friction available on URL <http://materialeducation.org> 1999/01/11.
- [13.] Belt Pulley Slippage available on URL <http://www.carbinitracing.com/> 2006/05/12.

Short Term Load Forecasting Using Multi Layer Perceptron

S.Hema Chandra¹, B.Tejaswini², B.suneetha³, N.chandi Priya⁴, P.Prathima⁵
1,2,3,4,5(Department of E.Con.E, Sree Vidyanikethan Engineering College, India)

Abstract: Load forecasting is the method for prediction of Electrical load. Short term load forecasting is one of the important concerns of power system and accurate load forecasting is essential for managing supply and demand of electricity. The basic objective of STLF is to predict the near future load for example next hour load prediction or next day load prediction etc....There are various factors which influence the behaviour of the consumer load. The factors that we consider in this paper are Load, Temperature, humidity, time. The ANN is used to learn the relationship among past, current and future parameters like load, temp. In this paper we are using Multi parameter regression and comparing the results with the Artificial Neural network output. Finally, outcomes of the approaches are evaluated and compared by means of the Mean absolute Percentage error (MAPE). ANN outcomes are more fairly accurate to the actual loads than those of conventional methods. So it can be considered as the suitable tool to deal with STLF problems.

Keyword: Multi parameter regression, ANN, load, temperature, humidity, MLP. Short term load forecasting using Multi layer perceptron Network

I. Introduction

Load forecasting can be defined as the technique to estimate of how much electricity will be needed in the future. Load forecasting has always been important for planning and operational decisions conducted by utility companies. Electricity load forecasting is an important task for supply and demand management of electricity. Imprecise load forecasting will raise the operating cost of the utility company. Especially under a market environment, accuracy means money. It is estimated that a raise of 1% in prediction error caused an increase of a million pounds in operation costs per year for an electricity utility. Forecasting the load is a difficult task as the load series is complex and exhibits several levels of seasonality. The load at the present hour is dependent on load at the previous hour, load at the same hour on previous day and on the load at the same hour on the day with the similar denomination in the before week.

There are mainly five types of load

1. Domestic
2. Commercial
3. Industrial
4. Agricultural
5. Other loads like street lights, bulk supplies etc.

Commercial and agricultural loads are characterized by seasonal variations. Industrial loads are base loads and are weather dependent.

II. Load Forecasting Types

There are three types of load forecasting

1. Short term load forecasting :one hour to one week
2. Medium term load forecasting: one week to one year
3. Long term load forecasting: longer than a year

In this paper the type of load forecasting we used is short term load forecasting (STLF). Short term load forecasting is used for day to day function and scheduling of the power system. Long term load forecasting is mainly used for system planning. It typically covers a period of 10 to 20 years. Medium term load forecasting is mainly used for the scheduling of fuel supplies and maintenance, which usually covers a few weeks. STLF is used to reduce the operating cost, electric supplier will use forecasted load to control the quantity of running generator units. It is important to supplier because they can use the forecasted load to control the number of generators in operation. STLF is very important for electricity trading. Hence, there is need to establish high accuracy models for STLF, which has many difficulties. The first reason is because the load series is complex and exhibits several levels of seasonality. Secondly, the load at a given hour is dependent not only on the load at the previous hour but also on many other factors.

III. Factors Effecting Self

It is important to consider several factors for short term load forecasting such as time factors, weather data, and possible customer classes. The most important factor in STLF is time as its impact on consumer load is highest. The time factor includes the time of the day, the day of the week, the hour of the day. The load is also influenced by Weather conditions, which is the most important variable for load forecasting. Temperature and humidity are the most frequently used load predictors. Temperature is the measure of degree of hotness or coldness of a body. Temperature is directly proportional to load during summer season and inversely proportional during winter season. Humidity is a word used for the amount of water vapours in air. The assortment of water vapours and humidity was defined as absolute humidity. It is expressed in terms of percentage. There are also factors like wind speed, precipitation, cloud cover etc...In this paper the factors that we consider are Time, load, Temperature and humidity.

IV. Conventional Methods

Many forecasting techniques have been applied to Short term load forecasting to improve accuracy and efficiency. They can be classified as either traditional methods or modern methods. The techniques that come under traditional method are

1. Similar day look up approach
2. Regression based approach
3. Time series analysis
4. Support vector machines

The modern load forecasting methods are

1. Artificial neural networks
2. Fuzzy logic
3. Expert system

In this paper we have taken one traditional method and one modern method to compare the results. The conventional method used here is Regression. The term "regression" was used in the nineteenth century to describe a natural phenomenon, namely that the progeny of exceptional individuals tend on average to be less exceptional than their parents and more like their more distant ancestors. Linear regression is one of the most widely used statistical techniques. By using this statistical relationship can be calculated between total load and weather conditions.

The objective in regression analysis is to identify a function that describes, as closely as possible, the relationship between these variables so that the value of the dependent variables can be predicted using a range of independent variables values. In the multiple linear regression method, the load is found in Short term load forecasting using Multi layer perceptron Network terms of explanatory (independent) variable such as weather and other variables which influence the electrical load.

V. Ann Approach for Load Forecasting

ANN is usually formed from many hundreds or thousands of simple processing units, connected in parallel. Artificial neural networks are developed since 1980 and extensively applied. ANN is the most efficient method for load forecasting because of many reasons like it is able to approximate numerically any continuous function to a desired accuracy. ANN is capable of mapping an automatic relation between input and output parameters. They learn the relationship and store this learning into their parameters. Multi layered perceptron is the most widely used ANN model.

It consists of one input Layer, one or more hidden layers and one output layer. Each layer employs several neurons and each neuron in a layer is connected to the neurons in the adjacent layer with different weights. Signals flow into the input layer, pass through the hidden layers, and arrive at the output layer. We used a fully connected feed forward type neural network consisting of one hidden layer. Back propagation algorithm was utilized for training. The optimal number of hidden neurons was obtained experimentally by changing the network design and running the training process several times until a good performance was obtained.

IV. Figures and Tables

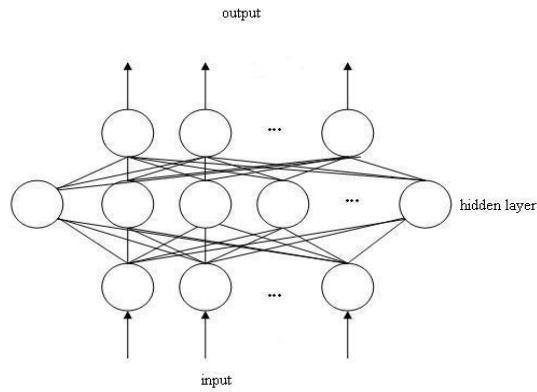
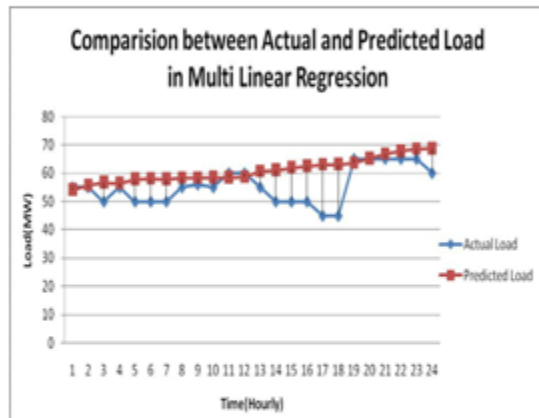


Fig. 1 Multi Layered Perceptron

Graph1: Multi linear regression

TIME	Actual Load	Predicted Load	MAPE
1	55	54.03545	0.073072259
2	55	55.7359	0.05575013
3	50	56.75779	0.563149263
4	55	56.47803	0.111971927
5	50	57.8264	0.65219994
6	50	57.97981	0.664984129
7	50	57.83448	0.652873327
8	55	58.36772	0.25513003
9	56	58.27573	0.16932534
10	55	58.42701	0.259621791
11	60	58.41611	0.109992353
12	60	58.62287	0.095634293
13	55	60.72875	0.433996456
14	50	61.06994	0.922495115
15	50	61.98087	0.998405737
16	50	62.51197	1.042664176
17	45	63.04307	1.670654757
18	45	63.11112	1.676956014
19	65	63.61662	0.088678147
20	65	65.20825	0.013349337
21	65	66.85322	0.118796422
22	65	67.90072	0.185943522
23	65	68.56839	0.228742788
24	60	68.77514	0.60938497

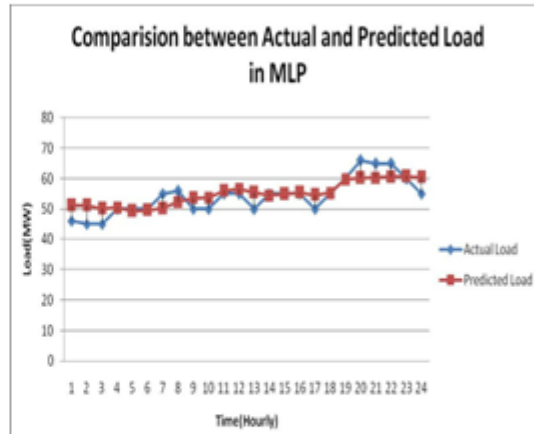


Graph1: Multi linear regression

Table1: Multi Linear Regression Comparison table

Graph 2: Multi layer perceptron

Time	Actual	Predicted	MaPe
1	46	51.21164	0.472068
2	45	51.21462	0.575428
3	45	50.16063	0.477836
4	50	50.50773	0.042311
5	50	49.3891	0.050908
6	50	49.65262	0.028948
7	55	50.20518	0.363244
8	56	52.3951	0.268221
9	50	53.51667	0.293056
10	50	53.72032	0.310026
11	55	55.89173	0.067555
12	55	56.62574	0.123162
13	50	55.46758	0.455632
14	55	54.49764	0.038058
15	55	54.90636	0.007094
16	55	55.42111	0.031903
17	50	54.62491	0.385409
18	55	55.31143	0.023593
19	60	59.76695	0.016184
20	66	60.13748	0.370108
21	65	60.33373	0.29912
22	65	60.52262	0.287011
23	60	60.75657	0.05254
24	55	60.50058	0.41671

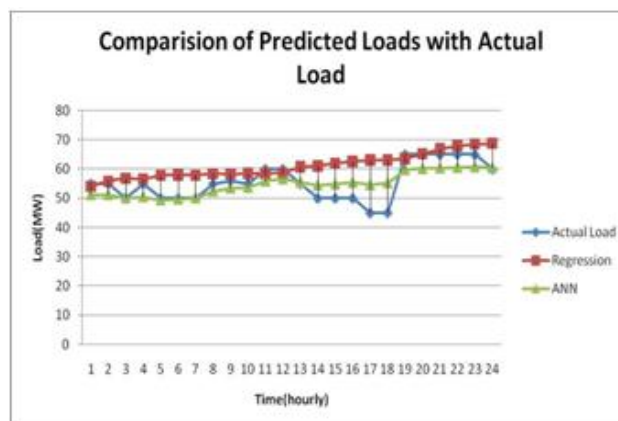


Graph 2: Multi layer perceptron

Table2: Multi layer Perceptron Comparison Table

METHOD	MAPE
MULTI LAYER PERCEPTRON NETWORK	0.227
MULTI LINEAR REGRESSION	0.4855

Table3: comparison of Map



Graph 3: Comparison table

VI. Conclusion

In this paper we have presented an electric load forecasting using two methods. The first method is the conventional method called multi linear regression and second method is the Artificial neural network. The result of MLP network model used for one day ahead STLF shows that the network has a good performance and reasonable prediction compared to conventional method. Mean absolute percentage error is calculated between actual and predicted loads for both the methods. The results suggest that ANN model with MLP structure can perform good prediction with least error and finally this neural network could be an important for short term load forecasting.

REFERENCES

Journal Papers:

- [1] Gross, G., Galiana, F.D, Short-Term Load Forecasting, Proceeding of IEEE, December 1987.
- [2] S. Rahman, "Formulation and analysis of a rule-based short-term load Forecasting algorithm," IEEE, vol. 78, pp. 805-816, 2002.
- [3] K.Y.Lee-J.H.Park, Short Term Load Forecasting Using An Artificial Neural Network, Transactions On Power Systems, Vol.7, No 1, February 1992
- [4] P.K.Dash – H.P.Satpathy – A.C.Liew, A Real-Time Short-Term Load Forecasting System Using Functional Link Network, IEEE Transactions On Power Systems, Vol.12, No.2, May 1999.
- [5] Moghram, S. Rahman, "Analysis and Evaluation of Five Short-Term Load Forecasting Techniques," Proceedings of the IEEE Transaction on Power Systems, pp. 1484-1491, Vol. 4, No. 4, October 1989.
- [6] D.Fay – J.V.Ringwood – M.Condon, On The Influence Of Weather Forecast Errors In Short-Term Load Forecasting Models, Control 2004, University Of Bath, Uk, September 2004.
- [7] T. W. S. Chow, C. T. Leung "Neural Networks Based Short Term Load Forecasting using weather Compensation," Proceedings of the IEEE, pp. 1736-1742, 1996. Note that the journal title, volume number and issue number are set in italics.

Calculating Voltage Instability Using Index Analysis in Radial Distribution System

J.K Garg¹, Pallavi Swami²

Abstract: This paper presents analysis of voltage stability index by a simple and efficient load flow method to find out the magnitude of voltage at each node in radial distribution system in that network. It shows the value of voltage stability index at each node in radial distribution network and predicts which node is more sensitive to voltage collapse. This paper also presents the effect on voltage stability index with variation in active power, reactive power, active and reactive power both. The voltage and VSI and effect of load variation on VSI for 33-node system & 28-node system are calculated in this paper with results shown.

Index Terms: Voltage Stability Index, Load Flow Method, Voltage Collapse.

I. Introduction

The distribution system provides connections for power transfer between transmission and the consumer point. It is essential to carry out the load flow analysis of a network in order to evaluate the performance of a power distribution network during operation and to examine the effectiveness of proposed alterations to a system in the planning stages. This paper presents two issue in RDS (a) load flow method (b) Voltage stability index. The load flow studies are normally carried out to determine: (a) node voltage and branch current, (b) the flow of active and reactive power in network branches, (c) no circuits are overloaded, and the node voltages are within acceptable limits, (e) effect of loss of circuits under emergency conditions, (f) optimum system loading condition, (g) optimum system losses.

Radial Distribution System(RDS) is that distribution system , which have separate feeders radiating from a single substation and feed the distribution at only one end . The radial distribution system have high R/X ratio. Due to this reason, conventional Newton-Raphson method and Fast Decoupled load flow method fails to converge in many cases. Kersting & Mendive (1) and Kersting(2) have developed load flow techniques based on ladder theory whereas Steven et al (3) modified it and proved faster than earlier methods. However, it fails to converge in 5 out of 12 case studies. Baran & Wu (4) have developed a load flow method based on Newton Raphson method, but it requires a Jacobian matrix, a series of matrix multiplication, and at least one matrix inversion. Hence, it is considered numerically cumbersome and computationally inefficient. The choice of solution method for particular application is difficult. It requires a careful analysis of comparative merits and demerits of those methods available. A new power flow method for radial distribution networks with improved converge characteristics have been reported in (5) which is passed on polynomial equation on forward process and backward ladder equation for each branch of RDS. The author of (6) utilizes forward and backward sweep algorithm based on Kirchoff's current and voltage law for evaluating the node voltage iteratively which avoids repetitive computation at each branch and thus makes it computationally efficient and resulted in improved speed. B. Venkatesh (7) formulates a set of equations to describe radial distribution system by high R/X ratio. The benefits of this set of equation are that it is insensitive to the R/X ratio of distribution system and possesses an ability to seek an accurate solution.

First part of this paper makes an effort to modify the load flow algorithm developed in (8) for balanced three-phase RDS to make it computationally efficient. This method can also be used to calculate the energy loss in each branch of Radial Distribution System. The proposed method is simple and mathematically less complex due to non-involvement of matrices.

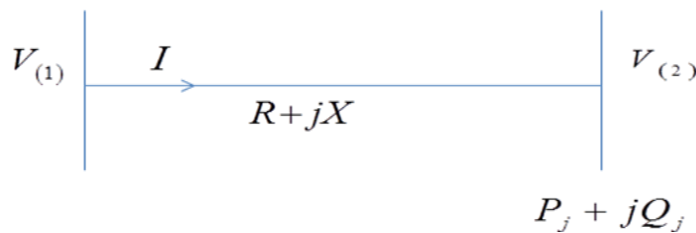
Voltage Stability Index is presented in the second part of this paper. Voltage Stability Index is numerical solution which helps the operator to monitor how close the system is to collapse. The purpose of finding Voltage Stability Index is to find most sensitive node of system that will predict the node which is more sensitive to voltage collapse. The problem of voltage stability & voltage collapse have increased because of the increased loading, exploitation and improved optimization operation of power transmission system. The problem of voltage collapse is the inability of power system to supply the reactive power or by an excessive absorption of reactive power by the system itself. Thus the voltage collapse is a reactive problem and it is strongly affected by the load behavior. Voltage collapse has become an increasing threat to power system security and reliability. One of the serious consequences of voltage stability problem is a system blackout. A fast

method for finding the maximum load, especially the reactive power demand, at a particular bus through thevenin's equivalent circuit before reaching the voltage stability limit is developed in (9) for general power system. Voltage instability in power network is a phenomenon of highly non-linear nature posing operational as well as prediction problem in power system control. The voltage instability is a local phenomenon, variables and network parameters contain sufficient information to assess proximity to instability. Hence a direct analytical approach to voltage instability assessment for radial network is presented in (10). Voltage collapse is characterized by slow variations in system operating point due to increase in loads in such a way that the voltage magnitude gradually decreases until a sharp accelerated change occurs. The voltage stability analysis, using different methods are described in(11) which presents a comparative study and analysis of performance of some on line static voltage collapse indices. Line indices provide accurate information with regard to stability condition of lines. In(12) a new and simple voltage stability margin of a radial distribution system to get a better estimation of distance to voltage collapse is developed.

This paper also presents the effect on VSI and voltage collapse point with increase of active power, reactive power and both active & reactive power. The results for 33-node system & 28 node system with magnitude of voltage, VSI, effect on VSI are shown along with their graphs.

II. Load Flow Calculation

Load flow calculation is an important and basic tool in the field of power system engineering. It is used in planning and designing stages as well operation stages of the power system. Some applications especially in the field of optimization of power system need fast converging load flow solution. To calculate the magnitude of voltage in a network, consider a line connected between two nodes as shown in figure given below.



Where $V^{(1)}$ is sending end of jth branch and $V^{(2)}$ is the receiving end of jth branch.

For flat voltage profile, consider $V^{(1)} = 1$ p.u.

Where R = resistance of branch between node 1 and 2.

X = Reactance of branch between node 1 and 2.

P_j = Total active power loads beyond the node 2.

Q_j = Total reactive power loads beyond the node 2.

$$A_j = (P_j R + Q_j X) - \frac{1}{2} V_1^2$$

$$B_j = \sqrt{A_j^2 - (P_j^2 + Q_j^2)(R^2 + X^2)}$$

$$V_2 = \sqrt{B_j - A_j}$$

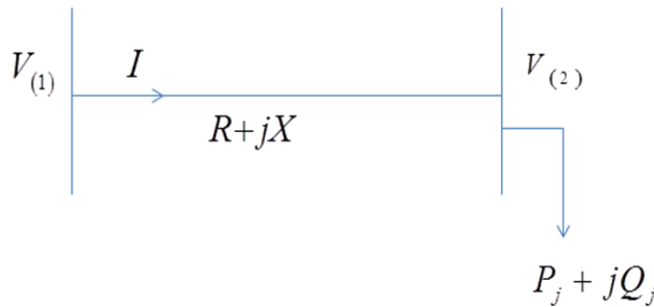
$$P_{loss(j)} = \frac{(P_j^2 + Q_j^2)}{V_2^2} R$$

$$Q_{loss(j)} = \frac{(P_j^2 + Q_j^2)}{V_2^2} X$$

P_{loss} =real power loss of branch

Q_{loss} =reactive power loss of branch

Voltage stability index:-



The proposed voltage stability index will be formulated in this section. The sending end voltage can be written as

$$\begin{aligned}
 V_1 &= V_2 + I(R + jX) \\
 &= V_2 + \frac{S_j^*}{V_2^*} (R + jX) \\
 &= V_2 + \frac{(P_j - jQ_j)}{V_2^*} (R + jX) \\
 &= \frac{|V_2|^2 + P_j R + Q_j X + j(P_j X - Q_j R)}{V_2^*} \quad \dots 1
 \end{aligned}$$

Now substitute the voltage by its magnitude, equation 1 can be written as

$$\begin{aligned}
 |V_1| &= \sqrt{\frac{(|V_2|^2 + P_j R + Q_j X)^2 + (P_j X - Q_j R)^2}{|V_2|}} \\
 |V_1||V_2| &= \sqrt{V_2^4 + (P_j R + Q_j X)^2 + 2|V_2|^2(P_j R + Q_j X) + (P_j X - Q_j R)^2} \quad \dots 2
 \end{aligned}$$

Rearranging equation 2, it will become

$$\begin{aligned}
 V_2^4 + (P_j R + Q_j X)^2 + (P_j X - Q_j R)^2 + 2|V_2|^2(P_j R + Q_j X) - |V_1|^2|V_2|^2 &= 0 \\
 V_2^4 + (P_j R + Q_j X)^2 + (P_j X - Q_j R)^2 + |V_2|^2[2(P_j R + Q_j X) - |V_1|^2] &= 0 \quad \dots 3
 \end{aligned}$$

The equation 3 is in form of $ax^2 + bx + c = 0$. To guarantee that 3 is solvable, the following inequality constraint should be satisfied

$$\begin{aligned}
 b^2 - 4ac &\geq 0 \\
 \text{i.e.,} \\
 V_1^4 - 4|V_1|^2(P_j R + Q_j X) - 4(P_j X - Q_j R)^2 &\geq 0 \quad \dots 4
 \end{aligned}$$

With the increase of receiving end power demand, the left hand side of equation 4 approaches zero, and the two bus network reaches its maximum power transfer limit. So the voltage stability index is

$$VSI = V_1^4 - 4|V_1|^2(P_j R + Q_j X) - 4(P_j X - Q_j R)^2 \quad \dots 5$$

III. Case study

In this paper we are testing the eq.4. by increasing the receiving end power demand.

Case(1):

When active & reactive power both increases with a multiplier K. Then eq.5. will be

$$VSI(P \ \& \ Q) = V_1^4 - 4|V_1|^2(KP_j R + KQ_j X) - 4(KP_j X - KQ_j R)^2$$

Case(2):

When only active power increases with the multiplier K. Then eq.5. will be

$$VSI(P) = V_1^4 - 4|V_1|^2 (KP_j R + Q_j X) - 4(KP_j X - Q_j R)^2$$

Case(3):

When only reactive power increases with the multiplier K. Then eq5. Will be

$$VSI(Q) = V_1^4 - 4|V_1|^2 (P_j R + KQ_j X) - 4(P_j X - KQ_j R)^2$$

IV. Results of System Study

The 33-bus RDS and 28-bus RDS has been considered for the study. The load data and transmission line details, are presented in table 5 in Appendix-C and Fig 1 along with a single line diagram for 33 node system, Table 6 in Appendix-C presents the details of data for 28-bus system along with single line diagram in fig4 . The details of results are presented in table 1 and table 2 in Appendix-A along with their graphical representation in fig 2 and fig 3 respectively for 33-bus system and details of results for 28-bus system are presented in table 3 and in table 4 in Appendix-B along with their graphical representation in fig 5 and fig 6.

NOTE: In Each Graph X-Axis Represents Nodes And Y-Axis Represents Voltage In Per Unit.

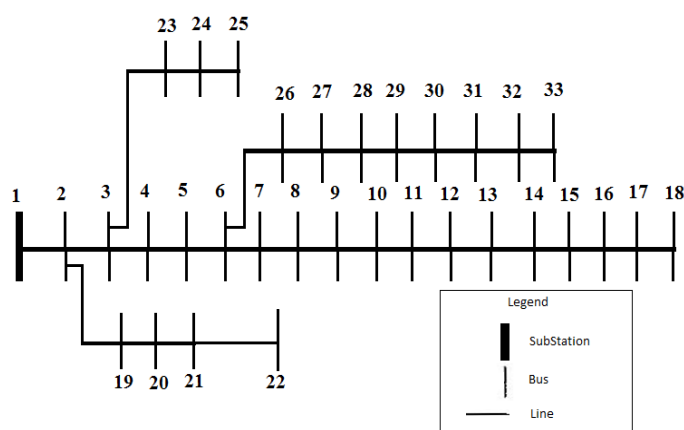
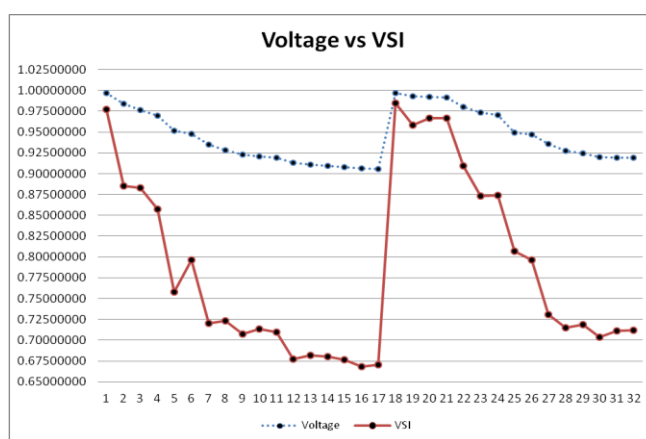


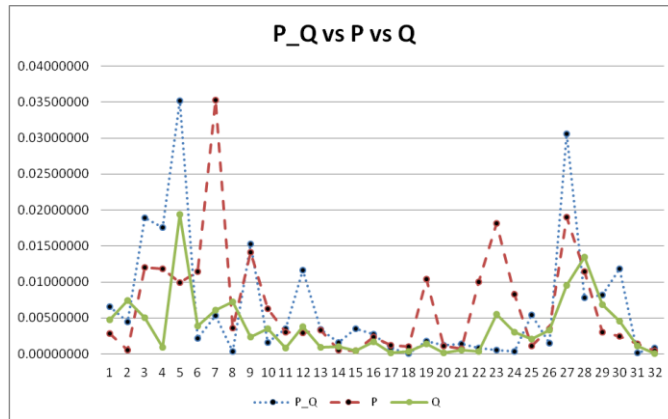
FIG 1: SINGLE LINE DIAGRAM FOR 33 NODE SYSTEM



X-Axis – Number of nodes

Y-Axis – Voltage vs VSI

FIG 2: The graph indicating that both voltage & VSI have same minimum & maximum



X-Axis – Number of nodes
Y-Axis – VSIP_Q vs VSIP vs VSIQ

FIG 3: This graph shows the value of (VSIP_Q) i.e. the values of vsi when we are using multiplier both with p,q to increase the value of receiving end power demand so that the left hand side eq. approaches to zero. Beyond these values at each node result becomes negative

minimum value is at node = 18

VSIP = Varying the equation of VSI by using multiplier with P
minimum value is at node = 15

VSIQ = Varying the equation of VSI by using multiplier with Q
minimum value is at node = 32

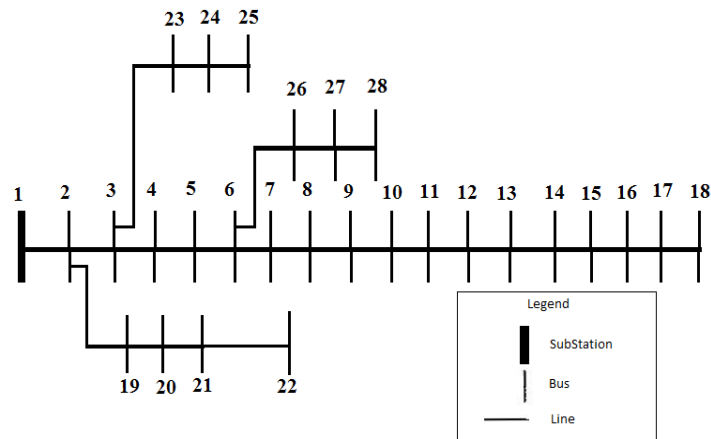
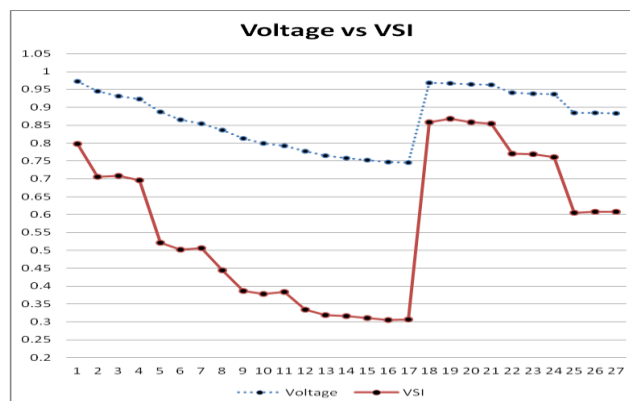
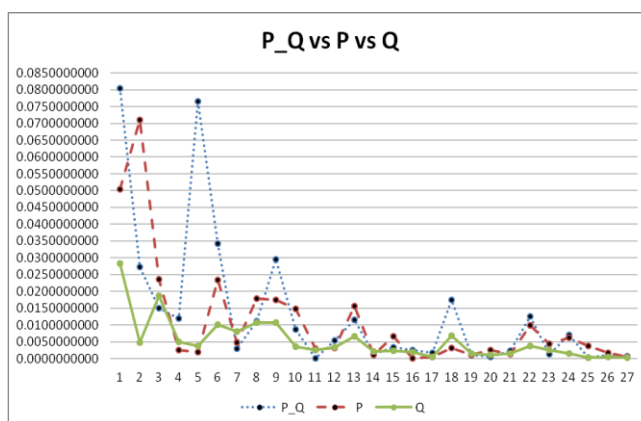


FIG 4: SINGLE LINE DIAGRAM FOR 28 NODE SYSTEM



X-Axis – Number of nodes
Y-Axis – Voltage vs VSI

FIG 5: In this graph both voltage & VSI have same minimum & maximum points
 Minimum voltage is at node n= 17
 Maximum voltage is at node = 18



X-Axis – Number of nodes
 Y-Axis – VSIP_Q vs VSIP vs VSIQ

FIG 6: This graph shows the value of (VSIP_Q) i.e. the values of vsi when we are using multiplier both with p,q to increase the value of receiving end power demand so that the left hand side eq. approaches to zero. Beyond these values at each node result becomes negative.

Minimum value is at node = 11
 VSIP = Varying the equation of VSI by using multiplier with P
 Minimum value is at node = 16
 VSIQ = Varying the equation of VSI by using multiplier with Q
 Minimum value is at node = 25

NOTE: (minimum value node is the voltage collapse point)

V. Conclusion

This paper presents simple and efficient load flow method to find out the magnitude of voltage at each node in Radial Distribution System which is mathematically less complex. The method is tested on 33 node system and 28 node system and the results are shown along with their graphs. Hence minimum voltage node can be located.

A new voltage stability index for RDS is developed which indicates that the node having minimum voltage is highly susceptible to voltage collapse. This equation is tested on 33 node and 28 node system. The results obtained for 33 node system and 28 node systems show the value of VSI at each node and indicate the voltage collapse point. The effect of variation in receiving end power demand on VSI is also tested on both the RDS Systems for the cases when:

- a) Increase in both active and reactive power.
- b) Increase in only active power.
- c) Increase in only reactive power.

It is observed that for above three cases the value of VSI at each node beyond the calculated point will become negative means the system will terminate. It is concluded that with only increase in reactive power it will largely affect on voltage collapse point, as compared to increment in only active power and, with both active and reactive power taken together.

REFERENCES

- [1.] W.H.Kersting and Mendive, "An application of Ladder Network Theory to the solution of three phase Radial Load Flow Problem," IEEE PES Winter Meeting, 1976.
- [2.] W.H.Kersting, "A Method To Design And Operation of Distribution system," IEEE Trans., vol.PAS-103, pp 1945-1952, 1984.
- [3.] R.A.Stevens, D.T.Rizy, and S.L.Puruker, "Performance of Conventional Power Flow Routines for Real Time Distribution Automations Application," Proceeding of 18th southeastern Symposium on System Theory, (IEEE), pp. 196-200, 1986.

- [4.] M.E.Baran and F.F.Wu, "Optimal Sizing of Capacitor Placed on Radial Distribution System," IEEE Trans., vol.PWRD-2,PP 735-743, 1989.S
- [5.] Ulas Eminoglu and M.Hacaoglu, " A New Power Flow Method for radial distribution system including Voltage Dependent Load Flow Modal," Electric Power System Research, vol.76,pp 106-114,2005.
- [6.] K.Vinoth kumar,M.P.Selvan,"A Simplified approach for Load Flow Analysis of Radial Distribution Network"International journal of computer, Information and system Science, and Engineering march 2008.
- [7.] B. Venkatesh, A. Dukpa and L. Chang " An accurate voltage solution method for radial distribution system" Can.J.Elect.Comput.Eng.,Vol.34,No.1/2, Winter/Spring 2009
- [8.] Ranjan R. and D.Das, "Novel computer Algorithm for solving radial distribution network," Journal of electric power component and system, vol.31, no.1,pp 95-107,jan 2003.
- [9.] M.H.Haque, "A Fast Method for determining the voltage stability limit of a power system,"Electric Power System Reaserch, vol.32, pp 35-43,1995.
- [10.] F. Gubina and B Strmcnic, "A Simple approach to voltage stability assessment in radial networks," IEEE Transaction of power system,vol.12,no.3,pp 1121-1128,AUG 1997.
- [11.] Claudia Reis and F.P. Maciel Barbosa " A Comparision of Voltage Stability Indices" IEEE MELECON 2006, May 16-19, Spain
- [12.] M.H.Haque, "A Linear Static Voltage Stability Margin for Radial Distribution Systems" IEEE 2006

APPENDIX-A

TABLE-1

Details of Magnitude of Voltage & Vsi at Each Node of 33 Node Systems

NODES	Voltage	VSI
1	0.99717062	0.97750862
2	0.98367898	0.88492637
3	0.97655889	0.88295501
4	0.96948503	0.85762879
5	0.95158811	0.75827594
6	0.94818000	0.79663604
7	0.93480205	0.71989823
8	0.92858852	0.72361773
9	0.92281261	0.70703595
10	0.92088209	0.71310664
11	0.91938468	0.70982353
12	0.91325271	0.67692071
13	0.91097514	0.68180369
14	0.90955564	0.68013802
15	0.90817935	0.67615419
16	0.90613619	0.66809386
17	0.90552406	0.67053897
18	0.99664426	0.98456008
19	0.99307008	0.95856285
20	0.99236598	0.96705921
21	0.99194108	0.96649308
22	0.98012458	0.90945010
23	0.97347089	0.87347550
24	0.97014866	0.87370057
25	0.94971573	0.80711546
26	0.94722385	0.79655438
27	0.93597383	0.73055688

28	0.92782522	0.71504245
29	0.92428631	0.71865483
30	0.92013904	0.70389943
31	0.91922608	0.71114872
32	0.91894317	0.71222868

TABLE-2
Results for Effect of Change in Receiving End Power on Vsi Of 33 Node System

NODES	P_Q	P	Q
1	0.00651695	0.00277727	0.00472652
2	0.00440307	0.00050815	0.00737475
3	0.01889712	0.01199109	0.00504944
4	0.01759400	0.01182700	0.00089393
5	0.03515700	0.00990620	0.01939355
6	0.00213052	0.01144139	0.00390332
7	0.00533382	0.03528813	0.00611866
8	0.00036554	0.00356275	0.00723163
9	0.01528803	0.01415792	0.00233480
10	0.00158603	0.00622429	0.00345392
11	0.00346256	0.00299202	0.00079843
12	0.01158961	0.00287664	0.00375195
13	0.00342967	0.00332398	0.00088147
14	0.00158177	0.00056778	0.00104808
15	0.00345284	0.00040951	0.00039598
16	0.00268090	0.00230304	0.00171501
17	0.00082822	0.00119108	0.00009532
18	0.00003531	0.00101203	0.00037417
19	0.00176814	0.01037072	0.00137989
20	0.00114780	0.00109940	0.00014189
21	0.00135825	0.00069830	0.00051139
22	0.00077607	0.01000156	0.00028852
23	0.00050740	0.01814790	0.00547364
24	0.00029280	0.00827969	0.00300178
25	0.00540307	0.00106780	0.00210112
26	0.00145815	0.00350658	0.00328727
27	0.03063027	0.01901449	0.00955204
28	0.00783061	0.01140097	0.01344417
29	0.00814267	0.00305458	0.00688019
30	0.01185659	0.00244253	0.00450016
31	0.00017201	0.00137474	0.00108570
32	0.00080713	0.00045312	0.00005946

APPENDIX-B

TABLE-3

Details of Magnitude of Voltage & Vsi At Each Node Of 28-Bus System

NODES	Voltage	VSI
1	0.973127117	0.797673997
2	0.945389387	0.705037231
3	0.931467896	0.70777414
4	0.922580044	0.696541018
5	0.887322139	0.521350467
6	0.865082321	0.502450032
7	0.854435069	0.50641817
8	0.835783547	0.444384184
9	0.812771463	0.386954148
10	0.798668748	0.378121214
11	0.792867162	0.383615455
12	0.776906775	0.334355042
13	0.764546365	0.319556679
14	0.757251394	0.316145152
15	0.751991018	0.31083112
16	0.747473473	0.30461443
17	0.745942826	0.30707373
18	0.967768266	0.857739708
19	0.966399397	0.867278648
20	0.964555752	0.85896559
21	0.963013601	0.854552058
22	0.941146243	0.770414227
23	0.938686848	0.768258322
24	0.936187575	0.759956409
25	0.88474105	0.605573185
26	0.883922235	0.608196588
27	0.883512643	0.608197974

TABLE-4

Details of Results for Effect of Change in Receiving End Power on Vsi Of 28 Node Systems

NODES	P_Q	P	Q
1	0.0803396545	0.0503454	0.028211576
2	0.0271909944	0.070972628	0.004768841
3	0.0151153707	0.023538207	0.018743386
4	0.0119562662	0.002554366	0.005021475
5	0.0765888293	0.001911007	0.003775704

6	0.0341933061	0.023390061	0.010178326
7	0.0028865674	0.004837756	0.008043718
8	0.0111861563	0.017849625	0.01073459
9	0.0295596189	0.017449489	0.010636168
10	0.0087606930	0.014744798	0.003512189
11	0.0000412946	0.002937983	0.00251565
12	0.0053930670	0.003186235	0.00340622
13	0.0115142797	0.015728189	0.006737277
14	0.0012318403	0.001117193	0.002230367
15	0.0033455252	0.006706155	0.002361746
16	0.0025793336	0.000179466	0.001917427
17	0.0017861154	0.000539772	0.000524395
18	0.0174343501	0.003231937	0.00693262
19	0.0010999386	0.001148699	0.001480455
20	0.0005982575	0.002556389	0.001093885
21	0.0024153735	0.001253786	0.001583127
22	0.0126126113	0.009813919	0.003868215
23	0.0013314007	0.004435565	0.002614562
24	0.0069653688	0.006321335	0.001503738
25	0.0003562311	0.003731343	0.00029578
26	0.0010813418	0.001797301	0.000407927
27	0.0006234999	0.00045139	0.000365597

APPENDIX-C

DATA FOR 33 NODE SYSTEMS

Line no	Sending Bus	Receiving Bus	Resistance	Reactance	Load at Receiving End Bus	
					Real Power (kW)	Reactive Power (kVAr)
1	1 Mai	2	0.0922	0.0477	100.0	60.0

	n	SS				
2	2	3	0.4930	0.2511	90.0	80.0
3	3	4	0.3660	0.1864	120.0	30.0
4	4	5	0.3811	0.1941	60.0	20.0
5	5	6	0.1890	0.7070	60.0	100.0
6	6	7	0.1872	0.6188	200.0	100.0
7	7	8	1.7114	1.2351	200.0	20.0
8	8	9	1.0300	0.7400	60.0	20.0
9	9	10	1.0400	0.7400	60.0	30.0
10	10	11	0.1966	0.0650	45.0	35.0
11	11	12	0.3744	0.1238	60.0	35.0
12	12	13	1.4680	1.1550	60.0	35.0
13	13	14	0.5416	0.7129	120.0	80.0
14	14	15	0.5910	0.5260	60.0	10.0
15	15	16	0.7463	0.5450	60.0	20.0
16	16	17	1.2890	1.7210	60.0	20.0
17	17	18	0.7320	0.5740	90.0	40.0
18	2	19	0.1640	0.1565	90.0	40.0
19	19	20	1.5042	1.3554	90.0	40.0
20	20	21	0.4095	0.4784	90.0	40.0
21	21	22	0.7089	0.9373	90.0	40.0
22	3	23	0.4512	0.3083	90.0	50.0
23	23	24	0.8980	0.7091	420.0	200.0
24	24	25	0.8960	0.7011	420.0	200.0
25	6	26	0.2030	0.1034	60.0	25.0
26	26	27	0.2812	0.1447	60.0	25.0
27	27	28	1.0590	0.9337	60.0	20.0
28	28	29	0.8042	0.7006	120.0	70.0
29	29	30	0.5075	0.2585	200.0	600.0
30	30	31	0.9744	0.9630	150.0	70.0
31	31	32	0.3105	0.3619	210.0	100.0
32	32	33	0.3410	0.5302	60.0	40.0

TABLE-6
DATA FOR 28 NODE SYSTEMS

Line Number	Sending Bus	Receiving Bus	Resistance	Reactance	Load at Receiving End Bus	Reactive Power (kVAr)
					Real Power (kW)	
1	1	2	1.8	0.7	140	90
2	2	3	2.2	0.9	80	50
3	3	4	1.3	0.5	80	60
4	4	5	0.9	0.3	100	60
5	5	6	3.6	1.5	80	50
6	6	7	2.7	1.1	90	50
7	7	8	1.4	0.6	90	40
8	8	9	2.7	1.1	80	40
9	9	10	3.6	1.5	90	50
10	10	11	2.7	0.7	80	50
11	11	12	1.3	0.3	80	50
12	12	13	4.1	1.1	90	40

13	13	14	4.1	0.8	70	50
14	14	15	3	0.7	70	40
15	15	16	2.7	1.1	70	40
16	16	17	4.1	0.7	60	40
17	17	18	2.7	0.7	60	30
18	2	19	3.4	0.9	70	30
19	19	20	1.3	0.3	50	40
20	20	21	2.7	0.7	50	30
21	21	22	4.9	1.4	40	30
22	3	23	3.5	1	50	30
23	23	24	3	0.8	50	20
24	24	25	5.5	1.5	60	30
25	6	26	2.7	0.7	40	20
26	26	27	1.3	0.3	40	20
27	27	28	1.3	0.3	40	20

Modified Procedure for Construction and Selection of Sampling Plans for Variable Inspection Scheme

V. Satish Kumar¹, M. V. Ramanaiah², Sk. Khadar Babu³

^{1,2} (Research Scholar, Professor, Department of Statistics, Sri Venkateswara University, Tirupati-517502, India)

³ (Asst.Prof(Sr), SAS,VIT University, Vellore, Tamil Nadu, India)

Abstract: Linear Trend is Technique to generate the values for observed frequency distribution and it will give the accuracy of the smoothing obtained depends on the number of available data sets. In this article, an attempt was made to estimate the modified liner trend value generator for construction and selection of sampling plans for variable inspection scheme indexed through the MAAOQ over the Liner Trend. We compare the constructed sampling plans indexed through MAAOQ over Linear Trend with the basic sampling plans indexed with AOQL. And also obtain the performance of the operating characteristic curves.

Key Words: Sampling inspection plans, AOQL, MAAOQ etc.

I. Introduction

A Lot Acceptance Sampling Plan (LASP) is a sampling scheme and a set of rules for making decisions. The decision, based on counting the number of defects in a sample, can be to accept the lot, reject the lot or even, for multiple or sequential sampling schemes, to take another sample and then repeat the decision process. These types of Lot Acceptance Sampling Plans are given below.

In **Single sampling plans**, one sample is selected at random from a lot and disposition of the lot is determined from the resulting information. These plans are usually denoted as (n,c) plans for a sample size n, where the lot is rejected if there are more than c defectives. These are the most common (and easiest) plans to use although not the most efficient in terms of average number of samples needed.

In **Double sampling plans**, we take two samples. After the first sample is tested, there are the following three possible decisions about the lot.

- a. Accept the lot
- b. Reject the lot
- c. No decision

If the conclusion is 'no decision', and a second sample is taken, the procedure is to combine the results of both samples and make a final decision based on that of defects.

The **Multiple sampling plan** is an extension of the double sampling plans where more than two samples are needed for conclusion. The advantage of multiple sampling is to realise inspection of smaller sample sizes.

The **Sequential sampling plans** is the ultimate extension of multiple sampling where items are selected from a lot one at a time and after inspection of each item a decision is made to accept or reject the lot or select another unit.

The **Skip lot sampling** means that only a fraction of the submitted lots are inspected. Making a final choice between various types of sampling plans is a matter of deciding how much sampling will be done on a day-by-day basis. While selecting the type of various acceptance plans one must consider the factors such as administrative efficiency, the type of information by the procedure, and the impact of the procedure may have on the material flow in the manufacturing organization. In the following sections the methods to design single and double sampling plans and their interpretations are discussed in detail.

The Inspection of items is broadly divided into two viz., Inspection by Attributes and Variable Inspection. Inspection by Attributes is an inspection whereby certain characteristics of units of products are inspected and classified simply as conforming or non-conforming to the specified requirements.

In Acceptance Sampling by Attributes, each item tested is classified as conforming or non-conforming. A sample is taken and if it contains too many non-conforming items, the batch is rejected, otherwise it is accepted. Here, items used to be classified as defective or non-defective but these days no self respecting Variable Inspection or Continuous sampling inspection is the

examination or testing of units of product as they move past in inspection station. Only those units of the product found by the inspector to be non-conforming are corrected or replaced with conforming units. The rest of the production uninspected unit as well as units found to be non-conforming, is allowed to continue down the production line as conforming material.

The Acceptance Sampling by Variables can be carried out by measuring a variable rather than classifying an item as conforming or non-conforming. Variables such as thickness, strength or weight might be measured. Usually it is easier and quicker to classify an item as conforming or non-conforming than to make an exact measurement. However, the information gained from an exact measurement is greater and so smaller sample sizes are required. A decision as to whether to use Attribute or Variables will depend on the particular circumstances of each case.

The average outgoing quality limit (AOQL) is designated as the worst average quality that the consumer will receive in the long run, when the defective items are replaced by non-defective items. The proportion defective corresponding to the inflection point of the OC curve denoted as P^* , and it is defined as the maximum allowable percent defective (MAPD). The desirability of developing a set of sampling plans indexed with P^* has been explained by Mandelson (1962) and Soundararajan (1975).

Dodge (1943) provided the concept of continuous sampling inspection and introduced the first continuous sampling plan, originally referred to as the random order plan, and later designated as CSP-1 plan by Dodge and Torrey (1951). The continuous sampling plans represent extensions and variations in the basic procedure of Dodge (1943). Dodge (1947) outlined several sampling plans for continuous production. MIL-STD-1235C (1988) is the latest US military standard on continuous sampling plans.

ANSI/ASQC standard A2 (1987) defines acceptance sampling as the methodology that deals with the procedures through which decisions of acceptance or non-acceptance are taken based on the results of the inspection of samples. According to Dodge (1969), the general areas of acceptance sampling are :

1. Lot-by-lot sampling by the method of attributes, in which each unit in a sample is inspected on a go-not-go basis for one or more characteristics.
2. Lot-by-lot sampling by the method of variables, in which each unit in a sample is measured for a single characteristic such as weight or strength.
3. Continuous sampling of a flow of units by the methods of attributes.
and
4. Special purpose plans, includes chain sampling, skip-lot sampling, small sample plans etc.

Inspired by the work done in this direction, an attempt was made in this Research paper to Design and Forecast of sampling plans for Variable Inspection scheme. The average outgoing quality limit (AOQL) is designated as the worst average quality that the consumer will receive in the long run, when the defective items are replaced by non-defective items. The proportion defective corresponding to the inflection point of the OC curve denoted as P^* , and it is defined as the maximum allowable percent defective (MAPD). The desirability of developing a set of sampling plans indexed with P^* , has been explained by Mandelson (1962) and Soundararajan (1975).

Dodge (1943) provided the concept of continuous sampling inspection and introduced the first continuous sampling plan, originally referred as the random order plan and later designated as CSP-1 plan by Dodge and Terry (1951).

II. Methodology

A sampling plan prescribes the sample size and the criteria for accepting, rejecting or taking another sample to be used in inspecting lot. The single sampling plan is the most widely used sampling plan in the area of acceptance sampling. A single sampling plan which has acceptance number zero, with a small sample size is often employed in a situations involving costly or destructive testing by attributes. The small sample size is warranted because of costly nature of testing and a zero acceptance number arises in practice. The Operating Characteristic (OC) curves of such plans have a uniquely poor shape, such that the probability of acceptance starts decreasing rapidly, even for small values of P , where P is the percent defective. The average outgoing quality limit (AOQL) is defined as the worst average quality that the consumer will receive in the long run, when defective items are replaced by non-defective items. Dodge and Romig (1959) have proposed a procedure for the selection of a Single Sampling Plan (SSP) indexed with AOQL by reduce the average total inspection. Mandelson (1962) has explained the desirability of developing a system of sampling plans indexed through the Maximum Allowable Average Percent Defective (MAPD) and shown that $P^* = \frac{c}{n}$ for an SSP with sample size 'n' and acceptance number 'c'.

One of the desirable properties of OC curve is that the decrease of $P_a(P)$ should be slower for lesser values of P (good quality) and steeper for larger values of P , which provides a better overall discrimination. If P^* is

considered as a standard quality measure, then the above property of a desirable OC curve is exactly followed. Since P^* corresponds to the inflection point of an OC curve, it implies that

$$\begin{aligned} \frac{\partial^2 \log L(P)}{\partial P^2} &< 0, & P < P^* \\ \frac{\partial^2 \log L(P)}{\partial P^2} &> 0, & P > P^* \\ \frac{\partial^2 \log L(P)}{\partial P^2} &= 0, & P = P^* \end{aligned}$$

Where $Pa(P)$ is the probability of acceptance at quality level p fraction defective.

The MAAOQ of an SSP is defined as the average outgoing quality (AOQ) the MAPD. Assuming Poisson conditions for quality characteristics, we have

$$\begin{aligned} \text{AOQ} &= P \cdot Pa(P) \frac{(N-n)}{N} \\ &= P \cdot Pa(P) \left(1 - \frac{n}{N}\right) \\ &= P \cdot Pa(P) \end{aligned}$$

Then we have $\text{MAAOQ} = \text{AOQ}$ at $P^* = P$

This can be written as

$$\begin{aligned} \text{MAAOQ} &= P^* \cdot Pa(P^*) \\ &= P^* \sum_{r=0}^c \frac{e^{-nP^*} (nP^*)^r}{r!} \end{aligned}$$

This study provides tables and procedures for designing and forecasting of certain Acceptance sampling plans using MAPD as a quality standard and $(\text{MAAOQ})_{LT}$ as a measure of outgoing quality. It also provides tables and procedures for the selection of SSPs, CSPs using the MAPD as a standard quality and the $(\text{MAAOQ})_{LT}$ as an average outgoing quality and then the parameters of SSP, CSP are determined. This study considers $(\text{MAAOQ})_{LT}$ in place of AOQL and then constructed tables through the different OC curves. It gives better measure to compare with Average Outgoing Quality Limit. This procedure protects the interests of the consumer in terms of incoming and outgoing quality.

The selection of sampling plans with this procedure is more advantageous to the producer and the consumer than the procedure adopted through AOQL. These procedures reduces the cost of inspection for the producer and the consumer gets quality items.

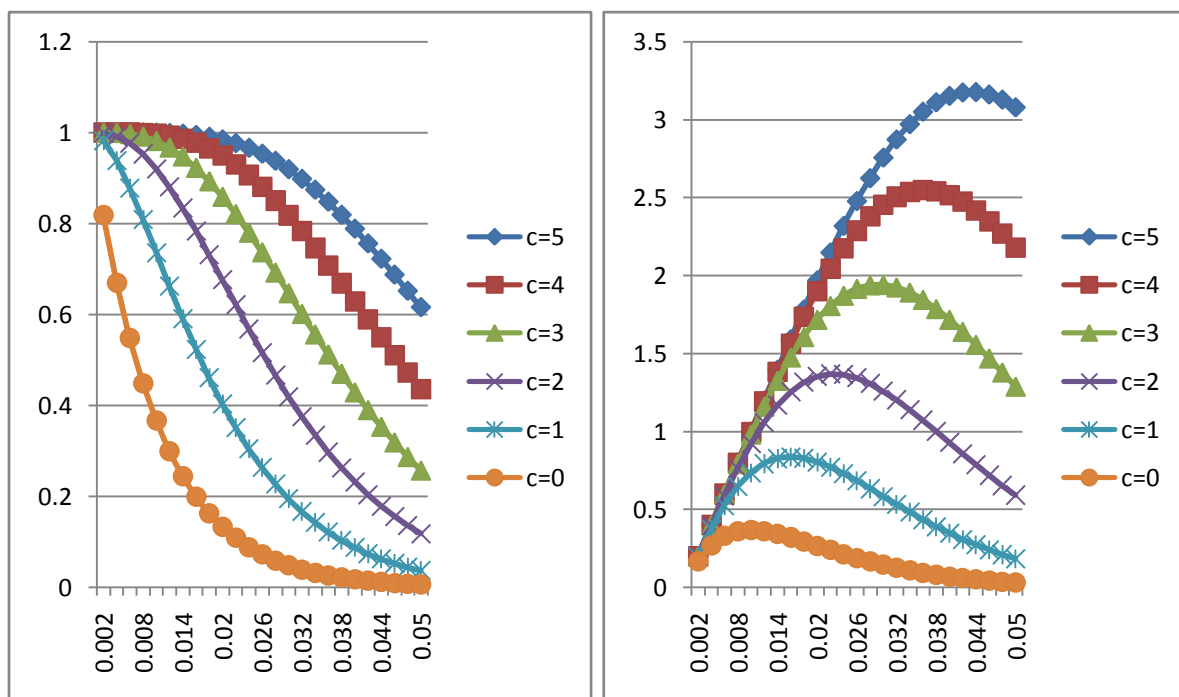
III. Tables and Discussions

For variable inspection scheme, we construct the possible tables indexed through the AOQL and also construct the tables indexed through the MAAOQ over Linear Trend. And also drawn the OC curves in the following manner.

P	Pa						AOQ					
	c=5	c=4	c=3	c=2	c=1	c=0	c=5	c=4	c=3	c=2	c=1	c=0
0.00		0.9999	0.9999	0.998	0.982	0.8185			0.199	0.1997	0.196	0.1637
2	1	98	46	881	608	67	0.2	0.2	989	76	522	13
0.00	0.99	0.9999	0.9992	0.992	0.938	0.6697	0.39999	0.3999	0.399	0.3968	0.375	0.2679
4	9996	44	61	245	772	83	9	78	704	98	509	13
0.00	0.99	0.9996	0.9967	0.977	0.878	0.5478	0.59997	0.5997	0.598	0.5863	0.527	0.3286
6	9966	35	83	301	497	21	9	81	07	81	098	92
0.00	0.99	0.9986	0.9912	0.953	0.809	0.4478	0.79986	0.7989	0.793	0.7626	0.647	0.3583
8	9836	85	57	272	084	86	8	48	005	17	267	09
0.01	0.99	0.9965	0.9816	0.920	0.735	0.3660	0.99946	0.9965	0.981	0.9206	0.735	0.3660
2	9465	68	26	627	762	32	5	68	626	27	762	32
0.01	0.99	0.9926	0.9671	0.880	0.662	0.2990	1.19836	1.1912	1.160	1.0566	0.794	0.3588
4	8639	89	73	541	193	16	7	27	607	49	632	19
0.01	0.99	0.9864	0.9475	0.834	0.590	0.2441	1.39590	1.3810	1.326	1.1683	0.827	0.3418
6	7073	64	49	529	861	7	2	49	568	4	205	37
0.01	0.99	0.9773	0.9227	0.784	0.523	0.1993	1.59109	1.5638	1.476	1.2547	0.837	0.3188
8	4434	79	49	202	368	01	4	06	398	24	389	82
0.01	0.99	0.9650	0.8930	0.731	0.460	0.1626	1.78265	1.7370	1.607	1.3160	0.829	0.2926
2	0366	34	53	118	675	11	9	61	496	12	215	99
0.02	0.98	0.9491	0.8589	0.676	0.403	0.1326	1.96903	1.8983	1.717	1.3533	0.806	0.2652
4	4516	7	62	686	272	2	3	39	923	71	543	39
0.02	0.97	0.9296	0.8211	0.622	0.351	0.1081	2.14842	2.0452	1.806	1.3686	0.772	0.2378
6	6559	75	21	124	318	15	9	84	467	73	9	53
0.02	0.96	0.9065	0.7802	0.568	0.304	0.0881	2.31892	2.1757	1.872	1.3642	0.731	0.2114

4	6218	81	68	443	743	01	2	94	642	64	384	43
0.02	0.95	0.8800	0.7371	0.516	0.263	0.0717	2.47853	2.2881	1.916	1.3427	0.684	0.1865
6	3281	51	7	446	325	62	2	33	642	61	644	82
0.02	0.93	0.8503	0.6925	0.466	0.226	0.0584	2.62532	2.3809	1.939	1.3068	0.634	
8	7615	57	9	744	742	29	2	98	252	84	878	0.1636
	0.91	0.8178	0.6472	0.419	0.194	0.0475	2.75748	2.4535	1.941	1.2593	0.583	0.1426
0.03	9163	55	49	775	622	53	9	64	748	25	866	58
0.03	0.89	0.7829	0.6018	0.375	0.166	0.0386	2.87343	2.5054	1.925	1.2026	0.533	0.1237
2	7948	66	08	829	567	84	4	9	787	51	013	9
0.03	0.87	0.7461	0.5568	0.335	0.142	0.0314	2.97183	2.5369	1.893	1.1392	0.483	0.1069
4	407	48	52	069	174	57	7	03	296	34	391	53
0.03	0.84	0.7078	0.5128	0.297	0.121	0.0255	3.05169	2.5483	1.846	1.0712	0.435	0.0920
6	7692	77	81	558	052	68	2	58	371	09	787	46
0.03	0.81	0.6686	0.4703	0.263	0.102	0.0207	3.11234	2.5407	1.787	1.0004	0.390	0.0789
8	9038	3	11	277	83	73	5	92	182	51	756	39
	0.78	0.6288	0.4294	0.232	0.087	0.0168	3.15349	2.5154	1.717	0.9285	0.348	0.0674
0.04	8375	64	76	143	163	7	9	56	902	7	653	81
	0.75	0.5890	0.3906	0.204	0.073	0.0136	3.17521	2.4738	1.640	0.8569	0.309	0.0575
	6003	12	28	028	734	95	4	52	637	16	682	18
0.04	0.72	0.5494	0.3539	0.178	0.062	0.0111	3.17788	2.4176	1.557	0.7865	0.273	0.0488
4	2246	69	5	77	255	12	5	65	379	89	921	92
0.04	0.68	0.5105	0.3195	0.156	0.052	0.0090	3.16221	2.3487	1.469	0.7184	0.241	0.0414
6	7438	87	59	188	468	12	6	01	972	64	353	57
0.04	0.65	0.4726	0.2875	0.136	0.044	0.0073	3.12918	2.2688	1.380	0.6532	0.211	0.0350
8	1913	72	17	085	145	06	5	24	084	1	894	7
	0.61	0.4359	0.2578	0.118	0.037	0.0059	3.07999	2.1799	1.289	0.5913	0.185	0.0296
0.05	5999	81	39	263	081	21	6	07	193	15	406	03

IV. OC CURVES and AOQ CURVES



V. Conclusions

From the above tables and curves, we observe that the procedure for construction and selection of sampling plans through MAAOQ over the Linear Trend is also applicable in variable inspection scheme. The performance of the operating characteristic curve is also agreeable. This procedure is the modified procedure for selection of sampling plans through MAAOQ over Linear Trend.

REFERENCES

- [1.] DODGE, H.F. (1970): Notes on the Evolution of Acceptance Sampling Plans, Part-IV, Journal of Quality Technology, Vol.2, No.1, pp.1-8.
- [2.] DODGE, H.F. (1943): A Sampling Inspection Plan for Continuous Production, The Annals of Mathematical Statistics, Vol.14, No.3, pp.264-279
- [3.] DODGE, H.F. (1947): Sampling Plans for Continuous Production, Industrial Quality Control, Vol.4, No.3, pp-5-9.
- [4.] DODGE, H.F. (1969): Evaluation of a Sampling Inspection System Having Rules for Switching Between Normal and Tightened Inspection, Rutgers – The State University, The Statistics Centre, Technical Report No.14.
- [5.] DODGE, H.F. and STEPHENS, K.S. (1966): Some New Chain Sampling Inspection Plans, Industrial Quality Control, Vol.23, No.2, pp.61-67.
- [6.] DODGE, H.F. (1955): Chain Sampling Inspection Plan, Industrial Quality Control, Vol.11, No.4, pp. 10-13. (also in Journal of Quality Technology, Vol.9, No.3, July 1977, pp. 139-142)
- [7.] DODGE, H.F., and ROMIG, H.G. (1959): Sampling Inspection Tables – Single And Double Sampling, 2nd Edition, John Wiley and Sons, New York.
- [8.] DODGE, H.F., and TORREY, M.N. (1951): Additional Continuous Sampling Inspection Plans, Industrial Quality Control, Vol. 7, No.5, pp.7-12.
- [9.] Duncan, (1986): “Quality control and industrial statistics”, 5th ed., Irwin, Homewood, 111.
- [10.] DUNCAN, A.J. (1986): Quality Control and Industrial Statistics, 5th Edition, Homewood, Illinois.
- [11.] MANDELSON, J. (1962): the statistician, the engineer and sampling plans, industrial quality control, Vol. 19, No.5, pp. 12-15.
- [12.] MONTGOMERY C.DOUGLAS, “Introduction To Statistical Quality Control”, 3 rd ed., john wiley & sons, inc, New York.
- [13.] MONTGOMERY, D.C(1991): Introduction to statistical quality control, 2nd edition, john wiley and sons inc., new York.
- [14.] Soundararajan, v. And gonvindaraju, k. (1983b): Construction And Selection Of Chain Sampling plans chsp-(0,1), journal of quality technology, vol.15, no.4, pp.180-185.
- [15.] SOUNDARARAJAN, V(1975):Maximum Allowable Percent Defective(MAPD) single sampling inspection by attributes plan, journal of quality technology, vol.7, no.4,pp.173-177.
- [16.] SOUNDARARAJAN, V and GOVINDARAJU, K. (1982): A Note on Designing Chain Sampling Plans chsp-1, The QR Journal, vol.9, no.3, pp.121-123.

Speech Compression Using Wavelets

P. srinivasa rao¹, G.krishnaveni², G. Prasanna kumar³, G.satyanandam⁴,
CH.parimala⁵, K.ramteja⁶

¹(Department of Electronics & Communication Engineering, Asst.professor, St.Ann's college of engineering & technology, India)

^{2, 3, 4, 5, 6}(Department of Electronics & Communication Engineering, Student, St.Ann's college of engineering & technology, India)

Abstract: In the recent years, large scale information transfer by remote computing and the development of massive storage and retrieval systems have witnessed a tremendous growth. To cope up with the growth in the size of databases, additional storage devices need to be installed and the modems and multiplexers have to be continuously upgraded in order to permit large amounts of data transfer between computers and remote terminals. This leads to an increase in the cost as well as equipment. One solution to these problems is "COMPRESSION" where the database and the transmission sequence can be encoded efficiently. In this we investigated for optimum wavelet, optimum level, and optimum scaling factor.

I. Introduction

Speech Compression is a method to convert human speech into an encoded form in such a way that it can later be decoded to get back the original signal. Compression is basically to remove redundancy between neighboring samples and between adjacent cycles. Major objective of speech compression is to represent signal with lesser number of bits. The reduction of data should be done in such a way that there is acceptable loss of quality.

II. Compression

Compression is a process of converting an input data stream into another data stream that has a smaller size. Compression is possible only because data is normally represented in the computer in a format that is longer than necessary i.e. the input data has some amount of redundancy associated with it. The main objective of compression systems is to eliminate this redundancy. When compression is used to reduce storage requirements, overall program execution time may be reduced. This is because reduction in storage will result in the reduction of disc access attempts. With respect to transmission of data, the data rate is reduced at the source by the compressor (coder), it is then passed through the communication channel and returned to the original rate by the expander(decoder) at the receiving end. The compression algorithms help to reduce the bandwidth requirements and also provide a level of security for the data being transmitted. A tandem pair of coder and decoder is usually referred to as codec.

2.1 Types of compression

There are mainly two types of compression techniques - Lossless Compression and Lousy Compression.

2.1.1 Lossless compression

It is a class of data compression algorithm that allows the exact original data to be reconstructed from the exact original data to be reconstructed from the compressed data. It is mainly used in cases where it is important that the original signal and the decompressed signal are almost same or identical. Examples of lossless compression are Huffman coding.

2.1.2 Lousy compression

It is a data encoding method that compresses data by removing some of them. The aim of this technique is to minimize the amount of data that has to be transmitted. They are mostly used for multimedia data compression. The rest of the paper is organized as follow; section 2 gives the Theoretical background about the speech compression schemes. The speech compression techniques are described in section 3& Section 4 evaluates the performance of the proposed technique followed by the conclusion.

III. Techniques for speech compression

Speech compression is classified into three categories,

3.1 Waveform coding

The signal that is transmitted as input is tried to be reproduced at the output which would be very similar to the original signal.

3.2 Parametric coding

In this type of coding the signals are represented in the form of small parameters which describes the signals very accurately. In parametric extraction method a preprocessor is used to extract some features that can be later used to extract the original signal.

3.3 Transform coding

This is the coding technique that we have used for our paper. In this method the signal is transformed into frequency domain and then only dominant feature of signal is maintained. In transform method we have used discrete wavelet transform technique and discrete cosine transform technique. When we use wavelet transform technique, the original signal can be represented in terms of wavelet expansion.

Similarly in case of DCT transform speech can be represented in terms of DCT coefficients. Transform techniques do not compress the signal, they provide information about the signal and using various encoding techniques compressions of signal is done. Speech compression is done by neglecting small and lesser important coefficients and data and discarding them and then using quantization and encoding techniques. Speech compression is performed in the following steps.

1. Transform technique
2. Thresholding of transformed coefficients
3. Quantization
4. Encoding

3.3.1 Transform technique

DCT and DWT methods are used on speech signal. Using DCT, reconstruction of signal can be done very accurately; this property of DCT is used for data compression. Localization feature of wavelet along with time frequency resolution property makes DWT very suitable for speech compression. The main idea behind signal compression using wavelets is linked primarily to the relative scarceness of the wavelet domain representation of signal.

A) Continuous wavelet transforms (CWT)

This chapter provides a motivation towards the study of wavelets as a tool for signal processing. The drawbacks inherent in the Fourier methods are overcome with wavelets. This fact is demonstrated here. It must be reiterated that the discussion in this chapter is by no means comprehensive and exhaustive. The concepts of time-frequency resolution have been avoided for the sake of simplicity. Instead, the development endeavors to compare the Wavelet methods with the Fourier methods as the reader is expected to be well conversant with the latter.

Consider the following figure which juxtaposes a sinusoid and a wavelet

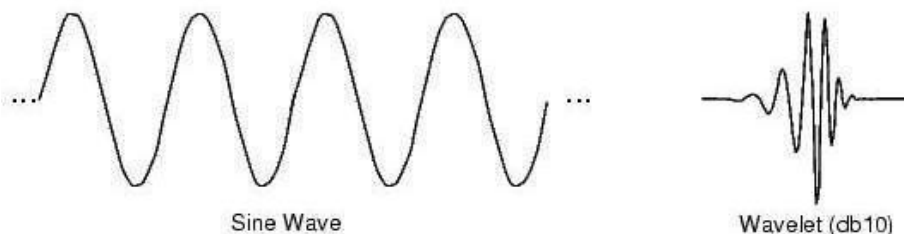


Fig 3.1: comparing sine wave and a wavelet

As has already been pointed out, wavelet is a waveform of effectively limited duration that has an average value of zero. Compare wavelets with sine waves, which are the basis of Fourier analysis. Sinusoids do not have limited duration -- they extend from minus to plus infinity. And where sinusoids are smooth and predictable, wavelets tend to be irregular and asymmetric.

Fourier analysis consists of breaking up a signal into sine waves of various frequencies. Similarly, wavelet analysis is the breaking up of a signal into shifted and scaled versions of the original (or mother) wavelet.

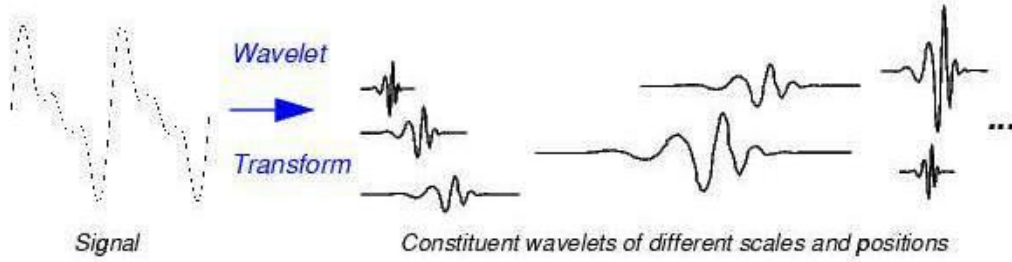


Fig3.2: constituent wavelets of different scales and positions

The above diagram suggests the existence of a synthesis equation to represent the original signal as a linear combination of wavelets which are the basis function for wavelet analysis (recollect that in Fourier analysis, the basic functions are sines and cosines). This is indeed the case. The wavelets in the synthesis equation are multiplied by scalars. To obtain these scalars, we need an analysis equation, just as in the Fourier case. We thus have two equations, the analysis and the synthesis equation. They are stated as follows:

1. Analysis equation or CWT equation:

$$C(a, b) = \int_{-\infty}^{\infty} f(t) \cdot \frac{1}{\sqrt{|a|}} \psi \left(\frac{t-b}{a} \right) dt \dots \dots \dots (3.1)$$

2. Synthesis equation or ICWT:

$$f(t) = \frac{1}{K} \int_{a=-\infty}^{\infty} \int_{b=-\infty}^{\infty} \frac{1}{|a|^2} C(a, b) \frac{1}{\sqrt{|a|}} \psi \left(\frac{t-b}{a} \right) \cdot d(a) \cdot d(b) \dots \dots \dots (3.2)$$

B) Continuous-time Wavelet

Consider a real or complex-valued continuous-time function y(t) with the following Properties:

1. The function integrates to zero

$$\int_{-\infty}^{\infty} \psi(t) \cdot dt = 0 \dots \dots \dots (3.3)$$

2. It is square integrable or, equivalently, has finite energy

$$\int_{-\infty}^{\infty} |\psi(t)|^2 \cdot dt < \infty \dots \dots \dots (3.4)$$

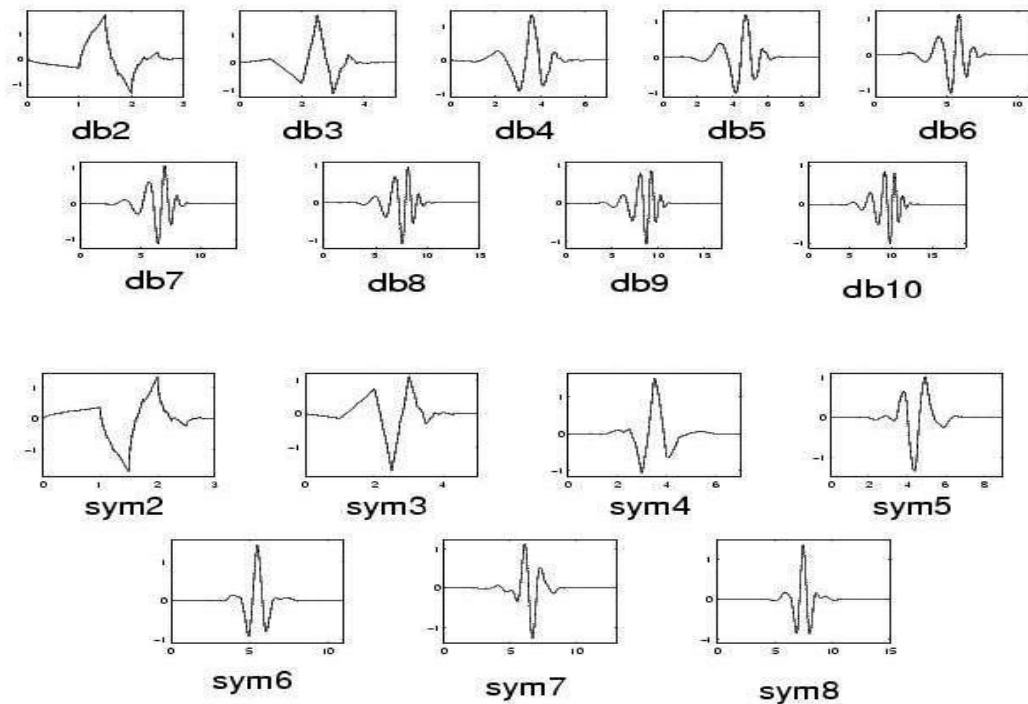


Fig3.3: some wavelet functions

C) Discrete wavelet transforms (DWT)

A discrete wavelet transform can be defined as a „small wave“ that has its energy concentrated in time, and it provides a tool for the analysis of transient, non-stationary or time varying phenomenon. It has oscillating wave like property. Wavelet is a waveform of limited duration having an average value zero. They are localized in space. Wavelet transform provides a time-frequency representation of the signal. In DWT, the signal is decomposed into set of basic functions also known as „WAVELETS“. Wavelets are obtained from a single MOTHER WAVELET by delay and shift in.

$$\psi(t) = \frac{1}{\sqrt{a}} \psi\left(\frac{t-b}{a}\right) \dots \dots \dots (3.5)$$

Where “a” is the scaling parameter and „b” is the shifting parameter. DWT uses multi resolution technique to analyze different frequencies. In DWT, the prominent information in the signal appears in the lower amplitudes. Thus compression can be achieved by discarding the low amplitude signals.

D) Discrete cosine transforms (DCT)

Discrete Cosine Transform can be used for speech compression because of high correlation in adjacent coefficient. We can reconstruct a sequence very accurately from very few DCT coefficients. This property of DCT helps in effective reduction of data.

DCT of 1-D sequence x (n) of length N is given by

$$X(m) = \left[\frac{2}{N} \right]^{1/2} C_m \sum_{n=0}^{N-1} X(n) \cos\left[\frac{(2n+1)m\pi}{2N} \right] \dots \dots \dots (3.6)$$

Where m=0, 1, -----, N-1

The inverse discrete cosine transform is

$$X(n) = \left[\frac{2}{N} \right]^{1/2} \sum_{m=0}^{N-1} C_m X(m) \cos\left[\frac{(2n+1)m\pi}{2N} \right] \dots \dots \dots (3.7)$$

In both equations Cm can be defined as

$$C_m = (1/2)^{1/2} \text{ for } m=0 \\ = 1 \text{ for } m \neq 0$$

3.3.2 Thresholding

After the coefficients are received from different transforms, thresholding is done. Very few DCT coefficients represent 99% of signal energy; hence Thresholding is calculated and applied to the coefficients. Coefficients having values less than threshold values are removed.

3.3.3 Quantization

It is a process of mapping a set of continuous valued data to a set of discrete valued data. The aim of quantization is to reduce the information found in threshold coefficients. This process makes sure that it produces minimum errors. We basically perform uniform quantization process.

3.3.4 Encoding

We use different encoding techniques like Run Length Encoding and Huffman Encoding. Encoding method is used to remove data that are repetitively occurring. In encoding we can also reduce the number of coefficients by removing the redundant data. Encoding can use any of the two compression techniques, lossless or lossy. This helps in reducing the bandwidth of the signal hence compression can be achieved. The compressed speech signal can be reconstructed to form the original signal by decoding followed by dequantization and then performing the inverse-transform methods. This would reproduce the original signal.

IV. Weaknesses of Fourier analysis

This chapter develops the need and motivation for studying the wavelet transform. Historically, Fourier Transform has been the most widely used tool for signal processing. As signal processing began spreading its tentacles and encompassing newer signals, Fourier Transform was found to be unable to satisfy the growing need for processing a bulk of signals. Hence, this chapter begins with a review of Fourier Methods. Detailed explanation is avoided to rid the discussion of insignificant details. A simple case is presented, where the shortcomings of Fourier methods is expounded. The next chapter concerns wavelet transforms, and shows how the drawback of FT is eliminated.

4.1 Review of Fourier Methods

For a continuous –time signal x(t), the Fourier Transform (FT) equations are

$$X(f) = \int_{-\infty}^{\infty} x(t) \cdot e^{-2j\pi ft} dt \dots \dots \dots (4.1)$$

$$x(t) = \int_{-\infty}^{\infty} X(f) \cdot e^{2j\pi ft} df \dots \dots \dots (4.2)$$

Equation (2.1) is the analysis equation and equation (2.2) is the synthesis equation.

The synthesis equation suggests that the FT expresses the signal in terms of linear combination of complex exponential signal. For a real signal, it can be shown that the FT synthesis equation expresses the signal in terms of linear combination of sine and cosine terms.

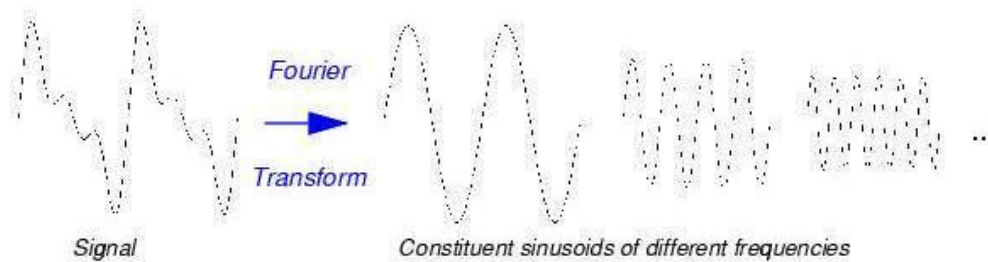


Fig 4.1: constituent sinusoids of different frequencies

The analysis equation represents the given signal in a different form; as a function of frequency. The original signal is a function of time, whereas the after the transformation, the same signal is represented as a function of frequency. It gives the frequency components



Fig4.2: Fourier transform

Thus the FT is a very useful tool as it gives the frequency content of the input signal. It however suffers from a serious drawback. It is explained through an example in the sequel.

4.2 Shortcomings of FT

Ex: 2.1- Consider the following 2 signals
 $x_1(t) = \sin(2\pi \cdot 100 \cdot t) \quad 0 \leq t < 0.1 \text{ sec}$
 $\quad = \sin(2\pi \cdot 500 \cdot t) \quad 0.1 \leq t < 0.2 \text{ sec}$
 $x_2(t) = \sin(2\pi \cdot 500 \cdot t) \quad 0 \leq t < 0.1 \text{ sec}$
 $\quad = \sin(2\pi \cdot 100 \cdot t) \quad 0.1 \leq t < 0.2 \text{ sec}$

A plot of these signals is shown below.

(Note: A time interval of 0 to 0.2 seconds was divided into 10,000 points. The sine of each point was computed and plotted. Since the signal is of 10,000 points, 16,384 point FFT was computed which represents the frequency domain of the signal.)

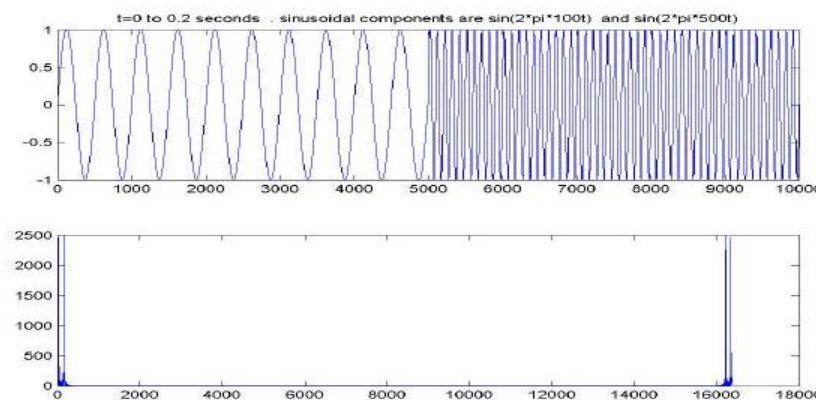


Fig4.3:signalX1 (t) and its FFT

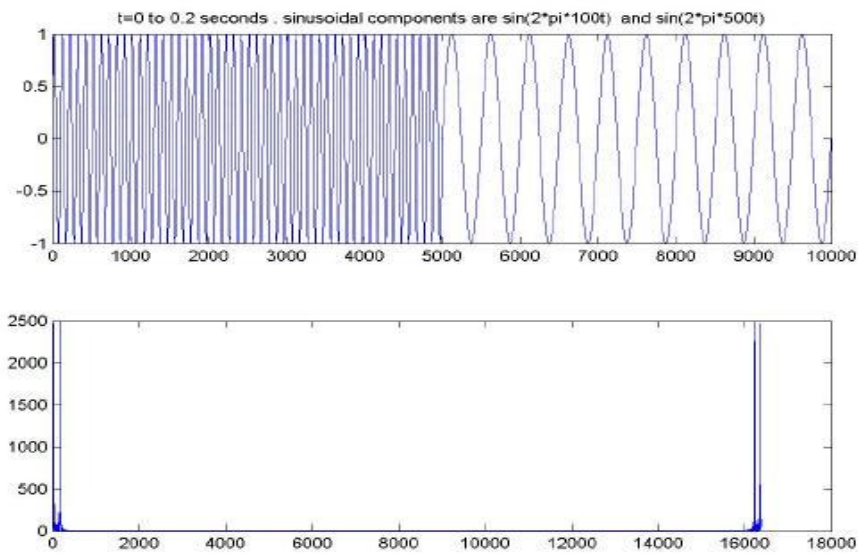


Fig4.4:signalX2 (t) and its FFT

The above example demonstrates the drawback inherent in the Fourier analysis of signals. It shows that the FT is unable to distinguish between two different signals. The two signals have same of giving time information of signals.

In general, FT is not suitable for the analysis of a class of signals called “Non stationary signals”. This led to the search of new tools for analysis of signals. One such tool that was proposed was the “Short time Fourier transforms” (STFT). This STFT too suffered from a drawback and was supplanted by “Wavelet transform”.

V. Procedure

5.1 Wavelet based compression techniques

Wavelets concentrate speech signals into a few neighboring coefficients. By taking the wavelet transform of a signal, many of its coefficients will either be zero or have negligible magnitudes. Data compression can then be done by treating the small valued coefficients as insignificant data and discarding them. Compressing a speech signal using wavelets involves the following stages.

5.2 Choice of wavelets

Choosing mother-wavelet function which is used in designing high quality speech coders is of prime importance. Choosing a wavelet having a compact support in time and frequency in addition to a significant number of vanishing moments is important for wavelet speech compressor. Different criteria can be used in selecting an optimal wavelet function. The objective is to minimize the error variance and maximize signal to noise ratio. They can be selected based on the energy conservation properties. Better reconstruction quality is provided by wavelets with more vanishing moments, as they introduce lesser distortion and concentrate more signal energy in neighboring coefficients.

However the computational complexity of DWT increases with the number of vanishing moments. Hence it is not practical to use wavelets with higher number of vanishing moments. Number of vanishing moments of a wavelet indicates the smoothness of a wavelet function and also the flatness of the frequency response of the wavelet filters. Higher the number of vanishing moments, faster is the decay rate of wavelet coefficients. It leads to a more compact signal representation and hence useful in coding applications. However, length of the filters increases with the number of vanishing moments and the hence complexity of computing the DWT coefficients increases.

5.3 Decomposition of wavelets

Wavelets decompose a signal into different resolutions or frequency bands. Signal compression is based on the concept that selecting small number of approximation coefficients and some of the detail coefficients can represent the signal components accurately. Choosing a decomposition level for the DWT depends on the type of signal being used or parameters like entropy.

5.4 Truncation of coefficients

Compression involves truncating wavelet coefficients below threshold. Most of the speech energy is high-valued coefficient. Thus the small valued coefficients can be truncated or zeroed and can then be used for reconstruction of the signal. This compression technique provided lesser signal-to-noise ratio.

5.5 Encoding coefficients

Signal compression is achieved by first truncating small-valued coefficients and then encoding these coefficients. High-magnitude coefficients can be represented by storing the coefficients along with their respective positions in the wavelet transform vector. Another method for compression is to encode consecutive zero valued coefficient with two bytes. One byte indicates the sequence of zeros in the wavelet transforms vector and the second byte represents the number of consecutive zeros. For further data compression a suitable bit-encoding format can be used. Low bit rate representation of signal can be achieved by using an entropy coder like Huffman coding.

5.6 Calculating threshold

Two different thresholding techniques are used for the truncation of coefficients i.e. global thresholding and level thresholding.

- ❖ **Global Thresholding-** It takes the wavelet expansion of the signal and keeps the largest absolute value coefficient. In this we manually set a global threshold. Hence only a single parameter needs to be selected in this case.
- ❖ **Level Thresholding-** It applies visually determined level dependent thresholds to each of the decomposition level in the wavelet transform.

5.7 Encoding zero value functions

In this method, consecutive zero valued coefficients are encoded with two bytes. One byte specifies the starting string of zeros and the second byte keeps record of the number of successive zeros. This encoding method provides a higher compression ratio.

VI. DCT based compression technique

The given sound file is read. The vector is divided into smaller frames and arranged into matrix form. DCT operation is performed on the matrix. DCT operation is performed and the elements are sorted in their matrix form to find components and their indices.

The elements are arranged in descending order. After the arrangement has been done, a Threshold value is decided. The coefficients below the threshold values are discarded. Hence reducing the size of the signal which results in compression. The data is then converted back into the original form by using reconstruction process. For this we perform IDCT operation on the signal. Now convert the signal back to its vector form. Thus the signal is reconstructed.

VII. Applications of compression

1. The use of compression in recording applications is extremely powerful. The playing time of the medium is extended in proportion to the compression factor.
2. In the case of tapes, the access time is improved because the length of the tape needed for a given recording is reduced and so it can be rewound more quickly.
3. In digital audio broadcasting and in digital television transmission, compression is Used to reduce the bandwidth needed.
4. The time required for a web page to be displayed and the downloading time in case of files is greatly reduced due to compression.

VIII. Compression terminology

- ❖ **Compression ratio:-** The compression ratio is defined as
Compression ratio = size of the output stream/size of the input stream. A value of 0.6 means that the data occupies 60% of its original size after compression. Values greater than 1 mean an output stream bigger than the input stream. The compression ratio can also be called bpb(bit per bit),since it equals the no. of bits in the compressed stream needed, on an average, to compress one bit in the input stream.
- ❖ **Compression factor:-** It is the inverse of compression ratio. Values greater than 1 indicate compression and less than 1 indicates expansion

8.1 Aim, scope and limitations of this thesis

The primary objective of this thesis is to present the wavelet based method for the compression of speech. The algorithm presented here was implemented in MATLAB the said software is provided in the accompanying CD. Readers may find it useful to verify the result by running the program

Since this thesis is an application of wavelets, it was natural to study the basics of wavelets in detail. The same procedure was adopted in writing this thesis, as it was felt that without minimal background in wavelets, it would be fruitless, and also inconvenient to explain the algorithm.

However, the wavelet itself is an engrossing field, and a comprehensive study was beyond the scope of our undergraduate level. Hence, attempt is made only to explain the very basics which are indispensable from the compression point of view.

This approach led to the elimination of many of the mammoth sized equations and vector analysis inherent in the study of wavelets.

At this stage, it is worthwhile mentioning two quotes by famous scientists

‘So far as the laws of mathematics refer to reality, they are not certain. And so far as they are certain, they do not refer to reality.’ --Albert Einstein ‘As complexity rises, precise statements lose meaning and meaningful statements lose precision.’ --Lotfi Zadeh [1]

The inclusion of the above quotes is to highlight the fact that simplicity and clarity are often the casualties of precision and accuracy, and vice-versa.

In this thesis, we have compromised on the mathematical precision and accuracy to make matters simple and clear. An amateur in the field of wavelets might find this work useful as it is relieved of most of the intimidating vector analysis and equations, which have been supplanted by simple diagrams. However, for our own understanding, we did find it necessary, interesting and exciting to go through some literature which deal with the intricate details of wavelet analysis, and sufficient references have been provided wherever necessary, for the sake of a fairly advanced reader. Some of the literature that we perused has been included in the CD.

The analysis that we undertook for wavelets includes only the orthogonal wavelets. This decision was based on the extensive literature we read on the topic, wherein the suitability of these wavelets for speech signals was stated. Another topic that has been deliberately excluded in this work is the concept of MRA, which bridges the gap between the wavelets and the filter banks and is indispensable for a good understanding of Mallet’s Fast Wavelet Transform Algorithm. Instead, we have assumed certain results and provided references for further reading.

Secondly, the sound files that we tested were of limited duration, around 5 seconds. Albeit the programs will run for larger files (of course, the computation time will be longer in this case), a better approach towards such large files is to use frames of finite length. This procedure is more used in real-time compression of sound files, and is not presented here.

Encoding is performed using only the Run Length Encoding. The effect of other encoding schemes on the compression factor has not been studied.

This thesis considers only wavelets analysis, wherein only approximation coefficients are split. There exists another analysis, called wavelet packet analysis, which splits detail coefficients. This is not explored in this thesis.

IX. Conclusion and future scope

In this project compress the data by optimization of wavelet, scale, and level. This technology is needed in the field of speech to satisfy transfer requirements of huge speech signals via communication companies and decreasing storage equipment is another need.

The main objective was to develop an appreciation for wavelet transforms, discuss their application in compression of human speech signals and study the effect of a few parameters on the quality of compression.

The parameters studied are: Sampling frequency, type of wavelet, threshold, file. Here using only Haar, Daubechies wavelets etc, if apply the advanced wavelets like biorthogonal wavelets achieve better performance.

Encoding is performed using only the Run Length Encoding. Higher compression ratios are expected with coding techniques like Huffman coding

REFERENCES

- [1.] Robi Polikar, “The Wavelet Tutorial Part I, Part II and Part III”.
- [2.] J. Pang, S. Chauhan, “FPGA Design of Speech
- [3.] Compression Using DWT” Proceeding of World
- [4.] Congress on Engineering and Computer science October 22-24, 2008, San Francisco, USA.
- [5.] Fundamentals of speech recognition by Lawrence Rabiner.

Accelerometer based Robot control using Renesas Microcontroller

S.Hemachandra¹, T.K.S Ravi Kiran², B.Gowri Prasad³, S.M Mazhar⁴

¹(Department of E.Con.E, Head of the department, Sree Vidyanikethan Engineering College, India)

^{2,3,4}(Department of E.Con.E, IV B.tech, Sree Vidyanikethan Engineering College, India)

Abstract: Tracking and attacking enemies at distant places is very much difficult for the soldiers. There may be a chance of loss of lives of the soldier during war and emergency situations. So the idea is to replace a real soldier with robot soldier completely controlled with a wireless network. The objective of this paper is to minimize human fatalities in terrorist attack. For this we design a robot that can monitor enemy remotely when required. It can silently enter into enemy area and send us all the information through its tiny camera, that can be mounted on top of it. For this purpose Renesas microcontroller was used to perform the control actions as per requirement.

Keywords: Renesas, Robot, Wireless

I. INTRODUCTION

Today, almost all the military organizations take the help of military robots to carry out many risky jobs that cannot be handled manually by soldier. We have also seen a great development in military robots when compare to military robots in earlier time. Military robots are autonomous robots or remote-controlled devices designed for military applications. Such systems are currently being researched by a number of militaries.

Broadly defined, military robots date back to World War II and the Cold War in the form of the German Goliath tracked mines and the Soviet teletanks. The MQ-1 Predator drone was when "CIA officers began to see the first practical returns on their decade-old fantasy of using aerial robots to collect intelligence."

The use of robots in warfare, although traditionally a topic for science fiction, is being researched as a possible future means of fighting wars. Already several military robots have been developed by various armies.

The field of artillery has also seen some promising research with an experimental weapons system named "Dragon Fire II" which automates the loading and ballistics calculations required for accurate predicted fire, providing a 12 second response time to fire support requests. However, weapons of warfare have one limitation in becoming fully autonomous: they require human input at certain intervention points to ensure that targets are not within restricted fire areas as defined by Geneva Conventions for the laws of war.

There have been some developments towards developing autonomous fighter jets and bombers. The use of autonomous fighters and bombers to destroy enemy targets is especially promising because of the lack of training required for robotic pilots, autonomous planes are capable of performing manoeuvres which could not otherwise be done with human pilots (due to high amount of G-Force), plane designs do not require a life support system, and a loss of a plane does not mean a loss of a pilot. However, the largest drawback to robotics is their inability to accommodate for non-standard conditions. Advances in artificial intelligence in the near future may help to rectify this.

II. LITERATURE SURVEY

We aim to develop a model which will be efficiently used to minimize terrorist causality. Being able to achieve reliable long distance communication with user-friendly robot control is an important open area of research to robotics.

2.1 Robot control

Programming and control of a robot through the use of the robot teach pendant is a tedious and time-consuming task that requires technical expertise. Therefore, new and more intuitive ways for robot programming and control are required. The goal is to develop methodologies that help users to control and program a robot, with a high-level of abstraction from the robot specific language.

In the robotics field, several research efforts have been made to create user-friendly teach pendants, implementing intuitive user interfaces such as color touch screens, a 3D joystick (ABB Robotics). But, neither of these techniques is efficient to control the robot as they do not give accurate results and have slow response time.

In the last few years the robot manufacturers have made great efforts towards creating “Human Machine Interfacing Device” -recognizing human gestures, recurring to vision-based systems [1], [2] or using finger gesture recognition systems based on active tracking mechanisms [3].

Using data glove is a better idea over camera as the user has flexibility of moving around freely within a radius limited by the range of wireless connecting the glove to the computer, unlike the vision based technique where the user has to stay in position before the camera [4]. The cause of light, electric or magnetic fields or any other interruption does not affect the performance of the glove [5].

So Accelerometer based gesture recognition has become increasingly popular over the last decade compared to vision based technique. The low- moderate cost and relative small size of the accelerometers make it an effective tool to detect and recognize human body gestures.

2.2 Communication

Wired communication is not suitable to transmit data over long distances as wiring itself is a problem. The next option is to adopt wireless communication which includes Bluetooth, WI-Fi, and ZigBee. Table 1 gives us the comparison between all the 3 kinds of techniques.

Category	Wi-Fi	Bluetooth	ZigBee
Distance	50m	10m	50-1600m
Extension	Depend on the existing network	None	Automatic
Power Supply	Hours	Days	Years
Complexity	Very Complicated	Complicated	Simple
Transmission Speed	1-54Mbps	1Mbps	250Kbps
Frequency Range	2.4GHz	2.4GHz	868MHz, 916MHz, 2.4GHz
Network Nodes	50	8	65535
Linking Time	Up to 3s	Up to 10s	30ms
Ease of Use	Hard	Normal	Easy

Table.1: Comparison between Wi-Fi, Bluetooth and ZigBee.

When it comes to robot communication the technique adopted should be such that it can cover wide distance and provide good battery backup. When these aspects are considered ZigBee is a better option than the others.

ZigBee is targeted at the applications that require a low data rate, long battery life. It operates over same 2.4GHz frequency range as Wi-Fi and Bluetooth. Unlike those technologies though, ZigBee transmits at much lower data rates, it's made for sending simple commands such as turning on a TV, rotating left etc., or small bits of data. Thanks to the low data rates, ZigBee tends to use far less power than other networking technologies. ZigBee's standard utilizes mesh networking, which allows ZigBee devices to automatically connect with and transmit data through one another without having to go through a central gateway like a

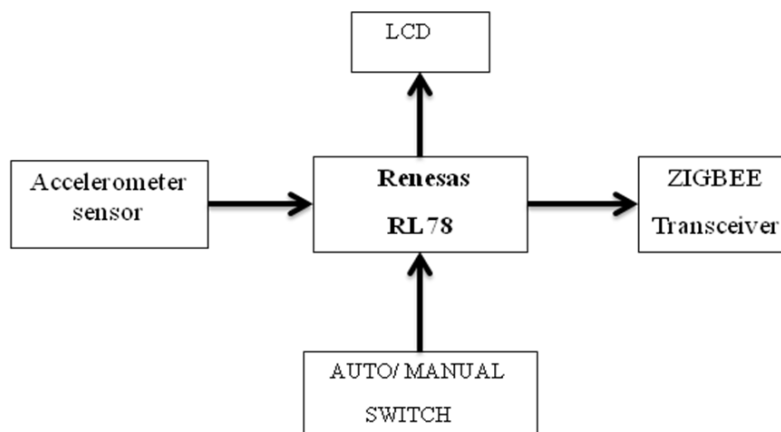
router. ZigBee uses IEEE 802.15.4 standard to allow wireless PAN (Personal Area Network) in home. It uses digital radio waves to transfer information between electric devices. It uses transistors in its electronic devices. The electronic devices communicate from a central computer that sends and receives data. It is more reliable, supports larger network and is more fully featured than other networking technologies.

In this paper we use accelerometer based gesture recognition technique to control robot and ZigBee networking technology to communicate.

2.3 Design

The block diagram of the Accelerometer controlled system using Zigbee-communication is shown in Figure 1.

Transmitter End:



Receiver End:

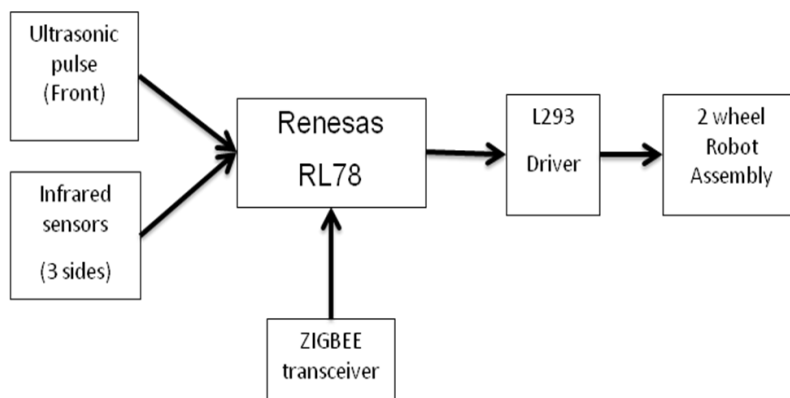


Figure 1: Block diagram of receiver and transmitter end of an accelerometer based robot motion and speed control with obstacle detection.

The brain of the robot is the transmitter i.e., Renesas microcontroller which acts as a master controller by giving commands to the slave controller. The second Renesas controller which acts as a slave controller is responsible for executing all the commands received from the master and also generating PWM pulse for the speed control. Based on the input codes given by the master, the slave i.e., the robot will behave as follows

- Moves in forward direction,
- Moves in reverse direction,
- Speed control in both directions,
- It can take a left or right turn while moving forward or in reverse direction,
- Instant reverse or stopping when obstacle is detected.

III. HARDWARE REQUIREMENTS

3.1 Accelerometer Sensor

The ADXL335 is a small, thin, low power, complete 3-axis accelerometer with signal conditioned voltage outputs. The product measures acceleration with a minimum full-scale range of $\pm 3g$. It can measure the static acceleration of gravity in tilt-sensing applications, as well as dynamic acceleration resulting from motion, shock, or vibration.

The ADXL335 is available in a small, low profile, $4\text{ mm} \times 4\text{ mm} \times 1.45\text{ mm}$, and 16-lead. Block diagram of the same is given in Figure 2.

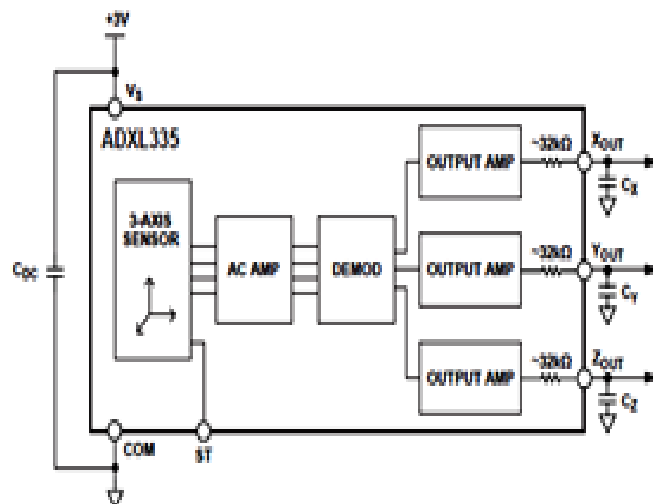


Figure 2: Functional block diagram of ADXL335 accelerometer.

They are typically used in Mobile devices, Gaming systems, Disk drive protection, Image stabilization, Sports and health devices applications.

3.2 Renesas Microcontroller

Renesas is a Japanese semiconductor manufacturer headquartered in Tokyo. It has manufacturing, design and sales operations in around 20 countries. Renesas is one of the world's largest manufacturers of semiconductor systems for mobile phones and automotive applications. It is the world's largest manufacturer of microcontrollers and the second largest manufacturer of application processors. Renesas is also known for LCD drivers, RF ICs, mixed-signal integrated circuits and system-on-a-chip semiconductors. "Renesas" is an invented name and a contraction of Renaissance Semiconductor for Advanced Solutions.

3.2.1 Renesas RL78 16-bit Microcontroller

The Renesas Electronics RL78 is a 16-bit CPU core with CISC architecture for embedded microcontrollers developed and manufactured by Renesas Electronics and introduced in 2011. Renesas Electronics is a developer and manufacturer of semiconductor devices especially microcontrollers, microprocessors, Power MOSFET, IGBTs, opt couplers, SRAMs and SOC devices. The RL78 was the first new MCU core to emerge from the new Renesas Electronics Company from the merger of NEC Electronics and Renesas Technology and incorporated the features of the NEC K0 and Renesas Technology R8C microcontrollers.

The RL78 was developed to address extremely low power but highly integrated microcontroller applications, to this end the core offered a novel low power mode of operation called "snooze mode" where the ADC or serial interface can be programmed to meet specific conditions to wake the device from the extreme low power STOP mode of $0.52\mu\text{A}$.

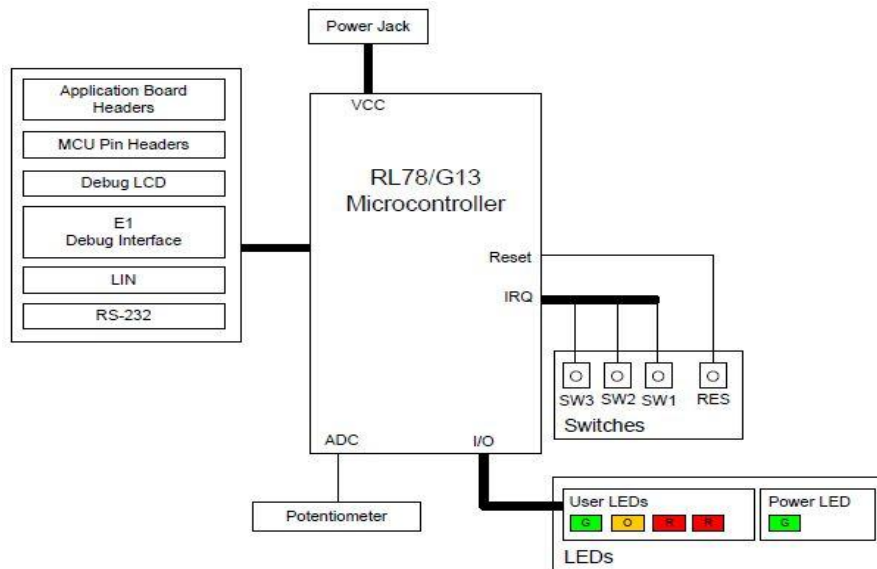


Figure 3 Block diagram of Renesas Microcontroller

3.3 Ultrasonic Motion Sensor

Figure 4 gives the clear idea of the GH-311 ultrasonic Motion sensor which provides precise, non-contact distance measurements from about 2 mm (0.8 inches) to 3 meters (3.3 yards) but with the sensing angle not greater than 15°.

The GH-311 sensor works by transmitting an ultrasonic (well above human hearing range) burst and providing an output pulse that corresponds to the time required for the burst echo to return to the sensor. By measuring the echo pulse width, the distance to target can easily be calculated.

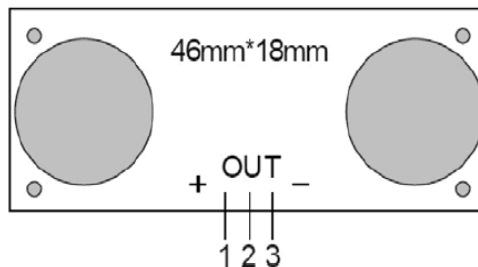


Fig 4: External connection schematic of GH-311 ultrasonic motion sensor.

The GH-311 sensor has a male 3-pin header used to supply ground, power (+5 VDC) and signal. It can be used to detect the move of human or object. Suitable for indoor and outdoor burglar-proof application, vehicle burglary-proof application, ATM surveillance camera, warehouse surveillance camera, and safety warning applications in dangerous site where high voltage and high temperature exist.

3.4 IR Transmitter & Receiver

To monitor the density of the traffic, we will be keeping a few sets of IR transmitter and receiver sensors on the side of the roads. On side IR transmitter will be placed & right opposite to the IR transmitter, an IR receiver will be kept. This set of IR transmitter & receiver will be kept on roads at different intervals. The IR transmitters are connected to supply, so that they will transmit high signal all the time. The IR receivers are connected to the comparator circuit, to get digital signals. A low power operational amplifier LM324 IC has been used to develop a comparator circuit. Two set of LM324 IC has been used in this project. The circuit diagram of the comparator is shown below:

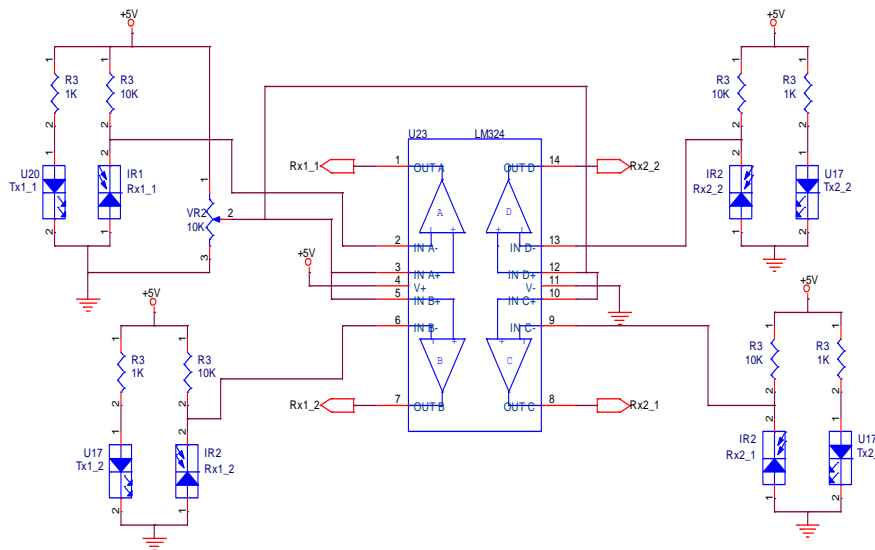


Figure5: Internal circuitry of IR sensors

3.4.1 Types of Infra-Red Sensors

Infra-red sensors are broadly classified into two types:

Thermal infrared sensors – These use infrared energy as heat. Their photo sensitivity is independent of wavelength. Thermal detectors do not require cooling; however, they have slow response times and low detection capability.

Quantum infrared sensors – These provide higher detection performance and faster response speed. Their photo sensitivity is dependent on wavelength. Quantum detectors have to be cooled so as to obtain accurate measurements. The only exception is for detectors that are used in the near infrared region.

3.4.2 Working Principle

A typical system for detecting infrared radiation using infrared sensors includes the infrared source such as blackbody radiators, tungsten lamps, and silicon carbide. In case of active IR sensors, the sources are infrared lasers and LEDs of specific IR wavelengths. Next is the transmission medium used for infrared transmission, which includes vacuum, the atmosphere, and optical fibers.

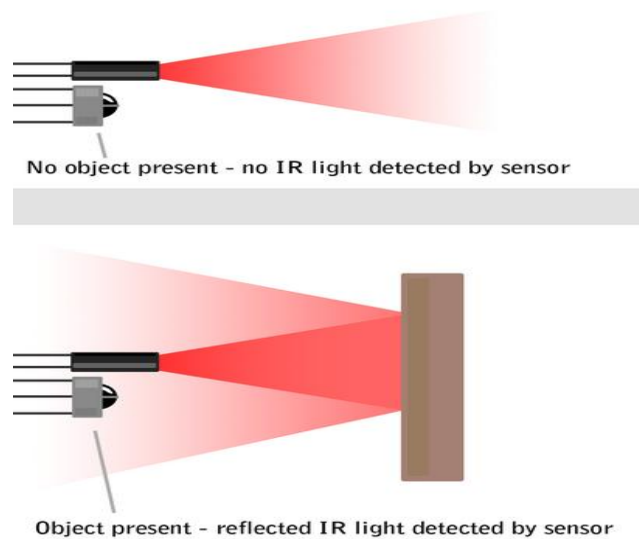


Fig 6: Working principle of IR sensors

IV. SOFTWARE REQUIREMENTS

For the software implementation, we deploy two software packages. First one is the Keil μ Vision 3.0, second is the Flash magic simulator.

4.1 Keil μ Vision

The debugger accurately simulates on-chip peripherals (I²C, CAN, UART, SPI, Interrupts, I/O Ports, A/D Converter, D/A Converter, and PWM Modules) of 89S52device. Simulation helps to understand hardware configurations and avoids time wasted on setup problems. With simulation, we can write and test applications before target hardware is available. The system program written in embedded C using Keil IDE software will be stored in Microcontroller. The industry-standard Keil C Compilers, Macro Assemblers, Debuggers, Real-time Kernels, Single- board Computers, and Emulators support all 89S52derivatives. The Keil Development Tools are designed to solve the complex problems facing embedded software developers.

4.2 Flash Magic

It is used to dump the code to microcontroller from PC. Flash Magic is a free, powerful, feature-rich Windows application that allows easy programming of Philips FLASH microcontrollers. Custom applications built for Philips microcontrollers on the Flash Magic platform can be used to create custom end-user firmware programming applications, or generate an in-house production line programming tool. The Flash Memory In-System Programmer is a tool that allows in-circuit programming of FLASH memories via a serial RS232 link. Computer side software called Flash Magic is executed that accepts the Intel HEX format file generated from compiler Keil to be sent to target microcontroller. It detects the hardware connected to the serial port

V. IMPLEMENTATION

It operates in two modes – manual and auto (predefined) mode. A Wireless camera mounted on the robot will send real time video signals, which could be seen on a remote monitor, and action can be taken accordingly.

5.1Algorithm for Auto mode

Once the controller gives the auto mode command to the robot, the robot uses its ultrasonic sensor to identify any obstacles in its path and navigates accordingly; it also displays the distance from the obstacle using its ALCD.

We can brief the algorithm for this mode as in figure 7.

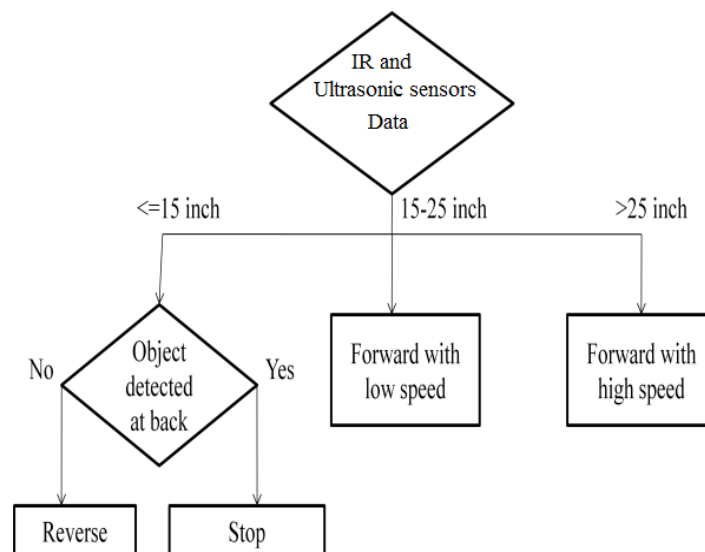


Figure 7: Algorithm for auto mode

5.2 Algorithm for manual mode

In this mode we control the robot movement manually using the accelerometer. Even a small tilt in the accelerometer sensor corresponds to the readings that are communicated to the robot through ZigBee for its navigation. We can request for the distance between the robot and obstacle in this mode and the algorithm for the same can be described in figure 8.

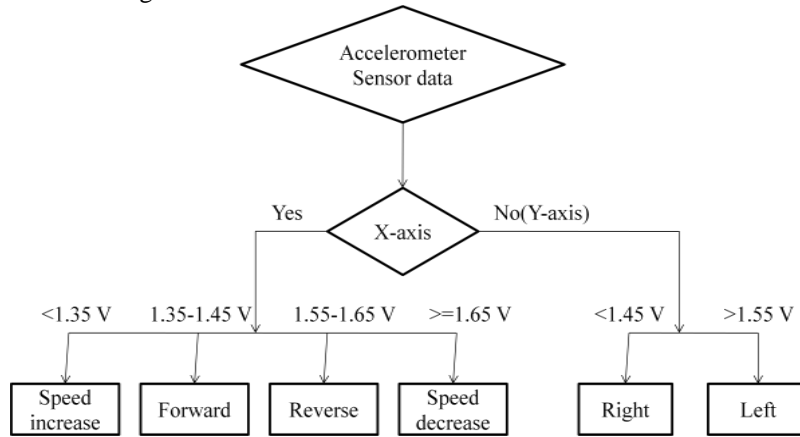


Figure 8: Algorithm for manual mode

5.3 Results

The top view of the robot and controller after the entire setup is shown in Figure 9 and 10.



Figure 9: Top view of robot.



Figure 10: Top view of controller.

Here the robot detects the obstacles using ultrasonic sensors and takes the path that is previously defined. When accelerometer is tilted in any of the 4 directions the ALCD displays its corresponding X and Y-axis value in terms of voltage (V) along with the command for the robot to traverse, the robot then moves in the specified path by displaying the distance from the obstacle along with the direction of movement.

VI. CONCLUSION

As we all know, these days our nation is sick of massive terror attacks and bomb explosions. To avoid such disasters technological power must exceed human power. Human life and time are priceless.

Acknowledgements

The authors wish to thank Prof. S. Hemachandra, Associate Professor and Head, Department of Electronics and Control Engineering and Mr.P.Ramesh, Embedded Software Engineer, Pragmatic Embedded Solutions, Bangalore for their moral support through the work.

REFERENCES

- [1] S. Waldherr, R. Romero, and S. Thrun, "A gesture based interface for human-robot interaction," in *Autonomous Robots*, vol. 9, no. 2, pp. 151-173, Springer, 2000.
- [2] I. Mihara, Y. Yamauchi, and M. Doi, "A real-time vision-based interface using motion processor and applications to robotics," in *Systems and Computers in Japan*, vol. 34, pp. 10-19, 2003.
- [3] S. Perrin, A. Cassinelli, and M. Ishikawa, "Gesture recognition using laser-based tracking system," in *Sixth IEEE International Conference on Automatic Face and Gesture Recognition*, pp. 541-546, 2004.
- [4] Martin Urban, Peter Bajcsy, Rob Kooper and Jean-Christophe "Recognition of Arm Gestures Using Multiple orientation sensors," *Lementec2004 IEEE Intelligent Transportation Systems conference Washington, D.C., USA, October 34, 2004.*
- [5] Tan Tian Swee, A.K. Ariff, Sh-Hussain.Salleh, Siew Kean Seng and Leong Seng Huat "Data Gloves Malay Sign Language Recognition System" 1-4244-0983-7/07/\$25.00 ©2007 IEEE.
- [6] Robert Lemoyne, Christian Coroian, and Timothy Mastroianni "Wireless accelerometer system for quantifying gait," 978-1-4244-3316-2/09/\$25.00©2009IEEE.
- [7] Pedro Neto, J. Norberto Pires, and A. Paulo Moreira, "Accelerometer-Based Control of an Industrial Robotic Arm", *IEEE International Symposium on Robot and Human Interactive Communication, Toyama, Japan, 2009.*

A New Technique of Extraction of Edge Detection Using Digital Image Processing

Balaji S.C.K¹

1, Asst Professor S.V.I.T

Abstract: Digital image Processing is one of the basic and important tool in the image processing and computer vision. In this paper we discuss about the extraction of a digital image edge using different digital image processing techniques. Edge detection is the most common technique for detecting discontinuities in intensity values. The input image or actual image have some noise that may cause the of quality of the digital image. Firstly, wavelet transform is used to remove noises from the image collected. Secondly, some edge detection operators such as Differential edge detection, Log edge detection, canny edge detection and Binary morphology are analyzed. And then according to the simulation results, the advantages and disadvantages of these edge detection operators are compared. It is shown that the Binary morphology operator can obtain better edge feature. Finally, in order to gain clear and integral image profile, the method of ordering closed is given. After experimentation, edge detection method proposed in this paper is feasible.

Index Terms: Image, Digital image, Edge, boundary, Edge detection, wavelet denoising, differential operators, and binary morphology.

I. Introduction

An edge in a digital image is a boundary or contour at which a significant change occurs in some physical aspect of an image, such as the surface reflectance, illumination or the distances of the visible surfaces from the viewer. Changes in physical aspects manifest themselves in a variety of ways, including changes in color, intensity and Texture. Edge always indwells in two neighboring areas having different grey level. It is the result of grey level being discontinuous. Edge detection is a kind of method of image segmentation based on range non-continuity. Image edge detection is one of the basal contents in the image processing and analysis, and also is a kind of issues which are unable to be resolved completely so far [1]. When image is acquired, the factors such as the projection, mix, aberrance and noise are produced. These factors bring on image feature is blur and distortion, consequently it is very difficult to extract image feature. Moreover, due to such factors it is also difficult to detect edge. The method of image edge and outline characteristic's detection and extraction has been research hot in the domain of image processing and analysis technique. Detecting edges is very useful in a number of contexts. For example in a typical image understanding task such as object identification, an essential step is to an image into different regions corresponded to different objects in the scene. Edge detection is the first step in the image segmentation. Edge feature extraction has been applied in many areas widely. This paper mainly discusses about advantages and disadvantages of several edge detection operators applied in the cable insulation parameter measurement. In order to gain more legible image outline, firstly the acquired image is filtered and denoised. In the process of denoising, wavelet transformation is used. And then different operators are applied to detect edge including Differential operator, Log operator, Canny operator and Binary morphology operator. Finally the edge pixels of image are connected using the method of bordering closed. Then a clear and complete image outline will be obtained.

II. Image Denoising

As we all know, the actual gathered images contain noises in the process of formation, transmission, reception and processing. Noises deteriorate the quality of the image. They make image blur. And many important features are covered up. This brings lots of difficulties to the analysis. Therefore, the main purpose is to remove noises of the image in the stage of pretreatment. The traditional denoising method is the use of a low-pass or band-pass filter to denoise. Its shortcoming is that the signal is blurred when noises are removed. There is irreconcilable contradiction between removing noise and edge maintenance. Yet wavelet analysis has been proved to be a powerful tool for image processing [2]. Because Wavelet denoising uses a different frequency band-pass filters on the signal filtering. It removes the coefficients of some scales which mainly reflect the noise frequency. Then the coefficient of every remaining scale is integrated for inverse transform, so that noise can be

suppressed well. So wavelet analysis widely used in many aspects such as image compression, image denoising [3][4], etc

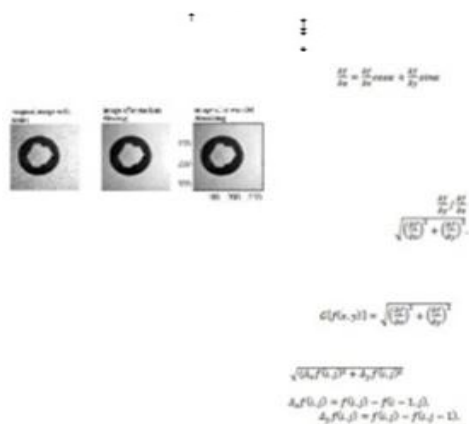


Image after denoising
fig1: Sketch of removing image noises with wavelet transformation

The basic process of denoising making use of wavelet transform is shown in Fig1, its main steps are [3][4] as follows:

- 1) Image is preprocessed (such as the gray-scale adjustment, etc.).
- 2) Wavelet multi-scale decomposition is adapted to process image.
- 3) In each scale, wavelet coefficients belonging to noises are removed and the wavelet coefficients are remained and enhanced.
- 4) The enhanced image after denoising is gained using wavelet inverse transform.

The common used operators are the Differential, Log, Canny operators and Binary morphology, etc. The simulation effect of wavelet denoising through Matlab is shown in Fig. 2.

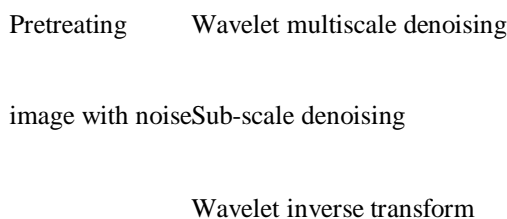


Fig.2.Comparison of denoising methods

Comparing with the traditional matched filter, the high-frequency components of image may not be destroyed using wavelet transform to denoise. In addition, there are Many advantages such as the strong adaptive ability, calculating quickly, completely reconstructed, etc. So the signal to noise ratio of image can be improved effectively making use of wavelet transform.

III. Edge Detection

The edge detection of digital image is quite important foundation in the field of image analysis including image division, identification of objective region and pick-up of region shape and so on. Edge detection is very important in the digital image processing, because the edge is boundary of the target and the background. And only when obtaining the edge we can differentiate the target and the background.

The basic idea of image detection is to outstand partial edge of the image making use of edge enhancement operator firstly. Then we define the „edge intensity“ of pixels and extract the set of edge points through setting threshold. But the borderline detected may produce interruption as a result of existing noise and image dark. Thus edge detection contains the following two parts:

- 1) Using edge operators the edge points set are extracted.
- 2) Some edge points in the edge points set are removed and a number of edge points are filled in the edge points set. Then the obtained edge points are connected to be a line.

A. Differential operator

Differential operator can outstand grey change. There are some points where grey change is bigger. And the value calculated in those points is higher applying derivative operator. So these differential values may be regarded as relevant „edge intensity“ and gather the points set of the edge through setting thresholds for these differential values. First derivative is the simplest differential coefficient. Suppose that the image is $f(x, y)$, and its derivative operator is the first order partial derivative $f\partial/\partial x, f\partial/\partial y$. They represent the rate-of-change that the gray f is in the direction of x and y . Yet the gray rate of change in the direction of α is shown in the equation (1):

(1)

Under consecutive circumstances, the differential of the function is:

$$df = \frac{\partial f}{\partial x} dx + \frac{\partial f}{\partial y} dy$$

The direction derivative of function $f(x, y)$ has maximum at a certain point. And the

direction of this point is $\arctan \left[\frac{\partial f / \partial y}{\partial f / \partial x} \right]$. The maximum

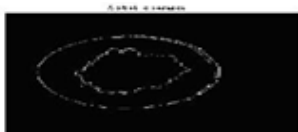
of direction derivative is $\sqrt{\left(\frac{\partial f}{\partial x}\right)^2 + \left(\frac{\partial f}{\partial y}\right)^2}$. The vector with

this direction and modulus is called as the gradient of the function f , that is, $\nabla f = \left(\frac{\partial f}{\partial x}, \frac{\partial f}{\partial y} \right)$. So the gradient modulus operator is designed in the equation (2).

(2)

For the digital image, the gradient template operator is designed as:

(3)



$$\begin{aligned} \nabla^2 f &= \nabla \cdot \nabla f \\ &= \frac{\partial}{\partial x} \left[\frac{\partial f}{\partial x} \right] + \frac{\partial}{\partial y} \left[\frac{\partial f}{\partial y} \right] \end{aligned}$$

$$\Delta^2 f = \frac{\partial^2 f}{\partial x^2} + \frac{\partial^2 f}{\partial y^2}$$



$$G[f(x, y)] = \left(\left[f(x+1, y+1) - f(x, y) \right]^2 + \left[f(x+1, y) - f(x, y+1) \right]^2 \right)^{1/2}$$

$$G[f(x, y)] \approx |f(x+1, y) - f(x, y)| + |f(x, y+1) - f(x, y)|$$

$$G[f(x, y)] \approx |f(x+1, y+1) - f(x, y)| + |f(x, y+1) - f(x+1, y)|$$

$$\sqrt{x^2 + y^2}$$



Differential operator mostly includes Roberts operator and Sobel operator.

(1) Roberts operator:

Roberts operator is a kind of the most simple operator which makes use of partial difference operator to look for edge. Its effect is the best for the image with steep low noise. But the borderline of the extracted image is quite thick using the Roberts operator, so the edge location is not very accurate. Roberts operator is defined as:(4)

But absolute deviation algorithm is usually used to predigest the equation (4) in practice. The following equations (5) and (6) are the process of reduction.

(5)

(6)

The template of the Roberts operator is shown in Fig. 3.

$$\begin{bmatrix} 1 & 0 & 0 & 1 \\ 0 & -1 & 1 & 0 \end{bmatrix}$$

Fig.3.Roberts Operator

(2) Sobel and Prewitt operator:

To reduce the influence of noise when detecting edge, the Prewitt operator enlarges edge detection operator template from two by two to three by three to compute difference operator. Using the Prewitt operator can not only detect edge points, but also restrain the noise. The Sobel operator counts difference using weighted for 4 neighborhoods on the basis of the Prewitt operator. The Sobel operator has the similar function as the Prewitt operator, but the edge detected by the Sobel operator is wider. Suppose that the pixel number in the 3×3 sub-domain of image is as follows:

$$\begin{matrix} A0A1 & A2 \\ A7f(x, y)A3 \\ A6A5 & A4 \end{matrix}$$

We order that

$$X = (A0+2A1 +A2) - (A6+2A5+A4)$$

$$\text{And } Y = (A0+2A7 +A6) - (A2+2A3+A4)$$

Then Prewitt operator is as follows:

$$G [f (i, j)] = (\quad) (7)$$

$$G [f (i, j)] = /X/+ /Y/ \quad (8)$$

Prewitt operator is said in Fig.4 in the form of the template.

$$\begin{matrix} 1-11 & & & & \\ & 1 & 1 & 1 & \end{matrix}$$

$$1-10 \quad 0 \quad 0 \quad 0$$

$$\begin{matrix} 1-1-1 \\ & -1-1-1 \end{matrix}$$

Fig.4.prewitt operator

Sobel operator can process those images with lots of noises and gray gradient well. We order that

$$X = (A0+2A1 +A2) - (A6+2A5+A4)$$

$$\text{And } Y = (A0+2A7 +A6)-(A2+2A3+A4).$$

Then Sobel operator is as follows:

$$G [f (i, j)] = (\quad) (9)$$

$$G [f (i, j)] = /X/+ /Y/ \quad (10)$$

The templates of sobel operator is shown in fig.5

$$1 \ 2 \ 1 \quad 10-1$$

$$0 \ 0 \ 0 \quad 20-2$$

$$-1-2- \ 1 \ 10-1$$

Fig.5.Sobel Operator

The original image of cable insulation layer and the edge detection drawing of Sobel operator gained using Mat Lab simulation are shown in Fig. 6 and Fig.7

Fig.6. Original image

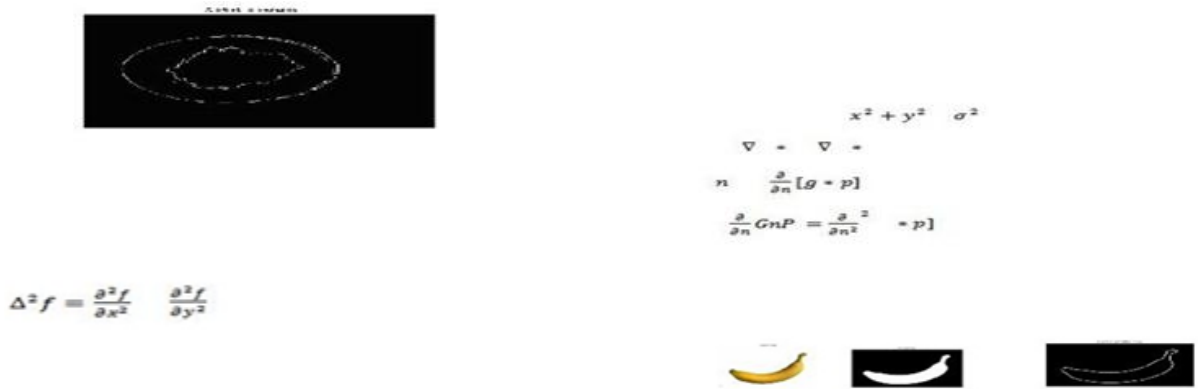


Fig. 7 the edge detection drawing of Sobel operator

From the simulation drawing Fig. we can know that the edge position is very accurate. And the effect of Sobel edge detection is very satisfying. In a word, the Sobel and Prewitt operators have a better effect for such images with grey level changing gradually and more noises.

B. Log operator

The Log operator is a linear and time-invariant operator. It detects edge points through searching for spots which two-order differential coefficient is zero in the image grey levels. For a continuous function $f(x, y)$, the Log operator is defined as at point (x, y) :

$$+(11)$$

The Log operator is the process of filtering and counting differential coefficient for the image. It determines the zero overlapping position of filter output using convolution of revolving symmetrical Log template and the image. The Log operator's template is shown in Fig. 8

$$\begin{matrix} -1 & -1 & 0 & -1 & 0 \\ -18 & -1 & -14 & -1 & \\ -1 & -1 & 0 & -1 & -1 \end{matrix}$$

Fig. 8 Log operator

In the detection process of the Log operator, we firstly pre-smooth the image with Gauss low-pass filter, and then find the steep edge in the image making use of the Log operator. Finally we carry on binarization with zero grey level to give birth to closed, connected outline and eliminate all internal spots. But double pixels boundary usually appears using the Log operator to detect edge, and the operator is very sensitive to noise. So the Log operator is often employed to judge that edge pixels lie in either bright section or dark section of the image.

C. Canny operator

The Canny operator is a sort of new edge detection operator. It has good performance of detecting edge, which has a wide application. The Canny operator edge detection is to search for the partial maximum value of image gradient. The gradient is counted by the derivative of Gauss filter. The Canny operator uses two thresholds to detect strong edge and weak edge respectively. And only when strong edge is connected with weak edge, weak edge will be contained in the output value. The theory basis of canny operator is shown in equations (12)-(15)

Gauss:

$$G(x, y) = \exp[-(x^2 + y^2)/2] \quad (12)$$

Edge normal

$$n1 = (g \cdot p) / |gp| \quad (13)$$

Edge strengths

$$G \cdot P = \quad (14)$$

Maximal strengths:

$$0 = [g \quad (15)$$

D. Binary morphology:

Mathematical morphology is a new method applied in image processing. The basic idea is to measure and extract the corresponding shape from image with structural elements having stated form. So that the image processing and analyzing can be completed [2]. Using mathematical morphology to detect the edge is better than using differential treatment. Because it is not sensitive to noise, and the edge extracted is relatively smooth. Binary image is also known as black-and-white image. The object can be easily identified from the image background. So we adopt the combination of binary image and mathematical morphology to detect edge. It is called Binary morphology. Suppose that the region is shown in form of the set A. Its border is $\beta(A)$. B is an appropriate structure element, and it is symmetrical around the origin. Firstly we corrupt A with

$$A \ominus B = \{x | (B)_x \subseteq A\}$$

Where $(B)_x$ is a translation B along the vector. The interior of region is available with $A \ominus B$. And $A - (A \ominus B)$ is the borderline naturally. Then $\beta(A)$ is obtained. The equation of edge extraction can be said,

$$\beta(A) = A - (A \ominus B)$$

Structuring element is larger, the edge gained will be wider.

E. Simulative results analysis

In order to know about the advantages and disadvantages of these edge detection operators, we detect edge using these different operators respectively. The simulation results are shown in Fig. 9 and Fig. 10.

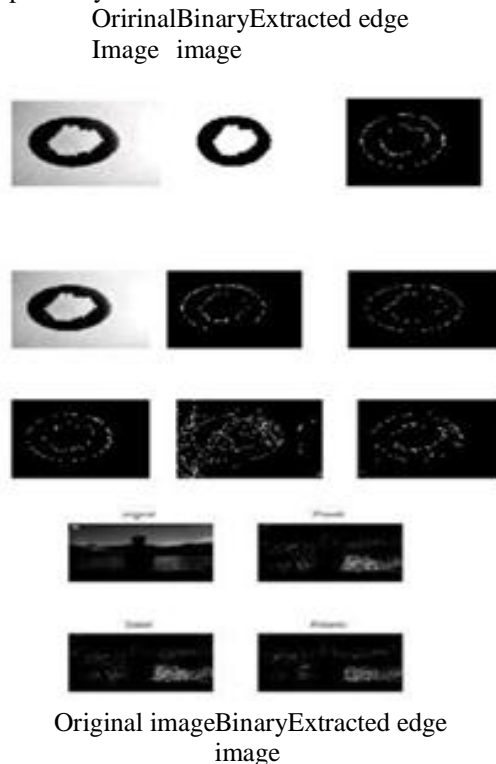


Fig.9. Detecting edge with binary morphology

Original image Roberts operators sobel operator
 Image
 prewitt operator canny operator log operator

pixels is that they have definite similarity. Two aspects one using gradient algorithm to process image. One is the magnitude of gradient; the other is direction of gradient.

According to edge pixels gradient's similarity on these two aspects, the edge pixels can be connected. Specific speaking, if Pixel(s,t) is in neighbor region of the pixel (x,y) and their gradient magnitudes and gradient directions must satisfy two conditions (16) and (17) respectively, then the pixels in (s,t) and the pixels in (x,y) can be connected. The closed boundary will be obtained if all pixels are judged and connected

$$|\nabla f(x,y) - \nabla f(s,t)| \leq T \tag{16}$$

$$|\varphi(x,y) - \varphi(s,t)| \leq A \tag{17}$$

Where T is magnitude threshold, A is angle threshold.

An Analytical Study of International Standards on Minority Rights

Vikrant Sopan Yadav¹

Abstract: The recognition and protection of minority rights under international law began with the establishment of the League of Nations which adopted several “minority treaties”. When the United Nations was set up in 1945 to replace the League of Nations, it too, gradually developed a number of norms, procedures and mechanisms with an aim to protect minorities. Apart from UN various international statutes and standards have provided the broad framework for the protection and promotion of these minorities.

This article is an endeavor by the author to ascertain the meaning of the term ‘Minority’ as enshrined in different international statutes. Author has also made an attempt to analyze the scope of minority rights at the international forum. Article also consist analysis of various international statutes providing array of rights to the minorities with help of relevant case laws.

Keywords: Minority, Rights, International Statutes

I. Introduction

The U.N. Sub-Commission on Prevention of Discrimination and Protection of Minorities has defined minority as under:

- 1) The term 'minority' includes only those non-dominant group of the population which possess and wish to preserve stable ethnic, religious or linguistic traditions or characteristics markedly different from those of the rest of the population;
- 2) Such minorities should properly include the number of persons sufficient by themselves to preserve such traditions or characteristics; and
- 3) Such minorities should be loyal to the state of which they are nationals.

The United Nations Minorities Declaration, 1992

Article 1 of this declaration refers minority as, ““based on national or ethnic, cultural, religious and linguistic identity, and provides that States should protect their existence. There is no internationally agreed definition as to which groups constitute minorities. It is often stressed that the existence of a minority is a question of fact and that any definition must include both objective factors (such as the existence of a shared ethnicity, language or religion) and subjective factors (including that individuals must identify themselves as members of a minority).”

Francesco Capotorti, Special Rapporteur of the United Nations Sub-Commission on Prevention of Discrimination and Protection of Minorities, has defined the term minority as,

“A group numerically inferior to the rest of the population of a State, in a non-dominant position, whose members—being nationals of the State—possess ethnic, religious or linguistic characteristics differing from those of the rest of the population and show, if only implicitly, a sense of solidarity, directed towards preserving their culture, traditions, religion or language.”¹

After considering the above definitions, the term minority can be said to refer to national or ethnic, religious and linguistic minorities, pursuant to the United Nations Minorities Declaration. All States have one or more minority groups within their national territories, characterized by their own national, ethnic, linguistic or religious identity, which differs from that of the majority population.

II. Scope Of Minority Rights

In 2005, the High Commissioner for Human Rights appointed an Independent Expert on Minority Issues, who has identified four broad areas of concern in relation to minority protection:

- a. protecting the existence of a minority;
- b. protecting the right of minorities to enjoy their cultural identities and reject forced assimilation;
- c. ensuring effective nondiscrimination and equality; and

¹ E/CN.4/Sub.2/384/Rev.1, para. 568

- d. Ensuring effective participation of members of minorities in public life.³¹ She also has called for increased attention to minority communities in the context of poverty reduction strategies and in the promotion of political and social stability.²

She also has called for increased attention to minority communities in the context of poverty reduction strategies and in the promotion of political and social stability.³

III. Physical Protection

The 2001 Durban Declaration while laying down the scope of protection of minority rights, affirms that, “the ethnic, cultural, linguistic and religious identity of minorities, where they exist, must be protected and that persons belonging to such minorities should be treated equally and enjoy their human rights and fundamental freedoms without discrimination of any kind”⁴.

The physical integrity of persons belonging to minority groups is at greatest risk during conflicts. As former United Nations Secretary- General Kofi Annan remarked at the Stockholm International Forum in January 2004: “We must protect especially the rights of minorities, since they are genocide’s most frequent targets.”⁵

IV. Equality And Non-Discrimination

The right against discrimination is paramount in protection of minorities around the world. Non-discrimination and equality before the law are two of the basic principles of international human rights law. The principle of nondiscrimination prohibits any distinction, exclusion, restriction or preference which has the purpose or effect of impairing or nullifying the recognition, enjoyment or exercise by all persons, on an equal footing, of all rights and freedoms.⁶

The International Convention on the Elimination of All Forms of Racial Discrimination permits the implementation of special measures “for the sole purpose of securing adequate advancement of certain racial or ethnic groups or individuals requiring such protection as may be necessary in order to ensure such groups or individuals equal enjoyment or exercise of human rights and fundamental freedoms.”⁷

The Convention on the Elimination of All Forms of Discrimination against Women allows for “temporary special measures” which accelerate de facto equality between men and women.⁸ The Human Rights Committee of the UN, held that, States parties are sometimes required to, “take affirmative action in order to diminish or eliminate conditions which cause or help to perpetuate discrimination prohibited by the Covenant and such action may involve granting for a time to the part of the population concerned certain preferential treatment in specific matters as compared with the rest of the population as long as such action is needed to correct discrimination in fact.”⁹

The Committee on the Elimination of Racial Discrimination in its general recommendation No. 32 (2009), provided further guidance on the scope of the principle of non-discrimination under article 1 (1) of the Convention¹⁰ and, more importantly, the meaning of “special measures”. The Committee specified that “the list of human rights to which the principle applies under the Convention is not closed and extends to any field of human rights regulated by the public authorities in the State party to address racial discrimination ‘by any persons, group or organization’.”¹¹

The European Court’s case law on the equality guarantee in Article 14¹² enables it to determine whether minority protection is necessary in a manner that is sensitive to the particular circumstances of minority communities. In *Thlimmenos v. Greece*,¹³ the Court, for the first time, expressly held that nondiscrimination in certain circumstances requires the differential treatment of “persons who are significantly different.” Greece was held to have discriminated against Thlimmenos, a Jehovah’s Witness who had been convicted of insubordination for refusing to enlist in the military for religious reasons, by failing to introduce appropriate exceptions to the rule barring persons convicted of a serious crime from the profession of chartered accountants. *Thlimmenos* effectively introduces the concept of indirect discrimination to Convention equality jurisprudence by treating a rule that is neutral on its face but which has a disparate impact on a religious minority as a

² UN Doc. E/CN.4/2006/74.

³ UN Doc. A/HRC/4/9.

⁴ Para. 66.

⁵ United Nations press release SG/SM/9126/Rev.1, 11 February 2004.

⁶ For details see, International Convention on the Elimination of All Forms of Racial Discrimination, Art. 1 (1).

⁷ Art. 1, Para. 4. See also art. 2, Para. 2.

⁸ For details see, Art. 4, Para. 1.

⁹ The Human Rights Committee, general comment No. 18 (1989) on non-discrimination

¹⁰ Supra note 4.

¹¹ See also art. 2 (1) (d) and (b).

¹² The European Convention on Human Rights

¹³ *Thlimmenos v. Greece*, (Application No. 34369/97) (2000) 31 E.H.R.R. 411, Para. 44.

violation of equality. It suggests that the equality guarantee in Article 14 of the European Convention, in certain circumstances, imposes positive obligations on states to treat some members of society, in this case, members of a religious minority, differently than others.

V. Effective And Meaningful Participation In Public Affairs

The participation in public affairs and in all aspects of the political, economic, social and cultural life of the country by the persons belonging to minorities is essential to preserve their identity and combating their social exclusion.

Article 2 (2) of the United Nations Minorities Declaration, provides for the right of persons belonging to national or ethnic, religious and linguistic minorities “to participate effectively in cultural, religious, social, economic and public life”. For the participation of persons belonging to minorities to be effective, it is not sufficient for States to ensure their formal participation; States must also ensure that the participation of representatives of minorities has a substantial influence on the decisions which are taken, so that there is, as far as possible, shared ownership of these decisions.¹⁴

VI. Promotion And Protection Of The Identity

Promoting and protecting the identity of minorities prevent forced assimilation and the loss of cultures, religions and languages—the basis of the richness of the world and therefore part of its heritage. The meaning of term minority as enshrined in The United Nations Minorities Declaration, 1992, also includes Protection, by States, of their existence and their national or ethnic, cultural, religious and linguistic identity.¹⁵

VII. International Statutes On Minority Rights:

1. The European Convention on Human Rights

The European Convention on Human Rights, perhaps the most significant regional human rights instrument in Europe, does not expressly enshrine minority rights. Its text is thoroughly individualistic in nature, and devoted overwhelmingly to the protection of civil and political rights.

The Convention was drafted in light of wartime atrocities primarily as an instrument that would safeguard interests associated with civil and political rights from the raw exercise of collective political power. The sole express exception to its focus on civil and political rights lies in its equality guarantee, which refers to minority membership, but the Convention enshrines only the right of an individual not to be discriminated as a member of a minority defined by language, religion or national origin.¹⁶

Numerous decisions of the European Court of Human Rights – the primary judicial body responsible for interpreting the European Convention – open this jurisprudential door, suggesting that certain civil and political rights protect interests associated with minority status. Such interests merit protection because of their universal value but only in circumstances where they will not lead to political instability and conflict in the region.¹⁷

For example, in *Serif v. Greece*,¹⁸ at issue was the conviction of a Muslim religious leader for officially representing a Muslim community in Greece without being designated as such by the Greek state. The European Court held the conviction to be an interference with the applicant’s freedom of religion. It noted that divisions within religious communities creates “tensions,” but it held that “the role of the authorities in such circumstances is not to remove the cause of tension by eliminating pluralism, but to ensure that the competing groups tolerate each other.”¹⁹ It noted further that Greece had not adduced any evidence to suggest that such tension had led to “disturbances” within the Muslim population, and that the risk of such tension beyond the Muslim population to affect relations between the Muslim and Greek populations, or between Greece and Turkey, was nothing more than “a remote possibility.”

¹⁴ See A/HRC/13/23, Para. 52, in which the independent expert on minority issues refers to: Council of Europe, Advisory Committee on the Framework Convention for the Protection of National Minorities, Commentary on the effective participation of persons belonging to national minorities in cultural, social and economic life and public affairs (ACFC/31DOC(2008)001, Para. 18 and 19).

¹⁵ See Art. 1

¹⁶ See, Art. 14.

¹⁷ *Serif v. Greece* (1999), 31 E.H.R.R. 56; *Case of Socialist Party and others v. Turkey*, App. No. 20/1997/804/1007, 27 EUR. H.R. REP. 51 (1998); *Thlimmenos v. Greece* (Application No. 34369/97) (2000) 31 E.H.R.R. 411, *Belgian Linguistic Case* (1967 and 1968) 1 E.H.R.R. 241 and 252; *G. and E. v. Norway* (Application nos. 9278/81 and 9415/81) DR 35, 1985 at 30 EComm HR ; *S. v. Sweden* (Application no. 16226/90) Report of 2 September 1991 EComm HR; *Sürek v. Turkey* (No.1)(1999) (Application no. 26682/95); *Könkämä and 38 other Saami Villages v. Sweden* (1996) (Application no. 27033/95); *Buckley v. United Kingdom* (1996) 23 E.H.R.R. 101; *Hasan and Chaush v. Bulgaria* (2000) (Application no. 30985/96). For a details see, Fernand de Varennes, *Using the European Court of Human Rights to Protect the Rights of Minorities, in Mechanisms For The Implementation Of Minority Rights* 83-108 (M. Weller & A. Morawa eds., Council of Europe Publishing, 2004).

¹⁸ (1999), 31 E.H.R.R. 56.

¹⁹ *Ibid*, at Para 53

2. International Covenant on Civil and Political Rights, 1966

Organization: United Nations

Nature: Legally binding

Article 27 of the Covenant deals with minority rights.

Art. 27 - In those States in which ethnic, religious or linguistic minorities exist, persons belonging to such minorities shall not be denied the right, in community with the other members of their group, to enjoy their own culture, to profess and practise their own religion, or to use their own language.

It frames minority rights in primarily individualistic terms. This is in keeping with the Covenant's stated purpose, which is to entrench a rich panoply of civil and political rights in "recognition of the inherent dignity and of the equal and inalienable rights of all members of the human family."²⁰

The rights enshrined in Article 27 are not only framed in individualistic terms. The interests they aspire to protect can be comprehended in universal terms, as features of existence that are essential to what it means to be a human being. The capacity to participate in one's culture, to hold and exercise spiritual beliefs, and to speak to others in a common language plausibly possess universal value. That is, cultural, religious and linguistic affiliations help to shape who we are. They constitute important features of what it means to be human.²¹

3. The International Covenant on Economic, Social and Cultural Rights

mentions explicitly in article 2 (2) that "the States Parties to the present Covenant undertake to guarantee that the rights enunciated in the present Covenant will be exercised without discrimination of any kind as to race, colour, sex, language, religion, political or other opinion, national or social origin, property, birth or other status." The Committee on Economic, Social and Cultural Rights on the right to the highest attainable standard of health states that,²² health facilities, goods and services must be within safe physical reach for all sections of the population, especially vulnerable or marginalized groups, including ethnic minorities. Furthermore, all health facilities, goods and services must be culturally appropriate, for instance respectful of the culture of minorities. "States are under the obligation to respect the right to health by, inter alia, refraining from denying or limiting equal access for all persons, including minorities, to preventive, curative and palliative health services".

Declaration on the Rights of Persons belonging to National or Ethnic, Religious and Linguistic Minorities, 1992

Organization: United Nations

Nature: Legally binding (adopted by the UN General Assembly in 1992)

Art. 1(1) - States shall protect the existence and the national or ethnic, cultural, religious and linguistic identity of minorities within their respective territories and shall encourage conditions for the promotion of that identity.

Inspired by the provisions of article 27 of the International Covenant on Civil and Political Rights, this declaration further develops and elaborates on the rights of minorities. Like Article 27 of the International Covenant, the Declaration casts these rights in individualistic terms, vesting in "persons belonging to minorities." In addition, the interests that the 1992 Declaration seeks to protect – cultural, religious and linguistic affiliation, political participation, and freedom of association – are the same as those underlying Article 27. Universal in significance, they are constituent features of human identity shared by members of majorities and minorities alike.²³

However, what the 1992 Declaration requires in terms of positive measures is far from clear. It calls on states to "protect the existence and the national or ethnic, cultural, religious and linguistic identities of minorities"²⁴ but requires states simply to "adopt appropriate legislative and other measures to achieve those ends."²⁵

Similar ambiguities plague Article 27 of the Covenant. On the one hand, its drafters, and states party to its terms, assumed that it obligates states to allow minority members to engage in religious, cultural and linguistic

²⁰ International Covenant on Civil and Political Rights (1966) 999 U.N.T.S. 171 in force 1976, first preambular paragraph.

²¹ See for example Will Kymlicka, *Multicultural Citizenship: A Liberal Theory Of Minority Rights* (Oxford Univ. Press, 1995) and Charles Taylor, *The Politics of Recognition*, in *Multiculturalism: Examining The Politics Of Recognition* 25-73 (A. Gutman ed., Princeton Univ. Press, 1994).

²² General comment No. 14 (2000), The Committee on Economic, Social and Cultural Rights on the right to the highest attainable standard of health states.

²³ Other UN instruments that extend minority rights protection include the 1951 Convention on the Prevention and Punishment of the Crime of Genocide, 78 U.N.T.S. 277; the 1960 UNESCO Convention Against Discrimination in Education, 429 U.N.T.S. 93; and the 1989 Convention on the Rights of the Child 1577 U.N.T.S. 43. See also the 1993 Vienna Declaration and Programme of Action A/CONF.157/23 (12 July 1993).

²⁴ Article 4(1).

²⁵ Article 4(2).

practices but does not require states to adopt positive measures to facilitate such practices.²⁶ He also argued that, argued that the implementation of Article 27 “calls for active and sustained intervention by states.”²⁷

Ivan Kitok v. Sweden,²⁸

Under Swedish law an ethnic Sami was denied rights to herd reindeer. Kitok was a Sami living in Sami territory, and had a herd of reindeer but he was not a Sami village member. Under Swedish law, a Sami village member possesses rights to hunt and fish on a large part of the territory. It also authorizes members’ reindeer herds to graze on public and private lands. The purpose of the restrictions is to ensure the future of reindeer breeding and the livelihood of those engaged in it. The village allowed, not as of right, Kitok to hunt and fish, and to be present when calves are marked and herds rounded up and reassigned to owners, to safeguard his interests.

The UN Human Rights Committee held that “reindeer husbandry is so closely connected to the Sami culture that it must be considered part of the Sami culture itself,” and where economic activity is “an essential element in the culture of an ethnic community” it falls under the protection of the Covenant.²⁹ In *Hopu and Bessert v. France*,³⁰

The Human Rights Committee heard a complaint by indigenous Polynesians who claimed to be the lawful owners of land in Tahiti where the French Polynesian authorities were constructing a resort. The resort was being built on an indigenous historical burial ground and around a lagoon that was still used by 30 indigenous families for subsistence fishing. The Covenant does not enshrine a right to property, and Article 27 (ICCPR) was not available because France had made a reservation against its application. Instead, at issue were Articles 17 and 23, which enshrine, respectively, rights to privacy and to a family life.

With respect to the right to a family life, the state argued that the authors could not prove that their families were buried there, that they had ancestral links to those buried in the site. The skeletons predate the arrival of Europeans on the island. The Committee ruled that the term family “is to be given a broad interpretation so as to include all those comprising the family as understood in the society in question. It follows that cultural traditions should be taken into account when defining the term ‘family’ in a specific situation.”³¹ It also noted that “the relationship to their ancestors [is] an essential element of their identity” and plays “an important role in their family life.”³² It concluded that the state was in violation of rights to privacy and a family life guaranteed by the Covenant.

VIII. The Convention On The Rights Of The Child

Article 30 provides that, “in those States in which ethnic, religious or linguistic minorities or persons of indigenous origin exist, a child belonging to such a minority or who is indigenous shall not be denied the right, in community with other members of his or her group, to enjoy his or her own culture, to profess and practice his or her own religion, or to use his or her own language”.

The Basic Principles and Guidelines on the Right to a Remedy and Reparation for Victims of Gross Violations of International Human Rights Law and Serious Violations of International Humanitarian Law³³, states that “restitution should, whenever possible, restore the victim to the original situation before the gross violations of international human rights law or serious violations of international humanitarian law occurred. Restitution includes, as appropriate: restoration of liberty, enjoyment of human rights, identity, family life and citizenship, return to one’s place of residence, restoration of employment and return of property.” This principle could be broadly interpreted to include the right to have one’s status as indigenous person or person belonging to a minority restored, in particular where this is provided for under national legislation and if such status is lost as a consequence of displacement.

IX. The Convention On The Prevention And Punishment Of The Crime Of Genocide³⁴

The convention is a legal source referred to in the United Nations Minorities Declaration for protecting

²⁶ See, report by UN Special Rapporteur Francesco Capotorti on *the rights of persons belonging to Ethnic, Religious and Linguistic Minorities*, 1979 para. 211-212.

²⁷ *Ibid*, para. 217.

²⁸ (Communication 197/1985), *Official Records of the Human Rights Committee* 1987/88, vol. II, p. 442 (U.N. Doc. A/43/40 (1988)).

²⁹ *Id.* Para. 9.2.

³⁰ Francis Hopu and Tepoaitu Bessert v. France (Communication no. 549/193) views of the Human Right Committee, 29 July 1997, UN doc. CCPR/C/60/D/549/1993), at 217-222.

³¹ *Id.* Para. 10.3.

³² *Id.* Para. 10.3. For commentary, see Martin Scheinin, *The Right to Enjoy a Distinct Culture: Indigenous and Competing Uses of Land*, in *The Jurisprudence of Human Rights Law: a Comparative Interpretive Approach* 159-222 (Theodore S. Orlin, Allan Rosas, and Martin Scheinin, eds., Institute for Human Rights Abo Akademi Univ., 2000).

³³ General Assembly resolution 60/147 of 16 December 2005.

³⁴ General Assembly resolution 260 A (III) of 9 December 1948)

the rights of minorities.

Article II of the Convention defines genocide as “any of the following acts committed with intent to destroy, in whole or in part, a national, ethnical, racial or religious group, as such:

- Killing members of the group;
- Causing serious bodily or mental harm to members of the group;
- Deliberately inflicting on the group conditions of life calculated to bring about its physical destruction in whole or in part;
- Imposing measures intended to prevent births within the group;
- Forcibly transferring children of the group to another group.”

X. Framework Convention For The Protection Of National Minorities, 1995

Organization: Council of Europe

Nature: Legally binding

The convention provides the extensive and elaborate protection to national minorities.

Art. 4(1) - The Parties undertake to guarantee to persons belonging to national minorities the right of equality before the law and of equal protection of the law. In this respect, any discrimination based on belonging to a national minority shall be prohibited.

Art. 4(2) -The Parties undertake to adopt, where necessary, adequate measures in order to promote, in all areas of economic, social, political and cultural life, full and effective equality between persons belonging to a national minority and those belonging to the majority. In this respect, they shall take due account of the specific conditions of the persons belonging to national minorities

The Framework Convention provides a rich description of its ideological origins, noting that “the upheavals of European history have shown that the protection of national minorities is essential to stability, democratic security and peace,” and that toleration and dialogue are necessary to enable “cultural diversity” to be a source of “enrichment” as opposed to “division.”³⁵

Like the ICCPR and the UN Declaration, the Framework Convention refers to the rights of persons belonging to national minorities, suggesting an emphasis on individual as opposed to collective interests. The Framework Convention also narrows the scope of protection to national minorities in contrast to the 1992 UN Declaration, which also provides protection to ethnic, religious and linguistic minorities.³⁶ This is a significant departure by the framework convention from the recommendations of the Council of Europe’s Parliamentary Assembly in 1990, which proposed the entrenchment of rights of national minorities to be recognized as such, by the states in which they are located, to maintain their own cultural, educational and religious institutions, and to participate in decisions about matters that affected their identities.³⁷

XI. European Charter For Regional Or Minority Languages, 1992³⁸

Organization: Council of Europe

Nature: Legally binding

The 1992 Charter seeks to protect regional and minority languages, and not linguistic minorities. It does not enshrine any individual or collective rights for the speakers of these languages.

XII. Copenhagen Document, 1990

Organization: Organization for Security and Co-operation in Europe (OSCE)

The Copenhagen Document was formulated in a very interesting time: 1990, when the communist regimes of Central and Eastern Europe were fast dissolving. Copenhagen went much further than existing documents in providing an entire catalogue of minority rights and committing participating States to protect the rights of ethnic, cultural, linguistic and religious minorities living on their territory.

XIII. Charter Of Fundamental Rights, 2000

Organization: European Union

Nature: Legally binding

The Charter of Fundamental Rights of the European Union is now the principal EU human rights document. It became part of core EU legislation with the entry into force of the Lisbon Treaty on 1 December 2009. Art. 21 of Charter deals with minority rights as follows;

³⁵ The preamble, Framework Convention for the Protection of National Minorities, 1995

³⁶ See, R. Hoffman, *Protecting the Rights of National Minorities in Europe*, 44 GER. YRBK. INT’L L. 237 (2001).

³⁷ Council of Europe, Parliamentary Assembly Recommendation 1134, On the Rights of Minorities (1990).

³⁸ Available at, <http://conventions.coe.int/Treaty/en/Treaties/Html/148.htm>, accessed on, 10th Feb. 2014

Art. 21(1): Any discrimination based on any ground such as sex, race, colour, ethnic or social origin, genetic features, language, religion or belief, political or any other opinion, membership of a national minority, property, birth, disability, age or sexual orientation shall be prohibited.

Where the first five documents mentioned above speaks of collective rights for minority groups/communities, whereas, the EU Charter generally speaks of *individual* rights.

XIV. International Labour Organization (ILO) And Minority Rights

The **ILO Discrimination (Employment and Occupation) Convention**, 1958 (No. 111) requires States to adopt and implement national policies to promote and ensure equality of opportunity and treatment in employment and occupation, with a view to eliminating direct and indirect discrimination on grounds of race, colour, sex, religion, political opinion, national extraction or social origin.³⁹

The 1998 **ILO Declaration on Fundamental Principles and Rights at Work** provides that all members of the Organization have an obligation to respect, promote and realize the fundamental principles and rights at work (“core labour standards”). These include the principle of non-discrimination in employment and occupation, freedom of association and the right to collective bargaining, and the elimination of forced and compulsory labour, as well as child labour. The enjoyment of equality of opportunity and the treatment of minorities are monitored under this Declaration.

The application of ILO conventions is subject to supervision by the Committee of Experts on the Application of Conventions and Recommendations and the Conference Committee on the Application of Standards. In their periodic reports on the application of the Discrimination (Employment and Occupation) Convention, 1958 (No. 111), States are required to specify the action they have taken to eliminate discrimination and the results achieved. Trade unions and employers’ organizations have the right to submit observations on the Convention’s application to the supervisory bodies. In their comments and conclusions, the supervisory bodies monitor the application of the Convention in law and in practice. The Committee of Experts frequently provides comments on the enjoyment of equality of opportunity and the treatment of minorities.

Reports concerning Convention No. 111 are due every two years. The Committee meets once a year in November–December. Its report is published each year in March and discussed by the Committee on the Application of Standards during the annual session of the International Labour Conference in June.⁴⁰

The **1998 Declaration on Fundamental Principles and Rights at Work** provides for the submission of annual reports by ILO members, as well as the publication, by the Director-General, of a yearly global report on the fundamental principles and rights covered by the Declaration. The 2003 and 2007 global reports focused on eliminating discrimination at work, both considered minority issues.⁴¹

XV. The UNESCO And Mechanism For Protection Of Minority Rights

The 2003 **UNESCO Convention for the Safeguarding of the Intangible Cultural Heritage** provides safeguards and promotes the practices, representations, expressions, knowledge, skills—as well as the associated instruments, objects, arte facts and cultural spaces—that communities, groups and, in some cases, individuals recognize as part of their cultural heritage. For this purpose, the Convention establishes a fund and a listing system of representative and endangered heritage.

The 2005 **UNESCO Convention on the Protection and Promotion of the Diversity of Cultural Expressions** encourages States to incorporate culture as a strategic element in national and international development policies and to adopt measures aimed at protecting and promoting the diversity of cultural expressions within their territory. It emphasizes the importance of the recognition of equal dignity and respect for all cultures, including that of persons belonging to minorities, and of the freedom to create, produce, disseminate, distribute and have access to traditional cultural expressions, and asks States to endeavor to create environments conducive thereto.

The Committee on Conventions and Recommendations of the Executive Board examines confidential (group and individual) complaints regarding alleged human rights violations within the fields of competence of UNESCO (education, science, culture and information, especially relating to articles 18, 19, 20, 26 and 27 of the Universal Declaration of Human Rights) that occurred within the territories of UNESCO member States. The Committee is composed of 29 members and meets twice a year. It tries to resolve the reported problems in a spirit of cooperation, dialogue and mutual understanding rather than acting as a tribunal. In urgent cases, the

³⁹ See Arts. 1 and 2

⁴⁰ The comments and conclusions of the supervisory bodies are available from the International Labour Standards website of the International Labour Organization: www.ilo.org/public/english/standards/norm (accessed 24th Jan. 2013).

⁴¹ The global reports and further information on the Declaration follow-up are available on, www.ilo.org/declaration, accessed on 25th Jan 2014

Director-General may personally make humanitarian representations on behalf of alleged victims of human rights violations in UNESCO fields of competence.

XVI. Conclusion

From the above analysis it can be said that, International statutes recognizing and protecting various rights of minorities is broad enough to secure rights of minorities around the world. These rights are specifically important for the protection, development and upliftment of the minorities. The present international statutory framework for protection of the minorities, though an adequate one for effective protection of minorities, will have no effect if they are not implemented and applied in domestic laws by the concerned nations. The lack of effective implementation mechanism at the international level also adds to the restraints of these international standards. Un may, therefore take a lead in this regard, in framing the mechanism for implementation of these rights, coupled with sanction on state governments failing to observe these rights.

Image Denoising Based On Wavelet for Satellite Imagery: A Review

Bhosale Narayan P¹, Ramesh R. Manza², K. V. Kale³

^{1,2,3} (Research Scholar, Assistant professor, Professor and Head, Department of Computer Science and IT, Dr. Babasaheb Ambedkar Marathawada University, Aurangabad India.)

Abstract: In this paper studied the use of wavelet and their family to denoising images. Satellite images are extensively used in the field of RS and GIS for land possession, mapping use for planning and decision support. As of many Satellite image having common problem i.e. noise which hold unwanted information in an images. Different types of noise are addressing different techniques to denoising remotely sense images. Noise within the remote sensing images identifying and denoising them is big challenge before the researcher. Therefore we review wavelet for denoising of the remote sensing images. Thus implementing wavelet is essential to get much higher quality denoising image. However, they are usually too computationally demanding. In order to reduce the computational cost, we need to develop an efficient filter by using the wavelet for denoising the images.

Keywords: Remote Sensing Image. Wavelet. Denoising. Shrinking

I. Introduction

Wavelets have been widely used in signal and image processing for the past 20 years [1]. Many systems are monitored and evaluated for their behavior using time signals. Additional information about the properties of a time signal can be obtained by representing the time signal by a series of coefficients, based on an analysis function. One example of a signal transformation is the transformation from the time domain to the frequency domain. The oldest and probably best known method for this is the Fourier transform developed in 1807 by Joseph Fourier. An alternative method with some attractive properties is the wavelet transform, first mentioned by Alfred Haar in 1909. Since then a lot of research into wavelets and the wavelet transform is performed [2]. The basic concepts in remote sensing via satellites which show how characteristics of the satellites and onboard sensors affect the amount and quality of data collected. A sampling of ways to use the data for activities such as weather forecasting and scientific research still challenging task [3].

II. Motivation

The need of Remote Sensing Image Analysis trusted area according NASA, Temporal Resolution, Weather Forecasting, and Adjusting Contrast for Feature Identification, Lagrangian Animation, Channel Combination and color enhancement [23].

2.1 Digital library and met data analysis

The massive amount of data obtained from remote sensing sensors requires us to properly archive them and catalog for various purposes. One of the first concerns of data analysis is to see that the data is properly archived and accessed. It is being increasingly appreciated that the old methods of storing the data on digital tapes in 1600 or 6250 bpi are now obsolete for the reason that both the physical media as well as the storage pattern are inefficient. In order to see that the content and historical value of millions of RS images are not lost to future generations, research into storage media and processing for archival is pursued in the world vigorously [13].

2.2 Need of denoising satellite image

Satellite images are usually degraded by noise during image acquisition and transmission process. The main purpose of the noise reduction technique is to remove impulse noise by retaining the important feature of the images. For example, Synthetic Aperture Radar (SAR) imagery uses microwave radiation so that it can illuminate the earth surface. Synthetic Aperture Radar provides its own illumination. The intensity of impulse noise has the tendency of being either relatively high or low thereby causing loss of image details. It is important to eliminate noise in images before using them for other image processing techniques like edge detection, segmentation, registration etc. [14].

A sample MOD11 Level-2 Land Surface Temperature (LST) image generated from Terra MODIS data in bands 31 and 32 on April 4, 2000 (19:15 UTC) in California and Nevada, is displayed in an original color composite with LST, and brightness temperatures in bands 31 and 20 as RGB components. The dark area in lower left corner is Pacific Ocean. The noisy spots in grey are broken clouds as shown in Figure -1 [15]. Therefore, still satellite image processing is a challenging task for researchers.

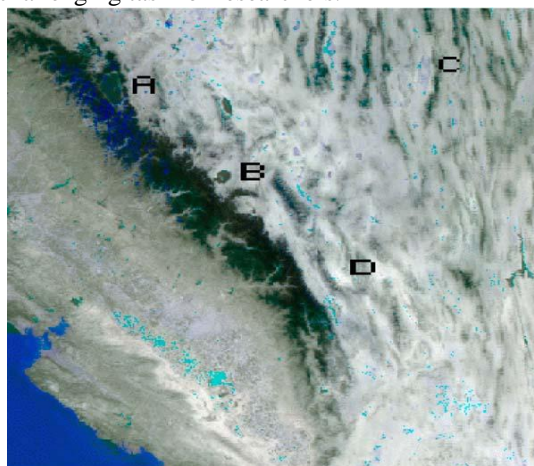


Figure: 1. MODIS Product: MOD11; Product Level: 2; MODIS Data Type: MODIS-PF.

III. Work Done So For

Jung C.R, Scharcanski J. and *et.al* [2010], In the proposed a new method for image denoising with edge preservation, based on image multiresolution decomposition by a redundant wavelet transform. In this approach, edges are implicitly located and preserved in the wavelet domain, while noise is filtered out. At each resolution, the coefficients associated to noise and coefficients associated to edges are modeled by Gaussians, and a shrinkage function is assembled. The shrinkage functions are combined in consecutive resolution, and geometric constraints are applied to preserve edges that are not isolated. Finally, the inverse wavelet transform is applied to the modified coefficients. This method is adaptive, and performs well for images contaminated by natural and artificial noise. However, these parameters could be fine-tuned to each individual image to produce optimal results. Future work will concentrate on improving our model for the wavelet coefficients, and extending our work to enhancement of noisy images [4].

Guo-shi Yang , Yun-xia Liu According [2010], they proposed new noise reduction method based on Wavelet modulus maximum for Chaotic signals and Noise, the numerical experiment results confirm the effectiveness of noise reduction for chaotic signals observed [5].

Hancheng Yu, Li Zhao and *et.al* [2009], in this paper they address an efficient algorithm for removing Gaussian noise from corrupted image by incorporating a wavelet-based trivariate shrinkage filter with a spatial-based joint bilateral filter. And In the wavelet domain, wavelet confidents are modeled as trivariate Gaussian distribution then a trivariate shrinkage filter is derived by using the maximum a posteriori (MAP) estimator. Although wavelet-based methods are efficient in image denoising, they are prone to producing salient artifacts such as low-frequency noise and edge ringing which relate to the structure of the underlying wavelet. On the other hand, most spatial-based algorithms output much higher quality denoising image with less artifacts. However, they are usually too computationally demanding. In order to reduce the computational cost, we develop an efficient joint bilateral filter by using the wavelet denoising result rather than directly processing the noisy image in the spatial domain. The filter could suppress the noise while preserve image details with small computational cost. Extension to color image denoising is also presented. We compare our denoising algorithm with other denoising techniques in terms of PSNR and visual quality. The experimental results indicate that our algorithm is competitive with other denoising techniques [10].

Sudha, S.,Suresh, G.R. and *et.al* [2007], the author has studied that the denoising of a natural image corrupted by Gaussian noise is a long established problem in signal or image processing. Even though much work has been done in the field of wavelet thresholding, most of it was focused on statistical modeling of wavelet coefficients and the optimal choice of thresholds. They proposed new method for suppression of noise in image by fusing the wavelet denoising technique with optimized thresholding function, improving the denoised results significantly. Simulated noise images are used to evaluate the denoising performance of proposed algorithm along with another wavelet-based denoising algorithm. Experimental result shows that the proposed denoising method outperforms standard wavelet denoising techniques in terms of the PSNR and the

preservation of edge information. They are compared with various denoising methods like Wiener filter, Visu shrink, Oracle shrink and Bayes shrink [11].

Zhen-Xian Lin, and *et.al* [2007], the Wavelet image denoising has been well acknowledged as an important method of denoising in Image Processing. In this paper, the principle of several wavelet denoising methods are described including the Mallat forced denoising, the wavelet transform modulus maximum method, the nonlinear wavelet threshold denoising method and the denoising based on the interrelation of wavelet domain. Also they compare with these methods and give two kinds of improved methods. The results show that it is practicable and effective for image Denoising [12].

Bingsheng Wu, Chaozhi Cai and *et.al* [2013], In the process of signal testing, often exposed to interference and influence of all kinds of noise signal, such as data collection and transmission and so may introduce noise. So in practical applications, before analysis of the data measured, the need for de-noising processing. At present, there are two de-noising methods, the traditional Filtering method and the wavelet denoising method, when in the actual test, different noise and signal with the choice of different denoising methods. Wavelet methods using denoising is an important aspect of wavelet analysis applied to the actual. This article described several commonly used principles of wavelet denoising methods, and achieved wavelet denoising method based on threshold in the Lab VIEW Which is a develop software of virtual instrument. Finally, compared to the wavelet denoising and traditional FFT denoising, and verified the superiority of the wavelet denoising [16].

Di Zhigang, Zhang Jingxuan, Jia Chunrong and *et.al* [2013], in this paper they took the hard threshold method is discontinuous on the threshold value, and soft threshold method also has defects, A new threshold function is presented to overcome the defects, and the Simulation results indicate that the new method has improved the effect of Denoising [17].

Yan Wang, Haibin Wang and *et.al* [2010], they studied to compensate for the deficiencies of traditional wavelet threshold shrinkage denoising algorithm and obtain the heart sounds with high SNR, an improved wavelet threshold shrinkage algorithm is proposed in this paper. Finally, the improved threshold shrinkage denoising algorithm is used to do noise reduction for 20 cases of the clinical heart sounds. The results indicate that the improved wavelet threshold shrinkage demonizing algorithm can eliminate noise more effectively, and has strong clinical value [18].

Ma Liyuan, Duan Yonggang, Li Yongjun and *et.al* [2010], A new threshold demonizing method is presented in this paper, which is based on the soft and hard-threshold denoising method and named by 'high-order approach method'. This method is flexible and extensively applicable. The principle and applicability of the new method is analyzed. Two common signals in Matlab are chosen to compare the demonizing effect between the new method and others. The result shows that the new method has better demonizing effect and higher SNR [19].

Wei Liu, Zhengming Ma and *et.al* [2006], In this paper, they most commonly used denoising methods use low pass filters to get rid of noise. However, both edge and noise information is high-frequency information, so the loss of edge information is evident and inevitable in the demonizing process. Edge information is the most important high-frequency information of an image, so we should try to maintain more edge information while denoising. From this comes the thesis of this paper. Moreover, they present a new image denoising method: wavelet image threshold denoising based on edge detection. Before denoising, those wavelet coefficients of an image that correspond to an image's edges are first detected by wavelet edge detection. The detected wavelet coefficients will then be protected from denoising set the denoising thresholds based solely on the noise variances, without damaging the image's edges. The theoretical analyses and experimental results presented in this paper show that, compared to commonly-used wavelet threshold demonizing methods, our method can keep an image's edges from damage and can increase the PSNR up to 1~2 dB. Finally, they draw the conclusion that edge detection and denoising are two important branches of image processing. If we combine edge detection with demonizing, we can overcome the shortcomings of commonly-used denoising methods and do demonizing without notably blurring the edge [20].

Donoho, D.L. (1995), In this paper they studied that all the general procedures related to de-noising and compression of one- or two-dimensional signals, using wavelets or wavelet packets [8,9, 23].

IV. Denoising

Denoising should not be confused with smoothing. Smoothing removes high frequencies and retains low frequencies whereas denoising attempts to remove whatever noise is present and retain whatever signal is present regardless of the spectral content of the noisy signal.

In many signal or image processing applications, the input data is corrupted by some noise which needs to be removed or at least reduced [25-27]. Wavelet denoising techniques work by adjusting the wavelet coefficients of the signal in such a way that the noise is reduced while the signal is preserved.

The accuracy of this technique depends on data type and its quality: wave-band, perpendicular and temporal baselines, ground conditions (such as vegetation and snow coverage), tropospheric noise, various techniques have been developed in order to minimize atmospheric and ionographic noise [23].

4.1 Potential disadvantages of noise filters in images

Many types of distortions limit the quality of digital images during image acquisition, formation, storage and transmission. Often, images are corrupted by impulse noise. The intensity of impulse noise has the tendency of being either relatively high or low thereby causing loss of image details. It is important to eliminate noise in images before using them for other image processing techniques like edge detection, segmentation, registration etc. Several filtering methods have been proposed in the past to address impulse noise removal (Wang & Hang 1999). One of the more famous filters for gray scale images is the standard median filter which rank orders the pixel intensities within a filtering window and replaces the center pixel with the median value. Extending the idea of a scalar median filter to color images is not straightforward due to the lack of a natural concept of ranking among the vectors. Color distortion may occur when the scalar median filter is applied separately to every single component of the color vectors. A method called Vector Median Filter (VMF) which considers all the three color components and rank orders the vectors. Various modifications of the standard VMF have been introduced like Directional Median Filter and Central Weighted Vector Median Filter. The biggest drawback of the conventional vector median approaches is that they apply median operation to each pixel, irrespective of it being corrupted or not. An intuitive solution to overcome this disadvantage is to first detect the corrupt pixels and then to apply filtering on those pixels alone [Trygve & Hakon 1999]. One of the main problems with impulse noise detection is that it is difficult to differentiate between an edge and an impulse noise. In the intensity space, both these stand as peaks in their neighborhood. The difference between the center pixel with the minimum and maximum gray value in the filtering window is taken and if greater than a certain threshold, the center pixel is considered as noise. The disadvantage of this method is that the false positive rate is very high and most of the edges also get detected as noise. Coherent processing of synthetic aperture radar (SAR) data makes images susceptible to speckles (Lee, Jukervish 1994). Basically, the speckles are signal-dependent and, therefore, act like multiplicative noise. This report develops a statistical technique to define a noise model, and then successfully applies a local statistics noise filtering algorithm to a set of actual SEASAT SAR images. The smoothed images permit observers to resolve fine detail with an enhanced edge effect. Several SEASAT SAR images are used for demonstration.

V. Wavelet Analysis

When asked to justify the values of mathematics, mathematicians often point out that idea developed to solve a pure mathematical problem can lead to unexpected applications years later. But the story of wavelet paints a more complicated and somewhat more interesting picture. In a specific applied research led to new theoretical synthesis, which in turn opened scientist eyes to new application. Good science requires us to see both the theoretical forest and practical trees. Through wavelet is organized research topic, it is only decades old, and has been in use for long time in various disciplines under different names. Morlet and Grossman were first to use word 'wavelet. Stephan Mallat brought out the relation between wavelet methodology used by Morlet and filter bank theory used in image processing applications. One such dimension of progress is in our recent ability to look beyond Fourier analysis. Fourier analysis has coped up well with naturally occurring sinusoidal behavior like ocean waves, but has not performed well in tackling discontinuities - such as edges of image features. In the recent times, a new form of mathematical technique called wavelet analysis has stormed the corridors of data analysis and its entry into remote sensing information synthesis is also dominant and certain. In contrast to the Fourier sinusoid~ which oscillates forever, a wavelet is localized in time - lasting for a few cycles. The efficiency of wavelets in depicting discontinuities has helped in solving problems of data compression and noise removal Singularities [13].

The main advantage of wavelet analysis is that it allows the use of long time intervals where more precise low frequency information is wanted, and shorter intervals where high frequency information is sought.

- Wavelet analysis is therefore capable of revealing aspects of data that other image analysis techniques miss, such as trends, breakdown points, and discontinuities in higher derivatives and self-similarity.
- Wavelets are also capable of compressing or de-noising a image without appreciable degradation of the original image.

Instead of an infinite sine wave for the transform, use a wavelet:

$$\Psi(t) = e^{j\omega_0 t} e^{-t^2/2}$$



TYPE OF WAVELET

In this below table given list of wavelet families.

List wavelets families	
Haar	haar
Daubechies	db
Symlets	sym
Coiflets	coif
BiorSplines	bior
ReverseBior	rbio
Meyer	meyr
DMeyer	dmey
Gaussian	gaus
Mexican_hat	mexh
Morlet	morl
Complex Gaussian	cgau
Shannon	shan
Frequency B-Spline	fbsp
Complex Morlet	cmor
Lemarie	lem

Table 1. Wavelets families

Haar is the compactly support wavelet, oldest and simplest wavelet. It also supports orthogonal, symmetry, Biorthogonal, DWT and CWT [22].

Finding a solution for denoising in Satellite imagery using wavelet

The wavelet transform is a mathematical tool widely used in image processing. Some applications of the transform to remote sensing images have been investigated in the literature. It was found useful for texture analysis, image compression and noise reduction. The transform allows representation of a signal onto an orthonormal basis. Each term of the basis represents the signal at a given scale. In order to decompose the signal onto the basis, the algorithm developed is applied to the signal. It consists of iterations of one-dimensional highpass and low-pass filtering steps. The algorithm creates a pyramid of low-resolution approximations as well as a wavelet pyramid in which the details are stored as wavelet coefficients [6].

Hard Thresholding:

- Ignore signals below noise threshold.
- Sharp transition from on/off.

Soft Thresholding:

- Ignore signals below noise threshold.
- Attenuates low-level signals.
- Smooth transition between on/off.

The denoising estimator is then defined as Set the threshold value [21].

VI. Conclusion And Future Scope

Image denoising has a significant role in image pre processing. As the application areas of image denoising are more, there is a big demand for efficient denoising algorithms. The intention behind this study is to reduce the convergence time of conventional filter and thereby increase its performance. Wavelet based methods are always a good choice for image denoising and has been discussed widely in literatures for the past two decades. Wavelet shrinkage permits a more efficient noise removal while preserving high frequencies based on the disbalancing of the energy of such representation. The technique denoises image in the orthogonal wavelet domain, where each coefficient is thresholded by comparing against a threshold; if the coefficient is smaller than the threshold, it is set to zero, otherwise it is kept or modified. The future scope of study to seek or design robust wavelet filter to remove noise from satellite images very efficiently.

Acknowledgement

We are very thankful to Z. Wan and his MODIS land science team, land surface temperature over California from MODIS to available to Digital image processing [23].

REFERENCES

- [1] Yinpeng Jin, Elsa Angelini, and Andrew Laine, "Wavelets in Medical Image Processing: De-noising, Segmentation, and Registration".
- [2] R.J.E. Merry, "Wavelet Theory and Application", SCT, 2005.
- [3] Karen E. Joyce, "A review of satellite remote sensing and image processing techniques", *Progress in Physical Geography* 33(2), pp. 183–207, [2009].
- [4] Jung C.R, Scharcanski J., "Adaptive Image Denoising In Scale-Space Using the Wavelet Transform", IEEE, 2010.
- [5] Guo-shi Yang ; Yun-xia Liu, A New Wavelet Modulus Maximum Method for Noise Reduction of Chaotic Signals, Electrical and Control Engineering (ICECE), 2010 International Conference on Digital Object Identifier: 10.1109/iCECE.2010.1116 Publication Year: 2010 , Page(s): 4618 – 4622.
- [6] Parthasarathy Subashini, "Image Denoising Based on Wavelet Analysis for Satellite Imagery", INTECH, Open Access Publisher, Croatia, book of Wavelet Transform.
- [7] Donoho, D.L. (1995), "De-noising by soft-thresholding," IEEE, Trans. on Inf. Theory, 41, 3, pp. 613–627.
- [8] Donoho, D.L., I.M. Johnstone (1994), "Ideal spatial adaptation by wavelet shrinkage," *Biometrika*, vol 81, pp. 425–455.
- [9] Donoho, D.L., I.M. Johnstone (1994), "Ideal de-noising in an orthonormal basis chosen from a library of bases," *C.R.A.S. Paris, Ser. I*, t. 319, pp.
- [10] Hancheng Yu , Li Zhao , Image Denoising Using Trivariate Shrinkage Filter in the Wavelet Domain and Joint Bilateral Filter in the Spatial Domain, Image Processing, IEEE Transactions on Volume: 18 , Issue: 10 Digital Object Identifier: 10.1109/TIP.2009.2026685 Publication Year: 2009 , Page(s): 2364 - 2369
- [11] Sudha, S. Suresh, G.R., Sukanesh, R. Wavelet Based Image Denoising Using Adaptive Thresholding Conference on Computational Intelligence and Multimedia Applications, 2007. International Conference on Volume: 3, 10.1109/ICCIMA.2007.305 , Page(s): 296 – 300, 2007,.
- [12] Zhen-Xian Lin ; Guo-Xiang Song ; Wen Xue Two improved methods on wavelet image denoising Machine Learning and Cybernetics, 2003 International Conference on Volume: 5 , IEEE CONFERENCE , Page(s): 2979 - 2983 Vol.5, 2003.
- [13] B L DEEKSHATULU, "Recent Trends in Remote Sensing Data Analysis", *Journal of the Indian Society of Remote Sensing*, Vol, 26, No. 3, 1998.
- [14] V. Saradhadevi, "An Enhanced Two-Stage Impulse Noise Removal Technique for SAR Images Based on Fast ANFIS and Fuzzy Decision", *European Journal of Scientific Research* ISSN 1450-216X Vol.68 No.4, pp. 506-522, © Euro Journals Publishing, 2012.
- [15] Z. Wan, MODIS land science team, land surface temperature over California from MODIS, 2000.
- [16] Bingsheng Wu, Chaozhi Cai, "Wavelet Denoising and Its Implementation in LabVIEW", *Image and Signal Processing, IEEE, CISP '09*, 2nd International Congress on Digital Object, Page(s): 1 – 4 , 2009 .
- [17] Di Zhigang , Zhang Jingxuan , Jia Chunrong , "An Improved Wavelet Threshold Denoising Algorithm", *Intelligent System Design and Engineering Applications (ISDEA), IEEE Explore*, Page(s): 297 – 299, 2013.
- [18] Yan Wang, Haibin Wang , "Junxuan Qiao An Improved Wavelet Threshold Shrinkage Algorithm for Noise Reduction of Heart Sounds", *Electrical and Control Engineering (ICECE), International Conference on Digital Object Identifier: 10.1109/iCECE 1214 , Page 5018 – 5021, 2010.*
- [19] Ma Liyuan, Duan Yonggang , Li Yongjun , Wang Tianhui, "Improved Algorithm for Denoising Based on Wavelet Threshold and Performance Analysis", *Pervasive Computing Signal Processing and Applications (PCSPA), First International Conference on Digital Object Identifier: 10.1109/PCSPA..144 Page 572 - 575, 2010.*
- [20] Wei Liu, Zhengming Ma, "Wavelet Image Threshold Denoising Based on Edge Detection " , *IMACS Computational Engineering in Systems Applications, Multiconference on, Volume-1, 10.1109/CESA4281626 , Page(s): 72 – 78, 2006.*
- [21] ImagewithdenoisingWavelet, https://www.ceremade.dauphine.fr/~peyre/numericalour/tours/denoisingwav_2_wavelet_2d/#
- [22] Wavelet toolbox Version 4.9, The Matlab Works Inc., 2012.
- [23] Z. Wan and his MODIS land science team, http://www.ssec.wisc.edu/sose/pirs_activity.html.
- [24] Øyvind Ryan, "Applications of the wavelet transform in image Processing", 1994.
- [25] Narayan P. Bhosale, Ramesh R. Manza, "Analysis of effect of noise removal filters on noisy remote sensing images", *International Journal of Scientific & Engineering Research (IJSER)*, Volume 4, Issue 10, page-1151, ISSN 2229-5518, Oct-2013
- [26] Narayan P. Bhosale, Ramesh R. Manza, "Effect of Poisson noise on Remote sensing images and noise removal using filters, IBMRD's Journal of Management & Research, ISSN: 2277-7830, Sep, 2013.
- [27] Narayan P. Bhosale, Ramesh R. Manza, "A Review on Noise removal techniques from Remote sensing Images", *National Conference at Radhai College, Aurangabad, CMS-13, by 25, 26 April, 2013.*

Pose and Illumination in Face Recognition Using Enhanced Gabor LBP & PCA

Manit Kapoor¹, Sumit Kapoor²

¹Assistant Professor, Ramgarhia Institute of Engineering and Technology, Phagwara, Punjab.

²Sr. Software Engineer, Beckman Coulter, Florida, USA.

Abstract: This paper presents the face recognition based on Enhanced GABOR LBP and PCA. Some of the challenges in face recognition are occlusion, pose and illumination. In this paper, we are more focused on varying pose and illumination. We divided this algorithm into five stages. First stage finds the fiducial points on face using Gabor filter bank as this filter is well known for illumination compensation. Second stage applies the morphological techniques for reduce useless fiducial points. Third stage applies the LBP on reduced fiducial points with neighborhood pixel for improving the pose variation. Forth stage uses PCA to detect the best variance points which are necessary to characterize the training images. The last recognition stage includes finding the Euclidean norm of the feature weight vectors with the test weight vector. In this project, we used 20 images of 20 different persons from ORL database for training. For testing, we used images with varying illumination, pose and occluded images of the same training persons. Using this algorithm, testing results has shown significant improvement performance.

Keyword: Enhanced Gabor filter, Local binary pattern, Principal component analysis, Feature selection, Recognition

I. INTRODUCTION

Face recognition is a very active research topic in the field of pattern recognition and computer vision [1]. Face recognition systems are important systems that can be used in various application areas such as entertainment, smartcards, information security, and law enforcement and surveillance. From a problems point of view, there are five major problems in face recognition which affect performance of a system: 1) Illumination variations 2) Pose changes 3) expression variations 4) time delay 5) Occlusions. Algorithms presented for pose variation are divided in two main categories based on their type of gallery images [2]. First of all, Multi-view face recognition system (FRS) [3] that requires several poses for every subject in gallery. Another category identifies probe faces that has different poses with gallery face. In general situations, a frontal face in gallery is available, but probe faces have unpredicted pose variations. So, the system must be robust for these types of situations. A key issue in face recognition is to find effective descriptors for face appearance. Hence it is difficult to develop a system which can recognize human faces under variable conditions and environment.

Face recognition has drawn a great deal of attention from the researchers and industrial communities over the past several decades. Since the early 70's, face recognition has drawn the attention of researchers in various fields, which include security, psychology, image processing and computer vision. Research in automatic face recognition started in the 1960s. Numerous approaches have been proposed, including eigenfaces [4], laplacianfaces [5], neural networks [6], elastic bunch graph matching [7], to overcome the challenges for recognition. To recognize face under illumination and pose variation of face image we introduced an image computationally the first method came into existence was template based matching. It required the administrator to locate the feature such as eyes, nose, and mouth on the photographs before it calculated distance and ratios between common reference points. This initial method had poor performance as the results were calculated manually.

Holistic methods tend to blur out small details owing to residual spatial registration errors. On the other hand, local descriptor methods have drawn increasing attention because they can capture small appearance details. Local descriptor methods include Gabor wavelets [8], Local Binary Patterns (LBP) [9], Local Ternate Patterns (LTP) [10]. Gabor wavelets were successfully used in face recognition. Moreover this method was not adaptable in any kind of variations. The approaches afterwards can be classified into two categories; including subspace based holistic feature and local appearance feature which brought a new revolution in the field of face recognition. In holistic matching method, the whole face image is represented as a high-dimensional vector. Due to the size of dimensionality, such vectors cannot be compared directly. Hence, holistic methods use dimensionality reduction techniques to resolve this problem and thus derive lower-dimensional vectors for

subsequent classification. The most popular examples among such approaches are based on Principal Component Analysis (PCA) [11] and on Linear Discriminant Analysis (LDA) [12] Independent Component Analysis(ICA)[13].

The LBP is a powerful illumination invariant texture primitive. The histogram of the binary patterns computed over a region is used for texture description. LTP is a generalization of LBP. The Local Binary Pattern is originally proposed by Ojala for the aim of texture classification, and then extended for various fields, including face recognition, face detection[14], facial expression recognition. The Local Binary Pattern is a non parametric operator which is used for describing a local spatial structure of an image. Face image is divided into several regions and LBP is applied and features are extracted over the region. These Features are concatenated to form face descriptor. Although face recognition with local binary pattern has been Proven to be a robust algorithm, it suffers from heavy Computational load due to the very high dimensional feature vectors that are extracted by concatenating the LBP histograms from each local region[24].

In 1988, Kirby and Sirovich applied principal component analysis , a standard linear algebra technique, used to transform one set of variables into another smaller set, and the newly created variables are not usually easy to interpret. ICA is a generalization of PCA, which is sensitive to high order relationship among the image pixels. The primary advantages of these techniques are that it provides more robust to the effect of noise. The local approaches, such as Gabor filter extract information from local facial features to distinguish faces, and have the advantage of robustness to environmental changes like illumination and expressional variability, so are used extensively in face recognition. The local binary pattern (LBP) features are originally designed for texture description. The operator has been successfully applied to pose change and facial expression analysis and face recognition.

The idea behind using the LBP features is that a face can be seen as a composition of micro patterns. LBP in nature represents the first-order circular derivative pattern of images, a micro pattern generated by the concatenation of the binary gradient directions. However, the first-order pattern fails to extract more detailed information contained in the input object. To the best of our knowledge, no high-order local pattern operator has been investigated for face representation. In fact, the high-order operator can capture more detailed discriminative information. Some high-order non local pattern methods have been successfully used to solve the face recognition problem.

We work on face recognition with combining the holistic, local approach and LBP. Gabor wavelets capture the local structure corresponding to specific spatial frequency, spatial locality, and selective orientation which are demonstrated to be discriminative and robust to illumination and expression changes. LBP operator which describes the neighboring changes around the central point is a simple yet effective way to represent faces. In this paper, these combinations of LBP and Gabor features have improved the face recognition performance significantly compared to the individual representation. The feature points extracted using Gabor Filter and LBP on feature point that shows better response irrespective of the illumination, rotation and occlusion. The performances of three statistical face recognition techniques namely Principal Component Analysis (PCA) Combined LBP Gabor and PCA for selecting fiducial points gives better recognition result.

Facial feature point extraction is explained overview of Gabor Filter, LBP and PCA for better recognition. Last sections will give the comparison of experimental results and compare all the results with conclusion that how it improves illumination and pose variation recognition.

II. Enhanced Gabor Feature Extraction

Gabor filters are used in representation of face due to their biological relevance and computational properties. Gabor filters are principally band pass filters which exhibit desirable characteristics of spatial localization and orientation selectivity, spatial frequency selectivity and quadrature phase relationship. Gabor filter representations of face image are robust for illumination and expressional variability, so are used extensively in face recognition. Therefore, when the goal is the derivation of local and discriminating feature, adopting Gabor transformation has become a popular method of feature extraction. In our work, 2D Gabor wavelet is applied to create are presentation of facial features. The Gabor kernels can be defined as following:

$$\Psi_{\mu,v}(z) = \frac{\|k_{\mu,v}\|^2}{\sigma^2} e^{-(\|k_{\mu,v}\|^2 \|z\|^2 / 2\sigma^2)} \left[e^{ik_{\mu,v}z} - e^{-\left(\frac{\sigma^2}{2}\right)} \right] \quad (1)$$

Where μ and v define the orientation and scale of the Gabor kernels, $z=(x, y)$, $\| \cdot \|$ denotes the norm operator, and the wave vector $k_{\mu,v}$ is defined as follows:

$$k_{\mu,v} = k_v e^{i\Phi_\mu} \quad (2)$$

Where $k_v = \frac{k_{\max}}{f^v}$ and $\Phi_\mu = \frac{\pi\mu}{g}$. f is the spacing factor between kernels in the frequency domain. The Gabor Kernel is a product of Gaussian envelope which is shown outside the square brackets in and a complex plane wave which is the first term inside the square brackets determines the oscillatory part of the kernel and the second

term compensates for the dc value. The remaining kernels can be generated from the mother wavelet by scaling and rotating the mother wavelet.

The Gabor wavelet representation of an image has been designed image features at different locations having different frequency can be extracted by convolving the image $I(x, y)$ with the filters. Let $I(x, y)$ be a gray scale image, the convolution of image I and a Gabor kernel QPM is defined as follows

$$O_{\mu, \nu} = I(z) * \varphi_{\mu, \nu}(z) \tag{3}$$

Where $z=(x, y)^*$ denotes the convolution operator, and $O_{\mu, \nu}$ is the convolution result corresponding to the Gabor kernel at orientation μ and scale ν .

Enhanced Gabor filter is enhancement in Gabor filter with the use of morphological techniques that adjust the contrast and clearing the border in an image and label only the useful feature points. These are used for feature extraction, texture analysis and texture segmentation, target detection, fractal dimension management, Document analysis, edge detection, retina identification, image coding and image representation. The main advantage of this approach is that if prominent facial features are occluded, for instance due to facial hair, glasses or expressions even then the algorithm should still recognize the face optimally basing on the features extracted from other regions of the face. However, they perform poorly when classifying face images having even a slight side rotation.

III. Local Binary Pattern (LBP)

The LBP operator is one of the best performing texture Descriptors The standard version of the LBP of a pixel is formed by thresholding the 3X3 neighborhood of each pixel value with the center pixel's value and concatenating the results binomially to form a number. Let Z_0 be the center pixel gray level and Z_i ($i=0, 1, 7$) be the gray level of each surrounding pixel. Fig.1 illustrates the basic LBP operation. If Z_i is smaller than Z_0 , the binary result of the pixel is set to 0 otherwise set to 1 is in equation. The eight binary associated with eight neighbors are the read sequentially in clockwise direction to form binary equivalent. This binary equivalent in decimal system may be assigned to the central pixel and may be used to characterize to local texture is shown in fig 2.

$$f(I(Z_0), I(Z_i)) = \begin{cases} 0, & \text{if } I(Z_i) - I(Z_0) \leq \text{threshold} \\ 1, & \text{if } I(Z_i) - I(Z_0) > \text{threshold} \end{cases}, i=1, 2, \dots, 8$$

This method makes use of the most frequently occurred patterns to capture descriptive textural information. LBP is a grayscale invariant texture measure and is a useful tool to model texture images.

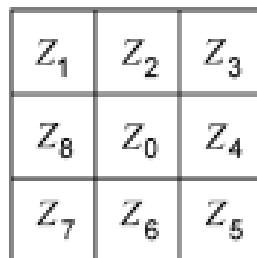


Figure 1. Eight neighborhood around central pixel Z_0

An LBP can also be considered as the concatenation of the binary gradient directions, and is called micro pattern. When the threshold is set to zero. The histograms of these micropatterns contain information of the distribution of the edges, spots, and other local features in an image. LBP has been successfully used for face recognition.

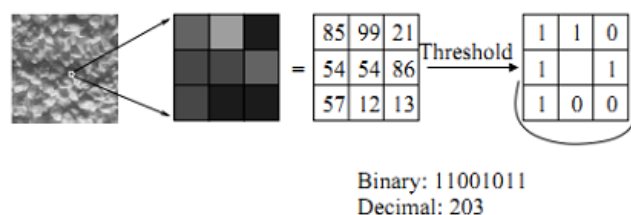


Figure 2. Calculating LBP from 3x3 window

IV. Principal Component Analysis

The Principal component analysis (PCA) is often referred to as a technique for reducing the number of variables in a data set without loss of information, and as a possible process for identifying new variables with greater meaning. Unfortunately, while PCA can be used to transform one set of variables into another smaller set, the newly created variables are not usually easy to interpret. PCA has been most successful in applications such as image compression. In many applications, PCA is used to reduce the dimensionality of a data set consisting of a large number of interrelated variables, while retaining as much as possible of the variation present in the data set. The most of the variation PCA identify directions in which there is very little variation. The eigenvectors correspond to the directions of principal components of the original data and their statistical significance is given by their corresponding eigenvalues. The eigenvectors constitute the transformation matrix. Eigen-vectors are unit vectors that identify the basic characteristics of the input data in a nonparametric format so eigenvectors are also called basis vectors. The eigenvectors form the basis of the feature space and the eigenvalues show the weightings of the individual contributions of the eigenvectors. Since the eigenvectors are unit vectors, their contribution incompletely normalized. However, the relative importance of the eigenvectors is indicated by the corresponding eigenvalues. The larger the eigenvalue the more the associated eigenvector contributes to explaining the variance of the input data. The significant eigenvalues and their associated eigenvector called principal components.

4.1. PCA Algorithm

As the standard PCA algorithm is well known, we briefly define in the algorithm. In Standard PCA consists of two stages, Training stage and Recognition stage. Training stage is used to convert the original space to subspace using basis vectors correspond to maximum variance direction in the original space is in fig 3. Let p-dimensional space data is transformed to q-dimensional data using the linear transformation. Where $q \ll p$ which is of key importance in case of large database. Let us see how the transformation function is derived and face space is formed. Suppose the given database consists of K number of $M \times N$ size images. We adjust these images column wise vectors of $((M \times N) \times K)$ size so that we can calculate the covariance matrix for one dimension signal which is of less complexity. We then calculate the mean vector of all images and mean adjusted them to ensure that the Eigen vector corresponding to Eigen value represents the dimension in Eigen space in which variance of vectors is maximized in correlation sense.

$$B = x_i - \bar{x}_i \tag{4}$$

$$\bar{x} = \frac{1}{K} \sum_{i=0}^K x_i \tag{5}$$

x_i is column vector of i^{th} image. The covariance matrix is found from the mean subtracted vectors.

$$C = B \times B^T \tag{6}$$

The linear transform function can be found using Eigen vectors corresponding to Eigen values (i.e., selected by thresholding process) found from the covariance matrix.

$$\lambda_i e_i = C e_i \tag{7}$$

By solving the equation 4 we get Eigen values (λ_i) and corresponding Eigen vectors (e_i). The Eigen values are arranged in decreasing order because the largest Eigen values one of more importance as they represent maximum variance in the space. We select the Eigen values by thresholding because not all Eigen values are necessary to represent the original space and this helps in dimension reduction. The corresponding Eigen vectors of selected Eigen values are used to linearly transform the original space to feature space or face space.

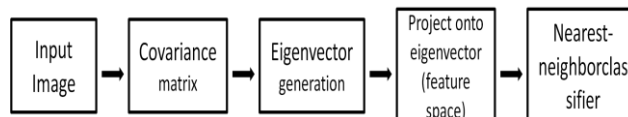


Figure 3. Principal Component analysis

The eigenvectors correspond to the directions of principal components of the original data and their statistical significance is given by their corresponding Eigenvalues. The database images are then projected onto this feature space (the feature space is the collection of parameters) or face space.

The recognition stage consists of mean adjusted test image projected onto face space. Then Euclidean distance is calculated between projected test image and all projected images in the face space. The image satisfying the minimum Euclidean distance will be the matched face. Thus the projected test image (noisy image) is gradually replaced by the stored image or restoring the image.

V. Combined Recognition With Enhanced Gabor LBP And PCA

In paper, Gabor filter bank is proposed and combined with the local binary pattern. Both the theoretical analysis and the experiment results show that the combined LBP Gabor filter is effective for illumination and pose variation. In our experiments, we choose 6 orientations and 5 frequencies and 30 Gabor filters are combined to form a Gabor filter bank. We are taking the 10 database images for training the recognition system. The noise is removed by applying the median filter and Gabor bank is used for extracting the feature points. The morphological enhancement is used to correct uneven illumination and reduce the useless feature points. This filtering can be used together to enhance contrast and clearing the border in an image and label only the useful feature points. Then take centroid of each labeled region of the image.

The LBP is applied on that features points. It automatically identify the feature points the neighborhood pixel of 3x3 windows threshold to the binary equivalent that improves the head rotated face image. In order to reduce the dimension further, Principal Component Analysis (PCA) is applied in which each image is represented by a t-dimensional feature vector. The PCA can be used to transform the t-dimensional vector into a f-dimensional vector, where normally $f \ll t$ then we can project the test vector to the lower space and calculate the minimal Euclidean distances between these vectors. Closest vector is the exact recognized face image.

The recognition process is occur in two stages testing stage having one test face image and training stage. In which the training the database of all the training face images and check the Euclidian distance between the test and trained image.

VI. Experiments And Results

6.1 Experimental Data

In the experiment we are taking the 10 training set database images as shown in Fig 4. We are testing the training database face images at different conditions light, crop, pose and expressions changes. We trained the database images with Gabor LBP and PCA algorithm and then test all the face images having different conditions is shown in fig 5. The degree of recognition is tested on expression and light gives better results in fig:6.



Figure 4. Sample Images for training set database



Figure 5. Experimental results of combined Gabor LBP and PCA



Figure 6. Face expression and light image with Gabor LBP & PCA

The comparison results of combined Local binary pattern (LBP) Enhanced Gabor filter and principal component analysis (PCA) shows the pose variation improves 79.48% and light effect improves 95.98% so recognition rate increases and recognition improves.

Table1: Test Results For LBP Enhanced Gabor+PCA and PCA

Database	LBP+Enhanced Gabor+PCA	Gabor+PCA	PCA	No. of Images
Light	95.98	90	50	20
Crop	70.25	65	50	20
Pose variation	79.48	55	46	10
Light + Crop	59	55	22.5	40
Expression	85.51	84.21	78.95	19
Expression+Light	53	45	40	20
Expression+Light+Crop Pose change	56	50	50	10

VII. Conclusion And Future Work

The Combined performance of Gabor LBP and traditional PCA algorithm gives better result on illumination and pose variation. The Gabor filter bank with different frequencies and orientations outputs finds the large number of important fiducial facial feature points all over the face. If some portion of the face is occluded then the remaining feature points are enough to represent the face. The LBP is applied on Gabor feature points and with neighborhood window improves the pose variation recognition result. In this way the proposed algorithm outperforms the traditional PCA algorithm in case of occlusion and non uniform pose and illumination changes. We also modified the selection criteria for the fiducial points by using morphological techniques. This gave good results compare to simple Gabor and PCA in case of combination attacks like illumination and occlusion, illumination and expression change. The combined performance improves efficient of face recognition but poor performance for large pose variation or orientation change.

REFERENCES

- [1] Roberto Brunelli and Tomaso Poggio, Face Recognition: Features versus Templates, IEEE transactions on pattern analysis and machine intelligence, vol. 15, no. 10, October 1993.
- [2] Ki-Chung Chung, Seok-Cheol Kee and Sang Ryong Kim, Face Recognition using Principal Component Analysis of Gabor Filter Responses, HCI Lab, Samsung Advanced Institute of Technology San 14, Nongseo-Ri, Kiheung-Eup, Yongin City, Kyungki-Do, 449-712, Korea.
- [3] Wei Zhao, Jeong-Sun Park, and Sang Woong Lee, fully automatic face detection and facial feature points extraction using local gabor filter bank and pca” Proceedings of the 2011 International Conference on Machine Learning and Cybernetics, Guilin, 10-13 July, 2011.
- [4] P.N. Belhumeur, J.P. Hespanha, and D.J. Kriegman, Eigenfaces vs Fisherfaces: Recognition using class specific linear projection, IEEE Trans. Pattern Anal. Mach. Intell., vol. 19, no. 7, pp. 711–720, Jul.
- [5] Weiqun Luo, ”Face Recognition Based on Laplacian Eigenmaps”. School of Information Engineering.
- [6] A. Torralba and A. Oliva. Statistics of natural image categories. Network: Computation in Neural Systems 14(3):391–412, 2003.
- [7] Laurenz Wiskott, Jean-Marc Fellous, ”Face Recognition by Elastic Bunch Graph Matching” University of Southern California, Los Angeles, CA
- [8] W. Choi, S. Tse, K. Wong, and K. Lam, ”Simplified Gabor wavelets for human face recognition,” Pattern Recognition, Vol. 41, pp. 1186–1199, 2008.
- [9] K. Meena & Dr. A. Suruliandi Assistant Professor, Computer Science & Engg. ”Performance Evaluation Of Local Binary Patterns And It’s Derivatives For Face Recognition” ICETECT 2011.
- [10] Baochang Zhang, Yongsheng Gao, Senior Member, IEEE, ”Local Derivative Pattern Versus Local Binary Pattern: Face Recognition With High-Order Local Pattern Descriptor” IEEE transactions on image processing, vol. 19, No. 2, february 2010.
- [11] Victor-Emil Neagoe, Ioan-Anton Stanculescu, Face Recognition using PCA versus ICA versus LDA cascaded with the Neural Classifier of Concurrent Self-Organizing Maps, 978-1-4244-6363-3/10/\$26.00c 2010 IEEE
- [12] Juwei Lu, Kostantinos N. Plataniotis, and Anastasios N. Venetsanopoulos, ”Face Recognition Using LDA-Based Algorithms,” IEEE transactions on neural networks, vol. 14, no. 1, January 2003.
- [13] M. S. Bartlett, J. R. Movellan, and T. J. Sejnowski, ”Face recognition by independent component analysis,” IEEE Trans. Neural Netw., vol. 13, no. 6, pp. 1450–1464, Jun. 2002.
- [14] S. A. Pardeshi and S. N. Talbar, ”Face recognition by automatic detection of important facial feature points,” Proc. IEEE sponsored 1st international conference on signal and image processing, India, Vol. 2, 2006, pp. 687–691.
- [15] Zhen Lei, Shengcai Liao, Matti Pietikäinen, Senior Member, IEEE, ”Face Recognition by Exploring Information Jointly in Space, Scale and Orientation” IEEE transactions on image processing, vol. 20, no. 1, january 2011.



International Journal of Modern Engineering Research (IJMER)

Volume : 4 Issue : 4 (Version-5)

ISSN : 2249-6645

April - 2014

Contents :

- | | |
|---|-------|
| Review of Intrusion and Anomaly Detection Techniques
<i>Qamar Rayees Khan, Muheet Ahmed Butt, Majid Zaman, Mohammad Asger</i> | 01-07 |
| Seasonal Variational Impact of the Physical Parameters On Mohand Rao River
Flowing In the Doon Valley
<i>Prashant-Dwivedi, Purandara Bekal, Kartikeya Dwivedi, D. N. Pandey</i> | 08-26 |
| Feature Extraction from the Satellite Image Gray Color and Knowledge Discovery
Using Association Rule Mining
<i>Yusuf Khan, Ravindra Gupta</i> | 27-35 |
| Numerical Analysis Of Header Configuration Of Plate-Fin Heat Exchanger
<i>Pardeep, Dr. M. K. Sinha</i> | 36-40 |
| Structural Analysis of Ladder Chassis Frame for Jeep Using Ansys
<i>Vishal Francis, Rajnish Kumar Rai, Anup Kumar Singh, Pratyush Kumar Singh, Himanshu Yadav</i> | 41-47 |
| Data Mining Techniques in Higher Education an Empirical Study for the
University of Palestine
<i>Rasha Ragheb Atallah, Samy S. Abu Naser</i> | 48-52 |
| Advanced Micro-Grids
<i>Raveesha S. H., Ashoka H. N.</i> | 53-65 |

Review of Intrusion and Anomaly Detection Techniques

Qamar Rayees Khan¹, Muheet Ahmed Butt², Majid Zaman³,
Mohammad Asger⁴

^{1,4} Baba Ghulam Shah Badshah University, Rajouri (J&K), India.

^{2,3} University of Kashmir, Srinagar, (J&K), India

Abstract: *Intrusion detection is the act of detecting actions that attempt to compromise the confidentiality, integrity or availability of a resource. With the tremendous growth of network-based services and sensitive information on networks, network security is getting more and more importance than ever. Intrusion poses a serious security threat in a huge network environment. The increasing use of internet has dramatically added to the growing number of threats that inhabit within it. Intrusion detection does not, in general, include prevention of intrusions. Now a days Network intrusion detection systems have become a standard component in the area of security infrastructure. This review paper tries to discuss various techniques which are already being used for intrusion detection.*

Keywords: *Anomaly, Data Confidentiality, False Positive, Intrusion, Misuse.*

I. Introduction

Intrusion detection starts with instrumentation of a computer network for data collection. Pattern-based software sensors monitor the network traffic and raise alarms when the traffic matches a saved pattern. Security analysts decide whether these alarms indicate an event serious to warrant a response. A response might be to shut down a part of a network, to phone the internet service provider associated with suspicious traffic, or to simply make note of usual traffic for future reference [19].

This paper presents overview in the area of intrusion detection. We have divided the work into three sections: the first section analyzes anomaly detection systems and their performance. It gives a short overview of statistical methods for anomaly detection, Predictive pattern generation for anomaly detection and program based anomaly detection. The second section presents an overview of misuse detection techniques: language base misuse detection, expert systems and high level state machines for misuse detection. The third section presents an overview of specification based approaches to intrusion detection: process, behavior monitoring and process state analysis. Each of the subsections gives a short overview of the techniques of interest and then presents the data set used.

Background

If the network is small and signatures are kept up to date, the human analyst solution to intrusion detection works well. But when organizations have a large, complex network the human analyst quickly become overwhelmed by the number of alarms they need to review [19]. The sensors on the large networks, will generate over millions alarm per day and that number is increasing. This situation arises from ever increasing attacks on the commercial tools typically do not provide an enterprise level view of alarms generated by multiple sensor vendors. Commercial intrusion detection software packages tend to be signature oriented with little or no state information maintained. These limitations led us to investigate the application of data mining to this problem.

A secure network must provide the following:

1. **Data Confidentiality:** Data that are being transferred through the network should be **accessible** only to those that have been properly authorized.
Data integrity: Data should maintain their integrity from the moment they are transmitted to the moment they are actually received. No corruption or data loss is accepted either from random events or malicious activity.
2. **Data availability:** The network should be resilient to Denial of Service attacks.

The first threat for a computer network system was realized in 1988 when 23-year old Robert Morris launched the first worm, which override over 6000 PCs of the ARPANET network. On February 7th, 2000 the first DoS attacks of great volume were launched, targeting the computer systems of large companies like Yahoo!, eBay, Amazon, CNN, ZDnet and Dadet. More details on these attacks can be found at [20].

The ideal approach to securing the network is to remove all security flaws from individual hosts, but less expensive and more feasible approaches are used for securing the computer systems. Most computer systems have some kind of security flaw that may allow intruders or legitimate users to gain unauthorized access to sensitive information. Moreover, many computer systems have widely known security flaws that are not fixed due to cost and some other limitations. Even a supposedly secure system or network can still be vulnerable to insiders misusing their privileges or it can be compromised by improper operating practices. So the ideal approach to secure a system can be to identify the process (system) with abnormal behavior and try to fix it.

II. Techniques

The two basic approaches to intrusion detection are misuse intrusion detection and anomaly intrusion detection. In *misuse intrusion* detection, known patterns of intrusion (intrusion signatures) are used to try to identify intrusions when they happen.

In *anomaly intrusion* detection, it is assumed that the nature of the intrusion is unknown, but that the intrusion will result in behavior different from that normally seen in the system. Many detection systems combine both approaches

1.1 Anomaly Detection

1.1.1 Statistical Methods for Anomaly Detection

In statistical Method for Anomaly detection, the NIDS observes the activity of systems under study and generates some valuable information that is stored in the form of profiles to represent the behavior of the system. The profile contains four different sets of measures i.e. activity intensity measure, audit record distribution measure, categorical measures and ordinal measures. At every point of time two profiles are maintained for each system a current profile and a stored profile. As the records are processed the NIDS updates the current profile and calculates the abnormal behavior if any by comparing the current profile with the stored profile using a function of abnormality for all the measures in the profile. The stored profile is updated from time to time by merging it with the current profile. Statistical methods suffers from a major drawback i.e. a skilled attacker can train the method so that it can accept an abnormal behavior as normal secondly not all the behaviors can be modeled as (Kumar 95).

a) Haystack

Haystack [1] is an example of statistical anomaly-based IDS. It uses both user and group-based anomaly detection. It models system parameters as independent, Gaussian random variables. Parameters are considered as abnormal when they fall out of 90% of the data range for the variable. It maintains a database of user groups and individual profiles. If a user has not previously been detected, a new user profile with minimal capabilities is created using restrictions based on the user's group membership. It is designed to detect six types of intrusions: attempted break-ins by unauthorized users, masquerade attacks, penetration of the security control system, leakage, DoS attacks and malicious use.

b) Bayesian classification

Bayesian classification automatically determines the most probable number of classes for the data, continuous and discrete measures can be freely mixed. On the other hand, this approach does not take into account the interdependence of the measures, it is unclear whether the algorithm can perform classification incrementally as needed for on-line processing, suffers from difficulty to determine thresholds, susceptibility to be trained by a skillful attacker etc.

1.1.2 Predictive Pattern Generation for Anomaly Detection

Predictive pattern generation for anomaly detection takes into account the relationship and ordering between events. It assumes that events are not random, but follow a distinguishable pattern. Such methods learn to predict future activities based on the most recent sequence of events and flag events that deviate significantly from the predicted.

a) Machine learning

T. Lane and C. Brodley applied the machine learning approach to anomaly detection in [2]. They built user profiles based on input sequences and compared current input sequences to stored profiles using a similarity measure. To form a user profile, the approach learns characteristic sequences of actions generated by users. For learning patterns of actions the system uses the sequence as the unit of comparison. A sequence is defined as an ordered, fixed-length set of temporally adjacent actions, where actions consist of UNIX shell commands and their arguments. To characterize user behavior they used only

positive examples. For the purpose of classification, sequences of new actions are classified as consistent or inconsistent in reference to sequence history using a similarity measure. To classify the attack, they classify the similarity of each input sequence, yielding a stream of similarity measures. If the mean value of the current window is greater than the threshold then it is classified as normal.

b). Time-based inductive generalization

Teng, Chen and Lu [3] developed a technique that applies a time-based inductive learning approach to security audit trail analysis. The system developed sequential rules. The technique uses time-based inductive engine to generate rule-based patterns that characterize the normal behavior of users. Each event is one single entry in the audit trail and is described in terms of a number of attributes (event type, image name, object name, object type, privileges used, status of execution, process ID, etc). The events in the audit trail are considered to be sequentially related. Rules identify common sequences of events and the probability of each sequence being followed by other events. Rules with a high level of accuracy and high confidence are kept, less useful rules are dropped. They define two types of anomaly detection: deviation detection and detection of unrecognized activities. Low probability events are also flagged, using a threshold. Anomaly is detected if either deviation or unrecognized activity is detected. This method can identify the relevant security items as suspicious rather than the entire login session and it can detect some anomalies that are difficult to detect with traditional approaches. It's highly adaptive to changes, can detect users who try to train the system, activities can be detected and reported within seconds. On the other hand, some unrecognized patterns might not be flagged since the initial, predicting portion of the rule may be matched.

2.1.3. Program-Based Anomaly Detection

a) Program Modeling

The program modeling approach (Garth Barbour Ph.D. thesis [4]) presents an algorithm that efficiently learns the program behavior. The author claims that the number of false positives never increases with additional training. If there is a false positive, the representation can learn to accept the run in the future without negatively impacting the performance of other runs. He also claims that his technique can detect novel attacks as they occur, without manual specification of program behavior or attack signatures. His algorithm learns an approximation of the program's behavior. The number of false positives decreases with training set size. He uses a non-statistical method since statistical methods would miss minor deviations. Barbour presents an algorithm that learns program behavior, without any input parameters presented in addition to his algorithm, which would add more reliability to his results. Input parameters may add additional reliability to detection because in programs with significant number of system calls, we may have different arguments associated with those system calls. If a program with limited capabilities is observed, it does not generate too many different system calls and, hence it is easy to detect any misuse of that program. On the other hand, if we are dealing with a powerful program, it generates a significant number of system calls and therefore, it is more difficult to detect misuse of that program.

b) Computational Immunology

Stephanie Forrest is investigating anomaly detection on system processes from the perspective of immunology [6], [7], [8]. In [6] the authors base their approach on the immunological mechanism of distinguishing self from non-self and [7] use look ahead pairs. They take short sequences of system calls, called n-grams that represent samples of normal runs of programs and compare them to sequences of system calls made by a test program. If any run has a number of mismatches that is higher than a certain number (percent), it is flagged as anomalous. They extended their work to variable length sequences, based on random generation of examples of invalid network traffic to detect anomalous behavior. Unlike Barbour [4], where there is no delay in detecting anomalies, the approach of Forrest has a certain delay due to the fact that the program computes the percent mismatch to be able to flag or not flag the run as anomalous. Hofmeyr [7] used the rule of r contiguous bits and showed that fixed length sequences give better discrimination than look-ahead pairs. Christina Warrender [8] modelled normal behavior of data sets described below using stide, t-stide, RIPPER and HMMs. She compared learning methods for application to n-grams: enumerating sequences using look-ahead pairs and contiguous sequences, methods based on relative frequency of different sequences, RIPPER (a rule-learning system) and HMMs. They used RIPPER to learn rules representing the set of n-grams. Training samples consisted of set of attributes describing the object to be classified and a target class to which the object belongs. RIPPER takes training samples and forms a list of rules to describe normal sequences. For each rule a violation score is established. Each set that violates a high confidence rule is a mismatch. They created HMMs so that there is one state for each n-gram.

The results showed that HMMs performed marginally better than other methods. She showed that HMMs performed only marginally better than other simple and not computationally expensive methods and concluded that the choice of data stream (short sequences of system calls) was more important than the particular method of analysis.

c). Variable-length audit trail patterns

Wespi [9] points out that usage of fixed-length patterns to represent the process model in [6] has no rule for selecting the optimal pattern length. On the other hand, Forrest *et.al.* [7], [8] point out that the pattern length has an influence on the detection capabilities of the IDS. Wespi *et al.* Initially were not able to prove significant advantage of variable-length patterns in [10]. Later, in [9] they showed that the previously stated method outperforms the method of Forrest *et. Al* [7], [8]. They use functionality verification test (FVT) suites provided by application developers to generate a training set based on the normal program's specified behaviors. Their system consists of an off-line and on-line part.

In the next step they apply the Teiresias algorithm [11] to generate the list of maximal variable-length patterns followed by some pruning during their preprocessing. During operation, a recursive pattern matching algorithm attempts to find the best matches for the test run. The measure of anomaly is the longest sequence of unmatched events (more than six consecutive unmatched events are treated as an intrusion). Initial work generated variable-length patterns using a suffix-tree constructor, a pattern pruner, and a pattern selector. ID based on this technique can detect the attacks but is prone to issue false alarms. Then they used a modified version of the pattern generator to create variable-length patterns that reduce the number of false alarms substantially without reducing the ability to detect intrusions. The authors claim that their algorithm performs better than the fixed-length sequences of Stephanie Forrest, but they compare their algorithm only for the ftpd process and then claim that their algorithm outperforms algorithms presented in [6],[7]. This is arguable because it might be the case that they presented one example where their algorithm outperformed the other algorithms and did not present the instances where their algorithm failed. Hence, we can conclude that on that specific process algorithm of Wespi *et. al.* [9] did outperform the algorithm of Forrest *et. al.* [6], [7] but, on the other hand, that may or may not be true for other processes.

d) Program Behavior Profiles

The work of Ghosh *et. al.* [5] is based on the work of the UNM group. The goal of their approach was to employ machine learning techniques that can generalize from past behavior so that they are able to detect new attacks and reduce the false positive rate. The first approach they used was equality matching. The database used was the normal behavior of programs. Instead of using trace, they use BSM data to collect the system call information and collect them into fixed size windows. They used the fact that the attacks cause anomalous behavior in clusters, like Kosoresow in [12]. Their decision choice looks for local clustering of the mismatches. The second model was the feed-forward topology with back propagation learning rules. Database was not on per-user basis like in [2], but they built profiles of software behavior and malicious software behavior. During training many networks were trained for each program and the network that performed the best was selected. The training process consisted of exposing networks to four weeks of labeled data and performing back propagation algorithm to adjust weights. They trained Artificial Neural Networks (ANN) to recognize whether small, fixed sequences of events are characteristic of the programs in which they occur. For each sequence, the ANN produces an output value that represents how anomalous the sequence is the leaky bucket algorithm was used to classify the program behavior and using leaky bucket they made use of the rule that two close anomalies have higher influence than when they are apart. The final approach was Elman network, developed by Jeffrey Elman, since they wanted to add information about the prior sequences (DFA approach lacked flexibility and ANNs have the ability to learn and generalize). In order to generalize they employ a recurrent ANN topology of an Elman network. They train the network to predict the next sequence that will occur at any point in time. The Elman network approach had the best results, with 77.3% detection and no false positives and 100% detection and fewer false positives than in two other cases. They also tried two approaches in which they used FSMs for their representation. Audit data was condensed into a stream of discrete events, where events are system calls recorded in data. Separate automata are constructed for different programs whose audit data are available for training. The training algorithm is presented with a series of n-grams taken from non-intrusive BSM data for a given program. The audit data is split into sub-sequences of size $n + 1$ (n elements define a state and 1 element is used to label a transition coming out of that state). The second FA-like approach, called a string transducer makes an attempt to detect subtler statistical deviations from normal behavior. It associates a sequence of input symbols with a series of output symbols. During training they estimate the probability distribution of the symbols at each state and during testing, deviations from this probability distribution indicate anomalous behavior. They use FA whose states correspond to n-grams in the BSM data. For each state they also record information about successor n -grams that are observed in the training data. During training their goal is to gather statistics about successor n -grams. They estimate the probability of each n -gram by counting.

1.1.3 Anomaly detection using data mining

The ADAM (Audit Data Analysis and Mining) system [13] is an anomaly detection system. It uses a module that classifies the suspicious events into false alarms or real attacks. It uses data mining to build a customizable profile of rules of normal behavior and then classifies attacks (by name) or declares false alarms. ADAM is a real-time system. To discover attacks in TCPdump audit trail, ADAM uses a combination of association rules, mining and classification. The system builds a repository of normal frequent item sets that hold during attack-free periods. Then it runs a sliding window online algorithm that finds frequent item sets in the last D connections and compares them with those stored in the normal item set repository. With the rest, ADAM uses a classifier which has previously been trained to classify the suspicious connections as a known type of attack, unknown type or a false alarm.

Association rules are used to gather necessary knowledge about the nature of the audit data. They derive a set of rules in form $X \rightarrow Y$, where X and Y are sets of attributes. There are two parameters associated with a rule: *support* s and *confidence* c . The definitions of s and c are as follows. The rule $X \rightarrow Y$ has support s in the transition set T if $s\%$ of transactions in T contains X or Y . The rule $X \rightarrow Y$ has confidence c if $c\%$ of transactions in T that contain X also contain Y . If the item set's support surpasses a threshold, that item set is reported as suspicious. The system annotates suspicious item sets with a vector of parameters. Since the system knows where the attacks are in the training set, the corresponding suspicious item set along with their feature vectors are used to train a classifier. The trained classifier will be able to, given a suspicious item set and a vector of features, classify it as a known attack (and label it with the name of attack), as an unknown attack or a false alarm.

1.2 Misuse Detection

1.2.1 Language-based Misuse Detection

Language-based Misuse Detection systems accept a description of the intrusions in a formal language and use this to monitor for the intrusions. Most languages for misuse systems, including the one used by NIDES, are low-level and have limited expressiveness.

a) ASAX

Habra *et al.* define Advanced Security audit trail Analysis for universal audit trail analysis [14]. ASAX (Advanced Security audit trail Analysis on UNIX) uses RUSSEL, a rule-based language, specifically appropriate for audit trail analysis. ASAX sequentially analyzes records using a collection of rules that are applied to each audit record. A subset of rules is active at any time. They define a normalized audit data format (NADF) as a canonical format of the Operating System's audit trail.

1.2.2 Expert Systems

Expert systems use lists of conditions that, if satisfied, indicate that an intrusion is taking place. The conditions are rules that are evaluated based on system or network events. These rules are specified by experts familiar with the intrusions, generally working closely with the developers of the system.

1.2.3 High-level state machines for misuse detection

The State Transition Analysis **Tool (STAT)** [15] describes computer penetrations as attack scenarios. It represents attacks as a sequence of actions that cause transitions that lead from a safe state to a compromised state. A state represents snapshot of the system's security-relevant properties that are characterized by means of assertions, which are predicates on some aspects of the security state of the system. The initial state of a transition diagram does not have any assertions. Each state transition diagram starts with a signature action that triggers monitoring of the intrusion scenario. Transitions between states are labeled by the actions required to switch from one state to another. These actions do not necessarily correspond to audit records. The resulting state transition diagram forms the basis of a rule-based intrusion detection algorithm.

a). USTAT [16] is an implementation of the STAT tool developed for Solaris BSM. It reads specifications of the state transitions necessary to complete an intrusion and evaluates an audit trail. Two preconditions must be met to use

USTAT: the intrusion must have a visible effect on the system state and the visible effect must be recognizable without knowing the attacker's true identity.

b). STATL [17] is a language that allows description of computer penetrations as sequences of actions that an attacker performs to compromise a computer system. The attack is modeled as a sequence of steps that bring a system from an initial safe state to a final compromised state. An attack is represented as a set of states and transitions, where each transition has an associated action. The notion of *timers* is used to

express attacks in which some events must happen with an interval following some other event (set of events). Times are declared as variables using the built-in type timer. STAT can detect cooperative attacks and attacks that span multiple user sessions, can specify rules at higher level than audit records, is easier to create and maintain than other rule-based methods, can represent a partial ordering among actions, can represent longer scenarios than other rule-based systems. On the other hand, it has no general-purpose mechanism to prune partial matches of attacks other than assertion primitives built into the model.

1.2.4 Emerald

EMERALD (Event monitoring enabling responses to anomalous live disturbances) [18] employs both anomaly and misuse detection. It includes *service analysis* that covers the misuse of individual components and network services within a single domain, *domain-wide analysis* that covers misuse visible across multiple services and components and *enterprise-wide analysis* that covers coordinated misuse across multiple domains. They also introduce the notion of *service monitors* that provide localized analysis of infrastructure and services. EMERALD consists of three analysis units: profiler engines, signature engines and resolver. Profiler engine performs statistical profile-based anomaly detection given a generalized event stream of an analysis target. Signature engine requires minimal state management and employs a rule-coding scheme. The profiler and signature engines receive large volumes of event logs and produce a smaller volume of intrusion/suspicion reports and send that data to the resolver. The signature analysis subsystem allows administrators to instantiate a rule set customized to detect known problem activity occurring on the analysis target.

III. Conclusion

This paper elaborates the foundations of the main anomaly based network intrusion detection technologies. Considering the surveyed literature, it is clear that in order to be able to secure a network against the novel attacks, the anomaly based intrusion detection is the best way out. However, due to its immaturity there are still problems with respect to its reliability. These problems will lead to high false positives in any anomaly-based IDS. In order to solve this problem, usually different anomaly detection techniques can be used. Method like Haystack can be used to detect a different set of attacks like break-in's Dos etc. In the same way some authors have used Machine Learning, Program based, and time based approaches for network intrusion detection. All the approaches that have been surveyed in the work perform better from one another in some cases but above all the techniques still need some improvements in terms of false positive rates and true negative rate.

However, there are still many challenges to overcome in the field of intrusion detection, But the presented information constitutes an important point to start for addressing Research & Development in the field of IDS. We find that the majority of surveyed works can be used as starting point for continuing research work in the field of intrusion detection.

BIBLIOGRAPHY

- [1] Stephen E. Smaha "Haystack: An Intrusion Detection System", Proc. of the IEEE 4th Aerospace Computer Security Applications Conference, Orlando, FL, Dec. 1988, 37 — 44 97
- [2] T. Lane, C. Brodley, "An application of machine learning to anomaly detection", Proc. 20th NIST-NCSC National Information Systems Security Conference, 1997.
- [3] H. Teng, K. Chen, S. Lu, "Security Audit Trail Analysis Using Inductively Generated Predictive Rules", Proceedings of the sixth conference on Artificial intelligence applications January 1990.
- [4] Garth Barbour "Program Modeling: A Machine Learning Approach To Intrusion Detection", PhD Thesis, University of Maryland at College Park, 2002.
- [5] A. K. Ghosh, A. Schwartzbard, M. Schatz, "Learning Program Behavior Profiles for Intrusion Detection", Proceedings of the Workshop on Intrusion Detection and Network monitoring, USENIX 1999.
- [6] S. Forrest, S. A. Hofmeyr, A. Somayaji and T. A. Longstaff "A sense of self for Unix processes". In Proceedings of the 1996 IEEE Symposium on security and Privacy, pages 120-128, Los Alamitos, CA, 1996. IEEE Computer Society Press
- [7] S. A. Hofmeyr, S. Forrest, A. Somayaji "Intrusion detection using sequences of system calls" Journal of Computer Security Vol. 6, pp. 151-180 (1998).
- [8] C. Warrender, S. Forrest, B. Pearlmutter "Detecting Intrusions Using System Calls: Alternative Data Models", 1999 IEEE Symposium on Security and Privacy, May 9-12, 1999.
- [9] A. Wespi, M. Dacier, H. Debar "Intrusion Detection Using Variable-Length Audit Trail Patterns", Recent Advances in Intrusion Detection — Lecture Notes in Computer Science ed. by H. Debar, L. M, S.F. Wu., Berlin, Springer-Verlag, vol.1907, p.110-29 in 2000
- [10] A. Wespi, M. Dacier, H. Debar "An Intrusion-Detection System Based on the Teiresias Pattern Discovery Algorithm ", Technical Report RZ3103, Zurich Research Laboratory, IBM Research Division, 1999.
- [11] I. Rigoutsos, A. Floratos "Combinatorial Pattern Discovery in Biological Sequences: the TEIRESIAS Algorithm",

- Bioinformatics, Vol. 14, No. 1, 1998, pp. 55-67.
- [12] A. P. Kosoresow, S. A. Hofmeyr, "Intrusion Detection via System Call Traces", IEEE Software, vol. 14, pp. 24-42, 1997.
- [13] D. Barbara, *et al*, "ADAM: Detecting Intrusions by Data Mining", proceedings of the 2001 IEEE Workshop on Information Assurance and Security, June 2001.
- [14] J. Habra, B. Charlier, A. Mounji, I. Mathieu, "ASAX: Software architecture and rule-based language for universal audit trail analysis", Second European Symposium on Research in Computer Security (ESORICS 92).
- [15] G. Vigna, S. T. Eckmann, R. A. Kemmerer, "The STAT Tool Suite", in Proceedings of DISCEX 2000, Hilton Head, South Carolina, January 2000, IEEE Press.
- [16] K. Ilgun, "USTAT: A real-time intrusion detection system for UNIX", in Proceedings of the 1993 IEEE Symposium on Security and Privacy, Oakland, CA, May 1993.
- [17] S. T. Eckmann, G. Vigna, R. A. Kemmerer, "STATL: An Attack Language for State-based Intrusion Detection", in Proceedings of the ACM Workshop in Intrusion Detection, Athens, Greece, November 2000.
- [18] A. Porras and P. G. Neumann, "EMERALD: Event monitoring Enabling Responses to Anomalous Live Disturbances", In Proceedings of the National Information Systems Security Conference, 1997, pp. 353- 365.
- [19] Eric Bloedorn, Alan D. Christiansen, William Hill, Clement Skorupka, Lisa M. Talbot, Jonathan Tivel "Data Mining for Network Intrusion Detection: How to Get Started"
- [20] <http://www.securityfocus.com/news/2445>.

Seasonal Variational Impact of the Physical Parameters On Mohand Rao River Flowing In the Doon Valley

Prashant-Dwivedi¹, Purandara Bekal², Kartikeya Dwivedi³, D.N.Pandey⁴

^{1,3} M.S. College, Saharanpur, Uttar Pradesh.

² National Institute of Hydrology, Hard Rock Regional Center, Belgaum Karnataka.

⁴ Sarojini Naidu Medical College, Agra, Uttar Pradesh.

Abstract: The paper depicts the seasonal variational impact on water quality of Doon Valley. Study was proposed to analyze the various water sample of Mohand-Rao river flowing in the Mohand Anticline in the lower parts of Shivalik hills in Doon Valley for physico-chemical characteristics of water quality parameters such as pH; Temperature; Conductivity; Hardness; Alkalinity; Total Solids; Total Dissolved Solids; Total Suspended Solids..To analyze the physical, chemical, and toxicological parameters of Streams and rivers.

Keywords: Anticline, physico-chemical, conductivity, solids, toxicological.

I. Introduction

The importance of understanding the relationship between man and environment has never been so great as it is realized at present. Industrial and technological advancement being made throughout the world are undoubtedly contributing towards our property but creating problems of depletion of environmental resources and increasing pollution. Therefore, the need for conservations of resources and environmental protection which are so intimately connected with our survival and sustainable development is being globally recognized. Pollution may be defined as any undesirable change in physical, chemical or biological characteristics of air, land or water affecting the life in harmful way. Pollutant get dispersed in air, water and soil. The dispersion and movement of pollutant in the biosphere is a complex process and it also accumulates within organism and causes toxic effects. Comprising over 80% of the earth's surfaces water is undoubtedly the most precious natural resources that exist on our planet. It is essential for all form of life on our planet-Earth. Owing to increasing industrialization on one hand and exploding population on the other, the demand of water supply have been increasing tremendously. The pollution is objectionable and damaging for varied reasons of primary importance and is possible hazard to the public health. In many countries, legislation mandates assessment of the water chemistry, biota, and physical environment of rivers, many of which have been highly impacted by human activities. Aquatic bodies can be fully assessed by three major components, hydrology, physico-chemical, and biology. A complete assessment of water quality is based on appropriate monitoring of these components. Aquatic quality assessment is the overall process of evaluation of the physical, chemical and biological nature of the water in relation to natural quality, human effects and intended uses, particularly which may affect human health and health of the aquatic ecosystem. In recent years non-point sources of pollution are being recognized as a major source of pollution to surface water.

II. Description Of The Study Area

Geology of Area

Dun; Doon: Dhoon in the Sanskrit and Hindi languages means a "Valley" which has not been made by river soil erosion, but is formed by tectonic activity within the earth that causes movements of its crusts, as earthquakes, folds, faults or the like.

The Oxford Dictionary defined it as – "Valley in Shivalik Hills". There are number of valleys large and small between the Sub-Himalayas and the Shivalik Hills. "Valley of Doon" is on the North-West part of the Indian states of Uttar-Pradesh. The Doon Valley is situated between the latitude of 30° to 30° 32' and longitude of 77° 43' to 78° 24'. It is nearly 75Km long from North-West to South-West.

Region of Dun Valley involves two distinct styles and amplitudes of folding. In the Northern part, the overturned SANTAURGARH - ANTICLINE with both limbs dipping steep to moderate was developed as fault propagated fold over the SANTUARGARH –THRUST (ST).

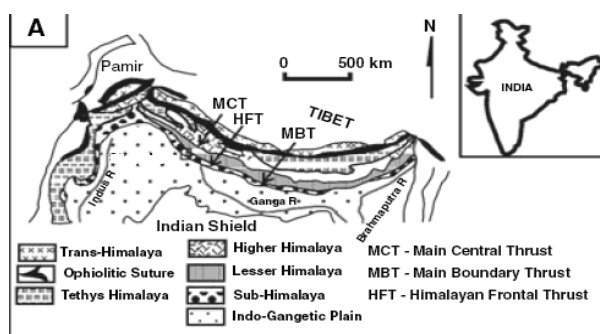


Fig-1 Regional geological map of the Himalaya showing tectonic subdivision

The uplifted hanging wall of the Santuargarh-thrust constituted the dissect Shiwalik and the down faulted footwall formed the pedimented Shiwalik. To the South in the frontal range, the Shiwalik strata were folded into MOHAND – ANTICLINE. MOHAND-ANTICLINE as fault-bend folds over the HIMALAYAN-FRONTAL-THRUST (HFT).

The Garhwal Himalaya geographically forms the central part of the Himalayan tectonic region.

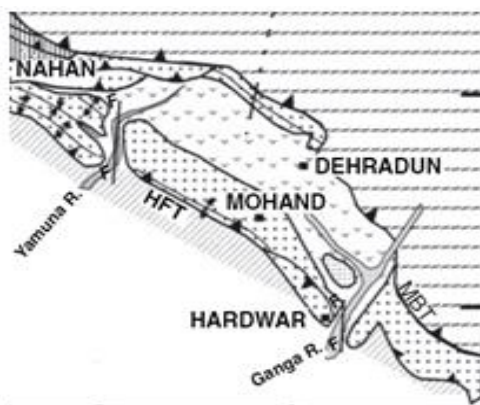


Fig-2 MOHAND ANTICLINE between the two main river of Indo-Gangetic plain along with HIMALAYAN FRONTAL THRUST and the valley of Dehradun

In environment characterized by active tectonic, it is widely accepted that river morphology will be affected by active fault displacement. For example, there is documented evidence of change in channel slope, channel width, channel braiding patterns, grain size distribution trend, and stream power in response to active faults. Therefore, river morphology can carry a measurable signature of tectonic activity. Furthermore, it can be hypothesized that fluvial systems are in fact more sensitive to local faulting than raw topographic expression. This would mean that young active faults will affect river morphology before they are expressed in the local topography. Therefore, detailed morphological measurements of rivers in tectonic setting could allow for an early detection of faulting which is not yet expressed in the landscape.

The Dehradun region of the Northwest Himalayan foothills is an ideal test case for this hypothesis. In this area, the Ganges and Yamuna rivers flow across an active thrust fault system; this is not yet clearly visible in the landscape. Ganges and Yamuna reaches flowing from the MAIN BOUNDARY THRUST, through the alluvial Dehradun valley and across the suspected active HIMALAYAN FRONTAL THRUST, and 35Km out into the Indo-Gangetic Foreland and Hinterland and Foreland (brown indicating lower lying elevation, rising to white then blue representing the highest elevation). The white lines represents drainage networks in the study region, the yellow lines represent the upstream and downstream ends of the river reaches.

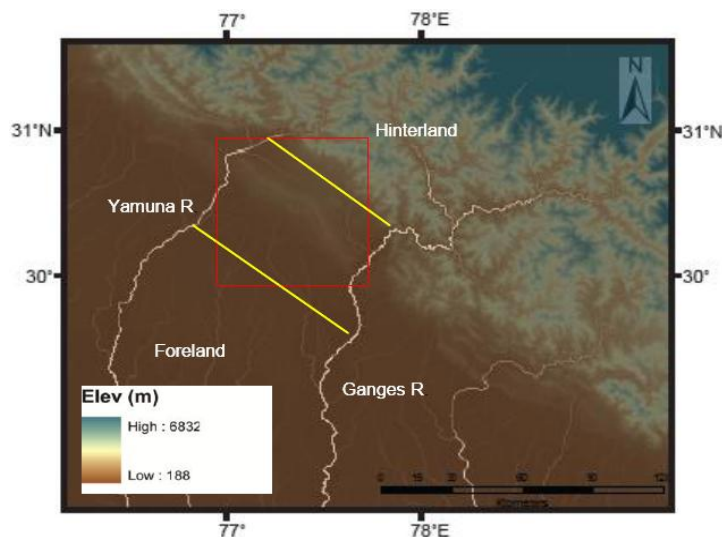


Fig-3 Clipped DEM coverage of Dehradun Basin and Mohand (Red Box), Ganges and Yamuna rivers.

III. Drainage System Of Area

A drainage system is the pattern formed by the streams, river, and lakes in a particular drainage basin. They are governed by the topography of the land, whether a particular region is dominated by hard or soft rocks, and the gradient of the land. Geomorphologists and hydrologists often view streams as being part of drainage basins. A drainage basin is the topographic region from which a stream receives runoff, through flow and ground water flow. Drainage basins are divided from each other by topographic barriers called watershed. A watershed represents all of the stream tributaries that flow to some location along the stream channel.

The ‘Garhwal Himalaya’ demarcates more or less Western and Eastern boundaries by the rivers Yamuna and Ramganga. The region is mainly covered by the drainage basin of the ‘Holy-Ganga’ and its tributaries which have carved out stupendous gorges for most part of their length and thus presented one of the best exposed sections of the Himalaya for study. From Shiwalik many river flows through the district Saharanpur, among these are the river Mohand-Rao (district Saharanpur, Uttar-Pradesh). District Saharanpur is situated in the North of Uttar-Pradesh. In the North of district Saharanpur on the Shiwalik Range, there is district Dehradun, in the south there is district Muzzafarnagar and district Haridwar in the east. Yamuna River lies in the west made boundaries with district Karnal and YamunaNagar means the district lies in doab basin of Ganga and Yamuna.

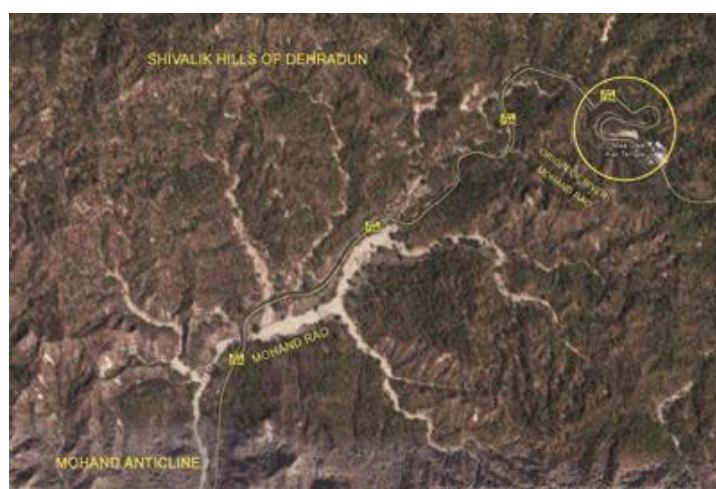


Fig-4 Dendrites pattern of drainage system of river Mohand-Rao from the origin i.e. Dat-Temple

Mohand Rao River originates from near a temple Dat-Temple it is about 18 km in length and flow from Dat-Temple via Iron – Bridge Mohand Village; Khushalipur; Ganeshpur; Tanda-Man-Singh; Biharigarh and then falls in Solani river near Amanatgarh village which then via khedi-Shikhopur; Hasanpur ; Madanpur; Khubbanpur-choli; Bhagwanpur; Roorkee; Landhora; and then falls in Ganga river near Luxor. The location of

Saharanpur on globe is on latitude $29^{\circ}58'$ North and longitude $77^{\circ}33'$. The length of the river is 20 km with a width varying between 5 to 100 m. The mean depth of the river is only 0.3 m.

(From the sea-level) = 270.50 meters
 Latitude $29^{\circ} 58'$

Longitude $77^{\circ} 33'$

Length of river 20 Km

Width of the river 5 to 100 meters

Minimum depth 0.10 meters

Maximum depth 0.50 meters

Mean depth 0.30 meters

Eight samples from each selected centers were taken in three season (summer; winter; Monsoon) 144 samples were the samples of the present studies. On the forest road to Shakumbra Devi about 1Km from forest toll post on the right bank of Mohand Rao river section the main HIMALAYAN FRONTAL THRUST (HFT) is exposed where the middle Shiwalik sandstone is overriding the recent alluvium. The sandstone is steeply about 70° dipping due N 21° S where as after moving upstream along the Rao for about 500m the dip changes to 35° due N 70° E forming a fault bend type antiformal structure referred as Mohand antiform. Further the sandstone is continuing with a uniform northerly dip upwards. 19Km milestone on Mohand-Dehradun road traversing upstream in the Rao section from this place the boulder conglomerate sequence of upper Shiwalik is encountered that marks the confirmable contact between middle and upper Shiwalik which continue up to Doon valley.

Map of the Study - Area

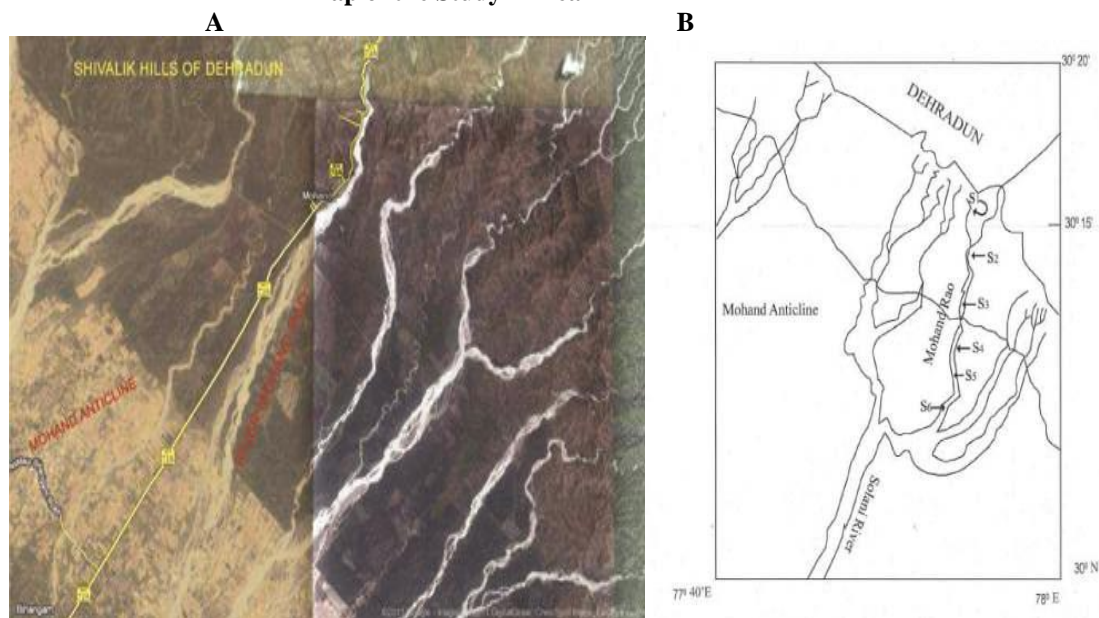


Fig-5 A-Shows the location of flowing of river Mohand-Rao B- Shows the sample stations selected on the river stream Mohand-Rao for the study purpose; S-1,S-2,S-3,S-4,S-5,S-6 are the various sample stations selected for our study on river Mohand-Rao

IV. Methodology

Methodology

Surface water Analysis for Chemical Mass Balance

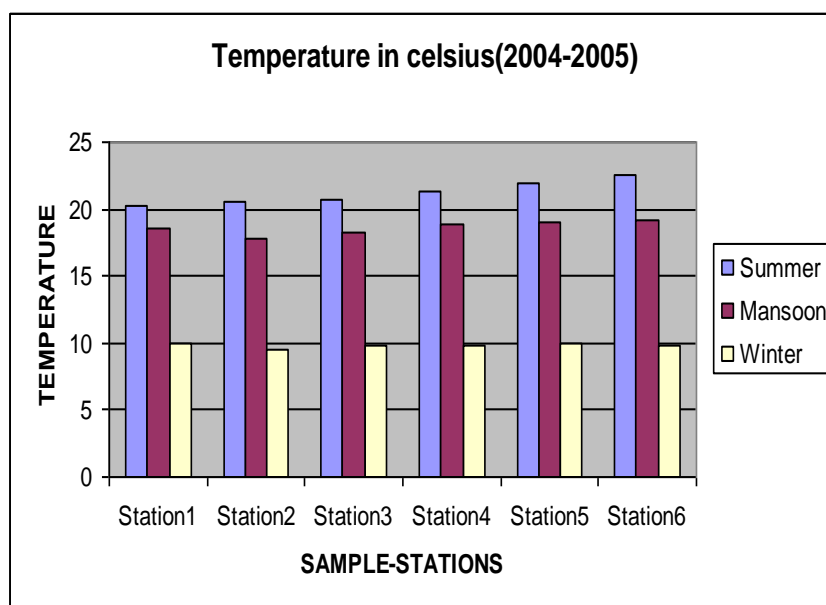
Six surface water samples were collected from selected locations In the present study only major physical parameters were determined by using standard methods.

V. Results

Surface Water Characteristics

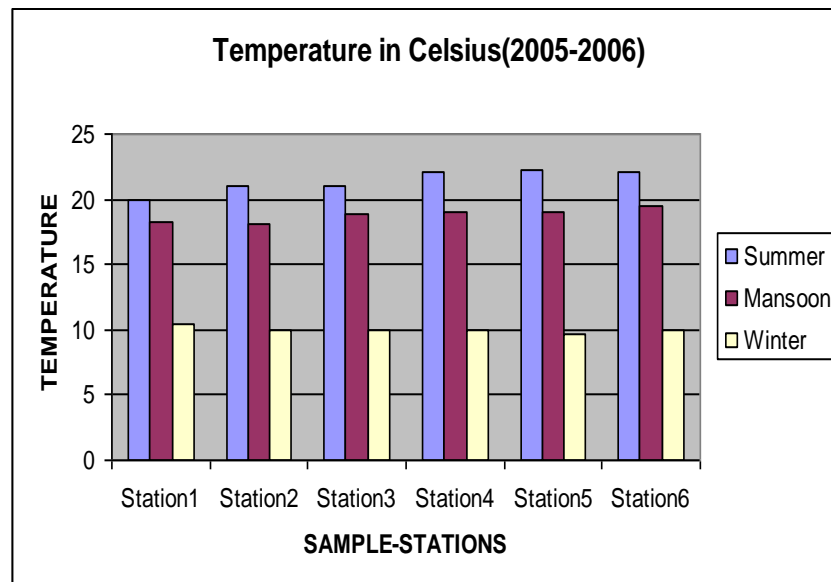
Assessment of water quality today in global terms implies the need for a reference point against which the results of monitoring can be measured and weighted. An attempt is made to define and describe natural water quality to the extent possible and scientifically justifiable. Aquatic ecosystems as a part of the natural environment are balanced both within themselves and other environmental compartments and this equilibrium is subject to natural variations and evolutions as well as variations caused by human interventions. It is the ambition of the present assessment to identify the anthropogenic influences over time against a natural baseline situation.

Temperature of the river Mohand Rao varies according to the three season in the region as in Summer varied maximum while it varied minimum during Winter and is medium in Monsoon thus the temperature of the stream varied with season in the year 2004-2005. Similarly temperature of the stream varied accordingly to station it is maximum at station -6 and minimum at station -1



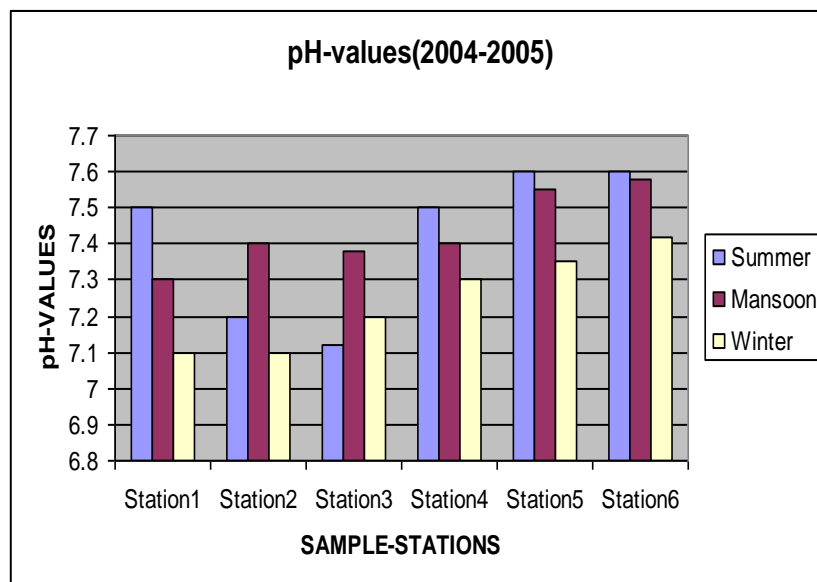
Graph-1: Seasonal variation of Temperature in the year 2004-2005

Same trend of variation in temperature was followed in the year 2005-2006. Temperature of the river Mohand Rao varies according to the three season in the region as in Summer varied maximum while it is varied minimum during Winter and is medium in Monsoon thus the temperature of the stream varied with season in the year 2005-2006. Similarly temperature of the stream varied accordingly to station it is maximum at station -6 and minimum at station -1



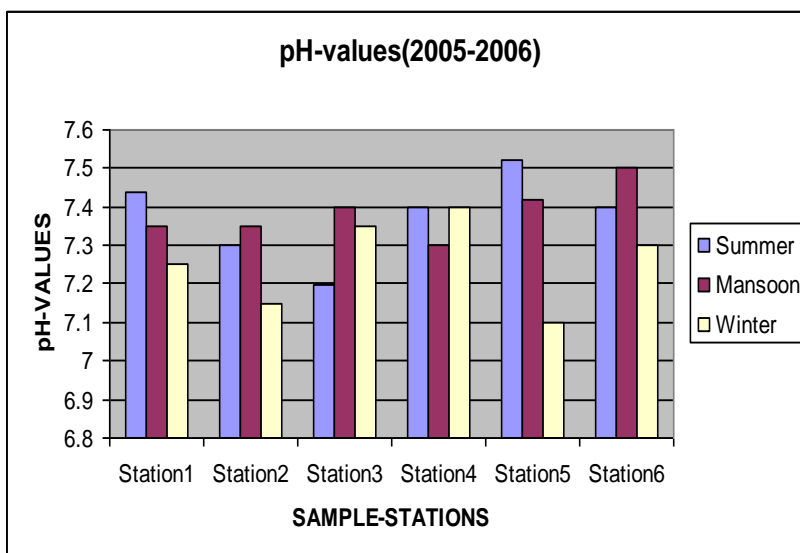
Graph -2: Seasonal variation of Temperature in the year 2005-2006

pH values varied according to the season and station both in 2004-2005. pH value of the stream is maximum at station 6 in summer season and minimum in monsoon although pH value is minimum at station 2 & station3 in all the three seasons. On these two stations the pH value is low in summer & maximum in monsoon. Although at all the six sample stations there is seasonal variation in pH accordingly.



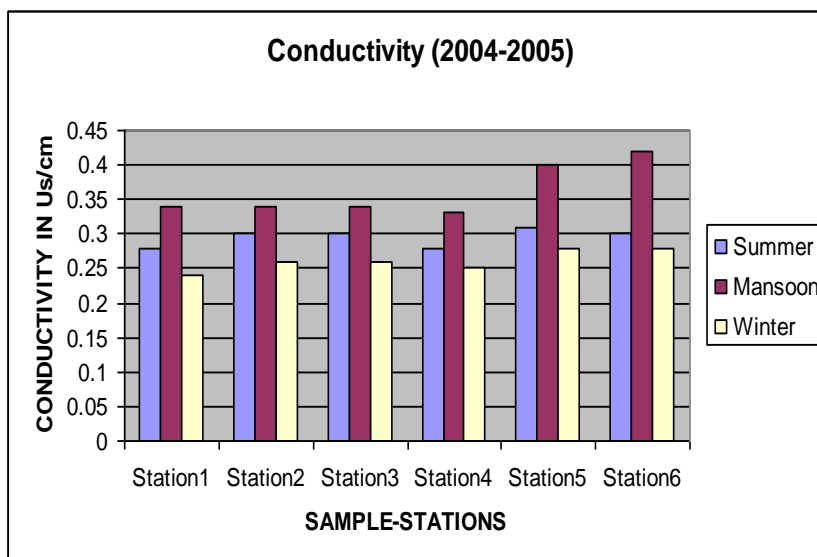
Graph -3: Seasonal variation of pH in the year 2004-2005

In 2005-2006 the value of pH was found to be maximum in the summer at sample station 5 and minimum in winter of the sample station5. The trend followed by the pH value of the stream gets varied accordingly with the season.



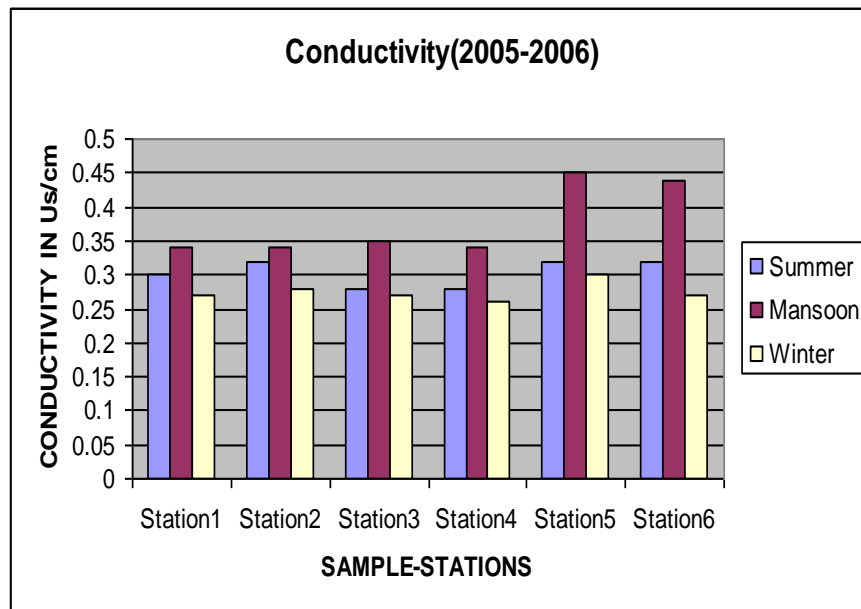
Graph -4: Seasonal variation of pH in the year 2005-2006

In 2004-2005 the conductivity is maximum in monsoon season of sample station-6 although it is minimum in winter season of sample station-1 while in summer season it follows medium trend though the conductivity varies in all the six sample stations accordingly with season.



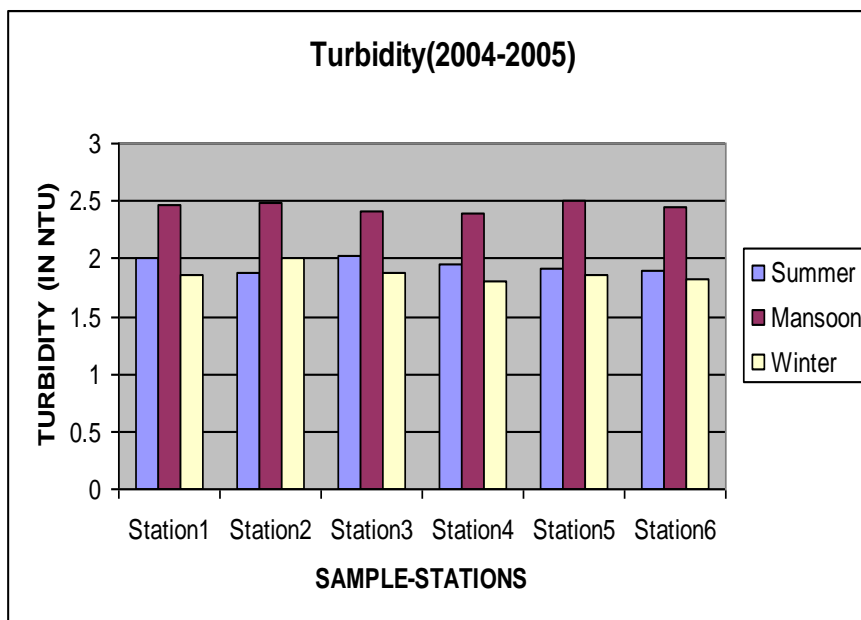
Graph -5: Seasonal variation of conductivity in the year 2004-2005

In 2005-2006 the conductivity is maximum in monsoon season of sample station-5 although it is minimum in winter season of sample station-4 while in summer season it follows medium trend though the conductivity varies in all the six sample stations accordingly with season.



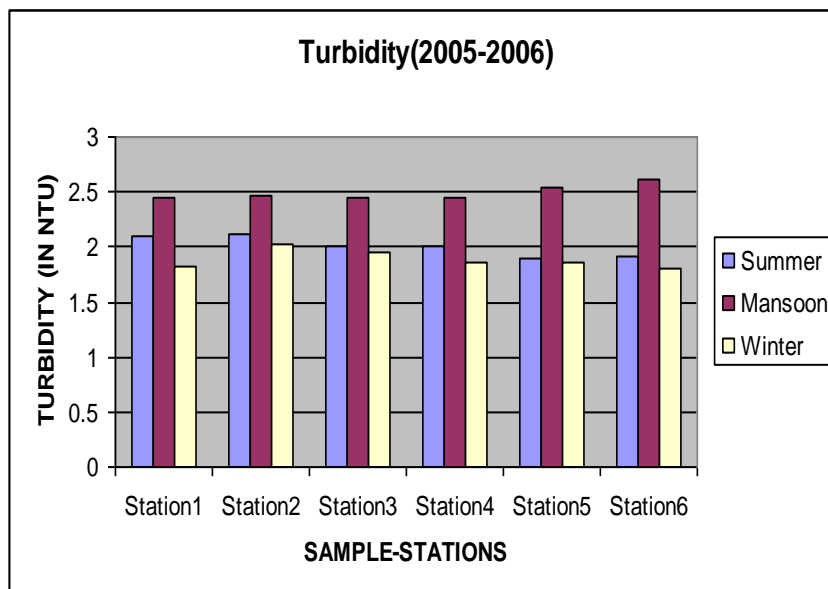
Graph-6:Seasonal variation of conductivity in the year 2005-2006

In 2004-2005 the turbidity value is maximum at sample station-5 of monsoon while it is minimum at sample station-4 in winter season although in summer the turbidity follows median trend. In monsoon the turbidity increases as lots of solids comes into stream along with flow of water coming from the higher mountain.



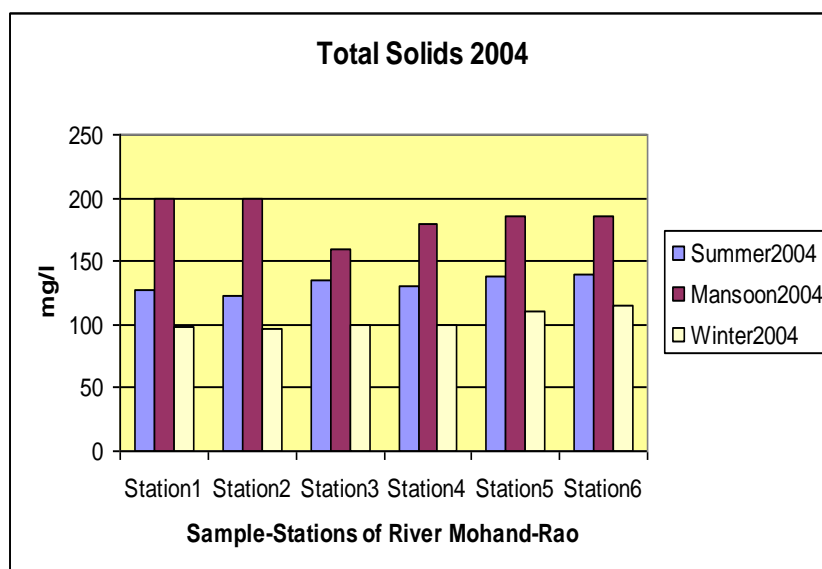
Graph-7:Seasonal variation of turbidity in the year 2004-2005

In 2005-2006 the turbidity value is maximum at sample station-6 of monsoon while it is minimum at sample station-6 in winter season although in summer the turbidity follows median trend. In monsoon the turbidity increases as lots of solids comes into stream along with flow of water coming from the higher mountain.

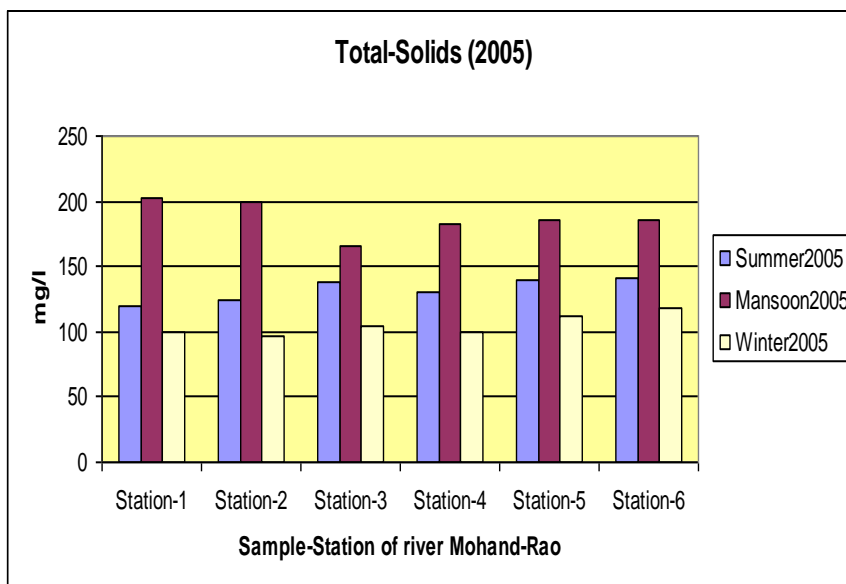


Graph -8: Seasonal variation of turbidity in the year 2005-2006

Water quality analysis results on the distribution of Total-Solids along the stretch of the river , showed an overall increase in the percentage of Total-Solids from year 2004-2005 except station 5 and station 6 during summer season. Similar trends was continued in the rainy season without any trend of decrease in any station except station 3 where the solids are gets decreases in rainy seasons , however in winter season Total Solids increases on station 5 and station 6 whereas in the remaining four station a normal trends was observed Figure-9 and Figure-10 shows the variation of Total-Solids along the stretch of the river during the year of 2004-2005

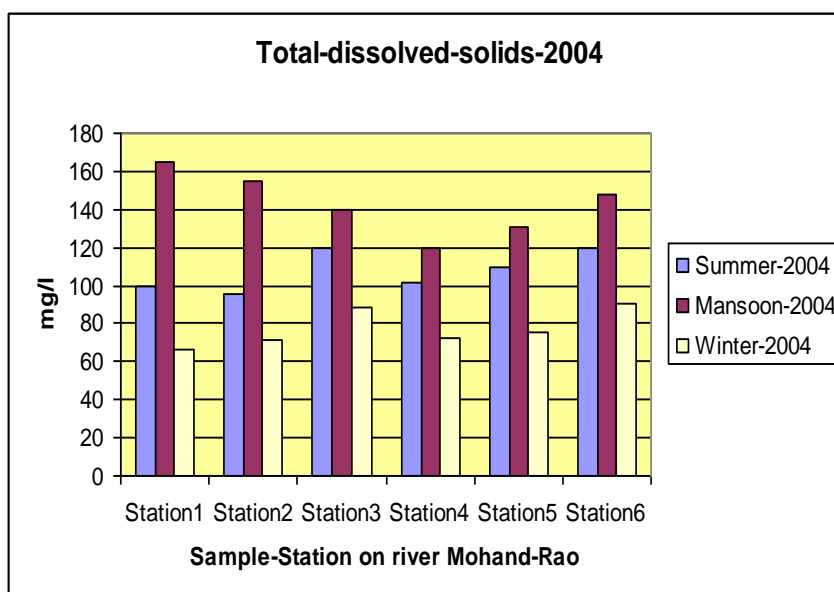


Graph-9 Seasonal Variation of Total-Solids during the year 2004-2005

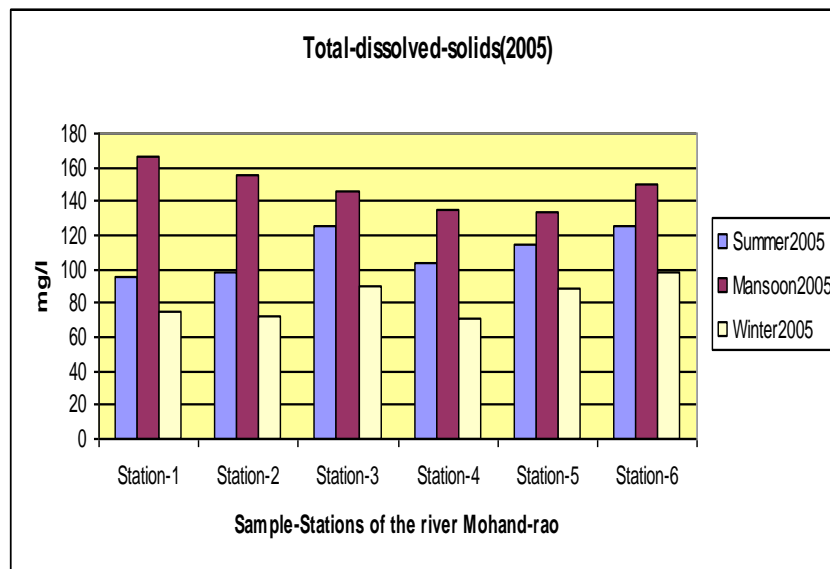


Graph-10 Seasonal Variation of Total-Solids during the year 2005-2006

Total –dissolved –solids are quite prominent in all the sample . The percentage was less during the Summer and winter months . Total dissolved solids showed a considerable increase during the rainy season followed by drastic decline during winter season In summer season Total dissolved solids are lower at station-2 while in rainy season Total dissolved solids are lower at station-4 and winter season this Total dissolved solids are lower at station-1 and station- 2 Figure 11 and Figure 12 shows the distribution of Total-dissolved – solids in different seasons along the stretch of the river.

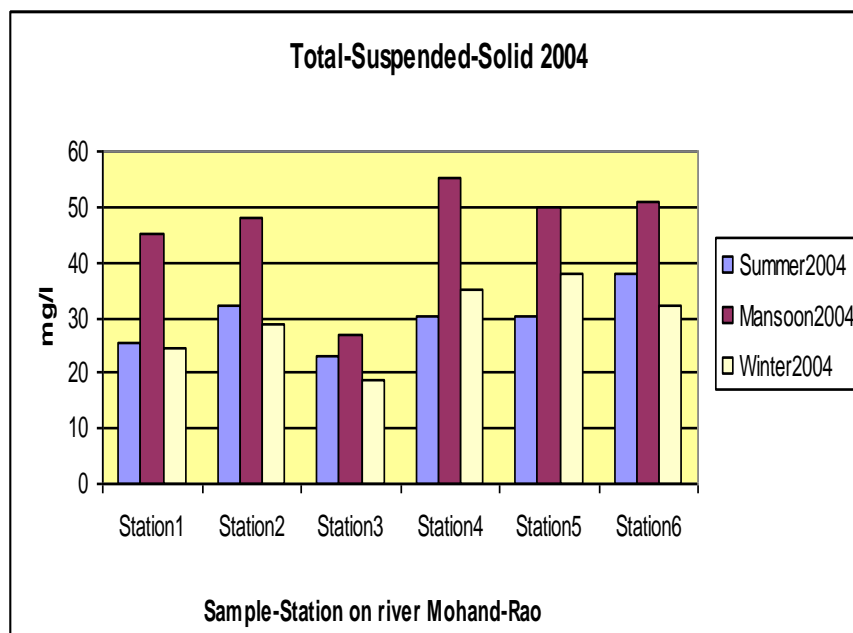


Graph-11 Seasonal variation of Total-Dissolved-Solids during the year 2004 -2005

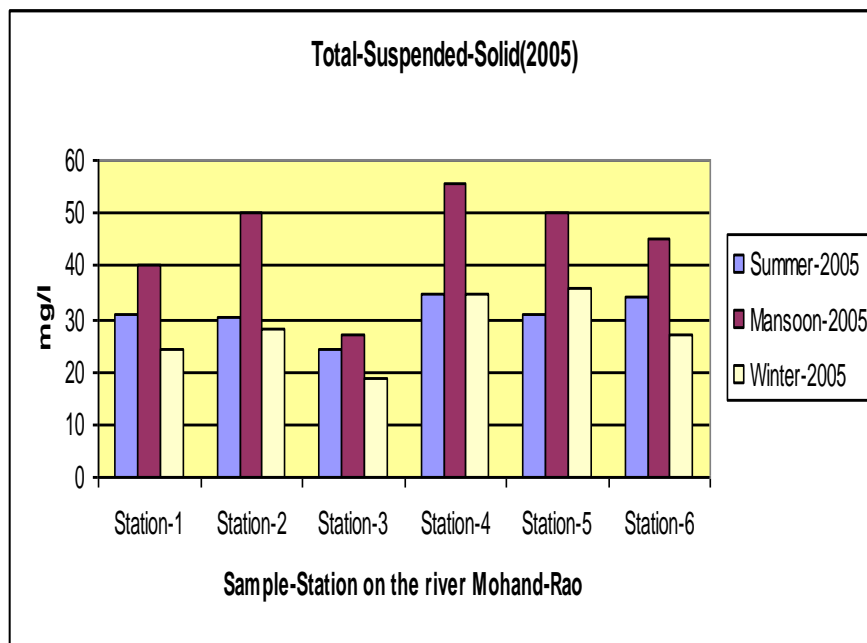


Graph-12 Seasonal variation of Total-Dissolved-Solids during the year 2005-2006

Total Suspended Solids are one of the important physical parameters that studied to understand the water quality conditions of the stream flowing mostly through hilly area. Here Total-Suspended-Solids are gets varied in the summer season it is maximum on station-6 although it gets varied from station 1 to station 6. In monsoon season it gets maximum as lots of solids flows through stream with pressure from the above hilly places from where the river originated, although it is maximum at station 4. In winter the solids gets lowered down the maximum quantity of the Total-Suspended-Solids are found to be at station 4 and station 5. Figure 13 and Figure 14 shows the seasonal variations of the Total-Suspended-Solids during the year 2004-2006

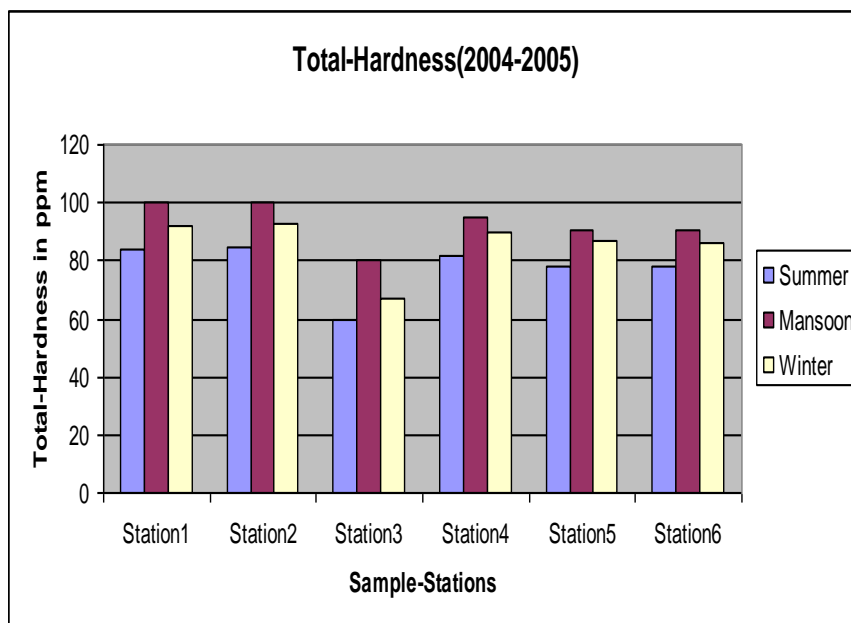


Graph-13 Seasonal variation of Total-Suspended-Solid in the year-2004-2005



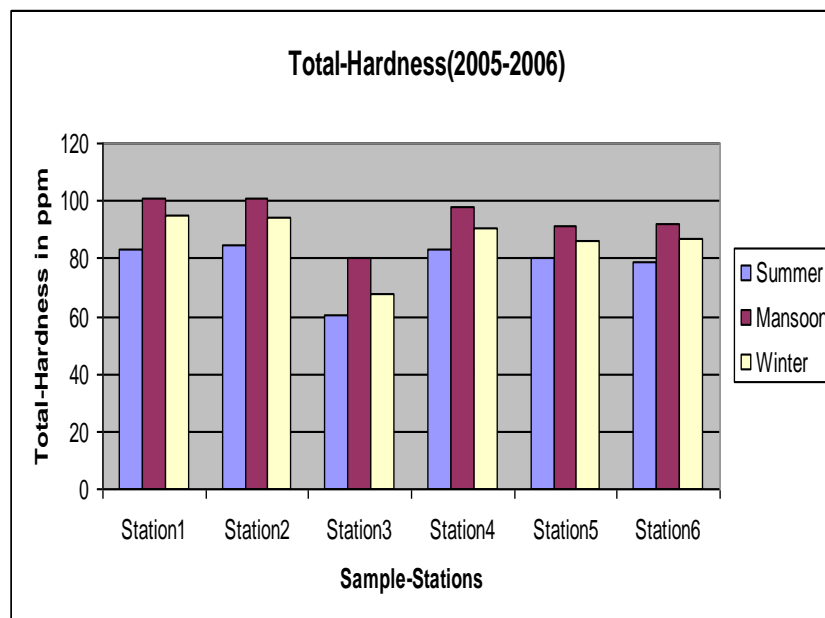
Graph-14 Seasonal variation of Total-Suspended-Solids in the year 2005-2006

Total-hardness of the stream Mohand-rao is maximum in monsoon at station-2 as most of the ions comes into the stream from the upper hills of Himalayas while it is minimum in the summer at station-3 although the Total-Hardness varied in the year 2004-2005 seasonally.



Graph-15 Seasonal variation of Total-Hardness in the year 2004-2005

In the year 2005-2006 the Total-Hardness followed the similar trend as in the previous year means maximum in monsoon at station-2 while minimum in summer at station-3.



Graph-16 Seasonal variation of Total-Hardness in the year 2005-2006

Hardness in water is defined as concentration of multivalent cations. Multivalent cations are cations (positively charged metal complexes) with a charge greater than 1+. They mainly have the charge of +2. These cations include Ca^{2+} & Mg^{2+} . These ions enter a water supply by leaching from minerals within an aquifer. Common calcium-containing minerals are calcite and gypsum. A common magnesium mineral is dolomite (which also contains calcium). Rainwater and distilled water are soft water, because they contain few ions.

VI. Discussion

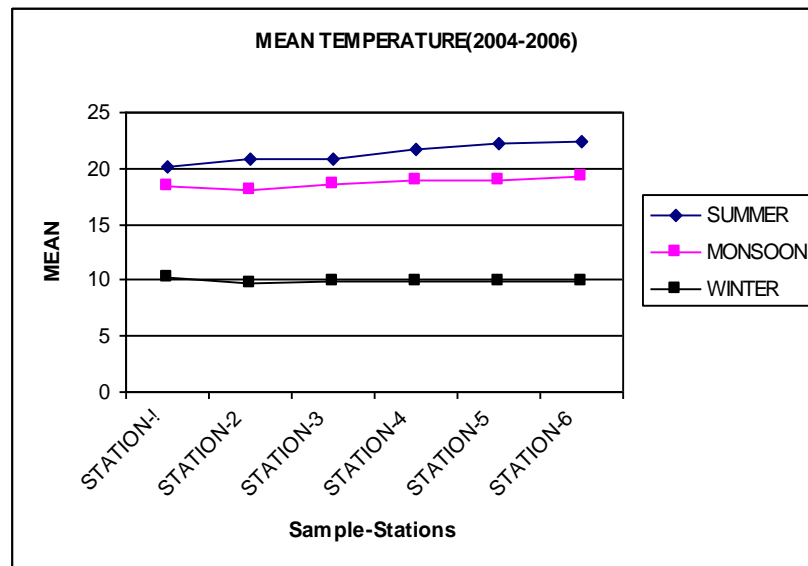
The above result so obtained from the chemico-physical analysis of the water of flowing stream in the hilly areas of Himalayas. These data's so obtained are gets involved to determine the STANDARD DEVIATION (S.D) in statistical data analysis –

$$S.D = \sqrt{\frac{\sum x^2}{n} - \frac{(\sum x)^2}{n^2}}$$

On this formula of standard deviations the mean and Analysis of variation were calculated, hence whole data analysis depends upon the above stated formula.

Table-1:-Mean of Temperature in the river at six sample-stations accordingly to season Sample

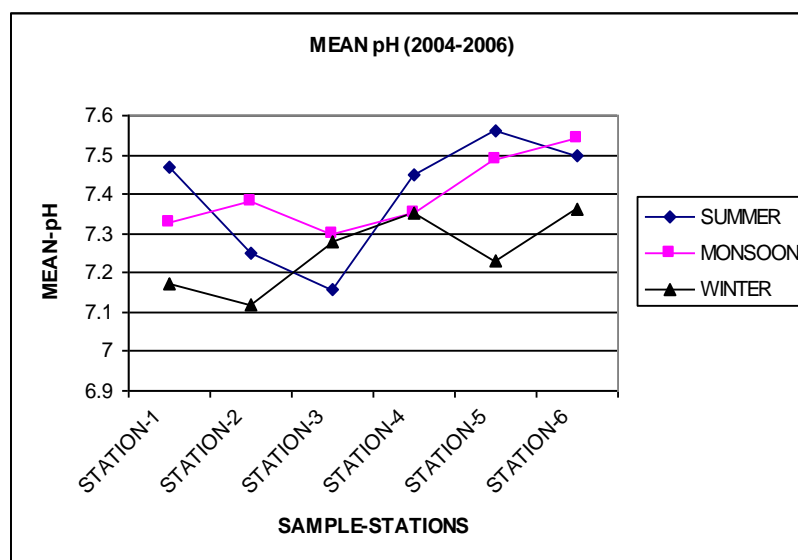
Sample Station	SUMMER		MANSOON		WINTER	
	Mean	S.D	Mean	S.D	Mean	S.D
1.	20.10	0.16	18.35	0.16	10.23	0.24
2.	20.75	0.30	17.99	0.17	9.70	0.23
3.	20.85	0.17	18.54	0.32	9.90	0.13
4.	21.67	0.38	18.93	0.26	9.90	0.15
5.	22.15	0.33	18.99	0.19	9.85	0.31
6.	22.31	0.31	19.32	0.20	9.86	0.14



Graph-17: Mean Temperature at different Sample Station in three different Season in the year – (2004-2006)

Table-2:- Mean pH in the river at six Sample-Stations accordingly to Season Sample

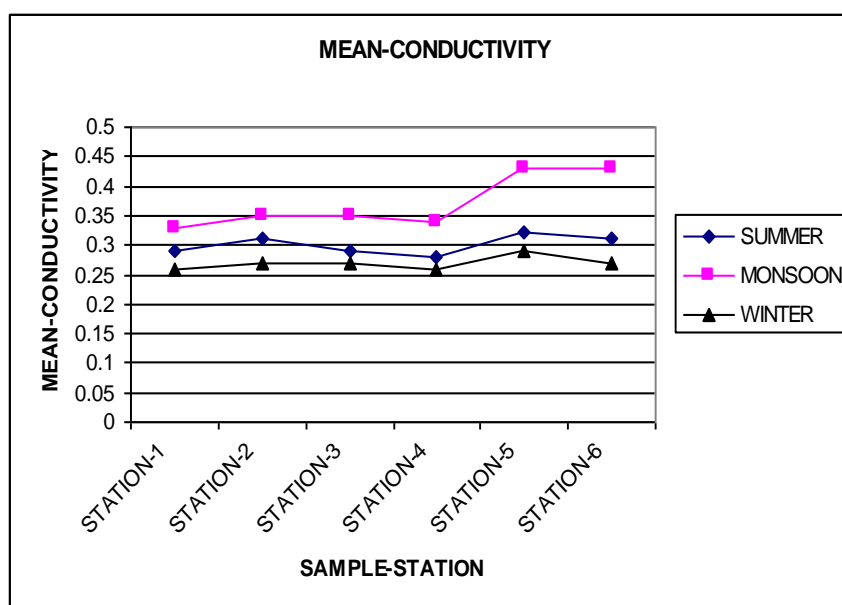
Sample Stations	Summer		Monsoon		Winter	
	Mean	S.D	Mean	S.D	Mean	S.D
1.	7.47	0.02	7.33	0.07	7.17	0.14
2.	7.25	0.09	7.38	0.11	7.12	0.07
3.	7.16	0.06	7.30	0.02	7.28	0.08
4.	7.45	0.09	7.35	0.06	7.35	0.07
5.	7.56	0.08	7.49	0.11	7.23	0.14
6.	7.50	0.12	7.54	0.05	7.36	0.12



Graph-18: Mean pH at different Sample Station in three different Season in the year – (2004-2006)

Table-3:-Mean Total Conductivity in the river at six Sample-Stations accordingly to Season Sample

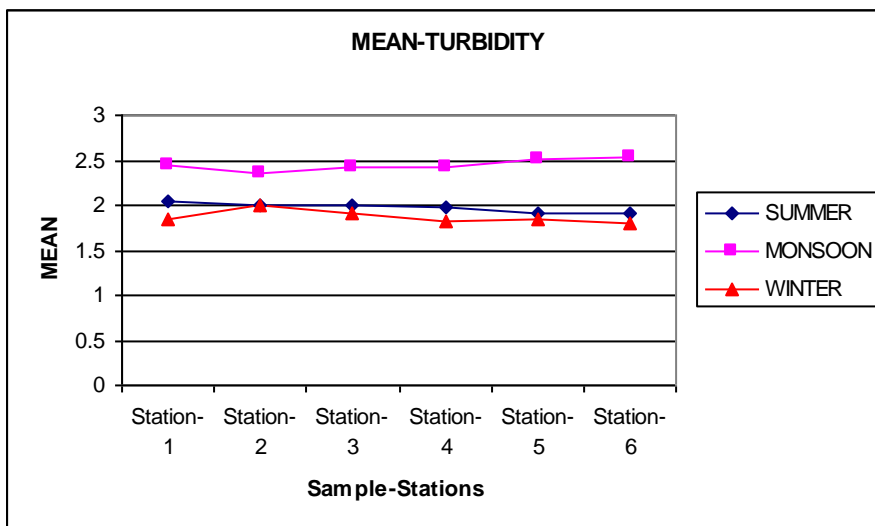
Sample Station	Summer		Monsoon		Winter	
	Mean	S.D	Mean	S.D	Mean	S.D
1.	0.29	0.01	0.33	0.04	0.26	0.01
2.	0.31	0.01	0.35	0.04	0.27	0.05
3.	0.29	0.01	0.35	0.04	0.27	0.03
4.	0.28	0.02	0.34	0.04	0.26	0.01
5.	0.32	0.03	0.43	0.01	0.29	0.01
6.	0.31	0.02	0.43	0.03	0.27	0.03



Graph-19: Mean Conductivity at different Sample Station in three different Season in the year – (2004-006)

Table-4:-Mean Total Turbidity in the river at six Sample-Stations accordingly to Season Sample

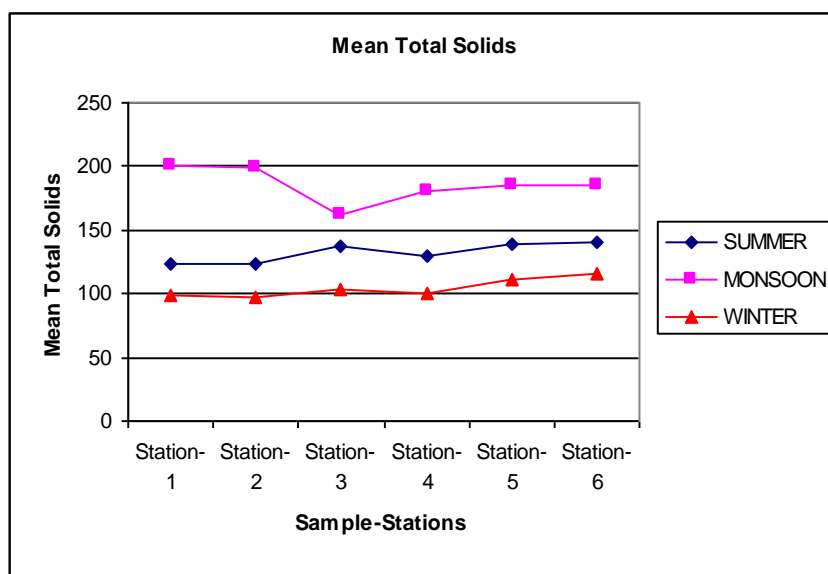
Stations	Summer		Monsoon		Winter	
	Mean	S.D	Mean	S.D	Mean	S.D
1.	2.05	0.12	2.45	0.01	1.84	0.07
2.	2.00	0.11	2.35	0.34	2.01	0.10
3.	2.01	0.05	2.43	0.01	1.91	0.10
4.	1.98	0.08	2.42	0.07	1.82	0.13
5.	1.91	0.03	2.52	0.03	1.85	0.04
6.	1.91	0.03	2.53	0.08	1.81	0.04



Graph-20: Mean Turbidity at different Sample Station in three different Season in the year – (2004-2006)

Table-5:-Mean Total Solids in the river at six Sample-Stations accordingly to Season Sample

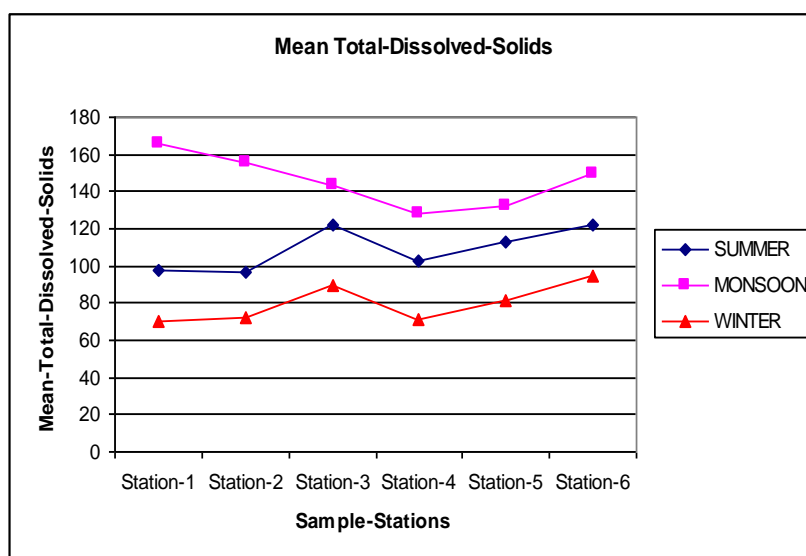
Sample Stations	Summer		Monsoon		Winter	
	Mean	S.D	Mean	S.D	Mean	S.D
1.	123.28	3.27	201.08	1.10	99.25	0.94
2.	123.50	1.66	199.54	0.83	96.92	0.53
3.	136.75	1.37	162.50	2.60	103.26	3.34
4.	130.25	0.83	181.00	1.22	100.00	0.71
5.	139.00	1.22	185.38	0.99	111.00	1.27
6.	140.50	1.03	185.38	0.56	116.50	1.66



Graph-21: Mean Total-Solids at different Sample Station in three different Season in the year – (2004-2006)

Table-6:- Mean Total Dissolved Solids in the river at six Sample-Station accordingly to Season Sample

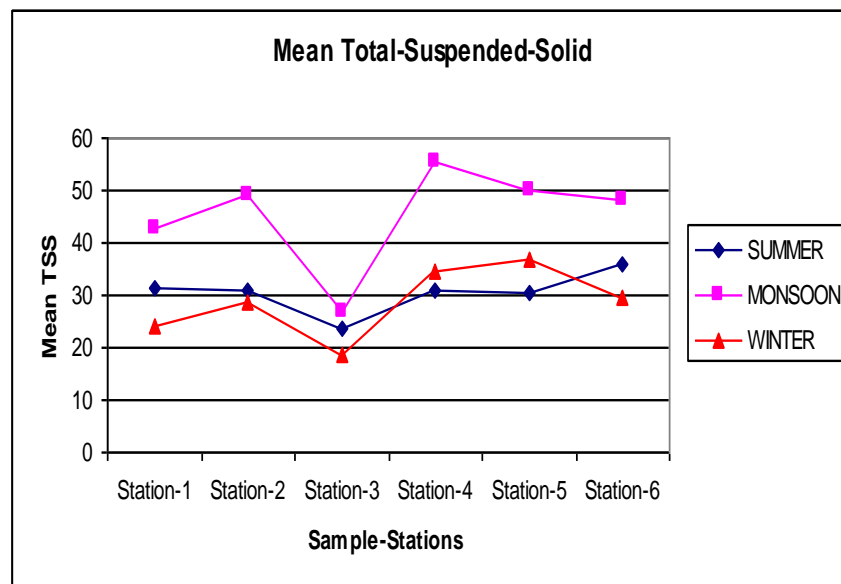
Station	Summer		Monsoon		Winter	
	Mean	S.D	Mean	S.D	Mean	S.D
1.	97.51	2.51	165.63	0.66	70.52	4.48
2.	96.75	1.39	155.50	0.87	71.75	0.97
3.	122.50	2.60	143.00	3.08	89.00	1.22
4.	102.60	0.79	127.63	7.70	71.50	0.87
5.	112.50	2.66	132.50	1.66	81.50	6.54
6.	122.50	2.62	149.10	1.10	94.50	3.57



Graph -22: Mean Total-Dissolved-Solids at different Sample Station in three different Season in the year – (2004-2006)

Table-7:- Mean Total-Suspended- Solids in the river at six Sample-Station accordingly to Seasons Sample

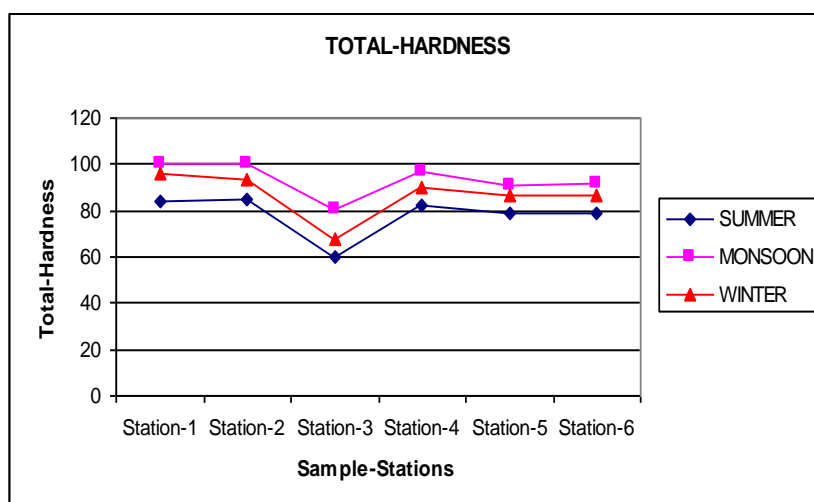
Stations	Summer		Monsoon		Winter	
	Mean	S.D	Mean	S.D	Mean	S.D
1.	31.50	0.54	42.53	2.49	24.29	0.36
2.	31.11	1.09	49.00	1.22	28.43	0.49
3.	23.55	0.51	26.92	0.19	18.68	0.30
4.	31.00	1.22	55.38	0.86	34.71	0.65
5.	30.50	1.22	50.00	0.71	37.00	1.22
6.	36.00	2.12	48.00	3.08	29.50	2.60



Graph -23: Mean Total-Suspended-Solids at different Sample Station in three different Season in the year – (2004-2006)

Table-7:- Mean Total-Hardness in the river at six Sample-Stations accordingly to Season Sample

Station	Summer		Monsoon		Winter	
	Mean	S.D	Mean	S.D	Mean	S.D
1.	83.80	0.45	100.27	0.57	96.18	2.50
2.	84.64	0.65	100.40	0.46	93.50	0.87
3.	60.26	0.62	80.21	0.57	67.53	0.83
4.	82.52	0.86	96.50	1.66	90.25	0.61
5.	79.10	1.12	90.75	0.68	86.75	0.69
6.	78.50	1.22	91.35	0.89	86.51	0.85



Graph -24: Mean Total-Hardness at different Sample Station in three different Season in the year – (2004-2006)

VII. Conclusions

- (1) Water quality analysis of alkali and alkaline earth metals show that water of the studied river is very good for drinking purpose
- (2) Study also revealed that there is an increase in measured parameters from year 2004 and 2005 which may need a long term monitoring station for further conclusion.
- (3) A clearcut impact of manmade disturbance is evident in certain stations which showed a declining trend of water quality.

Acknowledgement

First of all my deep sense of gratitude goes to Dr Rajan Vats; National Institute of Hydrology; Roorkee ;Uttarakhand for suggestion criticism evaluation encouragement in each step of this work. I am deeply indebted to Dr I.P.Pandey Reader ;Department of Chemistry; D.A.V College ; Dehradun Uttarakhand.

REFERENCES

- [1.] 1-Acero P., Mandado, J.M.A., Gomez , J.et.al.,(2002) "Environmental impact of heavy-metal dispersion in the Huerva River (Iberian Range, NE Spain) . Env'tal, Geo (Berlin); p10-20.
- [2.] 2-Ara Shoukat , Khan M.A. and Zavger, (2003), Physico-chemical characteristics of Dal Lake Water of Kashmir Valley, India India J. Environ and Ecoplan 7(1) ,47-50
- [3.] 3-Baxter, C.W. Stanley , S.J., Zhang , W. and Smith, D.W. ,(2002), " Developing artificial neural networks models of water treatment processes : a guide for utilities ". J. Environ . Eng . Sci. 1(3): p201-211
- [4.] 4-Beeton A.M., (2002), "Large Freshwater lakes : present state trends and future" . Env. Conser .29(1): p21-38
- [5.] 5-CPCB,(2003), A report on color problem of river Ganga , Central Pollution Control Board Zonal Kanpur p19
- [6.] 6-Sinha , D.K. and Saxena ,R.(2006). Statistical assessment of underground drinking water contamination and effect of monsoon at Hasanpur , J.P.Nagar (Uttar-Pradesh ,India),Journal of Environmental Science and Engineering ,48(3);157-164.
- [7.] 7-Asadi,S.S.,Vuppala,P., and Anji Reddy,M.(2007). Remote sensing and GIS techniques for evaluation of ground water quality in Municipal Corporation of Hyderabad (Zone-V), India . International Journal of Environmental Research and Public Health 4(1); 45-52
- [8.] 8-PICKERING, JACK (2010) Alluvial river response to active tectonics in the Dehradun region, North-West India : A case study of the Ganga and Yamuna rivers . Masters thesis Durham University.
- [9.] 9-Wasson , R.J. 2003 A sediment budget for the Ganga-Brahmaputra catchment Current Science .84,1041-1047
- [10.] 10-Jain,C.K.,K.K.S.Bhatia,C.P.Kumar and B.P.Purandara,2001. Ground Water Quality in Malprabha River Basin , Karnataka,Technical-Report ,2000-2001. National Institute of Hydrology,Roorkee.
- [11.] 11-Bist & Choudhry,1993 Lithotectonic sequence of Outer ,Lesser and Higher Himalaya from Rishikesh to Badrinath , along Alaknanda river , Garhwal Himalaya Uttaranchal .WIHG spl publ2,p1-17
- [12.] 12-Sharma, S. K. (2004), 'Ground water pollution of Sanganer block of Jaipur district in Rajasthan',Environment and Ecology 22(4): 934-940.
- [13.] 13- Shrestha, R. R., M. P. Shrestha, N. P. Upadhyay, R. Pradhan, R. Khadka, R. Maskey et al. (2003), 'Groudwater arsenic contamination, its health impact and mitigation program in Nepal', Journal of Environmental Science and Health A38(1): 185-200.
- [14.] 14. Eaton A. D., L. S. Clesceri and A.E. Greenberg (1995), 'Standard methods for the examination of water and wastewater', 19th ed. American Public Health Association, Washington, DC.
- [15.] 15. Howarth, W. and D. McGillivray (2001), Water pollution and water quality law, Shaw & Sons, 2001,cxiii + 1212pp, ISBN 0-7219-1102-1.
- [16.] 16. Poppe, W.and R. Hurst (1997), 'Water pollution',Water Quality International, pp. 39-43.
- [17.] 17. Chaudhury, S. (2004), 'Soil and ground water pollution in Faridabad', Environment and Ecology 22(3):636-641.

Feature Extraction from the Satellite Image Gray Color and Knowledge Discovery Using Association Rule Mining

Yusuf Khan¹, Ravindra Gupta²

^{1,2} (M. Tech Scholar, Software Engineering, Assistant Professor, Computer Science & Engineering
RKDF IST, Bhopal)

Abstract: Satellite take images of the Earth in selected spectral bands that are in both the visible and the infrared portions of the electromagnetic spectrum. Many Satellites provide three types of Satellite Images. These Images are Visible Satellite Image, Infrared Satellite Image, and Water Vapor Satellite Image. These images are important for different reasons, and, in some cases, all three are needed to accurately interpret atmospheric conditions. These Satellite images contain different types of cloud. This paper shows cloud feature extraction using Histogram. A table that shows cloud existence in different image is created, called Association table in which Y represents cloud is exist and N represent not exist. Association rule mining is applied to this table to make relations between different clouds and discover the knowledge about cloud existence.

I. Introduction

Satellite images are a pictorial representation measuring the electromagnetic energy recorded by a sensor, not by photography. A photograph is normally taken within a certain spectral range (visible light). Satellites take images outside this limited range [5].

The Satellite Images may look like an actual picture of the Earth; a weather satellite image is composed of thousands of points known as pixels. There are three types of satellite image Visible, Infrared, and water vapor. All three types of imagery are important for different reasons, and, in some cases, all three are needed to accurately interpret atmospheric conditions [7].

Satellite images are often described in term of their resolution. Resolution refers to the size of the smallest feature that can be seen in an image. Since one pixel is the smallest element in an image, the area represented by one pixel is equal to the image resolution. Each pixel represents the average brightness over an area. Image resolution is determined by the satellite sensor, the type of transmission used, and also type of display hardware used to view the imagery.

Knowledge discovery is extraction of implicit knowledge, image data relationship or other pattern not explicitly stored in images and uses ideas from computer vision, image processing, image retrieval, data mining and machine learning database [3].

A. Types of Satellite Images

Based on the Image Channel satellite Images are of three types:

i) Visible Satellite Images: Visible images show the visible light that is reflected off of clouds and the surface of the earth. Visible imagery is only taken during the day (in the area where the satellite is located). They show all types of clouds and are the best type of images for seeing low level systems, which do not show up well on infrared imagery. Visible satellite images are photographs of the earth that provide information about cloud cover. Areas of white indicate clouds while shades of gray indicate generally clear skies. Thicker clouds have a higher reflectivity (or albedo) and appear brighter than thinner clouds on a visible image. However, it is difficult to distinguish among low, middle, and high level clouds in a visible satellite image, since they can all have a similar albedo and for this distinction, infrared satellite images are useful [5][6][7].

ii) Infrared Satellite Images: Infrared imagery shows the amount of heat emitted by the different cloud features and the surface of the earth. Infrared images show clouds at higher levels better because they are colder. Infrared satellite measurements are related to the brightness temperature. The images shows really negatives of the images, because areas that are white are ones that are colder (emit less infrared light), and areas that are dark are warmer. This is done so that the images look similar to visible images. Since temperature in the troposphere decreases with height, high level clouds are colder than low level clouds. Therefore, low clouds appear darker on an infrared image and higher clouds appear brighter [5][6][7].

ii) Water Vapor Satellite Images: Water Vapor images are images that show water vapor in the upper troposphere. This troposphere is the only area of the atmosphere generally important in everyday weather

forecasting. The systems shown by water vapor images are upper level systems and are often different from those found at the surface. These systems have a large effect on the systems that are found at the surface. Water vapor images are useful for pointing out regions of moist and dry air, which also provides information about the swirling middle troposphere wind patterns and jet streams. Brighter area on the image represents greater area of moisture in the mid and upper level of atmosphere. Darker area represents drier area of moisture in the mid and upper levels. Very cold air can also show up fairly bright [5][6][7].

B. Visible Vs Infrared Vs Water Vapor Satellite Images

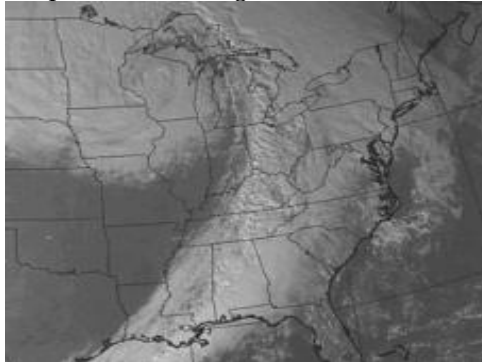


Figure 1: Visible Satellite Image

Visible images measure scattered light and the above figure 1 depicts a wide line of clouds stretching across the southeastern United States and then northward into Ontario and Quebec.

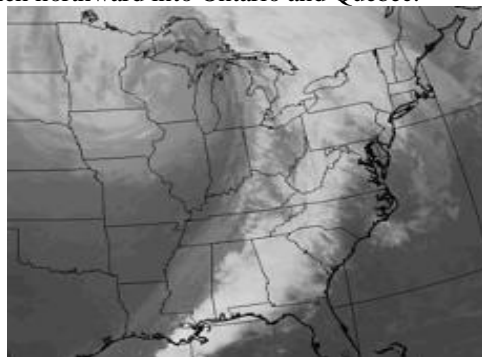


Figure 2: Infrared Satellite Image

In contrast, infrared images are related to brightness. Therefore, the clouds in image appear gray in the infrared image because of they are lower and have relatively warm cloud tops. The warmer the temperature, the lower the clouds, the darker the color.

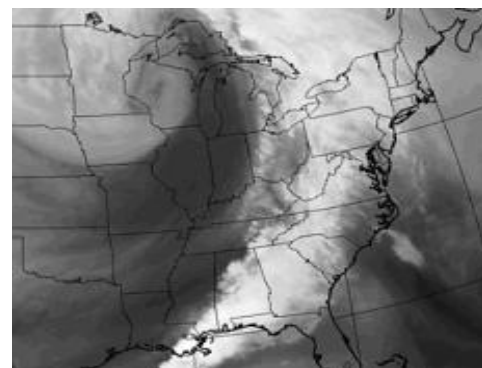


Figure 3: Water Vapor Satellite Image

These clouds are associated with a large area of moist air covering most of the eastern third of the United States visible in the water vapor image as the extensive area of white [5][6][7]. This paper, uses a widely accepted MATLAB for image processing and cloud feature extraction, and data mining tool called Weka[20] for applying Apriori algorithm for finding relationship between different attributes and useful information is derived from the results.

II. Literature Survey

Using fuzzy SOM strategy for satellite image retrieval and information mining projected by yo-ping hung, tsun-wei and li-jen kao. They proposed a model for efficient satellite image retrieval and knowledge discovery. It has two major parts. First, it uses computation algorithm for off-line satellite image feature extraction, image data representation and image retrieval. Important parameter can be extracted from the satellite image by the CBIR (content based image retrieval) technique to discover knowledge about the current whether condition. The extracted features are high pressure, cloud layer, linear cloud and typhoon. A dataset is created by these parameters to apply the association rule. A self organization feature is used to construct a two layer satellite image concept hierarchy. The events are stored in one layer and the corresponding feature vectors are categorized in the other layer. Second, a user friendly interface is developed that retrieves images of interest and mines useful information based on the event in concept hierarchy [1].

“Content Based Image Retrieval of Satellite Imageries Using Soft Query Based Color Composite Techniques” by Y N Mamatha and A.G Ananth, focused on developing image indexing techniques which have the capability to retrieve image based on their contents. The technologies are now generally referred to as Content-Based Image Retrieval (CBIR). Due to its extensive potential applications, CBIR has attracted a great amount of attention in recent years. Using colors as the content, content based image processing have been carried out for a sample of high resolution urban image and low resolution rural image scenes obtained from satellites. The color based processing has been utilized to identify important urban features such as buildings and gardens and rural features such as natural vegetation, water bodies and fields applying various techniques. The techniques included color based extractions using neighborhood rules and histograms. An estimation of the features and available resources from the imageries have been made using the color spectral graphs [17].

Wavelet based features for color texture Classification with application to CBIR. This paper describes an algorithm for texture feature extraction using wavelet decomposed coefficients of an image and its complement. Four different approaches to color texture analysis are tested on the classification of images from the VisTex database. The first method employs multispectral approach, in which texture features are extracted from each channel of the RGB color space. The second method uses HSV color space in which texture features are extracted from the luminance channel V and color features from the chromaticity channels H and S. The third method uses YCbCr color space, in which texture features are extracted from the luminance channel Y and color features from the chromaticity channels Cb and Cr. The last one uses gray scale texture features computed for a color image. The classification results show that the multispectral method gives the best percentage of 97.87%. Further, this multispectral method for texture classification is applied to RBIR system. Experiments are carried out on Wang’s dataset using JSEG for segmentation. The results are encouraging. Experiments are also carried out to study the effect of segmentation on the retrieval performance [18].

YU Changhui , Yuan Yuan ,Miao Minjing , Zhu Menglu “ Cloud detection method based on feature extraction in remote Sensing images” presented a cloud detection method based on feature extraction for remote sensing images. At first, they find out effective features through training pattern, the features are selected from gray, frequency and texture domains. The different features in the three domains of the training samples are calculated. Through the result of statistical analysis of all the features, the useful features are picked up to form a feature set. In concrete, the set includes three feature vectors, respectively, the gray feature vector constituted of average gray, variance, first-order difference, entropy and histogram, the frequency feature vector constituted of DCT high frequency coefficient and wavelet high frequency coefficient, and the texture feature vector constituted of the hybrid entropy and difference of the gray-gradient co-occurrence matrix and the image fractal dimension. Secondly, a thumbnail will be obtained by down sampling the original image and its features of gray, frequency and texture are computed. Then the cloud region judged by the comparison between the actual feature values and the thresholds determined by the sample training process. Experimental results show that the clouds and ground objects can be separated efficiently, and our method can implement rapid clouds detection and cloudiness calculation [15].

Noureldin Laban, Ayman Nasr, Motaz ElSaban, Hoda Onsi “Spatial Cloud Detection and Retrieval System for Satellite Images ” developed spatial cloud detection and retrieval system (SCDRS) that introduce a complete framework for specific semantic retrieval system. It uses a Query by polygon (QBP) paradigm for the content of interest instead of using the more conventional rectangular query by image approach. First, they extract features from the satellite images using multiple tile sizes using spatial and textural properties of cloud regions. Second, they retrieve tiles using a parametric statistical approach within a multilevel refinement process. This approach has been experimentally validated against the conventional ones yielding enhanced precision and recall rates in the same time [16].

III. Method Used To Extract Cloud Features From Satellite Images And Knowledge Discovery

A. Histogram to extract the cloud features

A histogram is bar graph that shows a distribution of data. In image processing, histograms are used to show how many of each pixel value are present in an image. Histograms can be very useful in determining which pixel values are important in an image. From this data we can manipulate an image to meet our specifications. Data from a histogram can aid you in contrast enhancement and thresholding. The gray-scale histogram of an image represents the distribution of the pixels in the image over the gray-level scale. It can be visualised as if each pixel is placed in a bin corresponding to the colour intensity of that pixel. All of the pixels in each bin are then added up and displayed on a graph. The histogram is a key tool in image processing. It is one of the most useful techniques in gathering information about an image. It is especially useful in viewing the contrast of an image. If the grey-levels are concentrated near a certain level the image is low contrast. Likewise if they are well spread out, it defines a high contrast image

The gray-scale histogram of an image represents the distribution of the pixels in the image over the gray-level scale. It can be visualised as if each pixel is placed in a bin corresponding to the colour intensity of that pixel. All of the pixels in each bin are then added up and displayed on a graph. The histogram is a key tool in image processing. It is one of the most useful techniques in gathering information about an image. It is especially useful in viewing the contrast of an image. If the grey-levels are concentrated near a certain level the image is low contrast. Likewise if they are well spread out, it defines a high contrast image.

B. Knowledge Discovery using Association Rule Mining

Association rule learning is a popular and well researched method for discovering interesting relations between variables in large databases. It is intended to identify strong rules discovered in databases using different measures of interestingness. Based on the concept of strong rules, association rules for discovering regularities between products in large-scale transaction data. For a given transaction database T, an association rule is an expression of the form $X \rightarrow Y$, where X and Y are subsets of A and $X \rightarrow Y$ holds with confidence τ , if $\tau\%$ of transaction in D that support X also support Y. The rule $X \rightarrow Y$ has support σ in the transaction set T if $\sigma\%$ of transaction in T supports XUY [11].

IV. Proposed Work

Most weather satellite images are collected in a gray tone display. In this format, each pixel is assigned a tone that represents a level of energy (called the brightness value) sensed by the satellite. The tone is white, black, or an array of intermediate gray shades (known as gray scale). Typically, there are 256 possible brightness values or shades of gray in a satellite image. Different features on the Earth or in the atmosphere have different brightness values, therefore the relative brightness aids in the identification of feature in a satellite image [7]. In all types of imagery the degree of contrast, or gray tone difference, between an object and its background is important. The greater the contrast, the easier it is to identify features in satellite imagery. When contrast is poor, enhancement techniques can be used to make accurate interpretation easier. To enhance an image, all the pixels in a specific range of brightness values are highlighted to locate the features of interest. For example, flood forecasters use IR imagery to look for specific cloud top temperatures that indicate heavy precipitation. By highlighting all the pixels with the corresponding brightness values, one can locate the area within a storm where heavy precipitation is most likely [7].

The proposed work extracts the cloud feature from all types of satellite images. To extract High Cloud and Low Cloud, IR images are used. Visible Image gives to cloud feature, Thin Cloud and Thick Cloud. Likewise Water Vapor satellite image is used to extract Moisture and drier. These can also be seen in table 1.

Table 1: the features that will be extracted

Features to be extracted	How to identify feature	From which image
High cloud	Bright white	IR Images
Low Cloud	Very dark	
Thin Cloud	White	Visible Image
Thick Cloud	Bright White	
Moisture	Brighter area	Water Vapor Image
Drier	Darker Area	

Table 1 contains feature in the first column, in second column how to identify that feature and in last column from which image that particular feature will be extracted [5][6][7].

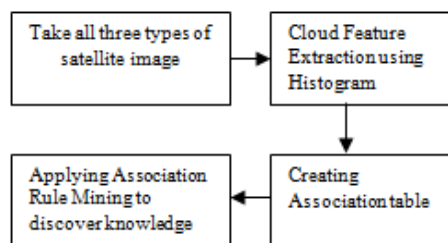


Figure 4: Block Diagram of proposed work

Figure 4 showing the block diagram of the proposed work. All the imagery used in the work are taken as input in the system.

A. Cloud Feature Identification

Generally all the satellite images grey color. Above discussed feature can be identified by there intensity value of histogram. We normally can that the specified feature exists in the image or not by seeing a satellite image. As shown in table 1, High cloud can be identified by Bright White. We can say that high cloud exists in the infrared image if we see a bright white area in image. We can say the same think for visible image and Water vapor image. Bright white in visible image means thick cloud exists otherwise thin cloud. In the same way, brighter in water vapor is the moisture area [5][6][7].

B. Cloud Feature Extraction

To extract the entire feature discussed above histogram is used. Histogram of each images are calculated and all the histogram values are stored in the database. These values are used to decide which cloud feature is existing in an image. There is a fixed threshold value is chosen on the basis of experiment on no. of satellite images. This threshold value is 4300 pixel in 255 bin.

If no. of pixel is greater than 4300 in 255 bin in histogram of infrared image then image contain high cloud otherwise low cloud. If in histogram of visible satellite image, no. of pixel is greater than 4300 it contain thick cloud other wise thin cloud. Likewise if there is no. of pixel is greater than 4300 in histogram of water vapor then there is moisture is exists in the image otherwise drier.

C. Knowledge Discovery using Association Rule

All the features extracted from three types of satellite image using Histogram method, collected in a table to create an Association Transaction table. In this table row represents image ID and column represents extracted cloud feature from satellite images. If feature exists in image there is Y in the respective cell otherwise N. This table helps to get the knowledge about the weather. Association Rule mining is applied on this table which help to know that which event can occur together.

Below are some general rules to determine cloud characteristics when comparing visible and infrared satellite images [19].

1. If the cloud is bright white on infrared then it is a high cloud or has a cloud top that is developed high into the troposphere.
2. If a cloud is bright white on visible but is not bright on infrared then it is likely this is a cloud that is close to the earth's surface. This can happen when there is a thick layer of fog or stratus near the surface.
3. If cloud is seen on visible but very hard to see on infrared then it could be a layer of fog or shallow stratus nears the surface.
4. Thunderstorms will show bright white on both visible and infrared. A thick cloud will be bright white on visible and cold cloud tops will show bright white on infrared. Look for other features also to make sure it is a thunderstorm such as anvil blowoff, overshooting top and extremely textured on visible imagery.
5. If a cloud is not very white on visible then it is likely a thin cloud. If a cloud is not very white on infrared then it is likely a cloud near the surface or it is a very thin cloud.
6. When the sun is close to setting, clouds will not show up as white on visible imagery due to less reflection.
7. Wispy looking clouds on visible that are very white on infrared are likely high level clouds such as cirrus or anvil blow off.
8. Cumulus clouds have a lumpy texture. Stratus clouds have a flat texture especially on infrared. Cirrus clouds tend to be thin and show up white on infrared [19].

D. Proposed work algorithm

Algorithm

1. Input satellite images
2. Translate and resize images
3. Calculate histogram and store histogram values in a table with there bin as index.
4. Check no. pixel in 255bin of each image histogram
 - A. For infrared image
 - a. If no. of pixel in 255 bin of infrared histogram < 4300
<Low Cloud>
 - b. Otherwise
<High Cloud>
 - B. For Visible Image
 - a. If no. of pixel in 255 bin of visible image histogram < 4300
<Thin cloud>
 - b. Otherwise
<Thin Cloud>
 - C. For Water Vapor Image
 - a. If no. of pixel in 255 bin of Water Vapor image histogram < 4300
<Drier>
 - b. Otherwise
<Moisture>
5. Put Y in the association table if feature found otherwise put N.
6. Repeat step 4 and 5 for different images.
7. Apply association rule and discover knowledge.
8. End

V. Result And Discussion

All the images used in this work are downloaded from the website of Indian metrological department www.imd.gov.in

A. Input images

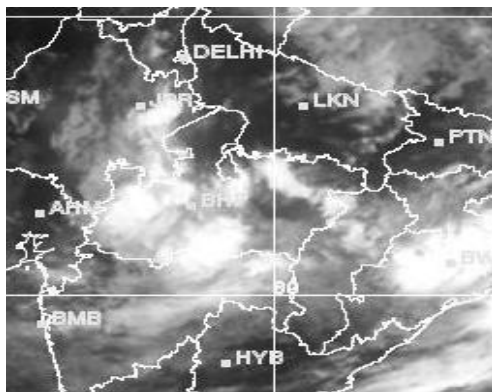


Figure 5: Infrared Satellite image

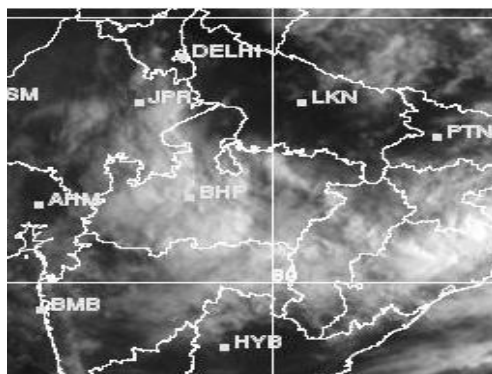


Figure 6: Visible Satellite image

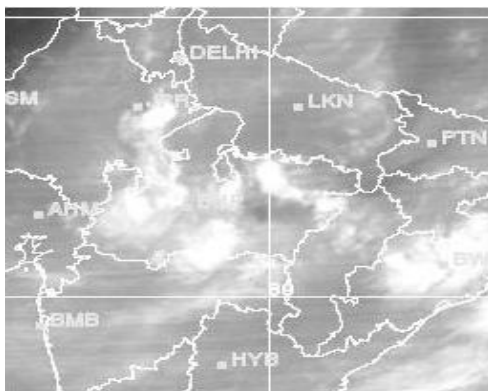


Figure 7: Water Vapor Satellite Image

All the satellite images used in this work are taken as input. In the proposed work all three types of satellite imagery are used which are downloaded from the website of Indian Metrological Department and this website is <http://www.imd.gov.in/section/satmet/dynamic/insat.htm>

B. Feature table

Table 2 The features that will be extracted

High Cloud	Low Cloud	Moisture	Drier	Thick cloud	Thin cloud	Rainfall
Y	N	N	Y	N	Y	No
N	Y	Y	N	Y	N	No
Y	N	N	Y	N	Y	No
N	Y	N	Y	N	Y	No
Y	N	Y	N	Y	N	Yes
Y	N	Y	N	Y	N	Yes
N	Y	Y	N	Y	N	No
Y	N	Y	N	Y	N	Yes
Y	N	Y	N	Y	N	Yes
N	Y	Y	N	Y	N	No

Table 2 represents six attributes which are High cloud, Low cloud, Thick Cloud, Thin Cloud, Moisture, and Drier. Here, Y is representing the cloud exist in image and N is representing not exist the cloud.

C. Association Rule

Minimum support: 0.75 (7 instances)

- Thick cloud=Y 7 ==> Moistured=Y 7 <conf:(1)> lift:(1.43) lev:(0.21) [2] conv:(2.1)
- Moistured=Y 7 ==> Thick cloud=Y 7 <conf:(1)> lift:(1.43) lev:(0.21) [2] conv:(2.1)
- Thin cloud=N 7 ==> Drier=N 7 <conf:(1)> lift:(1.43) lev:(0.21) [2] conv:(2.1)
- Drier=N 7 ==> Thin cloud=N 7 <conf:(1)> lift:(1.43) lev:(0.21) [2] conv:(2.1)
- Drier=N Thick cloud=Y 7 ==> Moistured=Y 7 <conf:(1)> lift:(1.43) lev:(0.21) [2] conv:(2.1)
- Thick cloud=Y 7 ==> Moistured=Y Drier=N 7 <conf:(1)> lift:(1.43) lev:(0.21) [2] conv:(2.1)
- Drier=N Thin cloud=N 7 ==> Moistured=Y 7 <conf:(1)> lift:(1.43) lev:(0.21) [2] conv:(2.1)
- Drier=N 7 ==> Moistured=Y Thin cloud=N 7 <conf:(1)> lift:(1.43) lev:(0.21) [2] conv:(2.1)
- Moistured=Y 7 ==> Drier=N Thin cloud=N 7 <conf:(1)> lift:(1.43) lev:(0.21) [2] conv:(2.1)
- Moistured=Y Thick cloud=Y 7 ==> Thin cloud=N 7 <conf:(1)> lift:(1.43) lev:(0.21) [2] conv:(2.1)

Minimum support: 0.35 (3 instances)

- Thick cloud=Y 7 ==> Moistured=Y 7 <conf:(1)> lift:(1.43) lev:(0.21) [2] conv:(2.1)
- Moistured=Y 7 ==> Thick cloud=Y 7 <conf:(1)> lift:(1.43) lev:(0.21) [2] conv:(2.1)
- High Cloud=N 4 ==> Rainfall=No 4 <conf:(1)> lift:(1.67) lev:(0.16) [1] conv:(1.6)
- High Cloud=Y Thick cloud=Y 4 ==> Moistured=Y 4 <conf:(1)> lift:(1.43) lev:(0.12) [1] conv:(1.2)
- High Cloud=Y Moistured=Y 4 ==> Thick cloud=Y 4 <conf:(1)> lift:(1.43) lev:(0.12) [1] conv:(1.2)
- High Cloud=Y Moistured=Y 4 ==> Rainfall=Yes 4 <conf:(1)> lift:(2.5) lev:(0.24) [2] conv:(2.4)

7. High Cloud=Y Thick cloud=Y 4 ==> Rainfall=Yes 4 <conf:(1)> lift:(2.5) lev:(0.24) [2] conv:(2.4)
8. High Cloud=Y Moistured=Y Thick cloud=Y 4 ==> Rainfall=Yes 4 <conf:(1)> lift:(2.5) lev:(0.24) [2] conv:(2.4)
9. High Cloud=Y Thick cloud=Y 4 ==> Moistured=Y Rainfall=Yes 4 <conf:(1)> lift:(2.5) lev:(0.24) [2] conv:(2.4)
10. High Cloud=Y Moistured=Y 4 ==> Thick cloud=Y Rainfall=Yes 4 <conf:(1)> lift:(2.5) lev:(0.24) [2] conv:(2.4)
11. High Cloud=N Moistured=Y 3 ==> Rainfall=No 3 <conf:(1)> lift:(1.67) lev:(0.12) [1] conv:(1.2)
12. High Cloud=N Thick cloud=Y 3 ==> Rainfall=No 3 <conf:(1)> lift:(1.67) lev:(0.12) [1] conv:(1.2)
13. Moistured=N Thick cloud=N 3 ==> Rainfall=No 3 <conf:(1)> lift:(1.67) lev:(0.12) [1] conv:(1.2)
14. Thin cloud=N 7 ==> Drier=N 7 <conf:(1)> lift:(1.43) lev:(0.21) [2] conv:(2.1)
15. Drier=N 7 ==> Thin cloud=N 7 <conf:(1)> lift:(1.43) lev:(0.21) [2] conv:(2.1)
16. Low Cloud=N Thin cloud=N 4 ==> Drier=N 4 <conf:(1)> lift:(1.43) lev:(0.12) [1] conv:(1.2)
17. Thin cloud=Y 3 ==> Drier=Y 3 <conf:(1)> lift:(3.33) lev:(0.21) [2] conv:(2.1)
18. Drier=Y 3 ==> Thin cloud=Y 3 <conf:(1)> lift:(3.33) lev:(0.21) [2] conv:(2.1)
19. Drier=Y 3 ==> Rainfall=No 3 <conf:(1)> lift:(1.67) lev:(0.12) [1] conv:(1.2)
20. Low Cloud=Y Thin cloud=N 3 ==> Drier=N 3 <conf:(1)> lift:(1.43) lev:(0.09) [0] conv:(0.9)
21. Drier=Y Thin cloud=Y 3 ==> Rainfall=No 3 <conf:(1)> lift:(1.67) lev:(0.12) [1] conv:(1.2)

Interpretation of above rules:

1. An important conclusion of these rules is that if High cloud, thick cloud and moisture are high then rainfall is high.
2. These rules represent if low cloud, thin cloud and drier are high then rainfall is low.
3. These rules show the strong relationship between High cloud, thick cloud and moisture.
4. These rules also show the relation between low cloud, thin cloud and drier attributes.
5. Rainfall and moisture is associated with thick cloud.
6. If thick cloud is exist in the visible satellite image then there is possible that moisture is available in the water vapor image.
7. This is possible that if drier exists in the satellite image then thin cloud is available in the visible image.
8. High cloud is associated with the moisture. This is possible that if high cloud is high then moisture will also high.
9. Thin cloud and low cloud are associated with drier.
10. Thick cloud and moisture play an important role for rainfall.

VI. Conclusion

This paper discovers different types of cloud from three types of satellite image and associates them to discover the relation between them. This paper has two results. One is association table that is create by histogram of satellite images and second is getting knowledge by applying association rule mining. The association table shows different cloud attributes and cell contain Y and N. Y shows existence of cloud and N shows not existence of cloud. Final results show the relation between the different clouds. An important conclusion of these rules is that if High cloud, thick cloud and moisture are high then rainfall is high.

REFERENCES

- [1] Yo-Ping Huang, Tsun-Wei Chang and Li-Jen Kao "Using Fuzzy SOM Strategy for Satellite Image Retrieval and Information Mining" CITSA 2007, Florida, USA. ISBN 1-934272-10-8.
- [2] Y. Li, T. Bretschneider "Semantics-Based Satellite Image Retrieval Using Low-Level Features" IEEE 2004.
- [3] Senduru Srinivasulu, P. Sakthivel "Extracting Spatial Semantics in Association Rules For Weather Forecasting Image" IEEE 2010.
- [4] Image Mining: Trends and Developments <http://www.comp.nus.edu.sg/~whsu/publication/2002/JIIS.pdf>.
- [5] <http://www.imd.gov.in/section/satmet/dynamic/insat.htm>
- [6] [http://ww2010.atmos.uiuc.edu/\(Gh\)/guides/rs/sat/img/vis.rxml](http://ww2010.atmos.uiuc.edu/(Gh)/guides/rs/sat/img/vis.rxml)
- [7] An Introduction to Satellite Imagery Interpretation by Eric.
- [8] Mahendra Kumar Gurve, Jyoti Sarup "Satellite Clout Image Processing and Information Retrieval System" IEEE 2012.
- [9] R.M. Haralick, K. Shanmugam, I. Dinstein. Textural features for image classification. IEEE Transactions on Systems, Man, and Cybernetics, Vol.3, No. 6, 1973, 610–621.
- [10] Mahendra Kumar Gurve, Jyoti Sarup. "Satellite Cloud Image Processing And Information Retrieval System" 978-1-4673-4805-8 IEEE 2012.
- [11] Data Mining Techniques by Arun K Pujari.
- [12] Getachew Berhan, Tsegaye Tadesse, Solomon Atnafu, Shawndra Hill, "Drought Information Mining from Satellite Images for Improved Climate Mitigation" 987-1-4673-4805-8/12 IEEE 2012.

- [13] Yikun Li and Timo R. Bretschneider, "Semantic-Sensitive Satellite Image Retrieval" 0196-2892 IEEE 2007.
- [14] Seema H.Jadhav¹, Dr.Shah Aqueel Ahmed "A Content Based Image Retrieval System using homogeneity Feature extraction from Recency-based Retrieved Image Library" IOSRJCE, ISSN: 2278-0661, ISBN: 2278-8727 Volume 7, Issue 6 (Nov-Dec. 2012), PP 13-24.
- [15] YU Changhui , Yuan Yuan ,Miao Minjing , Zhu Menglu " Cloud detection method based on feature extraction in remote Sensing images" International Archives of the Photogrammetry, Remote Sensing and Spatial Information Sciences, Volume XL-2/W1, 2013 8th International Symposium on Spatial Data Quality , 30 May - 1 June 2013, Hong Kong.
- [16] Noureldin Laban, Ayman Nasr, Motaz ElSaban, Hoda Onsi "Spatial Cloud Detection and Retrieval System for Satellite Images " (IJACSA), Vol. 3, No. 12, 2012
- [17] Y N Mamatha and A.G Ananth," Content Based Image Retrieval of Satellite Imageries Using Soft Query Based Color Composite Techniques", IJCA (0975 – 8887) Volume 7– No.5, September 2010.
- [18] P.S.Hiremath, S. Shivashankar, and Jagadeesh Pujari, "wavelet based features for color texture Classification with application to CBIR", IJCSNS International Journal of Computer Science and Network Security, VOL.6 No.9A, September 2006.
- [19] <http://www.theweatherprediction.com/habyhints2/512/>
- [20] Web reference: <http://www.cs.waikato.ac.nz/ml/weka/> "Weka's website" as accessed on [05/08/2013].

Numerical Analysis of Header Configuration of the Plate-Fin Heat Exchanger

Pardeep¹, Dr. M.K.Sinha²

¹MTech,²Associate Professor, Department of Mechanical Engineering, NIT Jamshedpur
Email: mail2pardeebishnoi@gmail.com, mksinha.me@nitjsr.ac.in

Abstract: Numerical analysis of a plate fin heat exchanger accounting for the effect of fluid flow maldistribution on the inlet header configuration of the heat exchanger is investigated. In this analysis, it was found that flow maldistribution has effect on the flow perpendicular to its velocity direction. The peak velocity occurs in the central zone of the header while the velocity along the perpendicular direction of the inlet flow diminishes more and more. By this investigation, the results of the flow maldistribution are presented for a plate fin heat exchanger which is reduced as compared to the existing configuration of the plate fin heat exchanger.

Keywords: Plate fin heat exchanger, Flow maldistribution, Header configuration, Computational Fluid Dynamics (CFD).

I. Introduction

Plate fin heat exchanger is specially designed for transferring the heat between medium and low pressure fluids. It is small in size but having high efficiency heat exchanger. It uses the metal plates to transfer heat between two fluids. A major advantage of the plate fin heat exchanger over a conventional heat exchanger is that the fluids are exposed to a much larger surface area because the fluids spread out over the plates. This facilitates the transfer of heat and greatly increases the speed of the temperature change. With the characteristics of compact structure, light weight and high heat transfer efficiency. The aluminum plate fin heat exchanger is widely used in various industries such as industrial gas separation plant, LNG plant, petrochemical, transportation and refrigeration plant, aerospace, chemical engineering, artificial organs. In the design of the plate fin heat exchanger, it is generally assumed that the fluid flow distribution is uniformly distributed among all the parallel fin passages through the heat exchanger core. But in actual practices, it is impossible to distribute the fluid flow uniformly because of flow maldistribution. Flow maldistribution is a non-uniform distribution of mass flow rate in a heat exchanger core. Flow maldistribution depends on several factors such as heat exchanger's geometrical configuration (i.e. mechanical design, channel and header geometry and dimensions, manufacturing tolerances or imperfections), operating conditions (flow velocity changes along the headers, fluid viscosity, and multiphase flow). Flow maldistribution is a very important factor that affects the performance of heat exchanger to a great extent [1].

A number of researchers have studied the maldistribution problem analytically and experimentally. Ch. Ranganayakulu et al [2] studied a cross flow plate-fin compact heat exchanger, accounting for the combined effects of two-dimensional longitudinal heat conduction through the exchanger wall and non-uniform inlet fluid flow and temperature distribution is being carried out by using a finite element method. Koen Grijspeerdt et al [3] analyzed the flow pattern of milk between two corrugated plates that was carried out using 2D and 3D computational fluid dynamics (CFD). The results obtained can be helped identifying those regions where turbulent backflows and thus higher temperature regions near the wall can occur. L. J. Shah et al. [4] developed a three block model for the analysis purposes through which revealed that fluid distribution along the mantle is being affected by recirculation produced due to buoyancy force in the mantle in case of high and low temperature inputs, respectively. Jian Wen and Yan Zhong Li [5] analyzed the fluid flow maldistribution for the conventional header used in industry. According to him, a baffle with small holes of three different kinds of diameters is recommended to be installed in the header to control the flow maldistribution in the heat exchanger. The numerical result obtained effectively improved the performance of the heat exchanger. Zhe Zhang and Yan Zhong Li [6] found that the flow maldistribution is very serious in the perpendicular to the flow of header for the conventional header used in industry. By the investigation, two modified headers with a two-stage-distributing structure are proposed and simulated. It is verified that the fluid flow distribution in plate-fin heat exchangers is more uniform if the ratios of the outlet and inlet equivalent diameters for both headers are

equal. Li-Zhi Zhang [7] analyzed that the inlet and outlet duct geometry in an air to air compact heat exchanger is always irregular. The results indicated that flow distribution depends upon the channel pitch size. V. V. Dharaiya et al [8] studied the flow distribution through a plate-fin heat exchanger (straight Z-type flow) with parallel micro-channels and mini-channels by using a CFD code FLUENT. They suggested that the flow maldistribution was quite severe with constant cross-sectional area headers. Myoung II Kim et al. [9] estimated the flow pattern characteristics of the shell-and-tube type heat exchanger. Different header types were considered and results indicated that the smallest header length and minimum flow rate (655 mm and $0.54 \text{ m}^3\text{s}^{-1}$) is not sufficient in distributing the flow uniformly along the length whereas the larger length header (1092.5 mm and $1.62 \text{ m}^3\text{s}^{-1}$) yields the best results.

The main objective behind this present work is to investigate the previously developed header configuration systematically and to optimize the design for the plate fin heat exchangers regarding flow distribution i.e. to reduce the effect of flow maldistribution for the Reynolds number from $\text{Re}=4000\text{-}6000$.

Noneclature

k - turbulent kinetic energy(m^2s^{-2})

n – channel number

S – flow nonuniformity

s_Φ -source term for generalized transport variable Φ

SIMPLEC – Simple Implicit Method for the Pressure Linked Equation Consistent

Greek Symbol

ε -turbulent energy dissipation rate(m^2s^{-3})

Γ - effective diffusivity(m^2s^{-1})

ρ -density of the fluid(kgm^{-3})

Φ -a generalized transport variable.

II. Analysis of the Flow Maldistribution in Plate-Fin Heat Exchanger

2.1 CFD Model

Fig 1 shows a parametric view of the plate fin heat exchanger with its geometrical dimensions. The section of the plate fin heat exchanger has the dimension of $200 \times 250 \times 178 \text{ mm}$. The inlet tube of header is of 40 mm in diameter and the length of the header is 250 mm . The header consists of a hemicylindrical tube of 60 mm diameter and 250 mm in length. It has T-shaped connection with the inlet tube.

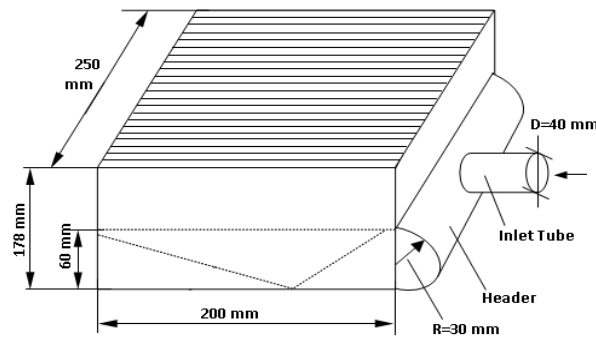


Plate -fin heat exchanger
Fig. 1

2.2 Mathematical Model Equation:

In this design process, to determine the flow motion a nonlinear Partial differential equation i.e. Reynolds transport equation is used.

$$\frac{\partial y}{\partial x} (\rho u \Phi) + \frac{\partial}{\partial r} (r \rho v \Phi) + \frac{\partial}{\partial \theta} (r \rho w \Phi) = \frac{\partial}{\partial x} \left(\Gamma \frac{\partial \Phi}{\partial x} \right) + \frac{\partial}{\partial r} \left(\Gamma r \frac{\partial \Phi}{\partial r} \right) + \frac{\partial}{\partial \theta} \left(\Gamma r \frac{\partial \Phi}{\partial \theta} \right) + S_\Phi$$

Where, Φ stands for a generalized transport variable, which is used for all conserved variables in a fluid flow problem, including mass, momentum, and the turbulence variables k and ε . Γ represents the effective

diffusivity (sum of the eddy diffusivity and the molecular diffusivity). s_{ϕ} is the source term for the respective dependent variable. The initial step for solving a partial differential equation is to discretize the equation. Here, Gauss Seidel method is used. The accuracy of the solution depends upon the mesh size. The solution of above equation develops the velocity and turbulence levels in the header.

2.3 Boundary Conditions

Initial conditions are given as follows:

At inlet the axial velocity is specified i.e. no radial or swirl components, outlet is considered as pressure outlet and for walls adiabatic and non slip boundary condition are applied. Convergent condition is specified to scaled residuals $\leq 10^{-6}$. The solution converges when the change in the solution variable in consecutive iterations are negligible.

2.4 Analysis of Flow maldistribution

2.4.1 Numerical Solution Procedure

The whole analysis is performed on ANSYS-FLUENT version 14.0 developed by ANSYS inc. In today's industry sector, ANSYS is one of the widely used software for the analysis purposes. The turbulence flow problem is solved through pressure-based segregated algorithm i.e. SIMPLEC scheme (Simple Implicit Method for the Pressure Linked Equation Consistent). For spatial discretization Least Square Cell Based scheme is used. The geometry is created in Solid Edge developed by UGS Corps as shown in Fig.2.

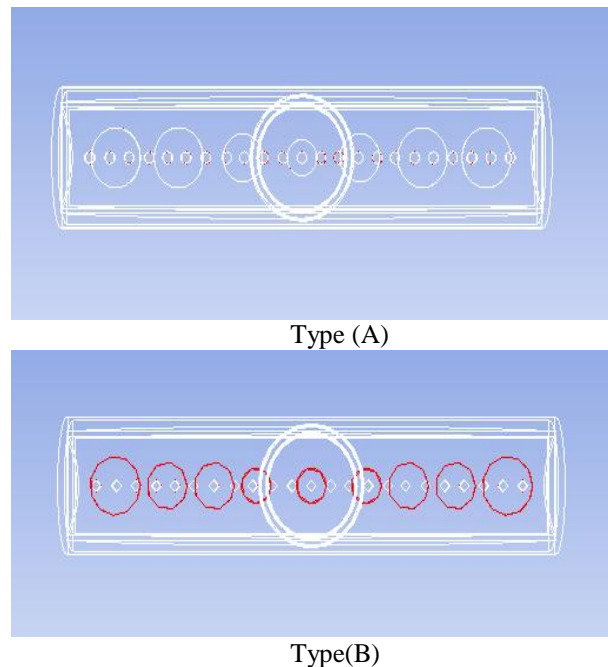


Fig.2 Schematic model of modified header configurations with type(A) and type(B)

Here, two types of header have been designed which are named as type(A) and type(B). Both headers are different in their structural design. Type A represents the header configuration with 7 outlets at the first header and 23 channels at the main outlet while Type B represents the header configuration having 9 outlets at the first header and 23 channels at the main outlet.

2.4.2 Grids

In the present model, a triangular surface mesh is implemented. The number of nodes created is 20134 while the elements are 81432 in number. For the modest geometries, quad/hex meshes provide a good solution as compared to the tri/tet mesh while for the complex geometries, tri/tet shows the good result.

2.4.3 Solver

In this analysis we uses segregated algorithm under the pressure-based solver. In the segregated algorithm the governing equations are solved sequentially, segregated from one another.

2.4.4 Evaluation of flow maldistribution

To evaluate the flow maldistribution in 23 passages , the flow non uniformity for the individual section and the whole section is given as follows:

$$Si = \frac{Vi - Va}{Va}$$

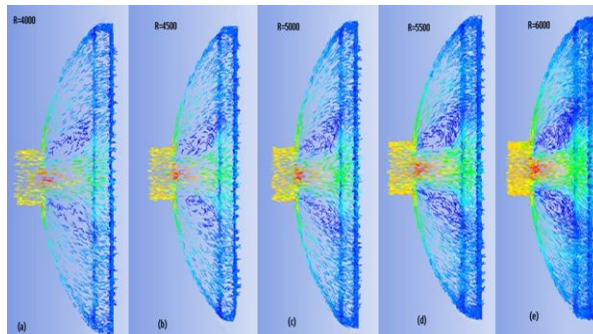
$$S = \sum_{i=1}^n |(Vi - Va)/Va|$$

Where Si and S is the individual flow non uniformity and the total nonuniformity of the crossection .Vi and Va is the flow velocity at the individual section and the average velocity for the whole crossection.

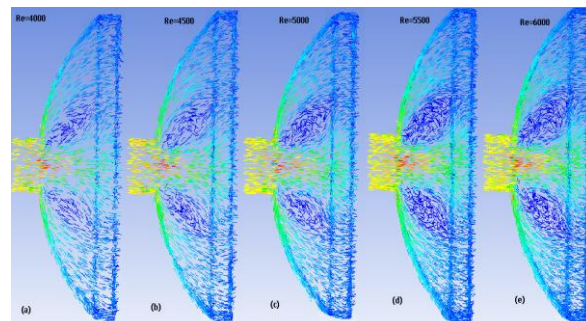
III. Results And Discussion

Flow distribution in the Plate fin heat exchanger with modified header:

In this analysis, we investigate the flow distribution in modified header within the turbulence range i.e.Reynolds number from Re=4000-6000.Figures 3 shows the flow distribution at different Reynolds Number for the modified header configuration.



Type (A)



Type (B)

Fig. 3 Velocity vector distribution for the Type (A) and Type (B) configurations at (a) Re=4000 (b) Re=4500 (c) Re=5000 (d) Re=5500 (e) Re=6000

As shown in the fig. 3 , the yellow coloured portion shows the maximum velocity while the light blue colour shows the minimum velocity. Flow maldistribution increases as the value of Reynolds number increases but it is less as compared with the conventional header configuration. We can also see the uniform distribution of flow along its length. Also, the eddy losses developed due to the reverse flow in the conventional header is being

reduced in the above shown header configuration. The efficiency of the heat exchanger and the flow distribution depends upon the geometrical configuration of the header.

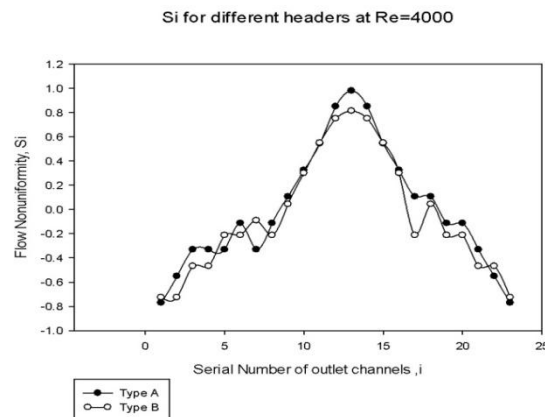


Fig. 4 Flow nonuniformity for the different headers at Re=4000

Comparison of the flow nonuniformity between the both Type A and Type B header configuration has been illustrated in Fig. 4. The flow distribution of Type B is much better than as compared to that of Type A. Also the flow maldistribution reduces from the 0.98 to 0.81 at Reynolds number i.e. at Re=4000. The optimization of the geometrical configuration improves the flow distribution in the heat exchanger. Also, with the increased smooth spread of flow along the length outlet increases the performance of the heat exchanger.

IV. Conclusion

In the present paper, a modified header configuration with two-stage distributing structure is developed and flow distribution in the range of Reynolds Number, Re= 4000-6000 is simulated by CFD. The proposed modified header configuration plays a remarkable role in the flow distribution. The flow nonuniformity has been reduced from 0.98 to 0.81 at Reynolds number, Re=4000. This simulation shows that CFD is a suitable tool for predicting the flow distribution and to optimizing the design of header configuration of the plate fin heat exchanger.

REFERENCES

- [1.] Lalot S, Florent P, Lang SK, Bergles AE. Flow maldistribution in heat exchanger. Applied Thermal Engg. 1999; 26:847-863.
- [2.] Ranganayakulu CH, Seetharamu K N. The combined effects of longitudinal heat conduction flow non uniformity and temperature non uniformity in cross flow in plate fin heat exchanger. IntComm Heat Mass Transfer 1999;26(5):669-678.
- [3.] Koen Grijspeerd et al. Application of CFD to model of the hydrodynamics of plate heat exchangers for milk processing. J. Food Eng. 57 (2003) 237-242.
- [4.] Shah L J et al. Heat Transfer correlation for vertical mantle heat exchanger. Elsevier volume 69, July-Dec 2001, Page 157-171.
- [5.] Jian Wen, Yanzhong Li. Study of flow distribution and its improvement on the header of Plate - fin heat exchanger. Cryogenics 44 (2004) 823-831.
- [6.] Zhang Zhe, Zhong Yan Li. CFD simulation on inlet configuration of plate-fin heat exchangers. Cryogenics 43 (2003) 673-678.
- [7.] ZhangLi-Zhi. Flow maldistribution and thermal performance deterioration in a cross-flow air to air heat exchanger with plate-fin cores. Volume 52, Issues 19-20, Pages 4500-4509.
- [8.] VV Dharaiya. Evaluation of a tapered header configuration to reduce flow maldistribution in mini channels and micro channels. ICNMM2009 June 22-24, Pohang, South Korea.
- [9.] Myoung II Kim et al. CFD Modeling of shell and tube heat exchanger header for uniform distribution among tubes, Korean J. Chem. Eng. 26 (2009) 359-363.
- [10.] User Guide ANSYS FLUENT version 14.0.
- [11.] ANSYS Customer Training Tutorials version 13.0.

Structural Analysis of Ladder Chassis Frame for Jeep Using Ansys

Vishal Francis¹, Rajnish Kumar Rai², Anup Kumar Singh³, Pratyush Kumar Singh⁴, Himanshu Yadav⁵

¹Assistant professor, Department of Mechanical Engineering, SSET, SHIATS Allahabad, Uttar Pradesh, India

^{2, 3, 4, 5}UG students, Department of Mechanical Engineering, SSET, SHIATS Allahabad, Uttar Pradesh, India

Abstract: Automotive chassis frame is an important part of an automobile. The automotive chassis frame is the structural backbone of any vehicle. The main function of chassis frame is to support the body, different parts of an automobile and topayload placed upon it. The chassis frame has to withstand the stresses developed as well as deformation occurs in it and to withstand the shock, twist vibration and other stresses. Its principle function is to carry the maximum load for all designed operating condition safely that should be within a limit. On chassis, frame maximum shear stress and deflection under maximum load are important criteria for design and analysis. In these projects, we have calculated the von mises stress and shear stress for the chassis frame and the finite element analysis has been done for the validation on the chassis frame model of jeep. We have taken certain material as Mild sheet steel, aluminium alloy and titanium alloy for the rectangular hollow box type to design chassis frame of jeep.

Software used in this project, CATIA V5-[Product 1] for design purpose and ANSYS 14 is used for analysis.

Keywords: ladder chassis frame, mild steel, aluminium alloy, titanium alloy, Rectangular Box (Hollow) type cross sections.

I. Introduction

Chassis is a French term and was initially used to denote the frame parts or Basic Structure of the vehicle. It is the backbone of the vehicle. A vehicle without body is called Chassis. The components of the vehicle like Power plant, Transmission System consisting of clutch gearbox, propeller shaft and rear axle, Wheels and Tyres, Suspension, Controlling Systems like Braking, Steering etc., and electrical system parts are also mounted on the Chassis frame. It is the main mounting for all the components including the body. So it is also called as Carrying Unit. Chassis of Automotive helps to keep an automobile rigid, stiff and unbending. Automobile chassis ensures less noise, vibrations and harshness throughout the automobile. The chassis frame consists of side members attached with a series of cross members. Along with the strength, an important consideration in the chassis design is to increase the stiffness (bending and torsion) characteristics. Adequate torsional stiffness is required to have good handling characteristics. Normally the chassis are designed on the basis of strength and stiffness. In the conventional design procedure the design is based on the strength and emphasis is then given to increase the stiffness of the chassis, with very little consideration to the weight of the chassis. One such design procedure involves the adding of structural cross member to the existing chassis to increase its torsional stiffness. As a result weight of the chassis increases. This increase in weight reduces the fuel efficiency and increases the cost due to extra material. The design of the Chassis with adequate stiffness and strength is necessary.

The different types of automobile chassis are as follows.

Conventional control chassis:

In which engine is mounted in front of the driver's cabin. This type of arrangement avoids full utilization of the space.

Semi-forward control chassis:-

In which engine is mounted that half of it is in the driver's cabin whereas the other half is in front, outside the driver's cabin.

Full-forward control chassis:-

In which engine is mounted completely inside the driver's cabin. Obviously maximum utilization of space is achieved in this type of arrangement.

The Different Types Of Automobile Chassis Frame Are As Follows:

Conventional Frame:-

It is non-load carrying frame. The loads of the vehicle are transferred to the suspensions by the frame. This suspension is the main skeleton of the vehicle, which is supported on the axles through springs. The body is made of flexible material like wood and isolated frame by inserting rubber mountings in between. The frame is made of channel section or tubular section of box section.

Ladder Chassis:-

Ladder chassis is one of the oldest forms of automotive chassis these are still used in most of the SUVs today. It is clear from its name that ladder chassis resembles a shape of a ladder having two longitudinal rails inter linked by lateral and cross braces.



Fig. 1 Model of rectangular box (hollow) type of ladder chassis frame.

Types of ladder frame:

Ladder frame are classified as follows.

1. C cross section type of ladder chassis frame
2. I cross-section type of ladder chassis frame.
3. Rectangular Box (Hollow) cross section type of ladder chassis frame.
4. Rectangular Box (Intermediate) cross section type of ladder chassis frame.

II. Literature Review

MohdAzizi Muhammad Nor et al. (2012) This paper aims to model, simulate and perform the stress analysis of an actual low loader structure consisting of I-beams design application of 35 tonne trailer designed in-house by Sumai Engineering Sdn. Bhd, (SESB). The material of structure is LowAlloy Steel A 710 C (Class 3) with 552 MPa of yield strength and 620 MPa of tensile strength. The scope of this study concern on structural design of the I-beams for info and data gathering, which will be used for further design improvement. Finite element modelling (FEM), simulations and analysis are performed using a modelling software i.e. CATIA V5R18. Firstly, a 3-D model of low loader based on design from SESB is created by using CATIA. Stress and displacement contour are later constructed and the maximum deflection and stress are determined by performing stress analysis. Computed results are then compared to analytical calculation, where it is found that the location of maximum deflection agrees well with theoretical approximation but varies on the magnitude aspect. Safety factor for the low loader structure has also been calculated. In the end, the current study is important for further improvement of the current low loader chassis design.

Swami K.I. et al. (Jan. 2014) The Automotive chassis is considered as the backbone of the vehicle. On chassis, different parts are provided with strength, an important consideration in chassis design is to have adequate bending stiffness for better handling characteristics. So, strength and stiffness are two important criteria for the design of the chassis. This paper related with work performed towards the static structural analysis of the truck chassis. Structural systems like the chassis can be easily analysed using the finite element techniques. So a proper finite element model of the chassis is to be developed. The chassis is modelled in ANSYS. Analysis is done using the same software.

Roslan Abd Rahman: does stress analysis on heavy duty truck chassis by finite element package ABAQUS. To improve the fatigue life of components at critical point by design modifications the stresses can be reduced. He uses ASTM low alloy steel a 710 C (Class 3) with 552 MPa of yield strength and 620 MPa of tensile strength for chassis finds the maximum stress 386.9 MPa at critical point occurred at opening of chassis. This critical point is located at element 86104 and node 16045, which was in contact with the bolt from it he concludes, that this critical point is an initial to probable failure

III. Methodology

Finite element analysis is performed to find the von mises stress and shear stress using ansys workbench 14. Three dimensional model of frame was designed using catia software). The design verification can be achieved without elaborate need for prototypes at each phase saving time and effort. A final prototype for the final design review can be employed for verifying the analytical results.

Specification of Ladder chassis:

Wheel Base (WB) = 2380 mm.
 Rear Overhang (ROH) = 1020 mm.
 Front Overhang (FOH) = 450/470 mm.
 Gross Vehicle Weight (GVW) = 3000 kg = 3 ton.
 Length = 3860mm.
 Width = 900mm.

Basic Calculation for Chassis:-

Weight of passengers = Weight per passenger × No. of passengers
 = 75kg × 8
 = 600kg = 0.6 ton

Total load acting on chassis =

Gross vehicle weight + Weight of passengers
 = 3000 kg + 600 kg = 3600 kg
 = 3ton + 0.6 ton
 = 3.6 ton

Chassis has two longitudinal members so load will be acted upon these two longitudinal members. Therefore, load acting on each member will be half of the total load acting on chassis.

Load acting on one longitudinal member = 3.6 ton ÷ 2
 = 1.8 ton.

Specification of Material

A. Mild Sheet Steel:-

Mass density = 7.85 g/cm³
 Yield strength = 225 MPa
 Ultimate Tensile Strength = 450-500 MPa
 Young's Modulus = 200 GPa
 Poisson's ratio = 0.28
 Share modulus = 78.125 GPa

B. Aluminium alloy:-

Mass density = 2.64-2.8 g/cm³
 Yield strength = 35-500 MPa
 Ultimate Tensile Strength = 100-550 MPa
 Young's Modulus = 70-79 (70) GPa
 Poisson's ratio = 0.33
 Share modulus = 26.32 GPa

C. Titanium alloy:-

Mass density = 4.51 g/cm³
 Yield strength = 40-450 MPa.
 Ultimate Tensile Strength = 900-970 MPa
 Young's Modulus = 110-120 (120) GPa
 Poisson's ratio = 0.33
 Share modulus = 45.13 GPa

Design of chassis frame through CATIA



Fig. 2 ladder type chassis frame.

IV. Finite Element Analysis

There are three main steps, namely: pre-processing, solution and post processing. In pre-processing (model definition) includes: define the geometric domain of the problem, the element type(s) to be used, the material properties of the elements, the geometric properties of the elements (length, area, and the like), the element connectivity (mesh the model), the physical constraints (boundary conditions) and the loadings.

In solution includes: the governing algebraic equations in matrix form and computes the unknown values of the primary field variable(s) are assembled. The computed results are then used by back substitution to determine additional, derived variables, such as reaction forces, element stresses and heat flow. Actually, the features in this step such as matrix manipulation, numerical integration and equation solving are carried out automatically by commercial software.

In post processing, the analysis and evaluation of the result is conducted in this step. Examples of operations that can be accomplished include sort element stresses in order of magnitude, check equilibrium, calculate factors of safety, plot deformed structural shape, animate dynamic model behaviour and produce color-coded temperature plots. The large software has a pre-processor and postprocessor to accompany the analysis portion and the both processor can communicate with the other large programs. Specific procedures of pre and post are different dependent upon the program.

The model of existing chassis as per the dimension is as shown in Figure2. The model is then saved in IGES format which can be directly imported into ANSYS workbench. Figure 3 shows the imported model in ANSYS workbench.

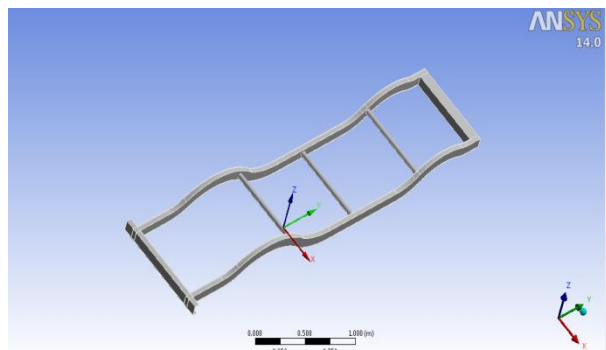


Fig.3 Imported Model in ANSYS Workbench

Meshing of Chassis Frame

The meshing is done on the model with 22996 No. of nodes and 11385 No. of Tetrahedral elements. Figures 3.4 show meshing of model.

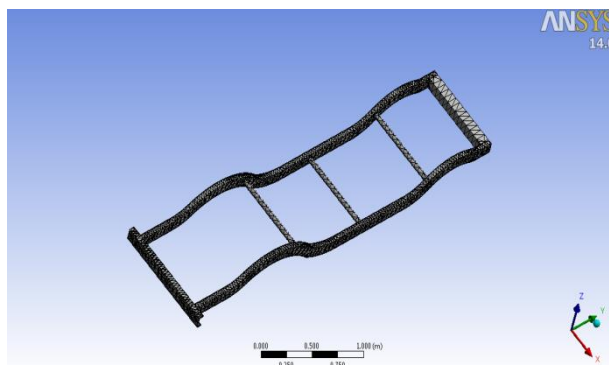


Fig.4 after generating mesh

Loading Condition of Chassis Frame

The jeep chassis model is loaded by static forces from the jeep body and load. For this model, the maximum loaded weight of jeep and body is 3,600 kg. The load is assumed as a uniform distributed obtained from the maximum loaded weight divided by the total length of chassis frame. Detail loading of model is shown in Figure 4.1 and 4.2. The magnitude of force on the upper side of chassis is 35316 N, which is carried by two side bars so load on one side bar is 17658 N.

The formula of design stress is defined by,

$$\text{Design Stress} = \frac{\text{Yield Stress}}{\text{Factor of Safety}}$$

considering factor of safety = 3 for design.

Stress analysis of ladder type chassis frame

1) Mild sheet steel

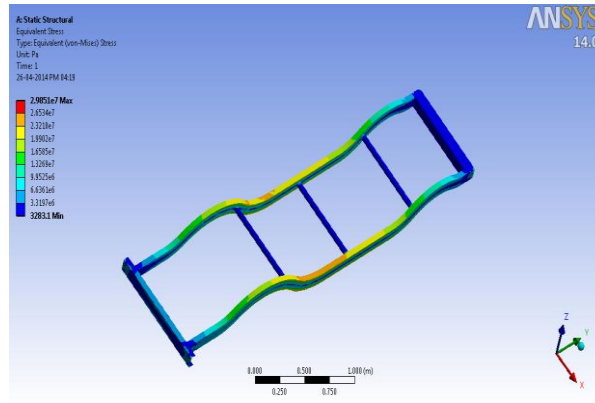


Fig. 5 Von misses stress on chassis frame

Von mises stress maximum value is 29.8 MPa.

Von mises stress minimum value is 0.032 MPa.

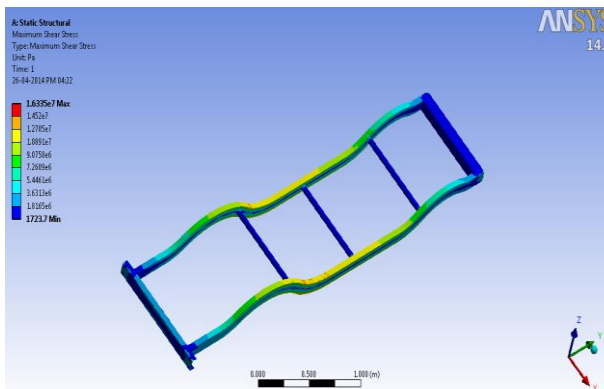


Fig. 6 Shear stress on chassis frame

Shear stress maximum value is 16.33 MPa.

Shear stress minimum value is 0.00173 MPa.

$$\text{Design Stress} = \frac{225}{3}$$

$$\text{Design Stress} = 75 \text{ MPa.}$$

2) Aluminium alloy

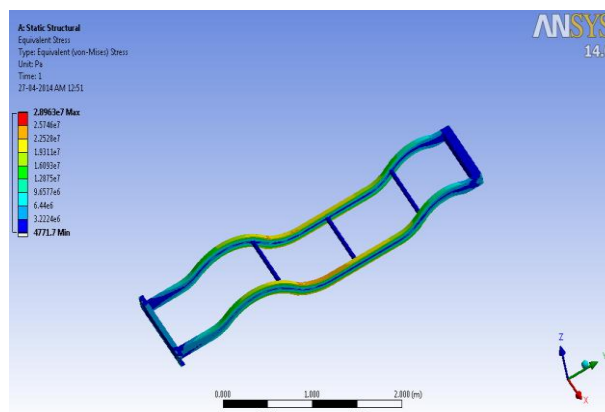


Fig. 7 Von misses stress on chassis frame

Von mises stress maximum value is 28.96 MPa.

Von mises stress minimum value is 0.0047 MPa.

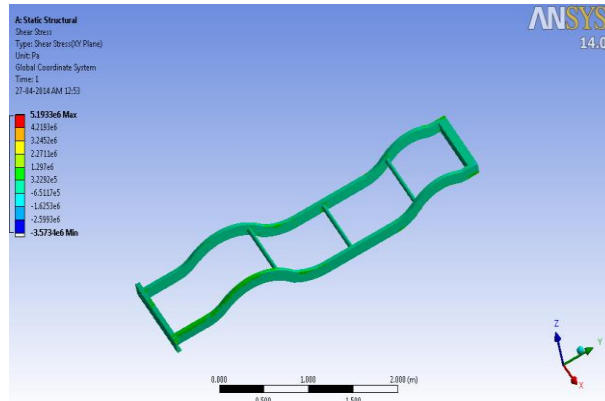


Fig. 8 Shear stress on chassis frame

Shear stress maximum value is 5.19 MPa.
 Shear stress minimum value is -3.57 MPa.

$$\text{Design Stress} = \frac{35}{3}$$

$$\text{Design Stress} = 11.67 \text{ MPa.}$$

3) Titanium alloy

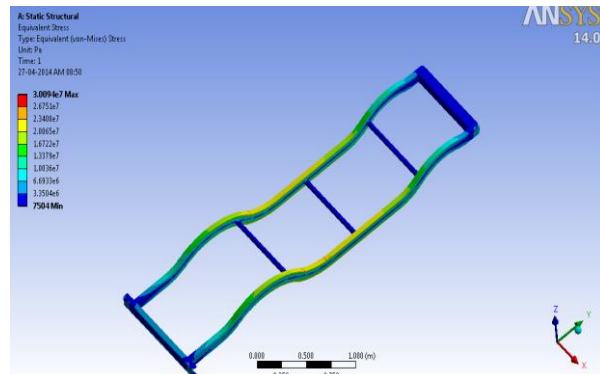


Fig. 9 Von misses stress on chassis frame

Von mises stress maximum value is 30.09MPa.
 Von mises stress minimum value is 0.0075 MPa.

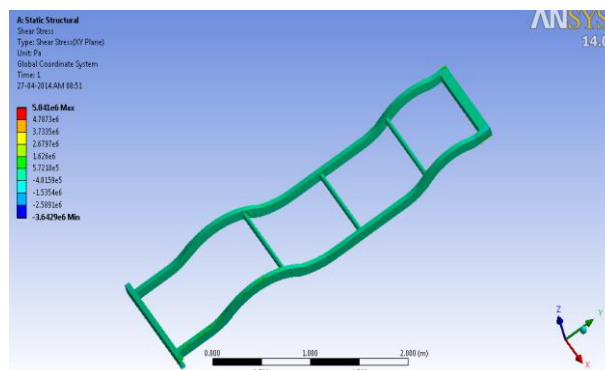


Fig. 10 Shear stress on chassis frame.

Shear stress maximum value is 5.84 MPa.
 Shear stress minimum value is -3.64 MPa

$$\text{Design Stress} = \frac{55}{3}$$

$$\text{Design Stress} = 18.33 \text{ MPa.}$$

stress	Mild sheet steel		Aluminium alloy		Titanium alloy	
	Max. MPa	Min. MPa	Max MPa	Min. MPa	Max MPa	Min. MPa
Von mises stress	29.8	0.032	28.96	0.0047	30.09	0.0075
Shear stress	16.33	0.00173	5.19	-3.57	5.84	-3.64
Design stress	75.00		11.67		18.33	

Table 1 Result

V. Conclusion

In the present work, ladder type chassis frame for jeep was analysed using ANSYS 14 software, based on the analysis following conclusion can be done.

- 1) The generated shear stresses are less than the permissible value so the design is safe for all three materials.
- 2) shear stress was found minimum in aluminium alloy and maximum in mild sheet steel under given boundary conditions.
- 3) Von mises stress was found minimum in aluminium alloy and maximum in titanium alloy under given boundary conditions.

REFERENCES

- [1.] Yucheng Liu, —Crashworthiness Analysis of Finite Element Truck Chassis Model Using LS-DYNAI, 11th International LS-DYNA Users Conference, Department of Mechanical Engineering, University of Louisiana, Lafayette, LA 70504, USA.
- [2.] Vijaykumar V. Patel, R. I. Patel, —Structural analysis of a ladder chassis frameI, World Journal of Science and Technology 2012, 2(4):05-08, ISSN: 2231 – 2587.
- [3.] HemantB.Patil, SharadD.Kachave, EknathR.Deore, —Stress Analysis of Automotive Chassis with Various ThicknessesI, IOSR Journal of Mechanical and Civil Engineering (IOSR-JMCE), Vol. 6, Issue 1 (Mar. - Apr. 2013), PP 44-49
- [4.] A. Rahman, R. Tamin, M. N., Kurdi, O., 2008, “Stress Analysis of Heavy Duty Truck Chassis using Finite Element Method,” Journal Mechanical, No26, 76-85.
- [5.] Monika S. Agrawal, Md. Razik, —A Review on Study of Analysis of ChassisI, International Journal of Modern Engineering Research (IJMER), Vol.3, Issue.2, March-April. 2013, pp-1135-113.
- [6.] N.K.Ingole, D.V. Bhope —Stress analysis of tractor trailer chassis for self-weight reductionI International Journal of Engineering Science and Technology (IJEST), ISSN: 0975-5462 Vol. 3 No. 9 September 2011
- [7.] Manpreet Singh Bajwa, SinthyaPundir, Amit Joshi ”Static Load Analysis of TATA Super Ace Chassis And Stress Optimisation Using Standard Techniques”,International J of Mechanical And Production Engineering. ISSN: 2320-2092,vol-1, No.2(Aug-2013).
- [8.] Joseph Edward Shigley, Charles R. Mischke “Mechanical Engineering Design”, McGraw-Hill Book Company, New York, 2000, Sixth Edition.
- [9.] M. F. Spotts, “Design of Machine Elements”, Prentice Hall of India Pvt. Ltd, New delhi, 2004.
- [10.] Reddy J.N, “An Introduction to Finite Element Method”, Tata McGraw-Hill Publication, Fifth Edition.

Data Mining Techniques in Higher Education an Empirical Study for the University of Palestine

Rasha Ragheb Atallah¹, Professor Samy S. Abu Naser²

¹(Faculty of Information Technology, The University of Palestine, Gaza, Palestine)

²(Department of Information Technology, Faculty of Engineering & Information Technology, Al Azhar)

Abstract: Nowadays, ones of the biggest challenges that educational institutions face is the explosive growth of educational data. and how to use these data to improve the quality of managerial decisions. Data mining, as an analytical tools that can be used to extract meaningful knowledge from large data sets, can be used to achieve this goal.

This paper addresses the applications of Educational Data Mining (EDM) to extract useful information from registration information of student at university of Palestine in Gaza strip. The data include five years period [2005-2011] by providing analytical tool to view and use this information for decision making processes by taking real life example such as grade and GPA for the students. abstract should summarize the content of the paper.

Keywords: Association, Classification, Clustering, Data mining, Higher education, Knowledge discovery, rules, Outlier analysis

I. INTRODUCTION

Educational Data Mining (EDM) is an emerging discipline, concerned with developing methods for exploring the unique types of data that come from educational setting ,and using those methods to better understand students, and the settings which they learn in [1]. Educational data mining can mine student GPA, student address, enrollment data, and applying it any college. Also with data mining the university can predicate which student will graduated and whose will not., So the university can use this result for improving the education behavior and improving student performance.

This paper applicant at University of Palestine which is a Palestinian private institution of higher education located in Al-Zahra' (south of Gaza City), the university was established in 2005.

In the paper, we try to extract useful knowledge from the registration system at University of Palestine during 5 years from [2005-2011]. After data preprocessing, we applied the association rules, Classification rules, and outlier analysis mining techniques.

II. RELATED WORKS

Hsu and Schombert in [3] analyze a data set comprised of academic records of undergraduates at the University of Oregon from 2000-2004. They found correlations of roughly 0.35 to 0.5 between SAT(predictive power of tests for college admissions) scores and upper division, in-major GPA (henceforth, GPA).

Interestingly, low SAT scores do not preclude high performance in most majors. The paper hypothesizes that over achievers overcome cognitive deficits through hard work, and discusses to what extent they can be identified from high school records. Only a few majors seem to exhibit a cognitive threshold – such that high GPA (mastery of the subject matter) is very unlikely below a certain SAT threshold (i.e., no matter how dedicated or hard working the student). There results suggest that almost any student admitted to university can achieve academic success, if they work hard enough. Also the paper found that the best predictor of GPA is a roughly equally weighted sum of SAT and high school GPA, measured in standard deviation units. Finally, the paper observe that one SAT scores fluctuate little on retest (very high reliability), two SAT and GRE scores (where available) correlate at roughly 0.75 (consistent with the notion that both tests measure a stable general cognitive ability) and three SAT distribution of students that obtained a degree does not differ substantially from that of the entering class.

Romero and Ventura in [4] introduced a survey of the specific application of data mining in learning management systems and a case study tutorial with the Moodle system. It is objective is to introduce it both

theoretically and practically to all users interested in this new research area, and in particular to online instructors and e-learning administrators, they describe the full process for mining e-learning data step by step as well as how to apply the main data mining techniques used, such as statistics, visualization, classification, clustering and association rule mining of Moodle data. They have described how different data mining techniques can be used in order to improve the course and the students' learning. All these techniques can be applied separately in a same system or together in a hybrid system.

Vialardi et. al in [5] focused on how university students can take the right decision in relation to their academic itinerary based on available information such as courses, schedules, section. This paper proposes use the recommendation system based on data mining techniques to help students to take decision on their academic itineraries, as example how many and which courses to enroll on ,having as basis the experience of previous students with similar academic achievements, they analyzed real data corresponding to seven years of student enrolment at the school of system Engineering at Universidad de Lima ,According to this analysis they developed a system.

Hongjie in [6] described how data mining techniques can be used to determine the student learning result evaluation system is an essential tool and approach for monitoring and controlling the learning quality. From the perspective of data analysis, this paper conducts a research on student learning result based on data mining.

III. CONCEPTS IN DATA MINING

The objective of this research is to identify the data mining techniques which can be applied in the field of Higher education.

3.1. Data Mining Definition and Techniques

Data mining refers to extracting or "mining" knowledge from large amounts of data [7]. Data mining techniques are used on large volumes of data to discover hidden patterns and relationships to help in decision making. The sequences of steps identified in extracting knowledge from data as shown in figure 1.

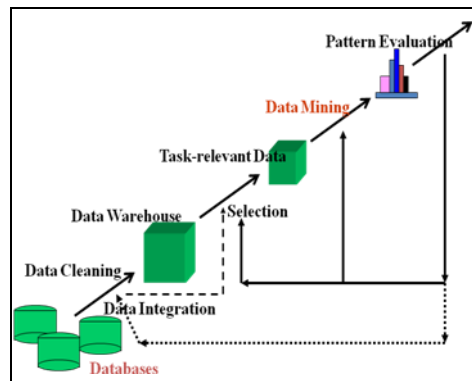


Fig 1: The steps of extracting knowledge from data

3.2. Data Collection

Initially the university provided us with 65536 records corresponding to 2493 students. The data supplied was students data at 5 faculties: Engineering, Information Technology, Management, Low and Media enrolled through the years of 2005 to 2011.

3.3. Data Preprocessing

In the entire data mining process it is of great relevance the data cleaning process in order to eliminate irrelevant item, as section number. ID of student , mid grade and final grade because in this paper the grade of the course is the needed also to fill the missing values in the data.

IV. CASE STUDY APPLICATION

This section represents the various techniques of data mining which applicant in the data of the registration at University of Palestine.

4.1. Association

Association analysis is the discovery of association rules showing attribute-value conditions that occur frequently together in a given set of data. Association rules used to discover the relationship between the grade of the course and the GPA of the student using FP-Growth operator. Figure 2 shows some resulting rules by association rules model with their evaluation factors support, confidence, and lift.

No.	Premises	Conclusion	Support	Confid.	LePlice	Gain	p-s	Lift	Comvit.
12	Total	GPA	0.967	0.999	0.999	-0.070	0.001	1.001	1.657
11	CourseID, Total	GPA	0.953	0.999	0.999	-0.066	0.001	1.001	1.632
10	CourseID	GPA	0.983	0.999	0.999	-0.088	-0.000	1.000	0.985
9	GPA	CourseID	0.983	0.985	0.983	-1.012	-0.000	1.000	0.988
8	Total	CourseID	0.954	0.985	0.983	-0.984	-0.000	1.000	0.969
7	GPA, Total	CourseID	0.953	0.985	0.983	-0.982	-0.000	1.000	0.967
6	Total	GPA, CourseID	0.953	0.983	0.982	-0.985	0.000	1.000	1.028
5	GPA	Total	0.967	0.970	0.985	-1.028	0.001	1.001	1.030
4	GPA, CourseID	Total	0.953	0.969	0.985	-1.013	0.000	1.000	1.015
3	CourseID	Total	0.954	0.969	0.984	-1.016	-0.000	1.000	0.985
2	CourseID	GPA, Total	0.953	0.967	0.984	-1.018	-0.000	1.000	0.985
1	GPA	CourseID, Total	0.953	0.985	0.978	-1.042	0.001	1.001	1.018

Fig. 2 Some Resulting Rules from Association Rules Model

Table 1: Associations rules for grade of the student data

Rule		Confidence
1#	[CourseID, Total] --> [GPA]	0.999
2#	[Total] --> [GPA]	0.999
3#	[GPA, Total] --> [CourseID]	0.985
4#	[Total] --> [CourseID]	0.985
5#	[GPA] --> [CourseID]	0.985
6#	[GPA, CourseID] --> [Total]	0.969

According to the rules in table1 for example from rule 1# if the course ID and total founded so the GPA founded. [not clear], also according to rule 3# from the total for the course and the GPA we can know the course because some course know that the general path for this course are high mark as Arabic but as principle of law it is mark as low.

Rule 6 help us in extract the grade of the course if we know the GPA and the Course that help the Academic advisor in the Faculty which courses registered to the student and how many hours he can registered.

4.2. Classification

Classification is the processing of finding a set of models (or functions) which describe and distinguish data classes or concepts, for the purposes of being able to use the model to predict the class of objects whose class label is unknown. The derived model may be represented in various forms, such as classification (IF-THEN) rules, decision trees, mathematical formulae, or neural networks. Classification can be used for predicting the class label of data objects.

In this work classification used to label is the student pass or fail according to the grade of the student, the grade type was the label in the operators which used to implemented the classification, In this paper two methods for the classification were implemented: the K_NN (k=10) with training data 60% and k =10 the result of K_NN is accuracy: 99.82%. In Decision Tree operator, it achieved 99.97% accuracy as shown in figure 3 below, the Decision tree of pass or fail student.

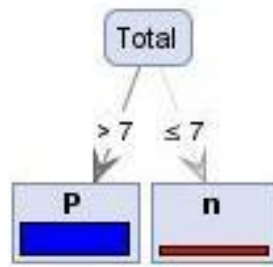


Fig. 3: Resulting Decision Tree

4.3. Outlier Analysis

A Database can contain data objects that do not obey the general behavior of the data and are identified as outliers[9]. The analysis of these outliers may help in fraud detection and predicting abnormal values.

In the EDM, outlier can be used to detect whether a student cheated in the exams according to his grade in the course and his GPA or detect the student phenomenon that he act in some courses better than other, or to guide the student in choosing the proper major in the university.

In this paper outlier founded to show the relation between the grade of the course and the GPA for the student, it was used to detect outlier (distance) operator.

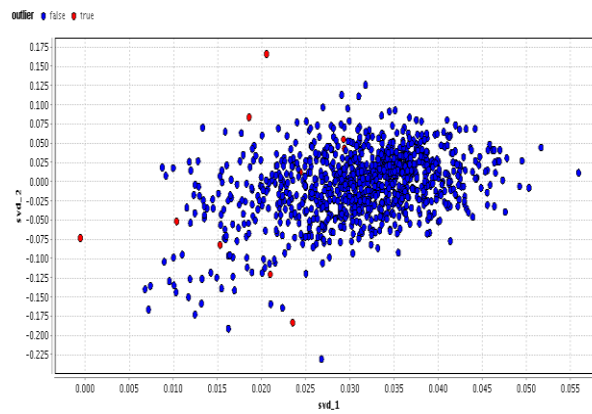


Fig. 4: Outliers Distribution

As we noted in Table 2 that there were three type of outliers :

- 1- The Grade was 99 and the GPA =60 here we can note that this student may be interested in this course so he can change his major.
- 2- The GPA was 95.95 and his grade 0, in this case the grade was not entered so must be entered by the teacher that help the Registration department in solving this problem.
- 3- The GPA = 0 and grade 99, in this situation the student registered zero credit hour course only.

Table 2: presented the analysis for the outliers

Number of outlier	Analysis
2	One of the outlier that student grade was 99 and his GPA 60
6	One of the outlier that student grade zero and this GPA 95.95 because here grade not entered
2	One of the outlier that student grade 99 and this GPA 0

V. CONCLUSION

In this study, a discussion of various data mining techniques which can support education system were presented. Since the application of data mining have a lot of advantages in higher learning institution, it is recommended to apply these techniques in the areas like guide student in chose his faculty. Furthermore, it enhances the performance of student in terms of his grade, detect the fraud of student in grade also can detect if student grades were changed in the database.

Acknowledgements

We would like to thank all people who provided any type of help in this paper, especially Mr. Sameh Abu Hassera from the University of Palestine.

REFERENCES

- [1] "EducationalDataMining.org". 2010 <http://www.educationaldatamining.org/>. Retrieved 26-4-2014
- [2] Han Jiawei, Micheline Kamber, Data Mining: Concepts and Technique. Morgan Kaufmann Publishers, 2000
- [3] Data Mining the University: College GPA Predictions from SAT Scores. Stephen D.H. Hsu, James Schombert
- [4] C. Romero, S. Ventura, E. Garcia, "Datamining in course management systems: Moodle case study and tutorial", Computers & Education, Vol. 51, No. 1, pp. 368-384, 2008.
- [5] César Vialardi, Javier Bravo, Leila Shafti, Elvaro, Recommendation in Higher Education Using Data Mining Techniques, Educational Data Mining, 2009.
- [6] Sun Hongjie, "Research on Student Learning Result System based on Data Mining", IJCSNS International Journal of Computer Science and Network Security, Vol.10, No. 4, April 2010.
- [7] http://en.wikipedia.org/wiki/Data_mining 25/4/2014.
- [8] http://en.wikipedia.org/wiki/Educational_data_mining, 26-4-2014.
- [9] Sakthi Nathiarasan A , Algorithm for Outlier Detection Based onUtility and Clustering (ODUC), International Journal of Advanced Research in Computer Science and Software Engineering, Volume 3, Issue 7, July 2013.

Advanced Micro-Grids

Raveesha.S.H¹, Ashoka.H.N²

¹*Asst.Professor, SBIT Tiptur,*

²*Associate Professor, UBDTCE Davanagere*

Abstract: *In modern society every sector needs continuous power on demand. To achieve this voltage, current and frequency, these parameters of the power system should be at rated values. Because of remote generation, transmission and distribution, we are failing to receive the reliable power. To overcome this problem, the Distribution energy sources (DES) become more suitable solution. This generated power from DES is supplied to local loads and this can be connected to the main grid through the Micro-Grid (MG). Micro-grids will operate in two modes, A Grid-connected mode and in an Islanded mode. During islanding mode, one Distributed Generation (DG) unit should share output generation power with other unit in exact accordance with the load. Need to control Real and Reactive power effectively for the load to operate without disturbance. Hence in the present work, Voltage Source Inverter (VSI) and Proportional Integral Derivative(PID) controller in power conversion process to get required real and reactive power for the normal operation of micro-grid. The proposed method has been applied to a designed test Simulink model for different types of Grid connected and Isolated modes. The simulation results obtained show that, this method can improve the reliability and smooth operation of the micro-grid system.*

Index Terms: *Distributed generation, PID control, micro-grids,*

I. Introduction

Distributed generation also called local generation [1]-[4]. Where the power is generated there itself distributed the power, generates power from many small energy sources, Solar power , Wind power, Bio-gas, Fuel cell etc. Distributed generation (DG) identified as one of the mechanism for ensuring supply of power in rural areas, remote areas, and hilly areas by way of setting up small generating units based on a variety of local fuel along with localized distribution. Usually conventional plants are far away from the populated area, so to transmit the power from generation plant to distribution power network, cost of transmission will be more and protection for this system is needed more compared to the Distributed generation.

Distributed generation used to supply the power continuously and quality of power supply, Distributed generation it is more necessary in the power system. Distributed generation for flexible operation Micro grid, mainly classified into three types, Distributed generation, Micro-Grid and control system [4].

A micro grid is designed to seamlessly separate from the grid when problems in the utility grid arise, reconnecting again once these problems are resolved [15]. Normally in grid connected mode, the micro sources act as constant power sources, which are controlled to inject the demanded power into the network. In autonomous mode, micro sources are controlled to supply all the power needed by the local loads while maintaining the voltage and frequency within the acceptable operating limits.

II. Control Required

Reactive power is essential to maintain and control voltage in AC electrical systems. The ability to meet the demand for rapid changes in reactive power prevents instability, voltage sags, even voltage collapse. Newer technology, such as the DSTATCOM Distribute Static Compensator offers a better solution to voltage stability problems. In that DSTATCOM includes Voltage source Inverter (VSI), Current Converter(C-C). PID [12]. The DSTATCOM generates a variable voltage V_d , that is very nearly in phase with the source voltage V_s . The inductance in this simplified circuit, L , consists of the inductance of the coupling transformer and filter. The voltage across the inductance, V_L , equals $V_s - V_d$. If $V_s > V_d$, V_L is in phase with V_s and current I_L lags V_s by 90° , DSTATCOM acting as a generator produces leading reactive current. If $V_s < V_d$, V_L is anti phase with V_s and current I_L leads V_s by 90° , DSTATCOM produces lagging reactive current[5].

DSTATCOM used to control the inner loop and outer loop. DSTATCOM is an Independent control of these quantities can be achieved with the using Clark transformation

$$P = v_q \cdot i_q + v_d \cdot i_d \dots\dots\dots (1.1)$$

$$Q = v_q \cdot i_d - v_d \cdot i_q \dots\dots\dots (1.2)$$

Where P =Active power,
 Q =Reactive power
 v_d =Real voltage
 v_q =Imaginary voltage,
 i_d =Real current,
 i_q =Imaginary current

Normally, for rotating machines the d-axis of the d_q -reference system is chosen at the rotor of the machine. This leads to $v_d = VSTATCOM$ and $v_q = 0$ and hence for the active and reactive power using equation (1.1 and 1.2)

$$P = v_d \cdot i_d \dots\dots\dots (1.3)$$

$$Q = -v_d \cdot i_q \dots\dots\dots (1.4)$$

The transformation into the rotating d -reference frame leads to the possibility to control the two current components i_d and i_q independently and hence control the active and reactive power independently.

Therefore static errors in the control system can be removed by applying PID controllers. The STATCOM controls the voltage by injecting or absorbing reactive power and q-axis current component of the current has to be controlled.. The output of the controllers is brought to a limiter block which limits the output of the controllers and provides the reference values for the inner controller loop. The output signal i_{dref} is limited

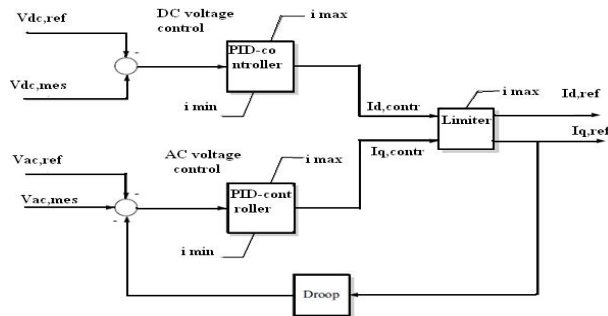


Figure.1.10. STATCOM outer control loop

$$i_{d,ref} = \left\{ \begin{array}{ll} -i_{max} & \text{if } i_{d,contr} < -i_{max} \\ i_{max} & \text{if } i_{d,contr} > i_{max} \\ i_{d,contr} & \text{if } -i_{max} < i_{d,contr} < i_{max} \end{array} \right\} \dots(1.5)$$

For the limitation of i_{qref} as follows

$$i_{q,ref} = \left\{ \begin{array}{ll} -i_{max} + |i_{d,ref}| & \text{if } i_{q,contr} < -i_{max} + |i_{d,ref}| \\ i_{max} - |i_{d,ref}| & \text{if } i_{q,contr} > i_{max} - |i_{d,ref}| \\ i_{q,contr} & \text{if } -i_{max} + |i_{d,ref}| < i_{q,contr} < i_{max} - |i_{d,ref}| \end{array} \right\} \dots\dots\dots(1.6)$$

The block scheme of the inner controller loop is given in figure 1.11. The inner controllers consist of two regular PID-controllers which are much faster than the outer loop controllers. The output of the inner controllers is the modulation index M_d and M_q which actually control the converter

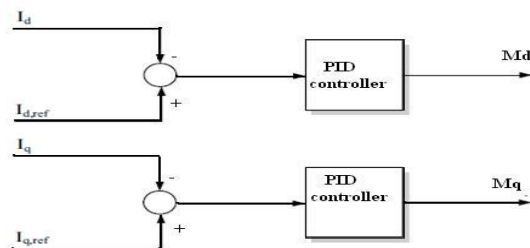


Figure 1.11. STATCOM inner loop control

III. Control system Design

3.1. Physical Model Design

3.1.1 System Configuration

Fig.3.1. shows the micro-grid system under study, which is adapted from the IEEE 1559 standard for low voltage applications [17]. The adopted study system represents a general low voltage distribution system, where different types of loads and different numbers of DG units can be considered to be connected to the main feeder. The DG units can be employed to work either parallel to the utility grid, or in isolated mode to serve sensitive loads connected to the main feeder when the main breaker (BR) is open. Without loss of generality, the performance of the micro-grid system is studied under the presence of two DG units, supplying general types of loads. The load on the second feeder is an inductive load where a 2.5-KVAr power factor correction capacitor bank is also considered to be connected to the main feeder. The adopted load model is in line with the IEEE 1547 test load used in DG applications. The nonlinear load is a three-phase diode rectifier with an R-L load at the dc-side. The addition of the diode rectifier helps in assessing the effectiveness of the proposed controller in rejecting voltage harmonics associated with nonlinear loading, and rejecting load-DG-unit-grid interactions at harmonic frequencies. The schematic diagram of a single DG unit as the building block of the sample micro-grid system is also shown in Fig.3.1. When the DG unit is connected to the grid, the voltage and frequency at the point of common coupling are dominantly dictated by the grid. However, in case of weak grids, the voltage is prone to voltage sags and disturbances. In this case, the DG unit can be controlled to support the grid voltage. Therefore, both PQ and PV operational modes can be adopted in the grid- connected mode. Subsequent to an islanding event, DG

$$Z_{\alpha\beta} = Z_{\alpha} + jZ_{\beta} \dots \dots \dots (3.2)$$

Using (3.2), the state space model of the system in the $\alpha\beta$ frame is as follows

$$\frac{di_{L,\alpha\beta}}{dt} = -\frac{V_{o,\alpha\beta}}{L} + \frac{V_{inv,\alpha\beta}}{L}$$

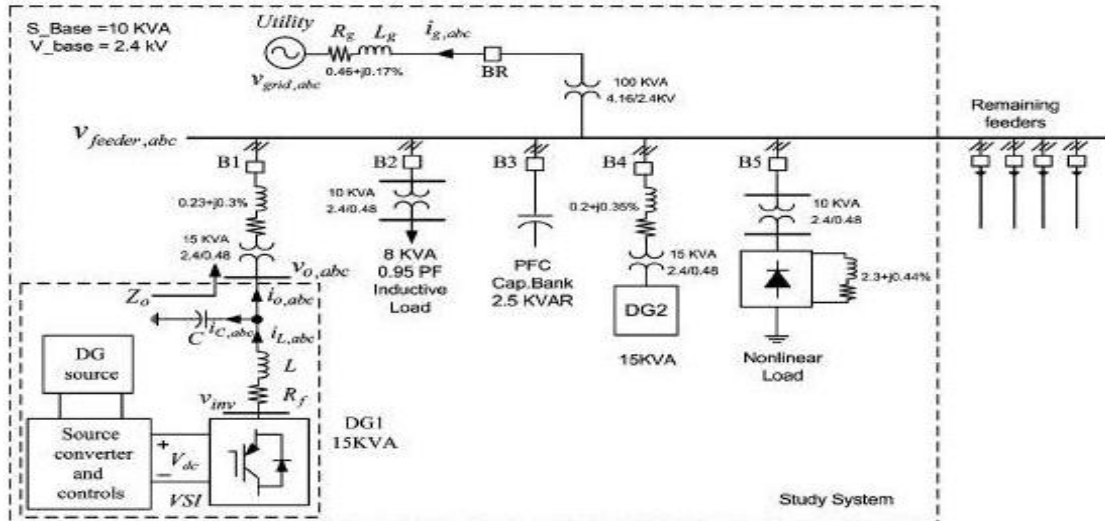


Fig.3.1. IEEE 1559 Single line diagram of the micro-grid study system

units can form an autonomous micro-grid system to enhance the reliability of sensitive loads[13]-[15]. In both grid connected and isolated modes, the state space presentation of the DG interface dynamics can be given in the natural frame

$$V_{inv,abc} = L \left(\frac{di_{L,abc}}{dt} \right) + V_{o,abc}$$

$$i_{L,abc} = i_{o,abc} + i_{c,abc} = i_{o,abc} + C \left(\frac{dv_{o,abc}}{dt} \right) \dots (3.1)$$

where L and C are the filter inductance and capacitance, $V_{inv,abc}$ is the inverter output voltage, $i_{L,abc}$ is the inverter output current, $V_{o,abc}$ is the voltage at the point of common coupling, and $i_{o,abc}$ is the network-side current. Note that $V_{inv,abc}$, $i_{L,abc}$, $V_{o,abc}$ and $i_{o,abc}$ are 3×1 vectors representing phase quantities corresponding to each phase, and the filter-inductor resistance is ignored. In order to decrease the number of differential equations and simplify system presentation, (3.1) can be rewritten in a stationary $\alpha\beta$ reference frame system by applying the following a b c to $\alpha\beta$ transformation.

$$Z_{\alpha\beta} = Za_e^{j0} + Zb_e^{j(-\frac{2\pi}{3})} + Zc_e^{j(\frac{2\pi}{3})}$$

$$\frac{d v_{o,\alpha\beta}}{dt} = \frac{i_{L,\alpha\beta}}{L} - \frac{i_{o,\alpha\beta}}{L} \dots \dots \dots (3.3)$$

Fig.3.2 the block diagram representation of the differential equations derived in (3.3) where models the disturbance caused by connecting the system to the utility grid. The block diagram suggests that the output current (i.e. i_o) can be regarded as an external disturbance caused by unknown load or grid behavior either in islanded or grid connected mode. Along with these disturbances, control mode switching in conventional DG controllers generates internal disturbances within the control structure.

3.1.2. Control Structure

As indicated in Fig. 3.2, external disturbances will be imposed on the DG interface during mode transition and network/load disturbances. On the other hand, internal disturbances will be generated due to control function switching between different modes in the conventional hierarchical control structure. To overcome these issues and to achieve a flexible and robust operation of DG units under the smart grid environment while maintaining the hierarchical control structure, the proposed control scheme, shown in Fig.3.2, utilizes a fixed hierarchical power–voltage–current control structure in both grid-connected and isolated modes[4]-[11]. This will minimize the undesired voltage transients generated by switching from a current-controlled interface to a voltage-controlled interface in conventional control techniques. Further, the proposed power controller works under grid-connected and isolated micro-grid modes. This feature provides a flexible interface for the DG unit to be used in different operational modes with minimal switching. Due to the proposed design strategy, both external and internal disturbances can be eliminated or remarkably attenuated within the DG interface. Moreover, the fixed control structure increases the robustness of the control structure to islanding detection delays. The voltage control is designed by considering an augmented model that includes the LC-filter active damping and inner current control loop dynamics to ensure robustness and coordinated control design. Theoretical analysis and design procedure of the proposed control scheme are described in the following sections.

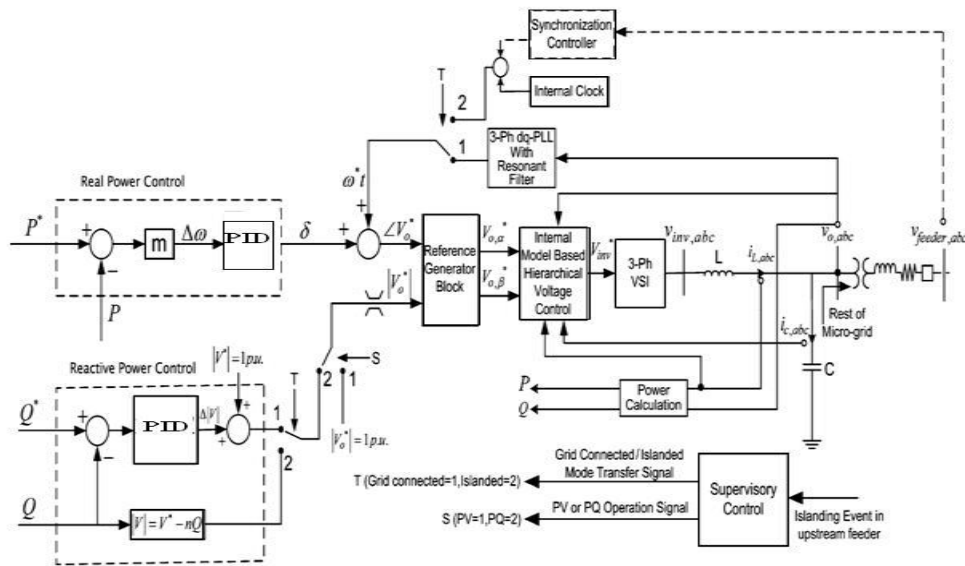


Fig.3.2. Control scheme

In resonance damping applying an LC filter at the output stage introduces a resonance peak to the frequency response of the system, which can limit the achievable bandwidth of the current controller in a multi loop hierarchical control approach. Besides, as the filter and grid parameters change, the corresponding resonance frequency also shifts, resulting in potential harmonic excitations at low-order harmonics affecting system stability. Therefore converter resonance damping is essential to maintain stability and facilitate high bandwidth current control design. Active damping resonance damping can be a viable option, particularly in DG applications and effective technique to actively damp filter resonance is to introduce a damping voltage that is proportional to the capacitor current. The dynamic equations corresponding to the actively damped system can be given as follows

$$L \frac{di_{L\alpha\beta}}{dt} = (v_{inv,\alpha\beta} - v_d) - v_{o,\alpha\beta} \dots\dots\dots (3.4)$$

$$v_d = R_d i_c \dots\dots\dots (3.5)$$

Where V_d represents the current-dependent voltage source injected in series with the original inverter output voltage and R_d is the virtual damping coefficient. With the active damping voltage modeled as a current-controlled voltage source, the open loop transfer function of the system is driven

$$G(s) = \frac{V_{o,\alpha\beta}}{V_{inv,\alpha\beta}} = \frac{1}{LCs^2 + R_d C_s + 1} \dots\dots\dots (3.6)$$

on the open loop system frequency characteristics. The resonance peak can be completely damped, and accordingly high control band width R_d can be achieved can provide the desired damping performance. A newly designed augmented internal model control (IMC) structure is proposed to provide internal model dynamics for harmonic, unbalanced, and random voltage disturbances.

Under exact model matching (i.e., $G_m(s) = G(s)$) and the absence of system disturbances, the feedback signal, which is influenced by the disturbance or any model uncertainties, would be zero. In this case, the IMC structure [16], shown in Fig.3.3, regarded as an open loop system where the feed-forward compensator should be designed to ensure close tracking performance. On the other hand, disturbance rejection achieved via the feedback compensator design. Since the tracking and disturbance rejection performances can be designed independently, the IMC control scheme. The sensitivity function (S) and the complementary sensitivity function (T), which represents tracking and Disturbance rejection capabilities of the system, respectively, driven as follows

$$S(s) = \frac{y(s)}{d(s)} r = 0$$

$$S(s) = \frac{1}{1 + G_m(s) Q_d(s)} \dots\dots\dots (3.7)$$

$$T(s) = \frac{Y(s)}{r(s)} d = 0$$

$$T(s) = \frac{G(s) Q_r(s) (1 + G_m(s) Q_d(s))}{1 + G_m(s) Q_d(s)} \dots\dots\dots (3.8)$$

The design goal is then to propose and such that and within a reasonably large range of frequencies of interest. This assures both disturbance rejection and tracking ability of the system. Assuming and then the model following error (e) is zero and the control scheme is reduced to an open loop one with $T(s) = Q(r(s))G(s)$ Performance stability constraints require an improper transfer function and cannot be realized practically. Therefore, a low pass filter is used to yield a proper feed-forward compensator

$$Q_r(s) = \frac{1}{(\tau s + 1)^n} \cdot G_m^{-1}(s) \dots\dots\dots (3.9)$$

Where τ corresponds to the bandwidth of the filter, and n is an integer selected in such a way that $Q_r(s)$ is a proper function. The disturbance rejection is achieved via $Q_d(s)$ which produces a compensating input to cancel out disturbances. To overcome the computational burden associated with frame a transformation, the proposed controller is performed in $\alpha\beta$ - frame. Proportional Integral derivative resonant controller used removes the harmonic.

The augmented model simplified as shown in Fig.3.5, where $G(s)$ models the transfer function between V_{inv} and v in the presence of the active damping loop. The output/input transfer function is given by

$$\frac{V_o}{i_L} = \frac{K_c L}{L^2 C_s^2 + (K_c L_c + R_d L C)s + (L + K_c R_d C)} \dots\dots\dots (3.10)$$

IMC-based multi loop voltage control structure. Considering the output/input relation calculated in (3.10) and the design approach introduced in (3.9), $Q_r(s)$ given by (3.11), where “m” denotes nominal model parameters.

$$Q_r(s) = \frac{L_m^2 C_m^2 + (K_c L_m C_m + R_d L_m C_m)s + (L_m + R_d K_c C_m)}{K_c L_m (\tau s + 1)^2} \dots\dots\dots (3.11)$$

It can be noted that the feed-forward compensator is both stable and proper. The time constant τ dictates the tracking bandwidth of the system. It can be also noted that mismatch in system parameters can be considered as disturbances and it will be attenuated by the feedback compensators. The sensitivity transfer function of the proposed system, which represents the frequency response of the $\frac{V_o}{I_o}$ transfer function, can be also obtained from

$$\frac{V_o}{I_o} = \frac{L_s}{K_c Q_d(s) + L C_s^2 + (R_d C + K_c C)s + 1} \dots\dots\dots (3.12)$$

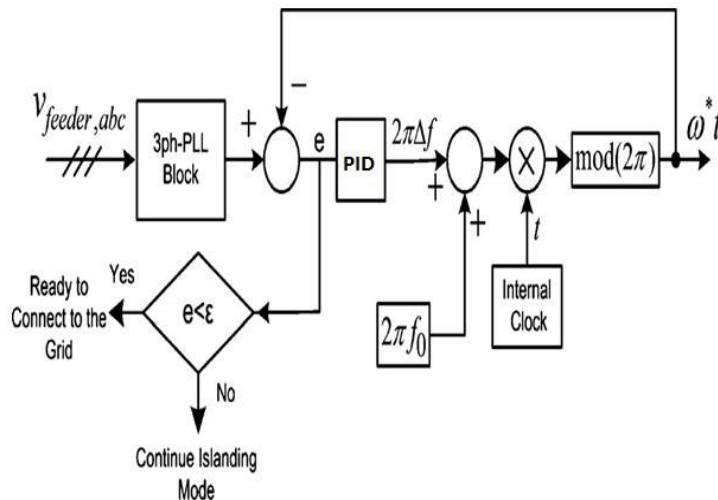


Fig.3.8. Synchronization controller

Power flow control adopted hierarchical design approach provides flexible operation of the DG unit in grid-connected mode [17]-[20]. To minimize the control switching actions between grid-connected and isolated modes, a single active power control structure is used in both modes. The proposed active power controller, shown in Fig.3.2, consists of a slow integrator, which generates frequency deviations $\Delta\omega$ according to the power-frequency characteristics presented in (3.13)

$$\Delta\omega = m(P^* - P) \dots\dots\dots (3.13)$$

The above equation (3.13) is very similar to the frequency-power droop equation in autonomous micro-grid system by adopting an appropriate slope coefficient (i.e., m) based on a reasonably small frequency deviation range, in the grid-connected mode, the phase angle of the grid $\omega^* t$ is generated via a dq three-phase phase-locked loop[5]. PLL during islanded operation, the processor internal clock is used to generate the a signal ω^* while is assumed to be 100. Considering the voltage and reactive power controller, the voltage amplitude can be either set to 1.0 p. u. for PV-bus operation. In the grid-connected mode, a Proportional integral derivative (PID) controller is adopted to provide the magnitude of the output voltage $|V|$. Therefore, the voltage control signal can be generated in islanded operation; however, a voltage droop function is adopted to share the reactive power among different DG units. Accordingly, the voltage magnitude is generated according to

$$|V_o| = V^* - nQ \dots \dots \dots (3.14)$$

Where n is the reactive power droop gain PLL configuration and Synchronization Fig. 3.8 can be realized by applying small frequency deviations in the voltage command to decrease the phase mismatching between the two voltages.

IV. Results And Discussion

To evaluate the performance of the proposed control scheme, the study system depicted in Fig.3.1 is implemented for time domain simulation under the Mat lab/Simulink. The proposed flexible control structure, shown in Fig. 3.2. Different modes are tested results are presented as follows

4.1. Grid-Connected Mode

Fig.4.1 and 4.2 shows the control performance under PQ-bus operation mode for one of the DG units. The inductive load and the capacitor bank are activated in this scenario. The reactive power command is set to zero, whereas the active power command experiences a step change from 6 to 10 kW at $t=1$ s. Fig.4.1 (1) and (2) shows the active and reactive powers generated by the unit. Close active power tracking performance. On the other hand, the coupling between active and reactive power dynamics is minimal. Fig.4.2 (1) depicts how the output voltage amplitude changes to maintain the unity power factor condition while increasing the active power injection. Voltage fluctuation in this mode is the natural result of the absence of voltage control at the point of common coupling. The instantaneous phase-a output voltage is shown in Fig.4.2 (2). In addition to active power regulation, the DG unit can contribute to the voltage reliability at the point of common coupling by allowing bus voltage control i.e., PV mode. This mode can be activated once voltage sags are detected. Under these conditions, the voltage control mode is activated to inject reactive power during the sag period to provide fault-ride-through performance. Accordingly, the economic operation of the DG unit will not be compromised. On the other hand, in long radial feeders and weak grids, existing DG units can be used for continuous voltage support.

Fig.4.3 & 4.4 shows the effectiveness of the proposed control strategy in terms of providing the DG unit with the fault-ride-through capability. The grid voltage encounters a 10% sag from $t=1$ s to $t=1.25$ s due to an upstream fault in the main feeder. The R-L-C load is Fig.4.3 & 4.4 shows the effectiveness of the proposed control strategy in terms of providing the DG unit with

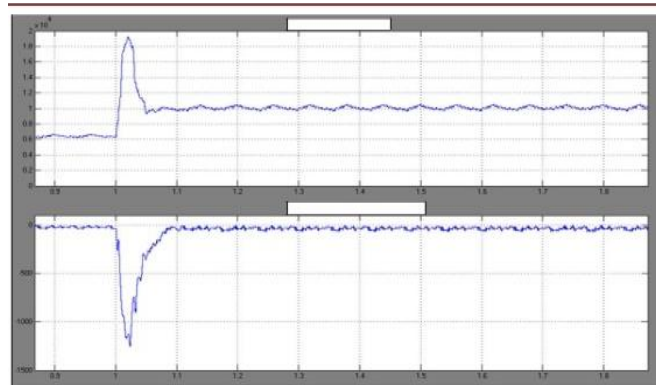


Fig. 4.1. (1) Converter active power. (2) Converter reactive power

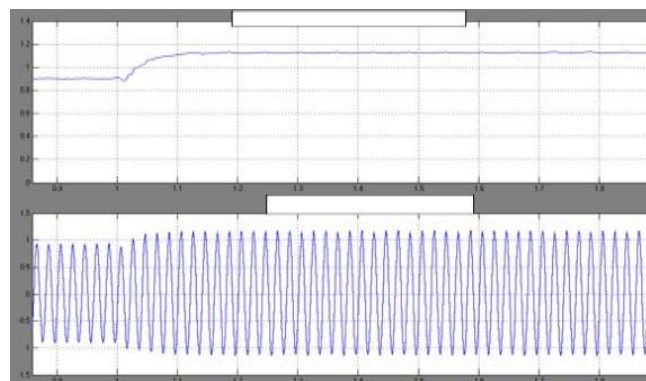


Fig.4.2. (1) Output voltage magnitude. (2) Instantaneous phase-a output voltage

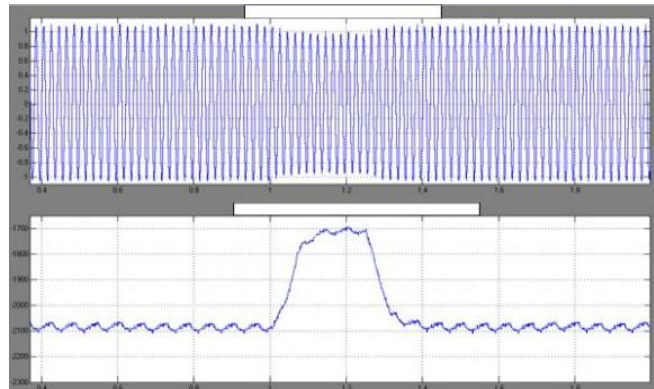


Fig. 4.3(1) Instantaneous output voltage. (2) Converter reactive power

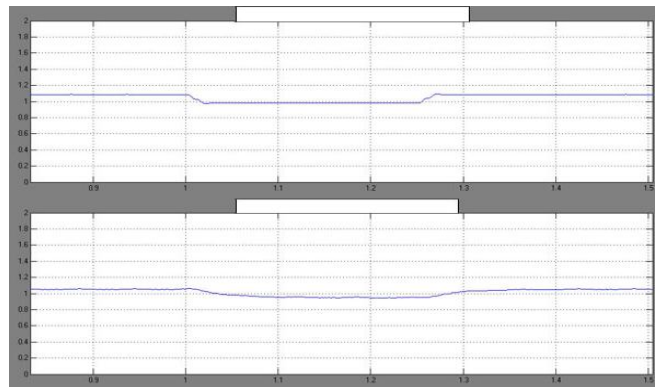


Fig.4.4 (1)Feeder voltage in p.u. (2) DG output voltage

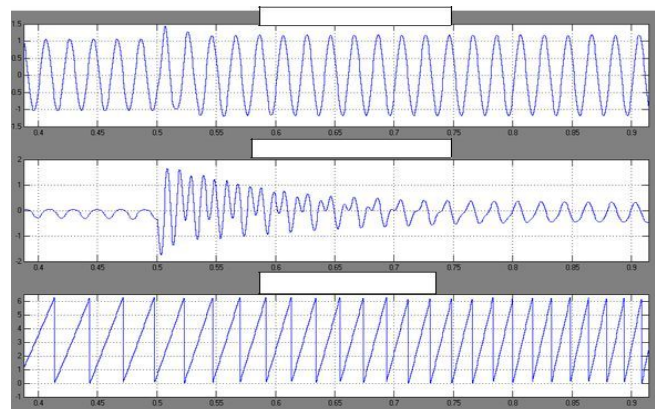


Fig.4.5. (1) Phase- a output voltage. (2) Phase-a load current (3) PLL output,

the fault-ride-through capability. The grid voltage encounters a 10% sag from $t=1s$ to $t=1.25s$ due to an upstream fault in the main feeder. The R-L-C load is assumed to be the locally connected load. Fig.4.3 (1) shows the phase-voltage during the voltage disturbance. Fig.4.3 (2) shows the reactive power injected by the unit during the fault period. Fig.4.4 (1) shows the magnitude of the output voltage of the main feeder. Fig.4.4 (2) shows the magnitude of the output voltage of the DG unit. Provided that there is enough reactive power rating, larger voltage sags can be mitigated by the DG interface.

To test the disturbance rejection against loading transient's band harmonic loading, the nonlinear load is switched ON at $t=0.5s$. The controller response to the addition of the nonlinear load is shown in Fig.4.5. Fig.4.5 (1) shows the output voltage waveform of phase-a, whereas Fig.4.5 (2) shows the load current. The proposed controller acts fast enough to reject the sudden loading disturbance yielding close voltage regulation at the local ac bus voltage. On the other hand, the harmonic disturbance rejection ability of the proposed controller is obvious. In spite of the heavily distorted load current, the total harmonic distortion (THD) of the phase-a voltage is 0.67% and 0.81% before and after adding the nonlinear load, respectively. The PLL output in the presence of harmonics is also shown in Fig.4.5 (3). Note that the PLL output is robust even after adding the rectifier load to the system. This is because of the resonant filter which provides robust phase tracking in the

presence of harmonics. These results confirm the high disturbance rejection performance of the proposed controller.

4.2 Isolated Mode

The transitional performance of the study system under the proposed control scheme from grid connected to islanded mode is evaluated by emulating an islanding event via opening the breaker switch (BR) at the upstream feeder in Fig.3.1. Initially, the micro-grid system is connected to the grid and both DG units are working in the PV-bus mode. The study system is islanded at $t=0.8s$ by opening the breaker BR. feeder breaker goes open and this event is signaled to the supervisory control unit shown in Fig.3.2. The detection delay is assumed to be 20 ms, therefore, the islanding event is detected at $t=0.82s$.

Fig.4.6 the dynamic response of the system before and after the islanding event. DG units utilize the same control structure, which is applied for both grid connected and islanded modes. Reactive power sharing is adopted in the isolated mode. The load voltage waveform and magnitude are shown in Fig.4.6 (1) and (2), respectively. In Fig.4.6 (1), the voltage response associated with the conventional method (i.e., from current-controlled to switching voltage-controlled interface) is also shown. As it can be seen, without applying the proposed method, the system is experiencing much higher over voltages due to the internal disturbance generated by switching from

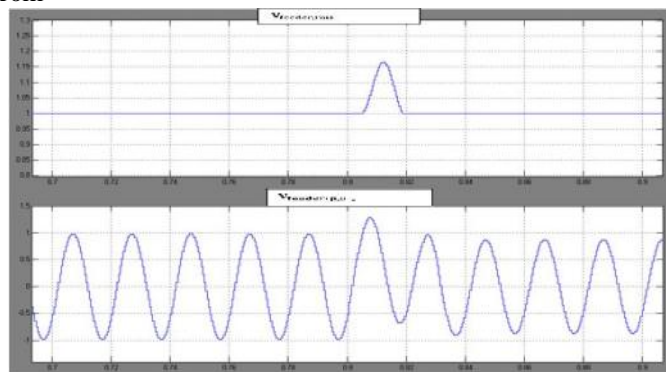


Fig.4.6. (1) RMS feeder voltage with proposed controller. (2) Instantaneous phase- a grid voltage with proposed controller

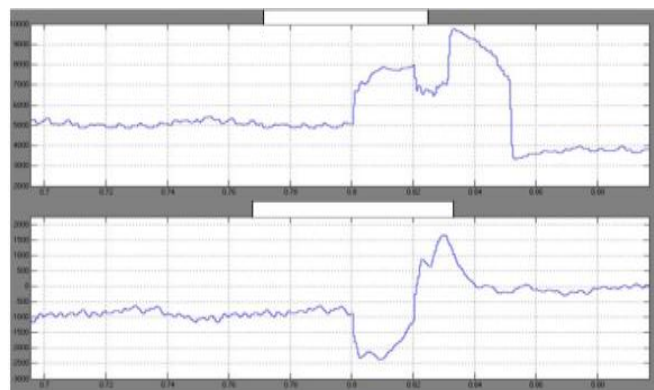


Fig.4.7. (1) Active converter powers of DG1 unit, (2) Reactive converter powers of each DG1 unit

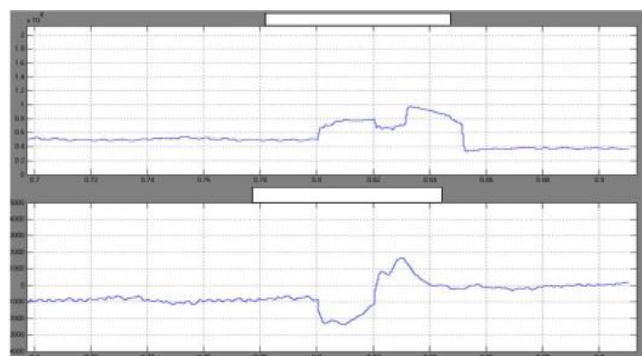


Fig. 4.8. (1) Active converter powers of DG2 unit, (2) Reactive converter powers of each DG2 unit

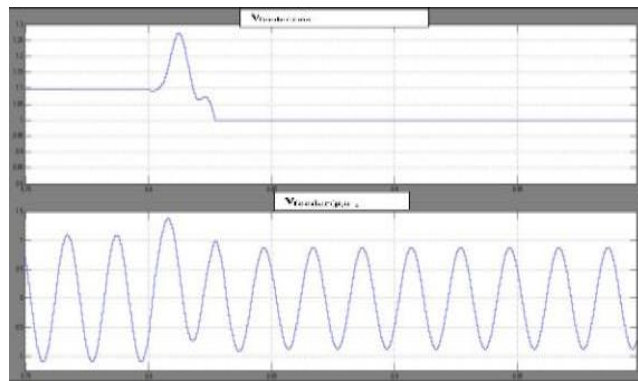


Fig.4.9. (1) RMS feeder voltage with proposed controller.. (2) Instantaneous phase- a grid voltage with proposed controller

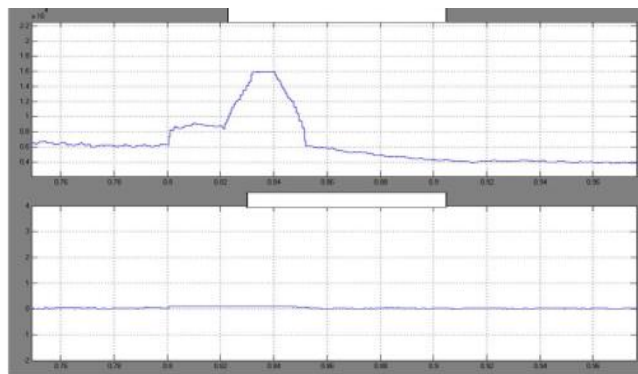


Fig.4.10.. (1) Active converter powers DG1 unit,(2) Reactive converter powers of each DG1 unit

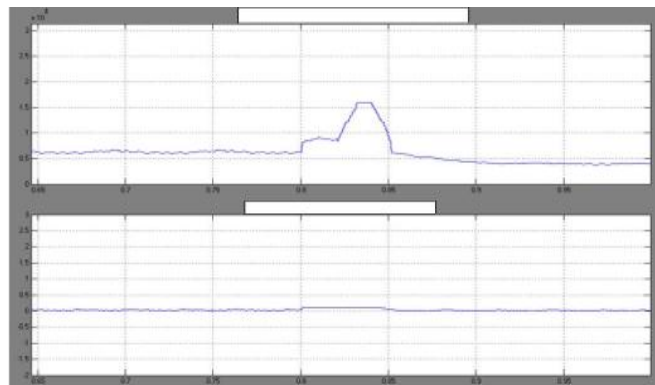


Fig.4.11. (1) Active converter powers of DG2 unit,(2) Reactive converter powers of each DG2 unit

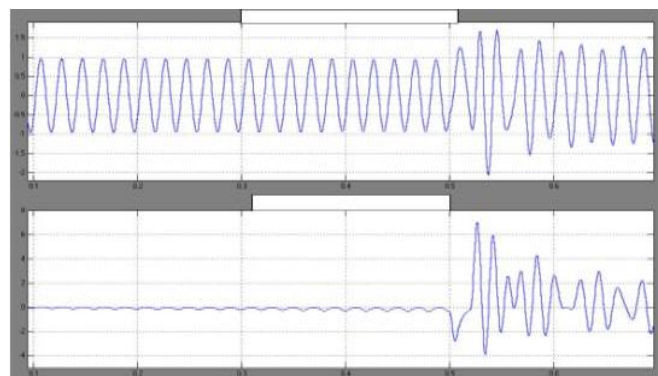


Fig.4.12. (1)Instantaneous phase-a output voltage. (2) Phase-a load current

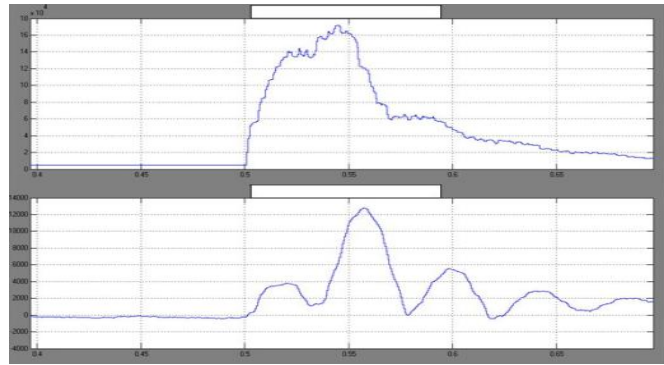


Fig.4.13. (1) Active converter powers for DG1. (2) Reactive converter powers for DG1

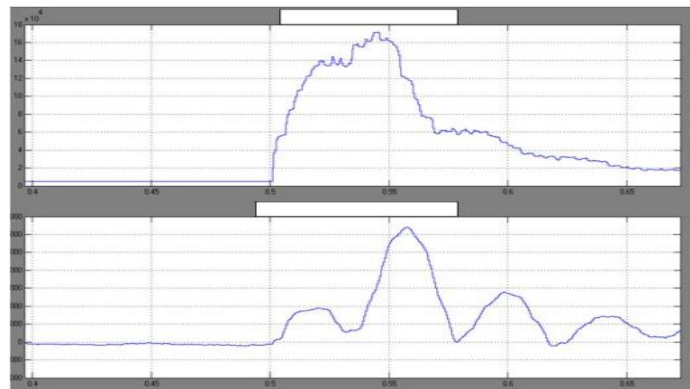


Fig.4.14. (1) Active converter powers for DG2. (2) Reactive converter powers for DG2

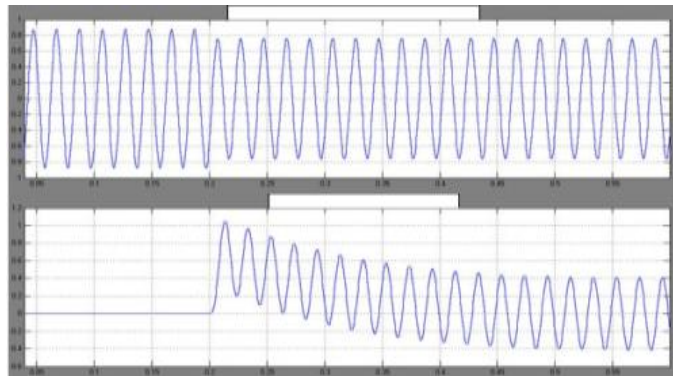


Fig.4.15. (1) Instantaneous phase-a output voltage. (2) Instantaneous phase-a grid current

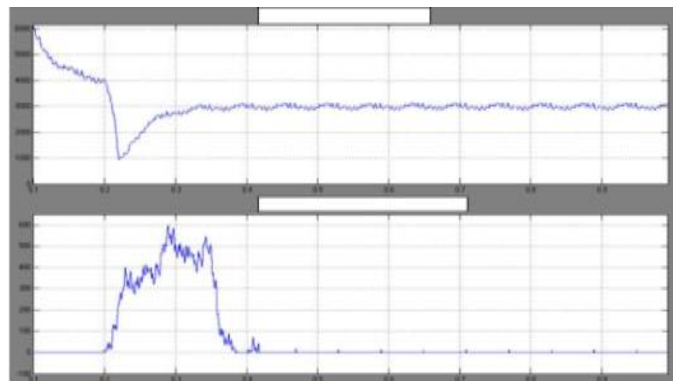


Fig.4.16 (1) Active converter powers for each DG1 unit.(2)Reactive converter powers for each DG1 unit

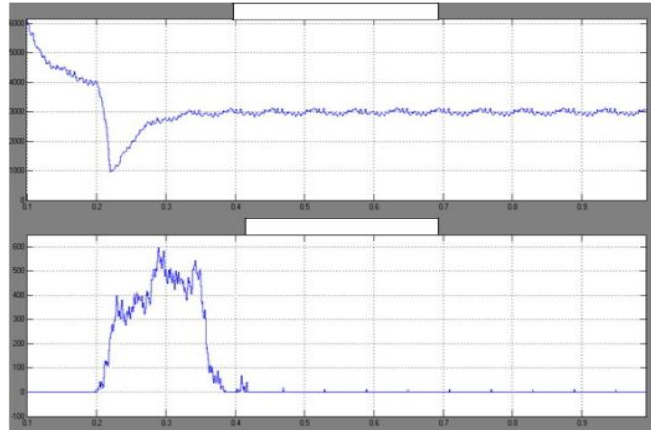


Fig.4.17. (1) Active converter powers for each DG2 unit, (2) Reactive converter powers for each DG2 unit.

Current-controlled interface to a voltage-controlled subsequent to an islanding event. The dynamics responses of the active and reactive power components for each DG unit are shown in Fig. 4.7 and 4.8, where the initial active power generated by each DG1 and DG2, dictated by the power controller in the grid connected mode. However, subsequent to the islanding event, the generated active power is decreased in order to meet the load consumption. For further performance, the micro-grid system is connected to the grid and both DG units are working in the PQ-bus mode with unity power factor. The utility supply is lost at $t=0.8$ s. The islanding is detected after 20 ms by the supervisory control unit at $t=0.82$ s. Fig.4.6, 4.7 & 4.8 depicts the dynamic response of the system prior and after the islanding event. The magnitude and load voltage waveform are shown in 4.9(1) and 4.9(2) respectively. Close voltage control characteristics are yielded subsequent to the islanding event. Once again the system response in the absence of the proposed scheme is shown in Fig.4.9 (2), where the higher transient over-voltage is obvious. The active and reactive power responses for DG units are shown in Fig.4.10 and 4.11, where the initial active power generated by each DG is 6.0 kW at unity power factor. Subsequent to the islanding event, the generated active power decreases in order to meet the load demand

Fig.4.12, 4.13 and 4.14 shows the load voltage and current responses of the islanded system when the nonlinear load is added at $t=0.5$ s. Fig.4.12 (1) shows the load voltage, whereas Fig. 4.12(2) shows the load current. It can be seen that the controller is well capable of maintaining the output voltage quality despite the highly distorted current going through the load. The THD of the load voltage is 2.7%. Fig. 4.13 shows the active and reactive power profiles of both DG1 units.4.14 Shows the active and reactive power profiles of DG2 units accurate power sharing performance is yielded even in the presence of harmonic loading, which demands reactive power injection by both DG units.

Fig.4.15, 4.16 and 4.17 shows the grid current, the load voltage, and power responses during a supply restoration scenario at $t=0.2$ s. Once the utility supply is restored, both DG units operate as a PQ bus with unity power factor and with a power command of 3.0 kW for each unit. In spite of grid-current transients, the load voltage is closely controlled to facilitate seamless restoration. Similar to the micro-grid formation event, the proposed control scheme yield seamless connection performance under the supply restoration event by rejecting the generated disturbances internally and externally within the control structure

PID,VSI used control the different mode of operation, maintaining constant real and reactive power during islanding and grid connected mode condition, compared to the PI controller PID controller utilizes a fixed power-voltage-current cascade control structure with robust internal model voltage controller to maximize the disturbance rejection performance within the DG interface and to minimize control function switching and also facilitates flexible DG operation in the grid-connected mode and autonomous micro grid.

V. CONCLUSION

The Simulink model has been design for the proposed test system and analyzed the simulation results for isolated mode and grid connected mode of the proposed test system. Be the simulation results we can conclude that, the following parameters can be controlled efficiently and in better way;

- It provides current limit capability for the Converter during grid faults.
- DGs shared the proper amount of power via proposed method.
- A start-up PLL based turn ON techniques to eliminate the circulating current completely during the turn ON the new incoming unit.
- Fast voltage regulation and effective mitigation dynamic, unbalanced voltage and harmonic voltage

disturbances.

- The proposed voltage and power sharing controller provide high disturbance rejection performance against voltage disturbances and power angle swing.
- It provides smooth transition capability between grid-connected and autonomous (islanded) modes.

The proposed control scheme enhances the flexibility of Micro-grid operation under the dynamic nature of future smart distribution system.

REFERENCES

- [1.] E.M.Lightener and S. E. Widergren, "An orderly transition to a transformed electricity systems," IEEE Trans. Smart Grid, vol. 1, no. 1, pp.3–10, Jun. 2010
- [2.] K.Molehill and R. Kumar, "A reliability perspective of smart grid,"IEEE Trans. Smart Grid, vol. 1, no. 1, pp. 57–64, Jun. 2010.
- [3.] G.T.Heydt, "The next generation of power distribution systems,"IEEE Trans. Smart Grid, vol. 1, no. 3, pp. 225–235, Nov. 2010
- [4.] A.Timbus, M. Liserre, R. Teodorescu, P. Rodriquez, and F. Blaabjerg,"Evaluation of current controllers for distributed power generation systems,"IEEE Trans. Power Electron., vol. 24, no. 3, pp. 654–664, Mar.2009
- [5.] J.M.Guerrero, J. C.Vasquez, J.Matas, K.Vicuna, and M. Castilla, "Hierarchical control of droop-controlled ac and dc micro grids A general approach towards standardization," IEEE Trans. Ind. Electron., to be published.
- [6.] M.Liserre, R. Teodorescu, and F. Blaabjerg, "Multiple harmonics control for three-phase grid converter systems with the use of PI-RES current controller in a rotating frame," IEEE Trans. Power Electron., vol.21, no. 3, pp. 836–841, May 2006.
- [7.] Y.A.-R.I.Mohamed, "Mitigation of dynamic, unbalanced and harmonic voltage disturbances using grid-connected inverters with LCL filter," IEEE Trans. Ind. Electron., vol. 58, no. 9, pp. 3914–3924, Sep.2011.
- [8.] S.Ahn,"Power-sharing method of multiple distributed generators considering modes and configurations of a micro grid," IEEE Trans. Power Del., vol. 25, no. 3, pp. 2007–2016, Jul. 2010.
- [9.] Twinning and D.G. Holmes, "Grid current regulation of a three phase voltage source inverter with an LCL input filter," IEEE Trans. Power Electron., vol. 18, no. 3, pp. 888– 895, May 2003
- [10.] D.De and V. Ramanarayanan, "Decentralized parallel operation of inverters sharing unbalanced and nonlinear loads," IEEE Trans. Power Electron., vol. 25, no. 12, pp. 3015–3022, Dec. 2010.
- [11.] H.Kim,T.Yu, and S. Choi, "Indirect current control algorithm for utility interactive inverters in distributed generation systems," IEEE Trans. Power Electron., vol. 23, no. 3, pp.1342–1347, May 2008
- [12.] Y.A.-R.I. Mohamed, "Mitigation of grid-converter resonance, grid-induced distortion and parametric instabilities in converter-based distributed generation," IEEE Trans. Power Electron., vol. 26, no. 3, pp.983–996, Mar. 2011.
- [13.] Z.Yao,L.Xiao, and Y.Yan, "Seamless transfer of single-phase grid interactive inverters between grid connected and stand-alone modes,"IEEE Trans. Power Electron., vol. 25, no. 6, pp. 1597–1603, Jun. 2010.
- [14.] F.Gao and R.Iravani, "A control strategy for a distributed generation unit in grid-connected and autonomous modes of operation," IEEE Trans. Power Del., vol. 23, no. 2,pp.850–859, Apr. 2008.
- [15.] Y.A.-R.I.Mohamed and A. Radwan, "Hierarchical control system for robust micro-grid operation and seamless mode-transfer in active distribution systems," IEEE Trans. Smart Grid, vol. 2, no. 2, pp. 352–362, Jun. 2011.
- [16.] M.Morari and E. Zafrious, Robust Process Control. Englewood Cliffs, NJ: Prentice Hall, 1989, ch. 2–3.
- [17.] F.Blaabjerg, R.Teodorescu, M.Liserre, and A.V.Timbus, "Overview of control and grid synchronization for distributed power generation systems," IEEE Trans. Ind. Electron., vol. 53, no. 5, pp. 1398–1409,Oct. 2006.
- [18.] Draft Guide for Design, Operation, and Integration of Distributed Resource Island Systems With Electric Power Systems, IEEE P1547.4.
- [19.] W. Xu,G. Zhang, C.Li,W.Wang, G.Wang, and J. Kliber, "A power line signaling based technique for anti-islanding protection of distributed generators–Part I: Scheme and analysis," in Proc. 2007 IEEE Power Engineering Society General Meeting, Jun. 24–28, 2007, p. 1.
- [20.] M.A.Redfern, O. U.Usta, and G. Fielding, "Protection against loss of utility grid supply for a dispersed storage and generation unit," IEEE Trans Power Del., vol. 8, no. 3, pp. 948–954, Jul. 1993